

**NATIONAL ADVISORY COMMITTEE  
FOR AERONAUTICS**

---

**REPORT No. 824**

**SUMMARY OF AIRFOIL DATA**

**By IRA H. ABBOTT, ALBERT E. VON DOENHOFF,  
and LOUIS S. STIVERS, Jr.**



**1945**

## AERONAUTIC SYMBOLS

### 1. FUNDAMENTAL AND DERIVED UNITS

	Symbol	Metric		English	
		Unit	Abbrevia- tion	Unit	Abbrevia- tion
Length.....	<i>l</i>	meter.....	m	foot (or mile).....	ft (or mi)
Time.....	<i>t</i>	second.....	s	second (or hour).....	sec (or hr)
Force.....	<i>F</i>	weight of 1 kilogram.....	kg	weight of 1 pound.....	lb
Power.....	<i>P</i>	horsepower (metric).....		horsepower.....	hp
Speed.....	<i>V</i>	{kilometers per hour.....	kph	miles per hour.....	mph
		{meters per second.....	mps	feet per second.....	fps

### 2. GENERAL SYMBOLS

<p><i>W</i> Weight = <math>mg</math></p> <p><i>g</i> Standard acceleration of gravity = <math>9.80665 \text{ m/s}^2</math> or <math>32.1740 \text{ ft/sec}^2</math></p> <p><i>m</i> Mass = <math>\frac{W}{g}</math></p> <p><i>I</i> Moment of inertia = <math>mk^2</math>. (Indicate axis of radius of gyration <i>k</i> by proper subscript.)</p> <p><math>\mu</math> Coefficient of viscosity</p>	<p><math>\nu</math> Kinematic viscosity</p> <p><math>\rho</math> Density (mass per unit volume)</p> <p>Standard density of dry air, <math>0.12497 \text{ kg-m}^{-3}\text{-s}^2</math> at <math>15^\circ \text{ C}</math> and <math>760 \text{ mm}</math>; or <math>0.002378 \text{ lb-ft}^{-3}\text{ sec}^2</math></p> <p>Specific weight of "standard" air, <math>1.2255 \text{ kg/m}^3</math> or <math>0.07651 \text{ lb/cu ft}</math></p>
---	--

### 3. AERODYNAMIC SYMBOLS

<p><i>S</i> Area</p> <p><i>S<sub>w</sub></i> Area of wing</p> <p><i>G</i> Gap</p> <p><i>b</i> Span</p> <p><i>c</i> Chord</p> <p><i>A</i> Aspect ratio, <math>\frac{b^2}{S}</math></p> <p><i>V</i> True air speed</p> <p><i>q</i> Dynamic pressure, <math>\frac{1}{2}\rho V^2</math></p> <p><i>L</i> Lift, absolute coefficient <math>C_L = \frac{L}{qS}</math></p> <p><i>D</i> Drag, absolute coefficient <math>C_D = \frac{D}{qS}</math></p> <p><i>D<sub>0</sub></i> Profile drag, absolute coefficient <math>C_{D_0} = \frac{D_0}{qS}</math></p> <p><i>D<sub>i</sub></i> Induced drag, absolute coefficient <math>C_{D_i} = \frac{D_i}{qS}</math></p> <p><i>D<sub>p</sub></i> Parasite drag, absolute coefficient <math>C_{D_p} = \frac{D_p}{qS}</math></p> <p><i>C</i> Cross-wind force, absolute coefficient <math>C_c = \frac{C}{qS}</math></p>	<p><i>i<sub>w</sub></i> Angle of setting of wings (relative to thrust line)</p> <p><i>i<sub>t</sub></i> Angle of stabilizer setting (relative to thrust line)</p> <p><i>Q</i> Resultant moment</p> <p><math>\Omega</math> Resultant angular velocity</p> <p><i>R</i> Reynolds number, <math>\rho \frac{Vl}{\mu}</math> where <i>l</i> is a linear dimension (e.g., for an airfoil of 1.0 ft chord, 100 mph, standard pressure at <math>15^\circ \text{ C}</math>, the corresponding Reynolds number is 935,400; or for an airfoil of 1.0 m chord, 100 mps, the corresponding Reynolds number is 6,865,000)</p> <p><math>\alpha</math> Angle of attack</p> <p><math>\epsilon</math> Angle of downwash</p> <p><math>\alpha_0</math> Angle of attack, infinite aspect ratio</p> <p><math>\alpha_i</math> Angle of attack, induced</p> <p><math>\alpha_a</math> Angle of attack, absolute (measured from zero-lift position)</p> <p><math>\gamma</math> Flight-path angle</p>
--	---

---

---

**REPORT No. 824**

**SUMMARY OF AIRFOIL DATA**

**By IRA H. ABBOTT, ALBERT E. VON DOENHOFF,  
and LOUIS S. STIVERS, Jr.**

**Langley Memorial Aeronautical Laboratory  
Langley Field, Va.**

---

---

# National Advisory Committee for Aeronautics

*Headquarters, 1500 New Hampshire Avenue NW., Washington 25, D. C.*

Created by act of Congress approved March 3, 1915, for the supervision and direction of the scientific study of the problems of flight (U. S. Code, title 49, sec. 241). Its membership was increased to 15 by act approved March 2, 1929. The members are appointed by the President, and serve as such without compensation.

JEROME C. HUNSAKER, Sc. D., Cambridge, Mass., *Chairman*

LYMAN J. BRIGGS, Ph. D., *Vice Chairman*, Director, National Bureau of Standards.

CHARLES G. ABBOT, Sc. D., *Vice Chairman, Executive Committee*, Secretary, Smithsonian Institution.

HENRY H. ARNOLD, General, United States Army, Commanding General, Army Air Forces, War Department.

WILLIAM A. M. BURDEN, Assistant Secretary of Commerce for Aeronautics.

VANNEVAR BUSH, Sc. D., Director, Office of Scientific Research and Development, Washington, D. C.

WILLIAM F. DURAND, Ph. D., Stanford University, California.

OLIVER P. ECHOLS, Major General, United States Army, Chief of Matériel, Maintenance, and Distribution, Army Air Forces, War Department.

AUBREY W. FITCH, Vice Admiral, United States Navy, Deputy Chief of Naval Operations (Air), Navy Department.

WILLIAM LITTLEWOOD, M. E., Jackson Heights, Long Island, N. Y.

FRANCIS W. REICHELDERFER, Sc. D., Chief, United States Weather Bureau.

LAWRENCE B. RICHARDSON, Rear Admiral, United States Navy, Assistant Chief, Bureau of Aeronautics, Navy Department.

EDWARD WARNER, Sc. D., Civil Aeronautics Board, Washington, D. C.

ORVILLE WRIGHT, Sc. D., Dayton, Ohio.

THEODORE P. WRIGHT, Sc. D., Administrator of Civil Aeronautics, Department of Commerce.

---

GEORGE W. LEWIS, Sc. D., *Director of Aeronautical Research*

JOHN F. VICTORY, LL. M., Secretary

HENRY J. E. REID, Sc. D., Engineer-in-Charge, Langley Memorial Aeronautical Laboratory, Langley Field, Va.

SMITH J. DEFRANCE, B. S., Engineer-in-Charge, Ames Aeronautical Laboratory, Moffett Field, Calif.

EDWARD R. SHARP, LL. B., Manager, Aircraft Engine Research Laboratory, Cleveland Airport, Cleveland, Ohio

CARLTON KEMPER, B. S., Executive Engineer, Aircraft Engine Research Laboratory, Cleveland Airport, Cleveland, Ohio

---

## TECHNICAL COMMITTEES

AERODYNAMICS

OPERATING PROBLEMS

POWER PLANTS FOR AIRCRAFT

MATERIALS RESEARCH COORDINATION

AIRCRAFT CONSTRUCTION

*Coordination of Research Needs of Military and Civil Aviation*

*Preparation of Research Programs*

*Allocation of Problems*

*Prevention of Duplication*

---

LANGLEY MEMORIAL AERONAUTICAL LABORATORY

Langley Field, Va.

AMES AERONAUTICAL LABORATORY

Moffett Field, Calif.

AIRCRAFT ENGINE RESEARCH LABORATORY, Cleveland Airport, Cleveland, Ohio

*Conduct, under unified control, for all agencies, of scientific research on the fundamental problems of flight*

---

OFFICE OF AERONAUTICAL INTELLIGENCE, Washington, D. C.

*Collection, classification, compilation, and dissemination of scientific and technical information on aeronautics*

## CONTENTS

	Page		Page
SUMMARY.....	1	EXPERIMENTAL CHARACTERISTICS—Continued	
INTRODUCTION.....	1	Drag Characteristics of Smooth Airfoils—Continued	
SYMBOLS.....	1	Effects of type of section on drag characteristics.....	18
HISTORICAL DEVELOPMENT.....	2	Effective aspect ratio.....	21
DESCRIPTION OF AIRFOILS.....	3	Effect of surface irregularities on drag.....	22
Method of Combining Mean Lines and Thickness Distributions.....	3	Permissible roughness.....	22
NACA Four-Digit Series Airfoils.....	4	Permissible waviness.....	22
Numbering system.....	4	Drag with fixed transition.....	24
Thickness distributions.....	5	Drag with practical construction methods.....	24
Mean lines.....	5	Effects of propeller slipstream and airplane vibration.....	29
NACA Five-Digit Series Airfoils.....	5	Lift Characteristics of Smooth Airfoils.....	30
Numbering system.....	5	Two-dimensional data.....	30
Thickness distributions.....	5	Three-dimensional data.....	37
Mean lines.....	5	Lift Characteristics of Rough Airfoils.....	37
NACA 1-Series Airfoils.....	5	Two-dimensional data.....	37
Numbering system.....	5	Three-dimensional data.....	38
Thickness distributions.....	5	Unconservative Airfoils.....	39
Mean lines.....	5	Pitching Moment.....	40
NACA 6-Series Airfoils.....	5	Position of Aerodynamic Center.....	43
Numbering system.....	5	High-Lift Devices.....	43
Thickness distributions.....	6	Lateral-Control Devices.....	43
Mean lines.....	6	Leading-Edge Air Intakes.....	49
NACA 7-Series Airfoils.....	7	Interference.....	50
Numbering system.....	7	APPLICATION TO WING DESIGN.....	51
Thickness distributions.....	7	Application of Section Data.....	51
THEORETICAL CONSIDERATIONS.....	8	Selection of Root Section.....	51
Pressure Distributions.....	8	Selection of Tip Section.....	52
Methods of derivation of thickness distributions.....	8	CONCLUSIONS.....	52
Rapid estimation of pressure distributions.....	10	APPENDIX—METHODS OF OBTAINING DATA IN THE LANGLEY	
Numerical examples.....	12	TWO-DIMENSIONAL LOW-TURBULENCE TUNNELS.....	54
Effect of camber on pressure distribution.....	13	Description of Tunnels.....	54
Critical Mach Number.....	13	Symbols.....	54
Moment Coefficients.....	14	Measurement of Lift.....	55
Methods of calculation.....	14	Measurement of Drag.....	56
Numerical examples.....	14	Tunnel-Wall Corrections.....	57
Angle of Zero Lift.....	14	Correction for Blocking at High Lifts.....	59
Methods of calculation.....	14	Comparison with Experiment.....	59
Numerical examples.....	14	REFERENCES.....	60
Description of Flow around Airfoils.....	15	TABLES.....	64
EXPERIMENTAL CHARACTERISTICS.....	16	SUPPLEMENTARY DATA:	
Sources of Data.....	16	I—Basic Thickness Forms.....	69
Drag Characteristics of Smooth Airfoils.....	16	II—Data for Mean Lines.....	89
Drag characteristics in low-drag range.....	16	III—Airfoil Ordinates.....	99
Drag characteristics outside low-drag range.....	18	IV—Predicted Critical Mach Numbers.....	113
		V—Aerodynamic Characteristics of Various Airfoil Sections.....	129

# REPORT No. 824

## SUMMARY OF AIRFOIL DATA

By IRA H. ABBOTT, ALBERT E. VON DOENHOFF, and LOUIS S. STIVERS, JR.

### SUMMARY

Recent airfoil data for both flight and wind-tunnel tests have been collected and correlated insofar as possible. The flight data consist largely of drag measurements made by the wake-survey method. Most of the data on airfoil section characteristics were obtained in the Langley two-dimensional low-turbulence pressure tunnel. Detail data necessary for the application of NACA 6-series airfoils to wing design are presented in supplementary figures, together with recent data for the NACA 00-, 14-, 24-, 44-, and 230-series airfoils. The general methods used to derive the basic thickness forms for NACA 6- and 7-series airfoils and their corresponding pressure distributions are presented. Data and methods are given for rapidly obtaining the approximate pressure distributions for NACA four-digit, five-digit, 6-, and 7-series airfoils.

The report includes an analysis of the lift, drag, pitching-moment, and critical-speed characteristics of the airfoils, together with a discussion of the effects of surface conditions. Data on high-lift devices are presented. Problems associated with lateral-control devices, leading-edge air intakes, and interference are briefly discussed. The data indicate that the effects of surface condition on the lift and drag characteristics are at least as large as the effects of the airfoil shape and must be considered in airfoil selection and the prediction of wing characteristics. Airfoils permitting extensive laminar flow, such as the NACA 6-series airfoils, have much lower drag coefficients at high speed and cruising lift coefficients than earlier types of airfoils if, and only if, the wing surfaces are sufficiently smooth and fair. The NACA 6-series airfoils also have favorable critical-speed characteristics and do not appear to present unusual problems associated with the application of high-lift and lateral-control devices.

### INTRODUCTION

A considerable amount of airfoil data has been accumulated from tests in the Langley two-dimensional low-turbulence tunnels. Data have also been obtained from tests both in other wind tunnels and in flight and include the effects of high-lift devices, surface irregularities, and interference. Some data are also available on the effects of airfoil section on aileron characteristics. Although a large amount of these data has been published, the scattered nature of the data and the limited objectives of the reports have prevented adequate analysis and interpretation of the results. The purpose of this report is to summarize these data and to correlate and interpret them insofar as possible.

Recent information on the aerodynamic characteristics of NACA airfoils is presented. The historical development of NACA airfoils is briefly reviewed. New data are presented that permit the rapid calculation of the approximate pressure distributions for the older NACA four-digit and five-digit airfoils by the same methods used for the NACA 6-series airfoils. The general methods used to derive the basic thickness forms for NACA 6- and 7-series airfoils together with their corresponding pressure distributions are presented. Detail data necessary for the application of the airfoils to wing design are presented in supplementary figures placed at the end of the paper. The report includes an analysis of the lift, drag, pitching-moment, and critical-speed characteristics of the airfoils, together with a discussion of the effects of surface conditions. Available data on high-lift devices are presented. Problems associated with lateral-control devices, leading-edge air intakes, and interference are briefly discussed, together with aerodynamic problems of application.

Numbered figures are used to illustrate the text and to present miscellaneous data. Supplementary figures and tables are not numbered but are conveniently arranged at the end of the report according to the numerical designation of the airfoil section within the following headings:

- I—Basic Thickness Forms
- II—Data for Mean Lines
- III—Airfoil Ordinates
- IV—Predicted Critical Mach Numbers
- V—Aerodynamic Characteristics of Various Airfoil Sections

These supplementary figures and tables present the basic data for the airfoils.

### SYMBOLS

$A$	aspect ratio
$A_n, B_n$	Fourier series coefficients
$a$	mean-line designation, fraction of chord from leading edge over which design load is uniform; in derivation of thickness distributions, basic length usually considered unity
$b$	wing span
$b_{f_i}$	flap span, inboard
$b_{f_o}$	flap span, outboard
$C_D$	drag coefficient
$C_{D_{L=0}}$	drag coefficient at zero lift
$C_L$	lift coefficient
$\Delta C_{L_f}$	increment of maximum lift caused by flap deflection

$c$	chord	$x_L$	abscissa of lower surface
$c_a$	aileron chord	$x_U$	abscissa of upper surface
$c_d$	section drag coefficient	$\left(\frac{x}{c}\right)_{tr}$	chordwise position of transition
$c_{d_{min}}$	minimum section drag coefficient	$y$	distance perpendicular to chord
$c_{f_i}$	flap chord, inboard	$y_c$	mean-line ordinate
$c_{f_o}$	flap chord, outboard	$y_L$	ordinate of lower surface
$\frac{c_f}{c}$	flap-chord ratio	$y_t$	ordinate of symmetrical thickness distribution
$c_H$	section aileron hinge-moment coefficient $\left(\frac{h}{q_0 c^2}\right)$	$y_U$	ordinate of upper surface
$\Delta c_H$	increment of aileron hinge-moment coefficient at constant lift	$z$	complex variable in circle plane
$\Delta c_H \delta$	hinge-moment parameter	$z'$	complex variable in near-circle plane
$c_l$	section lift coefficient	$\alpha$	angle of attack
$c_{l_i}$	design section lift coefficient	$\frac{\Delta \alpha_0}{\Delta \delta}$	section aileron effectiveness parameter, ratio of change in section angle of attack to increment of aileron deflection at a constant value of lift coefficient
$c_{m_{a.c.}}$	moment coefficient about aerodynamic center	$\alpha_{l_0}$	angle of zero lift
$c_{m_{c/4}}$	moment coefficient about quarter-chord point	$\alpha_0$	section angle of attack
$c_n$	section normal-force coefficient	$\Delta \alpha_0$	increment of section angle of attack
$D$	drag	$\alpha_i$	section angle of attack corresponding to design lift coefficient
$\Delta H$	loss of total pressure	$\delta$	flap or aileron deflection; down deflection is positive
$H_0$	free-stream total pressure	$\delta_{f_i}$	flap deflection, inboard
$h$	section aileron hinge moment	$\delta_{f_o}$	flap deflection, outboard
$h_e$	exit height	$\epsilon$	airfoil parameter ( $\phi - \theta$ )
$k$	constant	$\epsilon_{TE}$	value of $\epsilon$ at trailing edge
$L$	lift	$\zeta$	complex variable in airfoil plane
$M$	Mach number	$\theta$	angular coordinate of $z'$ ; also, angle of which tangent is slope of mean line
$M_{cr}$	critical Mach number	$\lambda$	taper ratio $\left(\frac{\text{Tip chord}}{\text{Root chord}}\right)$
$0_U, 0_L$	typical points on upper and lower surfaces of airfoil	$\tau$	turbulence factor $\left(\frac{\text{Effective Reynolds number}}{\text{Test Reynolds number}}\right)$
$P$	pressure coefficient $\left(\frac{p - p_0}{q_0}\right)$	$\phi$	angular coordinate of $z$
$P_{cr}$	critical pressure coefficient	$\psi$	airfoil parameter determining radial coordinate of $z$
$P_R$	resultant pressure coefficient; difference between local upper- and lower-surface pressure coefficients	$\psi_0$	average value of $\psi$ $\left(\frac{1}{2\pi} \int_0^{2\pi} \psi d\phi\right)$
$p$	local static pressure; also, angular velocity in roll in $pb/2V$		
$p_0$	free-stream static pressure		
$pb/2V$	helix angle of wing tip		
$q_0$	free-stream dynamic pressure		
$R$	Reynolds number		
$R_{cr}$	critical Reynolds number		
$S$	pressure coefficient $\left(\frac{H_0 - p}{q_0}\right)$		
$t_1$	first airfoil thickness ratio		
$t_2$	second airfoil thickness ratio		
$V$	free-stream velocity		
$V_i$	inlet velocity		
$v$	local velocity		
$\Delta v$	increment of local velocity		
$\Delta v_a$	increment of local velocity caused by additional type of load distribution		
$\left(\frac{v}{V}\right)_{t_1}$	velocity ratio corresponding to thickness $t_1$		
$\left(\frac{v}{V}\right)_{t_2}$	velocity ratio corresponding to thickness $t_2$		
$x$	distance along chord		
$x_e$	mean-line abscissa		

#### HISTORICAL DEVELOPMENT

The development of types of NACA airfoils now in common use was started in 1929 with a systematic investigation of a family of airfoils in the Langley variable-density tunnel. Airfoils of this family were designated by numbers having four digits, such as the NACA 4412 airfoil. All airfoils of this family had the same basic thickness distribution (reference 1), and the amount and type of camber was systematically varied to produce the family of related airfoils. This investigation of the NACA airfoils of the four-digit series produced airfoil sections having higher maximum lift coefficients and lower minimum drag coefficients than those of sections developed before that time. The investigation also provided information on the changes in aerodynamic characteristics resulting from variations of geometry of the mean line and thickness ratio (reference 1).

The investigation was extended in references 2 and 3 to include airfoils with the same thickness distribution but with positions of the maximum camber far forward on the airfoil. These airfoils were designated by numbers having five digits, such as the NACA 23012 airfoil. Some airfoils of this family showed favorable aerodynamic characteristics except for a large sudden loss in lift at the stall.

Although these investigations were extended to include a limited number of airfoils with varied thickness distributions (references 1 and 3 to 6), no extensive investigations of thickness distribution were made. Comparison of experimental drag data at low lift coefficients with the skin-friction coefficients for flat plates indicated that nearly all of the profile drag under such conditions was attributable to skin friction. It was therefore apparent that any pronounced reduction of the profile drag must be obtained by a reduction of the skin friction through increasing the relative extent of the laminar boundary layer.

Decreasing pressures in the direction of flow and low air-stream turbulence were known to be favorable for laminar flow. An attempt was accordingly made to increase the relative extent of laminar flow by the development of airfoils having favorable pressure gradients over a greater proportion of the chord than the airfoils developed in references 1, 2, 3, and 6. The actual attainment of extensive laminar boundary layers at large Reynolds numbers was a previously unsolved experimental problem requiring the development of new test equipment with very low air-stream turbulence. This work was greatly encouraged by the experiments of Jones (reference 7), who demonstrated the possibility of obtaining extensive laminar layers in flight at relatively large Reynolds numbers. Uncertainty with regard to factors affecting separation of the turbulent boundary layer required experiments to determine the possibility of making the rather sharp pressure recoveries required over the rear portion of the new type of airfoil.

New wind tunnels were designed specifically for testing airfoils under conditions closely approaching flight conditions of air-stream turbulence and Reynolds number. The resulting wind tunnels, the Langley two-dimensional low-turbulence tunnel (LTT) and the Langley two-dimensional low-turbulence pressure tunnel (TDT), and the methods used for obtaining and correcting data are briefly described in the appendix. In these tunnels the models completely span the comparatively narrow test sections; two-dimensional flow is thus provided, which obviates difficulties previously encountered in obtaining section data from tests of finite-span wings and in correcting adequately for support interference (reference 8).

Difficulty was encountered in attempting to design airfoils having desired pressure distributions because of the lack of adequate theory. The Theodorsen method (reference 9), as ordinarily used for calculating the pressure distributions about airfoils, was not sufficiently accurate near the leading edge for prediction of the local pressure gradients. In the absence of a suitable theoretical method, the 9-percent-thick symmetrical airfoil of the NACA 16-series (reference 10)

was obtained by empirical modification of the previously used thickness distributions (reference 4). These NACA 16-series sections represented the first family of the low-drag high-critical-speed sections.

Successive attempts to design airfoils by approximate theoretical methods led to families of airfoils designated NACA 2- to 5-series sections (reference 11). Experience with these sections showed that none of the approximate methods tried was sufficiently accurate to show correctly the effect of changes in profile near the leading edge. Wind-tunnel and flight tests of these airfoils showed that extensive laminar boundary layers could be maintained at comparatively large values of the Reynolds number if the airfoil surfaces were sufficiently fair and smooth. These tests also provided qualitative information on the effects of the magnitude of the favorable pressure gradient, leading-edge radius, and other shape variables. The data also showed that separation of the turbulent boundary layer over the rear of the section, especially with rough surfaces, limited the extent of laminar layer for which the airfoils should be designed. The airfoils of these early families generally showed relatively low maximum lift coefficients and, in many cases, were designed for a greater extent of laminar flow than is practical. It was learned that, although sections designed for an excessive extent of laminar flow gave extremely low drag coefficients near the design lift coefficient when smooth, the drag of such sections became unduly large when rough, particularly at lift coefficients higher than the design lift. These families of airfoils are accordingly considered obsolete.

The NACA 6-series basic thickness forms were derived by new and improved methods described herein in the section "Methods of Derivation of Thickness Distributions," in accordance with design criteria established with the objective of obtaining desirable drag, critical Mach number, and maximum-lift characteristics. The present report deals largely with the characteristics of these sections. The development of the NACA 7-series family has also been started. This family of airfoils is characterized by a greater extent of laminar flow on the lower than on the upper surface. These sections permit low pitching-moment coefficients with moderately high design lift coefficients at the expense of some reduction in maximum lift and critical Mach number.

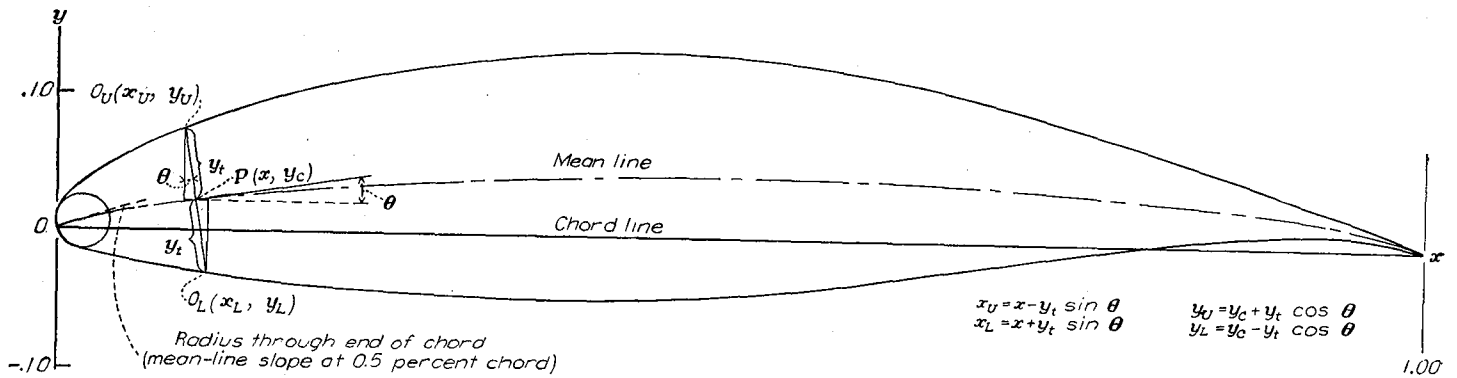
Acknowledgement is gratefully expressed for the expert guidance and many original contributions of Mr. Eastman N. Jacobs, who initiated and supervised this work.

## DESCRIPTION OF AIRFOILS

### METHOD OF COMBINING MEAN LINES AND THICKNESS DISTRIBUTIONS

The cambered airfoil sections of all NACA families considered herein are obtained by combining a mean line and a thickness distribution. The necessary geometric data and some theoretical aerodynamic data for the mean lines and thickness distributions may be obtained from the supplementary figures by the methods described for each family of airfoils.



SAMPLE CALCULATIONS FOR DERIVATION OF THE NACA 65,3-818,  $a=1.0$  AIRFOIL

$x$	$y_t$ ( $c$ )	$y_c$ ( $c$ )	$\tan \theta$	$\sin \theta$	$\cos \theta$	$y_t \sin \theta$	$y_t \cos \theta$	$x_U$	$y_U$	$x_L$	$y_L$
0	0	0				0	0	0	0	0	0
.005	.01324	.00200	$c$ 0.33696	0.31932	0.94765	.00423	.01255	.00077	.01455	.00923	-.01055
.05	.03831	.01264	.18744	.18422	.98288	.00706	.03765	.04294	.05029	.05706	-.02501
.25	.08093	.03580	.06996	.06979	.99756	.00565	.08073	.24435	.11653	.25565	-.04493
.50	.08593	.04412	0	0	1.00000	0	.08593	.50000	.13005	.50000	-.04181
.75	.04456	.03580	-.06996	-.06979	.99756	-.00311	.04445	.75311	.08025	.74689	-.00865
1.00	0	0				0	0	1.00000	0	1.00000	0

<sup>a</sup> Thickness distribution obtained from ordinates of the NACA 65,3-018 airfoil.  
<sup>b</sup> Ordinates of the mean line, 0.8 of the ordinate for  $c_t=1.0$ .  
<sup>c</sup> Slope of radius through end of chord.

FIGURE 1.—Method of combining mean lines and basic thickness forms.

The process for combining a mean line and a thickness distribution to obtain the desired cambered airfoil section is illustrated in figure 1. The leading and trailing edges are defined as the forward and rearward extremities, respectively, of the mean line. The chord line is defined as the straight line connecting the leading and trailing edges. Ordinates of the cambered airfoil are obtained by laying off the thickness distribution perpendicular to the mean line. The abscissas, ordinates, and slopes of the mean line are designated as  $x_c$ ,  $y_c$ , and  $\tan \theta$ , respectively. If  $x_U$  and  $y_U$  represent, respectively, the abscissa and ordinate of a typical point of the upper surface of the airfoil and  $y_t$  is the ordinate of the symmetrical thickness distribution at chordwise position  $x$ , the upper-surface coordinates are given by the following relations:

$$x_U = x - y_t \sin \theta \quad (1)$$

$$y_U = y_c + y_t \cos \theta \quad (2)$$

The corresponding expressions for the lower-surface coordinates are

$$x_L = x + y_t \sin \theta \quad (3)$$

$$y_L = y_c - y_t \cos \theta \quad (4)$$

The center for the leading-edge radius is found by drawing a line through the end of the chord at the leading edge with the slope equal to the slope of the mean line at that point and laying off a distance from the leading edge along this line equal to the leading-edge radius. This method of construction causes the cambered airfoils to project slightly forward

of the leading-edge point. Because the slope at the leading edge is theoretically infinite for the mean lines having a theoretically finite load at the leading edge, the slope of the radius through the end of the chord for such mean lines is usually taken as the slope of the mean line at  $\frac{x}{c}=0.005$ . This

procedure is justified by the manner in which the slope increases to the theoretically infinite value as  $x/c$  approaches 0. The slope increases slowly until very small values of  $x/c$  are reached. Large values of the slope are thus limited to values of  $x/c$  very close to 0 and may be neglected in practical airfoil design.

Tables of ordinates are included in the supplementary data for all airfoils for which standard characteristics are presented.

#### NACA FOUR-DIGIT-SERIES AIRFOILS

**Numbering system.**—The numbering system for the NACA airfoils of the four-digit series (reference 1) is based on the airfoil geometry. The first integer indicates the maximum value of the mean-line ordinate  $y_c$  in percent of the chord. The second integer indicates the distance from the leading edge to the location of the maximum camber in tenths of the chord. The last two integers indicate the airfoil thickness in percent of the chord. Thus, the NACA 2415 airfoil has 2-percent camber at 0.4 of the chord from the leading edge and is 15 percent thick.

The first two integers taken together define the mean line, for example, the NACA 24 mean line. The symmetrical airfoil sections representing the thickness distribution for a family of airfoils are designated by zeros for the first two integers, as in the case of the NACA 0015 airfoil.

**Thickness distributions.**—Data for the NACA 0006, 0008, 0009, 0010, 0012, 0015, 0018, 0021, and 0024 thickness distributions are presented in the supplementary figures. Ordinates for intermediate thicknesses may be obtained correctly by scaling the tabulated ordinates in proportion to the thickness ratio (reference 1). The leading-edge radius varies as the square of the thickness ratio. Values of  $(v/V)^2$ , which is equivalent to the low-speed pressure distribution, and of  $v/V$  are also presented. These data were obtained by Theodorsen's method (reference 9). Values of the velocity increments  $\Delta v_a/V$  induced by changing angle of attack (see section "Rapid Estimation of Pressure Distributions") are also presented for an additional lift coefficient of approximately unity. Values of the velocity ratio  $v/V$  for intermediate thickness ratios may be obtained approximately by linear scaling of the velocity increments obtained from the tabulated values of  $v/V$  for the nearest thickness ratio; thus,

$$\left(\frac{v}{V}\right)_{t_2} = \left[\left(\frac{v}{V}\right)_{t_1} - 1\right] \frac{t_2}{t_1} + 1 \quad (5)$$

Values of the velocity-increment ratio  $\Delta v_a/V$  may be obtained for intermediate thicknesses by interpolation.

**Mean lines.**—Data for the NACA 62, 63, 64, 65, 66, and 67 mean lines are presented in the supplementary figures. The data presented include the mean-line ordinates  $y_c$ , the slope  $dy_c/dx$ , the design lift coefficient  $c_{li}$  and the corresponding design angle of attack  $\alpha_i$ , the moment coefficient  $c_{m_{c/4}}$ , the resultant pressure coefficient  $P_R$ , and the velocity ratio  $\Delta v/V$ . The theoretical aerodynamic characteristics were obtained from thin-airfoil theory. All tabulated values for each mean line, accordingly, vary linearly with the maximum ordinate  $y_c$ , and data for similar mean lines with different amounts of camber within the usual range may be obtained simply by scaling the tabulated values. Data for the NACA 22 mean line may thus be obtained by multiplying the data for the NACA 62 mean line by the ratio 2:6, and for the NACA 44 mean line by multiplying the data for the NACA 64 mean line by the ratio 4:6.

#### NACA FIVE-DIGIT-SERIES AIRFOILS

**Numbering system.**—The numbering system for airfoils of the NACA five-digit series is based on a combination of theoretical aerodynamic characteristics and geometric characteristics (references 2 and 3). The first integer indicates the amount of camber in terms of the relative magnitude of the design lift coefficient; the design lift coefficient in tenths is thus three-halves of the first integer. The second and third integers together indicate the distance from the leading edge to the location of the maximum camber; this distance in percent of the chord is one-half the number represented by these integers. The last two integers indicate the airfoil thickness in percent of the chord. The NACA 23012 airfoil thus has a design lift coefficient of 0.3, has its maximum camber at 15 percent of the chord, and has a thickness ratio of 12 percent.

**Thickness distributions.**—The thickness distributions for airfoils of the NACA five-digit series are the same as those for airfoils of the NACA four-digit series.

**Mean lines.**—Data for the NACA 210, 220, 230, 240, and 250 mean lines are presented in the supplementary figures in the same form as for the mean lines given herein for the four-digit series. All tabulated values for each mean line vary linearly with the maximum ordinate or with the design lift coefficient. Thus, data for the NACA 430 mean line may be obtained by multiplying the data for the NACA 230 mean line by the ratio 4:2 and for the NACA 640 mean line by multiplying the data for the NACA 240 mean line by the ratio 6:2.

#### NACA 1-SERIES AIRFOILS

**Numbering system.**—The NACA 1-series airfoils are designated by a five-digit number—as, for example, the NACA 16-212 section. The first integer represents the series designation. The second integer indicates the distance in tenths of the chord from the leading edge to the position of minimum pressure for the symmetrical section at zero lift. The first number following the dash indicates the amount of camber expressed in terms of the design lift coefficient in tenths, and the last two numbers together indicate the thickness in percent of the chord. The commonly used sections of this family have minimum pressure at 0.6 of the chord from the leading edge and are usually referred to as the NACA 16-series sections.

**Thickness distributions.**—Data for the NACA 16-006, 16-009, 16-012, 16-015, 16-018, and 16-021 thickness distributions (reference 10) are presented in the supplementary figures. These data are similar in form to the data for those airfoils of the NACA four-digit series, and data for intermediate thickness ratios may be obtained in the same manner.

**Mean lines.**—The NACA 16-series airfoils as commonly used are cambered with a mean line of the uniform-load type ( $a=1.0$ ), which is described under the section for the NACA 6-series airfoils that follows. If any other type of mean line is used, this fact should be stated in the airfoil designation.

#### NACA 6-SERIES AIRFOILS

**Numbering system.**—The NACA 6-series airfoils are usually designated by a six-digit number together with a statement showing the type of mean line used. For example, in the designation NACA 65,3-218,  $a=0.5$ , the "6" is the series designation. The "5" denotes the chordwise position of minimum pressure in tenths of the chord behind the leading edge for the basic symmetrical section at zero lift. The "3" following the comma gives the range of lift coefficient in tenths above and below the design lift coefficient in which favorable pressure gradients exist on both surfaces. The "2" following the dash gives the design lift coefficient in tenths. The last two digits indicate the airfoil thickness in percent of the chord. The designation " $a=0.5$ " shows the type of mean line used. When the mean-line designation is not given, it is understood that the uniform-load mean line ( $a=1.0$ ) has been used.

When the mean line used is obtained by combining more than one mean line, the design lift coefficient used in the designation is the algebraic sum of the design lift coefficients of the mean lines used, and the mean lines are described in the statement following the number as in the following case:

$$\text{NACA } 65,3-218 \left\{ \begin{array}{l} a=0.5, c_{li}=0.3 \\ a=1.0, c_{li}=-0.1 \end{array} \right\}$$

Airfoils having a thickness distribution obtained by linearly increasing or decreasing the ordinates of one of the originally derived thickness distributions are designated as in the following example:

$$\text{NACA } 65(318)-217, a=0.5$$

The significance of all of the numbers except those in the parentheses is the same as before. The first number and the last two numbers enclosed in the parentheses denote, respectively, the low-drag range and the thickness in percent of the chord of the originally derived thickness distribution.

The more recent NACA 6-series airfoils are derived as members of thickness families having a simple relationship between the conformal transformations for airfoils of different thickness ratios but having minimum pressure at the same chordwise position. These airfoils are distinguished from the earlier individually derived airfoils by writing the number indicating the low-drag range as a subscript; for example,

$$\text{NACA } 65_3-218, a=0.5$$

For NACA 6-series airfoils having a thickness ratio less than 0.12 of the chord, the subscript number indicating the low-drag range should be less than unity. Rather than use a fractional number, a subscript of unity was originally employed for these airfoils. Since this usage is not consistent with the previous definition of a number indicating the low-drag range, the designations of airfoil sections having a thickness ratio less than 0.12 of the chord are now given without such a number. As an example, an NACA 6-series airfoil having a thickness ratio of 0.10 of the chord would be designated:

$$\text{NACA } 65-210$$

Ordinates for the basic thickness distributions designated by a subscript are slightly different from those for the corresponding individually derived thickness distributions. As before, if the ordinates of the basic thickness distribution have been changed by a factor, the low-drag range and thickness ratio of the original thickness distribution are enclosed in parentheses as follows:

$$\text{NACA } 65_{(318)}-217, a=0.5$$

If, however, the ordinates of a basic thickness distribution having a thickness ratio less than 0.12 of the chord have been changed by a factor, the number indicating the low-drag range is eliminated and only the original thickness ratio is enclosed in parentheses as follows:

$$\text{NACA } 65_{(10)}-211$$

If the design lift coefficient in tenths or the airfoil thickness in percent of chord are not whole integers, the numbers giving these quantities are usually enclosed in parentheses as in the following designation:

$$\text{NACA } 65_{(318)}-(1.5)(16.5), a=0.5$$

Some early experimental airfoils are designated by the insertion of the letter "x" immediately preceding the hyphen as in the designation 66,2x-115.

**Thickness distributions.**—Data for available NACA 6-series thickness forms are presented in the supplementary figures. These data are comparable with the similar data for airfoils of the NACA four-digit series, except that ordinates for intermediate thicknesses may not be correctly obtained by scaling the tabulated ordinates proportional to the thickness ratio. This method of changing the ordinates by a factor will, however, produce shapes satisfactorily approximating members of the family if the change in thickness ratio is small. Values of  $v/V$  and  $\Delta v_a/V$  for intermediate thickness ratios may be approximated as described for the NACA four-digit series.

**Mean lines.**—The mean lines commonly used with the NACA 6-series airfoils produce a uniform chordwise loading from the leading edge to the point  $\frac{x}{c}=a$  and a linearly decreasing load from this point to the trailing edge. Data for NACA mean lines with values of  $a$  equal to 0, 0.1, 0.2, 0.3, 0.4, 0.5, 0.6, 0.7, 0.8, 0.9, and 1.0 are presented in the supplementary figures. The ordinates were computed by the following formula, which represents a simplification of the original expression for mean-line ordinates given in reference 11:

$$\begin{aligned} \frac{y_c}{c} = \frac{c_{li}}{2\pi(a+1)} \left\{ \frac{1}{1-a} \left[ \frac{1}{2} \left( a - \frac{x}{c} \right)^2 \log_e \left| a - \frac{x}{c} \right| \right. \right. \\ \left. \left. - \frac{1}{2} \left( 1 - \frac{x}{c} \right)^2 \log_e \left( 1 - \frac{x}{c} \right) + \frac{1}{4} \left( 1 - \frac{x}{c} \right)^3 - \frac{1}{4} \left( a - \frac{x}{c} \right)^2 \right] \right. \\ \left. - \frac{x}{c} \log_e \frac{x}{c} + g - h \frac{x}{c} \right\} \end{aligned} \quad (6)$$

where

$$g = -\frac{1}{1-a} \left[ a^2 \left( \frac{1}{2} \log_e a - \frac{1}{4} \right) + \frac{1}{4} \right]$$

$$h = \frac{1}{1-a} \left[ \frac{1}{2} (1-a)^2 \log_e (1-a) - \frac{1}{4} (1-a)^2 \right] + g$$

The ideal angle of attack  $\alpha_i$  corresponding to the design lift coefficient is given by

$$\alpha_i = -h \frac{c_{li}}{2\pi(a+1)}$$

The data are presented for a design lift coefficient  $c_{li}$  equal to unity. All tabulated values vary directly with the design lift coefficient. Corresponding data for similar mean lines with other design lift coefficients may accordingly be obtained simply by multiplying the tabulated values by the desired design lift coefficient.

In order to camber NACA 6-series airfoils, mean lines are usually used having values of  $a$  equal to or greater than the distance from the leading edge to the location of minimum pressure for the selected thickness distribution at zero lift. For special purposes, load distributions other than those corresponding to the simple mean lines may be obtained by combining two or more types of mean line having positive or negative values of the design lift coefficient. The geometric

and aerodynamic characteristics of such combinations may be obtained by algebraic addition of the values for the component mean lines.

NACA 7-SERIES AIRFOILS

**Numbering system.**—The NACA 7-series airfoils are designated by a number of the following type (reference 12):

NACA 747A315

The first number "7" indicates the series number. The second number "4" indicates the extent over the upper surface, in tenths of the chord from the leading edge, of the region of favorable pressure gradient at the design lift coefficient. The third number "7" indicates the extent over the lower surface, in tenths of the chord from the leading edge, of the region of favorable pressure gradient at the design lift coefficient. The significance of the last group of three numbers is the same as for the previous NACA 6-series airfoils. The letter "A" which follows the first three numbers is a serial letter to distinguish different airfoils having parameters that would correspond to the same numerical designation. For example, a second airfoil having the same extent of favorable pressure gradient over the upper and lower surfaces, the same design lift coefficient, and the same maximum thickness as the original airfoil but having a different mean-line combination or thickness distribution would have the

serial letter "B." Mean lines used for the NACA 7-series airfoils are obtained by combining two or more of the previously described mean lines. A list of the thickness distributions and mean lines used to form these airfoils is presented in table I. The basic thickness distribution is given a designation similar to those of the final cambered airfoils. For example, the basic thickness distribution for the NACA 747A315 and 747A415 airfoils is given the designation NACA 747A015 even though minimum pressure occurs at 0.4c on both upper and lower surfaces at zero lift. Combination of this thickness distribution with the mean lines listed in table I for the NACA 747A315 airfoil changes the pressure distribution to the desired type as shown in figure 2.

**Thickness distributions.**—Data for available NACA 7-series thickness distributions are presented in the supplementary figures. These thickness distributions are individually derived and do not form thickness families. The thickness ratio may, however, be changed a moderate amount—say 1 or 2 percent—by multiplying the tabulated ordinates by a suitable factor without seriously altering their characteristic features. Values of  $(v/V^2)$  and of  $v/V$  for thinner or thicker thickness distributions may be approximated by the method of equation (5). If the change in thickness ratio is small, tabulated values of  $\Delta v_a/V$  may be applied directly with reasonable accuracy.

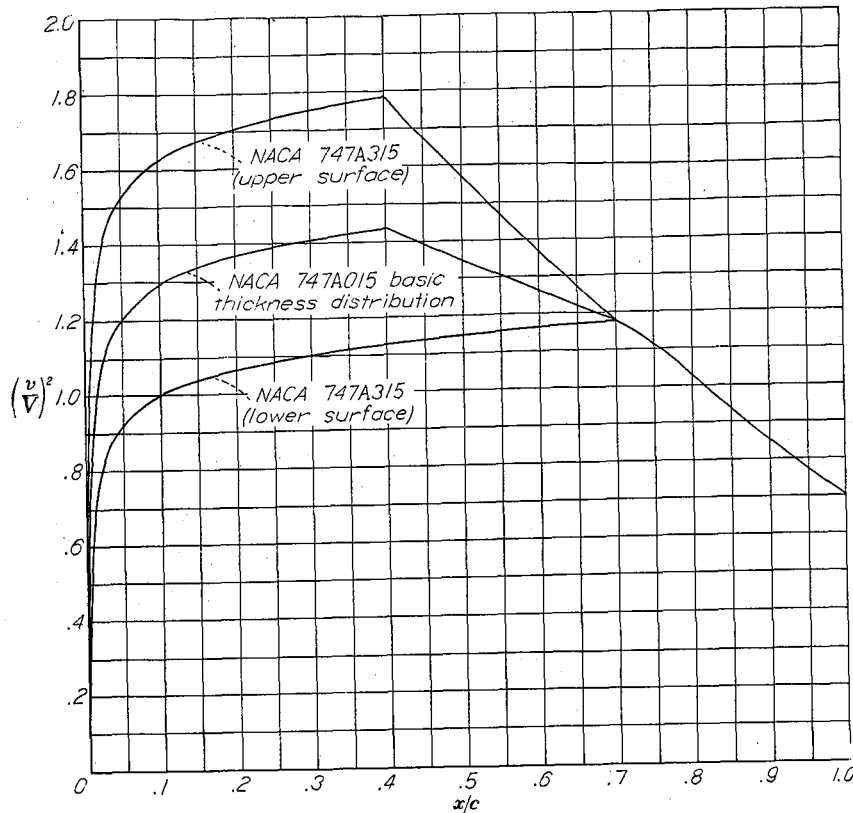


FIGURE 2.—Theoretical pressure distribution for the NACA 747A315 airfoil section at the design lift coefficient and the NACA 747A015 basic thickness distribution.

TABLE I.—ANALYSIS OF AIRFOIL DERIVATION

Airfoil designation	Basic thickness form	Mean-line combination <sup>1</sup>										
		a=0	a=0.1	a=0.2	a=0.3	a=0.4	a=0.5	a=0.6	a=0.7	a=0.8	a=0.9	a=1.0
747A315	747A015	-----	-----	-----	-----	0.763	-----	-----	-----	-----	-----	-----
747A415	747A015	-----	-----	-----	-----	.763	-----	-----	-----	-----	-----	0.100

<sup>1</sup> The numbers in the various columns headed "Mean-line combination" indicate the magnitude of the design lift coefficient used.

## THEORETICAL CONSIDERATIONS

## PRESSURE DISTRIBUTIONS

A knowledge of the pressure distribution over an airfoil is desirable for structural design and for estimation of the critical Mach number and moment coefficient if tests are not available. The pressure distribution also exerts a strong or predominant influence on the boundary-layer flow and, hence, on the airfoil characteristics. It is therefore usually advisable to relate the airfoil characteristics to the pressure distribution rather than directly to the airfoil geometry.

**Methods of derivation of thickness distributions.**—As mentioned in the section "Historical Development," the basic symmetrical thickness distributions of the NACA 6- and 7-series airfoils, together with their corresponding pressure distributions, are derived by means of conformal transformations. The transformations used to relate the known flow about a circle to that about an airfoil section were developed by Theodorsen in reference 9. Figure 3 shows schematically the significance of the various phases of the process.

The circle about which the flow is originally calculated has its center at the origin and a radius of  $ae^{\psi_0}$ . The equation of

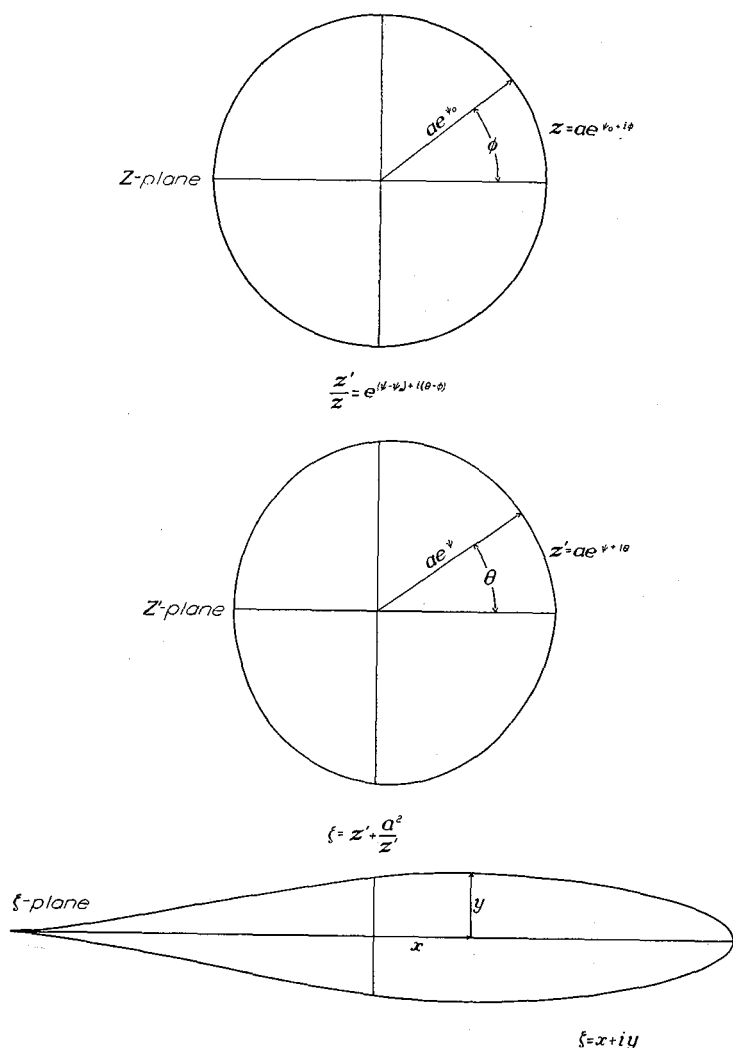


FIGURE 3.—Transformations used to derive airfoils and calculate pressure distributions.

this circle in complex coordinates is

$$z = ae^{\psi_0 + i\phi} \quad (7)$$

where

- $z$  complex variable in circle plane
- $\phi$  angular coordinate of  $z$
- $a$  basic length usually considered unity
- $\psi_0$  constant determining radius of circle

This true circle is transformed into an arbitrary, almost circular curve by the relation

$$\frac{z'}{z} = e^{(\psi - \psi_0) + i(\theta - \phi)} \quad (8)$$

the equation of the almost circular curve is

$$z' = ae^{\psi + i\theta} \quad (9)$$

where

- $z'$  complex variable in near-circle plane
- $ae^{\psi}$  radial coordinate of  $z'$
- $\theta$  angular coordinate of  $z'$

In order for the transformation (8) to be conformal, it is necessary that the quantity  $(\theta - \phi)$  (given the symbol  $-\epsilon$ ) be the conjugate function of  $(\psi - \psi_0)$ ; that is, if  $\epsilon$  is represented by a Fourier series of the form

$$\epsilon = \sum_1^{\infty} A_n \sin n\phi - \sum_1^{\infty} B_n \cos n\phi$$

then  $(\psi - \psi_0)$  is given by the relation

$$(\psi - \psi_0) = \sum_1^{\infty} A_n \cos n\phi + \sum_1^{\infty} B_n \sin n\phi$$

This relationship indicates that, if the function  $\epsilon(\phi)$  is given,  $(\psi - \psi_0)$  can be calculated as a function of  $\phi$ . Means of performing this calculation are presented in reference 13. The transformation relating the almost circular curve to the airfoil shape is

$$\zeta = z' + \frac{a^2}{z'} \quad (10)$$

where  $\zeta$  is the complex variable in the airfoil plane. The coordinates of the airfoil  $x$  and  $y$  are the real and imaginary parts of  $\zeta$ , respectively. These coordinates are given by the relations

$$x = 2a \cosh \psi \cos \theta \quad (11)$$

$$y = 2a \sinh \psi \sin \theta \quad (12)$$

The velocity distribution in terms of the airfoil parameters  $\psi$  and  $\epsilon$  is given exactly for perfect fluid flow by the expression

$$\frac{v}{V} = \frac{[\sin(\alpha_0 + \phi) + \sin(\alpha_0 + \epsilon)] e^{\psi_0}}{\sqrt{(\sinh^2 \psi + \sin^2 \theta) \left[ \left(1 - \frac{d\epsilon}{d\phi}\right)^2 + \left(\frac{d\psi}{d\phi}\right)^2 \right]}} \quad (13)$$

where

$v$  local velocity over surface of airfoil

$V$  free-stream velocity

$\alpha_0$  section angle of attack

$\psi_0$  average value of  $\psi$   $\left( \frac{1}{2\pi} \int_0^{2\pi} \psi d\phi \right)$

$\epsilon_{TE}$  value of  $\epsilon$  at trailing edge

The basic symmetrical shapes were derived by assuming suitable values of  $d\epsilon/d\phi$  as a function of  $\phi$ . These values were chosen on the basis of previous experience and are subject to the conditions that

$$\int_0^\pi \frac{d\epsilon}{d\phi} = 0$$

and  $d\epsilon/d\phi$  at  $\phi$  is equal to  $d\epsilon/d\phi$  at  $-\phi$ . These conditions are necessary for obtaining closed symmetrical shapes.

Values of  $\epsilon(\phi)$  were obtained simply by integrating  $\frac{d\epsilon}{d\phi} d\phi$ .

Values of  $\psi(\phi)$  were found by obtaining the conjugate of the curve of  $\epsilon(\phi)$  and adding a value  $\psi_0$  sufficient to make the value of  $\psi$  equal to zero at  $\phi = \pi$ . This condition assures a sharp trailing-edge shape.

Inasmuch as small changes in the velocity distribution at any point of the surface are approximately proportional to  $1 + \frac{d\epsilon}{d\phi}$  (see reference 14), the initially assumed values of  $d\epsilon/d\phi$  were altered by a process of successive approximations until the desired type of velocity distribution was obtained. After the final values of  $\psi$  and  $\epsilon$  were obtained, the ordinates of the basic thickness distribution were computed by equations (11) and (12).

When these computations were made, it appeared that there was an optimum value of the leading-edge radius dependent upon the airfoil thickness and the position of minimum pressure. If the leading-edge radius was too small, a premature peak in the pressure distribution occurred in the immediate vicinity of the leading edge as the angle of attack was increased. If the leading-edge radius was too large, a premature peak occurred a few percent of the chord behind the leading edge. With the correct leading-edge radius, the pressure distribution became nearly flat over the forward portion of the airfoil before the normal leading-edge peak formed at the higher lift coefficients. Curves of the parameters  $\psi$ ,  $\epsilon$ ,  $d\psi/d\phi$ ,  $d\epsilon/d\phi$  plotted against  $\phi$  for the NACA 64<sub>3</sub>-018 airfoil section are given in figure 4.

Experience has shown that, when the thickness ratio of an originally derived basic form was increased merely by multiplying all the ordinates by a constant factor, an unnecessarily large decrease in the critical speed of the resulting section occurred. Reducing the thickness ratio in a similar manner caused an unnecessarily large decrease in the low-drag range. For this reason, each of the earlier NACA 6-series sections was individually derived. It was later found that it was possible

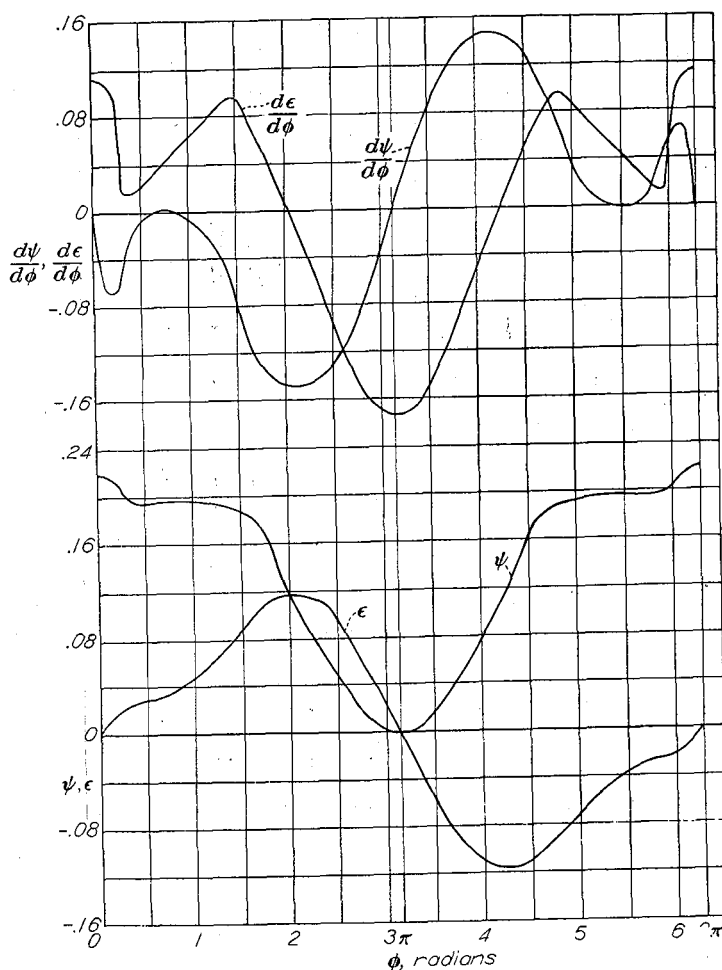


FIGURE 4.—Variation of airfoil parameters  $\psi$ ,  $\epsilon$ ,  $\frac{d\psi}{d\phi}$ ,  $\frac{d\epsilon}{d\phi}$  with  $\phi$  for the NACA 64<sub>3</sub>-018 airfoil-section basic thickness form.

to derive basic airfoil parameters  $\psi$  and  $\epsilon$  that could be multiplied by a constant factor to obtain airfoils of various thickness ratios, without having the aforementioned limitations in the resulting sections. Each of the more recent families of NACA 6-series airfoils, in which numerical subscripts are used in the designation, having minimum pressure at a given chordwise position was obtained by scaling up and down the basic values of the airfoil parameters  $\psi$  and  $\epsilon$ .

Theoretical pressure distributions (indicated by  $\left(\frac{v}{V}\right)^2$ ) for a family of NACA 65-series airfoils covering a range of thickness ratios are given in figure 5 (a). This figure shows the typical increase in the magnitude of the favorable pressure gradient, increase in maximum velocity over the surface, and increase in the relative pressure recovery over the rear portion of the airfoil with increase in thickness ratio. Figure 5 (b) shows the pressure distribution for a series of basic thickness forms having a thickness ratio of 0.15 and having minimum pressure at various chordwise positions. The value of the minimum pressure coefficient is seen to decrease and the magnitude of the pressure recovery over the rear portion of the airfoil to increase with the rearward movement of the point of minimum pressure.

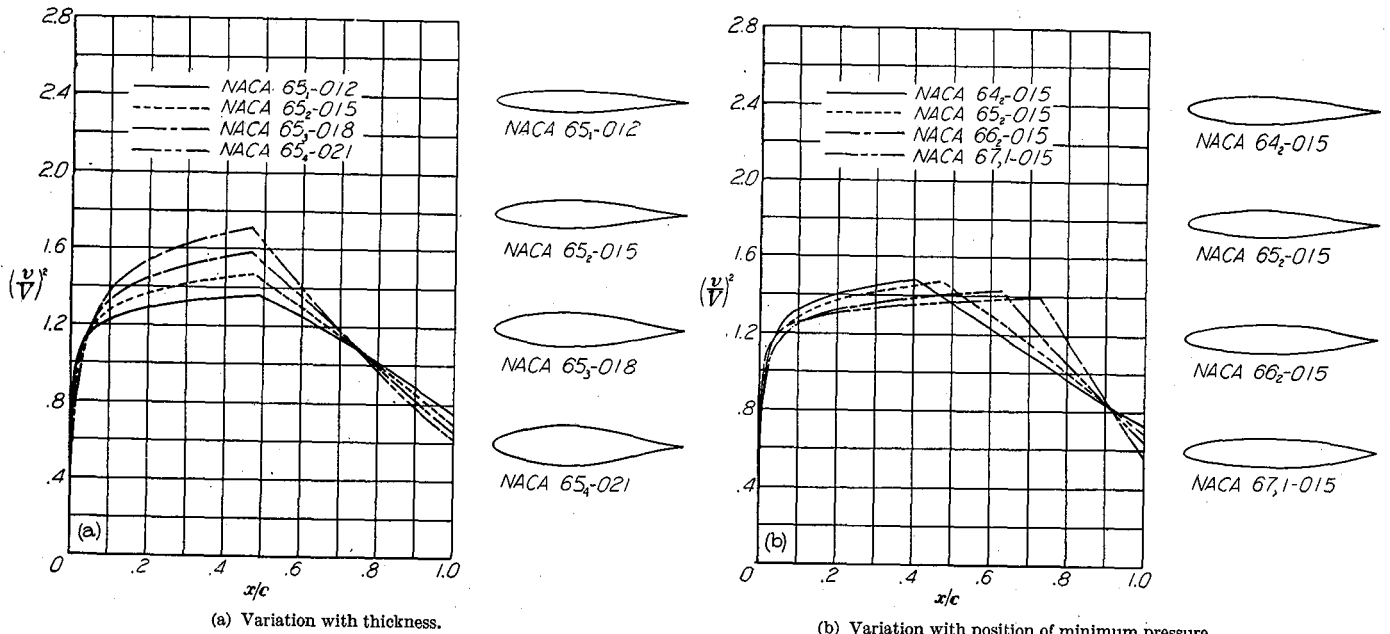


FIGURE 5.—Theoretical pressure distributions for some basic symmetrical NACA 6-series airfoils at zero lift.

The pressure distribution for one of the basic symmetrical thickness distributions at various lift coefficients is shown in figure 6. At zero lift the pressure distributions over the upper and lower surfaces are the same. As the lift coefficient is increased, the slope of the pressure distribution over the forward portion of the upper surface decreases until it becomes flat at a lift coefficient of 0.22 (the end of the low-drag range). As the lift coefficient is increased beyond this value, the usual peak in the pressure distribution forms at the leading edge.

**Rapid estimation of pressure distributions.**—In the discussion that follows, the term “pressure distribution” is used to signify the distribution of the static pressures on the upper

and lower surfaces of the airfoil along the chord. The term “load distribution” is used to signify the distribution along the chord of the normal force resulting from the difference in pressure on the upper and lower surfaces.

The pressure distribution about any airfoil in potential flow may be calculated accurately by a generalization of the methods of the previous section. Although this method is not unduly laborious, the computations required are too long to permit quick and easy calculations for large numbers of airfoils. The need for a simple method of quickly obtaining pressure distributions with engineering accuracy has led to the development of a method (reference 15) combining features of thin- and thick-airfoil theory. This simple method makes use of previously calculated characteristics of a limited number of mean lines and thickness distributions that may be combined to form large numbers of airfoils.

Thin-airfoil theory (references 16 to 18) shows that the load distribution of a thin airfoil may be considered to consist of: (1) a basic distribution at the ideal angle of attack and (2) an additional distribution proportional to the angle of attack as measured from the ideal angle of attack.

The first load distribution is a function only of the shape of the thin airfoil, or (if the thin airfoil is considered to be a mean line) of the mean-line geometry. Integration of this load distribution along the chord results in a normal-force coefficient which, at small angles of attack, is substantially equal to a lift coefficient  $c_{l_i}$ , which is designated the ideal or design lift coefficient. If, moreover, the camber of the mean line is changed by multiplying the mean-line ordinates by a constant factor, the resulting load distribution, the ideal or design angle of attack  $\alpha_i$ , and the design lift coefficient  $c_{l_i}$  may be obtained simply by multiplying the original values by the same factor. The characteristics of a large number of mean lines are presented in both graphical and tabular form in the supplementary figures. The load-distribution data are presented both in the form of the resultant pressure coefficient  $P_R$  and in the form of the corresponding velocity-increment ratios  $\Delta v/V$ . For positive design lift coefficients, these velocity-increment ratios are positive on the upper

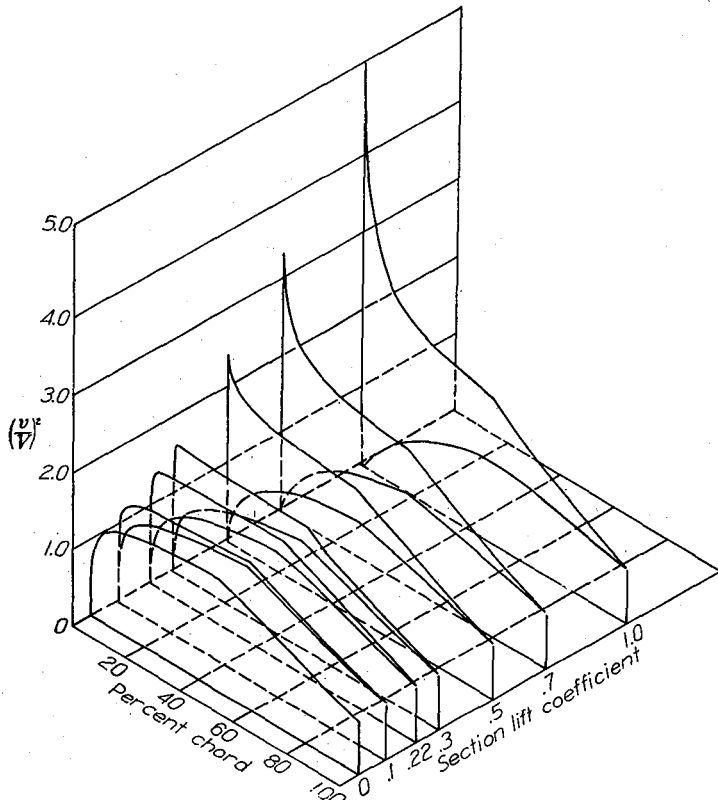


FIGURE 6.—Theoretical pressure distribution for the NACA 65-015 airfoil at several lift coefficients.

surface and negative on the lower surface; the opposite is true for negative design lift coefficients.

The second load distribution, which results from changing the angle of attack, is designated herein the "additional load distribution" and the corresponding lift coefficient is designated the "additional lift coefficient." This additional load distribution contributes no moment about the quarter-chord point and, according to thin-airfoil theory, is independent of the airfoil geometry except for angle of attack. The additional load distribution obtained from thin-airfoil theory is of limited practical application, however, because this simple theory leads to infinite values of the velocity at the leading edge. This difficulty is obviated by the exact thick-airfoil theory (reference 9) which also shows that the additional load distribution is neither completely independent of the airfoil shape nor exactly a linear function of the lift coefficient. For this reason, the additional load distribution has been calculated by the methods of reference 9 for each of the thickness distributions presented in the supplementary figures. These data are presented in the form of velocity-increment ratios  $\Delta v_a/V$  corresponding to an additional lift coefficient of approximately unity. For positive additional lift coefficients, these velocity-increment ratios are positive on the upper surfaces and negative on the lower surfaces; the opposite is true for negative additional lift coefficients.

In addition to the pressure distributions associated with these two load distributions, another pressure distribution exists which is associated with the basic symmetrical thickness form or thickness distribution of the airfoil. This pressure distribution has been calculated by the methods described in the previous section for the condition of zero lift and is presented in the supplementary figures as  $\left(\frac{v}{V}\right)^2$ , which is equivalent at low Mach numbers to the pressure coefficient  $S$ , and as the local velocity ratio  $v/V$ . This local velocity ratio is always positive and is the same for corresponding points on the upper and lower surfaces of the thickness form.

The velocity distribution about the airfoil is thus considered to be composed of three separate and independent components as follows:

(1) The distribution corresponding to the velocity distribution over the basic thickness form at zero angle of attack

(2) The distribution corresponding to the design load distribution of the mean line

(3) The distribution corresponding to the additional load distribution associated with angle of attack

The velocity-increment ratios  $\Delta v/V$  and  $\Delta v_a/V$  corresponding to components (2) and (3) are added to the velocity ratio corresponding to component (1) to obtain the total velocity at one point, from which the pressure coefficient  $S$  is obtained; thus,

$$S = \left( \frac{v}{V} \pm \frac{\Delta v}{V} \pm \frac{\Delta v_a}{V} \right)^2 \quad (14)$$

When this formula is used, values of the ratios corresponding to one value of  $x$  are added together and the resulting value of the pressure coefficient  $S$  is assigned to the airfoil surface at the same value of  $x$ .

The values of  $v/V$  and of  $\Delta v/V$  in equation (14) should, of course, correspond to the airfoil geometry. Methods of obtaining the proper values of these ratios from the values tabulated in the supplementary figures are presented in the previous section "Description of Airfoils."

When the ratio  $\Delta v_a/V$  has the value of zero, the resulting distribution of the pressure coefficient  $S$  will correspond approximately to the pressure distribution of the airfoil section at the design lift coefficient  $c_{li}$  of the mean line, and the lift coefficient may be assigned this value as a first approximation. If the pressure-distribution diagram is integrated, however, the value of  $c_l$  will be found to be greater than  $c_{li}$  by an amount dependent on the thickness ratio of the basic thickness form.

The pressure distribution will usually be desired at some specified lift coefficient not corresponding to  $c_{li}$ . For this purpose the ratio  $\Delta v_a/V$  must be assigned some value obtained by multiplying the tabulated value of this ratio by a factor  $f(\alpha)$ . For a first approximation this factor may be assigned the value

$$f(\alpha) = c_l - c_{li} \quad (15)$$

where  $c_l$  is the lift coefficient for which the pressure distribution is desired. If greater accuracy is desired, the value of  $f(\alpha)$  may be adjusted by trial and error to produce the actual desired lift coefficient as determined by integration of the pressure-distribution diagram.

Although this method of superposition of velocities has inadequate theoretical justification, experience has shown that the results obtained are adequate for engineering use. In fact, the results of even the first approximations agree well with experimental data and are adequate for at least preliminary consideration and selection of airfoils. A comparison of a first-approximation theoretical pressure distribution with an experimental distribution is shown in figure 7.

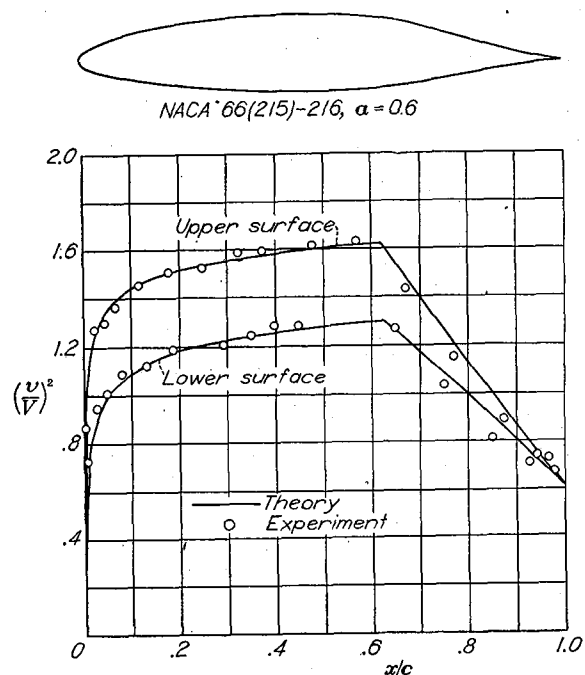


FIGURE 7.—Comparison of theoretical and experimental pressure distributions for the NACA 66(215)-216,  $\alpha = 0.6$  airfoil.  $c_l = 0.23$ .



Some discrepancy naturally occurs between the results of experiment and of any theoretical method based on potential flow because of the presence of the boundary layer. These effects are small, however, over the range of lift coefficients for which the boundary layer is thin and the drag coefficient is low.

**Numerical examples.**—The following numerical examples are included to illustrate the method of obtaining the first-approximation pressure distributions:

**Example 1:** Find the pressure coefficient  $S$  at the station  $x=0.50$  on the upper and lower surfaces of the NACA 65<sub>3</sub>-418 airfoil at a lift coefficient of 0.2.

From the description of the NACA 6-series airfoils, it is determined that this airfoil is obtained by combining the NACA 65<sub>3</sub>-018 basic thickness form with the  $a=1.0$  type mean line cambered to a design lift coefficient of 0.4. The following data are obtained from the supplementary figures for this thickness form and mean line at  $x=0.50$ :

$$\frac{v}{V} = 1.235$$

$$\frac{\Delta v_a}{V} = 0.157$$

$$\frac{\Delta v}{V} = 0.250$$

The desired value of  $\Delta v_a/V$  is computed as follows by use of equation (15):

$$\begin{aligned} \frac{\Delta v_a}{V} &= (0.157) (0.2 - 0.4) \\ &= -0.031 \end{aligned}$$

The desired value of  $\Delta v/V$  is obtained by multiplying the tabulated value by the design lift coefficient as stated in the description of the NACA 6-series airfoils. Thus,

$$\begin{aligned} \frac{\Delta v}{V} &= (0.250) (0.4) \\ &= 0.100 \end{aligned}$$

Substituting these values in equation (14) gives the following values of  $S$ :

For the upper surface

$$\begin{aligned} S &= (1.235 + 0.100 - 0.031)^2 \\ &= 1.700 \end{aligned}$$

For the lower surface

$$\begin{aligned} S &= (1.235 - 0.100 + 0.031)^2 \\ &= 1.360 \end{aligned}$$

**Example 2:** Find the pressure coefficient  $S$  at the station  $x=0.25$  on the upper and lower surfaces of the NACA 65<sub>(215)</sub>-214,  $a=0.5$  airfoil at a lift coefficient of 0.6.

The airfoil designation shows that this airfoil was obtained by combining a thickness form obtained by multiplying the ordinates of the NACA 65<sub>2</sub>-015 form by the factor 14/15 with the  $a=0.5$  type mean line cambered to a design lift coefficient of 0.2.

The supplementary figures give a value of 1.182 for  $v/V$  at  $x=0.25$  for the NACA 65<sub>2</sub>-015 basic thickness form. The desired value of  $v/V$  is obtained by applying formula (5) as follows:

$$\begin{aligned} \frac{v}{V} &= (1.182 - 1) \frac{14}{15} + 1 \\ &= 1.170 \end{aligned}$$

From the supplementary figures the following values of  $\Delta v_a/V$  are obtained at  $x=0.25$  for the following basic thickness forms:

Thickness form	$\frac{\Delta v_a}{V}$ at $x=0.25$
NACA 65 <sub>2</sub> -015	0.290
NACA 65 <sub>1</sub> -012	.282

By interpolation the value of  $\Delta v_a/V$  of 0.287 may be assigned to the 14-percent-thick form. The desired value of  $\Delta v_a/V$  is then computed as follows by use of equation (15):

$$\begin{aligned} \frac{\Delta v_a}{V} &= (0.287) (0.6 - 0.2) \\ &= 0.115 \end{aligned}$$

Data presented in the supplementary figures for the  $a=0.5$  type mean lines give the value of 0.333 for  $\Delta v/V$  at  $x=0.25$ . As stated in the description of the NACA 6-series airfoils, the desired value of  $\Delta v/V$  is obtained by multiplying the tabulated value by the design lift coefficient. Thus,

$$\begin{aligned} \frac{\Delta v}{V} &= (0.333) (0.2) \\ &= 0.067 \end{aligned}$$

Substituting the foregoing values in equation (14) gives the values of  $S$  as follows:

For the upper surface

$$\begin{aligned} S &= (1.170 + 0.067 + 0.115)^2 \\ &= 1.828 \end{aligned}$$

For the lower surface

$$\begin{aligned} S &= (1.170 - 0.067 - 0.115)^2 \\ &= 0.976 \end{aligned}$$

**Example 3:** Find the pressure coefficient  $S$  at the station  $x=0.30$  on the upper and lower surfaces of the NACA 2412 airfoil at a lift coefficient of 0.5.

The description of airfoils of the NACA four-digit series shows that the necessary data may be found from the NACA 0012 thickness form and 64 mean line in the supplementary figures. From these figures the following data are obtained:

At  $x=0.30$

$$\frac{v}{V} = 1.162$$

At  $x=0.30$

$$\frac{\Delta v_a}{V} = 0.239$$

For the NACA 64 mean line at  $x=0.30$

$$\frac{\Delta v}{V} = 0.260$$

For the NACA 64 mean line

$$c_{i_t} = 0.76$$

The values of  $\Delta v/V$  and  $c_{i_t}$  corresponding to the airfoil geometry are obtained by multiplying the foregoing values by the factor  $2/6$  as explained in the description of these airfoils; thus,

$$\frac{\Delta v}{V} = (0.260) \left( \frac{2}{6} \right)$$

$$= 0.087$$

$$c_{i_t} = (0.76) \left( \frac{2}{6} \right)$$

$$= 0.253$$

The desired value of  $\Delta v_a/V$  is obtained from equation (15) as follows:

$$\frac{\Delta v_a}{V} = (0.239)(0.5 - 0.253)$$

$$= 0.059$$

Substituting the proper values in equation (14) gives the values of  $S$  as follows:

For the upper surface

$$S = (1.162 + 0.087 + 0.059)^2$$

$$= 1.712$$

For the lower surface

$$S = (1.162 - 0.087 - 0.059)^2$$

$$= 1.032$$

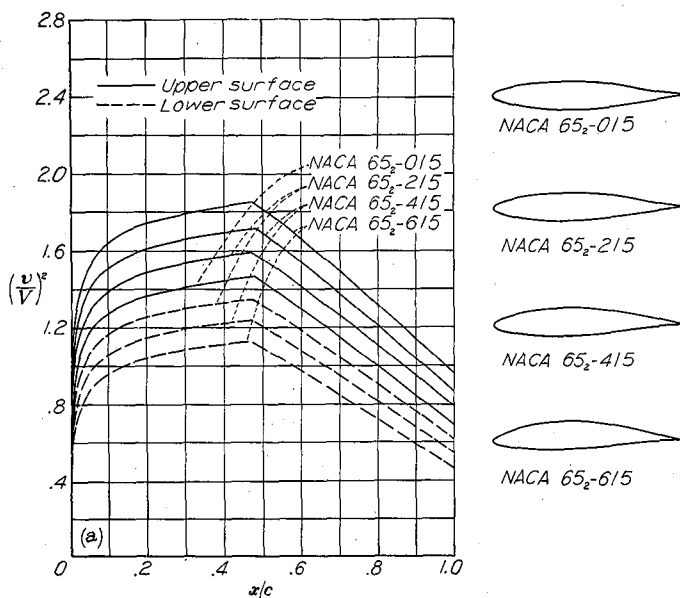
**Effect of camber on pressure distribution.**—At zero lift the pressure distributions over the upper and lower surfaces of a basic symmetrical thickness distribution are, of course, identical. The effect of camber on the pressure distribution

at the design lift coefficient is to separate the pressures on the upper and lower surfaces by an amount corresponding approximately to the design load distribution of the mean line. When the local value of the design load distribution is positive, the pressure coefficient  $S$  on the upper surface is increased (decreased absolute pressure) whereas that on the lower surface is decreased. This effect is shown in figure 8 (a) for various amounts of camber.

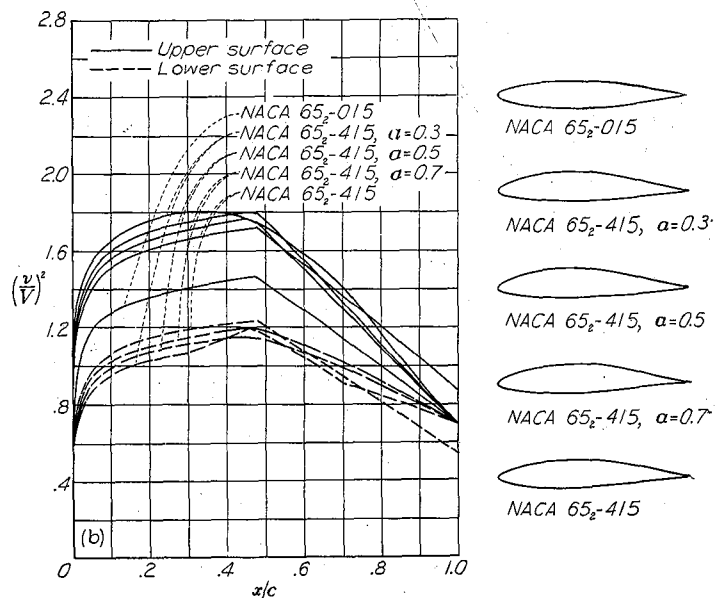
The maximum value of the pressure coefficient on the upper surface at the design lift coefficient increases with the design lift coefficient and for a given design lift coefficient increases with decreasing values of  $\alpha$ . The result is to cause the critical Mach number at the design lift coefficient to decrease with increasing camber or with the use of types of mean line concentrating the load near the leading edge. Figure 8 (b) shows that the location of minimum pressure on both surfaces is not affected if a type of mean line is used having a value of  $\alpha$  at least as large as the value of  $x/c$  at the position of minimum pressure on the basic thickness distribution. If a mean line with a smaller value of  $\alpha$  is used, the possible extent of laminar flow along the upper surface will be reduced.

CRITICAL MACH NUMBER

The critical speed is defined as the free-stream speed at which the velocity at any point along the surface of the airfoil reaches the local velocity of sound. If the maximum value of the low-speed pressure coefficient  $S$  is known either experimentally or from theoretical methods, the critical Mach number may be predicted approximately by the Von Kármán method (reference 19). A curve relating the critical Mach number and the low-speed pressure coefficient  $S$  has been calculated from the equations of reference 19 and included in the supplementary figures. These predicted critical Mach numbers are useful for preliminary considerations in the absence of test data and appear to correspond fairly well to the Mach numbers at which the local velocity of sound is reached in the high-critical-speed range of lift coefficient. This criterion does not, however, appear to predict accurately



(a) Amount of camber.



(b) Type of camber.

FIGURE 8.—Effect of amount and type of camber on pressure distribution at design lift.

the Mach numbers at which large changes in airfoil characteristics occur, especially when sharp pressure peaks exist at the leading edge. A discussion of the characteristics of airfoil sections at supercritical Mach numbers is beyond the scope of this report.

For convenience, curves of predicted critical Mach number plotted against the low-speed section lift coefficient have been included in the supplementary figures for a number of airfoils. High-speed lift coefficients may be obtained by multiplying the low-speed lift coefficient by the factor  $\frac{1}{\sqrt{1-M^2}}$ . The critical Mach numbers have been predicted from theoretical pressure distributions. For airfoils of the NACA four- and five-digit series and for the NACA 7-series airfoils, the theoretical pressure distributions were obtained by Theodorsen's method. For the other airfoils the theoretical pressure distributions were obtained by the approximate method described in the preceding section.

The data in the supplementary figures show that, for any one type of airfoil, the maximum critical Mach number decreases rapidly as the thickness is increased. The effect of camber is to lower the maximum critical Mach number and to shift the range of high critical Mach numbers in the same manner as for the low drag range. For common types of camber the minimum reduction in critical speed for a given design lift coefficient is obtained with a uniform load type of mean line. A comparison of the data presented in the supplementary figures shows that NACA 6-series sections have considerably higher maximum critical Mach numbers than NACA 24-, 44-, and 230-series airfoils of corresponding thickness ratios.

#### MOMENT COEFFICIENTS

**Methods of calculation.**—Theoretical moment coefficients may be approximated directly from the values presented in the supplementary figures for the various mean lines. These values were obtained from thin-airfoil theory and may be scaled up or down linearly with the design lift coefficient or with the mean-line ordinates. These theoretical values are sufficiently accurate for preliminary considerations, but experimental values should be used for stability and control calculations.

**Numerical examples.**—The following numerical examples illustrate the methods of calculating the moment coefficients:

**Example 1:** Find the theoretical moment coefficient about the quarter-chord point for the NACA 65<sub>2</sub>-215,  $a=0.5$  airfoil.

The designation of the airfoil shows that the design lift coefficient of this airfoil is 0.2. From the data on the NACA  $a=0.5$  type mean line included in the supplementary figures, the value of  $c_{m_{c/4}}$  is  $-0.139$  for a design lift coefficient of 1.0. The desired value of the moment coefficient is accordingly

$$\begin{aligned} c_{m_{c/4}} &= (-0.139) (0.2) \\ &= -0.028 \end{aligned}$$

**Example 2:** Find the theoretical moment coefficient about the quarter-chord point for the NACA 4415 airfoil.

From the description of the NACA four-digit series airfoils, the required data is found to be presented for the

NACA 64 mean line in the supplementary figures. The moment coefficient for this mean line is  $-0.157$ . The required value is then

$$\begin{aligned} c_{m_{c/4}} &= (-0.157) \frac{4}{6} \\ &= -0.105 \end{aligned}$$

#### ANGLE OF ZERO LIFT

**Methods of calculation.**—Values of the ideal or design angle of attack  $\alpha_i$  corresponding to the design lift coefficient  $c_{li}$  are included among the data for the various mean lines presented in the supplementary figures. The approximate values of the angle of zero lift may be obtained from the data by using the theoretical value of the lift-curve slope for thin airfoils,  $2\pi$  per radian. The value of  $\alpha_{i_0}$  in degrees is then

$$\alpha_{i_0} = \alpha_i - \frac{57.3}{2\pi} c_{li} \quad (16)$$

The tabulated values of  $\alpha_i$  may be scaled linearly with the design lift coefficient or with the mean-line ordinates.

Although these theoretical angles of zero lift may be useful in preliminary design, they should not be used without experimental verification for such purposes as establishing the washout of a wing.

**Numerical examples.**—The method of computing  $\alpha_{i_0}$  is illustrated in the following examples:

**Example 1:** Find the theoretical angle of zero lift of the NACA 65<sub>2</sub>-515,  $a=0.5$  airfoil.

This airfoil number indicates a design lift coefficient of 0.5. Data for the NACA  $a=0.5$  mean line indicate that  $\alpha_i=3.04^\circ$  when  $c_{li}=1.0$ . The desired value of  $\alpha_i$  is then

$$\begin{aligned} \alpha_i &= (3.04) (0.5) \\ &= 1.52^\circ \end{aligned}$$

Substituting in equation (16) gives

$$\begin{aligned} \alpha_{i_0} &= 1.52 - \frac{(57.3) (0.5)}{2\pi} \\ &= -3.0^\circ \end{aligned}$$

**Example 2:** Find the theoretical angle of zero lift for the NACA 2415 airfoil.

The description of the NACA four-digit-series airfoils shows that the required values of  $\alpha_i$  and  $c_{li}$  may be obtained by multiplying the corresponding values for the NACA 64 mean line (see supplementary figures) by a factor  $2/6$ ; then

$$\begin{aligned} \alpha_i &= (0.74) \left(\frac{2}{6}\right) \\ &= 0.25^\circ \\ c_{li} &= (0.76) \left(\frac{2}{6}\right) \\ &= 0.253 \end{aligned}$$

and from equation (16)

$$\begin{aligned} \alpha_{i_0} &= 0.25 - \frac{(57.3) (0.253)}{2\pi} \\ &= -2.0^\circ \end{aligned}$$

## DESCRIPTION OF FLOW AROUND AIRFOILS

Perfect-fluid theory postulates that the flow follow the airfoil contour smoothly at all angles of attack with no loss of energy. Consequently, perfect-fluid theory itself gives no information concerning the profile drag or the maximum lift of airfoil sections. The explanation of these phenomena is found from a consideration of the effects of viscosity, which are of primary importance in a thin region near the surface of the airfoil called the boundary layer.

Boundary layers in general are of two types, namely, laminar and turbulent. The flow in the laminar layer is smooth and free from any eddying motion. The flow in the turbulent layer is characterized by the presence of a large number of relatively small eddies. Because the eddies in the turbulent layer produce a transfer of momentum from the relatively fast-moving outer parts of the boundary layer to the portions closer to the surface, the distribution of average velocity is characterized by relatively higher velocities near the surface and a greater total boundary-layer thickness in a turbulent boundary layer than in a laminar boundary layer developed under otherwise identical conditions. Skin friction is therefore higher for turbulent boundary-layer flow than for laminar flow.

When the pressures along the airfoil surface are increasing in the direction of flow, a general deceleration takes place. At the outer limits of the boundary layer this deceleration takes place in accordance with Bernoulli's law. Closer to the surface, no such simple law can be given because of the action of the viscous forces within the boundary layer. In general, however, the relative loss of speed is somewhat greater for particles of fluid within the boundary layer than for those at the outer limits of the layer because the reduced kinetic energy of the boundary-layer air limits its ability to flow against the adverse pressure gradient. If the rise in pressure is sufficiently great, portions of the fluid within the boundary layer may actually have their direction of motion reversed and may start moving upstream. When this reverse occurs, the flow in the boundary layer is said to be "separated." Because of the increased interchange of momentum from different parts of the layer, turbulent boundary layers are much more resistant to separation than are laminar layers. Laminar boundary layers can only exist for a relatively short distance in a region in which the pressure increases in the direction of flow. Formulas for calculating many of the boundary-layer characteristics are given in references 20 to 22.

After laminar separation occurs, the flow may either leave the surface permanently or reattach itself in the form of a turbulent boundary layer. Not much is known concerning the factors controlling this phenomenon. Laminar separation on wings is usually not permanent at flight values of the Reynolds number except when it occurs near the leading edge under conditions corresponding to maximum lift. The size of the locally separated region that is formed when the laminar boundary layer separates and the flow returns to the surface decreases with increasing Reynolds number at a given angle of attack.

The flow over aerodynamically smooth airfoils at low and moderate lift coefficients is characterized by laminar boundary layers from the leading edge back to approximately the location of the first minimum-pressure point on both upper and

lower surfaces. If the region of laminar flow is extensive, separation occurs immediately downstream from the location of minimum pressure (reference 20) and the flow returns to the surface almost immediately at flight Reynolds numbers as a turbulent boundary layer. This turbulent boundary layer extends to the trailing edge. If the surfaces are not sufficiently smooth and fair, if the air stream is turbulent, or perhaps if the Reynolds number is sufficiently large, transition from laminar to turbulent flow may occur anywhere upstream of the calculated laminar separation point.

For low and moderate lift coefficients where inappreciable separation occurs, the airfoil profile drag is largely caused by skin friction and the value of the drag coefficient depends mainly on the relative amounts of laminar and turbulent flow. If the location of transition is known or assumed, the drag coefficient may be calculated with reasonable accuracy from boundary-layer theory by use of the methods of references 23 and 24.

As the lift coefficient of the airfoil is increased by changing the angle of attack, the resulting application of the additional type of lift distribution moves the minimum-pressure point upstream on the upper surface, and the possible extent of laminar flow is thus reduced. The resulting greater proportion of turbulent flow, together with the larger average velocity of flow over the surfaces, causes the drag to increase with lift coefficient.

In the case of many of the older types of airfoils, this forward movement of transition is gradual and the resulting variation of drag with lift coefficient occurs smoothly. The pressure distributions for NACA 6-series airfoils are such as to cause transition to move forward suddenly at the end of the low-drag range of lift coefficients. A sharp increase in drag coefficient to the value corresponding to a forward location of transition on the upper surface results. Such sudden shifts in transition give the typical drag curve for these airfoils with a "sag" or "bucket" in the low-drag range. The same characteristic is shown to a smaller degree by some of the earlier airfoils such as the NACA 23015 when tested in a low-turbulence stream.

At high lift coefficients, a large part of the drag is contributed by pressure or form drag resulting from separation of the flow from the surface. The flow over the upper surface is characterized by a negative pressure peak near the leading edge, which causes laminar separation. The onset of turbulence causes the flow to return to the surface as a turbulent boundary layer. High Reynolds numbers are favorable to the development of turbulence and aid in this process. If the lift coefficient is sufficiently high or if the reestablishment of flow following laminar separation is unduly delayed by low Reynolds numbers, the turbulent layer will separate from the surface near the trailing edge and will cause large drag increases. The eventual loss in lift with increasing angle of attack may result either from relatively sudden permanent separation of the laminar boundary layer near the leading edge or from progressive forward movement of turbulent separation. Under the latter condition, the flow over a relatively large portion of the surface may be separated prior to maximum lift. A more extended discussion of the flow conditions associated with maximum lift is given in reference 5.

EXPERIMENTAL CHARACTERISTICS

SOURCES OF DATA

The primary source of the wind-tunnel data presented is from tests in the Langley two-dimensional low-turbulence pressure tunnel (TDT). The methods used to obtain and correct the data are summarized in the appendix. Design data obtained from tests of 2-foot-chord models in this tunnel are presented in the supplementary figures.

Some wind-tunnel data presented were obtained in other NACA wind tunnels. In each case, the source of the data is indicated and the testing techniques and corrections used were conventional unless otherwise indicated.

Most of the flight data consist of drag measurements made by the wake-survey method on either the airplane wing or a "glove" fitted over the wing as the test specimen. Whenever the measurements were obtained for a glove, this fact is indicated in the presentation of the data. All data obtained at high speeds have been reduced to coefficient form by compressible-flow methods. In the case of all such NACA flight data, precautions have been taken to ensure that the results presented are not invalidated by cross flows of low-energy air into or out of the survey plane.

DRAG CHARACTERISTICS OF SMOOTH AIRFOILS

**Drag characteristics in low-drag range.**—The value of the drag coefficient in the low-drag range for smooth airfoils is mainly a function of the Reynolds number and the relative extent of the laminar layer and is moderately affected by the airfoil thickness ratio and camber. The effect on minimum drag of the position of minimum pressure which determines the possible extent of laminar flow is shown in figure 9 for some NACA 6-series airfoils. The data show a regular decrease in drag coefficient with rearward movement of minimum pressure.

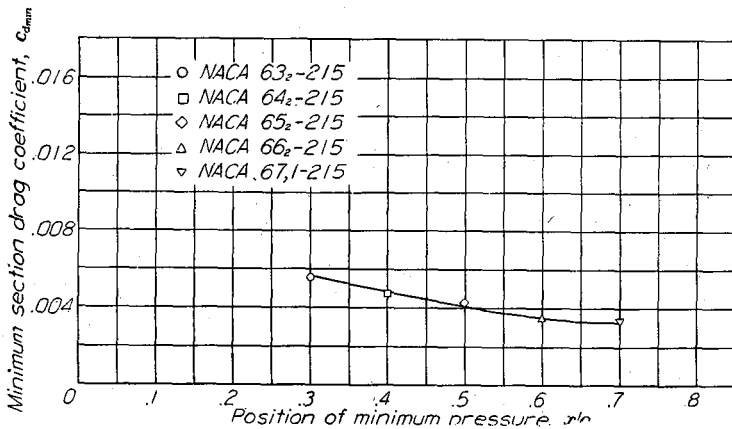


FIGURE 9.—Variation of minimum drag coefficient with position of minimum pressure for some NACA 6 series airfoils of the same camber and thickness.  $R = 6 \times 10^6$ .

The variation of minimum drag coefficient with Reynolds number for several airfoils is shown in figure 10. The drag coefficient generally decreases with increasing Reynolds number up to Reynolds numbers of the order of  $20 \times 10^6$ . Above this Reynolds number the drag coefficient of the NACA 65<sub>(421)</sub>-420 airfoil remained substantially constant up to a Reynolds number of nearly  $40 \times 10^6$ . The earlier increase in drag coefficient shown by the NACA 66(2x15)-116 airfoil may be caused by surface irregularities because the specimen

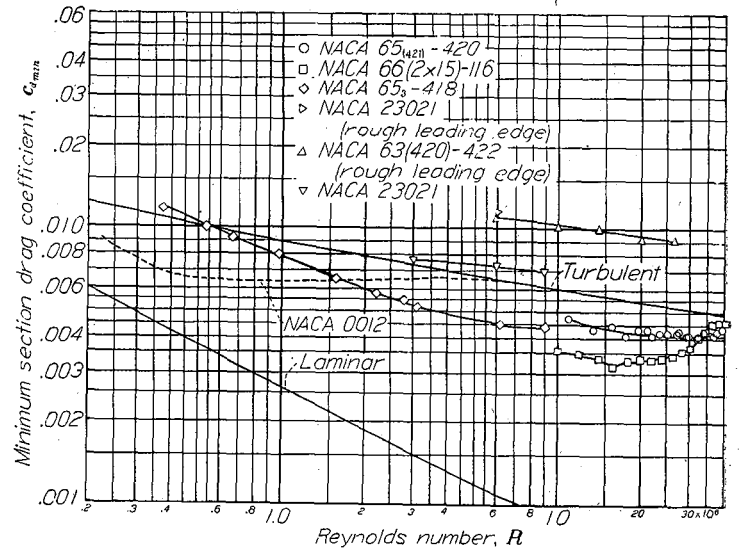


FIGURE 10.—Variation of minimum section drag coefficient with Reynolds number for several airfoils, together with laminar and turbulent skin-friction coefficients for a flat plate.

tested was a practical-construction model. It may be noted that the drag coefficient for the NACA 65<sub>3</sub>-418 airfoil at low Reynolds numbers is substantially higher than that of the NACA 0012, whereas at high Reynolds numbers the opposite is the case. The higher drag of the NACA 65<sub>3</sub>-418 airfoil section at low Reynolds numbers is caused by a relatively extensive region of laminar separation downstream of the point of minimum pressure. This region decreases in size with increasing Reynolds number. These data illustrate the inadequacy of low Reynolds number test data either to estimate the full-scale characteristics or to determine the relative merits of airfoil sections at flight Reynolds numbers (references 25 and 26).

The variation of minimum drag coefficient with camber is shown in figure 11 for a number of smooth 18-percent-thick NACA 6-series airfoils. These data show very little change

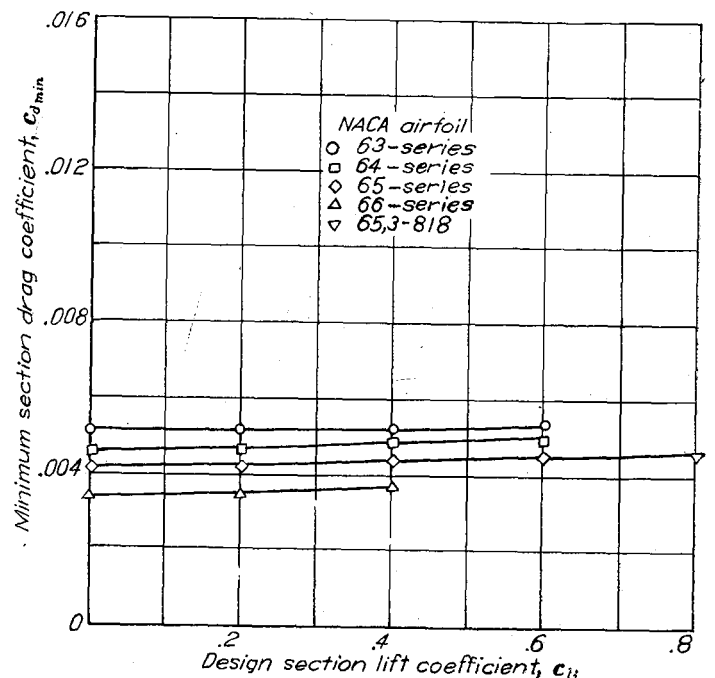


FIGURE 11.—Variation of minimum section drag coefficient with camber for several NACA 6-series airfoil sections of 18-percent thickness ratio.  $R = 9 \times 10^6$ .

in minimum drag coefficient with increase in camber. A large amount of systematic data is included in figure 12 to show the variation of minimum drag coefficient with thickness ratio for a number of NACA airfoil sections ranging in thickness from 6 percent to 24 percent of the chord. The minimum drag coefficient is seen to increase with increase in thickness ratio for each airfoil series. This increase, however, is greater for the NACA four- and five-digit-series airfoils (fig. 12 (a)) than for the NACA 6-series airfoils (figs. 12 (b) to 12 (e)).

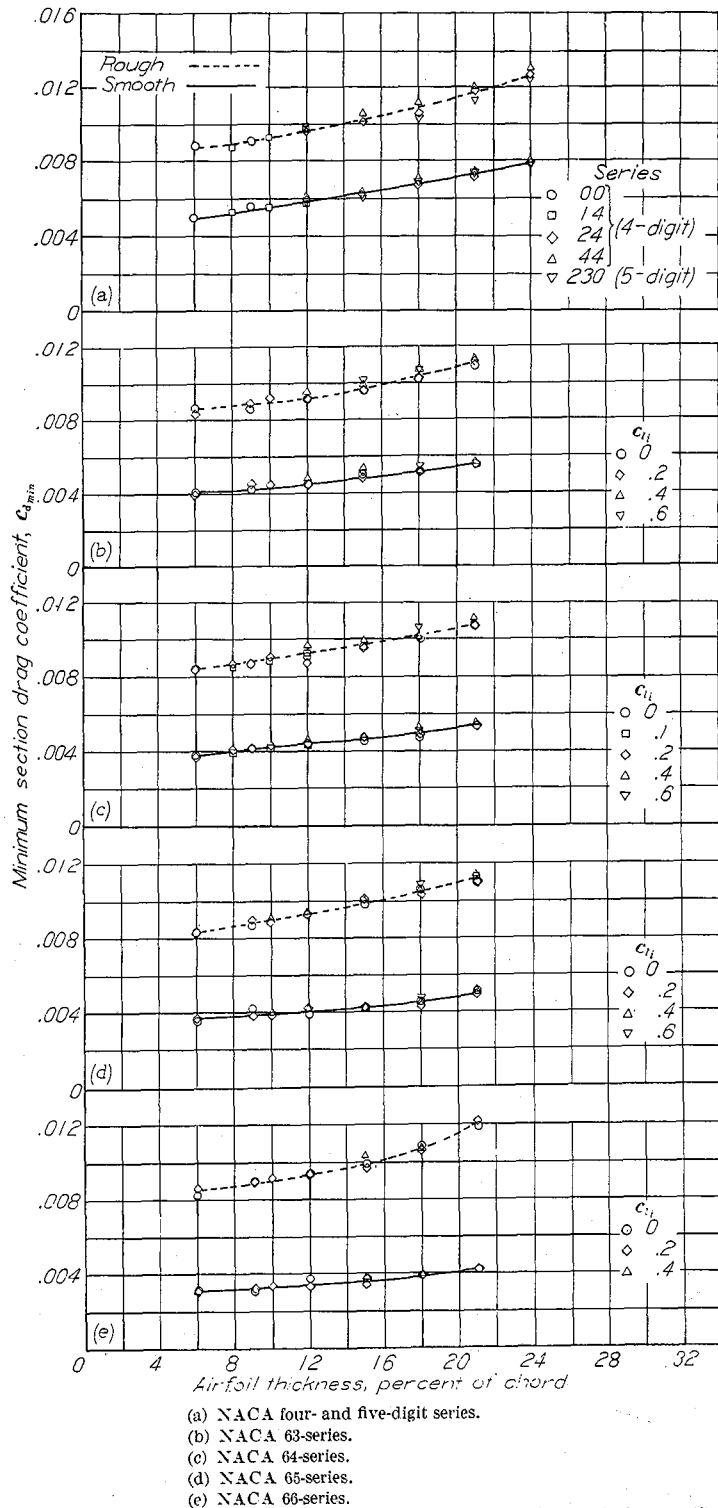


FIGURE 12.—Variation of minimum section drag coefficient with airfoil thickness ratio for several NACA airfoil sections of different cambers in both smooth and rough conditions.  $R = 6 \times 10^6$ .

The data presented in the supplementary figures for the NACA 6-series thickness forms show that the range of lift coefficients for low drag varies markedly with airfoil thickness. It has been possible to design airfoils of 12-percent thickness with a total theoretical low-drag range of lift coefficients of 0.2. This theoretical range increases by approximately 0.2 for each 3-percent increase of airfoil thickness. Figure 13 shows that the theoretical extent of the low-drag range is approximately realized at a Reynolds number of  $9 \times 10^6$ . Figure 13 also shows a characteristic tendency for the drag to increase to some extent toward the upper end of the low-drag range for moderately cambered airfoils, particularly for the thicker airfoils. All data for the NACA 6-series airfoils show a decrease in the extent of the low-drag range with increasing Reynolds number. Extrapolation of the rate of decrease observed at Reynolds numbers below  $9 \times 10^6$  would indicate a vanishingly small low-drag range at flight values of the Reynolds number. Tests of a carefully constructed model of the NACA 65<sub>(421)</sub>-420 airfoil showed, however, that the rate of reduction of the low-drag range with increasing Reynolds number decreased markedly at Reynolds numbers above  $9 \times 10^6$  (fig. 14). These data indicate that the extent of the low-drag range of this airfoil is reduced to about one-half the theoretical value at a Reynolds number of  $35 \times 10^6$ .

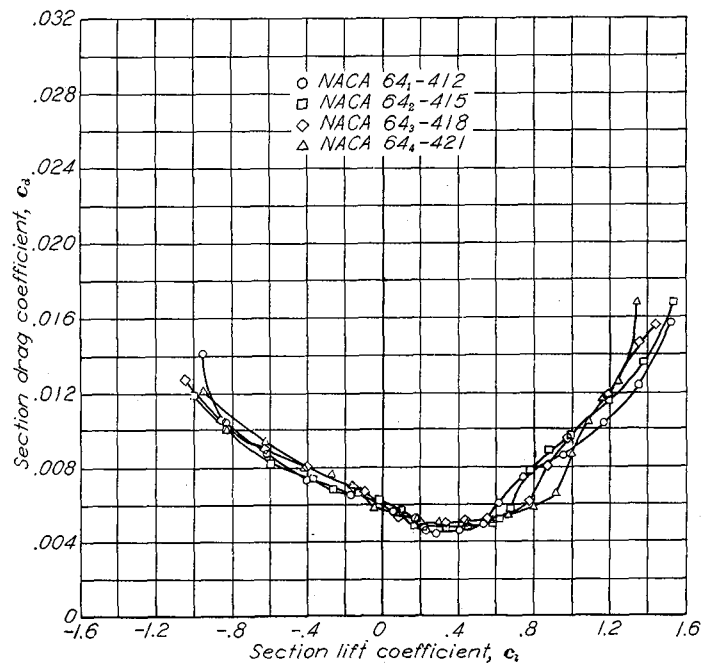
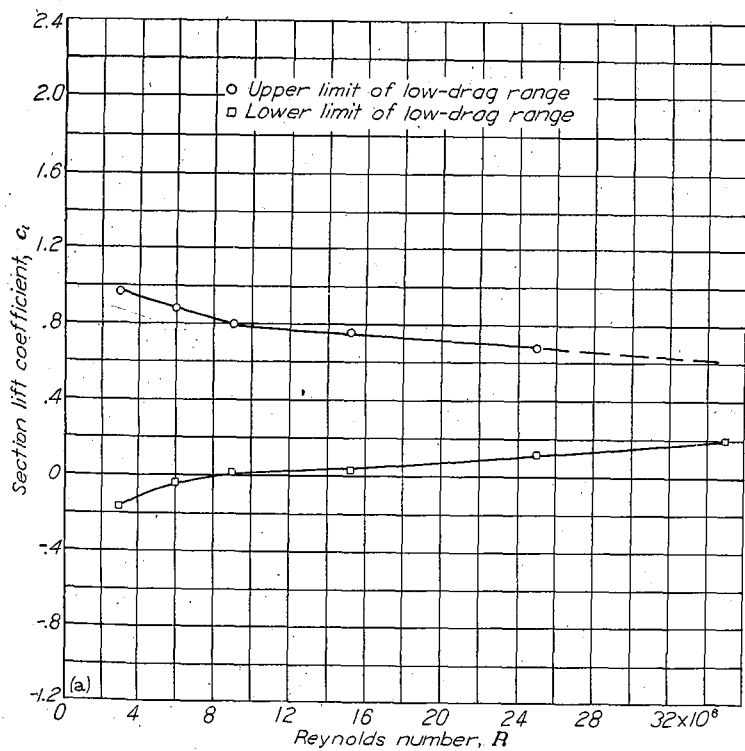
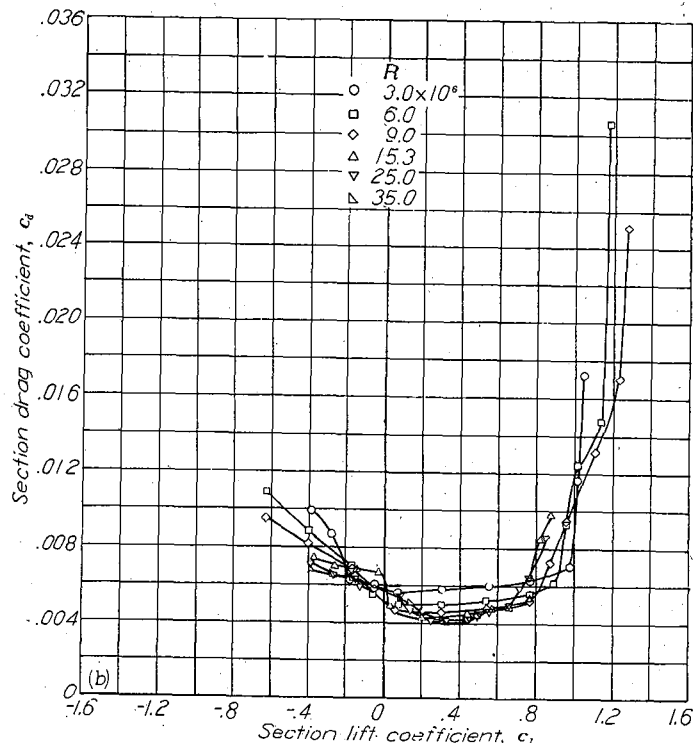


FIGURE 13.—Drag characteristics of some NACA 64-series airfoil sections of various thicknesses, cambered to a design lift coefficient of 0.4.  $R = 9 \times 10^6$ ; TDT tests 682, 733, 735, and 691.

The values of the lift coefficient for which low drag is obtained are determined largely by the amount of camber. The lift coefficient at the center of the low-drag range corresponds approximately to the design lift coefficient of the mean line. The effect on the drag characteristics of various amounts of camber is shown in figure 15. Section data indicate that the location of the low-drag range may be shifted by even such crude camber changes as those caused by small deflections of a plain flap. (See supplementary fig.)



(a) Variation of upper and lower limits of low-drag range with Reynolds number.



(b) Section drag characteristics at various Reynolds numbers.

FIGURE 14.—Variation of low-drag range with Reynolds number for the NACA 65(21)-420 airfoil. TDT tests 300, 312, and 328.

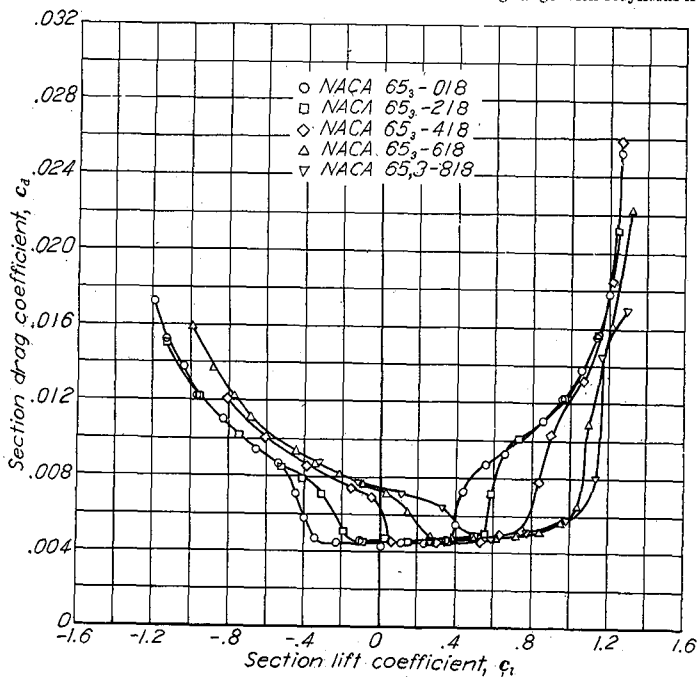


FIGURE 15.—Drag characteristics of some NACA 65-series airfoil sections of 18 percent thickness with various amounts of camber.  $R = 6 \times 10^6$ ; TDT tests 163, 314, 802, 813, and 830.

The location of the low-drag range shows some variation from that predicted by simple thin-airfoil theory. This departure appears to be a function of the type of mean line used (reference 27) and the airfoil thickness. The effect of airfoil thickness is shown in figure 13, from which the center of the low-drag range is seen to shift to higher lift coefficients with increasing airfoil thickness. This shift is partly explained by the increase in lift coefficient above the design lift coefficient for the mean line obtained when the velocity increments caused by the mean line are combined with the velocity distribution for the basic thickness form according to the approximate methods previously described.

**Drag characteristics outside low-drag range.**—At the end of the low-drag range the drag increases rapidly with increase in lift coefficient. For symmetrical and low-cambered airfoils, for which the lift coefficient at the upper end of the low-drag range is moderate, this high rate of increase does not continue. (See fig. 15.) For highly cambered sections, for which the lift at the upper end of the low-drag range is already high, the drag coefficient shows a continued rapid increase.

Comparison of data for airfoils cambered with a uniform-load mean line with data for airfoils cambered to carry the load farther forward shows that the uniform-load mean line is favorable for obtaining low drag coefficients at high lift coefficients (fig. 16 and reference 27).

Data for many of the airfoils given in the supplementary figures show large reductions in drag with increasing Reynolds number at high lift coefficients. This scale effect is too large to be accounted for by the normal variation in skin friction and appears to be associated with the effect of Reynolds number on the onset of turbulent flow following laminar separation near the leading edge (reference 28).

**Effects of type of section on drag characteristics.**—A comparison of the drag characteristics of the NACA 23012 and of three NACA 6-series airfoils is presented in figure 17. The drag for the NACA 6-series sections is substantially lower than for the NACA 23012 section in the range of lift coefficients corresponding to high-speed flight, and this margin may usually be maintained through the range of lift coefficients useful for cruising by suitable choice of camber. The NACA 6-series sections show the higher maximum values of the lift-drag ratio. At high values of the lift coefficient, however, the earlier NACA sections have generally lower drag coefficients than the NACA 6-series airfoils.

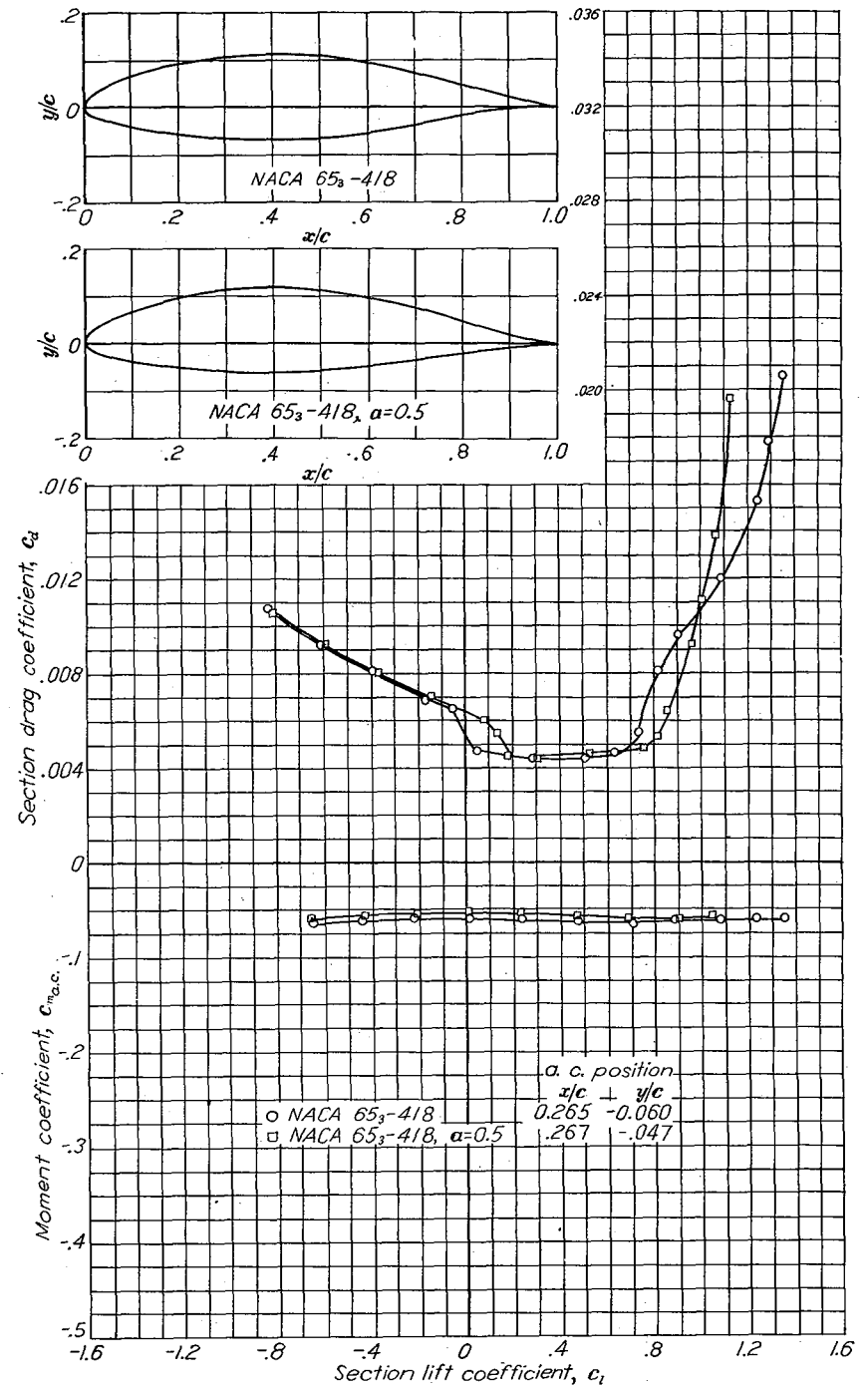
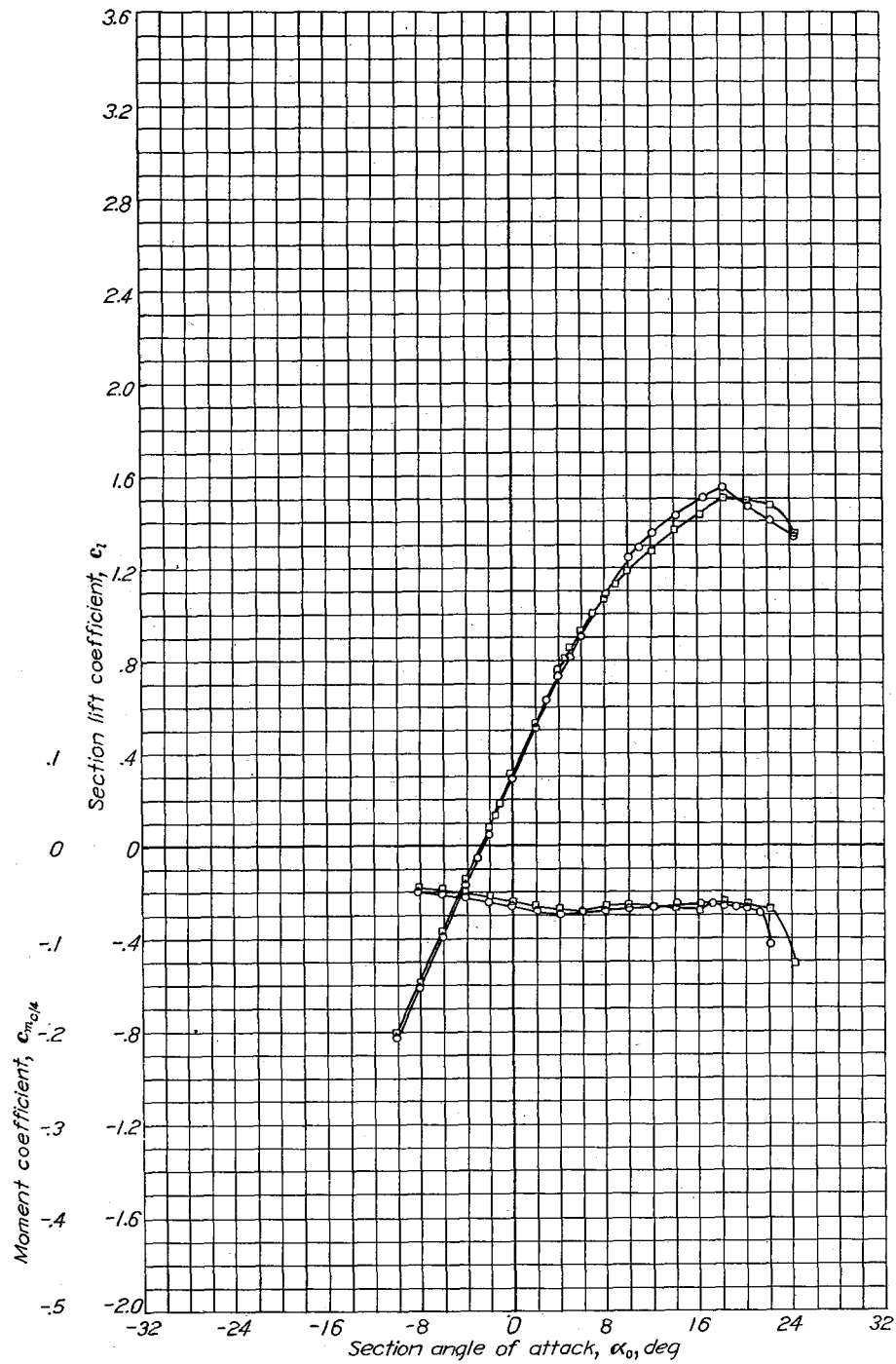


FIGURE 16.—Comparison of the aerodynamic characteristics of the NACA 653-418 and NACA 653-418,  $\alpha = 0.5$  airfoils at a Reynolds number of  $9 \times 10^6$ . TDT tests 314, 320, 406, and 411.



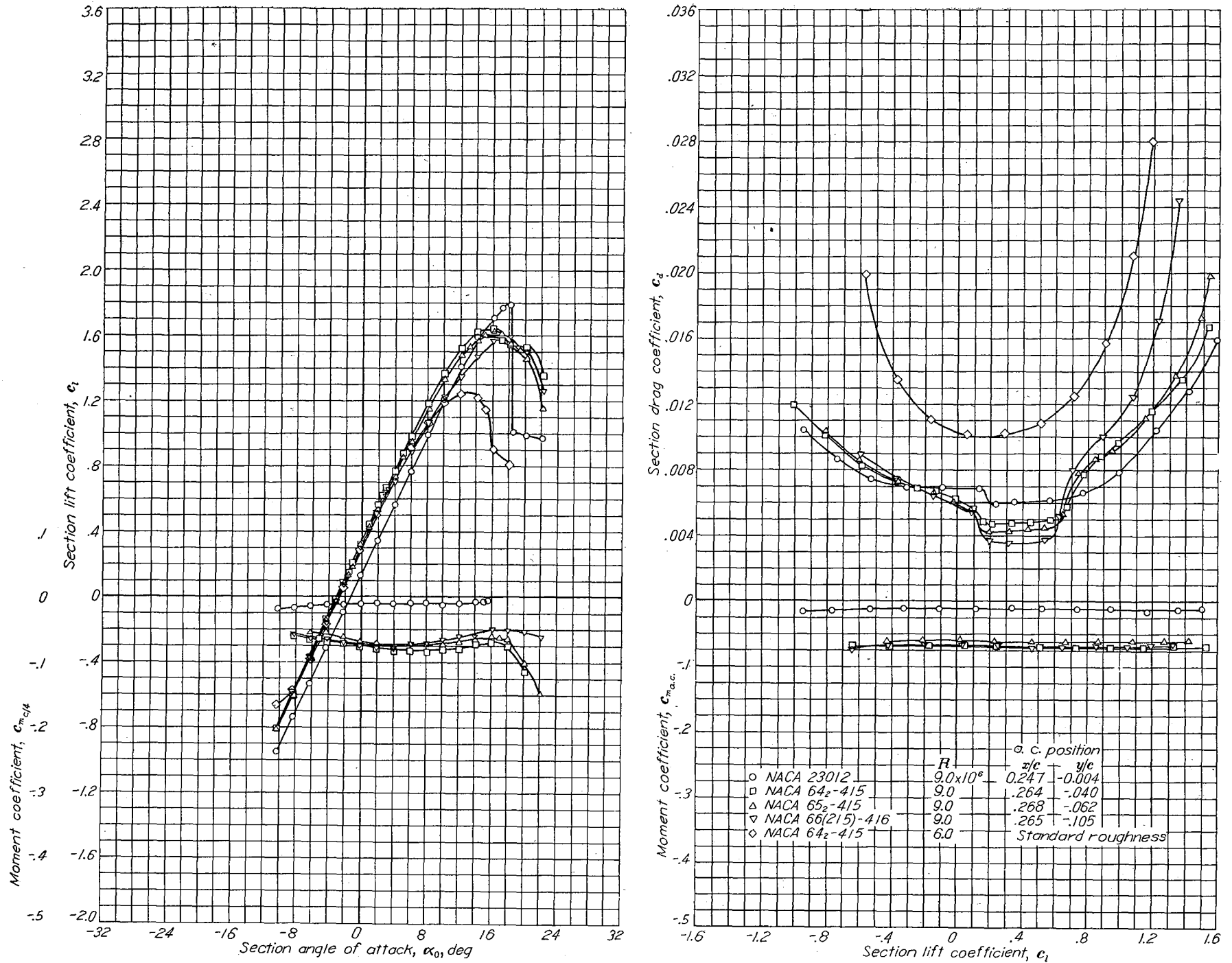


FIGURE 17.—Comparison of the aerodynamic characteristics of some NACA airfoils from tests in the Langley two-dimensional low-turbulence pressure tunnel.

**Effective aspect ratio.**—The combination of high drags at high lift coefficients, low drags at moderate lift coefficients, and the nonregular variation of drag with lift coefficient shown by the NACA 6-series airfoils may lead to paradoxical results when the span-efficiency concept (reference 29) is used for the calculation of airplane performance. In the usual application of this concept, the airplane drag characteristics are approximated by a curve of the type

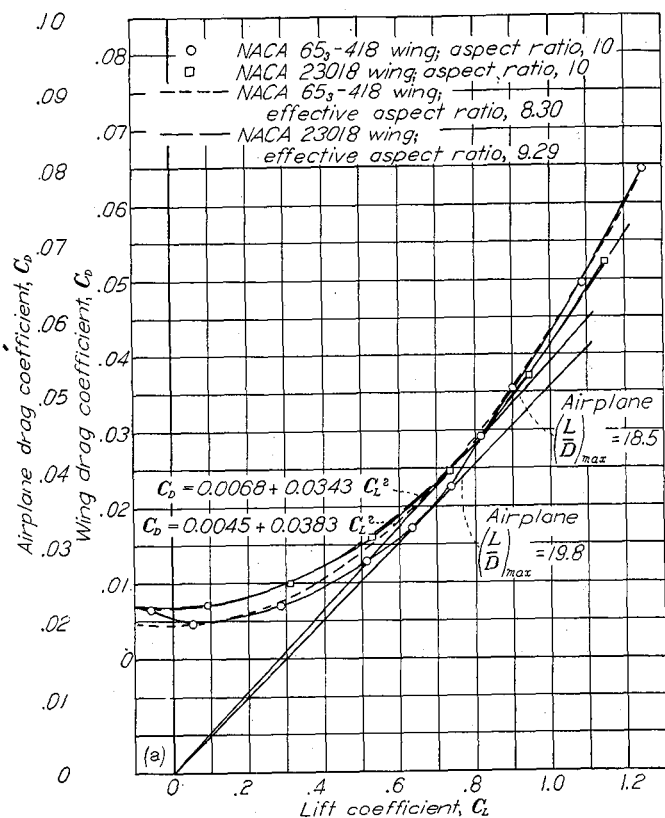
$$C_D = C_{D_{L=0}} + kC_L^2 \quad (17)$$

This curve is usually matched to the actual drag characteristics at a rather low and at a moderately high value of the lift coefficient (reference 30).

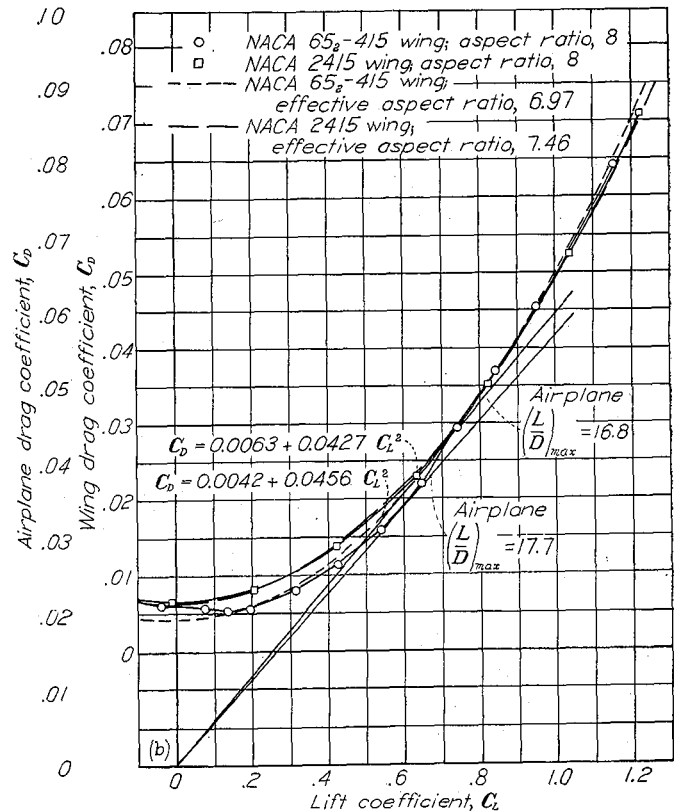
The application of this concept to two hypothetical airplanes with NACA 230- and 65-series sections, respectively, is illustrated in figure 18 (a). The wing drags of the airplanes have been calculated by adding the induced drags corresponding to an aspect ratio of 10 with elliptical loading to the profile-drag coefficients of the NACA 23018 and 65<sub>3</sub>-418 airfoils. These sections are considered representative of average wing sections for a large airplane of this aspect ratio. Ordinate scales are given in figure 18 (a) for the wing drag and for the total airplane drag coefficients obtained by adding a representative constant value of

0.0150 to the wing drag coefficients. The resulting drag coefficients have been approximated by two curves corresponding to equation (17) and matched to the drag curves at lift coefficients of 0.2 and 1.0. These two curves correspond to effective aspect ratios of 9.29 for the airplane with NACA 23018 sections and of 8.30 for the airplane with NACA 65<sub>3</sub>-418 sections and illustrate the typical large reduction in the effective aspect ratio obtained with such sections.

It should be noted, however, that although equation (17) provides a reasonably satisfactory approximation to the drag of the airplane with NACA 23018 sections, such is not the case for the airplane with the NACA 65<sub>3</sub>-418 section. The most important reason for using high aspect ratios on large airplanes is to reduce the drag at cruising lift coefficients and to obtain high maximum values of the lift-drag ratio. For the two wings considered, the maximum value of this ratio is appreciably higher for the airplane with NACA 65<sub>3</sub>-418 sections (19.8 as compared with 18.5) despite the fact that this airplane shows the lower effective aspect ratio. Figure 18 (b) shows a similar comparison with similar results for two airplanes of aspect ratio 8 and NACA 2415 and 65<sub>2</sub>-415 airfoils. It is accordingly concluded that the effective aspect ratio is not a satisfactory criterion for use in airfoil selection.



(a) NACA 65<sub>3</sub>-418 and 23018 wings of aspect ratio 10.



(b) NACA 65<sub>2</sub>-415 and 2415 wings of aspect ratio 8.

FIGURE 18.—Comparison of finite aspect-ratio drag characteristics for two types of airfoils obtained by adding the induced drag corresponding to an elliptical span loading to the section drag coefficients.

## EFFECT OF SURFACE IRREGULARITIES ON DRAG

**Permissible roughness.**—Previous work has shown large drag increments resulting from surface roughness (reference 31). Although a large part of these drag increments was shown to result from forward movement of transition, substantial drag increments resulted from surface roughness in the region of turbulent flow. It is accordingly important to maintain smooth surfaces even when extensive laminar flow cannot be expected, but the gains that may be expected from maintaining smooth surfaces are greater for NACA 6- or 7-series airfoils when extensive laminar flows are possible.

No accurate method of specifying the surface condition necessary for extensive laminar flow at high Reynolds numbers has been developed, although some general conclusions have been reached. It may be presumed that for a given Reynolds number and chordwise position, the size of the permissible roughness will vary directly with the chord of the airfoil. It is known, at one extreme, that the surfaces do not have to be polished or optically smooth. Such polishing or waxing has shown no improvement in tests in the Langley two-dimensional low-turbulence tunnels when applied to satisfactorily sanded surfaces. Polishing or waxing a surface that is not aerodynamically smooth will, of course, result in improvement and such finishes may be of considerable practical value because deterioration of the finish may be easily seen and possibly postponed. Large models having chord lengths of 5 to 8 feet tested in the Langley two-dimensional low-turbulence tunnels are usually finished by sanding in the chordwise direction with No. 320 carborundum paper when an aerodynamically smooth surface is desired. Experience has shown the resulting finish to be satisfactory at flight values of the Reynolds number. Any rougher surface texture should be considered as a possible source of transition, although slightly rougher surfaces have appeared to produce satisfactory results in some cases.

Wind-tunnel experience in testing NACA 6-series sections and data of reference 32 show that small protuberances extending above the general surface level of an otherwise satisfactory surface are more likely to cause transition than small depressions. Dust particles, for example, are more effective than small scratches in producing transition if the material at the edges of the scratches is not forced above the general surface level. Dust particles adhering to the oil left on airfoil surfaces by fingerprints may be expected to cause transition at high Reynolds numbers.

Transition spreads from an individual disturbance with an included angle of about  $15^\circ$  (references 31 and 33). A few scattered specks, especially near the leading edge, will cause the flow to be largely turbulent. This fact makes necessary an extremely thorough inspection if low drags are to be realized. Specks sufficiently large to cause premature transition on full-size wings can be felt by hand. The inspection procedure used in the Langley two-dimensional low-turbulence tunnels is to feel the entire surface by hand after which the surface is thoroughly wiped with a dry cloth.

It has been noticed that transition resulting from individual

small sharp protuberances, in contrast to waves, tends to occur at the protuberance. Transition caused by surface waviness appears to approach the wave gradually as the Reynolds number or wave size is increased. The height of a small cylindrical protuberance necessary to cause transition when located at 5 percent of the chord with its axis normal to the surface is shown in figure 19. These data were

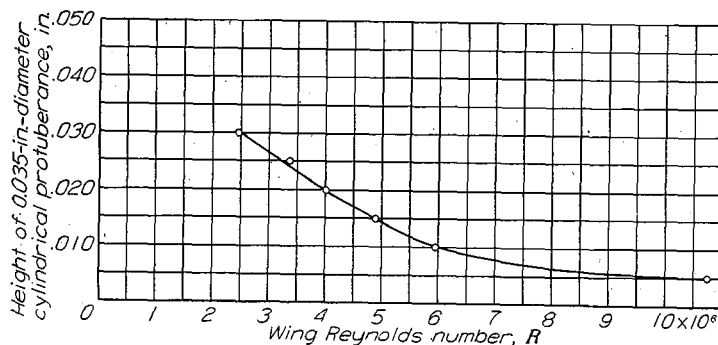


FIGURE 19.—Variation with wing Reynolds number of the minimum height of a cylindrical protuberance necessary to cause premature transition. Protuberance has 0.035-inch diameter with axis normal to wing surface and is located at 5 percent chord of a 90-inch-chord symmetrical 6-series airfoil section of 15-percent thickness and with minimum pressure at 70 percent chord.

obtained at rather low values of the Reynolds number and show a large decrease in allowable height with increase in Reynolds number. This effect of Reynolds number on permissible surface roughness is also evident in figure 20, in which a sharp increase in drag at a Reynolds number of approximately  $20 \times 10^6$  occurs for the model painted with camouflage lacquer.

The magnitude of the favorable gradient appears to have a small effect on the permissible surface roughness for laminar flow. Figure 21 shows that the roughness becomes more important at the extremities of the low-drag range where the favorable pressure gradient is reduced on one surface. The effect of increasing the Reynolds number for a surface of marginal smoothness, which has an effect similar to increasing the surface roughness for a given Reynolds number, is to reduce rapidly the extent of the low-drag range and then to increase the minimum drag coefficient (fig. 21). The data of figure 21 were specially chosen to show this effect. In most cases, the effect of Reynolds number predominates over the effect of decreasing the magnitude of the favorable pressure gradient to such an extent that the only effect is the elimination of the low-drag range (reference 34).

**Permissible waviness.**—More difficulty is generally encountered in reducing the waviness to permissible values for the maintenance of laminar flow than in obtaining the required surface smoothness. In addition, the specification of the required freedom from surface waviness is more difficult than that of the required surface smoothness. The problem is not limited merely to finding the minimum wave size that will cause transition under given conditions because the number of waves and the shape of the waves require consideration.

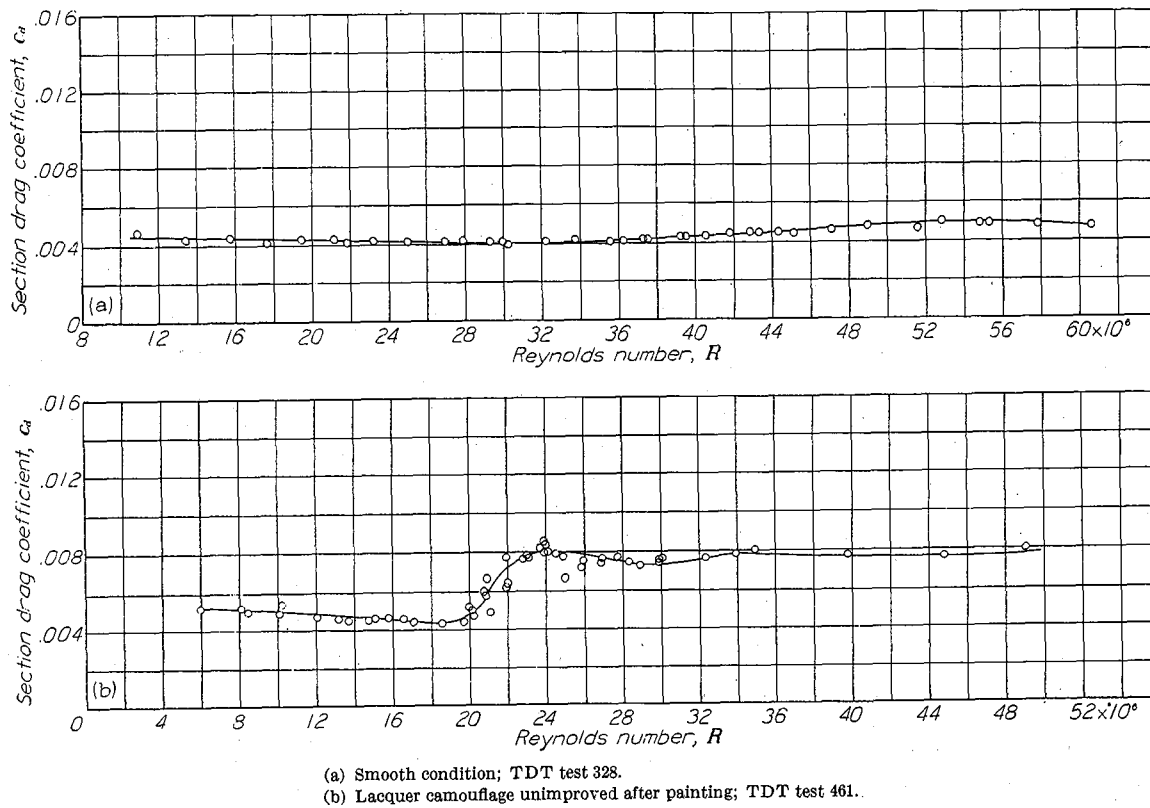


FIGURE 20.—Variation of drag coefficient with Reynolds number for a 60-inch-chord model of the NACA 65(421)-420 airfoil for two surface conditions.

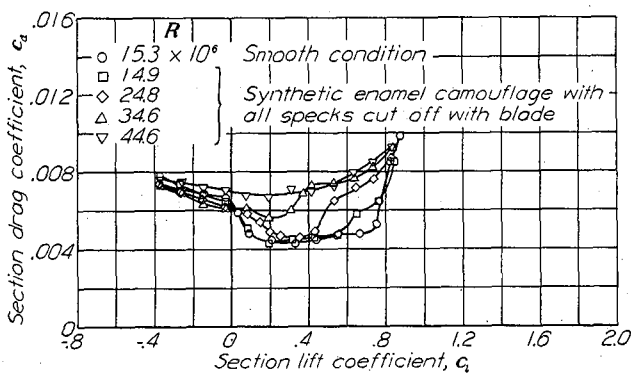


FIGURE 21.—Drag characteristics of NACA 65(421)-420 airfoil for two surface conditions. TDT tests 300 and 486.

If the wave is sufficiently large to affect the pressure distribution in such a manner that laminar separation is encountered, there is little doubt that such a wave will cause premature transition at all useful Reynolds numbers. A relation between the dimensions of a wave and the pressure distribution may be found by the method of reference 35. The size of the wave required to reverse the favorable pressure gradient increases with the pressure gradient. Large negative pressure gradients would therefore appear to be favorable for wavy surfaces. Experimental results have shown this conclusion to be qualitatively correct.

Little information is available on waves too small to cause

laminar separation or even reversal of the pressure gradient. Data for an airfoil section having a relatively long wave on the upper surface are given in figure 22. Marked increases in the drag corresponding to a rapid forward movement of the transition point were not noticeable below a Reynolds number of  $44 \times 10^6$ . On the other hand, transition has been caused at comparatively low Reynolds numbers by a series of small waves with a wave height of the order of a few ten-thousandths of an inch and a wave length of the order of 2 inches on the same 60-inch-chord model.

For the types of wave usually encountered on practical-construction wings, the test of rocking a straightedge over the surface in a chordwise direction is a fairly satisfactory criterion. The straightedge should rock smoothly without jarring or clicking. The straightedge test will not show the existence of waves that leave the surface convex, such as the wave of figure 22 and the series of small waves previously mentioned. Tests of a large number of practical-construction models, however, have shown that those models which passed the straightedge test were sufficiently free of small waves to permit low drags to be obtained at flight values of the Reynolds number.

It is not feasible to specify construction tolerances on airfoil ordinates with sufficient accuracy to ensure adequate freedom from waviness. If care is taken to obtain fair surfaces, normal tolerances may be used without causing serious alteration of the drag characteristics.

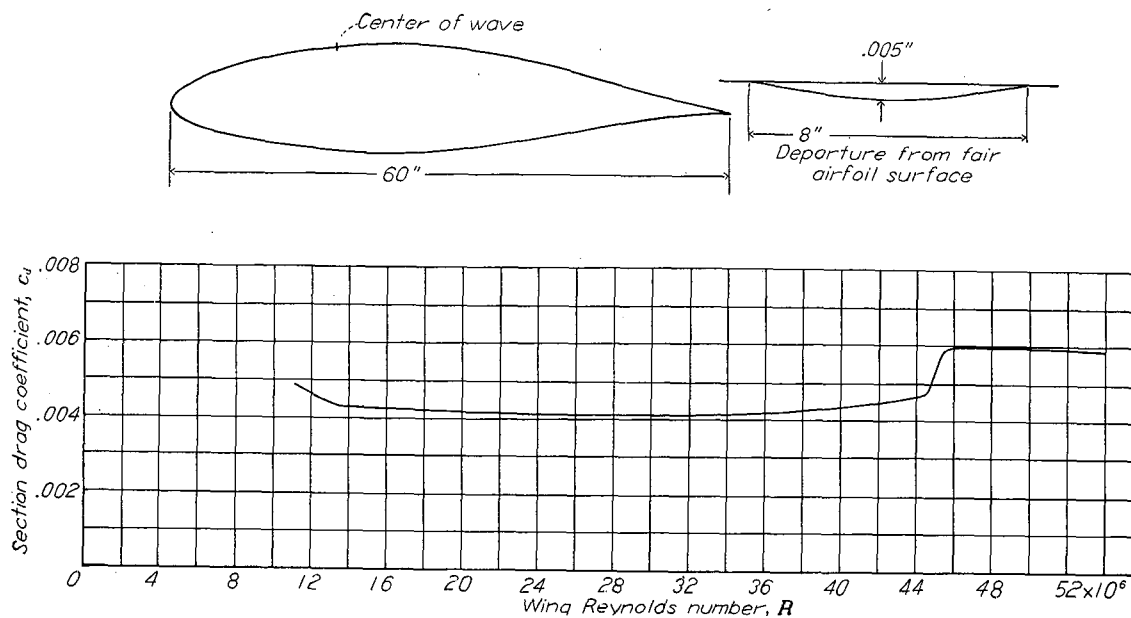


FIGURE 22.—Experimental curve showing variation of drag coefficient with Reynolds number for the NACA 65(421)-420 airfoil section with a small amount of surface waviness.

**Drag with fixed transition.**—If the airfoil surface is sufficiently rough to cause transition near the leading edge, large drag increases are to be expected. Figure 23 shows that, although the degree of roughness has some effect, the increment in minimum drag coefficient caused by the smallest roughness capable of producing transition is nearly as great as that caused by much larger grain roughness when the roughness is confined to the leading edge. The degree of roughness has a much larger effect on the drag at high lift coefficients. If the roughness is sufficiently large to cause transition at all Reynolds numbers considered, the drag of the airfoil with roughness only at the leading edge decreases with increasing Reynolds number (fig. 10 and reference 36).

The effect of fixing transition by means of a roughness strip of carborundum of 0.011-inch grain is shown in figure 24. The minimum drag increases progressively with forward movement of the roughness strip. The effect on the drag at high lift coefficients is not progressive; the drag increases rapidly when the roughness is at the leading edge. Figure 25 shows that the drag coefficients for the NACA 65(223)-422 and 63(420)-422 airfoils were nearly the same throughout most of the lift range when the extent of laminar flow was limited to 0.30c.

All recent airfoil data obtained in the Langley two-dimensional low-turbulence pressure tunnel include results with roughened leading edge, and these data are included in the supplementary figures. Tests with roughened leading edge were formerly made only for a limited number of airfoil sections, especially those having large thickness ratios (reference 37). The standard roughness selected for 24-inch-chord models consists of 0.011-inch carborundum grains applied to the airfoil surface at the leading edge over a surface length of 0.08c measured from the leading edge on both surfaces. The grains are thinly spread to cover 5 to 10 percent of this area. This standard roughness is considerably more severe than that caused by the usual manufacturing irregularities or deterioration in service but is considerably less severe than that likely to be encountered in service as a

result of accumulation of ice or mud or damage in military combat.

The variation of minimum drag coefficient with thickness ratio for a number of NACA airfoils with standard roughness is shown in figure 12. These data show that the magnitudes of the minimum drag coefficients for the NACA 6-series airfoils are less than the values for the NACA four- and five-digit-series airfoils. The rate of increase of drag with thickness is greater for the airfoils in the rough condition than in the smooth condition.

**Drag with practical construction methods.**—The section drag coefficients of several airplane wings have been measured in flight by the wake-survey method (reference 38), and a number of practical-construction wing sections have been tested in the Langley two-dimensional low-turbulence pressure tunnel at flight values of the Reynolds number. Flight data obtained by the NACA (reference 38) are summarized in figure 26 and some data obtained by the Consolidated Vultee Aircraft Corporation are presented in figure 27. Data obtained in the Langley two-dimensional low-turbulence pressure tunnel for typical practical-construction sections are presented in figures 28 to 32. Figure 33 presents a comparison of the drag coefficients obtained in this wind tunnel for a model of the NACA 0012 section and in flight for the same model mounted on an airplane. For this case, the wind-tunnel and flight data agree to within the experimental error.

All wings for which flight data are presented in figure 26 were carefully finished to produce smooth surfaces. Great care was taken to reduce surface waviness to a minimum for all the sections except the NACA 2414.5, the N-22, the Republic S-3,13, and the NACA 27-212. Curvature-gage measurements of surface waviness for some of these airfoils are presented in reference 38. Surface conditions corresponding to the data of figure 27 are described in the figure. These data show that the sections permitting extensive laminar flow had substantially lower drag coefficients when smooth than the other sections.

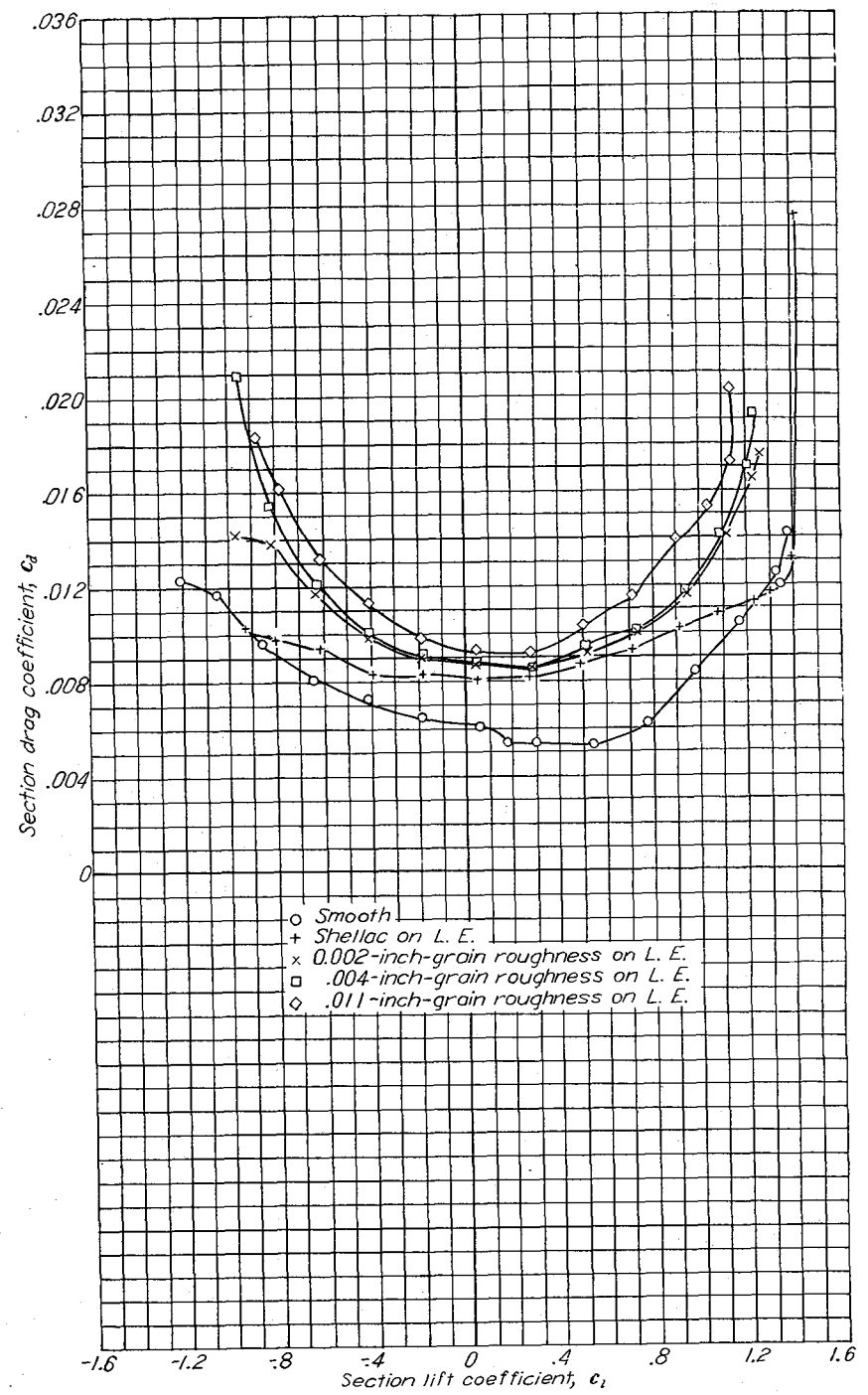
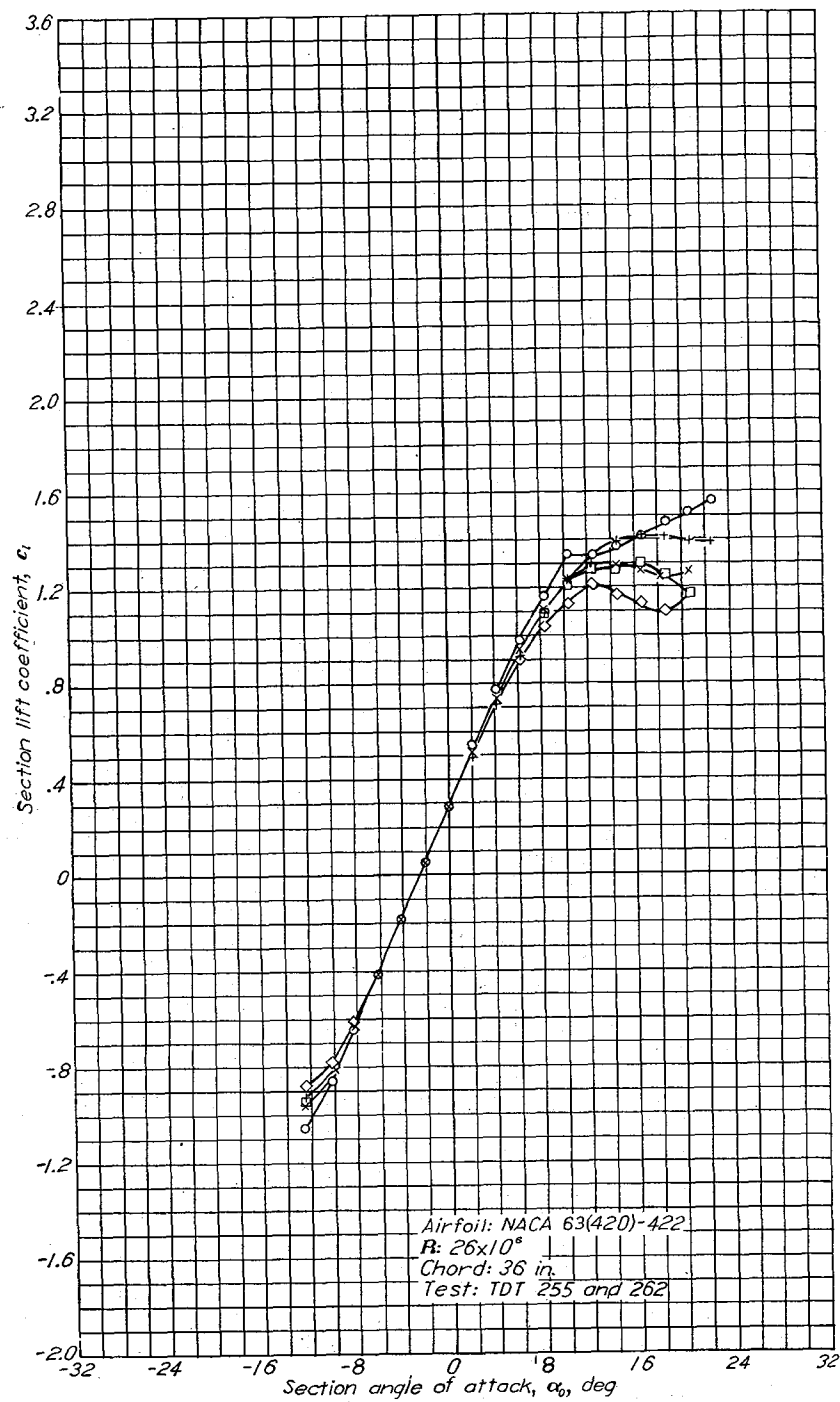


FIGURE 23.—Lift and drag characteristics of an NACA 63(420)-422 airfoil with various degrees of roughness at the leading edge.

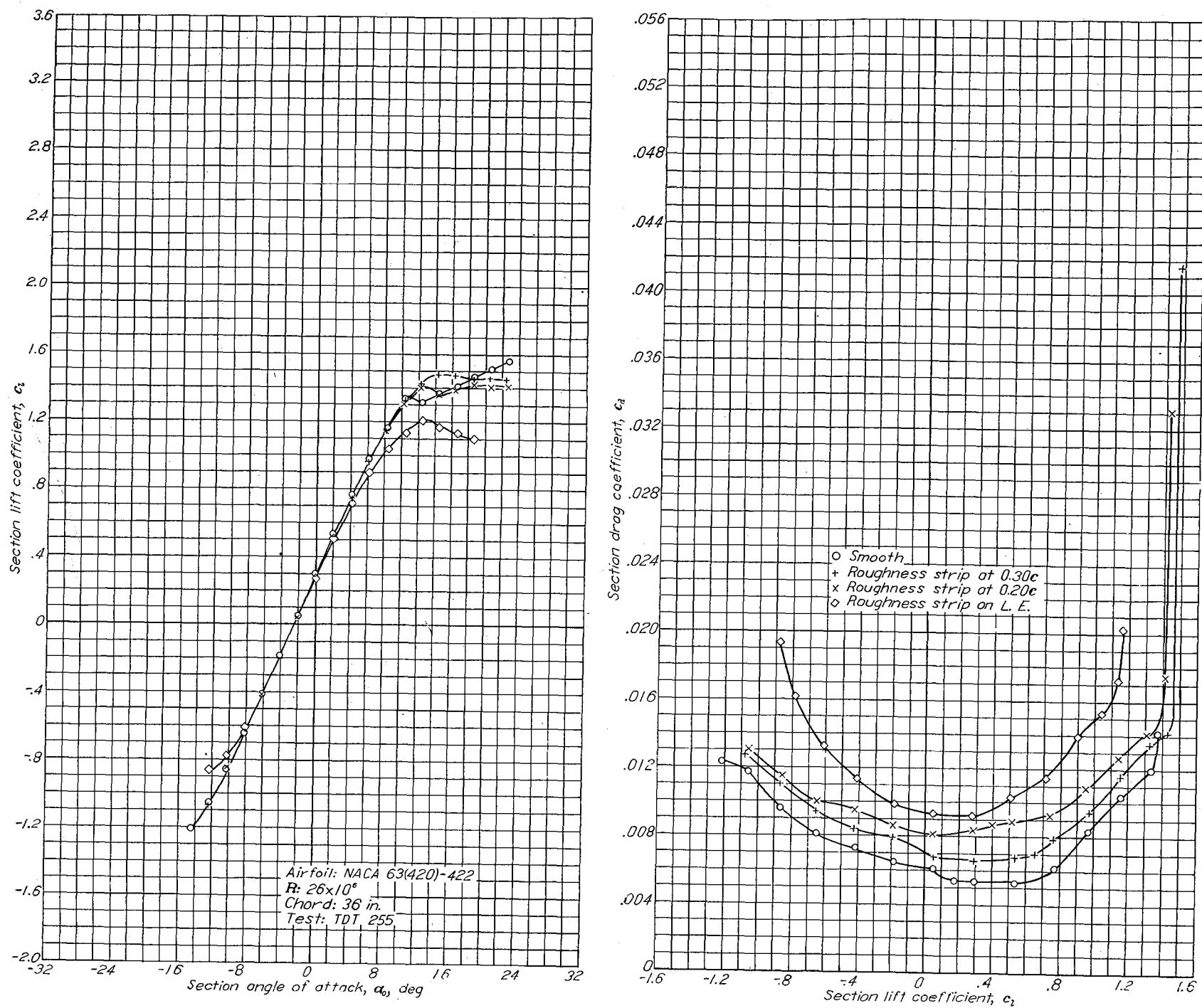


FIGURE 24.—Lift and drag characteristics of an NACA 63(420)-422 airfoil with 0.011-inch-grain roughness at various chordwise locations.

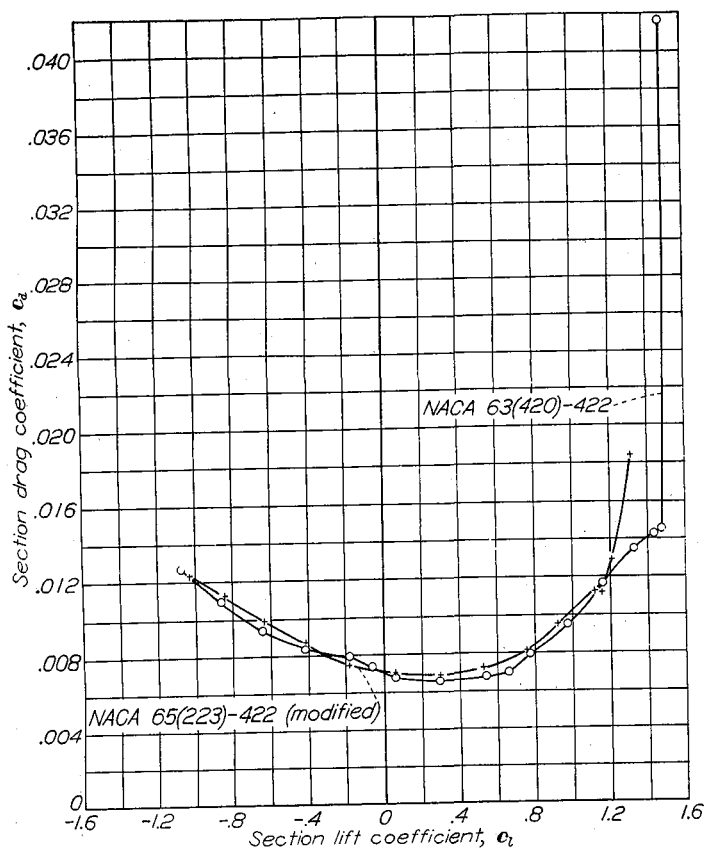


FIGURE 25.—Drag characteristics of two NACA 6-series airfoils with 0.011-inch-grain roughness at 0.30c.  $R=26 \times 10^6$ .

The wind-tunnel tests of practical-construction wing sections as delivered by the manufacturer showed minimum drag coefficients of the order of 0.0070 to 0.0080 in nearly all cases regardless of the airfoil section used (figs. 28 to 32). Such values may be regarded as typical for good current construction practice. Finishing the sections to produce smooth surfaces always produced substantial drag reductions although considerable waviness usually remained. None of the sections tested had fair surfaces at the front spar. Unless special care is taken to produce fair surfaces at the front spar, the resulting wave may be expected to cause transition either at the spar location or a short distance behind it. One practical-construction specimen tested with smooth surfaces maintained relatively low drags up to Reynolds numbers of approximately  $30 \times 10^6$  (NACA 66(2x15)-116 airfoil of fig. 10). This specimen had no spar forward of about 35 percent chord from the leading edge and no spanwise stiffeners forward of the spars. This type of construction resulted in unusually fair surfaces and is being used on some modern high-performance airplanes.

A comparison of the effect of airfoil section on the minimum drag with practical-construction surfaces is very difficult because the quality of the surface has more effect on the drag than the type of section. Probably the best comparison can be obtained from pairs of models constructed at

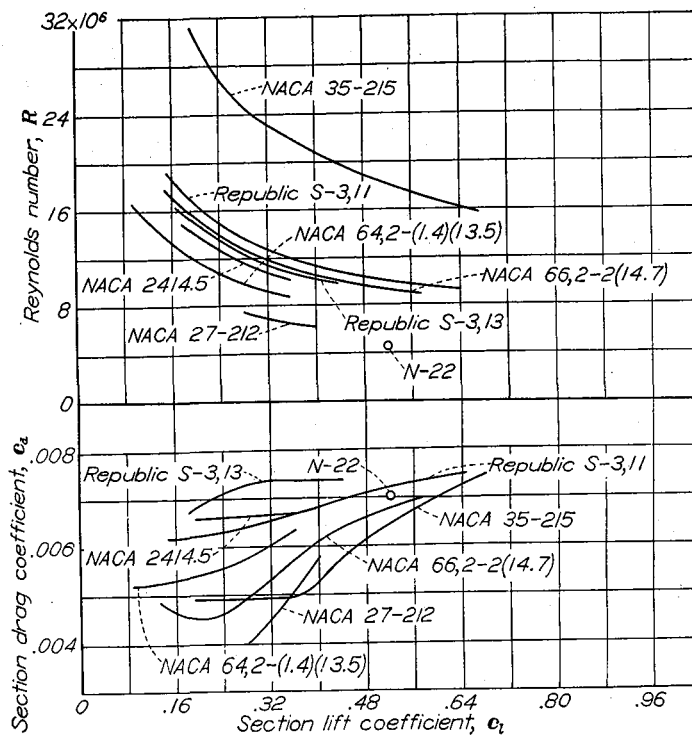


FIGURE 26.—Comparison of section drag coefficients obtained in flight on various airfoils. Tests of NACA 27-212 and 35-215 sections made on gloves.

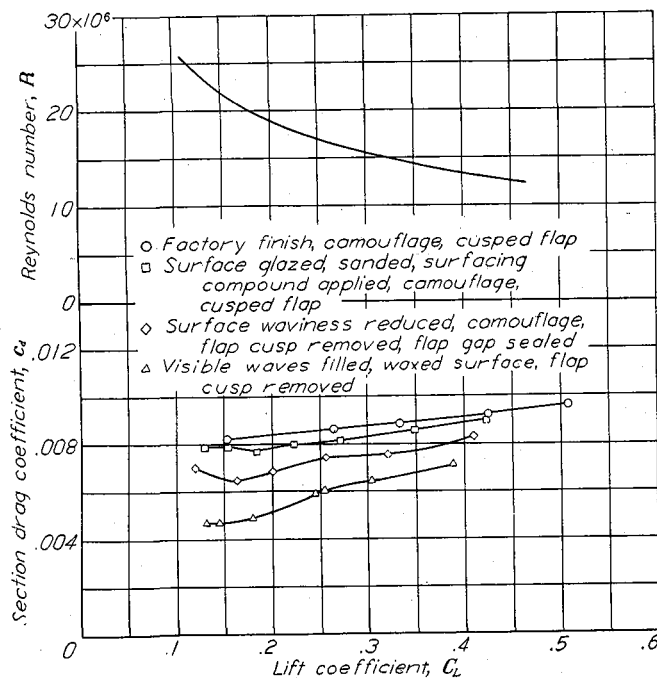


FIGURE 27.—Consolidated-Vultee flight measurements of the effect of wing surface condition on drag of an NACA 66(215)-1(14.5) wing section.

the same time by the same manufacturers. Data for such pairs of models are presented in figures 30 to 32. The results indicate that as long as current construction practices are used the type of section has relatively little effect at flight values of the Reynolds number for military airplanes.



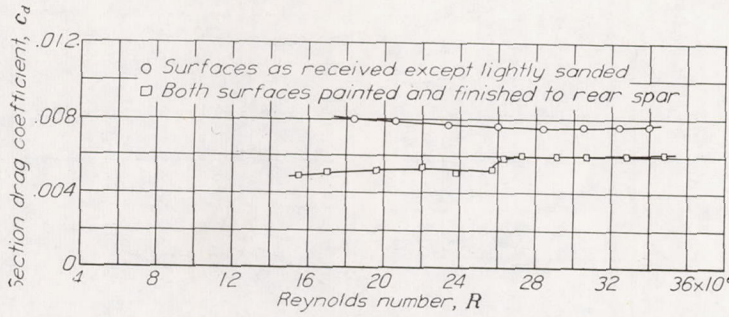
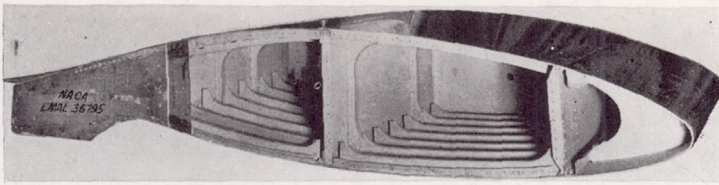


FIGURE 28.—Drag scale effect on 100-inch-chord practical-construction model of the NACA 65(216)-3(16.5) (approx.) airfoil section.  $c_l=0.2$  (approx.).

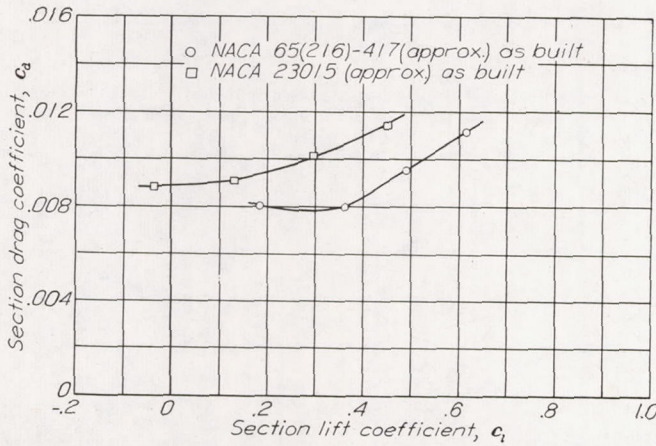


FIGURE 30.—Drag characteristics of the NACA 65(216)-417 (approx.) and NACA 23015 (approx.) airfoil sections built by practical-construction methods by the same manufacturer.  $R=10.23 \times 10^6$ .

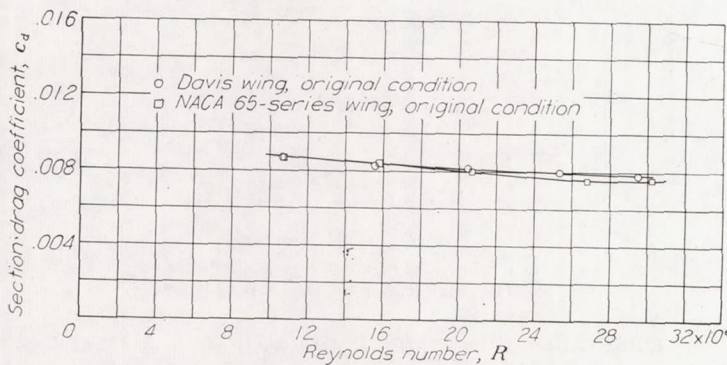


FIGURE 32.—Drag scale effect for a model of the NACA 65-series airfoil section, 18.27 percent thick, and the Davis airfoil section, 18.27 percent thick, built by practical-construction methods by the same manufacturer.  $c_l=0.46$  (approx.).

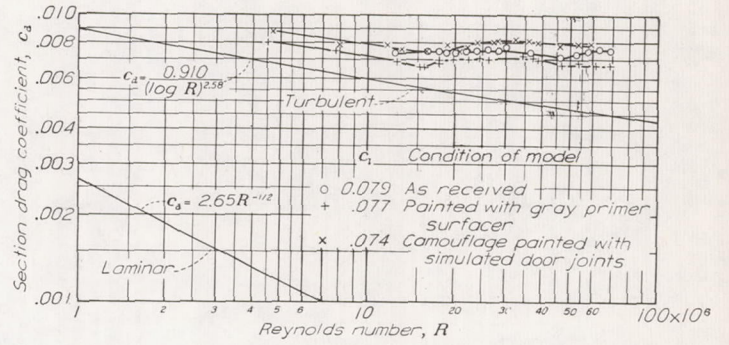
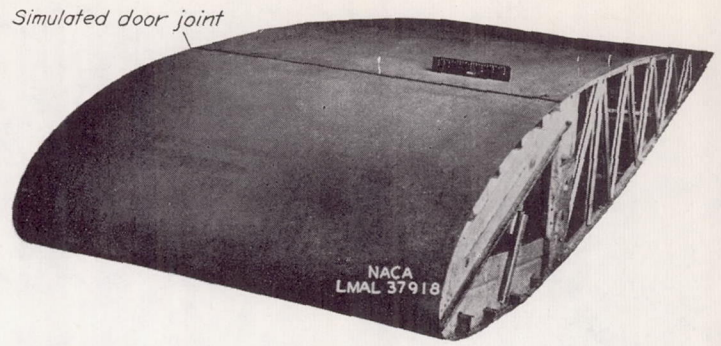


FIGURE 29.—Variation of drag coefficient with Reynolds number for the NACA 23016 airfoil section together with laminar and turbulent skin-friction coefficients for a flat plate.

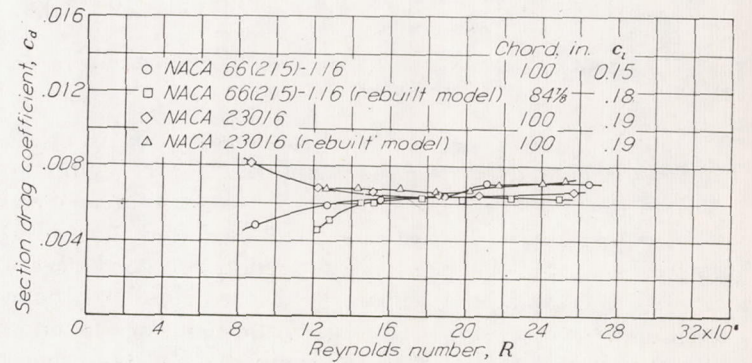


FIGURE 31.—Scale effect on drag of the NACA 66(215)-116 and NACA 23016 airfoil sections built by practical-construction methods by the same manufacturer and tested as received.

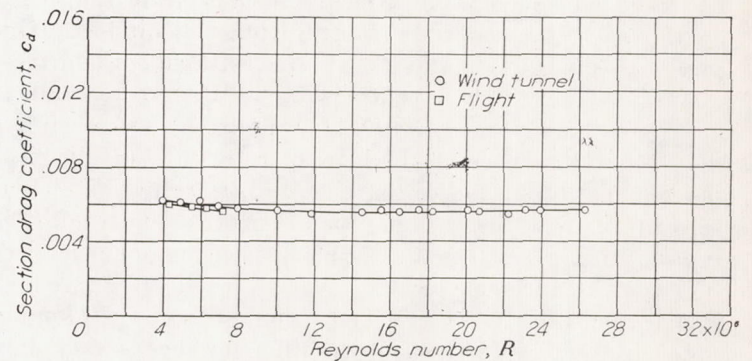


FIGURE 33.—Comparison of drag coefficients measured in flight and wind tunnel for the NACA 0012 airfoil section at zero lift.

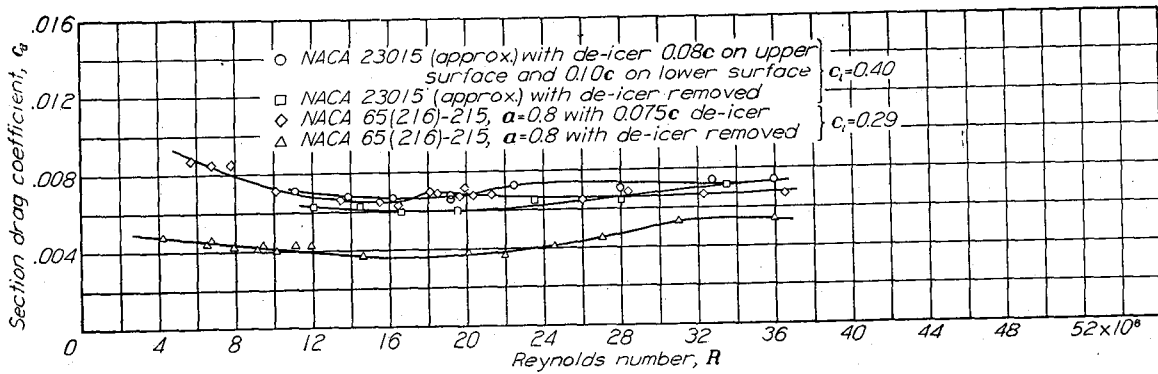


FIGURE 34.—Effect of de-icers on the drag of two practical-construction airfoil sections with relatively smooth surfaces.

Important savings in drag may be obtained at high Reynolds numbers by keeping the surfaces smooth even if extensive laminar flow is not realized. Drag increments resulting from surface roughness in turbulent flow have been shown to be important (reference 31). The effects of surface roughness on the variation of drag with Reynolds number are shown in figure 29, in which the favorable scale effect usually expected at high Reynolds numbers was not realized. This type of scale effect may be compared with that shown for the NACA 63(420)-422 airfoil with rough leading edge but otherwise smooth surfaces (fig. 10). Drag increments obtained in flight resulting from roughness in the turbulent boundary layer with fixed transition are presented in reference 39.

The effect of the application of de-icers to the leading edge of two smooth airfoils is shown in figure 34. The de-icer "boots" were installed in both cases by the manufacturer to

represent good typical installations. The minimum drag coefficients for both sections with de-icers installed were of the order of 0.0070 at high Reynolds numbers.

**Effects of propeller slipstream and airplane vibration.**— Very few data are available on the effect of propeller slipstream on transition or airfoil drag; the data that are available do not show consistent results. This inconsistency may result from variations in lift coefficient, surface condition, air-stream turbulence, propeller advance-diameter ratio, and number of blades. Tests in the Langley 8-foot high-speed tunnel indicated transition occurring from 5 to 10 percent of the chord from the leading edge (reference 40). Drag measurements made in the Langley 19-foot pressure tunnel (fig. 35) indicated only moderate drag increments resulting from a windmilling propeller. Although the data of figure 35 may not be very accurate because of the difficulty of making wake surveys in the slipstream, these data seem to preclude very large drag increments such as would result from movement of the transition to a position close to the leading edge. These data also seem to be confirmed by recent NACA flight data (fig. 36), which show transition as far back as 20 percent

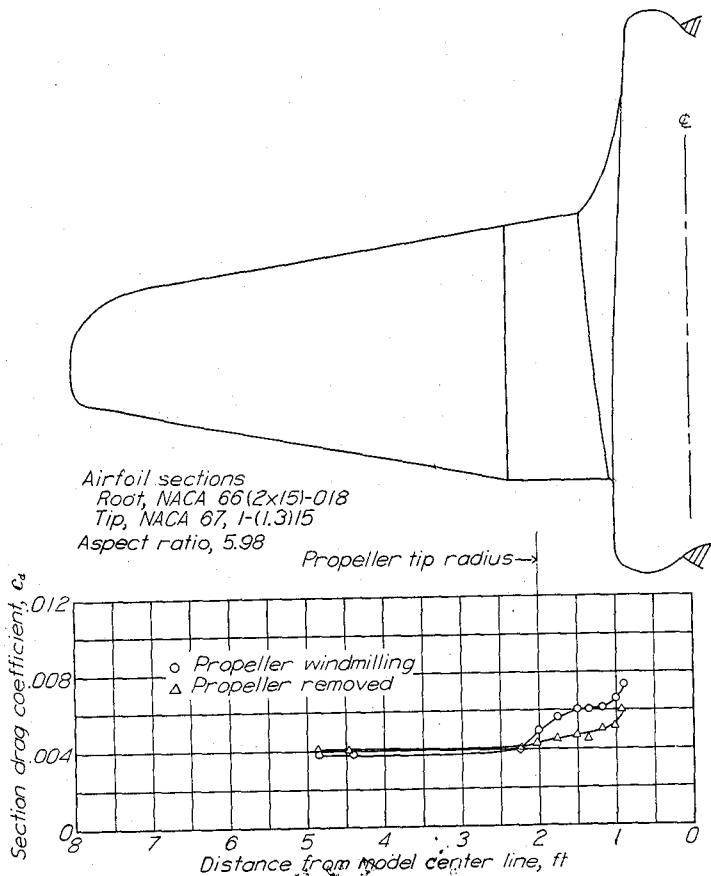


FIGURE 35.—The effect of propeller operation on section drag coefficient of a fighter-type airplane from tests of a model in the Langley 19-foot pressure tunnel.  $C_L=0.10$ ;  $R=3.7 \times 10^6$ .

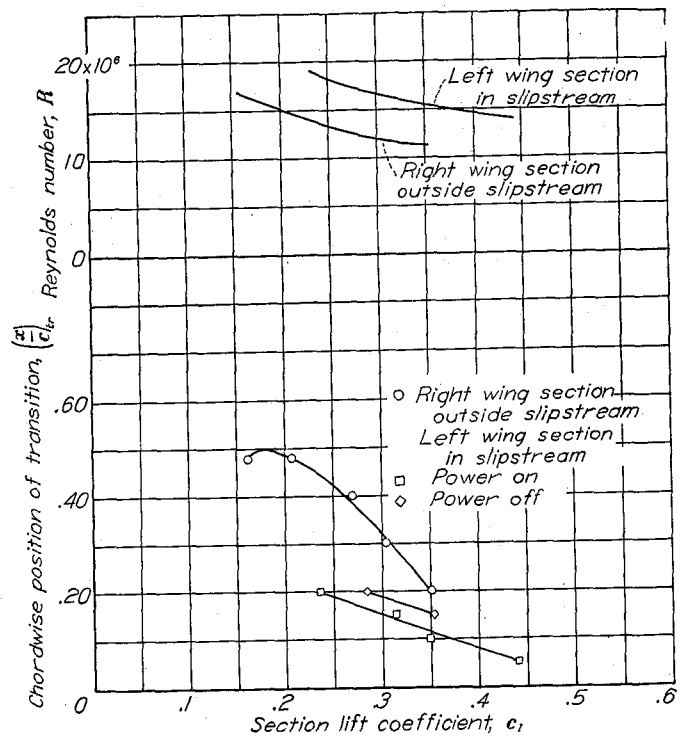


FIGURE 36.—Flight measurements of transition on an NACA 66-series wing within and outside the slipstream.

of the chord in the slipstream. Other unpublished NACA flight data on transition on an S-3,14.6 airfoil in the slipstream indicated that laminar flow occurred as far back as 0.2c.

Even less data are available on the effects of vibration on transition. Tests in the Langley 8-foot high-speed tunnel (reference 40) showed negligible effects, but the range of frequencies tested may not have been sufficiently wide. Some unpublished flight data showed small but consistent rearward movements of transition outside the slipstream when the propellers were feathered. This effect was noticed even when the propeller on the opposite side of the airplane from the survey plane was feathered and was accordingly attributed to vibration. Recent tests in the Ames full-scale tunnel showed premature adverse scale effect on drag coefficients measured by the wake-survey method when a model-support strut vibrated.

#### LIFT CHARACTERISTICS OF SMOOTH AIRFOILS

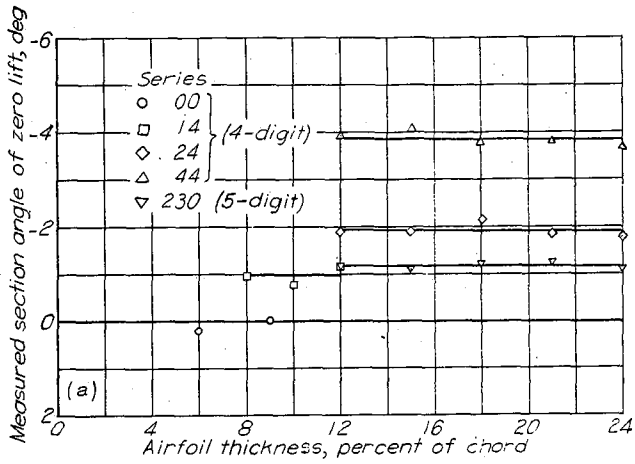
**Two-dimensional data.**—As explained in the section "Angle of Zero Lift," the angle of zero lift of an airfoil is largely determined by the camber. Thin-airfoil theory provides a means for computing the angle of zero lift from the mean-line data presented in the supplementary figures. The agreement between the calculated and the experimental angle of zero lift depends on the type of mean line used. Comparison of the experimental values of the angle of zero lift obtained from the supplementary figures and the theoretical values taken from the mean-line data shows that the agreement is good except for the uniform-load type ( $a=1.0$ ) mean line. The angles of zero lift for this type mean line generally have values more positive than those predicted. The experimental values of the angles of zero lift for a number of NACA four- and five-digit and NACA 6-series airfoils are presented in figure 37. The airfoil thickness appears to have little effect on the value of the angle of zero lift regardless of the airfoil series. For the NACA four-digit-series airfoils, the angles of zero lift are approximately 0.93 of the value given by thin-airfoil theory; for the NACA 230-series airfoils, this factor is approximately 1.08; and for the NACA 6-series airfoils with uniform-load type mean line, this factor is approximately 0.74.

The lift-curve slopes (fig. 38) for airfoils tested in the Langley two-dimensional low-turbulence pressure tunnel are higher than those previously obtained in the tests reported in reference 8. It is not clear whether this difference in slope is caused by the difference in air-stream turbulence or by the differences in test methods, since the section data of reference 8 were inferred from tests of models of aspect ratio 6. The present values of the lift-curve slope were measured for a Reynolds number of  $6 \times 10^6$  and at values of the lift coefficient approximately equal to the design lift coefficient of the

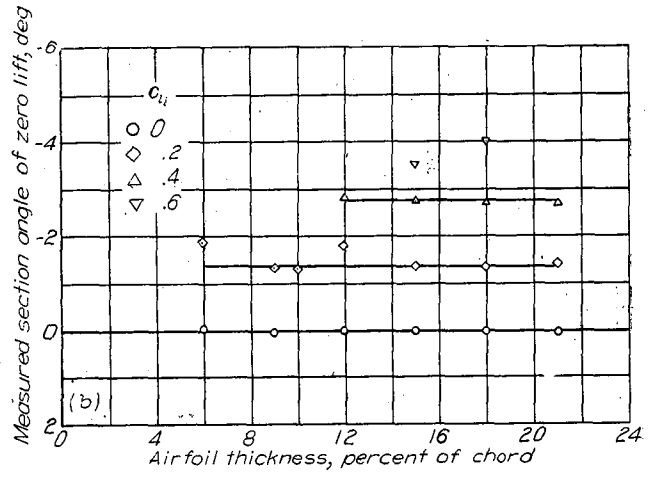
airfoil section. For the NACA 6-series airfoils this lift coefficient is approximately in the center of the low-drag range. For airfoils having thicknesses in the range from 6 to 10 percent, the NACA four- and five-digit series and the NACA 64-series airfoil sections have values of lift-curve slope very close to the value for thin airfoils ( $2\pi$  per radian or 0.110 per degree). Variation in Reynolds number between  $3 \times 10^6$  and  $9 \times 10^6$  and variations in airfoil camber up to 4 percent chord appear to have no systematic effect on values of lift-curve slope. The airfoil thickness and the type of thickness distribution appear to be the primary variables. For the NACA four- and five-digit-series airfoil sections, the lift-curve slope decreases with increase in airfoil thickness. For the NACA 6-series airfoil sections, however, the lift-curve slope increases with increase in thickness and forward movement of the position of minimum pressure of the basic thickness form at zero lift.

Some NACA 6-series airfoils show jogs in the lift curve at the end of the low-drag range, especially at low Reynolds numbers. This jog becomes more pronounced with increase of camber or thickness and with rearward movement of the position of minimum pressure on the basic thickness form. This jog decreases rapidly in severity with increasing Reynolds number, becomes merely a change in lift-curve slope, and is practically nonexistent at a Reynolds number of  $9 \times 10^6$  for most airfoils that would be considered for practical application. This jog may be a consideration in the selection of airfoils for small low-speed airplanes. An analysis of the flow conditions leading to this jog is presented in reference 28.

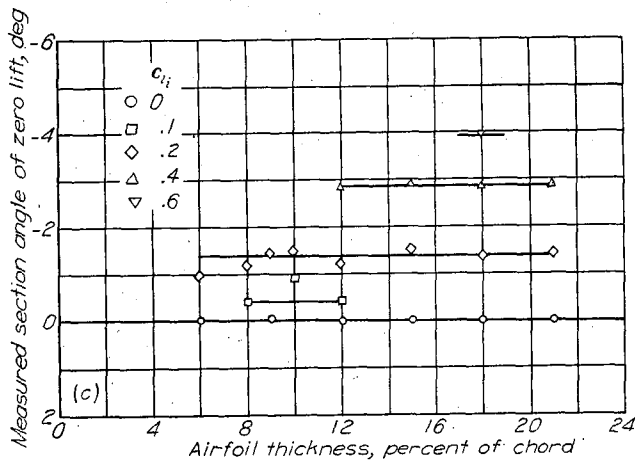
The variation of maximum lift coefficient with airfoil thickness ratio at a Reynolds number of  $6 \times 10^6$  is shown in figure 39 for a number of NACA airfoil sections. The airfoils for which data are presented in this figure have a range of thickness ratio from 6 to 24 percent and cambers up to 4 percent chord. From the data for the NACA four- and five-digit-series airfoil sections (fig. 39 (a)), the maximum lift coefficients for the plain airfoils appear to be the greatest for a thickness of 12 percent. In general, the rate of change of maximum lift coefficient with thickness ratio appears to be greatest for airfoils having a thickness less than 12 percent. The data for the NACA 6-series airfoils (figs. 39 (b) to 39 (e)) also show a rapid increase in maximum lift coefficient with increasing thickness ratio for thickness ratios of less than 12 percent. For NACA 6-series airfoil sections cambered to give a design lift coefficient of not more than 0.2, the optimum thickness ratio for maximum lift coefficient appears to be between 12 and 15 percent, except for the airfoils having the position of minimum pressure at 60 percent chord. The optimum thickness ratio for the NACA 66-series sections cambered for a design lift coefficient of not more than 0.2 appears to be 15 percent or greater.



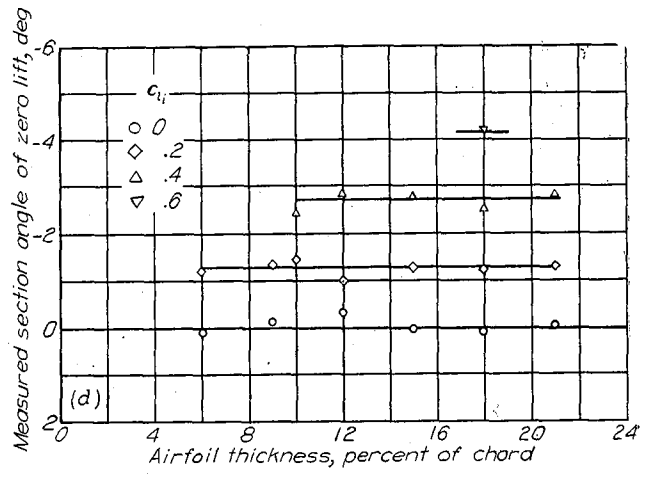
(a) NACA four- and five-digit series.



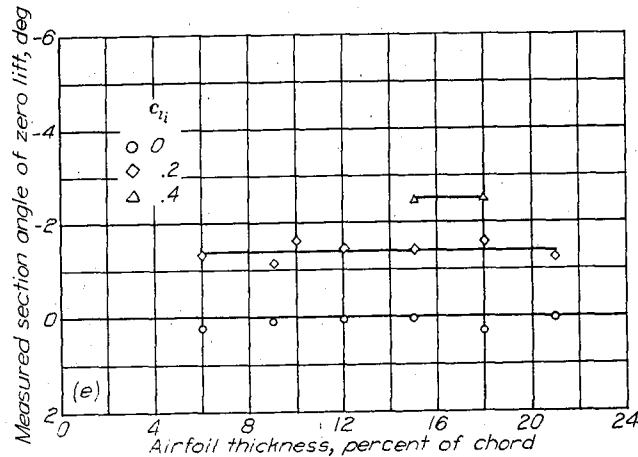
(b) NACA 63-series.



(c) NACA 64-series.



(d) NACA 65-series.



(e) NACA 66-series.

FIGURE 37.—Measured section angles of zero lift for a number of NACA airfoil sections of various thicknesses and camber.  $R=6 \times 10^6$ .

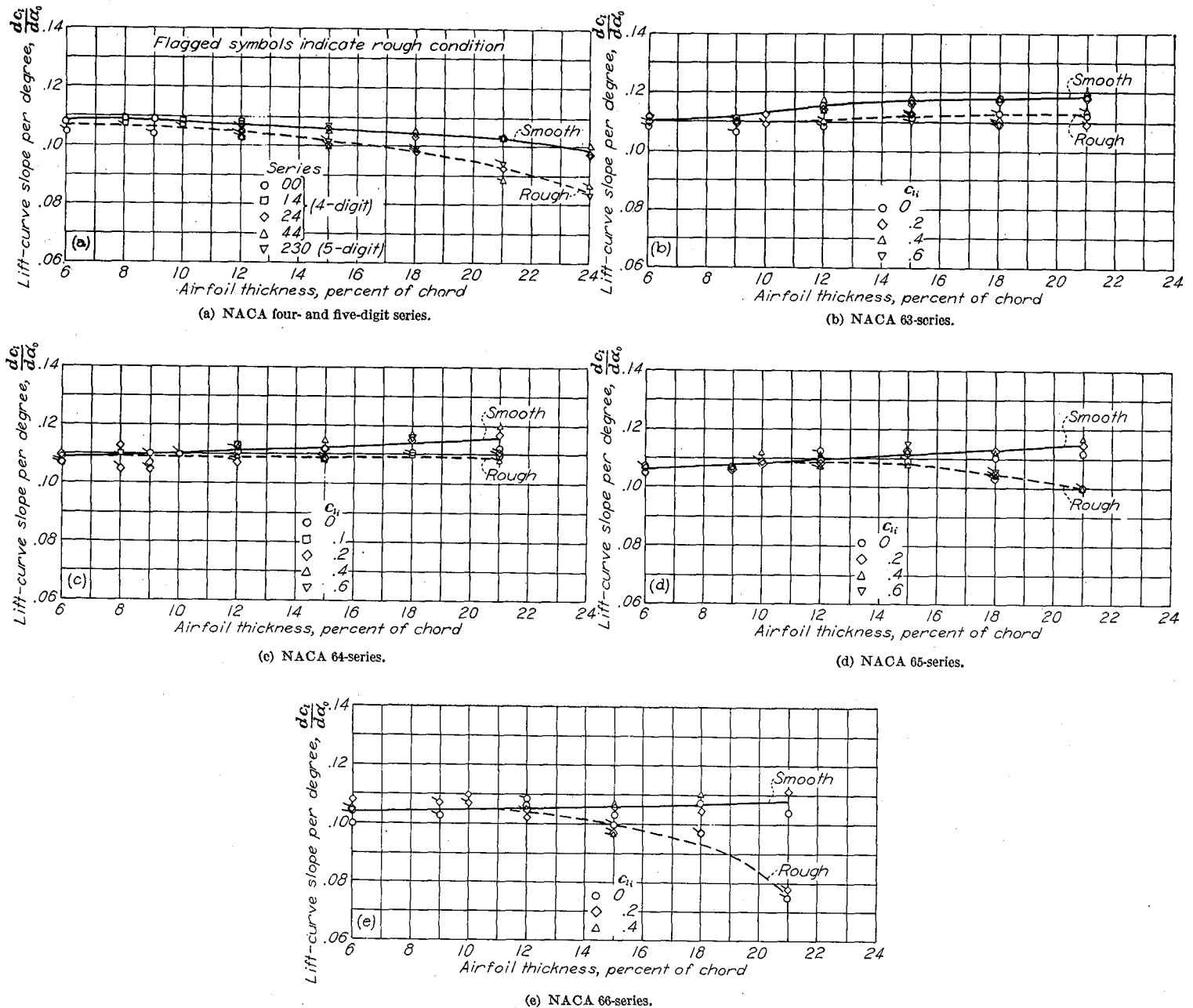


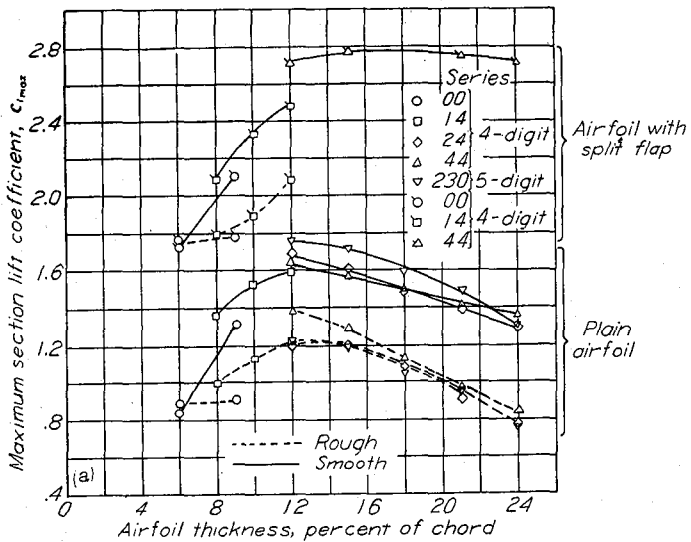
FIGURE 38.—Variation of lift-curve slope with airfoil thickness ratio and camber for a number of NACA airfoil sections in both the smooth and rough conditions.  $R=6 \times 10^6$ .

The available data indicate that a thickness ratio of 12 percent or less is optimum for airfoils having a design lift coefficient of 0.4.

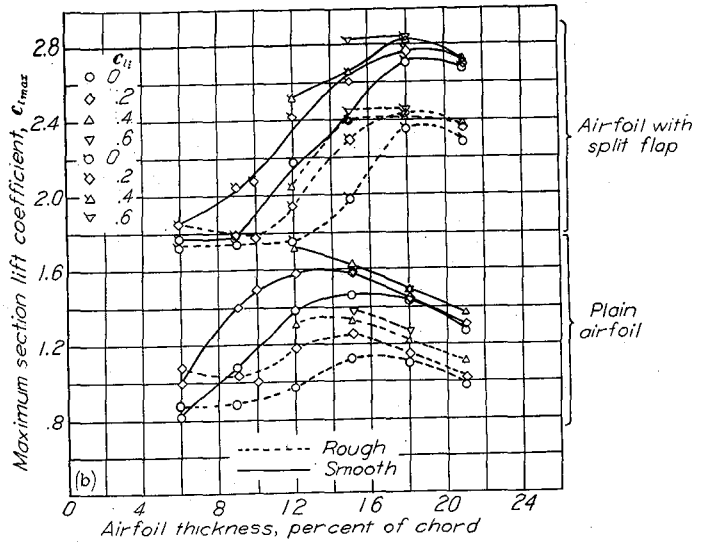
The maximum lift coefficient is least sensitive to variations in position of minimum pressure on the basic thickness form for airfoils having thickness ratios of 6, 18, or 21 percent. The maximum lift coefficients corresponding to intermediate thickness ratios increase with forward movement of the position of minimum pressure, particularly for those airfoils having design lift coefficients of 0.2 or less.

The maximum lift coefficients of moderately cambered

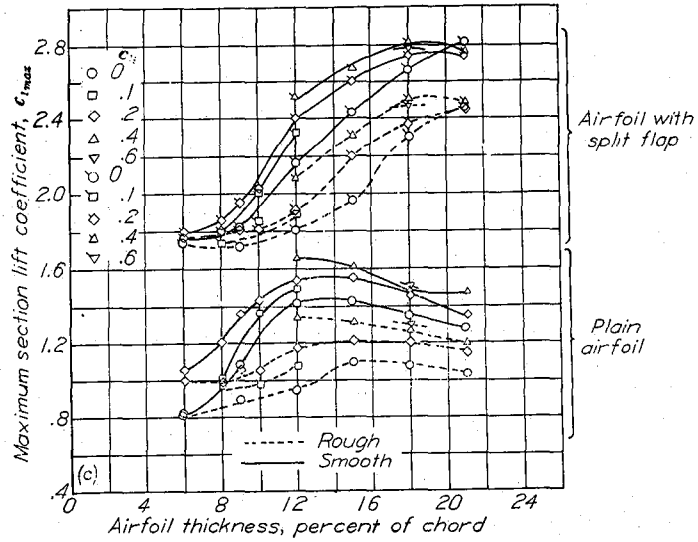
NACA 6-series sections increase with increasing camber (fig. 39 (b) to 39 (e)). The addition of camber to the symmetrical airfoils causes the greatest increments of maximum lift coefficient for airfoil thickness ratios varying from 6 to 12 percent. The effectiveness of camber as a means of increasing the maximum lift coefficient generally decreases as the airfoil thickness increases beyond 12 or 15 percent. The available data indicate that the combination of a 12-percent-thick section and a mean line cambered for a design lift coefficient of 0.4 yields the highest maximum lift coefficient.



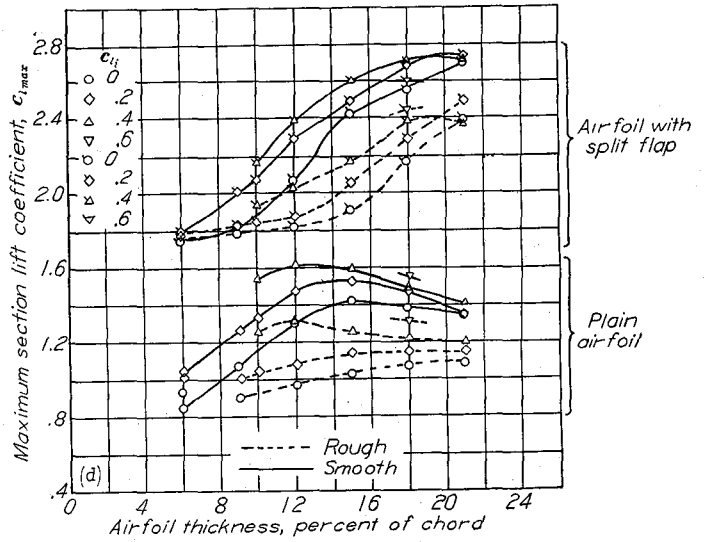
(a) NACA four- and five-digit series.



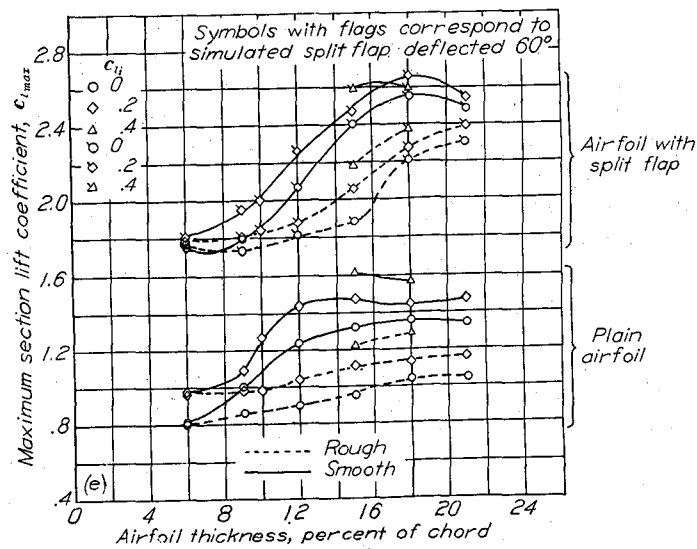
(b) NACA 63-series.



(c) NACA 64 series.



(d) NACA 65-series.



(e) NACA 66-series.

FIGURE 39.—Variation of maximum section lift coefficient with airfoil thickness ratio and camber for several NACA airfoil sections with and without simulated split flaps and standard roughness.  $R=6 \times 10^6$ .

The variation of maximum lift with type of mean line is shown in figure 40 for one 6-series thickness distribution. No systematic data are available for mean lines with values of  $a$  less than 0.5. It should be noted, however, that airfoils such as the NACA 230-series sections with the maximum camber far forward show large values of maximum lift. Airfoil sections with maximum camber far forward and with thickness ratios of 6 to 12 percent usually stall from the leading edge with large sudden losses in lift. A more desirable gradual stall is obtained when the location of maximum camber is farther back, as for the NACA 24-, 44-, and 6-series sections with normal types of camber.

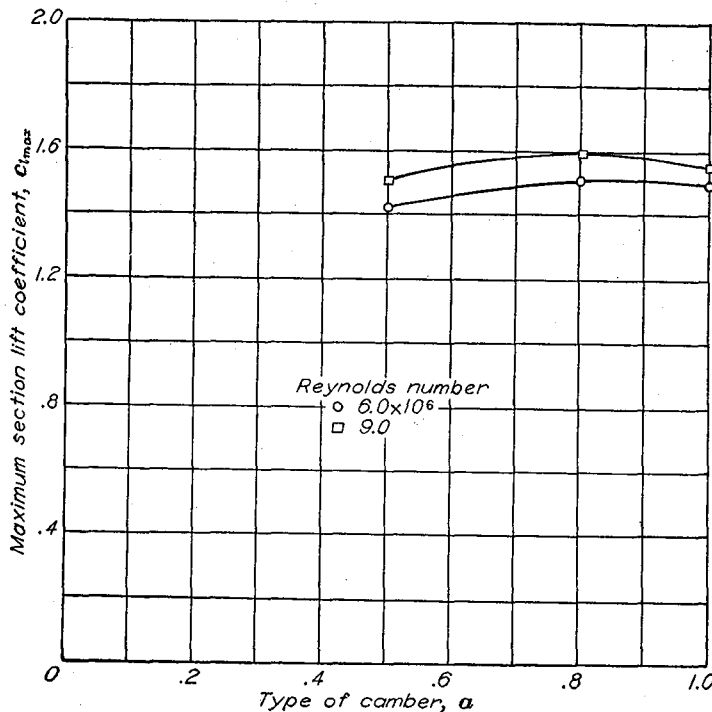


FIGURE 40.—Variation of maximum lift coefficient with type of camber for some NACA 65-418 airfoil sections from tests in the Langley two-dimensional low-turbulence pressure tunnel.

A comparison of the maximum lift coefficients of NACA 64-series airfoil sections cambered for a design lift coefficient of 0.4 with those of the NACA 44- and 230-series sections (fig. 39) shows that the maximum lift coefficients of the NACA 64-series airfoils are as high or higher than those of the NACA 44-series sections in all cases. The NACA 230-series airfoil sections have maximum lift coefficients somewhat higher than those of the NACA 64-series sections.

The scale effect on the maximum lift coefficient of a large number of NACA airfoil sections for Reynolds numbers from  $3 \times 10^6$  to  $9 \times 10^6$  is shown in figure 41. The scale effect for the NACA 24-, 44-, and 230-series airfoils (figs. 41 (a) and 41 (b)) having thickness ratios from 12 to 24 percent is favorable and nearly independent of the airfoil thickness. Increasing the Reynolds number from  $3 \times 10^6$  to  $9 \times 10^6$  results in an increase in the maximum lift coefficient of

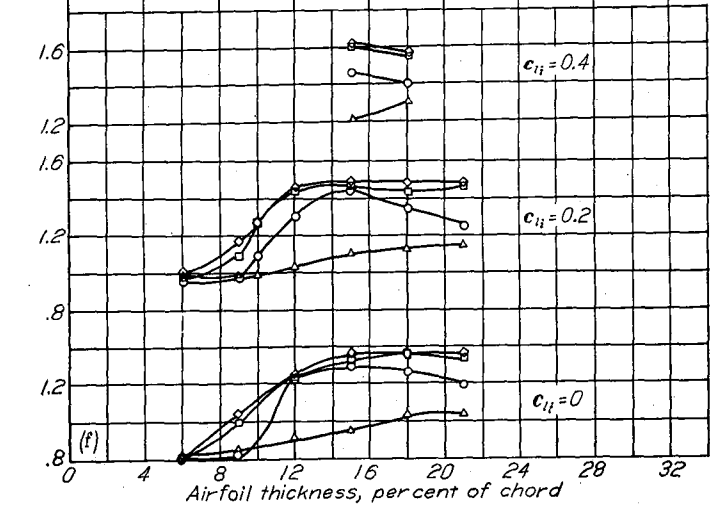
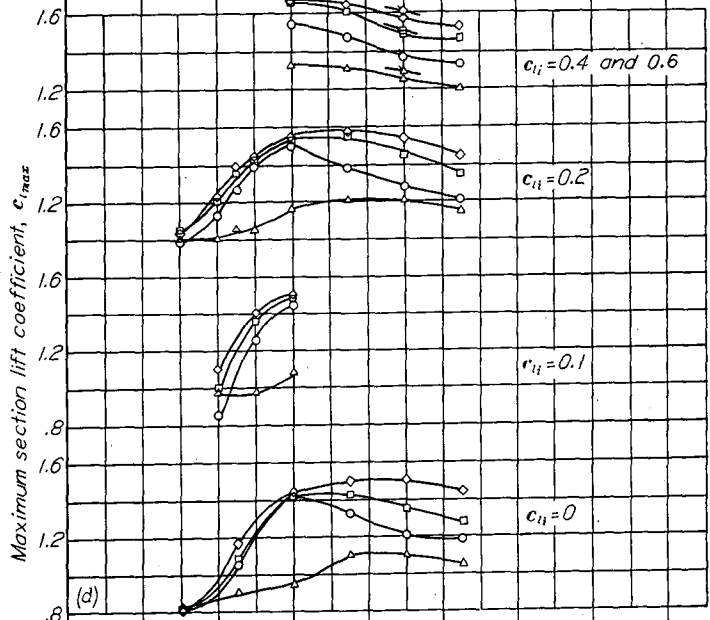
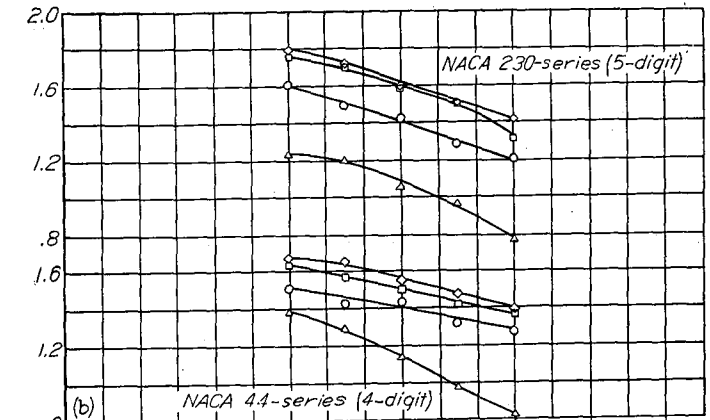
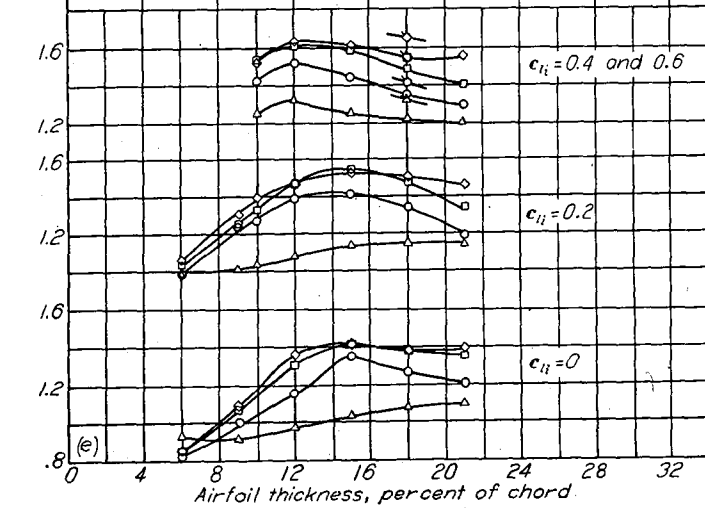
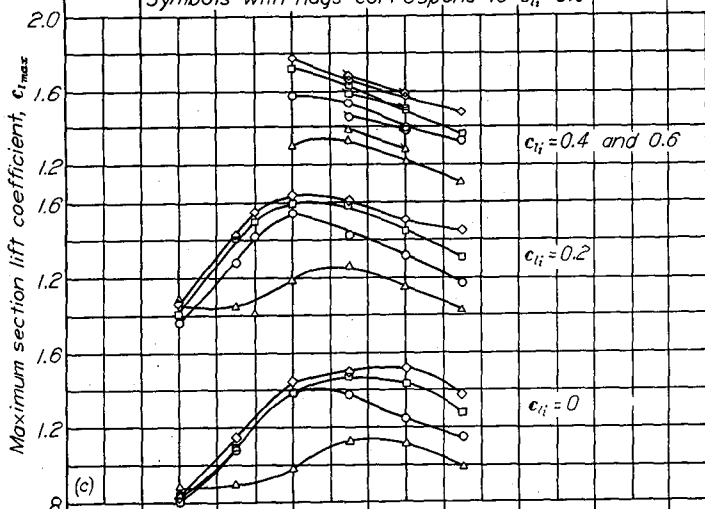
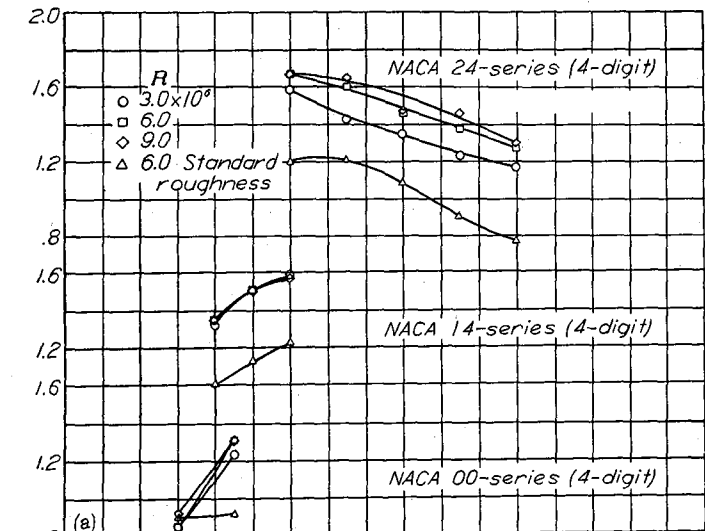
approximately 0.15 to 0.20. The scale effect on the NACA 00- and 14-series airfoils having thickness ratios less than 0.12c is very small.

The scale-effect data for the NACA 6-series airfoils (figs. 41 (c) to 41 (f)) do not show an entirely systematic variation. In general, the scale effect is favorable for these airfoil sections. For the NACA 63- and 64-series airfoils with small camber, the increase in maximum lift coefficient with increase in Reynolds number is generally small for thickness ratios of less than 12 percent but is somewhat larger for the thicker sections. The character of the scale effect for the NACA 65- and 66-series airfoil sections is similar to that for the NACA 63- and 64-series airfoils but the trends are not so well defined. In most cases the scale effect for NACA 6-series airfoil sections cambered for a design lift coefficient of 0.4 or 0.6 does not vary much with airfoil thickness ratio. The data of figure 42 show that the maximum lift coefficient for the NACA 63(420)-422 airfoil continues to increase with Reynolds number, at least up to a Reynolds number of  $26 \times 10^6$ .

The values of the maximum lift coefficient presented were obtained for steady conditions. The maximum lift coefficient may be higher when the angle of attack is increasing. Such a condition might occur during gusts and landing maneuvers. (See reference 41.)

The systematic investigation of NACA 6-series airfoils included tests of the airfoils with a simulated split flap deflected  $60^\circ$ . It was believed that these tests would serve as an indication of the effectiveness of more powerful types of trailing-edge high-lift devices although sufficient data to verify this assumption have not been obtained. The maximum lift coefficients for a large number of NACA airfoil sections obtained from tests with the simulated split flap are presented in figure 39.

The data for the NACA 00- and 14-series airfoils equipped with split flap for thickness ratios from 6 to 12 percent show a considerable increase in maximum lift coefficient with increase in thickness ratio. Corresponding data for the NACA 44-series airfoils with thickness ratios from 12 to 24 percent show very little variation in maximum lift coefficient with thickness. For NACA 6-series airfoils equipped with split flaps the maximum lift coefficients increase rapidly with increasing thickness over a range of thickness ratio, the range beginning at thickness ratios between 6 and 9 percent, depending upon the camber. The upper limit of this range for the symmetrical NACA 64- and 65-series airfoils appears to be greater than 21 percent and for the NACA 63- and 66-series airfoils, approximately 18 percent. Between thickness ratios of 6 and 9 percent the values of maximum lift coefficient for the symmetrical NACA 6-series airfoils are essentially the same regardless of thickness ratio and position of minimum pressure on the basic thickness form. The maximum lift coefficient decreases with rearward movement of minimum pressure for the airfoils having thickness ratios between 9 and 18 percent.



(a) NACA four-digit series.  
 (c) NACA 63-series.  
 (e) NACA 65-series.

(b) NACA four- and five-digit series.  
 (d) NACA 64-series.  
 (f) NACA 66-series.

FIGURE 41.—Variation of maximum section lift coefficient with airfoil thickness ratio at several Reynolds numbers for a number of NACA airfoil sections of different cambers.



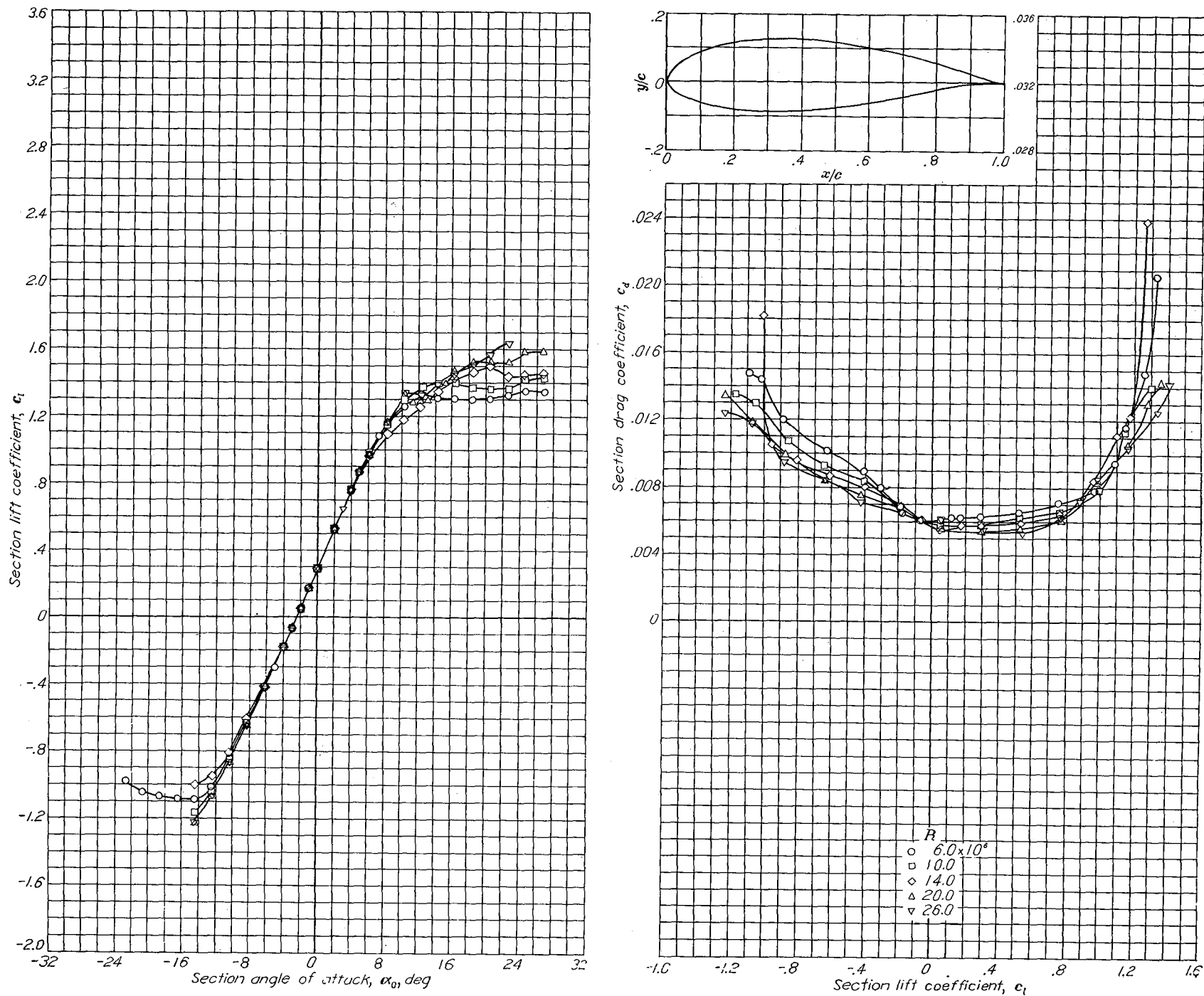


FIGURE 42.—Lift and drag characteristics of the NACA 63(420)-422 airfoil at high Reynolds number. TDT tests 228 and 255.

Substantial increments in maximum lift coefficient with increase in camber are shown for the NACA 6-series airfoils of moderate thickness ratios (10 to 15 percent chord) with split flaps. For the airfoils having thickness ratios of 6 percent and for the airfoils having thickness ratios of 18 or 21 percent, the maximum lift coefficient is affected very little by a change in camber. For thickness ratios greater than 15 percent, the maximum lift coefficients of the NACA 63- and 64-series airfoils cambered for a design lift coefficient of 0.4 equipped with split flaps are greater than the corresponding maximum lift coefficients of the NACA 44-series airfoils.

**Three-dimensional data.**—No recent systematic three-dimensional wing data obtained at high Reynolds numbers are available, so that it is difficult to make any comparison with the section data. When the maximum-lift data for three-dimensional wings are compared with section data, account should be taken of the span load distribution over the wing. The predicted maximum lift coefficient for the wing will be somewhat lower than the maximum lift coefficients of the sections used because of the nonuniformity of the spanwise distribution of lift coefficient. The difference amounts to about 4 to 7 percent for a rectangular wing with an aspect ratio of 6.

Maximum-lift data obtained from tests of a number of wings and airplane models in the Langley 19-foot pressure tunnel are presented in table II. Although section data at the Reynolds numbers necessary to permit a detailed comparison are not available, the maximum lift coefficient for plain wings given in table II appears to be in general agreement with values expected from section data. The data for the airplane models are presented to indicate the maximum lift coefficients obtained with various airfoils and configurations.

#### LIFT CHARACTERISTICS OF ROUGH AIRFOILS

**Two-dimensional data.**—Most recent airfoil tests, especially of airfoils with the thicker sections, have included tests with roughened leading edge (reference 37), and the available data are included in the supplementary figures.

The effect on maximum lift coefficient of various degrees of roughness applied to the leading edge of the NACA 63(420)–422 airfoil is shown in figure 23. The maximum lift coefficient decreases progressively with increasing roughness (reference 36). For a given surface condition at the leading edge, the maximum lift coefficient increases slowly with increasing Reynolds number (fig. 43). Figure 24 shows that roughness strips located more than 0.20c from the leading edge have little effect on the maximum lift coefficient or lift-curve slope. The results presented in figure 38 show that the effect of standard leading edge roughness is to decrease the lift-curve slope, particularly for the thicker airfoils having the position of minimum pressure far back. These data are for a Reynolds number of  $6 \times 10^6$ . Maximum-

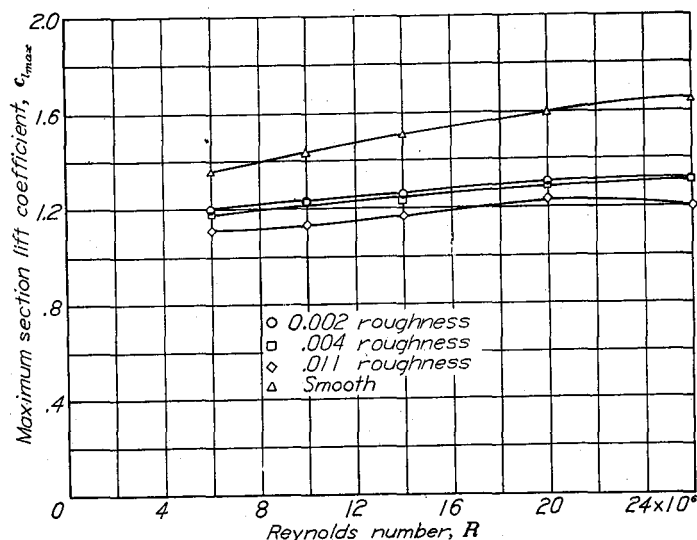


FIGURE 43.—Effects of Reynolds number on maximum section lift coefficient  $c_{l,max}$  of the NACA 63(420)–422 airfoil with roughened and smooth leading edge.

lift-coefficient data at a Reynolds number of  $6 \times 10^6$  for a large number of NACA airfoil sections with standard roughness are presented in figures 39 and 41. The variation of maximum lift coefficient with thickness for the NACA four- and five-digit-series airfoil sections shows the same trends for the airfoils with roughness as for the smooth airfoils except that the values are considerably reduced for all of these airfoils other than the NACA 00-series airfoils of 6 percent thickness. For a given thickness ratio greater than 15 percent, the values of maximum lift coefficient for the four- and five-digit-series airfoils are substantially the same.

Much less variation in maximum lift coefficient with thickness ratio is shown by the NACA 6-series airfoil sections in the rough condition than with smooth leading edge. The maximum lift coefficients of the 6-percent-thick airfoils are essentially the same for both smooth and rough conditions. The variation of maximum lift coefficient with camber, however, is about the same for the airfoils with standard roughness as for the smooth sections. The maximum lift coefficient of airfoils with standard roughness generally decreases somewhat with rearward movement of the position of minimum pressure except for airfoils having thickness ratios greater than 18 percent, in which case some slight gain in maximum lift coefficient results from a rearward movement of the position of minimum pressure.

Except for the NACA 44-series airfoils of 12 to 15 percent thickness, the present data indicate that the rough NACA 64-series airfoil sections cambered for a design lift coefficient of 0.4 have maximum lift coefficients consistently higher than the rough airfoils of the NACA 24-, 44-, and 230-series airfoils of comparable thickness. Standard roughness causes decrements in maximum lift coefficient of the airfoils with split flaps that are substantially the same as those observed for the plain airfoils.

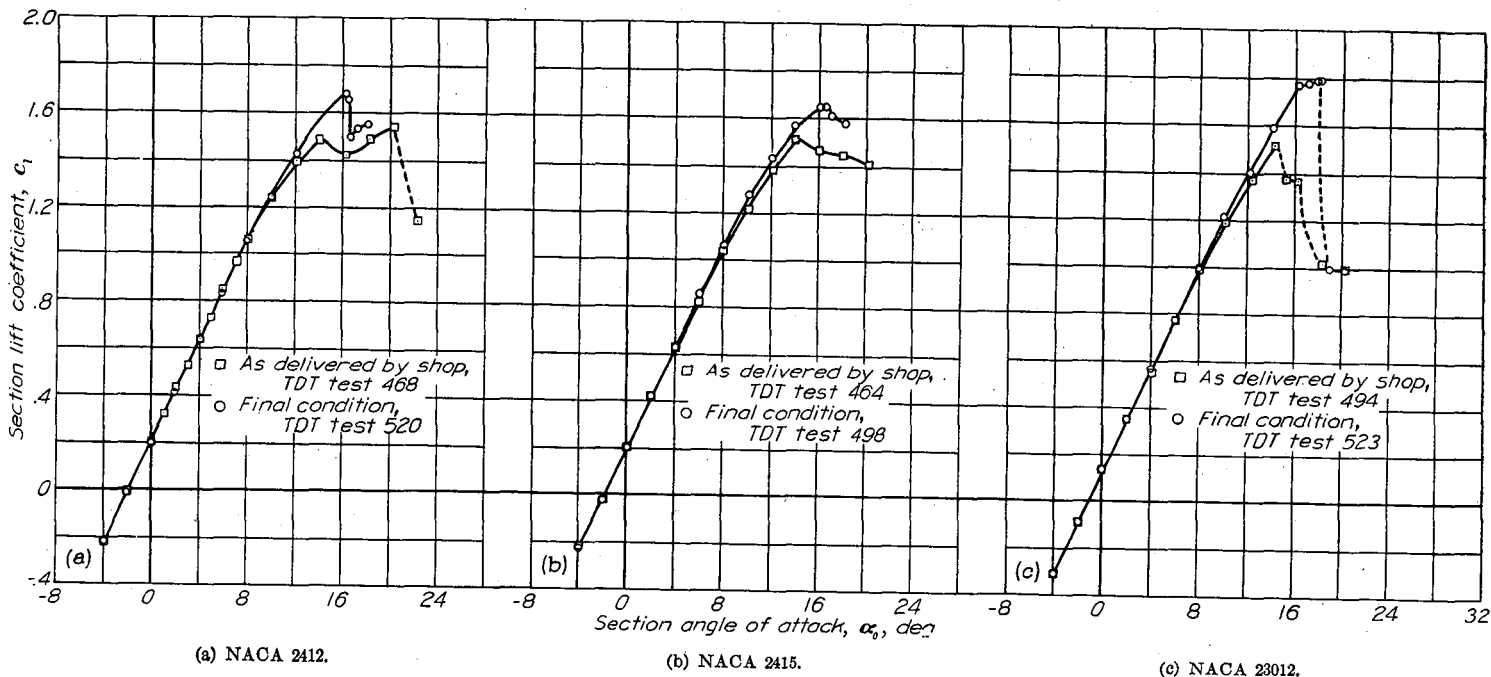


FIGURE 44.—Lift characteristics of the NACA 23012, 2412, and 2415 airfoil sections as affected by normal model inaccuracies.  $R=9 \times 10^6$  (approx.).

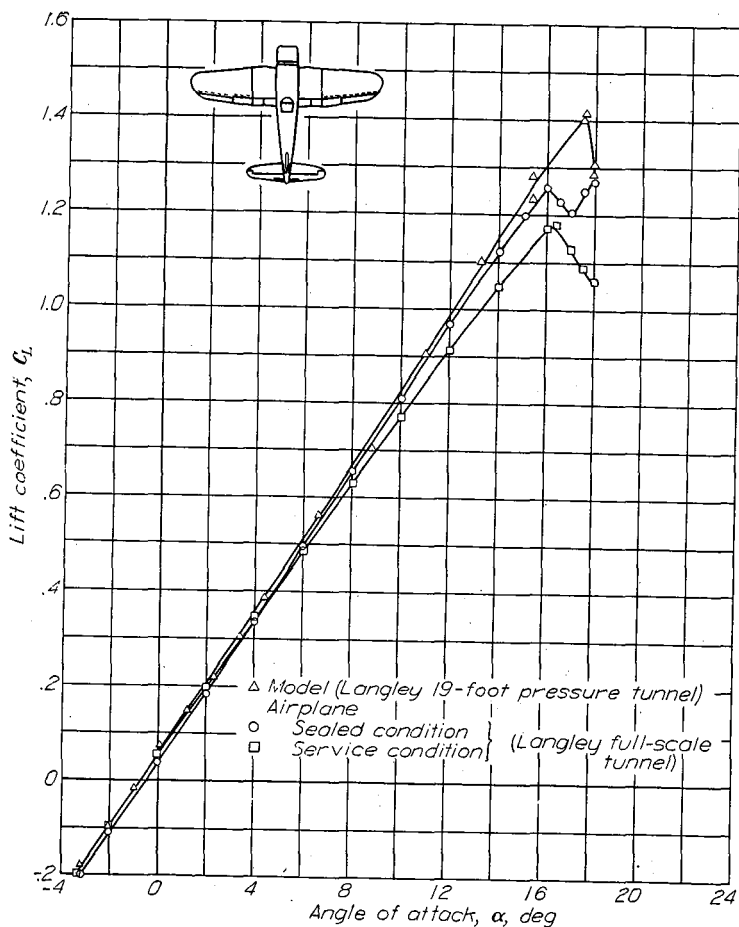


FIGURE 45.—The effects of surface conditions on the lift characteristics of a fighter-type airplane.  $R=2.8 \times 10^6$ .

The maximum lift coefficient may be lowered by failure to maintain the true airfoil contour near the leading edge, but no systematic data on this effect have been obtained. Examples of this effect that were accidentally encountered are presented in figure 44, in which lift characteristics are given for accurate and slightly inaccurate models. The model inaccuracies were so small that they were not found previous to the tests.

**Three-dimensional data.**—Tests of several airplanes in the Langley full-scale tunnel (reference 42) show that many factors besides the airfoil sections affect the maximum lift coefficient of airplanes. Such factors as roughness, leakage, leading-edge air intakes, armament installations, nacelles, and fuselages make it difficult to correlate the airplane maximum lift with the airfoils used, even when the flaps are retracted. The various flap configurations used make such a correlation even more difficult when the flaps are deflected. When the flaps were retracted, both the highest and the lowest maximum lift coefficients obtained in recent tests of airplanes and complete mock-ups of conventional configurations in the Langley full-scale tunnel were those obtained with NACA 6-series airfoils.

Results obtained from tests of a model of an airplane in the Langley 19-foot pressure tunnel and of the airplane in the Langley full-scale tunnel are presented in figure 45. Both tests were made at approximately the same Reynolds number. The results show that the airplane in the service condition had a maximum lift coefficient more than 0.2 lower than that of the model, as well as a lower lift-curve slope. Some improvement in the airplane lift characteristics was obtained by sealing leaks. These results show that airplane lift characteristics are strongly affected by details not reproduced on large-scale smooth models.

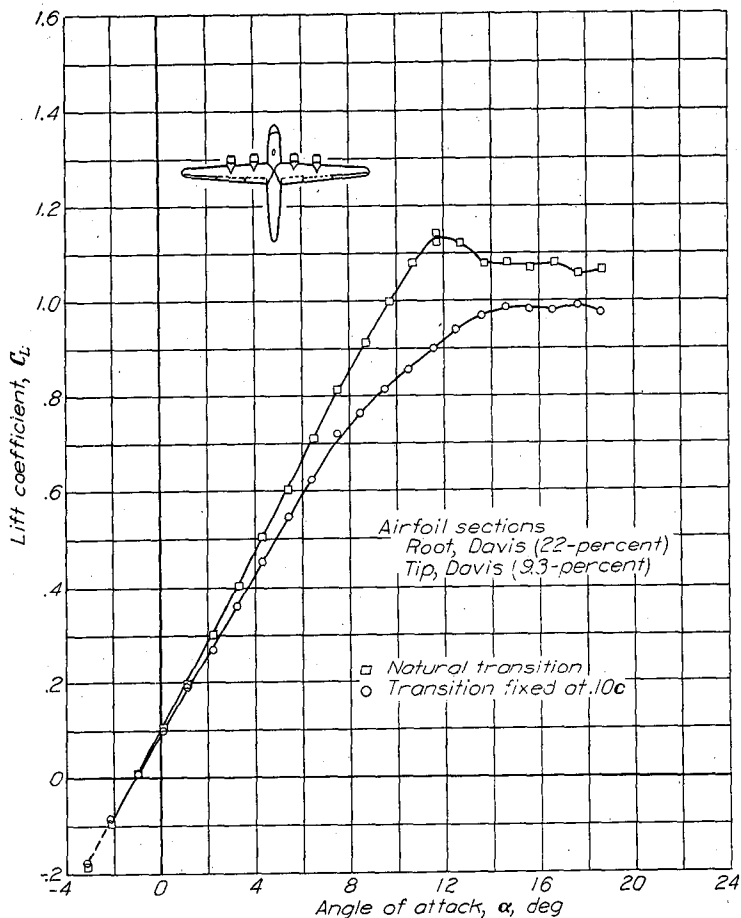


FIGURE 46.—The effect on the lift characteristics of fixing the transition on a model in the Langley 19-foot pressure tunnel.  $R=2.7 \times 10^6$ . (Model with Davis airfoil sections.)

Lift characteristics obtained in the Langley 19-foot pressure tunnel for two airplane models in the smooth condition and with transition fixed at the front spar are presented in figures 46 and 47. In both cases, the lift-curve slope was decreased throughout most of the lift range with fixed transition. The maximum lift coefficient was decreased in one case but was increased in the other case.

#### UNCONSERVATIVE AIRFOILS

The attempt to obtain low drags, especially for long-range airplanes, leads to high wing loadings together with relatively low span loadings. This tendency results in wings of high aspect ratio that require large spar depths for structural efficiency. The large spar depths require the use of thick root sections.

This trend to thick root sections has been encouraged by the relatively small increase in drag coefficient with thickness ratio of smooth airfoils (fig. 12). Unfortunately, airplane wings are not usually constructed with smooth surfaces and, in any case, the surfaces cannot be relied upon to stay smooth under all service conditions. The effect of roughening the leading edges of thick airfoils is to cause large increases in the

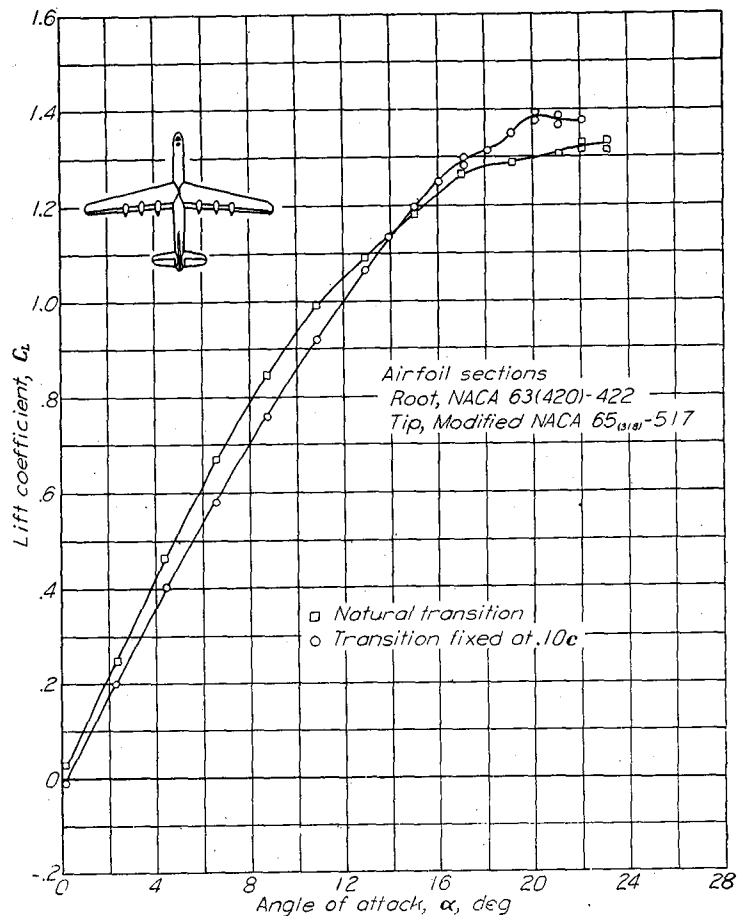


FIGURE 47.—The effect on the lift characteristics of fixing the transition on a model in the Langley 19-foot pressure tunnel.  $R=2.7 \times 10^6$ . (Model with NACA airfoil sections.)

drag coefficient at high lift coefficients. The resulting drag coefficients may be excessive at cruising lift coefficients for heavily loaded, high-altitude airplanes. Airfoil sections that have suitable characteristics when smooth but have excessive drag coefficients when rough at lift coefficients corresponding to cruising or climbing conditions are classified as unconservative.

The decision as to whether a given airfoil section is conservative will depend upon the power and the wing loading of the airplane. The decision may be affected by expected service and operating conditions. For example, the ability of a multiengine airplane to fly with one or more engines inoperative in icing conditions or after suffering damage in combat may be a consideration.

As an aid in judging whether the sections are conservative, the lift coefficient corresponding to a drag coefficient of 0.02 was determined from the supplementary figures for a large number of NACA airfoil sections with roughened leading edges. The variation of this critical lift coefficient with airfoil thickness ratio and camber is shown in figure 48. These data show that, in general, the lift coefficient at which the drag coefficient is 0.02 decreases with rearward movement of

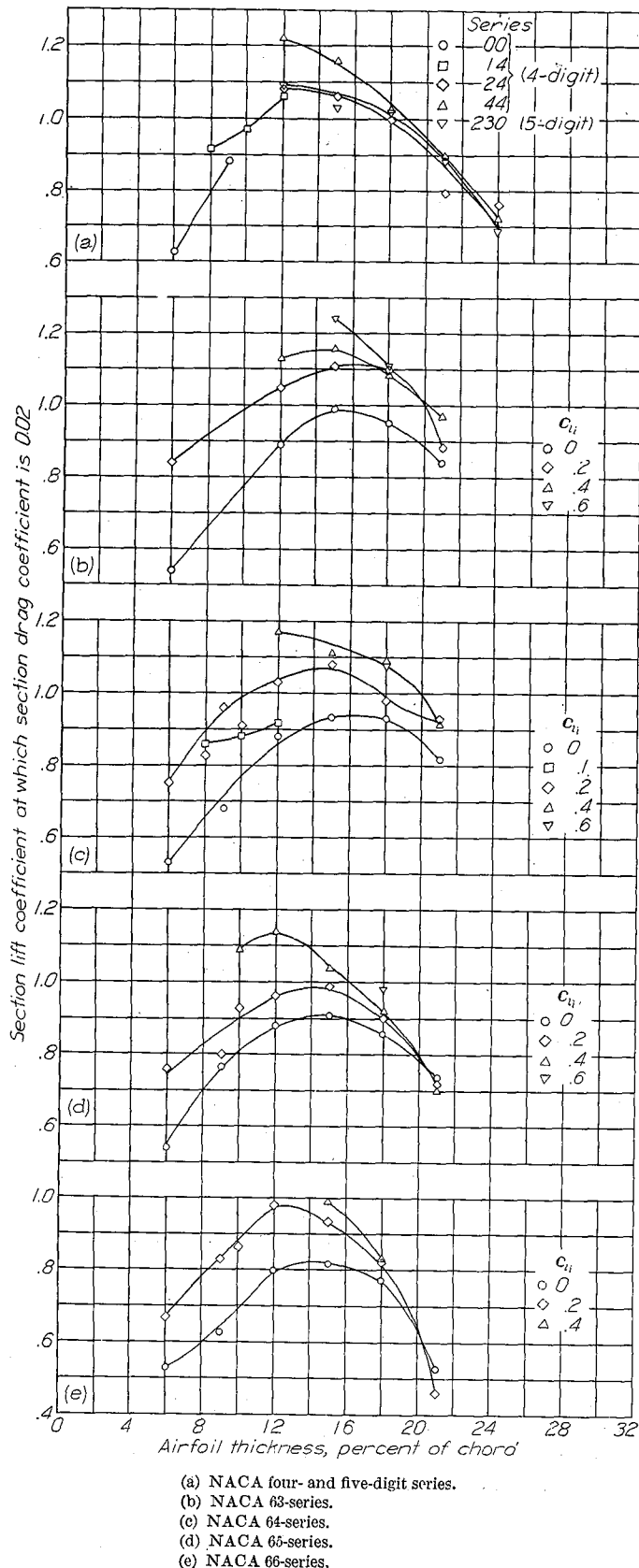


FIGURE 48.—Variation of the lift coefficient corresponding to a drag coefficient of 0.02 with thickness and camber for a number of NACA airfoil sections with roughened leading edges.  $R=6 \times 10^6$ .

position of minimum pressure. The thickness ratio for which this lift coefficient is a maximum usually lies between 12 and 15 percent; variations in thickness ratio from this optimum range generally cause rather sharp decreases in the critical lift coefficient. The addition of camber to the symmetrical airfoils usually causes an increase in the critical lift coefficient except for the very thick sections, in which case increasing the camber becomes relatively ineffectual and may be actually harmful. All the data of figure 48 correspond to a Reynolds number of  $6 \times 10^6$ . As shown in figure 49, the drag coefficient at flight values of the Reynolds number may be considerably lower than the drag coefficient at a Reynolds number of  $6 \times 10^6$  if the roughness is confined to the leading edge.

PITCHING MOMENT

The variation of the quarter-chord pitching-moment coefficient at zero angle of attack with airfoil thickness ratio and camber is presented in figure 50 for several NACA airfoil sections. The quarter-chord pitching-moment coefficients of the NACA four- and five-digit-series airfoils become less negative with increasing airfoil thickness. Almost no variation in quarter-chord pitching-moment coefficient with airfoil thickness ratio or position of minimum pressure is shown by the NACA 6-series airfoil sections. As might be expected, increasing the amount of camber causes an almost uniform negative increase in the pitching-moment coefficient.

As discussed previously, the pitching moment of an airfoil section is primarily a function of its camber, and thin-airfoil theory provides a means for estimating the pitching moment from the mean-line data presented in the supplementary figures. A comparison of the experimental moment coefficient and theoretical values for the mean lines is presented in figure 51. The experimental values of the moment coefficients for NACA 6-series airfoils cambered with the uniform-load type mean line are usually about three-quarters of the theoretical values (figs. 50 and 51). Airfoils employing mean lines with values of  $a$  less than unity, however, have moment coefficients somewhat more negative than those indicated by theory. The use of a mean line having a value of  $a$  less than unity, therefore, brings about only a slight reduction in pitching-moment coefficient for a given design lift coefficient when compared with the value obtained with a uniform-load type mean line. The experimental moment coefficients for the NACA 24-, 44-, and 230-series airfoils are also less negative than those indicated by theory but the agreement is closer than for airfoils having the uniform-load type mean line.

The pitching-moment data for the airfoils equipped with simulated split flaps deflected  $60^\circ$  (fig. 50) indicate that the value of the quarter-chord pitching-moment coefficient becomes more negative with increasing thickness for all the airfoils tested. For the thicker NACA 6-series sections the magnitude of the moment coefficient increases with rearward movement of the position of minimum pressure.

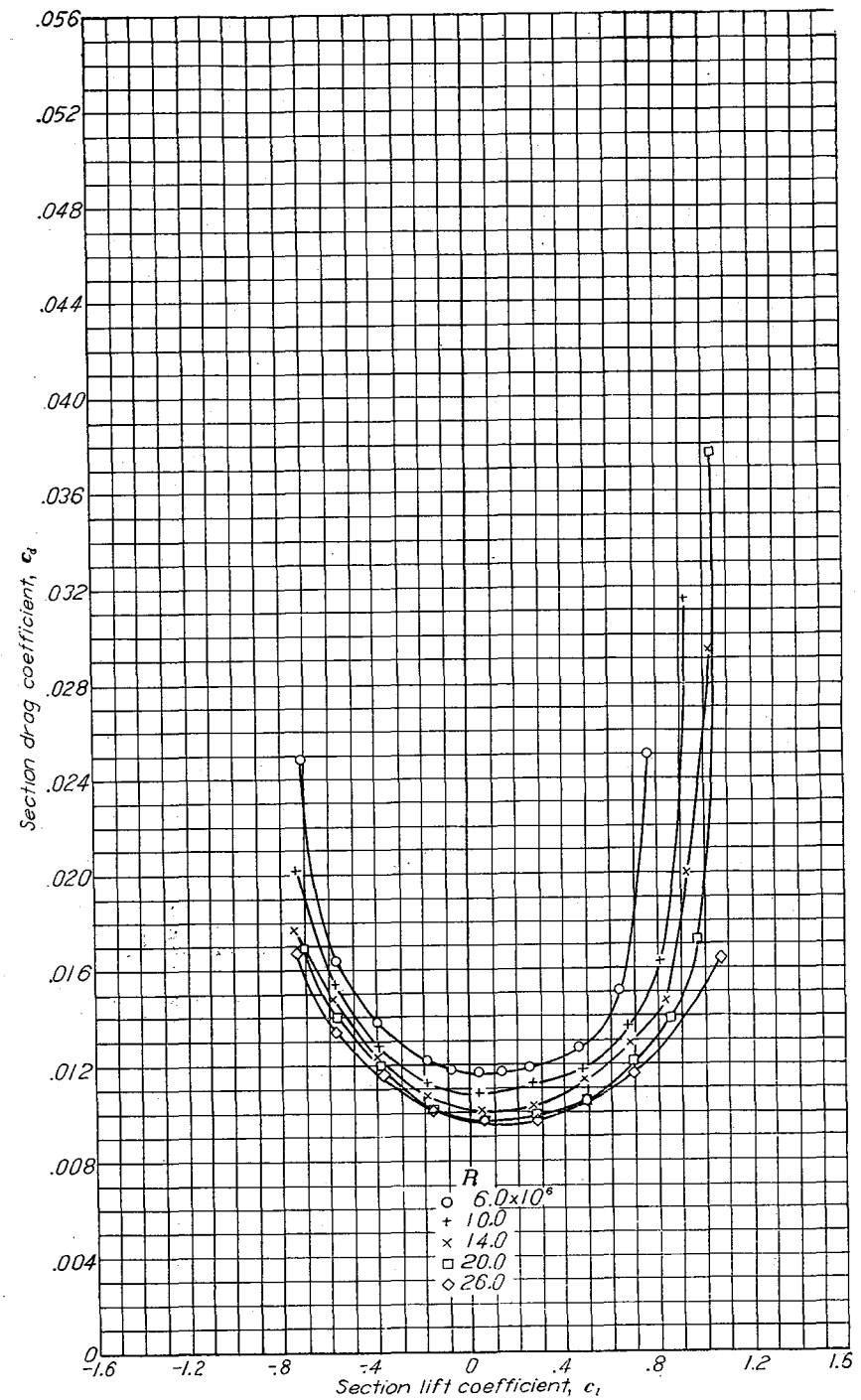
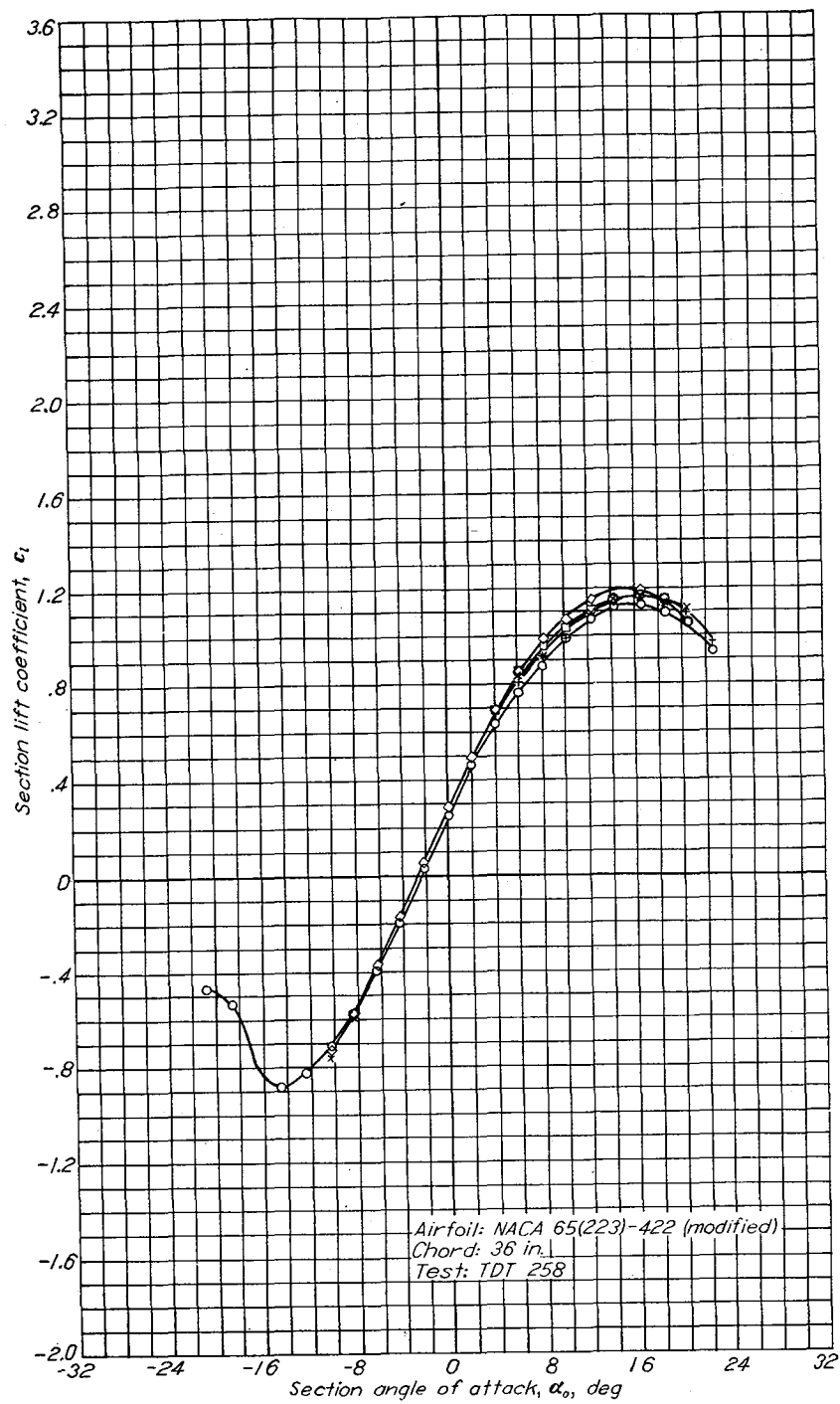


FIGURE 49.—Lift and drag characteristics of an NACA 65(223)-422 (modified) airfoil with standard roughness applied to the leading edge.

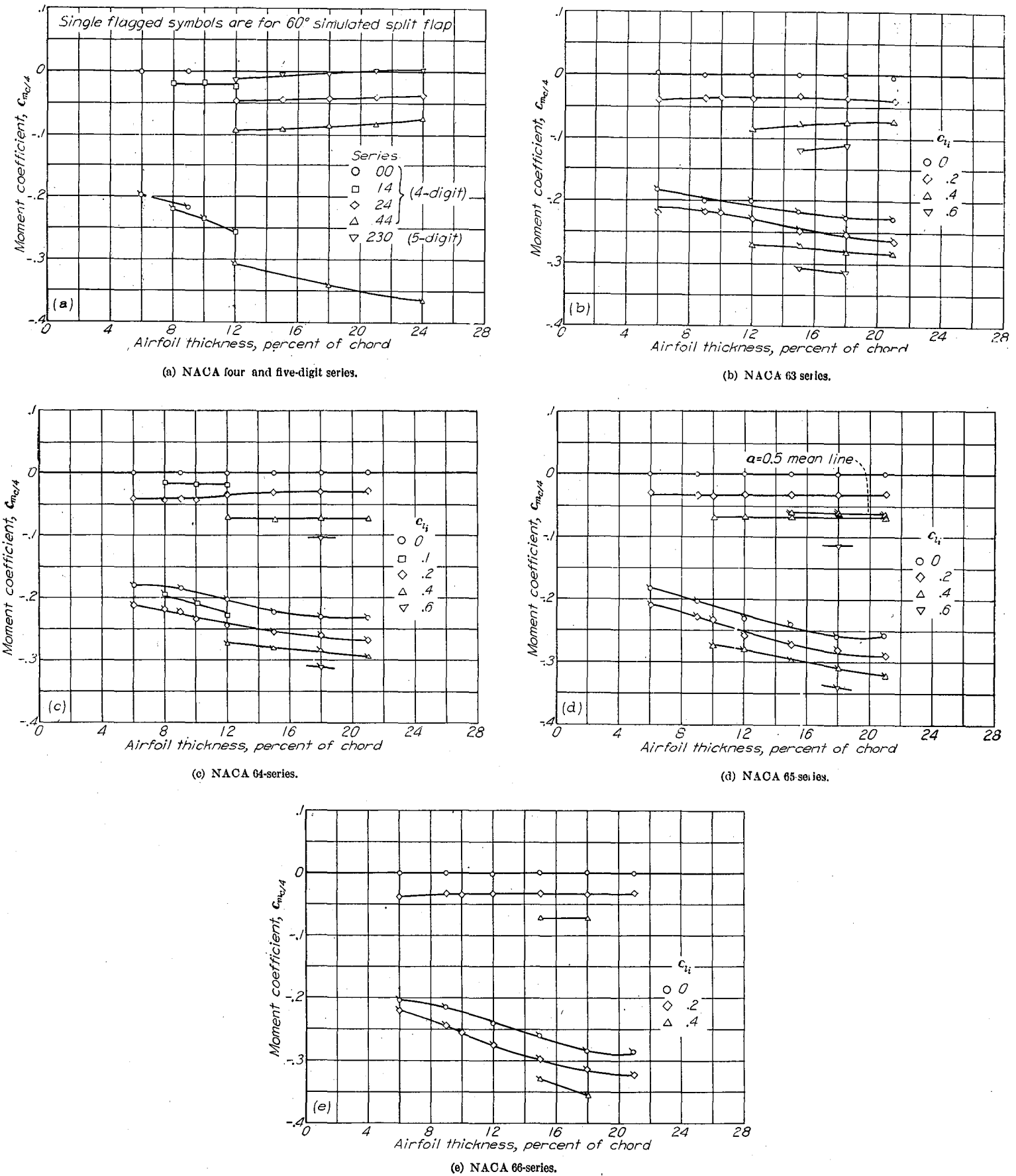


FIGURE 50.—Variation of section quarter-chord pitching-moment coefficient (measured at an angle of attack of 0°) with airfoil thickness ratio for several NACA airfoil sections of different camber  $R=6 \times 10^6$ .

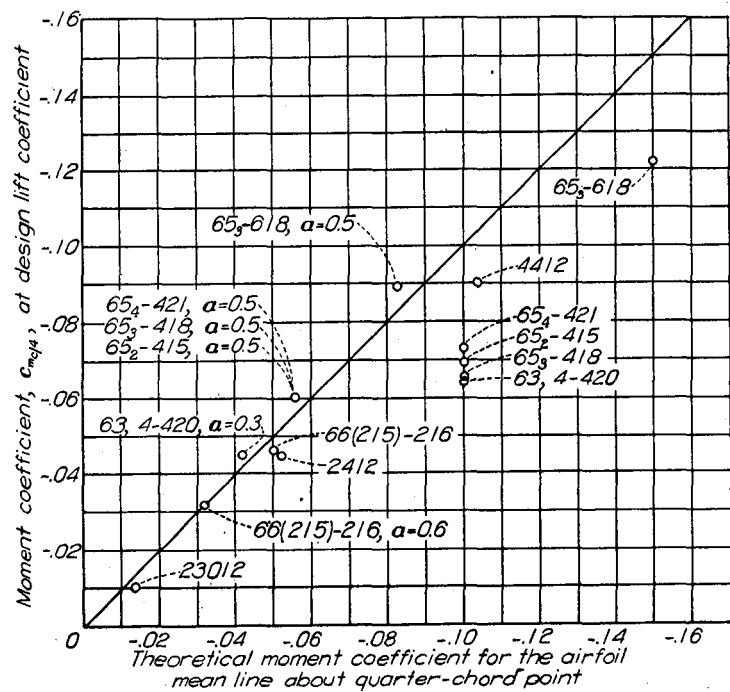


FIGURE 51.—Comparison of theoretical and measured pitching-moment coefficients for some NACA airfoils.  $R=6 \times 10^6$ .

#### POSITION OF AERODYNAMIC CENTER

The variation of chordwise position of the aerodynamic center corresponding to a Reynolds number of  $6 \times 10^6$  for a large number of NACA airfoils is presented in figure 52. From the data given in the supplementary figures there appears to be no systematic variation of chordwise position of aerodynamic center with Reynolds number. The data for the NACA 00- and 14-series airfoils, presented for thickness ratios less than 12 percent, show that the chordwise position of the aerodynamic center is at the quarter-chord point and does not vary with airfoil thickness. For the NACA 24-, 44-, and 230-series airfoils with thickness ratios ranging from 12 to 24 percent, the chordwise position of the aerodynamic center is ahead of the quarter-chord point and moves forward with increase in thickness ratio.

The chordwise position of the aerodynamic center is behind the quarter-chord point for the NACA 6-series airfoils and moves rearward with increase in airfoil thickness, which is in accordance with the trends indicated by perfect-fluid theory. There appears to be no systematic variation of chordwise position of the aerodynamic center with camber or position of minimum pressure on the basic thickness form for these airfoils.

The data of reference 43 show important forward movements of the aerodynamic center with increasing trailing-edge angle for a given airfoil thickness. For the NACA 24-, 44-, and 230-series airfoils (fig. 52) the effect of increasing trailing-edge angle is apparently greater than the effect of

increasing thickness. For the NACA 6-series airfoils, the opposite appears to be the case.

#### HIGH-LIFT DEVICES

Lift characteristics for two NACA 6-series airfoils equipped with plain flaps are presented in figure 53. These data show that the maximum lift coefficient increases less rapidly with flap deflection for the more highly cambered section. Lift characteristics of three NACA 6-series airfoils with split flaps are presented in reference 44 and figure 54. The maximum-lift increments for the 12-percent-thick sections were only about three-fourths of that increment for the 16-percent-thick section. The maximum lift coefficient for the thicker section with flap deflected is about the same as that obtained for the NACA 23012 airfoil in the now obsolete Langley variable-density tunnel (reference 45) and in the Langley 7- by 10-foot tunnel (reference 46).

Tests of a number of slotted flaps on NACA 6-series airfoils (supplementary figures and reference 47) indicate that the design parameters necessary to obtain high maximum lifts are essentially similar to those for the the NACA 230-series sections (references 48 and 49). Lift data obtained for typical hinged single slotted  $0.25c$  flaps (fig. 55 (a)) on the NACA 63,4-420 airfoil are presented in figure 55 (b). A maximum lift coefficient of approximately 2.95 was obtained for one of the flaps. Lift characteristics for the NACA 65<sub>3</sub>-118 airfoil fitted with a double slotted flap (reference 47 and fig. 56 (a)) are presented in figure 56 (b). A maximum lift coefficient of 3.28 was obtained. It may be concluded that no special difficulties exist in obtaining high maximum lift coefficients with slotted flaps on moderately thick NACA 6-series sections.

Tests of airplanes in the Langley full-scale tunnel (reference 42) have shown that expected increments of maximum lift coefficient are obtained for split flaps (fig. 57) but not for slotted flaps (fig. 58). This failure to obtain the expected maximum-lift increments with slotted flaps may be attributed to inaccuracies of flap contour and location, roughness near the flap leading edge, leakage, interference from flap supports, and deflection of flap and lip under load.

#### LATERAL-CONTROL DEVICES

An adequate discussion of lateral-control devices is outside the scope of this report. The following brief discussion is therefore limited to considerations of effects of airfoil shape on aileron characteristics.

The effect of airfoil shape on aileron effectiveness may be inferred from the data of figure 59 and reference 50. The section aileron effectiveness parameter  $\Delta\alpha_0/\Delta\delta$  is plotted against the aileron-chord ratio  $c_a/c$  for a number of airfoils of different type in figure 59. Also shown in this figure are the theoretical values of the parameter for thin airfoils.



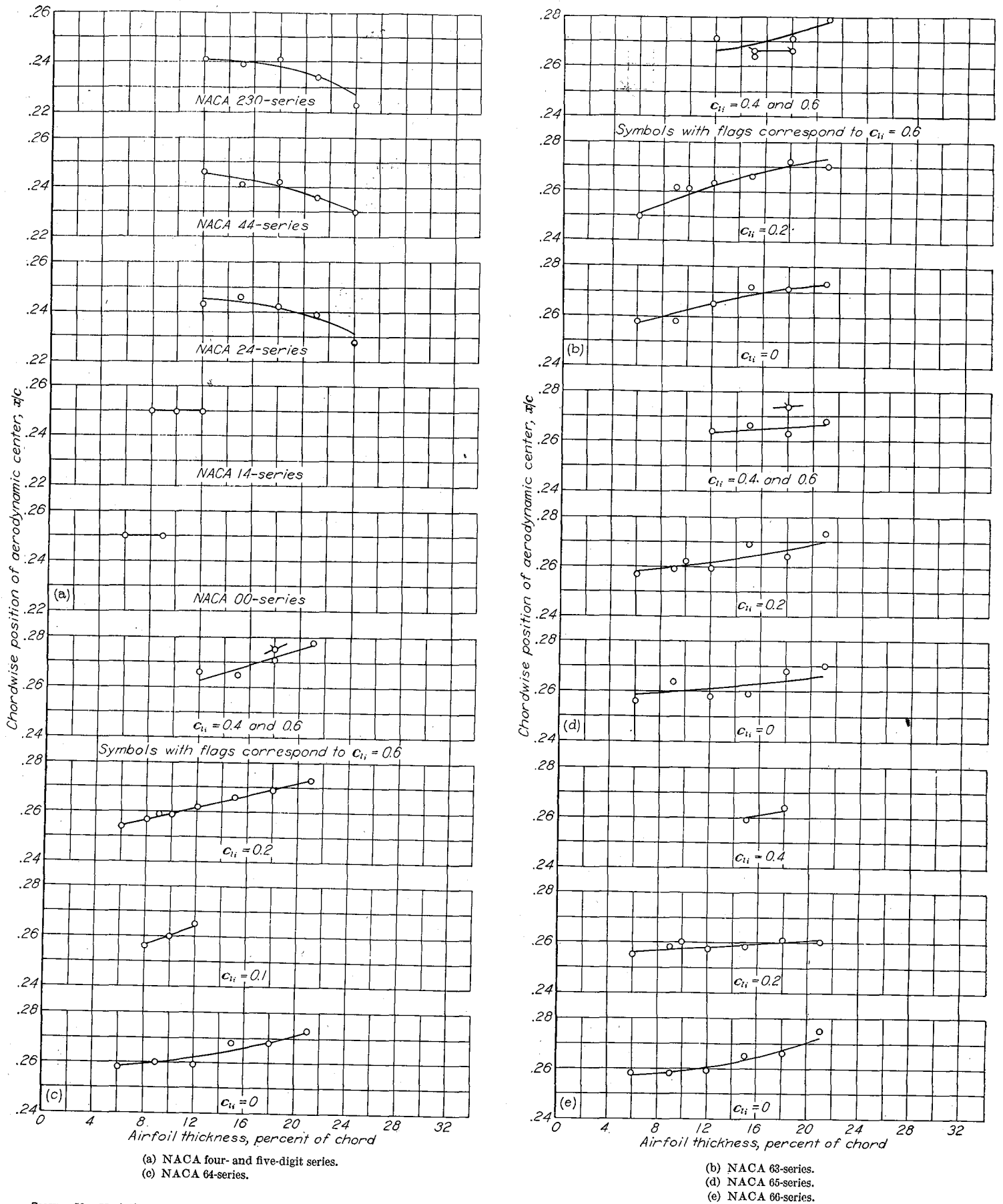


FIGURE 52.—Variation of section chordwise position of the aerodynamic center with airfoil thickness ratio for several NACA airfoil sections of different cambers.  $R=6 \times 10^6$ .

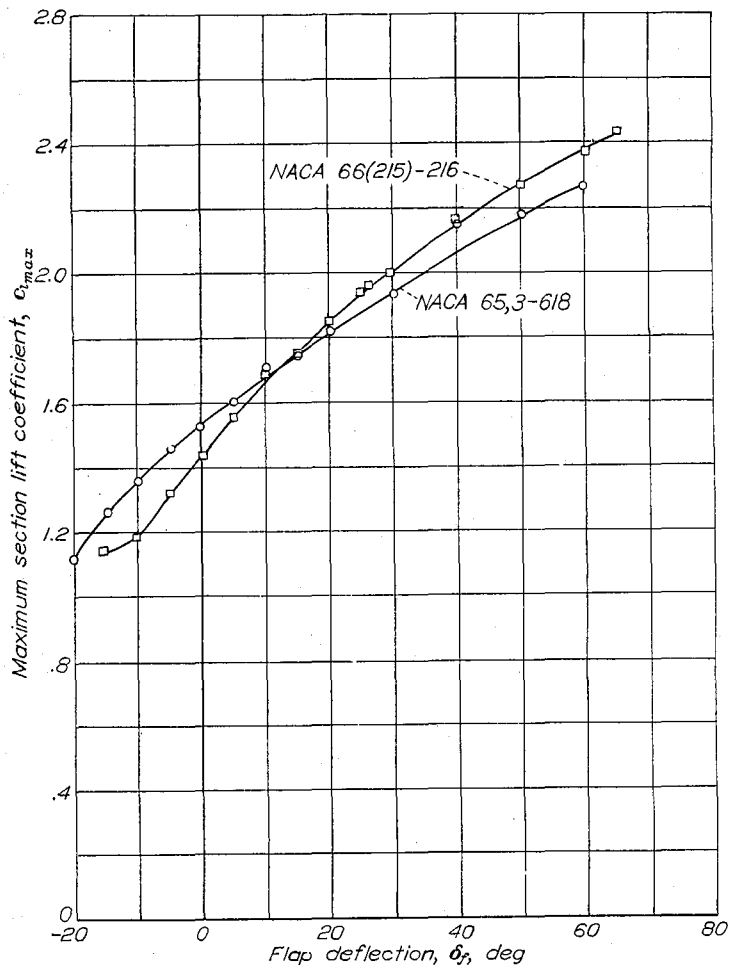


FIGURE 53.—Maximum lift coefficients for the NACA 65,3-618 and NACA 66(215)-216 airfoils fitted with 0.20-airfoil-chord plain flaps.  $R=6 \times 10^6$ .

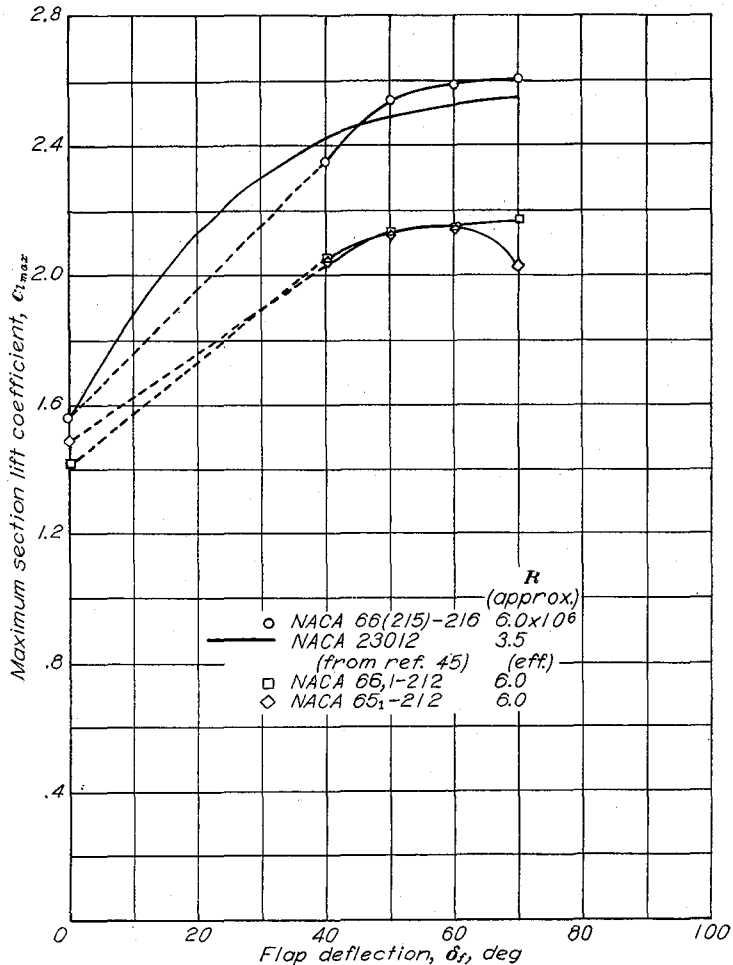
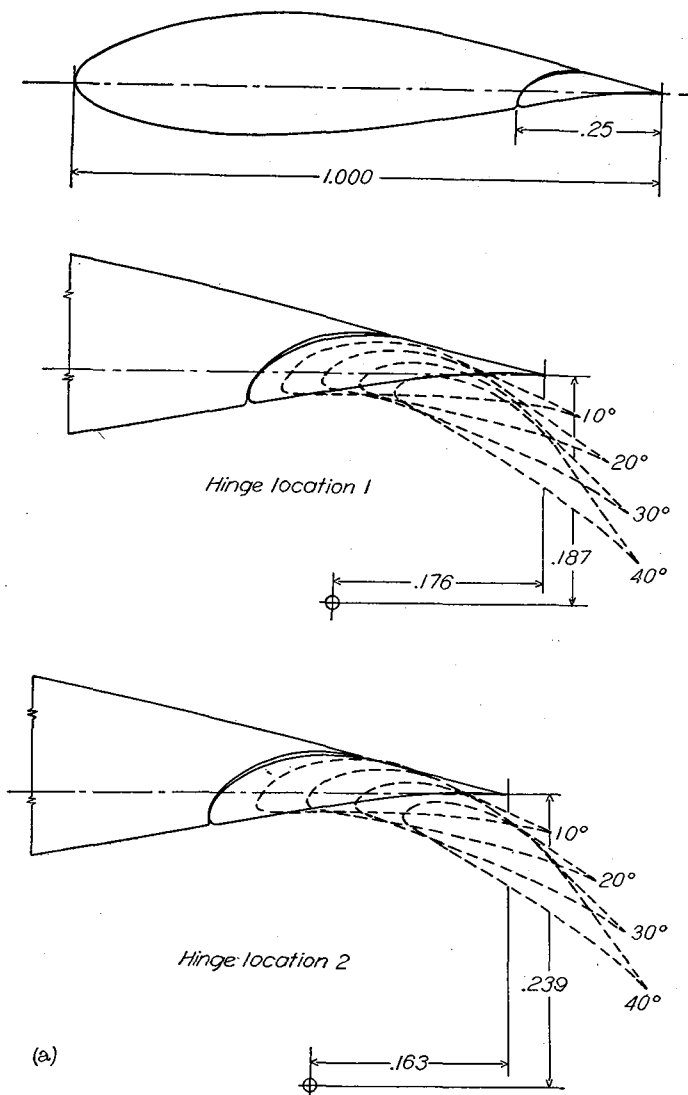


FIGURE 54.—Maximum lift coefficients for some NACA airfoils fitted with 0.20-airfoil-chord split flaps.

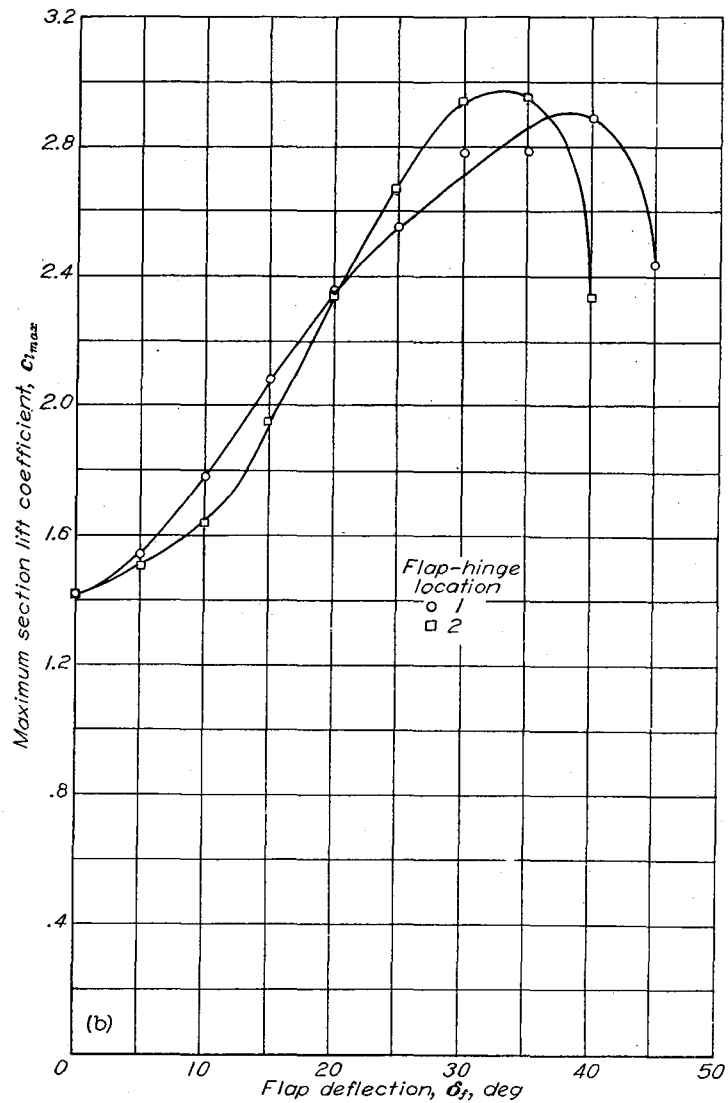
The data show no large consistent trends of aileron-effectiveness variation with airfoil section for a wide range of thickness distributions and thickness ratios. In order to evaluate aileron characteristics from section data, a method of analysis is necessary that will lead to results comparable to the usual curves of stick force against helix angle  $pb/2V$  for three-dimensional data. The analysis that follows is considered suitable for comparing the relative merits of ailerons from two-dimensional data.

Two-dimensional data are presented in the form of the equivalent change in section angle of attack  $\Delta\alpha_0$  required to maintain a constant section lift coefficient for various deflections of the aileron from neutral. This equivalent change in angle of attack is plotted against the hinge-moment parameter  $\Delta c_H \delta$ , which is the product of the aileron deflection from neutral and the resulting increment of hinge-moment

coefficient based on the wing chord. This method of analysis takes into account the aileron effectiveness, the hinge moments, and the possible mechanical advantage between the controls and the ailerons. The larger the value of  $\Delta\alpha_0$  for a given value of the hinge-moment parameter, the more advantageous the combination should be for providing a large value of  $pb/2V$  for a given control force. The assumption that the aileron operates at a constant lift coefficient as the airplane rolls is not entirely correct, however, and involves an overestimation of the effect of changing angle of attack on the hinge-moment coefficient. In addition, the span of the ailerons and other possible three-dimensional effects are not considered. In spite of these inaccuracies, the method provides a useful means of comparing the two-dimensional characteristics of different ailerons.

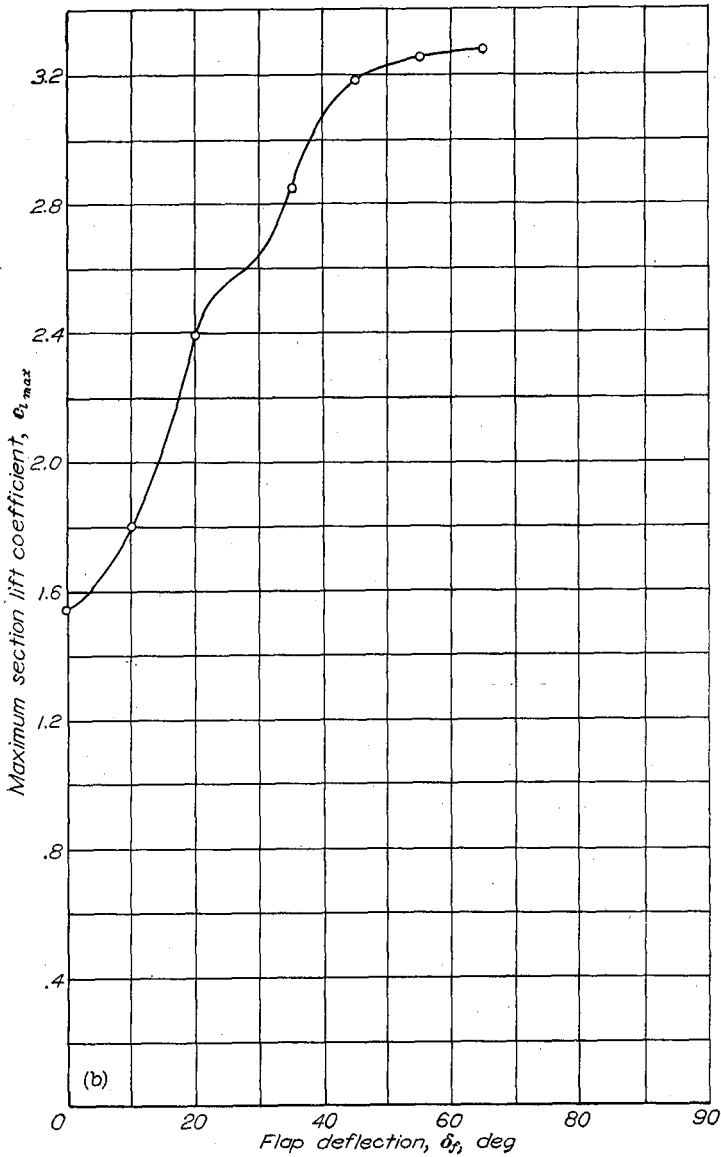
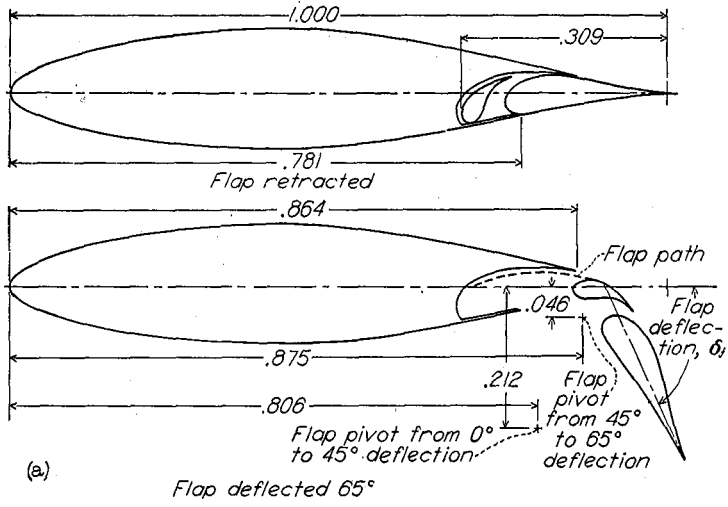


(a) Flap configuration.



(b) Maximum lift characteristics.

FIGURE 55.—Flap configuration and maximum lift coefficients for the NACA 63,4-420 airfoil with a 0.25-airfoil-chord hinged slotted flap.  $R=6 \times 10^6$ .



(a) Flap configuration.  
(b) Maximum lift characteristics.

FIGURE 56.—Flap configuration and maximum lift coefficients for the NACA 65s-118 airfoil with a double slotted flap.  $R=6 \times 10^6$ .

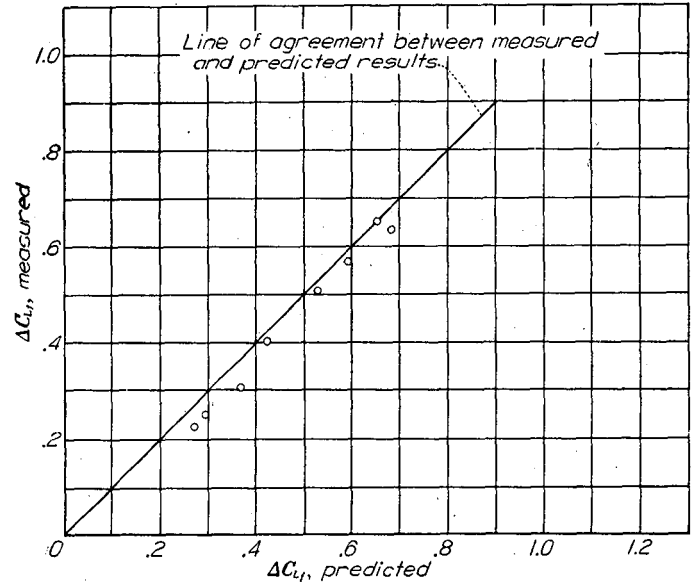


FIGURE 57.—Comparison between measured values of the increments in lift coefficients due to flap deflection and values predicted from two-dimensional data. Split flap.

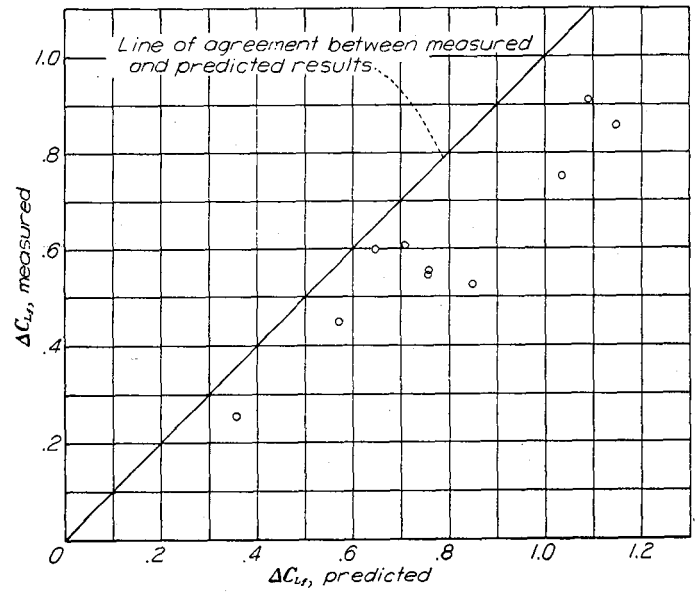
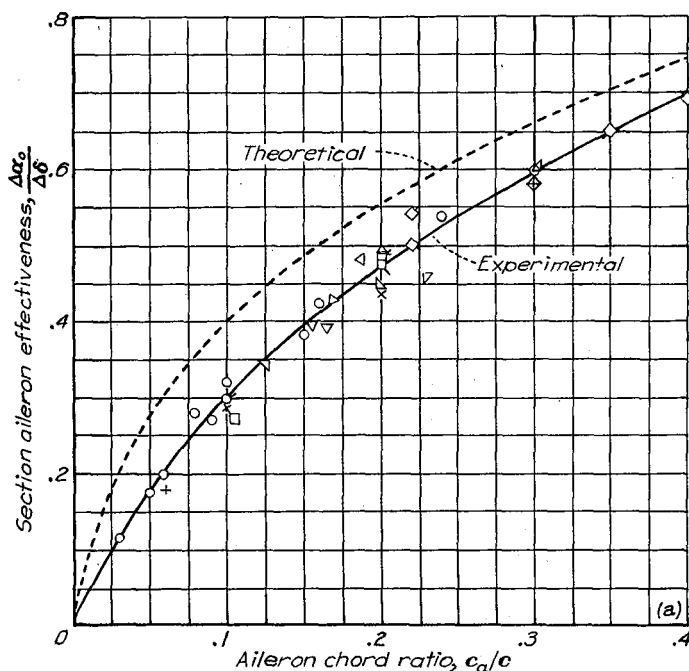


FIGURE 58.—Comparison between measured values of the increments in lift coefficients due to flap deflection and values predicted from two-dimensional data. Slotted flap.

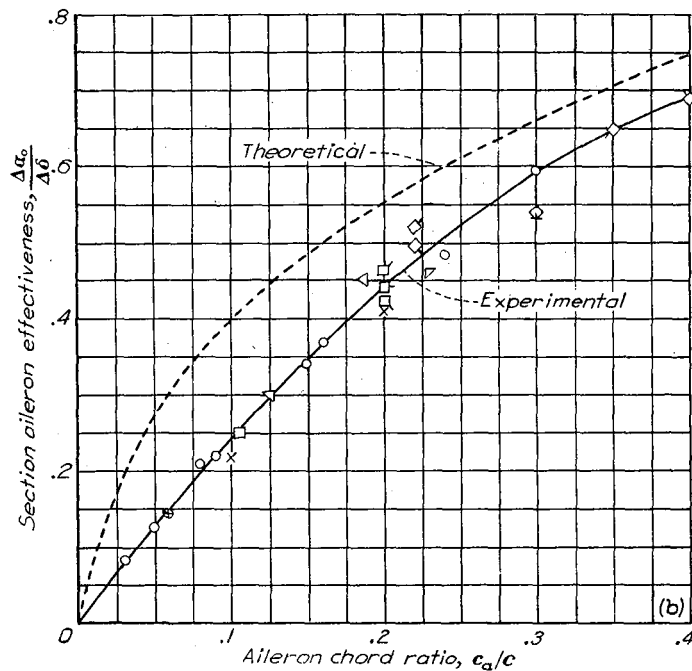
SUPPLEMENTARY INFORMATION REGARDING TESTS OF TWO-DIMENSIONAL MODELS

Symbol	Basic airfoil	Type of flap	Air-flow characteristics			Reference
			$r$	$M$	$R$	
○	NACA 0009.....	Plain.....	1.93	0.08	-----	51 to 55
+	NACA 0015.....	do.....	1.93	.10	$1.4 \times 10^6$	56
x	NACA 23012.....	do.....	1.60	.11	$2.2 \times 10^6$	57, 48
□	NACA 66(2x15)-0C9.....	Plain, straight contour.....	1.93	.10	$1.4 \times 10^6$	-----
◇	NACA 66-009.....	Plain.....	1.93	.11	$1.4 \times 10^6$	58
△	NACA 63,4-4(17.8) (approx.).....	Internally balanced.....	( <sup>1</sup> )	.17	$2.5 \times 10^6$	59
▽	NACA 66(2x15)-216, $\alpha=0.6$ .....	do.....	( <sup>1</sup> )	.18	$5.3 \times 10^6$	59
▽	NACA 66(2x15)-116, $\alpha=0.6$ .....	do.....	( <sup>1</sup> )	.14	$6.0 \times 10^6$	59
△	NACA 64,2-(1.4) (13.5).....	Plain.....	( <sup>1</sup> )	-----	$13.0 \times 10^6$	-----
▽	NACA 65,2-318 (approx.).....	Internally balanced.....	( <sup>1</sup> )	.14	$6.0 \times 10^6$	59
△	NACA 63(420)-521 (approx.).....	do.....	( <sup>1</sup> )	-----	$8.0 \times 10^6$	-----
▽	NACA 66(215)-216, $\alpha=0.6$ .....	do.....	( <sup>1</sup> )	.20 to .48	$2.8 \times 10^6$ to $6.8 \times 10^6$	60
△	NACA 66(215)-014.....	Plain.....	1.93	.09	$1.2 \times 10^6$	
○	NACA 66(215)-216, $\alpha=0.6$ .....	do.....	( <sup>1</sup> )	-----	$6.0 \times 10^6$	-----
□	NACA 65 <sub>s</sub> -415.....	do.....	( <sup>1</sup> )	.13	$6.0 \times 10^6$	62
□	NACA 65 <sub>s</sub> -418.....	do.....	( <sup>1</sup> )	.13	$6.0 \times 10^6$	62
□	NACA 65 <sub>s</sub> -421.....	do.....	( <sup>1</sup> )	.13	$6.0 \times 10^6$	62
◇	NACA 65 <sub>(112)</sub> -213.....	Internally balanced.....	( <sup>1</sup> )	.14	$8.0 \times 10^6$	-----
◇	NACA 745A317 (approx.).....	do.....	( <sup>1</sup> )	.13	$6.0 \times 10^6$	-----
◇	NACA 64,3-013 (approx.).....	do.....	( <sup>1</sup> )	.13	$6.0 \times 10^6$	-----
◇	NACA 64,3-1(15.5) (approx.).....	do.....	( <sup>1</sup> )	.13	$6.0 \times 10^6$	-----

<sup>1</sup> Approaching 1.00.



(a)  $\delta$  range from 0° to 10°.



(b)  $\delta$  range from 0° to 20°.

FIGURE 59.—Variation of section aileron effectiveness with aileron-chord ratio for true-airfoil-contour ailerons without exposed overhang balance on a number of airfoil sections. Gaps sealed;  $c_1=0$ .

Basic airfoil	$c_l$	Type of aileron (1)	Air-flow characteristics			Reference
			$r$	$M$	$R$	
NACA 0009	0	0.20c plain	1.93	0.10	$1.4 \times 10^6$	63
NACA 64,2-(1.4) (13.5)	.150	0.187c plain	(2)	.18	$4.0 \times 10^6$	---
NACA 66(215)-216, $\alpha=0.6$	.100	0.20c plain	(2)	.33	$9.0 \times 10^6$	64

<sup>1</sup> True airfoil contour.  
<sup>2</sup> Approaching 1.00.

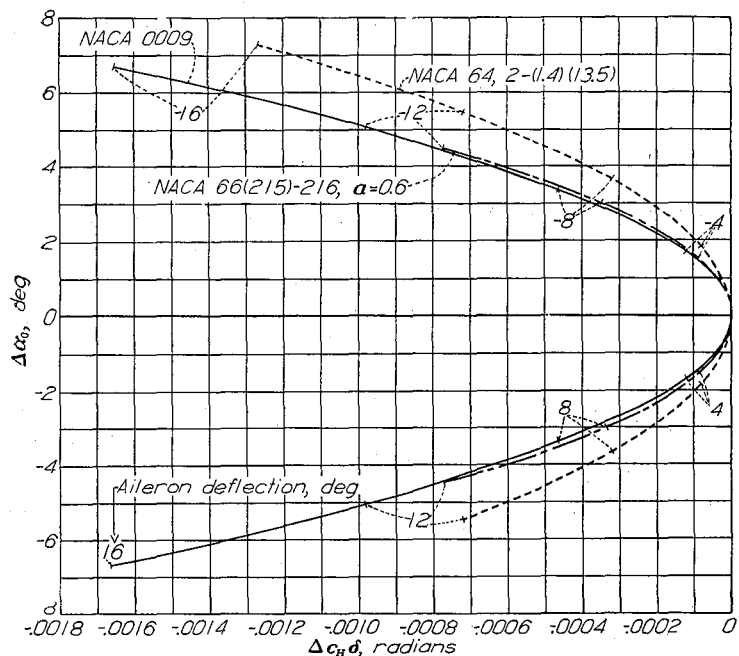


FIGURE 60.—Variation of the hinge-moment parameter  $\Delta c_H\delta$  with the equivalent change in section angle of attack required to maintain a constant section lift coefficient for deflection of the aileron on the NACA 0009, NACA 64,2-(1.4)(13.5), and NACA 66(215)-216,  $\alpha=0.6$  airfoil sections. Gaps sealed.

For the purpose of evaluating the effect of airfoil shape on the aileron characteristics, it is desirable to make the comparison with unbalanced ailerons to avoid confusion. Plots of the parameters for plain unbalanced flaps of true airfoil contour on three airfoil sections are shown in figure 60. The characteristics of the NACA 66(215)-216,  $\alpha=0.6$  section are essentially the same as those for the NACA 0009 airfoil within the range of deflection for which data are available. The NACA 64,2-(1.4)(13.5) airfoil shows appreciably smaller values of  $\Delta c_H\delta$  for a given value of  $\Delta\alpha_0$  than the other sections presented. No explanation for this difference can be offered, although some of the difference may result from the slightly smaller chord of the flap for this combination.

The effects of using straight-sided ailerons instead of ailerons of true airfoil contour are shown in figure 61 for two NACA 6-series airfoils. One of the two combinations for which data are available was provided with an internal balance whereas the other combination was without balance. This difference prevents any comparison between the two combinations but does not affect comparison of the two contours for each case. For the NACA 66(215)-216,  $\alpha=0.6$  airfoil, the straight-sided aileron has more desirable characteristics for the range of deflections for which data are avail-

Basic airfoil	$c_l$	Type of aileron	Reference
NACA 66(215)-216, $\alpha=0.6$	0.100	0.20c plain	64
NACA 63,4-4(17.8) (approx.)	.450	0.20c with 0.43c <sub>i</sub> internal balance	---

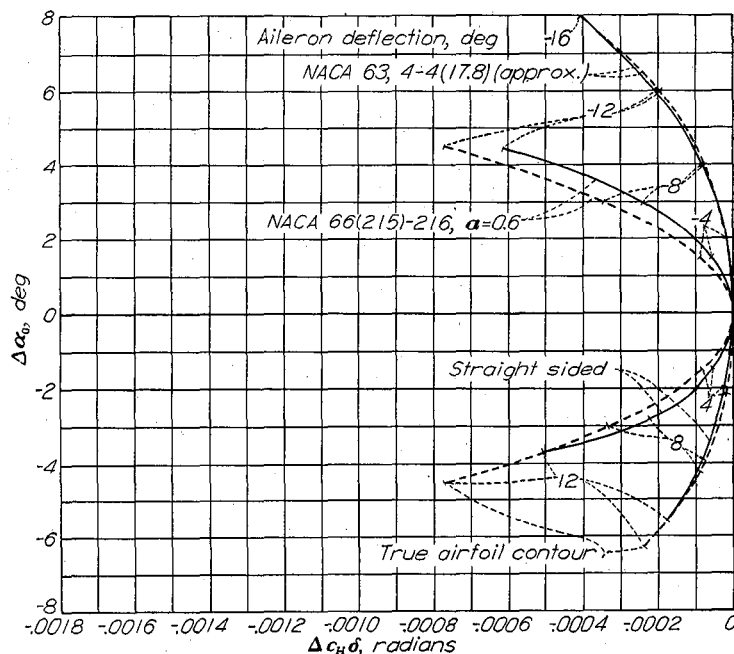


FIGURE 61.—Variation of the hinge-moment parameter  $\Delta c_H\delta$  with the equivalent change in section angle of attack required to maintain a constant section lift coefficient for deflection of true-airfoil-contour and straight-sided ailerons on the NACA 63,4-4(17.8) (approx.) and the NACA 66(215)-216,  $\alpha=0.6$  airfoil sections. Gaps sealed.

able. It appears, however, that the straight-sided aileron would be less advantageous than the aileron of true contour for positive deflections greater than 12°. In the case of the NACA 63,4-4(17.8) (approx.) airfoil, the straight-sided aileron appears to have no advantage over the aileron of true airfoil contour. The advantage of using straight-sided ailerons appears to depend markedly on the airfoil used but sufficient data are not available to determine the significant airfoil parameters. Figure 62 shows that in one case the effect of leading-edge roughness on the aileron characteristics is unfavorable.

#### LEADING-EDGE AIR INTAKES

The problem of designing satisfactory leading-edge air intakes is to maintain the lift, drag, and critical-speed characteristics of the sections while providing low intake losses over a wide range of lift coefficients and intake velocity ratios. The data of reference 65 show that desirable intake and drag characteristics can easily be maintained over a rather small range of lift coefficients for NACA 6-series airfoils. The data of reference 65 show that the intake losses increase rapidly at moderately high lift coefficients for the shapes tested. Unpublished data taken at the Langley Laboratory indicate that shapes such as those of reference 65 have low maximum lift coefficients. Recent data show

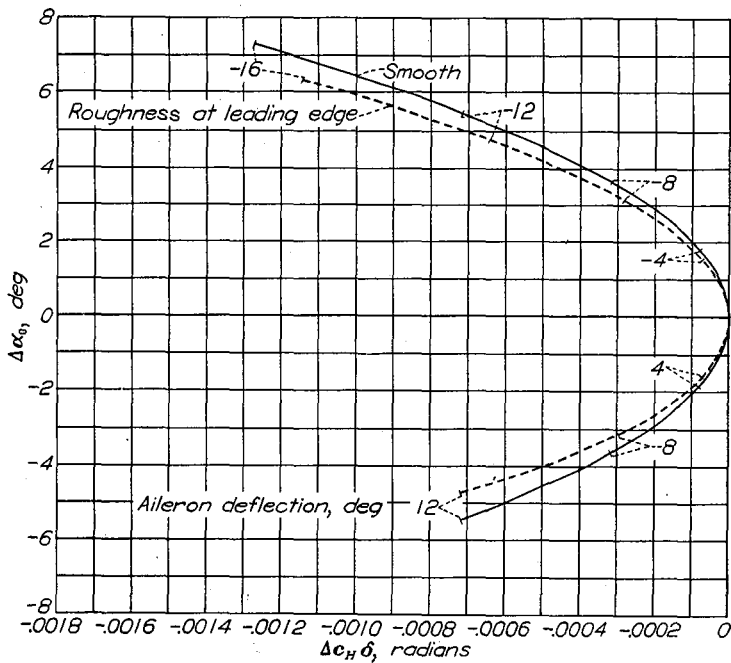


FIGURE 62.—Variation of the hinge-moment parameter  $\Delta c_H \delta$  with the equivalent change in section angle of attack required to maintain a constant section lift coefficient for deflection of the aileron on the NACA 64,2-(1.4)(13.5) airfoil section, smooth and with roughness at the leading edge of the airfoil. (For description of aileron, see fig. 60.)

that air-intake shapes can be provided for such airfoil sections with desirable air-intake characteristics and without loss in maximum lift coefficient (fig. 63). Some pressure-distribution data for the air intakes shown in figure 63 indicate that the critical speed of the section has been lowered only slightly and that falling pressures in the direction of flow were maintained for some distance from the leading edge on both surfaces at lift coefficients near the design lift coefficient for the section. Sufficient information is not available to permit such desirable configurations to be designed without experimental development.

INTERFERENCE

The main problem of interference at low Mach numbers is considered to be that of avoiding boundary-layer separation resulting from rapid flow expansions caused by the addition of induced velocities about bodies and the boundary-layer accumulations near intersections. No recent systematic investigations of interference such as the investigation of reference 66 have been made.

Some tests have been made of airfoil sections with intersecting flat plates (reference 67). These configurations may be considered to represent approximately the condition of a wing intersection with a large flat-sided fuselage. In

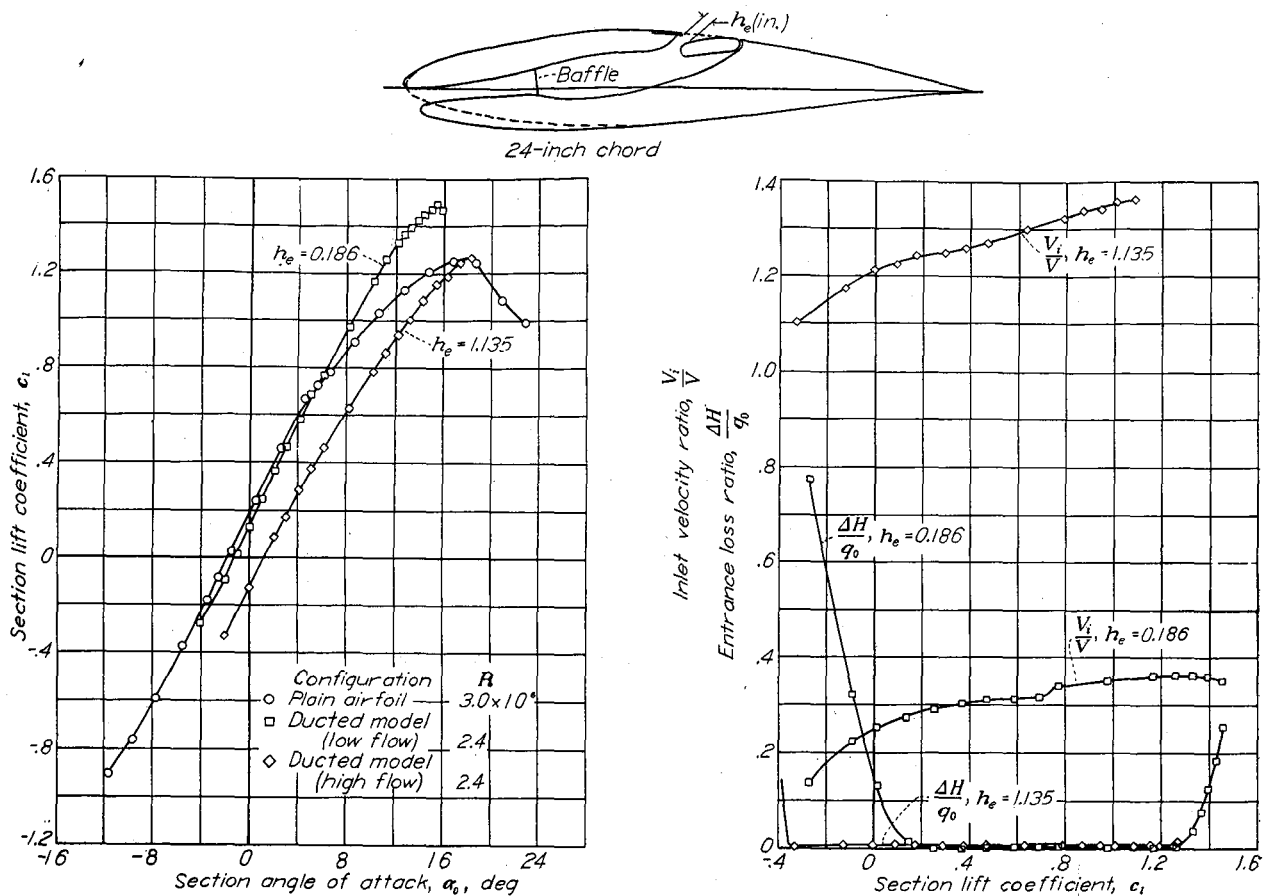


FIGURE 63.—Lift and flow characteristics of an NACA 7-series type airfoil section with leading-edge air intake.

this case, the interference may be considered to result from the effect on the wing of the fully developed turbulent boundary layer on the fuselage or flat plate and the accumulation of boundary layer in the intersection. These tests showed little interference except in cases for which the boundary layer on the airfoil alone was approaching conditions of separation such as were noted with the less conservative airfoils at moderately high lift coefficients.

Some scattered data on the characteristics of nacelles mounted on airfoils permitting extensive laminar flow are presented in references 68 to 70. The data appear to indicate that the interference problems for conservative NACA 6-series sections are similar to those encountered with other types of airfoil. The detail shapes for optimum interfering bodies and fillets may, however, be different for various sections if local excessive expansions in the flow are to be avoided.

Some lift and drag data for an airfoil with pusher-propeller-shaft housings are presented in reference 71. These results indicate that protuberances near the trailing edge of wings should be carefully designed to avoid unnecessary drag increments.

Another type of interference of particular importance for high-speed airplanes results in the reduction of the critical Mach number of the combination because of the addition of the induced velocities associated with each body (reference 72). This effect may be kept to a minimum by the use of bodies with low induced velocities, by separation of interfering bodies to the greatest possible extent, and by such selection and arrangement of combinations that the points of maximum induced velocity for each body do not coincide.

#### APPLICATION TO WING DESIGN

Detail consideration of the various factors affecting wing design lies outside the scope of this report. The following discussion is therefore limited to some important aerodynamic features that must be considered in the application of the data presented.

##### APPLICATION OF SECTION DATA

Wing characteristics are usually predicted from airfoil-section data by use of methods based on simple lifting-line theory (references 73 to 76). Application of such methods to wings of conventional plan form without spanwise discontinuities yields results of reasonable engineering accuracy (reference 77), especially with regard to such important characteristics as the angle of zero lift, the lift-curve slope, the pitching moment, and the drag. Basically similar methods not requiring the assumption of linear section lift characteristics (references 78 and 79) appear capable of yielding results of greater accuracy, especially at high lift coefficients. Further refinement may be made by consideration of the chordwise distribution of lift (reference 80). Wings with large amounts of sweep require special consideration (reference 81).

The usual wing theory assumes that the resultant air force and moment on any wing section are functions of only the section lift coefficient (or angle of attack) and the section shape. According to this assumption, the air forces and moments on any section are not affected by adjacent sections or other features of the wing except as such sections or features affect the lift distribution and thus the local lift of the section under consideration. These assumptions obviously are not valid near wing tips, near discontinuities in deflected flaps or ailerons, near disturbing bodies, or for wings with pronounced sweep or sudden changes in plan form, section, or twist. Under such circumstances, cross flows result in a breakdown of the concept of two-dimensional flow over the airfoil sections. In addition to these cross flows, induced effects exist that are equivalent to a change in camber. Such effects are particularly marked near the wing tips for wings of normal plan form and for wings of low aspect ratio or unusual plan form. Lifting-surface theory (see, for example, reference 81) provides a means for calculating wing characteristics more accurately than the simple lifting-line theory.

Although span load distributions calculated for wings with discontinuities such as are found with partial-span flaps (references 82 and 83) may be sufficiently accurate for structural design, such distributions are not suitable for predicting maximum-lift and stalling characteristics. Until sufficient data are obtained to permit the prediction of the maximum-lift and stalling characteristics of wings with discontinuities, these characteristics may best be estimated from previous results with similar wings or, in the case of unusual configurations, should be obtained by test.

The characteristics of intermediate wing sections must be known for the application of wing theory, but data for such sections are seldom available. Tests of a number of such intermediate sections obtained by several manufacturers for wings formed by straight-line fairing have indicated that the characteristics of such sections may be obtained with reasonable accuracy by interpolation of the root and tip characteristics according to the thickness variation.

##### SELECTION OF ROOT SECTION

The characteristics of a wing are affected to a large extent by the root section. In the case of tapered wings formed by straight-line fairing, the resulting nonlinear variation of section along the span causes the shapes of the sections to be predominantly affected by the root section over a large part of the wing area. The desirability of having a thick wing that provides space for housing fuel and equipment and reduces structural weight or permits large spans usually leads to the selection of the thickest root section that is aerodynamically feasible. The comparatively small variation of minimum drag coefficient with thickness ratio for smooth airfoils in the normal range of thickness ratios and the maintenance of high lift coefficient for thick sections with flaps deflected usually result in limitation of thickness ratio by characteristics other than maximum lift and minimum drag.



The critical Mach number of the section is the most serious limitation of thickness ratio for high-speed airplanes. It is desirable to select a root section with a critical Mach number sufficiently high to avoid serious drag increases resulting from compressibility effects at the highest level-flight speed of the airplane, allowance being made for the increased velocity of flow over the wing resulting from interference of bodies and slipstream. Available data indicate that a small margin exists between the critical Mach number and the Mach number at which the drag increases sharply. As airplane speeds increase, it becomes increasingly difficult and finally impossible to avoid the drag increases resulting from compressibility effects by reduction of the airfoil thickness ratio.

In the cases of airplanes of such low speeds that compressibility considerations do not limit the thickness ratio to values less than about 0.20, the maximum thickness ratio is limited by excessive drag coefficients at moderate and high lift coefficients with the surfaces rough. In these cases, the actual surface conditions expected for the airplane should be considered in selecting the section. Consideration should also be given to unusual conditions such as ice, mud, and damage caused in military combat, especially in the case of multiengine airplanes for which ability to fly under such conditions is desired with one or more engines inoperative. In cases for which root sections having large thickness ratios are under consideration to permit the use of high aspect ratios, a realistic appraisal of the drag coefficients of such sections with the expected surface conditions at moderately high lift coefficients will indicate an optimum aspect ratio beyond which corresponding increases in aspect ratio and root thickness ratio will result in reduced performance.

Inboard sections of wings on conventional airplanes are subject to interference effects and may be in the propeller slipstream. The wing surfaces are likely to be roughened by access doors, landing-gear retraction wells, and armament installations. Attainment of extensive laminar flows is, therefore, less likely on the inboard wing panels than on the outboard panels. Unless such effects are minimized, little drag reduction is to be expected from the use of sections permitting extensive laminar flow. Under these conditions, the use of sections such as the NACA 63-series will provide advantages if the sections are thick, because such sections are more conservative than those permitting more extensive laminar flow.

#### SELECTION OF TIP SECTION

In order to promote desirable stalling characteristics, the tip section should have a high maximum lift coefficient and a large range of angle of attack between zero and maximum lift as compared with the root section. It is also desirable that the tip section stall without a large sudden loss in lift. The attainment of a high maximum lift coefficient is often more difficult at the tip section than at the root section for tapered wings because of the lower Reynolds number of the tip section. For wings with small camber, the most effective way of increasing the section maximum lift coefficient is to increase the camber. The amount of camber used will be limited in most cases by either the critical-speed requirements or by the requirement that the section have low drag at the high-speed lift coefficient.

The selection of the optimum type of camber for the tip section presents problems for which no categorical answers can be given on the basis of existing data. The use of a type of camber that imposes heavy loads on the ailerons complicates the design of the lateral-control system and increases its weight. The use of a type of camber that carries the lift farther forward on the section and thus relieves the ailerons will, however, have little effect on the maximum lift coefficient of the section unless the maximum-camber position is well forward, as for the NACA 230-series sections. In this case a sudden loss of lift at the stall may be expected. The effects on the camber of modifications to the airfoil contour near the trailing edge, which may be made in designing the ailerons, should not be overlooked in estimating the characteristics of the wing.

If the root sections are at least moderately thick, it is usually desirable to select a tip section with a somewhat reduced thickness ratio. This reduction in thickness ratio, together with the absence of induced velocities from interfering bodies, gives a margin in critical speed that permits the camber of the tip section to be increased. This reduction in thickness ratio will probably be limited by the loss in maximum lift coefficient resulting from too thin a section.

A small amount of aerodynamic washout may also be useful as an aid in the avoidance of tip stalling. The permissible amount of washout may not be limited by the increase in induced drag, which is small for 1° or 2° of washout (reference 73). The limiting washout may be that which causes the tip section to operate outside the low-drag range at the high-speed lift coefficient. This limitation may be so severe as to require some adjustment of the camber to permit the use of any washout.

A change in airfoil section between the root and tip may be desirable to obtain favorable stalling characteristics or to take advantage of the greater extent of laminar flow that may be possible on the outboard sections. Thus, such combinations as an NACA 230-series root section with an NACA 44-series tip section or an NACA 63-series root section with an NACA 65-series tip section may be desirable.

It should be noted that the tip sections may easily be so heavily loaded by the use of an unfavorable plan form as to cause tip stalling with any reasonable choice of section and washout. Both high taper ratios and large amounts of sweepback are unfavorable in this respect and are particularly bad when used together, because the resulting tip stall promotes longitudinal instability at the stall in addition to the usual lateral instability.

#### CONCLUSIONS

The following conclusions may be drawn from the data presented. Most of the data, particularly for the lift, drag, and pitching-moment characteristics, were obtained at Reynolds numbers from 3 to  $9 \times 10^6$ .

1. Airfoil sections permitting extensive laminar flow, such as the NACA 6- and 7-series sections, result in substantial reductions in drag at high-speed and cruising lift coefficients as compared with other sections if, and only if, the wing surfaces are fair and smooth.

2. Experience with full-size wings has shown that extensive laminar flows are obtainable if the surface finish is as smooth as that provided by sanding in the chordwise direction with No. 320 carborundum paper and if the surface is free from small scattered defects and specks. Satisfactory results are usually obtained if the surface is sufficiently fair to permit a straightedge to be rocked smoothly in the chordwise direction without jarring or clicking.

3. For wings of moderate thickness ratios with surface conditions corresponding to those obtained with current construction methods, minimum drag coefficients of the order of 0.0080 may be expected. The values of the minimum drag coefficient for such wings depend primarily on the surface condition rather than on the airfoil section.

4. Substantial reductions in drag coefficient at high Reynolds numbers may be obtained by smoothing the wing surfaces, even if extensive laminar flow is not obtained.

5. The maximum lift coefficients for moderately cambered smooth NACA 6-series airfoils with the uniform-load type of mean line are as high as those for NACA 24- and 44-series airfoils. The NACA 230-series airfoils have somewhat higher maximum lift coefficients for thickness ratios less than 0.20.

6. The maximum lift coefficients of airfoils with flaps are about the same for moderately thick NACA 6-series sections as for the NACA 23012 section but appear to be considerably lower for thinner NACA 6-series sections.

7. The lift-curve slopes for smooth NACA 6-series airfoils are slightly higher than for NACA 24-, 44-, and 230-series airfoils and usually exceed the theoretical value for thin airfoils.

8. Leading-edge roughness causes large reductions in maximum lift coefficient for both plain airfoils and airfoils equipped with split flaps deflected  $60^\circ$ . The decrement in maximum lift coefficient resulting from standard roughness is essentially the same for the plain airfoils as for the airfoils equipped with the  $60^\circ$  split flaps.

9. The effect of leading-edge roughness is to decrease the lift-curve slope, particularly for the thicker sections having the position of minimum pressure far back.

10. Characteristics of airfoil sections with the expected surface conditions must be known or estimated to provide a satisfactory basis for the prediction of the characteristics of practical-construction wings and the selection of airfoils for such wings.

11. The NACA 6-series airfoils provide higher critical Mach numbers for high-speed and cruising lift coefficients than earlier types of sections and have a reasonable range of lift coefficients within which high critical Mach numbers may be obtained.

12. The NACA 6-series sections provide lower predicted critical Mach numbers at moderately high lift coefficients than the earlier types of sections. The limited data available suggest, however, that the NACA 6-series sections retain satisfactory lift characteristics up to higher Mach numbers than the earlier sections.

13. The NACA 6-series airfoils do not appear to present unusual problems with regard to the application of ailerons.

14. Problems associated with the avoidance of boundary-layer separation caused by interference are expected to be similar for conservative NACA 6-series sections and other good airfoils. Detail shapes for optimum interfering bodies and fillets may be different for various sections if local excessive expansions in the flow are to be avoided.

15. Satisfactory leading-edge air intakes may be provided for NACA 6-series sections, but insufficient information exists to allow such intakes to be designed without experimental development.

LANGLEY MEMORIAL AERONAUTICAL LABORATORY,  
NATIONAL ADVISORY COMMITTEE FOR AERONAUTICS,  
LANGLEY FIELD, VA., *March 5, 1945.*

## APPENDIX

### METHODS OF OBTAINING DATA IN THE LANGLEY TWO-DIMENSIONAL LOW-TURBULENCE TUNNELS

By MILTON M. KLEIN

#### DESCRIPTION OF TUNNELS

The Langley two-dimensional low-turbulence tunnels are closed-throat wind tunnels having rectangular test sections 3 feet wide and 7½ feet high and are designed to test models completely spanning the width of the tunnel in two-dimensional flow. The low-turbulence level of these tunnels, amounting to only a few hundredths of 1 percent, is achieved by the large contraction ratio in the entrance cone (approx. 20:1) and by the introduction of a number of fine-wire small-mesh turbulence-reducing screens in the widest part of the entrance cone. The chord of models tested in these tunnels is usually about 2 feet, although the characteristics at low lift coefficients of models having chords as large as 8 feet may be determined.

The Langley two-dimensional low-turbulence tunnel operates at atmospheric pressure and has a maximum speed of approximately 155 miles per hour. The Langley two-dimensional low-turbulence pressure tunnel operates at pressures up to 10 atmospheres absolute and has a maximum speed of approximately 300 miles per hour at atmospheric pressure. Standard airfoil tests in this tunnel are made of 2-foot-chord wooden models up to Reynolds numbers of approximately  $9 \times 10^6$  at a pressure of 4 atmospheres absolute.

The lift and drag characteristics of airfoils tested in these tunnels are usually measured by methods other than the use of balances. The lift is evaluated from measurements of the pressure reactions on the floor and ceiling of the tunnel. The drag is obtained from measurements of static and total pressures in the wake. Moments are usually measured by a balance.

#### SYMBOLS

$A_1, A_2, \dots, A_n$	coefficients of potential function for a symmetrical body
$a$	fraction of chord from leading edge over which design load is uniform
$B$	dimensionless constant determining width of wake
$c$	chord
$c_d$	drag coefficient corrected for tunnel-wall effects
$c_d'$	drag coefficient uncorrected for tunnel-wall effects
$c_{dT}$	drag coefficient measured in tunnel
$c_l$	section lift coefficient corrected for tunnel-wall effects

$c_l'$	section lift coefficient uncorrected for tunnel-wall effects
$c_{l_d}$	design lift coefficient
$c_{l_T}$	lift coefficient measured in tunnel
$c_{m_{c/4}}$	moment coefficient about quarter-chord point corrected for tunnel-wall effects
$c_{m_{c/4}}'$	moment coefficient about quarter-chord point measured in tunnel
$F$	average of velocity readings of orifices on floor and ceiling used to measure blocking at high lifts
$F_0$	average value of $F$ in low-lift range
$f$	potential function used to obtain $\eta$ -factor
$H_0$	total pressure in front of airfoil
$H_1$	total pressure in wake of airfoil
$H_c$	coefficient of loss of total pressure in the wake $\left(\frac{H_0 - H_1}{q_0}\right)$
$H_{c_{max}}$	maximum value of $H_c$
$h_T$	tunnel height
$K = \frac{c_d'}{c_{dT}}$	
$L$	true lift resulting from a point vortex
$L'$	lift associated with a point vortex as measured by integrating manometers
$m$	upstream limit of integration of floor and ceiling pressures
$n$	downstream limit of integration of floor and ceiling pressures
$P_R$	resultant pressure coefficient; difference between local upper- and lower-surface pressure coefficients
$p_1$	static pressure in the wake
$q_0$	free-stream dynamic pressure
$S$	static-pressure coefficient $\left(\frac{H_0 - p}{q_0}\right)$
$S_1$	static-pressure coefficient in the wake $\left(\frac{H_0 - p_1}{q_0}\right)$
$s$	distance along airfoil surface
$u$	velocity, due to row of vortices, at any point along tunnel walls
$V$	free-stream velocity
$\Delta V$	increment in free-stream velocity due to blocking

$V'$	corrected indicated tunnel velocity
$V''$	tunnel velocity measured by static-pressure orifices
$v$	local velocity at any point on airfoil surface
$w$	potential function for flow past a symmetrical body
$x$	distance along chord or center line of tunnel
$Y$	variable of integration $\left(\frac{By_w}{c}\right)$
$y$	distance perpendicular to stream direction
$y_t$	ordinate of symmetrical thickness distribution
$y_w$	distance perpendicular to stream direction from position of $H_{c_{max}}$
$\frac{dy_t}{dx}$	slope of surface of symmetrical thickness distribution
$z$	complex variable $(x+iy)$
$\alpha_{l_0}$	angle of zero lift
$\alpha_0$	section angle of attack corrected for tunnel-wall effects.
$\alpha_0'$	section angle of attack measured in tunnel
$\Gamma$	strength of a single vortex
$\eta$	ratio of measured lift to actual lift for any type of lift distribution
$\eta_a$	$\eta$ -factor for additional-type loading
$\eta_b$	$\eta$ -factor for basic mean-line loading
$\eta_x$	$\eta$ -factor applying to a point vortex
$\Delta$	component of blocking factor dependent on shape of body
$\xi$	quantity used for correcting effect of body upon velocity measured by static-pressure orifices
$\sigma$	component of blocking factor dependent on size of body
$\phi$	potential function
$\psi$	stream function

MEASUREMENT OF LIFT

The lift carried by the airfoil induces an equal and opposite reaction upon the floor and ceiling of the tunnel. The lift may therefore be obtained by integrating the pressure distribution along the floor and ceiling of the tunnel, the integration being accomplished with an integrating manometer. Because the pressure field theoretically extends to infinity in both the upstream and the downstream directions, not all the lift is included in the length over which the integration is performed. It is therefore necessary to apply a correction factor  $\eta$  that gives the ratio of the measured lift to the actual lift for any lift distribution. The calculation was performed by first finding the correction factor  $\eta_x$  applying to a point vortex and then determining the weighted average of this factor over the chord of the model.

The factor  $\eta_x$  was obtained as follows: The image system which gives only a tangential component of velocity along the tunnel walls is made up of an infinite vertical row of vortices of alternating sign as shown in figure 64. If the sign of the vortex at the origin is assumed to be positive, the complex potential function  $f$  for this image system is

$$f = \frac{i\Gamma}{2\pi} \log \sinh \frac{\pi z}{2h_T} - \frac{i\Gamma}{2\pi} \log \sinh \pi \left( \frac{z - ih_T}{2h_T} \right) \quad (18)$$

where

$\Gamma$  strength of a single vortex

$z$  complex variable  $(x+iy)$

$h_T$  tunnel height

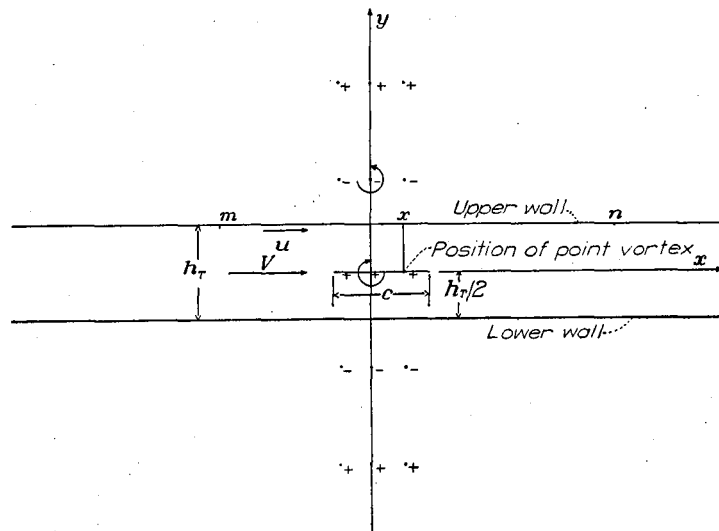


FIGURE 64.—Image system for calculation of  $\eta$ -factor in the Langley two-dimensional low-turbulence tunnels.

The velocity  $u$ , due to the row of vortices, at any point along the tunnel walls where

$$y = \frac{h_T}{2}$$

is then obtained as

$$u = \frac{\Gamma}{2h_T} \operatorname{sech} \frac{\pi x}{h_T} \quad (19)$$

where  $x$  is the horizontal distance from the point on the wall to the origin. The resultant pressure coefficient  $P_R$  is then given by

$$P_R = \frac{4u}{V} = \frac{2\Gamma}{h_T V} \operatorname{sech} \frac{\pi x}{h_T} \quad (20)$$

where  $V$  is the free-stream velocity.

The lift manometers integrate the pressure distribution along the floor and ceiling from the downstream position  $n$  to the upstream position  $m$  (fig. 64). For a point vortex

located a distance  $x$  from the origin along the center line of the tunnel, the limits of integration become  $n-x$  and  $m-x$ . The lift  $L'$  associated with a point vortex, as measured by the integrating manometers, is given by

$$L' = \int_{m-x}^{n-x} q_0 P_R dx \quad (21)$$

where  $q_0$  is the free-stream dynamic pressure.

The true lift  $L$  resulting from the point vortex is given by

$$L = \frac{2q_0\Gamma}{V}$$

The correction factor  $\eta_x$  is then

$$\begin{aligned} \eta_x &= \frac{L'}{L} \\ &= \frac{1}{h_T} \int_{m-x}^{n-x} \operatorname{sech} \frac{\pi x}{h_T} dx \end{aligned}$$

which yields

$$\eta_x = \frac{2}{\pi} \tan^{-1} \left[ \frac{e^{-\pi x/h_T} (e^{\pi n/h_T} - e^{\pi m/h_T})}{1 + e^{-2\pi x/h_T} e^{\pi(m+n)/h_T}} \right] \quad (22)$$

In the Langley two-dimensional low-turbulence tunnels, the orifices in the floor and ceiling of the tunnel used to measure the lift extend over a length of approximately 13 feet. A plot of  $\eta_x$  against  $x$  for the Langley two-dimensional low-turbulence pressure tunnel is shown in figure 65. The  $\eta$ -factor for a given lift distribution is obtained from the expression

$$\eta = \frac{\int_{\text{chord}} P_R \eta_x d\left(\frac{x}{c}\right)}{\int_{\text{chord}} P_R d\left(\frac{x}{c}\right)} \quad (23)$$

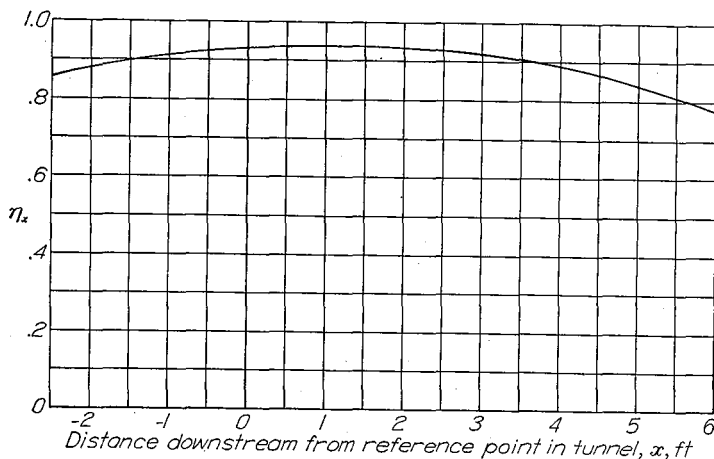


FIGURE 65.—Lift efficiency factor  $\eta_x$  for a point vortex situated at various positions along the center line of the tunnel.

The values of  $\eta_b$  and  $\eta_a$  for the Langley two-dimensional low-turbulence pressure tunnel are given in the following table for a model having a chord length of 2 feet, where  $\eta_b$  is the  $\eta$ -factor corresponding to the basic mean-line loading (indicated by the value of  $a$ ) and  $\eta_a$  is the  $\eta$ -factor for the additional type of loading as given by thin-airfoil theory:

$a$	$\eta_b$
1.0	0.9347
.8	.9342
.6	.9336
.4	.9330
.2	.9325
0	.9322

$\eta_a = 0.9296$

In order to check the variation of  $\eta_a$  with variations in the additional type of lift distribution, the value of  $\eta_a$  was recalculated for the class C additional lift distribution given in figure 6 of reference 74. The value of  $\eta_a$  for this case was 0.9304, as compared with 0.9296 for a thin airfoil. Because of the small variation of  $\eta_a$  with the type of additional lift, the value for thin-airfoil additional lift was used for all calculations. The lift coefficient of the model in the tunnel uncorrected for blocking  $c_{lT}$  is given in terms of the lift coefficient measured in the tunnel  $c_{lT}$  and the design lift coefficient of the airfoil  $c_{li}$  by the following expression:

$$c_{i'} = \frac{c_{lT}}{\eta_a} - \left( \frac{\eta_b}{\eta_a} - 1 \right) c_{li} \quad (24)$$

Because  $\eta_b$  does not differ much from  $\eta_a$ , it is not necessary that the basic loading or the design lift coefficient be known with great accuracy.

Because of tunnel-wall and other effects, the lift distribution over the airfoil in the tunnel does not agree exactly with the assumed lift distribution. Because of the small variations of  $\eta$  with lift distribution, errors caused by this effect are considered negligible. It can also be shown that errors caused by neglecting the effect of airfoil thickness on the distribution of the lift reaction along the tunnel walls are small.

#### MEASUREMENT OF DRAG

The drag of an airfoil may be obtained from observations of the pressures in the wake (reference 84). An approximation to the drag is given by the loss in total pressure of the air in the wake of the airfoil. The loss of total pressure is measured by a rake of total-pressure tubes in the wake. When the total pressures in front of the airfoil and in the wake are represented by  $H_0$  and  $H_1$ , respectively, the drag coefficient obtained from loss of total pressure  $c_{dT}$  is

$$c_{dT} = \int_{\text{wake}} H_c \frac{dy_w}{c} \quad (25)$$

where

$H_c$  coefficient of loss of total pressure in the wake  $\left( \frac{H_0 - H_1}{q_0} \right)$

$y_w$  distance perpendicular to stream direction from position of  $H_{c_{max}}$

If the static pressure in the wake is represented by  $p_1$ , the true drag coefficient uncorrected for blocking  $c_d'$  may be shown to be (reference 84)

$$c_d' = \int_{wake} 2\sqrt{S_1 - H_c}(1 - \sqrt{1 - H_c}) \frac{dy_w}{c} \quad (26)$$

where  $S_1$  is the static-pressure coefficient in the wake  $\frac{H_0 - p_1}{q_0}$ .

The assumption is made that the variation of total pressure across the wake can be represented by a normal probability curve. The drag coefficient  $c_d'$  is then easily obtainable from measurements of  $c_{dT}$  by means of a factor  $K$ , the ratio of  $c_d'$  to  $c_{dT}$ , which depends only on  $S_1$  and the maximum value of  $H_c$ . If the maximum value of  $H_c$  is represented by  $H_{c_{max}}$ , the equation of the normal probability curve is

$$H_c = H_{c_{max}} e^{-\left(\frac{By_w}{c}\right)^2}$$

where  $B$  is a dimensionless constant that determines the width of the wake. If a convenient variable of integration  $Y = \frac{By_w}{c}$  is used, the ratio  $K$  is

$$K = \frac{c_d'}{c_{dT}} = \frac{2}{\sqrt{\pi}} \frac{1}{H_{c_{max}}} \int_{-\infty}^{\infty} \sqrt{S_1 - H_c} (1 - \sqrt{1 - H_c}) dY \quad (27)$$

and is independent of the width of the wake. The quantity  $K$  has been evaluated for various values of  $H_{c_{max}}$  and  $S_1$  by assuming  $S_1$  to be constant across the wake. The drag coefficient  $c_d'$  may thus be obtained from tunnel measurements of  $c_{dT}$ ,  $H_{c_{max}}$ , and  $S_1$ . A plot of  $K$  as a function of  $H_{c_{max}}$  with  $S_1$  as parameter is given in figure 66. A parallel treatment of this problem is given in reference 85.

#### TUNNEL-WALL CORRECTIONS

In two-dimensional flow, the tunnel walls may be conveniently considered as having two distinct effects upon the flow over a model in a tunnel: (1) an increase in the free-stream velocity in the neighborhood of the model because of a constriction of the flow and (2) a distortion of the lift distribution from the induced curvature of the flow.

The increase in free-stream velocity caused by the tunnel walls (blocking effect) is obtained from consideration of an infinite vertical row of images of a symmetrical body as given in reference 86; the images represent the effect of the tunnel walls.

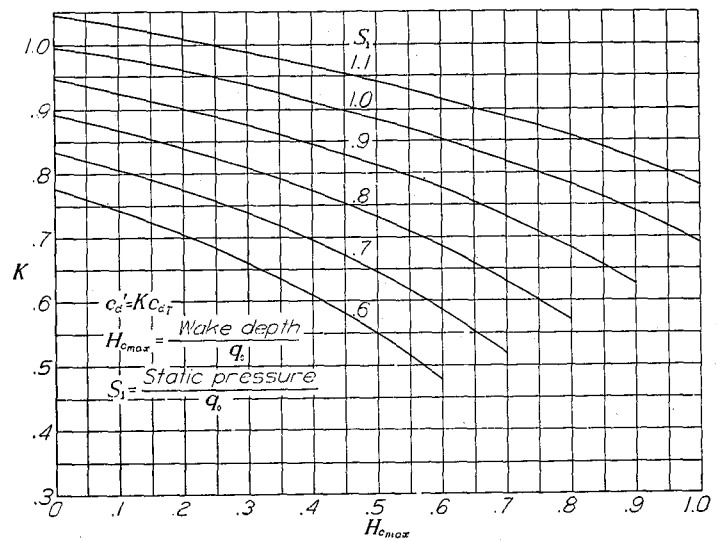


FIGURE 66.—Plot of  $K$  as a function of  $H_{c_{max}}$  with  $S_1$  as a parameter.

The potential function  $w$  for a symmetrical body is given by

$$w = Vz + \frac{A_1}{z} + \frac{A_2}{z^2} + \dots + \frac{A_n}{z^n} \quad (28)$$

where  $V$  is the free-stream velocity and the coefficients  $A_1, A_2, \dots$  are complex. If the tunnel height is large compared to the size of the body, powers of  $1/z$  greater than 1 may be neglected and

$$w = Vz + \frac{A_1}{z} \quad (29)$$

This operation is equivalent to replacing the body by a circle of which the doublet strength is  $2\pi A_1$ ; the term  $A_1/z$  represents the disturbance to the free-stream flow. The total induced velocity at the center of the body due to all the images is expressed in reference 86 as

$$\Delta V = \frac{A_1 \pi^2}{h_T^2} \frac{1}{3} \quad (30)$$

where the term  $A_1$  is the same as the term  $\frac{1}{4} \lambda l^2 V$  of reference 86.

For convenience in tunnel calculations, the expression of  $\Delta V$  may be written

$$\frac{\Delta V}{V} = \Lambda \sigma \quad (31)$$

where

$$\sigma = \frac{\pi^2}{48} \left(\frac{c}{h_T}\right)^2 \quad (32)$$

$$\Lambda = \frac{16A_1}{c^2 V} \quad (33)$$

The factor  $\sigma$  depends only on the size of the body and is easily calculated. The factor  $\Lambda$  depends on the shape of the body and is more difficult to calculate. For bodies such as

Rankine ovals and ellipses, simple formulas may be obtained for calculating  $\Lambda$ . In the general case, the value of  $\Lambda$  may be obtained from the velocity distribution over the body by the expression

$$\Lambda = \frac{16}{\pi} \int_0^1 \frac{y}{c} \frac{v}{V} \sqrt{1 + \left(\frac{dy_t}{dx}\right)^2} d\left(\frac{x}{c}\right) \quad (34)$$

where  $v$  is the velocity at any point on the airfoil surface and  $dy_t/dx$  is the slope of the airfoil surface at any point of which the ordinate is  $y_t$ .

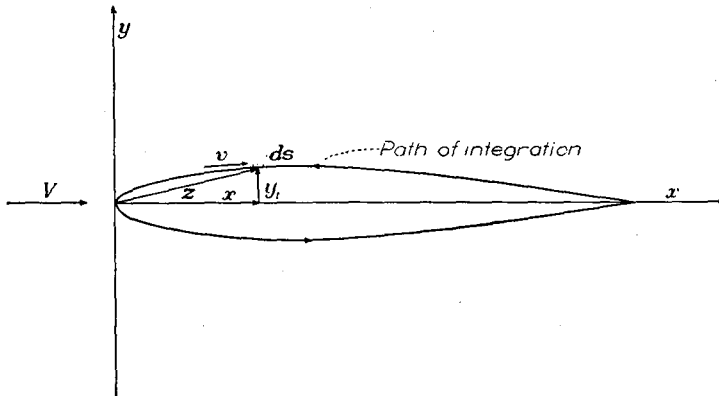


FIGURE 67.—Sketch for derivation of  $\Lambda$ -factor.

In order to obtain this expression, consider the flow past a symmetrical body as shown in figure 67. The potential function for this flow is given by equation (28). Differentiating and multiplying equation (28) by  $z$  gives

$$z \frac{dw}{dz} = Vz - \frac{A_1}{z} - \frac{2A_2}{z^2} \dots - \frac{nA_n}{z^n}$$

The line integral about a closed curve  $\int_C z \frac{dw}{dz} dz$  will depend only on the term  $-A_1/z$  and, from the theory of residues, is given by

$$\int_C z \frac{dw}{dz} dz = -2\pi i A_1$$

but

$$\begin{aligned} z \frac{dw}{dz} dz &= z dw \\ &= (x + iy)(d\phi + i d\psi) \end{aligned}$$

where  $\phi$  is the potential function and  $\psi$  is the stream function. On the surface of the body  $d\psi = 0$ , so that

$$\int_C z \frac{dw}{dz} dz = \int_C x d\phi + i \int_C y d\phi \quad (35)$$

Since the body is symmetrical, the term  $x d\phi$  will have equal numerical values but opposite signs at corresponding points of the upper and lower surfaces, and  $\int_C x d\phi$  will vanish. The term  $y d\phi$  will have equal values at corre-

sponding points of the upper and lower surfaces, and  $\int_C y d\phi$  may be replaced by an integration over the upper surface; therefore,

$$\int_C z \frac{dw}{dz} dz = 2i \int y d\phi \quad (\text{counterclockwise direction})$$

or

$$A_1 = -\frac{1}{\pi} \int y d\phi$$

Reversing the path of integration, replacing  $d\phi$  by  $v ds$ , replacing  $ds$  by  $\sqrt{1 + \frac{dy_t^2}{dx^2}} dx$ , and solving for  $\Lambda = \frac{16A_1}{c^2 V}$  gives

$$\Lambda = \frac{16}{\pi} \int_0^1 \frac{y}{c} \frac{v}{V} \sqrt{1 + \left(\frac{dy_t}{dx}\right)^2} d\left(\frac{x}{c}\right)$$

where the integration is taken from the leading edge to the trailing edge over the upper surface.

In addition to the error caused by blocking, an error exists in the measured tunnel velocity because of the interference effects of the model upon the velocity indicated by the static-pressure orifices located a few feet upstream of the model and halfway between floor and ceiling. In order to correct for this error, an analysis was made of the velocity distribution along the streamline halfway between the upper and the lower tunnel walls for Rankine ovals of various sizes and thickness ratios. The analysis showed that the correction could be expressed, within the range of conventional-airfoil thickness ratios, as a product of a thickness factor given by the blocking factor  $\Lambda$  and a factor  $\xi$  which depended upon the size of the model and the distance from the static-pressure orifices to the midchord point of the model. The corrected indicated tunnel velocity  $V'$  could then be written

$$V' = V''(1 + \Lambda\xi) \quad (36)$$

where  $V''$  is the velocity measured by the static-pressure orifices. In the Langley two-dimensional low-turbulence tunnels, the distance from the static-pressure orifices to the midchord point of the model is approximately 5.5 feet; the corresponding value of  $\xi$  for a 2-foot-chord model is approximately 0.002.

In order to calculate the effect of the tunnel walls upon the lift distribution, a comparison is made of the lift distribution of a given airfoil in a tunnel and in free air on the basis of thin-airfoil theory. It is assumed that the flow conditions in the tunnel correspond most closely to those in free air when the additional lift in the tunnel and in free air are the same (reference 87). On this basis the following corrections are derived (reference 87), in which the primed quantities refer to the coefficients measured in the tunnel:

$$c_l = [1 - 2\Lambda(\sigma + \xi) - \sigma]c_l' \quad (37)$$

$$\alpha_0 = (1 + \sigma)\alpha_0' + \frac{4\sigma c_{m_{c/4}}'}{dc_i'/d\alpha_0'} - \sigma\alpha_{i_0}' \quad (38)$$

$$c_{m_{c/4}} = [1 - 2\Lambda(\sigma + \xi)]c_{m_{c/4}}' + \sigma \frac{c_i'}{4} \quad (39)$$

In the foregoing equations, the terms  $\frac{4\sigma c_{m_{c/4}}'}{dc_i'/d\alpha_0'}$ ,  $\sigma\alpha_{i_0}'$ , and  $\sigma c_i'/4$  are usually negligible for 2-foot-chord models in the Langley two-dimensional low-turbulence tunnels.

When the effect of the tunnel walls on the pressure distribution over the model is small, the wall effect on the drag is merely that corresponding to an increase in the tunnel speed. The correction to the drag coefficient is therefore given by the following relation:

$$c_d = [1 - 2\Lambda(\sigma + \xi)]c_d' \quad (40)$$

Similar considerations have been applied to the development of corrections for the pressure distribution in reference 87.

Equation (40) neglects the blocking due to the wake, such blocking being small at low to moderate drags. The effect of a pressure gradient in the tunnel upon loss of total pressure in the wake is not easily analyzed but is estimated to be small. The effect of the pressure gradient upon the drag has therefore been disregarded. When the drag is measured by a balance, the effect of the pressure gradient upon the drag is directly additive and a correction should be applied. For large models, especially at high lift coefficients, the effect of the tunnel walls is to distort the pressure distribution appreciably. Such distortions of the pressure distribution may cause large changes in the boundary flow and no adequate corrections to any of the coefficients, particularly the drag, can be found.

#### CORRECTION FOR BLOCKING AT HIGH LIFTS

So long as the flow follows the airfoil surface, the foregoing relations account for the effects of the tunnel walls with sufficient accuracy. When the flow leaves the surface, the blocking increases because of the predominant effect of the wake upon the free-stream velocity. Since the wake effect shows up primarily in the drag, the increase in blocking would logically be expressed in terms of the drag. The accurate measurement of drag under these conditions by means of a rake is impractical because of spanwise movements of low-energy air. A method of correcting for increased blocking at high angles of attack without drag measurements has therefore been devised for use in the Langley two-dimensional low-turbulence tunnels.

Readings of the floor and ceiling velocities are taken a few inches ahead of the quarter-chord point and averaged to remove the effect of lift. This average  $F$ , which is a measure of the effective tunnel velocity, is essentially constant in the low-lift range. The quantity  $F/F_0$ , where  $F_0$  is the average value of  $F$  in the low-lift range, however, shows a variation

from unity in the high-lift range for any airfoil tested in the tunnel; this variation indicates a change in blocking at high lifts. A plot of  $F/F_0$  against angle of attack  $\alpha_0'$  for a 2-foot-chord model of the NACA 64<sub>3</sub>-418 airfoil is given in figure 68. The quantity  $F/F_0$  is nearly constant for values of  $\alpha_0'$  up to 12°; but for values of  $\alpha_0'$  greater than 12°,  $F/F_0$  increases and the increase is particularly noticeable at and over the stall.

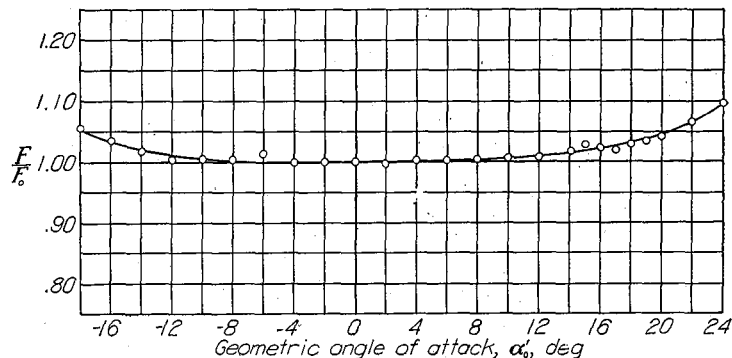


FIGURE 68.—Additional blocking factor at the tunnel walls plotted against angle of attack for the NACA 64<sub>3</sub>-418 airfoil.

A theoretical comparison was made of the blocking factor  $\Delta\sigma$  and the velocity measured by the floor and ceiling orifices for a series of Rankine ovals of various sizes and thickness ratios. The quarter-chord point of each oval was located at the pivot point, the usual position of an airfoil in the tunnel. The analysis showed the relation between the blocking factor  $\Delta\sigma$  and the change in  $F$  to be unique for chord lengths up to 50 inches in that different bodies having the same blocking factor  $\Delta\sigma$  gave approximately the same value of  $F$ . For chords up to 50 inches, the relationship is

$$\frac{\Delta V}{V} = 0.45 \left( \frac{F}{F_0} - 1 \right) \quad (41)$$

where  $\Delta V/V$  is the true increment in tunnel velocity due to blocking. The foregoing relation was adopted to obtain the correction to the blocking in the range of lifts where  $\frac{F}{F_0} > 1$ .

Considerable uncertainty exists regarding the correct numerical value of the coefficient occurring in equation (41). If a row of sources, rather than the Rankine ovals used in the present analysis, is considered to represent the effect of the wake, the value of the coefficient in equation (41) would be approximately twice the value used. Fortunately, the correction amounts to only about 2 percent at maximum lift for an extreme condition with a 2-foot-chord model. Further refinement of this correction has therefore not been attempted.

#### COMPARISON WITH EXPERIMENT

A check of the validity of the tunnel-wall corrections has been made in reference 87, which gives lift and moment curves for models having various ratios of chord to tunnel height, uncorrected and corrected for tunnel-wall effects.



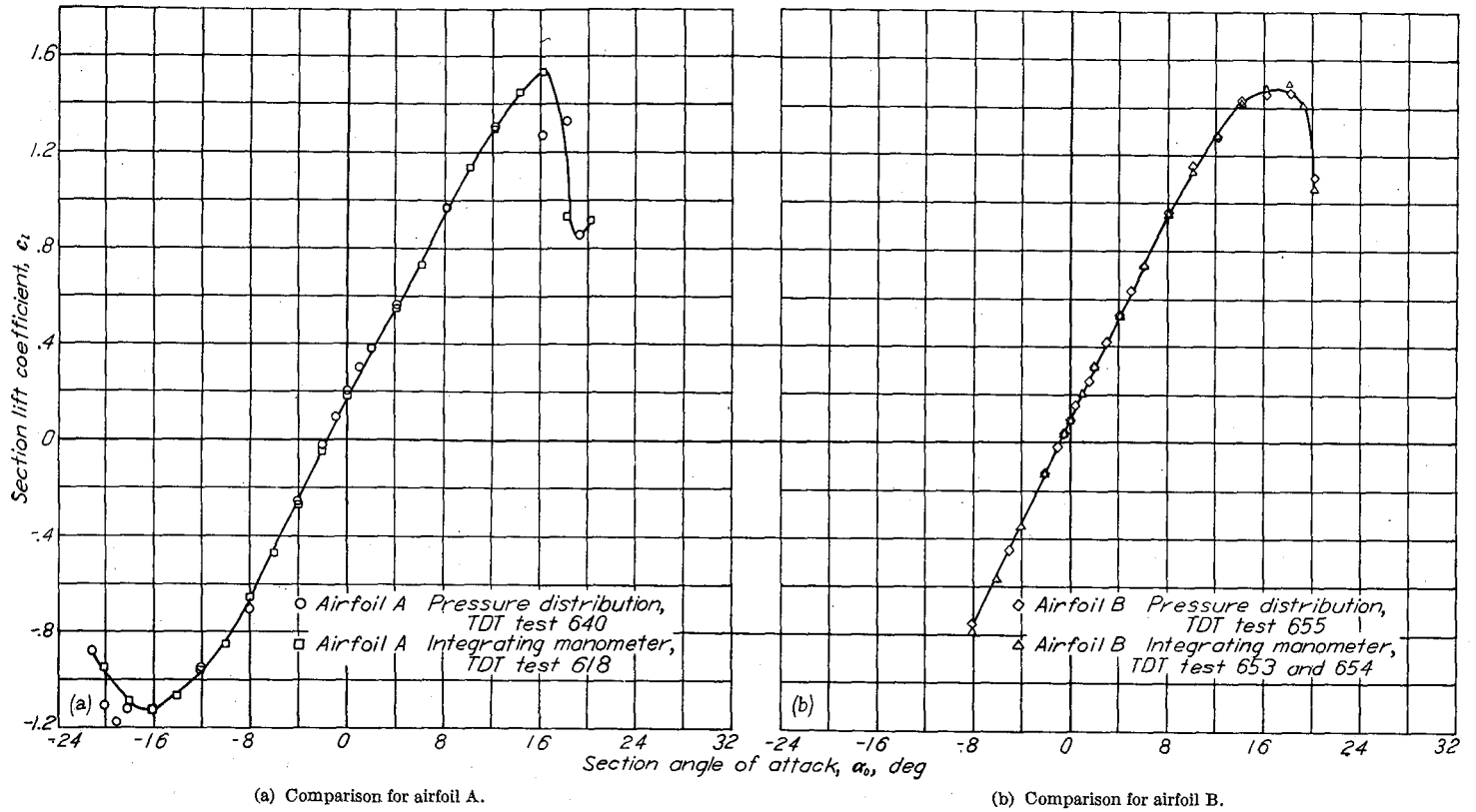


FIGURE 69.—Comparison between lifts obtained from pressure-distribution measurements and lifts obtained from reactions on the floor and ceiling of the tunnel.

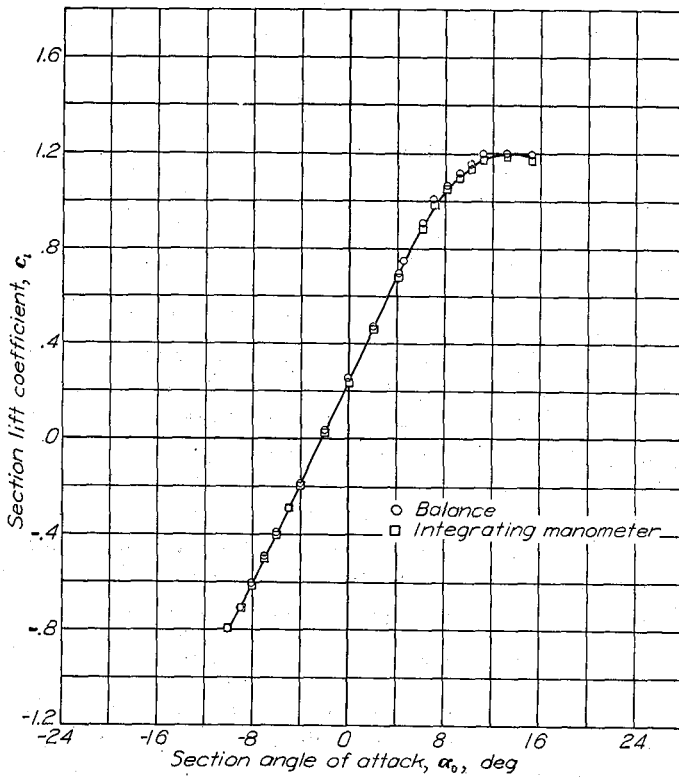


FIGURE 70.—Comparison between lifts obtained from balance measurements and from reactions on the floor and ceiling of the tunnel.

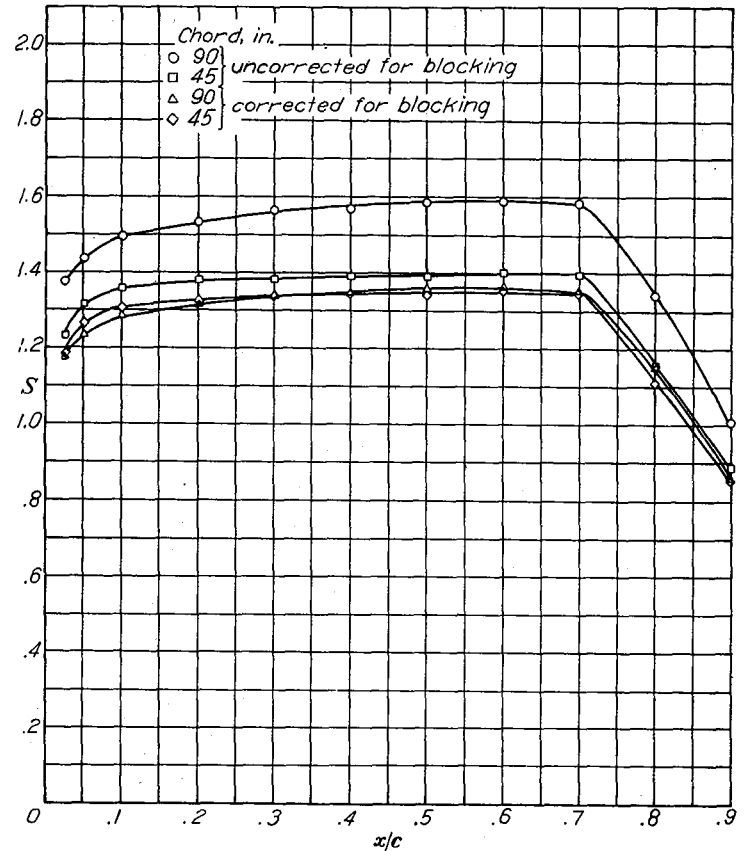


FIGURE 71.—Comparison between corrected and uncorrected pressure distributions for two chord sizes of a symmetrical NACA 6-series airfoil of 15-percent thickness.  $\alpha_0 = 0^\circ$ .

The general agreement of the corrected curves shows that the method of correcting the lifts and moments is valid.

A comparison is made in reference 87 between the theoretical correction factor (equation (40)) and the experimentally derived corrections of reference 88. The theoretical correction factors were found to be in good agreement with those obtained experimentally.

In order to check the validity of the  $\eta$ -factor, a comparison has been made of lift values obtained from pressure distributions with those obtained from the integration of the floor and ceiling pressures in the tunnel. A comparison for two airfoils given in figure 69 shows that the two methods of measuring lift give results that are in good agreement. The  $\eta$ -factor has also been checked by comparison of the lift obtained from balance measurements with the integrating-manometer values in figure 70.

Finally, a check has been made of the method of correcting pressure distributions (reference 87) for NACA 6-series airfoils of two chord lengths at zero angle of attack in figure 71, in which the pressure coefficients are plotted against chordwise position  $x/c$ . The agreement between the corrected pressure distributions for both models verifies the method of making the tunnel-wall corrections.

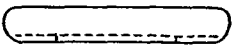









#### REFERENCES

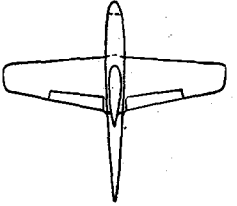

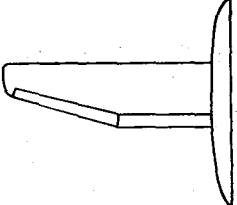

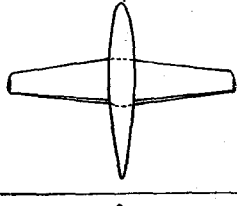
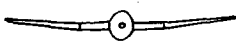
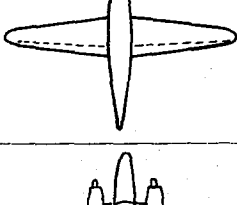
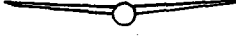
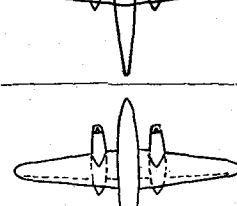

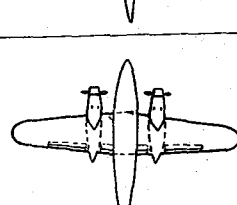

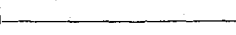
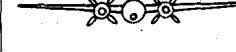
- Jacobs, Eastman N., Ward, Kenneth E., and Pinkerton, Robert M.: The Characteristics of 78 Related Airfoil Sections from Tests in the Variable-Density Wind Tunnel. NACA Rep. No. 460, 1933.
- Jacobs, Eastman N., and Pinkerton, Robert M.: Tests in the Variable-Density Wind Tunnel of Related Airfoils Having the Maximum Camber Unusually Far Forward. NACA Rep. No. 537, 1935.
- Jacobs, Eastman N., Pinkerton, Robert M., and Greenberg, Harry: Tests of Related Forward-Camber Airfoils in the Variable-Density Wind Tunnel. NACA Rep. No. 610, 1937.
- Stack, John, and Von Doenhoff, Albert E.: Tests of 16 Related Airfoils at High Speeds. NACA Rep. No. 492, 1934.
- Jacobs, Eastman N., and Sherman, Albert: Airfoil Section Characteristics as Affected by Variations of the Reynolds Number. NACA Rep. No. 586, 1937.
- Pinkerton, Robert M., and Greenberg, Harry: Aerodynamic Characteristics of a Large Number of Airfoils Tested in the Variable-Density Wind Tunnel. NACA Rep. No. 628, 1938.
- Jones, B. Melvill: Flight Experiments on the Boundary Layer. Jour. Aero. Sci., vol. 5, no. 3, Jan. 1938, pp. 81-94.
- Jacobs, Eastman N., and Abbott, Ira H.: Airfoil Section Data Obtained in the N.A.C.A. Variable-Density Tunnel as Affected by Support Interference and Other Corrections. NACA Rep. No. 669, 1939.
- Theodorsen, Theodore: Theory of Wing Sections of Arbitrary Shape. NACA Rep. No. 411, 1931.
- Stack, John: Tests of Airfoils Designed to Delay the Compressibility Burble. NACA Rep. No. 763, 1943.
- Jacobs, Eastman N.: Preliminary Report on Laminar-Flow Airfoils and New Methods Adopted for Airfoil and Boundary-Layer Investigations. NACA ACR, June 1939.
- Von Doenhoff, Albert E., and Stivers, Louis S., Jr.: Aerodynamic Characteristics of the NACA 747A315 and 747A415 Airfoils from Tests in the NACA Two-Dimensional Low-Turbulence Pressure Tunnel. NACA CB No. L4I25, 1944.
- Naiman, Irven: Numerical Evaluation by Harmonic Analysis of the  $\epsilon$ -Function of the Theodorsen Arbitrary-Airfoil Potential Theory. NACA ARR No. L5H18, 1945.
- Theodorsen, Theodore: Airfoil-Contour Modification Based on  $\epsilon$ -Curve Method of Calculating Pressure Distribution. NACA ARR No. L4G05, 1944.
- Allen, H. Julian: A Simplified Method for the Calculation of Airfoil Pressure Distribution. NACA TN No. 708, 1939.
- Munk, Max M.: Elements of the Wing Section Theory and of the Wing Theory. NACA Rep. No. 191, 1924.
- Glauert, H.: The Elements of Aerofoil and Airscrew Theory. Cambridge Univ. Press, 1926, pp. 87-93.
- Theodorsen, Theodore: On the Theory of Wing Sections with Particular Reference to the Lift Distribution. NACA Rep. No. 383, 1931.
- Von Kármán, Th.: Compressibility Effects in Aerodynamics. Jour. Aero. Sci., vol. 8, no. 9, July 1941, pp. 337-356.
- Von Doenhoff, Albert E.: A Method of Rapidly Estimating the Position of the Laminar Separation Point. NACA TN No. 671, 1938.
- Jacobs, E. N., and Von Doenhoff, A. E.: Formulas for Use in Boundary-Layer Calculations on Low-Drag Wings. NACA ACR, Aug. 1941.
- Von Doenhoff, Albert E., and Tetervin, Neal: Determination of General Relations for the Behavior of Turbulent Boundary Layers. NACA Rep. No. 772, 1943.
- Squire, H. B., and Young, A. D.: The Calculation of the Profile Drag of Aerofoils. R. & M. No. 1838, British A. R. C., 1938.
- Tetervin, Neal: A Method for the Rapid Estimation of Turbulent Boundary-Layer Thicknesses for Calculating Profile Drag. NACA ACR No. L4G14, 1944.
- Quinn, John H., Jr., and Tucker, Warren A.: Scale and Turbulence Effects on the Lift and Drag Characteristics of the NACA 65<sub>3</sub>-418,  $a=1.0$  Airfoil Section. NACA ACR No. L4H11, 1944.
- Tucker, Warren A., and Wallace, Arthur R.: Scale-Effect Tests in a Turbulent Tunnel of the NACA 65<sub>3</sub>-418,  $a=1.0$  Airfoil Section with 0.20-Airfoil-Chord Split Flap. NACA ACR No. L4I22, 1944.
- Davidson, Milton, and Turner, Harold R., Jr.: Effects of Mean-Line Loading on the Aerodynamic Characteristics of Some Low-Drag Airfoils. NACA ACR No. 3I27, 1943.
- Von Doenhoff, Albert E., and Tetervin, Neal: Investigation of the Variation of Lift Coefficient with Reynolds Number at a Moderate Angle of Attack on a Low-Drag Airfoil. NACA CB, Nov. 1942.
- Oswald, W. Bailey: General Formulas and Charts for the Calculation of Airplane Performance. NACA Rep. No. 408, 1932.
- Millikan, Clark B.: Aerodynamics of the Airplane. John Wiley & Sons, Inc., 1941, pp. 108-109.
- Hood, Manley J.: The Effects of Some Common Surface Irregularities on Wing Drag. NACA TN No. 695, 1939.
- Loftin, Laurence K., Jr.: Effects of Specific Types of Surface Roughness on Boundary-Layer Transition. NACA ACR No. L5J29a, 1946.
- Charters, Alex C., Jr.: Transition between Laminar and Turbulent Flow by Transverse Contamination. NACA TN No. 891, 1943.
- Braslow, Albert L.: Investigation of Effects of Various Camouflage Paints and Painting Procedures on the Drag Characteristics of an NACA 65<sub>(421)</sub>-420,  $a=1.0$  Airfoil Section. NACA CB No. L4G17, 1944.

35. Jones, Robert T., and Cohen, Doris: A Graphical Method of Determining Pressure Distribution in Two-Dimensional Flow. NACA Rep. No. 722, 1941.
36. Abbott, Frank T., Jr., and Turner, Harold R., Jr.: The Effects of Roughness at High Reynolds Numbers on the Lift and Drag Characteristics of Three Thick Airfoils. NACA ACR No. L4H21, 1944.
37. Jacobs, Eastman N., Abbott, Ira H., and Davidson, Milton: Investigation of Extreme Leading-Edge Roughness on Thick Low-Drag Airfoils to Indicate Those Critical to Separation. NACA CB, June 1942.
38. Zaloveik, John A.: Profile-Drag Coefficients of Conventional and Low-Drag Airfoils as Obtained in Flight. NACA ACR No. L4E31, 1944.
39. Zaloveik, John A., and Wood, Clotaire: A Flight Investigation of the Effect of Surface Roughness on Wing Profile Drag with Transition Fixed. NACA ARR No. L4I25, 1944.
40. Hood, Manley J., and Gaydos, M. Edward: Effects of Propellers and of Vibration on the Extent of Laminar Flow on the N. A. C. A. 27-212 Airfoil. NACA ACR, Oct. 1939.
41. Silverstein, Abe, Katzoff, S., and Hootman, James A.: Comparative Flight and Full-Scale Wind-Tunnel Measurements of the Maximum Lift of an Airplane. NACA Rep. No. 618, 1938.
42. Sweberg, Harold H., and Dingeldein, Richard C.: Summary of Measurements in Langley Full-Scale Tunnel of Maximum Lift Coefficients and Stalling Characteristics of Airplanes. NACA Rep. No. 829, 1945.
43. Purser, Paul E., and Johnson, Harold S.: Effects of Trailing-Edge Modifications on Pitching-Moment Characteristics of Airfoils. NACA CB No. L4I30, 1944.
44. Fullmer, Felicien F., Jr.: Wind-Tunnel Investigation of NACA 66(215)-216, 66,1-212, and 65,1-212 Airfoils with 0.20-Airfoil-Chord Split Flaps. NACA CB No. L4G10, 1944.
45. Abbott, Ira H., and Greenberg, Harry: Tests in the Variable-Density Wind Tunnel of the N. A. C. A. 23012 Airfoil with Plain and Split Flaps. NACA Rep. No. 661, 1939.
46. Wenzinger, Carl J., and Harris, Thomas A.: Wind-Tunnel Investigation of N. A. C. A. 23012, 23021, and 23030 Airfoils with Various Sizes of Split Flap. NACA Rep. No. 668, 1939.
47. Bogdonoff, Seymour M.: Wind-Tunnel Investigation of a Low-Drag Airfoil Section with a Double Slotted Flap. NACA ACR No. 3I20, 1943.
48. Wenzinger, Carl J., and Harris, Thomas A.: Wind-Tunnel Investigation of an N. A. C. A. 23012 Airfoil with Various Arrangements of Slotted Flaps. NACA Rep. No. 664, 1939.
49. Wenzinger, Carl J., and Harris, Thomas A.: Wind-Tunnel Investigation of an N. A. C. A. 23021 Airfoil with Various Arrangements of Slotted Flaps. NACA Rep. No. 677, 1939.
50. Swanson, Robert S., and Crandall, Stewart M.: Analysis of Available Data on the Effectiveness of Ailerons without Exposed Overhang Balance. NACA ACR No. L4E01, 1944.
51. Street, William G., and Ames, Milton B., Jr.: Pressure-Distribution Investigation of an N. A. C. A. 0009 Airfoil with a 50-Percent-Chord Plain Flap and Three Tabs. NACA TN No. 734, 1939.
52. Ames, Milton B., Jr., and Sears, Richard I.: Pressure-Distribution Investigation of an N. A. C. A. 0009 Airfoil with an 80-Percent-Chord Plain Flap and Three Tabs. NACA TN No. 761, 1940.
53. Ames, Milton B., Jr., and Sears, Richard I.: Pressure-Distribution Investigation of an N. A. C. A. 0009 Airfoil with a 30-Percent-Chord Plain Flap and Three Tabs. NACA TN No. 759, 1940.
54. Sears, Richard I.: Wind-Tunnel Investigation of Control-Surface Characteristics. I—Effect of Gap on the Aerodynamic Characteristics of an NACA 0009 Airfoil with a 30-Percent-Chord Plain Flap. NACA ARR, June 1941.
55. Jones, Robert T., and Ames, Milton B., Jr.: Wind-Tunnel Investigation of Control-Surface Characteristics. V—The Use of a Beveled Trailing Edge to Reduce the Hinge Moment of a Control Surface. NACA ARR, March 1942.
56. Sears, Richard I., and Liddell, Robert B.: Wind-Tunnel Investigation of Control-Surface Characteristics. VI—A 30-Percent-Chord Plain Flap on the NACA 0015 Airfoil. NACA ARR, June 1942.
57. Wenzinger, Carl J., and Delano, James B.: Pressure Distribution over an N. A. C. A. 23012 Airfoil with a Slotted and a Plain Flap. NACA Rep. No. 633, 1938.
58. Gillis, Clarence L., and Lockwood, Vernard E.: Wind-Tunnel Investigation of Control-Surface Characteristics. XIII—Various Flap Overhangs Used with a 30-Percent-Chord Flap on an NACA 66-009 Airfoil. NACA ACR No. 3G20, 1943.
59. Rogallo, F. M.: Collection of Balanced-Aileron Test Data. NACA ACR No. 4A11, 1944.
60. Denaci, H. G., and Bird, J. D.: Wind-Tunnel Tests of Ailerons at Various Speeds. II—Ailerons of 0.20 Airfoil Chord and True Contour with 0.60 Aileron-Chord Sealed Internal Balance on the NACA 66,2-216 Airfoil. NACA ACR No. 3F18, 1943.
61. Purser, Paul E., and Riebe, John M.: Wind-Tunnel Investigation of Control-Surface Characteristics. XV—Various Contour Modifications of a 0.30-Airfoil-Chord Plain Flap on an NACA 66(215)-014 Airfoil. NACA ACR No. 3L20, 1943.
62. Braslow, Albert L.: Wind-Tunnel Investigation of Aileron Effectiveness of 0.20-Airfoil-Chord Plain Ailerons of True Airfoil Contour on NACA 65,2-415, 65,2-418, and 65,2-421 Airfoil Sections. NACA CB No. L4H12, 1944.
63. Sears, Richard I., and Purser, Paul E.: Wind-Tunnel Investigation of Control-Surface Characteristics. XIV—NACA 0009 Airfoil with a 20-Percent-Chord Double Plain Flap. NACA ARR No. 3F29, 1943.
64. Crane, Robert M., and Holtzelaw, Ralph W.: Wind-Tunnel Investigation of the Effects of Profile Modifications and Tabs on the Characteristics of Ailerons on a Low Drag Airfoil. NACA Rep. No. 803, 1944.
65. Von Doenhoff, Albert E., and Horton, Elmer A.: Preliminary Investigation in the NACA Low-Turbulence Tunnel of Low-Drag-Airfoil Sections Suitable for Admitting Air at the Leading Edge. NACA ACR, July 1942.
66. Jacobs, Eastman N., and Ward, Kenneth E.: Interference of Wing and Fuselage from Tests of 209 Combinations in the N. A. C. A. Variable-Density Tunnel. NACA Rep. No. 540, 1935.
67. Abbott, Ira H.: Interference Effects of Longitudinal Flat Plates on Low-Drag Airfoils. NACA CB, Nov. 1942.
68. Ellis, Macon C., Jr.: Some Lift and Drag Measurements of a Representative Bomber Nacelle on a Low-Drag Wing—II. NACA CB, Sept. 1942.
69. Ellis, Macon C., Jr.: Effects of a Typical Nacelle on the Characteristics of a Thick Low-Drag Airfoil Critically Affected by Leading-Edge Roughness. NACA CB No. 3D27, 1943.
70. Allen, H. Julian, and Frick, Charles W., Jr.: Experimental Investigation of a New Type of Low-Drag Wing-Nacelle Combination. NACA ACR, July 1942.
71. Abbott, Frank T., Jr.: Lift and Drag Data for 30 Pusher-Propeller Shaft Housings on an NACA 65,3-018 Airfoil Section. NACA ACR No. 3K13, 1943.
72. Robinson, Russell G., and Wright, Ray H.: Estimation of Critical Speeds of Airfoils and Streamline Bodies. NACA ACR, March 1940.
73. Anderson, Raymond F.: Determination of the Characteristics of Tapered Wings. NACA Rep. No. 572, 1936.
74. Jacobs, Eastman N., and Rhode, R. V.: Airfoil Section Characteristics as Applied to the Prediction of Air Forces and Their Distribution on Wings. NACA Rep. No. 631, 1938.

75. Soulé, H. A., and Anderson, R. F.: Design Charts Relating to the Stalling of Tapered Wings. NACA Rep. No. 703, 1940.
76. Harmon, Sidney M.: Additional Design Charts Relating to the Stalling of Tapered Wings. NACA ARR, Jan. 1943.
77. Anderson, Raymond F.: The Experimental and Calculated Characteristics of 22 Tapered Wings. NACA Rep. No. 627, 1938.
78. Tani, Itiro: A Simple Method of Calculating the Induced Velocity of a Monoplane Wing. Rep. No. 111 (Vol. IX, 3), Aero. Res. Inst., Tokyo Imperial Univ., Aug. 1934.
79. Sherman, Albert: A Simple Method of Obtaining Span Load Distributions. NACA TN No. 732, 1939.
80. Jones, Robert T.: Correction of the Lifting-Line Theory for the Effect of the Chord. NACA TN No. 817, 1941.
81. Cohen, Doris: Theoretical Distribution of Load over a Swept-Back Wing. NACA ARR, Oct. 1942.
82. Pearson, H. A.: Span Load Distribution for Tapered Wings with Partial-Span Flaps. NACA Rep. No. 585, 1937.
83. Pearson, Henry A., and Anderson, Raymond F.: Calculation of the Aerodynamic Characteristics of Tapered Wings with Partial-Span Flaps. NACA Rep. No. 665, 1939.
84. The Cambridge University Aeronautics Laboratory: The Measurement of Profile Drag by the Pitot-Traverse Method. R. & M. No. 1688, British A. R. C., 1936.
85. Silverstein, A., and Katzoff, S.: A Simplified Method for Determining Wing Profile Drag in Flight. Jour. Aero. Sci., vol. 7, no. 7, May 1940, pp. 295-301.
86. Glauert, H.: Wind Tunnel Interference on Wings, Bodies and Airscrews. R. & M. No. 1566, British A. R. C., 1933.
87. Allen, H. Julian, and Vincenti, Walter G.: Interference in a Two-Dimensional-Flow Wind Tunnel with the Consideration of the Effect of Compressibility. NACA Rep. No. 782, 1944.
88. Fage, A.: On the Two-Dimensional Flow past a Body of Symmetrical Cross-Section Mounted in a Channel of Finite Breadth. R. & M. No. 1223, British A. R. C., 1929.

TABLE II.—MAXIMUM LIFT AND STALLING CHARACTERISTICS OF MODELS TESTED IN THE NACA 19-FOOT PRESSURE TUNNEL

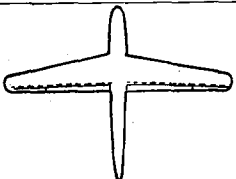
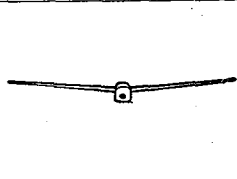
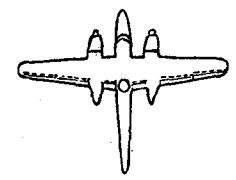
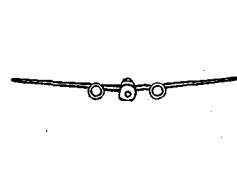
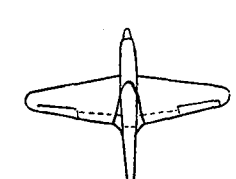
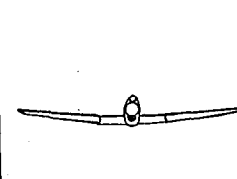
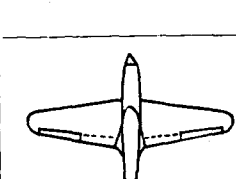
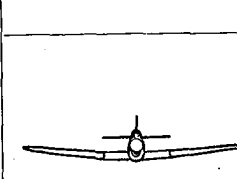
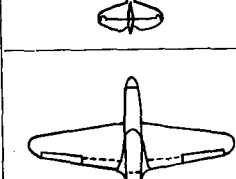
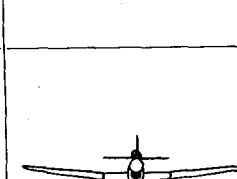
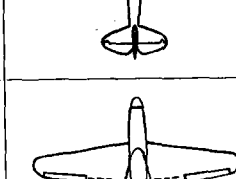
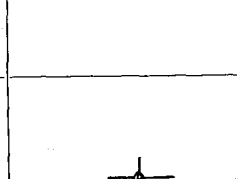
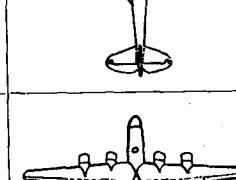
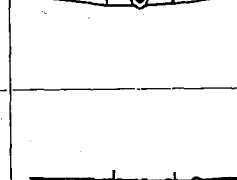
Model	Configuration		Geometric characteristics	Flap		Flap angle (deg)		Flap chord (percent c)		Flap span (percent b)		R	$C_{L_{max}}$	Stalling characteristics			
	Plan view	Front view		Inboard	Outboard	$\delta_{f_i}$	$\delta_{f_o}$	$c_{f_i}$	$c_{f_o}$	$b_{f_i}$	$b_{f_o}$						
I			Sections: Root: NACA 66(215)-216 Tip: NACA 66(215)-216 $A=7.00$ $\lambda=1.00$ Geometric washout, $0.0^\circ$	None	None	---	---	None	None	None	None	$2.6 \times 10^6$	1.26	Abrupt stall progresses from root toward tip for flaps neutral and partial-span flaps deflected; no data for full-span flaps			
				Split	↓	60	↓	10	↓	53	↓	2.6	1.72		3.6	1.36	
												3.6	1.78		4.6	1.84	
												2.6	1.94		3.6	1.98	
				↓	↓	60	↓	10	10	37	↓	2.6	2.04		3.6	2.11	
												3.6	2.15		4.6	2.15	
												2.6	2.40		3.6	2.50	
				↓	↓	30	↓	30	↓	↓	↓	2.6	2.43		3.6	2.49	
												3.6	2.49		4.6	2.52	
												2.6	2.51		3.6	2.51	
II			Sections: Root: NACA 66(215)-116 Tip: NACA 66(215)-216 $A=7.0$ $\lambda=0.5$ Geometric washout, $1.5^\circ$	Fowler	Fowler	0	0	30	30	53	37	$2.1 \times 10^6$	1.15	With flaps neutral, satisfactory; with flaps deflected, extremely abrupt stall envelops entire wing			
				↓	↓	30	↓	↓	↓	↓	↓	↓	↓		2.8	1.29	
															3.3	1.27	
															2.1	2.29	
				↓	↓	35	↓	↓	↓	↓	↓	↓	↓		↓	2.9	2.44
																3.4	2.49
																2.1	2.36
↓	↓	30	↓	30	↓	↓	↓	↓	↓	↓	2.9	2.49					
											3.4	2.54					
											2.1	3.13					
↓	↓	30	↓	↓	↓	↓	↓	↓	↓	↓	2.9	3.31					
											3.4	3.29					
											2.1	3.29					
III			Sections: Root: NACA 65(318)-019 Tip: NACA 65(318)-015 $A=7.36$ $\lambda=0.25$ Geometric washout; $3.6^\circ$	None	None	---	---	---	---	---	$3.0 \times 10^6$	1.18	Abrupt stall with satisfactory progression toward tips				
IV			Sections: Root: NACA 65(318)-019 Tip: NACA 65(318)-015 $A=7.36$ $\lambda=0.25$ Geometric washout, $4.0^\circ$ Sweepback of 0.25 chord line $21.93^\circ$	None	None	---	---	---	---	---	---	$3.3 \times 10^6$	1.17	Unsatisfactory stall; a strong outflow resulted in severe tip stall			
				↓	↓	---	---	---	---	---	---	---	---		5.6	1.31	
															7.2	1.34	
V			Sections: Root: NACA 66(215)-(1.8)(15.5), $a=0.6$ Tip: NACA 66(215)-(1.8)12, $a=0.6$ $A=5.82$ $\lambda=0.46$ Geometric washout, $2.5^\circ$	Plain	None	0	---	25	---	60	---	$3.2 \times 10^6$	1.40	Abrupt stall with satisfactory progression toward tips			
				↓	↓	50	---	↓	---	---	---	---	---		5.4	1.52	
															7.8	1.55	
															3.3	2.10	
															5.2	2.19	
5.8	2.21																
7.0	2.23																

VI			Sections: Root: NACA 66(215)-(1.8) (15.5), $\alpha=0.6$ Tip: NACA 66(215)-(1.8)12, $\alpha=0.6$ $A=5.82$ $\lambda=0.46$ Geometric washout, $2.5^\circ$	Plain ↓	None ↓	0 50	25 ↓	60 ↓	$3.3 \times 10^6$ 5.3 6.0 3.3 5.1 5.8	1.34 1.39 1.39 1.87 1.91 1.92	Abrupt stall with satisfactory progression toward tips			
VII			Sections: Root: Mod. NACA 65, 3-318, $\alpha=0.8$ Tip: Mod. NACA 65(318)-316, $\alpha=0.8$ $A=8.09$ $\lambda=0.5$ Geometric washout, $0.0^\circ$	Double slotted ↓	Double slotted ↓	0 55	0 30	25 ↓	25 ↓	50 ↓	48 ↓	$5.1 \times 10^6$ 5.1	1.33 2.85	Satisfactory
VIII			Sections: Root: NACA 67(115)-116 Tip: NACA 67, 1-115 $A=6.7$ $\lambda=0.4$ Geometric washout, $2.0^\circ$	Zap ↓ Split ↓	Zap ↓ None Split	0 48 60	0 48 60	35 ↓	35 ↓	60 ↓	38 ↓	$2.4 \times 10^6$ 2.4 2.4 2.5 2.5	1.32 2.25 2.77 1.91 2.22	No data
IX			Sections: Root: NACA 64(215)-418 Tip: NACA 66, 2x-415 $A=8.92$ $\lambda=0.33$ Geometric washout, $1.0^\circ$	None Split	None ↓	55	20	60	$3.5 \times 10^6$ 3.6	1.38 1.97	Satisfactory			
X			Sections: Root: NACA 64(215)-418 Tip: NACA 66, 2x-415 $A=8.92$ $\lambda=0.33$ Geometric washout, $1.0^\circ$	None Split ↓	None Split	55 ↓	55 ↓	20 ↓	60 ↓	30	$3.5 \times 10^6$ 3.6 3.5	1.42 1.87 2.11	Satisfactory	
XI			Sections: Root: NACA 64(215)-418 Tip: NACA 66, 2x-415 $A=8.92$ $\lambda=0.33$ Geometric washout, $1.0^\circ$	None Split	None ↓	55	20	60	$4.0 \times 10^6$ 4.1	1.47 1.95	Satisfactory			
XII			Sections: Root: NACA 63(420)-418, $\alpha=1.0$ Tip: NACA 65, 415, $\alpha=1.0$ $A=7.77$ $\lambda=0.50$ Geometric washout, $2.8^\circ$	Extensible slotted ↓ Split	None ↓	0 35 60	25 ↓	70 ↓	$3.1 \times 10^6$ 4.1 4.8 3.1 4.0 4.9 3.1 4.1 4.8	$\pm 1.37$ $\pm 1.42$ $\pm 1.45$ $\pm 2.19$ $\pm 2.20$ $\pm 2.21$ $\pm 2.00$ $\pm 2.06$ $\pm 2.06$	Satisfactory			

• Propellers windmilling.

TABLE II.—MAXIMUM LIFT AND STALLING CHARACTERISTICS OF MODELS TESTED IN THE NACA 19-FOOT PRESSURE TUNNEL—Concluded

Model	Configuration		Geometric characteristics	Flap		Flap angle (deg)		Flap chord (percent c)		Flap span (percent b)		R	$CL_{max}$	Stalling characteristics
	Plan view	Front view		Inboard	Outboard	$\delta_{fi}$	$\delta_{fo}$	$c_{fi}$	$c_{fo}$	$b_{fi}$	$b_{fo}$			
XIII			Sections: Root: NACA 66(215)-016 Tip: NACA 66(215)-016 $A=5.34$ $\lambda=0.68$ Geometric washout, $0.0^\circ$	None	None							2.4×10 <sup>6</sup>	1.21	Satisfactory
				Split	↓	60	↓	20	↓	65	↓	2.4	1.76	
				Extensible trailing edge	↓	45	↓					2.5	1.72	
				↓	Split	↓	60	↓	20	↓	30	2.4	1.86	
				Split	↓	60	↓					3.6	1.96	
XIV			Sections: Root: NACA 65(318)-1(18.5) Tip: NACA 66(215)-216 $A=5.52$ $\lambda=0.48$ Geometric washout, $3.0^\circ$	Extensible slotted	None	0		20		60		3.6×10 <sup>6</sup>	1.32	Abrupt stall with satisfactory progression toward tips
				↓		35					3.6	2.27		
				Slotted	↓	50					5.2	2.34		
				↓	Split	↓	50				6.3	2.37		
												3.5	2.04	
XV			Sections: Root: NACA 23015.6 Tip: NACA 23009 $A=5.5$ $\lambda=0.52$ Geometric washout, $0.0^\circ$	Slotted	None	0		20		60		3.4×10 <sup>6</sup>	1.55	Very abrupt stall, left wing stalling very rapidly, for all conditions
				↓		50					4.8	1.58		
												5.6	1.60	
												3.4	2.46	
												4.8	2.50	
XVI			Sections: Root: NACA 66,2-118 Tip: NACA 66(2x15)-116 $A=8.9$ Geometric washout, $2.0^\circ$	Extensible slotted	None	0		24		50		3.0×10 <sup>6</sup>	1.34	Extremely abrupt stall, left wing stalls first for the extensible slotted flap, satisfactory for split flap
				↓		38					4.1	1.47		
												5.0	1.50	
												2.9	2.01	
												4.0	2.15	
XVII			Sections: Root: NACA 65 (216)-215, $a=0.8$ Tip: NACA 65(216)-215, $a=0.5$ $A=9.08$ $\lambda=0.45$ Geometric washout, $1.0^\circ$ 0.2 chord line straight	Double slotted	Double slotted	0	0	25	25	65	31	3.6×10 <sup>6</sup>	1.38	Satisfactory
				↓	↓	55	↓	25	↓	↓	3.1	2.45		
												2.8	2.69	
XVIII			Sections: Root: NACA 65 (216)-215, $a=0.8$ Tip: NACA 65(216)-215, $a=0.5$ $A=9.08$ $\lambda=0.45$ Geometric washout, $1.0^\circ$ -0.10 chord line straight	Double slotted	Double slotted	0	0	25	25	65	31	3.6×10 <sup>6</sup>	1.37	Satisfactory
				↓	↓	55	↓	25	↓	↓	3.1	2.44		
												2.8	2.76	

XIX			Sections: Root: NACA 65(216)-215, $\alpha=0.8$ Tip: NACA 65(216)-215, $\alpha=0.5$ $A=9.08$ $\lambda=0.45$ Geometric washout, $1.0^\circ$ 1.1 chord line straight	Double slotted ↓	Double slotted ↓	0 55 ↓	0 25 ↓	25 ↓	25 ↓	65 ↓	31 ↓	$3.6 \times 10^6$ 3.1 2.8	1.45 2.57 2.86	Unsatisfactory, severe tip stall for all conditions except full-span flap
XX			Sections: Root: NACA 65(216)-215, $\alpha=0.8$ Tip: NACA 65(216)-215, $\alpha=0.5$ $A=9.08$ $\lambda=0.45$ Geometric washout, $1.0^\circ$ 0.20 chord line straight	Double slotted ↓	Double slotted ↓	0 55 ↓	0 55 ↓	25 ↓	25 ↓	65 ↓	31 ↓	$5.5 \times 10^6$ 5.5 5.5	1.45 2.37 2.65	Satisfactory
XXI			Sections: Root: NACA 66,2-118 Tip: NACA 66(2x15)-116 $A=6.25$ $\lambda=0.35$ Geometric washout, $2.5^\circ$ 0.375 chord line straight	None  Split ↓	None  ↓  Split ↓	45  60 ↓	20  ↓	50  ↓	40  ↓	$2.9 \times 10^6$ 4.0 4.9 3.0 4.0 4.9 3.0 4.3 5.1 5.2	1.23 1.43 1.51 1.80 1.85 1.96 1.90 2.01 2.04 2.43	Satisfactory		
XXII			Sections: Root: NACA 66,2-118 Tip: NACA 66(2x15)-116 $A=6.25$ $\lambda=0.35$ Geometric washout, $2.5^\circ$ 0.375 chord line straight	None  Split ↓	None  ↓	45  45	20  20	50  50		$4.1 \times 10^6$ 4.9 4.1	1.50 1.60 2.02	Satisfactory		
XXIII			Sections: Root: NACA 66,2-118 Tip: NACA 66(2x15)-116 $A=6.25$ $\lambda=0.35$ Geometric washout, $2.5^\circ$ 0.375 chord line swept for- ward $3.5^\circ$	None  Split ↓	None  ↓	45  45	20  20	50  50		$2.9 \times 10^6$ 4.1 4.9 2.9 4.1 5.0	1.38 1.57 1.61 1.83 1.99 2.02	Satisfactory		
XXIV			Sections: Root: NACA 66,2-118 Tip: NACA 66(2x15)-116 $A=6.1$ $\lambda=0.47$ Geometric washout, $2.5^\circ$ 0.375 chord line straight	None  Split ↓	None  ↓	45  45	20  20	50  50		$2.9 \times 10^6$ 4.2 5.0 3.0 4.2 5.1	1.34 1.56 1.63 1.85 1.92 2.01	Satisfactory		
XXV			Sections: Root: NACA 65(223)-221, $\alpha=1.0$ Tip: NACA 66(215)-316, $\alpha=0.6$ $A=12.8$ $\lambda=0.33$ Geometric washout, $0.0^\circ$	Fowler ↓	None ↓	0 40	18 ↓	53 ↓		$1.5 \times 10^6$ 2.2 2.8 1.4 1.9 2.7	1.17 1.27 1.37 2.21 2.23 2.30	Poor, initial stall occurs at tips		

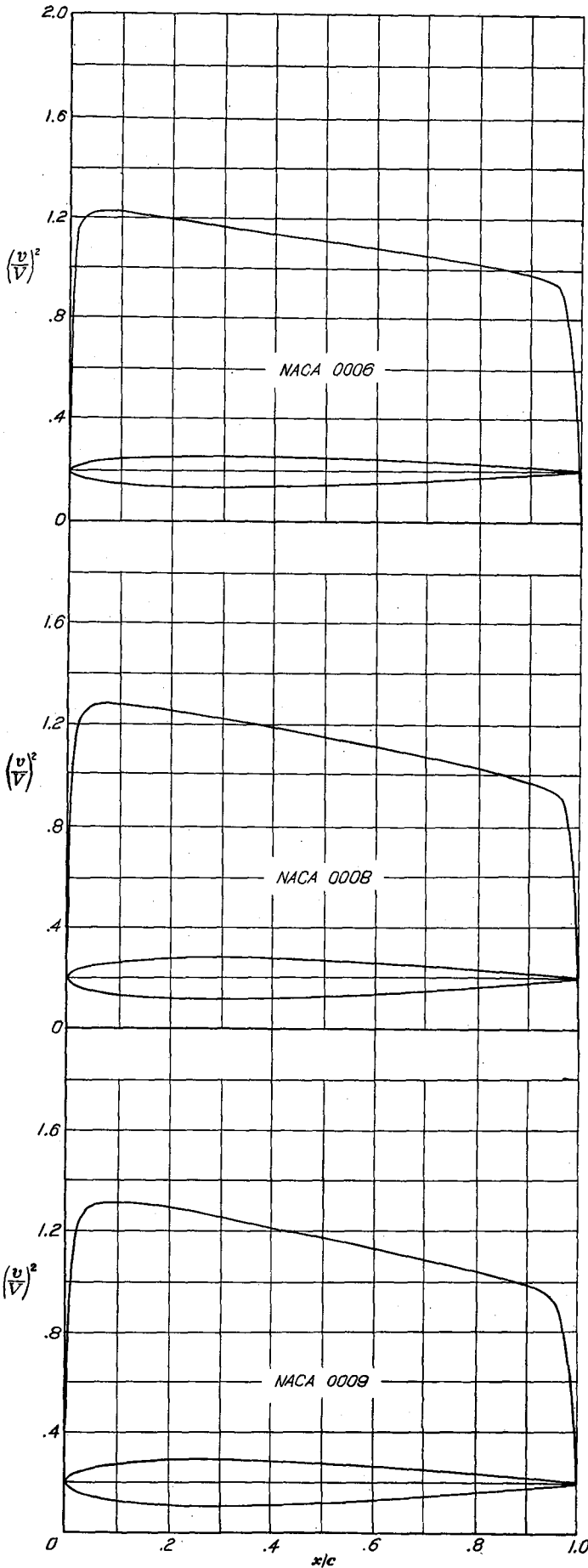
\* Fillets removed.



## SUPPLEMENTARY DATA

## I—BASIC THICKNESS FORMS

	Page		Page
NACA 0006.....	70	NACA 64 <sub>1</sub> -012.....	79
NACA 0008.....	70	NACA 64 <sub>2</sub> -015.....	79
NACA 0009.....	70	NACA 64 <sub>3</sub> -018.....	80
NACA 0010.....	71	NACA 64 <sub>4</sub> -021.....	80
NACA 0012.....	71	NACA 65 <sub>2</sub> -016.....	80
NACA 0015.....	71	NACA 65 <sub>2</sub> -023.....	81
NACA 0018.....	72	NACA 65 <sub>3</sub> -018.....	81
NACA 0021.....	72	NACA 65-006.....	81
NACA 0024.....	72	NACA 65-008.....	82
NACA 16-006.....	73	NACA 65-009.....	82
NACA 16-009.....	73	NACA 65-010.....	82
NACA 16-012.....	73	NACA 65 <sub>1</sub> -012.....	83
NACA 16-015.....	74	NACA 65 <sub>2</sub> -015.....	83
NACA 16-018.....	74	NACA 65 <sub>3</sub> -018.....	83
NACA 16-021.....	74	NACA 65 <sub>4</sub> -021.....	84
NACA 63 <sub>4</sub> -020.....	75	NACA 66 <sub>1</sub> -012.....	84
NACA 63-006.....	75	NACA 66 <sub>2</sub> -015.....	84
NACA 63-009.....	75	NACA 66 <sub>2</sub> -018.....	85
NACA 63-010.....	76	NACA 66-006.....	85
NACA 63 <sub>1</sub> -012.....	76	NACA 66-008.....	85
NACA 63 <sub>2</sub> -015.....	76	NACA 66-009.....	86
NACA 63 <sub>3</sub> -018.....	77	NACA 66-010.....	86
NACA 63 <sub>4</sub> -021.....	77	NACA 66 <sub>1</sub> -012.....	86
NACA 64 <sub>2</sub> -015.....	77	NACA 66 <sub>2</sub> -015.....	87
NACA 64-006.....	78	NACA 66 <sub>3</sub> -018.....	87
NACA 64-008.....	78	NACA 66 <sub>4</sub> -021.....	87
NACA 64-009.....	78	NACA 67 <sub>1</sub> -015.....	88
NACA 64-010.....	79	NACA 747A015.....	88



NACA 0006 BASIC THICKNESS FORM

$x$ (percent $c$ )	$y$ (percent $c$ )	$(v/V)^2$	$v/V$	$\Delta v_a/V$
0	0	0	0	3.992
.5	-----	.880	.938	2.015
1.25	.947	1.117	1.057	1.364
2.5	1.307	1.186	1.089	.984
5.0	1.777	1.217	1.103	.696
7.5	2.100	1.225	1.107	.562
10	2.341	1.212	1.101	.478
15	2.673	1.206	1.098	.378
20	2.869	1.190	1.091	.316
25	2.971	1.179	1.086	.272
30	3.001	1.162	1.078	.239
40	2.902	1.136	1.066	.189
50	2.647	1.109	1.053	.152
60	2.282	1.086	1.042	.123
70	1.832	1.057	1.028	.097
80	1.312	1.026	1.013	.073
90	.724	.980	.990	.047
95	.403	.949	.974	.032
100	.063	0	0	0

L. E. radius: 0.40 percent  $c$

NACA 0008 BASIC THICKNESS FORM

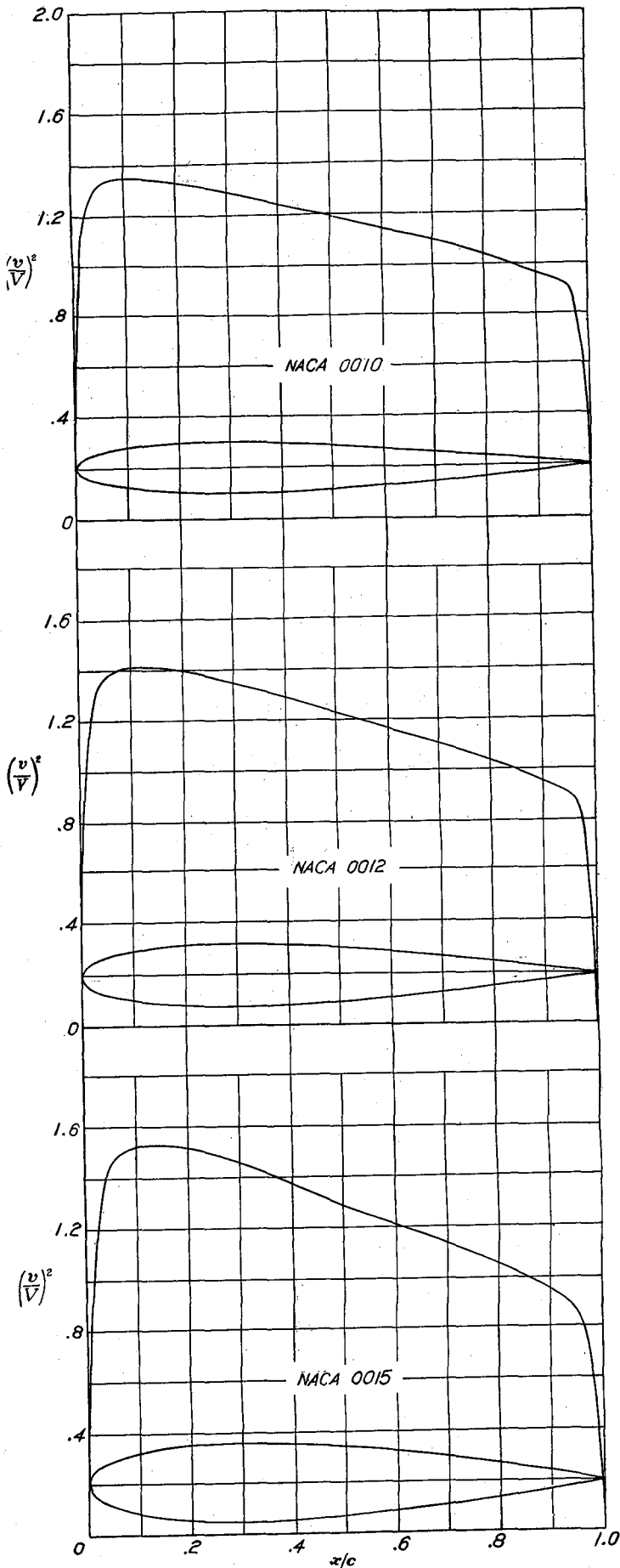
$x$ (percent $c$ )	$y$ (percent $c$ )	$(v/V)^2$	$v/V$	$\Delta v_a/V$
0	0	0	0	2.900
.5	-----	.792	.890	1.795
1.25	1.263	1.103	1.050	1.310
2.5	1.743	1.221	1.105	.971
5.0	2.369	1.272	1.128	.694
7.5	2.800	1.284	1.133	.561
10	3.121	1.277	1.130	.479
15	3.564	1.272	1.128	.379
20	3.825	1.259	1.122	.318
25	3.961	1.241	1.114	.273
30	4.001	1.223	1.106	.239
40	3.869	1.186	1.089	.188
50	3.529	1.149	1.072	.152
60	3.043	1.111	1.054	.121
70	2.443	1.080	1.039	.096
80	1.749	1.034	1.017	.071
90	.965	.968	.984	.047
95	.537	.939	.969	.031
100	.084	-----	-----	0

L. E. radius: 0.70 percent  $c$

NACA 0009 BASIC THICKNESS FORM

$x$ (percent $c$ )	$y$ (percent $c$ )	$(v/V)^2$	$v/V$	$\Delta v_a/V$
0	0	0	0	0.595
.5	-----	.750	.866	1.700
1.25	1.420	1.083	1.041	1.283
2.5	1.961	1.229	1.109	.963
5.0	2.666	1.299	1.140	.692
7.5	3.150	1.310	1.145	.560
10	3.512	1.309	1.144	.479
15	4.009	1.304	1.142	.380
20	4.303	1.293	1.137	.318
25	4.456	1.275	1.129	.273
30	4.501	1.252	1.119	.239
40	4.352	1.209	1.100	.188
50	3.971	1.170	1.082	.151
60	3.423	1.126	1.061	.120
70	2.748	1.087	1.043	.095
80	1.967	1.037	1.018	.070
90	1.086	.984	.982	.046
95	.605	.933	.966	.030
100	.095	0	0	0

L. E. radius: 0.89 percent  $c$



NACA 0010 BASIC THICKNESS FORM

$x$ (percent $c$ )	$y$ (percent $c$ )	$(v/V)^2$	$v/V$	$\Delta v_a/V$
0	0	0	0	2.372
.5	-----	.712	.844	1.618
1.25	1.578	1.061	1.030	1.255
2.5	2.178	1.237	1.112	.955
5.0	2.962	1.325	1.151	.690
7.5	3.500	1.341	1.158	.559
10	3.902	1.341	1.158	.479
15	4.455	1.341	1.158	.380
20	4.782	1.329	1.153	.318
25	4.952	1.309	1.144	.273
30	5.002	1.284	1.133	.239
40	4.837	1.237	1.112	.188
50	4.412	1.190	1.091	.150
60	3.803	1.138	1.067	.119
70	3.053	1.094	1.046	.094
80	2.187	1.040	1.020	.069
90	1.207	.960	.980	.045
95	.672	.925	.962	.030
100	.105	-----	-----	0

L. E. radius: 1.10 percent  $c$

NACA 0012 BASIC THICKNESS FORM

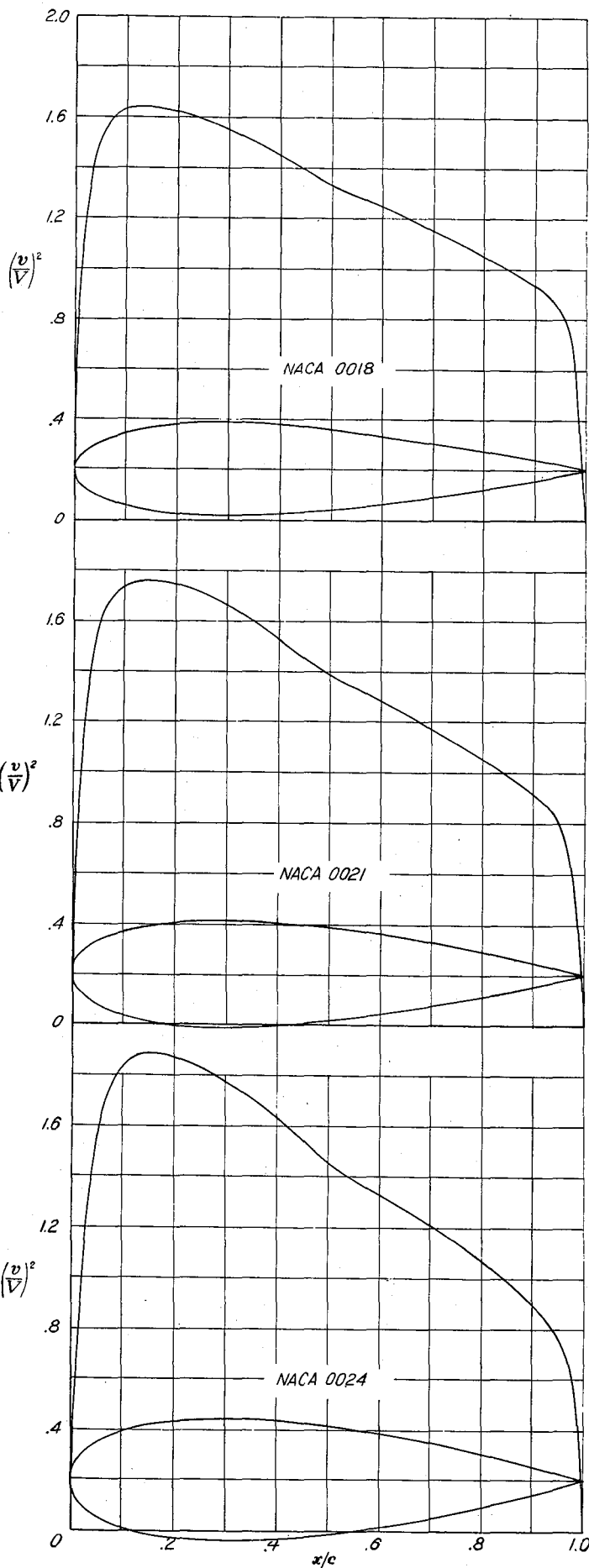
$x$ (percent $c$ )	$y$ (percent $c$ )	$(v/V)^2$	$v/V$	$\Delta v_a/V$
0	0	0	0	1.988
.5	-----	.640	.800	1.475
1.25	1.894	1.010	1.005	1.199
2.5	2.615	1.241	1.114	.934
5.0	3.555	1.378	1.174	.685
7.5	4.200	1.402	1.184	.558
10	4.683	1.411	1.188	.479
15	5.345	1.411	1.188	.381
20	5.737	1.399	1.183	.319
25	5.941	1.378	1.174	.273
30	6.002	1.350	1.162	.239
40	5.803	1.288	1.135	.187
50	5.294	1.228	1.108	.149
60	4.563	1.166	1.080	.118
70	3.664	1.109	1.053	.092
80	2.623	1.044	1.022	.068
90	1.448	.956	.978	.044
95	.807	.906	.952	.029
100	.126	0	0	0

L. E. radius: 1.58 percent  $c$

NACA 0015 BASIC THICKNESS FORM

$x$ (percent $c$ )	$y$ (percent $c$ )	$(v/V)^2$	$v/V$	$\Delta v_a/V$
0	0	0	0	1.600
.5	-----	.546	.739	1.312
1.25	2.367	.933	.966	1.112
2.5	3.268	1.237	1.112	.900
5.0	4.443	1.450	1.204	.675
7.5	5.250	1.498	1.224	.557
10	5.853	1.520	1.233	.479
15	6.682	1.520	1.233	.381
20	7.172	1.510	1.229	.320
25	7.427	1.484	1.218	.274
30	7.502	1.450	1.204	.239
40	7.254	1.369	1.170	.185
50	6.617	1.279	1.131	.146
60	5.704	1.206	1.098	.115
70	4.580	1.132	1.064	.090
80	3.279	1.049	1.024	.065
90	1.810	.945	.972	.041
95	1.008	.872	.934	.027
100	.158	0	0	0

L. E. radius: 2.48 percent  $c$



NACA 0018 BASIC THICKNESS FORM

$x$ (percent $c$ )	$y$ (percent $c$ )	$(v/V)^2$	$v/V$	$\Delta v_a/V$
0	0	0	0	1.342
.5	-----	.465	.682	1.178
1.25	2.841	.857	.926	1.028
2.5	3.922	1.217	1.103	.861
5.0	5.332	1.507	1.228	.662
7.5	6.300	1.598	1.264	.555
10	7.024	1.628	1.276	.479
15	8.018	1.633	1.278	.381
20	8.606	1.625	1.275	.320
25	8.912	1.592	1.262	.274
30	9.003	1.556	1.247	.238
40	8.705	1.453	1.205	.184
50	7.941	1.331	1.154	.144
60	6.845	1.246	1.116	.113
70	5.496	1.153	1.074	.087
80	3.935	1.051	1.025	.063
90	2.172	.933	.966	.039
95	1.210	.836	.914	.025
100	.189	0	0	0

L. E. radius: 3.56 percent  $c$

NACA 0021 BASIC THICKNESS FORM

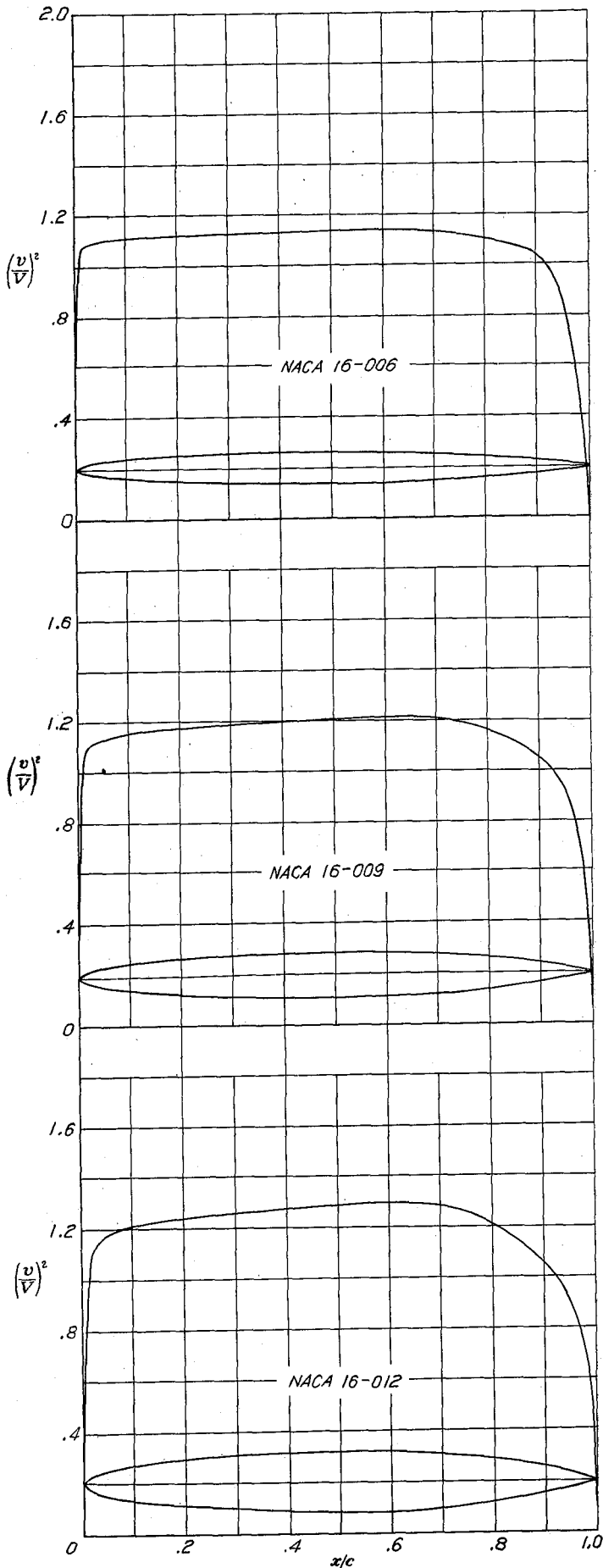
$x$ (percent $c$ )	$y$ (percent $c$ )	$(v/V)^2$	$v/V$	$\Delta v_a/V$
0	0	0	0	1.167
.5	-----	.397	.630	1.065
1.25	3.315	.787	.887	.946
2.5	4.576	1.182	1.087	.818
5	6.221	1.543	1.242	.648
7.5	7.350	1.682	1.297	.550
10	8.195	1.734	1.317	.478
15	9.354	1.756	1.325	.381
20	10.040	1.742	1.320	.320
25	10.397	1.706	1.306	.274
30	10.504	1.664	1.290	.238
40	10.156	1.538	1.240	.183
50	9.265	1.388	1.178	.142
60	7.986	1.284	1.133	.111
70	6.412	1.177	1.085	.084
80	4.591	1.055	1.027	.061
90	2.534	.916	.957	.037
95	1.412	.801	.895	.023
100	.221	0	0	0

L. E. radius: 4.85 percent  $c$

NACA 0024 BASIC THICKNESS FORM

$x$ (percent $c$ )	$y$ (percent $c$ )	$(v/V)^2$	$v/V$	$\Delta v_a/V$
0	0	0	0	1.050
.5	-----	.335	.579	.964
1.25	3.788	.719	.848	.870
2.5	5.229	1.130	1.063	.771
5.0	7.109	1.548	1.244	.632
7.5	8.400	1.748	1.322	.542
10	9.365	1.833	1.354	.476
15	10.691	1.888	1.374	.383
20	11.475	1.871	1.368	.321
25	11.883	1.822	1.350	.274
30	12.004	1.777	1.333	.238
40	11.607	1.631	1.277	.181
50	10.588	1.450	1.204	.140
60	9.127	1.325	1.151	.109
70	7.328	1.203	1.097	.082
80	5.247	1.065	1.032	.059
90	2.896	.891	.944	.035
95	1.613	.773	.879	.022
100	.252	0	0	0

L. E. radius: 6.33 percent  $c$



NACA 16-006 BASIC THICKNESS FORM

$x$ (percent $c$ )	$y$ (percent $c$ )	$(v/V)^2$	$v/V$	$\Delta v_a/V$
0	0	0	0	5.471
1.25	.646	1.059	1.029	1.376
2.5	.903	1.085	1.042	.980
5.0	1.255	1.097	1.047	.689
7.5	1.516	1.105	1.051	.587
10	1.729	1.108	1.053	.476
15	2.067	1.112	1.055	.379
20	2.332	1.116	1.057	.319
30	2.709	1.123	1.060	.244
40	2.927	1.132	1.064	.196
50	3.000	1.137	1.066	.160
60	2.917	1.141	1.068	.130
70	2.635	1.132	1.064	.104
80	2.099	1.104	1.051	.077
90	1.259	1.035	1.017	.049
95	.707	.962	.981	.032
100	.060	0	0	0

L. E. radius: 0.176 percent  $c$

NACA 16-009 BASIC THICKNESS FORM

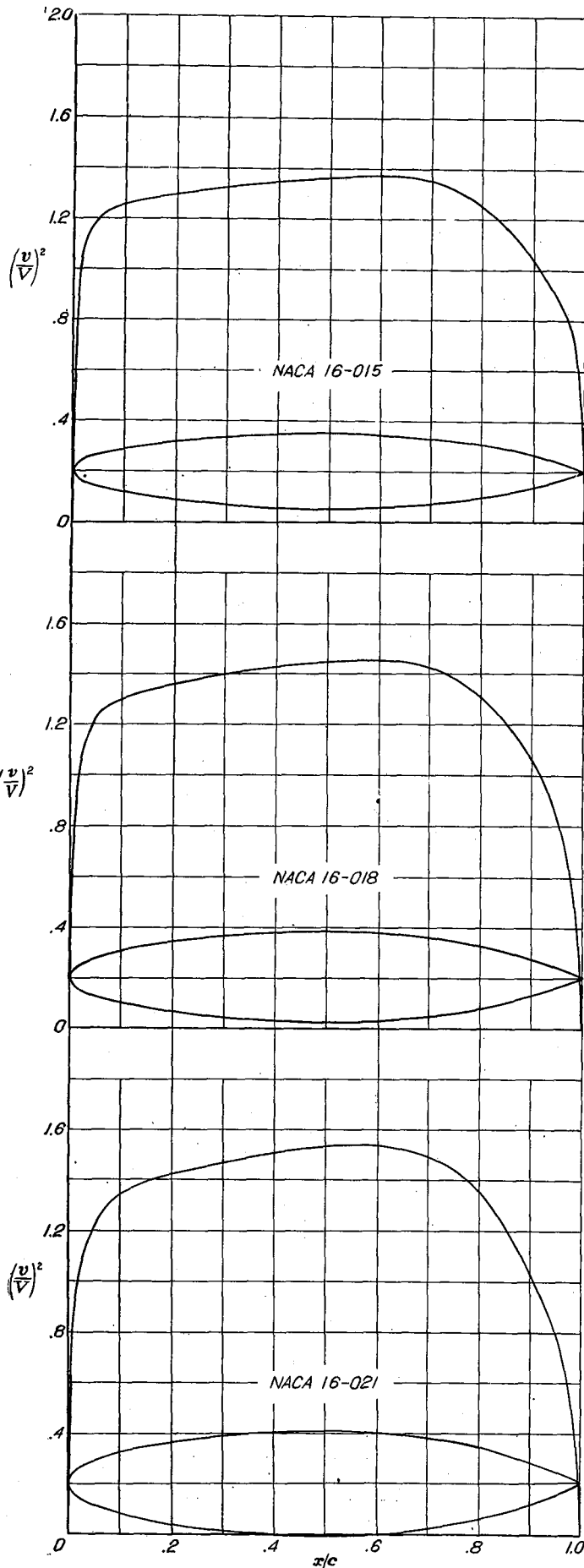
$x$ (percent $c$ )	$y$ (percent $c$ )	$(v/V)^2$	$v/V$	$\Delta v_a/V$
0	0	0	0	3.644
1.25	.969	1.042	1.021	1.330
2.5	1.354	1.109	1.053	.964
5.0	1.882	1.139	1.067	.684
7.5	2.274	1.152	1.073	.554
10	2.593	1.158	1.076	.475
15	3.101	1.168	1.081	.378
20	3.498	1.177	1.085	.319
30	4.063	1.190	1.091	.245
40	4.391	1.202	1.096	.197
50	4.500	1.211	1.100	.160
60	4.376	1.214	1.106	.131
70	3.952	1.206	1.099	.103
80	3.149	1.156	1.075	.076
90	1.888	1.043	1.022	.047
95	1.061	.939	.969	.030
100	.090	0	0	0

L. E. radius: 0.396 percent  $c$

NACA 16-012 BASIC THICKNESS FORM

$x$ (percent $c$ )	$y$ (percent $c$ )	$(v/V)^2$	$v/V$	$\Delta v_a/V$
0	0	0	0	2.624
1.25	1.292	1.002	1.001	1.268
2.5	1.805	1.109	1.053	.942
5.0	2.509	1.173	1.083	.677
7.5	3.032	1.197	1.094	.551
10	3.457	1.208	1.099	.478
15	4.135	1.223	1.106	.378
20	4.664	1.237	1.112	.319
30	5.417	1.257	1.121	.245
40	5.855	1.271	1.128	.197
50	6.000	1.286	1.134	.161
60	5.835	1.293	1.137	.131
70	5.269	1.275	1.129	.102
80	4.199	1.203	1.097	.075
90	2.517	1.051	1.025	.045
95	1.415	.908	.953	.027
100	.120	0	0	0

L. E. radius: 0.703 percent  $c$



NACA 16-015 BASIC THICKNESS FORM

$x$ (percent $c$ )	$y$ (percent $c$ )	$(v/V)^2$	$v/V$	$\Delta v_a/V$
0	0	0	0	2.041
1.25	1.615	.956	.978	1.209
2.5	2.257	1.105	1.051	.916
5.0	3.137	1.200	1.095	.668
7.5	3.790	1.239	1.113	.471
10	4.322	1.256	1.121	.377
15	5.168	1.278	1.130	.318
20	5.830	1.297	1.139	.245
30	6.772	1.327	1.152	.197
40	7.318	1.340	1.161	.161
50	7.500	1.364	1.168	.131
60	7.293	1.374	1.172	.102
70	6.587	1.348	1.161	.074
80	5.243	1.254	1.120	.043
90	3.147	1.053	1.026	.025
95	1.768	.875	.935	0
100	.150	0	0	0

L. E. radius: 1.100 percent  $c$

NACA 16-018 BASIC THICKNESS FORM

$x$ (percent $c$ )	$y$ (percent $c$ )	$(v/V)^2$	$v/V$	$\Delta v_a/V$
0	0	0	0	1.744
1.25	1.938	.903	.950	1.140
2.5	2.708	1.092	1.045	.883
5.0	3.764	1.217	1.103	.657
7.5	4.548	1.271	1.128	.541
10	5.186	1.302	1.141	.468
15	6.202	1.322	1.154	.376
20	6.996	1.337	1.165	.318
30	8.126	1.359	1.183	.245
40	8.782	1.426	1.194	.198
50	9.000	1.447	1.203	.162
60	8.752	1.452	1.205	.131
70	7.904	1.421	1.192	.102
80	6.298	1.306	1.143	.073
90	3.776	1.051	1.025	.042
95	2.122	.837	.915	.024
100	.180	0	0	0

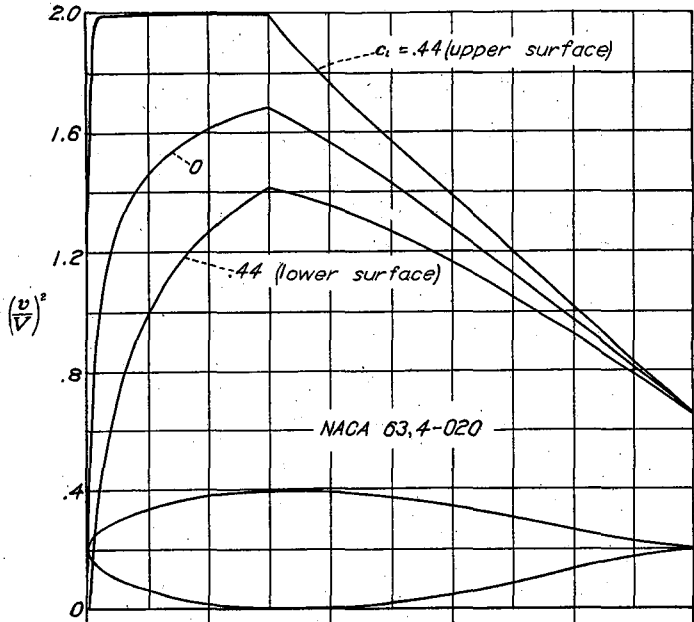
L. E. radius: 1.584 percent  $c$

NACA 16-021 BASIC THICKNESS FORM

$x$ (percent $c$ )	$y$ (percent $c$ )	$(v/V)^2$	$v/V$	$\Delta v_a/V$
0	0	0	0	1.574
1.25	2.261	.826	.909	1.069
2.5	3.159	1.062	1.031	.828
5.0	4.391	1.221	1.105	.640
7.5	5.306	1.295	1.138	.534
10	6.050	1.342	1.159	.463
15	7.236	1.391	1.179	.374
20	8.162	1.419	1.191	.317
30	9.480	1.474	1.214	.245
40	10.246	1.506	1.227	.198
50	10.500	1.535	1.239	.162
60	10.211	1.536	1.239	.131
70	9.221	1.495	1.223	.102
80	7.348	1.361	1.166	.072
90	4.405	1.039	1.019	.041
95	2.476	.801	.895	.023
100	.210	0	0	0

L. E. radius: 2.156 percent  $c$

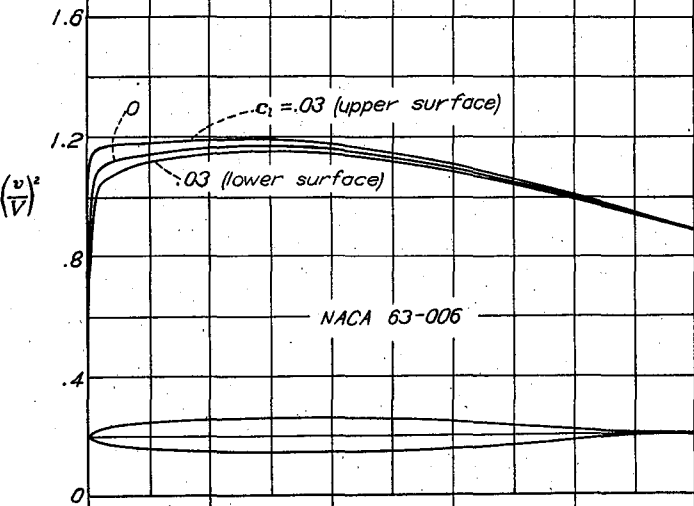
NACA 63,4-020 BASIC THICKNESS FORM



x (percent c)	y (percent c)	(v/V) <sup>2</sup>	v/V	Δv <sub>a</sub> /V
0	0	0	0	1.395
.5	1.714	.444	.666	1.280
.75	2.081	.605	.778	1.201
1.25	2.638	.820	.906	1.072
2.5	3.606	1.080	1.039	.846
5.0	4.947	1.277	1.130	.645
7.5	5.964	1.383	1.176	.543
10	6.800	1.456	1.207	.475
15	8.090	1.551	1.245	.386
20	9.006	1.614	1.270	.350
25	9.630	1.659	1.288	.289
30	9.955	1.689	1.300	.257
35	9.978	1.630	1.277	.219
40	9.765	1.567	1.252	.192
45	9.366	1.500	1.225	.168
50	8.819	1.433	1.197	.148
55	8.143	1.362	1.167	.128
60	7.351	1.288	1.135	.112
65	6.464	1.213	1.101	.097
70	5.496	1.137	1.066	.084
75	4.466	1.059	1.029	.071
80	3.401	.978	.989	.059
85	2.342	.896	.947	.046
90	1.348	.811	.901	.036
95	.501	.728	.853	.023
100	0	.651	.807	0

L. E. radius: 3.16 percent c

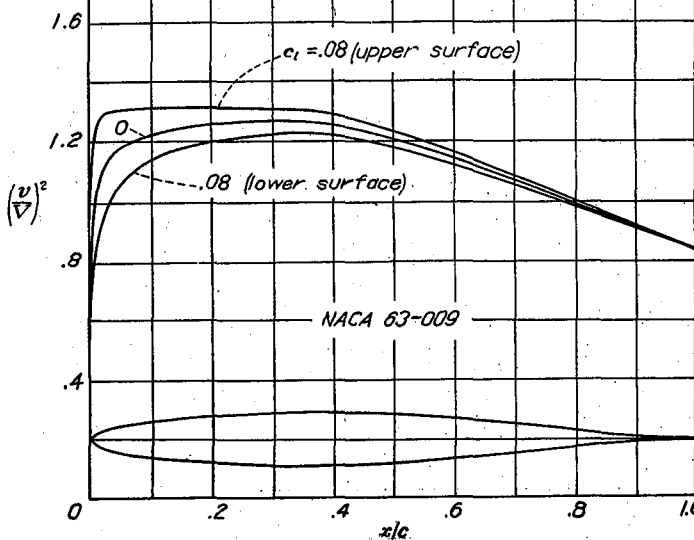
NACA 63-006 BASIC THICKNESS FORM



x (percent c)	y (percent c)	(v/V) <sup>2</sup>	v/V	Δv <sub>a</sub> /V
0	0	0	0	4.483
.5	.503	.973	.986	2.110
.75	.609	1.050	1.025	1.778
1.25	.771	1.080	1.039	1.399
2.5	1.057	1.110	1.054	.981
5	1.462	1.130	1.063	.692
7.5	1.706	1.142	1.069	.562
10	2.010	1.149	1.072	.484
15	2.386	1.159	1.077	.384
20	2.656	1.165	1.079	.321
25	2.841	1.170	1.082	.279
30	2.954	1.174	1.084	.245
35	3.000	1.170	1.082	.218
40	2.971	1.164	1.079	.196
45	2.877	1.151	1.073	.176
50	2.723	1.137	1.066	.158
55	2.517	1.118	1.057	.141
60	2.267	1.096	1.047	.125
65	1.982	1.074	1.036	.111
70	1.670	1.046	1.023	.098
75	1.342	1.020	1.010	.085
80	1.008	.994	.997	.073
85	.683	.965	.982	.060
90	.383	.936	.967	.047
95	.138	.910	.954	.032
100	0	.886	.941	0

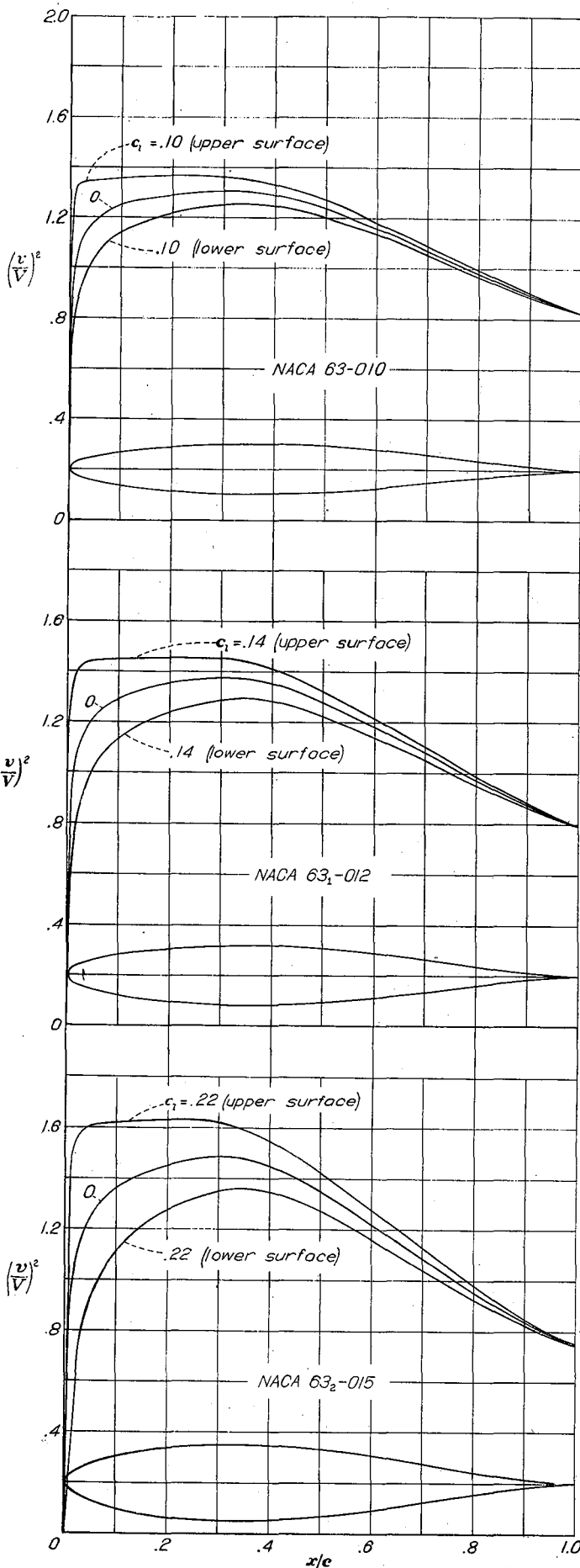
L. E. radius: 0.297 percent c

NACA 63-009 BASIC THICKNESS FORM



x (percent c)	y (percent c)	(v/V) <sup>2</sup>	v/V	Δv <sub>a</sub> /V
0	0	0	0	3.058
.5	.740	.885	.941	1.889
.75	.906	1.002	1.001	1.647
1.25	1.151	1.051	1.025	1.339
2.5	1.682	1.130	1.063	.961
5	2.196	1.180	1.086	.689
7.5	2.655	1.205	1.098	.560
10	3.024	1.221	1.105	.484
15	3.591	1.241	1.114	.386
20	3.997	1.255	1.120	.324
25	4.275	1.264	1.124	.281
30	4.442	1.269	1.126	.248
35	4.500	1.265	1.125	.220
40	4.447	1.255	1.120	.196
45	4.296	1.235	1.111	.175
50	4.056	1.208	1.099	.156
55	3.739	1.175	1.084	.140
60	3.358	1.141	1.068	.124
65	2.928	1.104	1.051	.109
70	2.458	1.065	1.032	.095
75	1.966	1.025	1.012	.082
80	1.471	.984	.992	.069
85	.990	.942	.971	.057
90	.550	.903	.950	.044
95	.196	.868	.932	.030
100	0	.838	.915	0

L. E. radius: 0.631 percent c



NACA 63-010 BASIC THICKNESS FORM

$x$ (percent $c$ )	$y$ (percent $c$ )	$(v/V)^2$	$v/V$	$\Delta v_a/V$
0	0	0	0	2.775
.5	.829	.841	.917	1.825
.75	1.004	.978	.989	1.603
1.25	1.275	1.037	1.018	1.316
2.5	1.756	1.131	1.063	.952
5.0	2.440	1.193	1.092	.687
7.5	2.950	1.223	1.106	.560
10	3.362	1.245	1.116	.484
15	3.994	1.270	1.127	.386
20	4.445	1.285	1.134	.325
25	4.753	1.296	1.138	.282
30	4.938	1.302	1.141	.248
35	5.000	1.299	1.140	.220
40	4.938	1.286	1.134	.196
45	4.766	1.262	1.123	.175
50	4.496	1.231	1.110	.156
55	4.140	1.193	1.092	.139
60	3.715	1.154	1.074	.123
65	3.234	1.113	1.055	.108
70	2.712	1.069	1.034	.094
75	2.166	1.025	1.012	.081
80	1.618	.979	.989	.069
85	1.088	.935	.967	.056
90	.604	.893	.945	.043
95	.214	.853	.924	.030
100	0	.822	.907	0

L. E. radius: 0.770 percent  $c$

NACA 63<sub>1</sub>-012 BASIC THICKNESS FORM

$x$ (percent $c$ )	$y$ (percent $c$ )	$(v/V)^2$	$v/V$	$\Delta v_a/V$
0	0	0	0	2.336
.5	.985	.750	.866	1.695
.75	1.194	.925	.962	1.513
1.25	1.519	1.005	1.003	1.263
2.5	2.102	1.129	1.063	.933
5	2.925	1.217	1.103	.682
7.5	3.542	1.261	1.123	.559
10	4.039	1.294	1.138	.484
15	4.799	1.330	1.153	.387
20	5.342	1.349	1.161	.326
25	5.712	1.362	1.167	.283
30	5.930	1.370	1.170	.249
35	6.000	1.366	1.169	.221
40	5.920	1.348	1.161	.196
45	5.704	1.317	1.148	.174
50	5.370	1.276	1.130	.155
55	4.935	1.229	1.109	.137
60	4.420	1.181	1.087	.121
65	3.840	1.131	1.063	.106
70	3.210	1.076	1.037	.091
75	2.556	1.023	1.011	.079
80	1.902	.969	.984	.067
85	1.274	.920	.959	.055
90	.707	.871	.933	.042
95	.250	.826	.909	.029
100	0	.791	.889	0

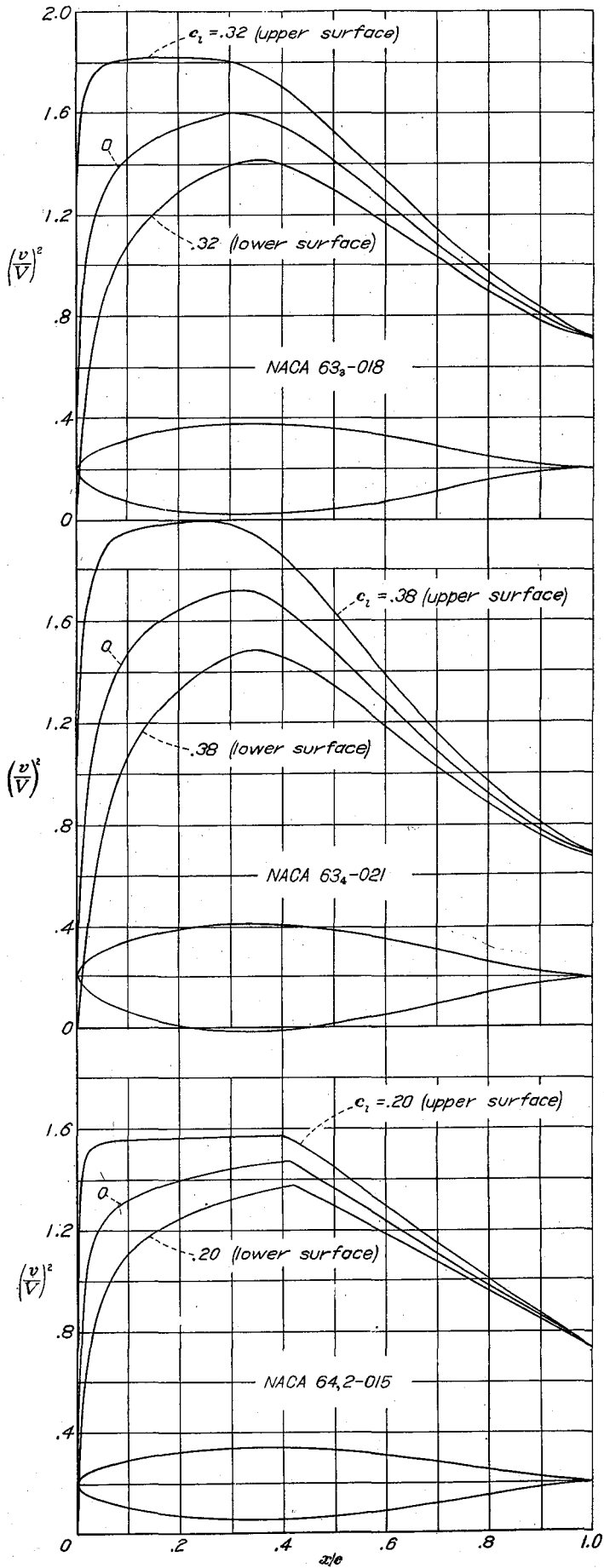
L. E. radius: 1.087 percent  $c$

NACA 63<sub>2</sub>-015 BASIC THICKNESS FORM

$x$ (percent $c$ )	$y$ (percent $c$ )	$(v/V)^2$	$v/V$	$\Delta v_a/V$
0	0	0	0	1.918
.5	1.204	.600	.775	1.513
.75	1.462	.822	.907	1.370
1.25	1.878	.938	.969	1.182
2.5	2.610	1.105	1.051	.903
5	3.648	1.244	1.115	.674
7.5	4.427	1.345	1.147	.557
10	5.055	1.390	1.166	.484
15	6.011	1.415	1.190	.388
20	6.693	1.446	1.202	.330
25	7.155	1.467	1.211	.286
30	7.421	1.481	1.217	.251
35	7.560	1.475	1.214	.222
40	7.386	1.446	1.202	.196
45	7.095	1.401	1.184	.174
50	6.665	1.345	1.160	.153
55	6.108	1.281	1.132	.135
60	5.453	1.220	1.105	.118
65	4.721	1.155	1.075	.102
70	3.934	1.085	1.042	.088
75	3.119	1.019	1.009	.076
80	2.310	.953	.976	.063
85	1.541	.894	.946	.051
90	.852	.839	.916	.039
95	.300	.789	.888	.028
100	0	.750	.866	0

L. E. radius: 1.594 percent  $c$





NACA 63-018 BASIC THICKNESS FORM

x (percent c)	y (percent c)	(v/V) <sup>2</sup>	v/V	Δv <sub>a</sub> /V
0	0	0	0	1.639
.5	1.404	.441	.664	1.361
.75	1.713	.700	.837	1.258
1.25	2.217	.848	.921	1.105
2.5	3.104	1.065	1.032	.871
5	4.362	1.260	1.122	.663
7.5	5.308	1.360	1.166	.553
10	6.068	1.424	1.193	.484
15	7.225	1.500	1.225	.390
20	8.048	1.547	1.244	.333
25	8.600	1.579	1.257	.289
30	8.913	1.598	1.264	.253
35	9.000	1.585	1.259	.223
40	8.845	1.550	1.245	.197
45	8.482	1.490	1.221	.173
50	7.942	1.411	1.188	.152
55	7.256	1.330	1.153	.133
60	6.455	1.252	1.119	.115
65	5.567	1.170	1.082	.099
70	4.622	1.087	1.043	.084
75	3.650	1.009	1.004	.072
80	2.691	.933	.966	.059
85	1.787	.868	.932	.048
90	.985	.807	.898	.036
95	.348	.753	.868	.024
100	0	.712	.844	0

L. E. radius: 2.120 percent c

NACA 63-021 BASIC THICKNESS FORM

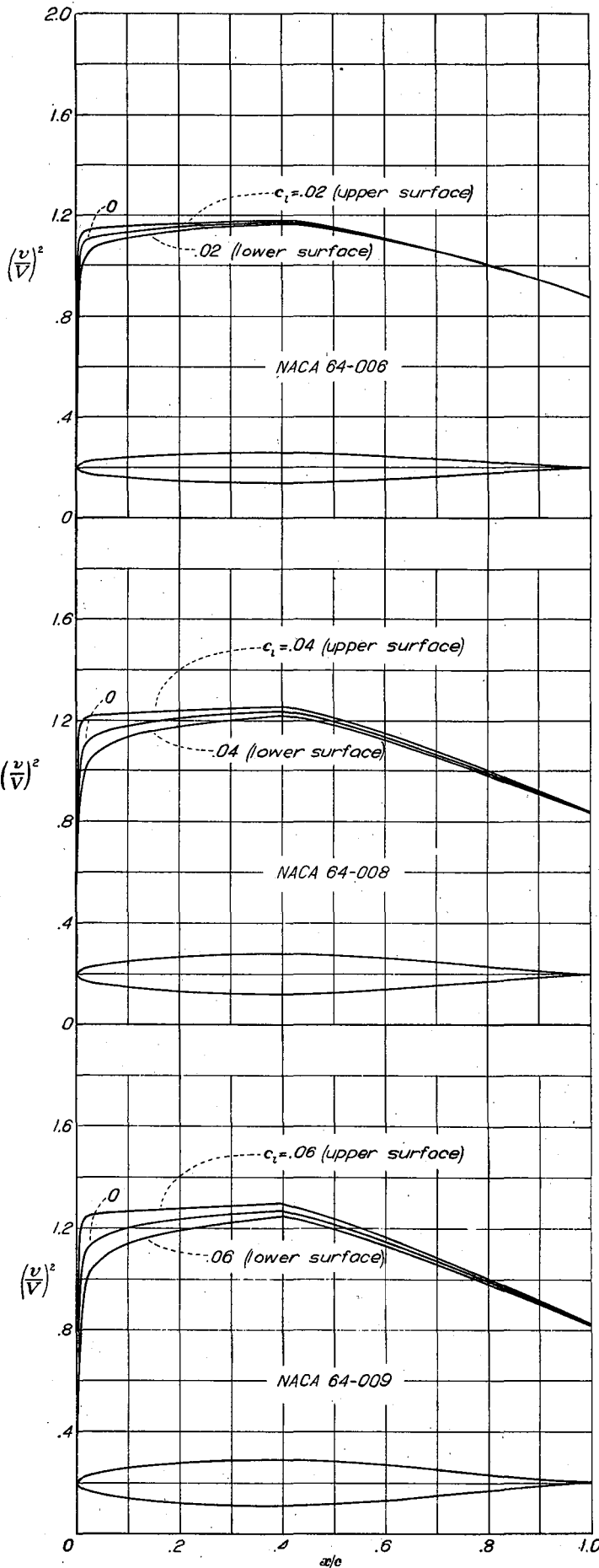
x (percent c)	y (percent c)	(v/V) <sup>2</sup>	v/V	Δv <sub>a</sub> /V
0	0	0	0	1.439
.5	1.583	.275	.524	1.236
.75	1.937	.564	.751	1.156
1.25	2.527	.725	.851	1.034
2.5	3.577	1.010	1.005	.842
5	5.065	1.260	1.122	.653
7.5	6.182	1.394	1.181	.550
10	7.080	1.487	1.219	.484
15	8.441	1.592	1.262	.392
20	9.410	1.655	1.286	.335
25	10.053	1.698	1.303	.291
30	10.412	1.721	1.312	.255
35	10.500	1.709	1.307	.225
40	10.298	1.654	1.286	.198
45	9.854	1.578	1.256	.173
50	9.206	1.479	1.216	.150
55	8.390	1.380	1.175	.130
60	7.441	1.281	1.132	.112
65	6.396	1.180	1.086	.096
70	5.290	1.084	1.041	.081
75	4.160	.994	.997	.068
80	3.054	.911	.954	.057
85	2.021	.839	.916	.046
90	1.113	.774	.880	.035
95	.392	.721	.849	.023
100	0	.676	.822	0

L. E. radius: 2.650 percent c

NACA 64,2-015 BASIC THICKNESS FORM

x (percent c)	y (percent c)	(v/V) <sup>2</sup>	v/V	Δv <sub>a</sub> /V
0	0	0	0	1.930
.5	1.216	.710	.843	1.500
.75	1.453	.825	.908	1.359
1.25	1.829	.962	.981	1.161
2.5	2.538	1.122	1.059	.911
5.0	3.514	1.234	1.111	.678
7.5	4.243	1.288	1.135	.553
10	4.838	1.323	1.150	.477
15	5.781	1.371	1.171	.383
20	6.464	1.401	1.184	.325
25	6.967	1.422	1.192	.285
30	7.307	1.441	1.200	.253
35	7.481	1.458	1.207	.227
40	7.480	1.471	1.213	.202
45	7.268	1.432	1.197	.175
50	6.850	1.366	1.169	.156
55	6.311	1.289	1.140	.137
60	5.670	1.234	1.111	.122
65	4.944	1.188	1.081	.102
70	4.158	1.102	1.050	.086
75	3.338	1.039	1.019	.080
80	2.508	.973	.986	.071
85	1.698	.910	.954	.056
90	.961	.849	.921	.039
95	.351	.791	.889	.027
100	0	.739	.860	0

L. E. radius: 1.65 percent c



NACA 64-006 BASIC THICKNESS FORM

$x$ (percent $c$ )	$y$ (percent $c$ )	$(v/V)^2$	$v/V$	$\Delta v_a/V$
0	0	0	0	4.623
.5	.494	.995	.997	2.175
.75	.596	1.058	1.029	1.780
1.25	.754	1.085	1.042	1.418
2.5	1.024	1.108	1.053	.982
5.0	1.405	1.119	1.058	.692
7.5	1.692	1.128	1.062	.560
10	1.928	1.134	1.065	.483
15	2.298	1.146	1.071	.385
20	2.572	1.154	1.074	.321
25	2.772	1.160	1.077	.279
30	2.907	1.164	1.079	.246
35	2.981	1.168	1.081	.220
40	2.995	1.171	1.082	.198
45	2.919	1.160	1.077	.178
50	2.775	1.143	1.069	.168
55	2.575	1.124	1.060	.142
60	2.331	1.102	1.050	.126
65	2.050	1.079	1.039	.112
70	1.740	1.054	1.027	.098
75	1.412	1.028	1.014	.085
80	1.072	1.000	1.000	.072
85	.737	.970	.985	.060
90	.423	.939	.969	.047
95	.157	.908	.953	.031
100	0	.876	.936	0

L. E. radius: 0.256 percent  $c$

NACA 64-008 BASIC THICKNESS FORM

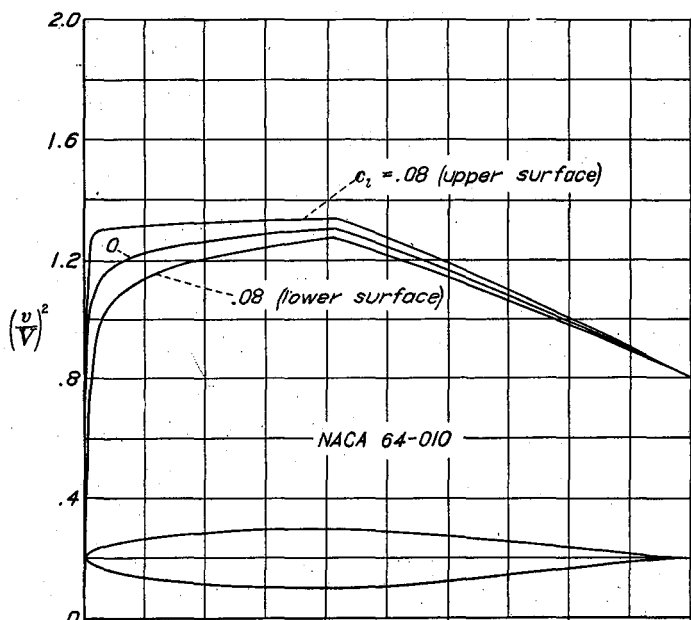
$x$ (percent $c$ )	$y$ (percent $c$ )	$(v/V)^2$	$v/V$	$\Delta v_a/V$
0	0	0	0	3.544
.5	.658	.912	.955	1.994
.75	.794	1.016	1.008	1.686
1.25	1.005	1.084	1.041	1.367
2.5	1.365	1.127	1.062	.969
5.0	1.875	1.152	1.073	.688
7.5	2.259	1.167	1.080	.560
10	2.574	1.179	1.086	.480
15	3.069	1.195	1.093	.385
20	3.437	1.208	1.099	.323
25	3.704	1.217	1.103	.279
30	3.884	1.225	1.107	.246
35	3.979	1.230	1.109	.220
40	3.992	1.235	1.111	.198
45	3.883	1.220	1.105	.176
50	3.684	1.191	1.091	.158
55	3.411	1.163	1.078	.141
60	3.081	1.133	1.064	.125
65	2.704	1.102	1.050	.110
70	2.291	1.069	1.034	.096
75	1.854	1.033	1.016	.083
80	1.404	.995	.997	.071
85	.961	.957	.978	.059
90	.550	.918	.958	.046
95	.206	.878	.937	.031
100	0	.839	.916	0

L. E. radius: 0.455 percent  $c$

NACA 64-009 BASIC THICKNESS FORM

$x$ (percent $c$ )	$y$ (percent $c$ )	$(v/V)^2$	$v/V$	$\Delta v_a/V$
0	0	0	0	3.130
.5	.739	.872	.934	1.905
.75	.892	.990	.995	1.637
1.25	1.128	1.075	1.037	1.340
2.5	1.533	1.131	1.063	.963
5.0	2.109	1.166	1.080	.686
7.5	2.543	1.186	1.089	.560
10	2.898	1.200	1.095	.479
15	3.455	1.221	1.105	.383
20	3.868	1.236	1.112	.323
25	4.170	1.246	1.116	.281
30	4.373	1.255	1.120	.248
35	4.479	1.262	1.123	.221
40	4.490	1.267	1.126	.198
45	4.364	1.246	1.116	.176
50	4.136	1.217	1.103	.158
55	3.826	1.183	1.088	.140
60	3.452	1.149	1.072	.125
65	3.026	1.112	1.055	.109
70	2.561	1.073	1.036	.095
75	2.069	1.033	1.016	.082
80	1.564	.992	.996	.070
85	1.069	.950	.975	.057
90	.611	.907	.952	.044
95	.227	.865	.930	.030
100	0	.822	.907	0

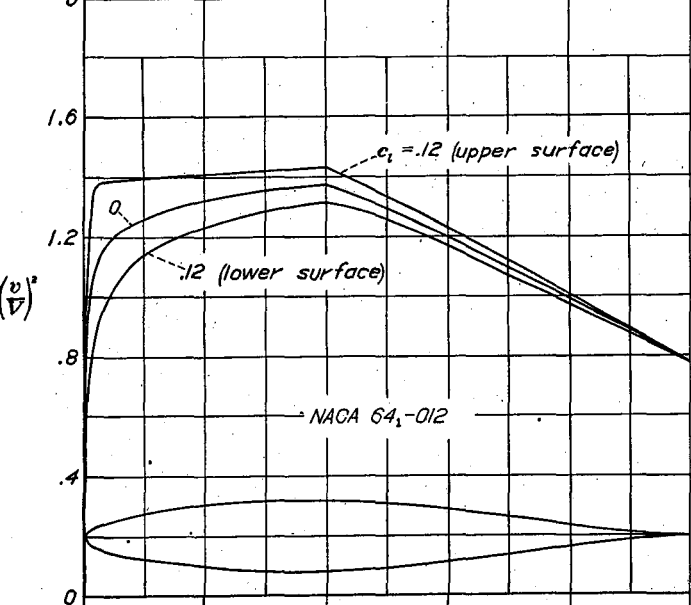
L. E. radius: 0.579 percent  $c$



NACA 64-010 BASIC THICKNESS FORM

$x$ (percent $c$ )	$y$ (percent $c$ )	$(v/V)^2$	$v/V$	$\Delta v_a/V$
0	0	0	0	2.815
.5	.820	.834	.913	1.817
.75	.989	.962	.981	1.886
1.25	1.250	1.061	1.030	1.813
2.5	1.701	1.130	1.063	.967
5	2.343	1.181	1.087	.684
7.5	2.826	1.206	1.098	.559
10	3.221	1.221	1.105	.480
15	3.842	1.245	1.116	.386
20	4.302	1.262	1.123	.325
25	4.639	1.275	1.129	.280
30	4.864	1.286	1.134	.246
35	4.980	1.295	1.138	.220
40	4.988	1.300	1.140	.199
45	4.843	1.279	1.131	.176
50	4.586	1.241	1.114	.158
55	4.238	1.201	1.096	.139
60	3.820	1.161	1.077	.124
65	3.345	1.120	1.058	.109
70	2.827	1.080	1.039	.095
75	2.281	1.036	1.018	.081
80	1.722	.990	.995	.069
85	1.176	.944	.972	.057
90	.671	.900	.949	.044
95	.248	.850	.922	.030
100	0	.805	.897	0

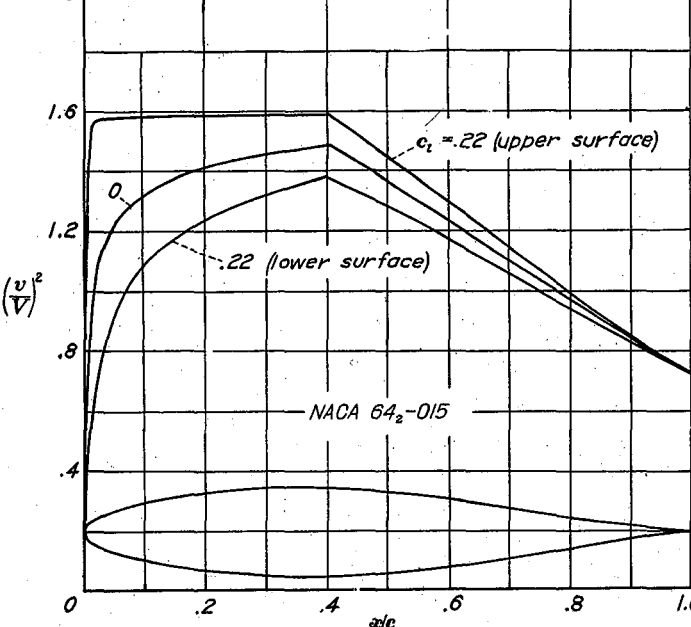
L. E. radius: 0.720 percent  $c$



NACA 64-012 BASIC THICKNESS FORM

$x$ (percent $c$ )	$y$ (percent $c$ )	$(v/V)^2$	$v/V$	$\Delta v_a/V$
0	0	0	0	2.379
.5	.978	.750	.866	1.663
.75	1.179	.885	.941	1.508
1.25	1.490	1.020	1.010	1.271
2.5	2.035	1.129	1.063	.945
5.0	2.810	1.204	1.097	.685
7.5	3.394	1.240	1.114	.559
10	3.871	1.264	1.124	.482
15	4.020	1.286	1.139	.386
20	5.173	1.320	1.148	.328
25	5.576	1.358	1.156	.281
30	5.844	1.351	1.162	.247
35	5.978	1.362	1.167	.221
40	5.981	1.372	1.171	.199
45	5.798	1.355	1.156	.177
50	5.480	1.289	1.136	.158
55	5.056	1.243	1.115	.138
60	4.545	1.195	1.092	.122
65	3.974	1.144	1.070	.108
70	3.350	1.091	1.044	.088
75	2.685	1.037	1.018	.074
80	2.029	.981	.990	.063
85	1.382	.928	.963	.052
90	.786	.874	.935	.045
95	.288	.825	.908	.028
100	0	.775	.880	0

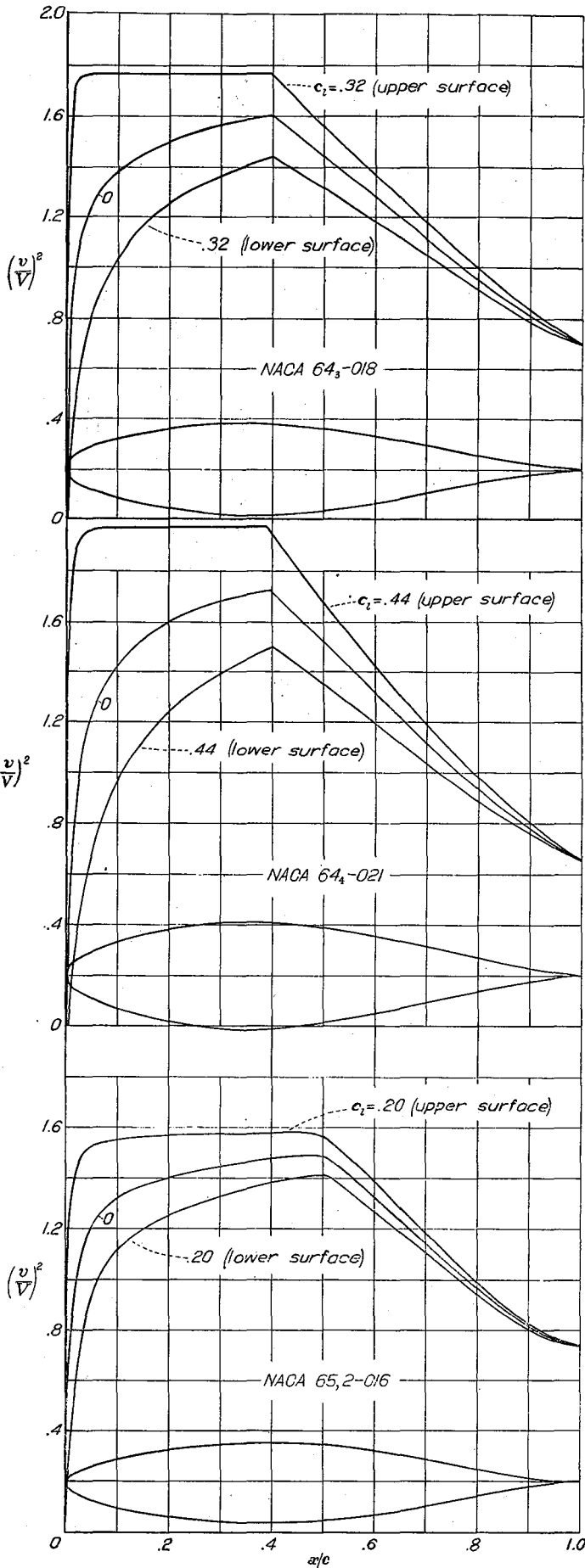
L. E. radius: 1.040 percent  $c$



NACA 64-015 BASIC THICKNESS FORM

$x$ (percent $c$ )	$y$ (percent $c$ )	$(v/V)^2$	$v/V$	$\Delta v_a/V$
0	0	0	0	1.939
.5	1.208	.670	.819	1.476
.75	1.456	.762	.873	1.354
1.25	1.842	.896	.947	1.188
2.5	2.528	1.113	1.055	.916
5.0	3.504	1.231	1.109	.670
7.5	4.240	1.284	1.133	.559
10	4.842	1.323	1.150	.482
15	5.785	1.375	1.172	.386
20	6.480	1.410	1.187	.325
25	6.985	1.434	1.198	.280
30	7.319	1.454	1.208	.250
35	7.482	1.470	1.213	.225
40	7.473	1.485	1.218	.202
45	7.224	1.426	1.195	.179
50	6.810	1.365	1.168	.158
55	6.266	1.300	1.140	.135
60	5.620	1.233	1.110	.121
65	4.895	1.167	1.080	.105
70	4.113	1.101	1.049	.090
75	3.296	1.033	1.016	.078
80	2.472	.967	.983	.065
85	1.677	.902	.950	.054
90	.950	.841	.917	.041
95	.346	.785	.886	.031
100	0	.730	.855	0

L. E. radius: 1.590 percent  $c$



NACA 64<sub>3</sub>-018 BASIC THICKNESS FORM

$x$ (percent $c$ )	$y$ (percent $c$ )	$(v/V)^2$	$v/V$	$\Delta v_a/V$
0	0	0	0	1.646
.5	1.428	.546	.739	1.360
.75	1.720	.705	.840	1.269
1.25	2.177	.862	.920	1.128
2.5	3.005	1.079	1.039	.904
5.0	4.186	1.244	1.115	.669
7.5	5.076	1.327	1.152	.558
10	5.803	1.380	1.175	.486
15	6.942	1.450	1.204	.391
20	7.782	1.497	1.224	.331
25	8.391	1.535	1.239	.288
30	8.789	1.562	1.250	.255
35	8.979	1.585	1.259	.228
40	8.952	1.600	1.265	.200
45	8.630	1.518	1.232	.177
50	8.114	1.436	1.198	.154
55	7.445	1.354	1.164	.134
60	6.658	1.272	1.128	.117
65	5.782	1.190	1.091	.102
70	4.842	1.109	1.053	.088
75	3.866	1.028	1.014	.074
80	2.888	.952	.976	.063
85	1.951	.879	.937	.051
90	1.101	.812	.901	.039
95	.400	.747	.864	.027
100	0	.695	.834	0

L. E. radius: 2.208 percent  $c$

NACA 64<sub>4</sub>-021 BASIC THICKNESS FORM

$x$ (percent $c$ )	$y$ (percent $c$ )	$(v/V)^2$	$v/V$	$\Delta v_a/V$
0	0	0	0	1.458
.5	1.646	.462	.680	1.274
.75	1.985	.603	.776	1.203
1.25	2.517	.759	.871	1.084
2.5	3.485	1.010	1.005	.878
5.0	4.871	1.248	1.117	.665
7.5	5.915	1.358	1.165	.557
10	6.769	1.431	1.196	.486
15	8.108	1.527	1.236	.395
20	9.095	1.593	1.262	.335
25	9.807	1.654	1.281	.293
30	10.269	1.681	1.297	.259
35	10.481	1.712	1.308	.232
40	10.431	1.709	1.307	.202
45	10.030	1.607	1.268	.178
50	9.404	1.507	1.228	.155
55	8.607	1.406	1.186	.134
60	7.678	1.307	1.143	.116
65	6.649	1.209	1.099	.099
70	5.549	1.112	1.055	.084
75	4.416	1.020	1.010	.071
80	3.287	.932	.965	.059
85	2.213	.851	.923	.047
90	1.245	.778	.882	.036
95	.449	.711	.844	.022
100	0	.653	.808	0

L. E. radius: 2.884 percent  $c$

NACA 65,2-016 BASIC THICKNESS FORM

$x$ (percent $c$ )	$y$ (percent $c$ )	$(v/V)^2$	$v/V$	$\Delta v_a/V$
0	0	0	0	1.950
.5	1.202	.560	.748	1.650
.75	1.423	.690	.831	1.500
1.25	1.796	.842	.918	1.275
2.5	2.507	1.068	1.033	.920
5.0	3.543	1.217	1.103	.680
7.5	4.316	1.287	1.134	.545
10	4.954	1.328	1.152	.480
15	5.958	1.379	1.174	.390
20	6.701	1.409	1.187	.325
25	7.252	1.433	1.197	.285
30	7.645	1.453	1.205	.255
35	7.892	1.469	1.212	.225
40	7.995	1.484	1.218	.200
45	7.938	1.497	1.224	.180
50	7.672	1.491	1.221	.160
55	7.184	1.421	1.192	.140
60	6.495	1.328	1.152	.125
65	5.647	1.235	1.111	.110
70	4.713	1.147	1.071	.095
75	3.738	1.056	1.028	.080
80	2.759	.970	.985	.066
85	1.817	.886	.941	.050
90	.982	.816	.903	.040
95	.340	.769	.877	.025
100	0	.733	.856	0

L. E. radius: 1.704 percent  $c$

NACA 65,2-023 BASIC THICKNESS FORM

$x$ (percent $c$ )	$y$ (percent $c$ )	$(v/V)^2$	$v/V$	$\Delta v_a/V$
0	0	0	0	1.414
.5	1.664	.400	.632	1.161
.75	2.040	.500	.707	1.084
1.25	2.628	.682	.826	.967
2.5	3.715	.943	.971	.811
5.0	5.300	1.232	1.110	.633
7.5	6.478	1.375	1.173	.539
10	7.433	1.467	1.211	.479
15	8.889	1.577	1.256	.380
20	9.917	1.628	1.276	.324
25	10.648	1.655	1.286	.281
30	11.142	1.677	1.295	.247
35	11.423	1.694	1.302	.220
40	11.499	1.708	1.307	.198
45	11.361	1.716	1.310	.178
50	10.949	1.712	1.308	.161
55	10.179	1.696	1.287	.147
60	9.108	1.428	1.195	.110
65	7.848	1.274	1.129	.096
70	6.461	1.135	1.065	.093
75	5.015	1.003	1.001	.090
80	3.618	.893	.945	.083
85	2.345	.803	.896	.085
90	1.258	.732	.856	.022
95	.439	.682	.826	.018
100	0	.651	.807	0

L. E. radius: 2.955 percent  $c$

NACA 65,3-018 BASIC THICKNESS FORM

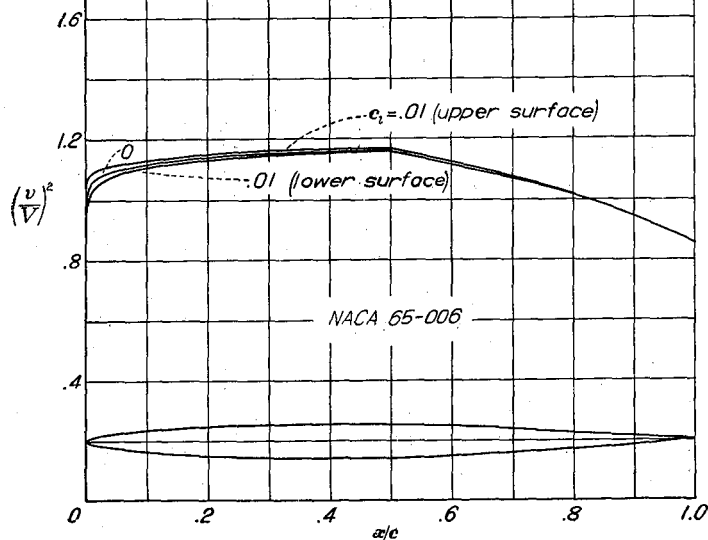
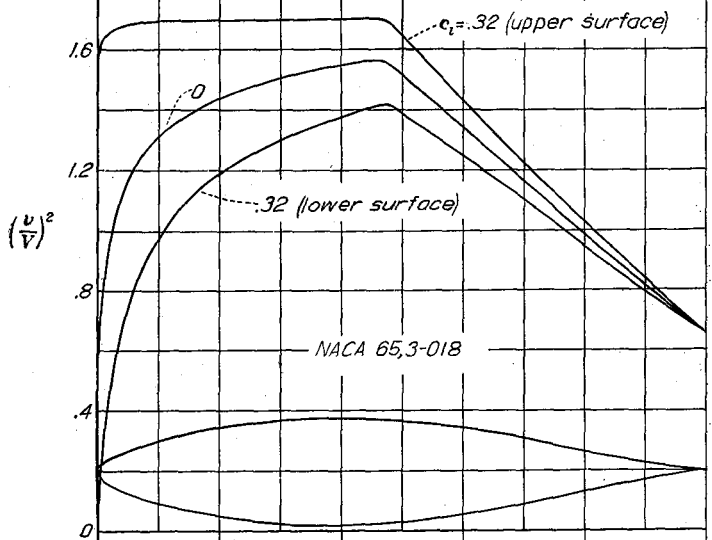
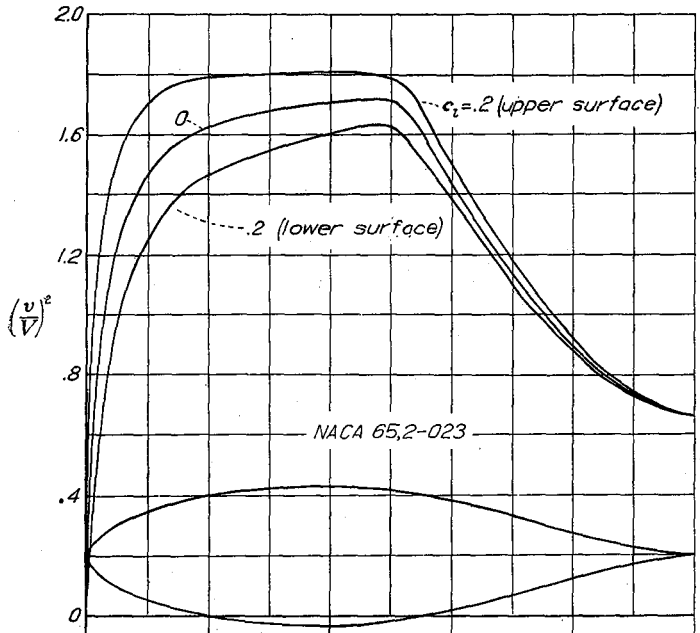
$x$ (percent $c$ )	$y$ (percent $c$ )	$(v/V)^2$	$v/V$	$\Delta v_a/V$
0	0	0	0	1.750
.5	1.324	.650	.806	1.387
.75	1.599	.750	.866	1.268
1.25	2.004	.872	.934	1.108
2.5	2.728	1.020	1.010	.890
5.0	3.831	1.179	1.086	.677
7.5	4.701	1.263	1.124	.568
10	5.424	1.320	1.149	.489
15	6.568	1.393	1.180	.395
20	7.434	1.439	1.200	.334
25	8.093	1.473	1.214	.292
30	8.568	1.502	1.226	.260
35	8.868	1.526	1.235	.232
40	8.990	1.546	1.243	.209
45	8.916	1.562	1.250	.186
50	8.593	1.513	1.230	.165
55	8.045	1.433	1.197	.142
60	7.317	1.348	1.161	.123
65	6.450	1.258	1.122	.107
70	5.486	1.169	1.081	.093
75	4.456	1.079	1.039	.080
80	3.390	.992	.996	.066
85	2.325	.905	.951	.054
90	1.324	.818	.904	.040
95	.492	.738	.859	.024
100	0	.658	.811	0

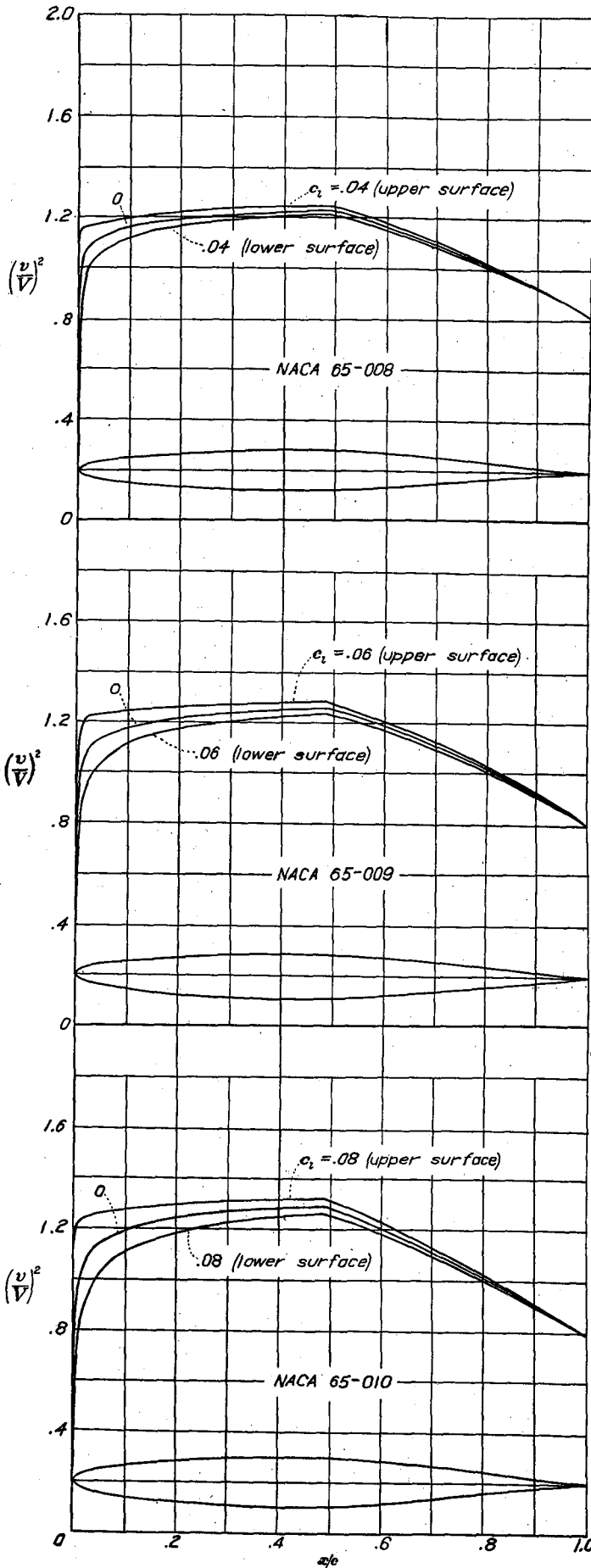
L. E. radius: 1.92 percent  $c$

NACA 65-006 BASIC THICKNESS FORM

$x$ (percent $c$ )	$y$ (percent $c$ )	$(v/V)^2$	$v/V$	$\Delta v_a/V$
0	0	0	0	4.815
.5	.476	1.044	1.022	2.110
.75	.574	1.055	1.027	1.780
1.25	.717	1.063	1.031	1.390
2.5	.956	1.081	1.040	.965
5.0	1.310	1.100	1.049	.695
7.5	1.589	1.112	1.055	.560
10	1.824	1.120	1.058	.474
15	2.197	1.134	1.065	.381
20	2.482	1.143	1.069	.322
25	2.697	1.149	1.072	.281
30	2.852	1.155	1.075	.247
35	2.952	1.159	1.077	.220
40	2.998	1.163	1.078	.198
45	2.983	1.166	1.080	.178
50	2.900	1.165	1.079	.160
55	2.741	1.145	1.070	.144
60	2.518	1.124	1.060	.128
65	2.246	1.100	1.049	.114
70	1.935	1.073	1.036	.100
75	1.594	1.044	1.022	.086
80	1.233	1.013	1.006	.074
85	.865	.981	.990	.060
90	.510	.944	.972	.046
95	.195	.902	.950	.031
100	0	.858	.926	0

L. E. radius: 0.240 percent  $c$





NACA 65-008 BASIC THICKNESS FORM

$x$ (percent $c$ )	$y$ (percent $c$ )	$(v/V)^2$	$v/V$	$\Delta v_a/V$
0	0	0	0	3.695
.5	.627	.978	.989	2.010
.75	.756	1.010	1.005	1.696
1.25	.945	1.043	1.021	1.340
2.5	1.267	1.086	1.042	.956
5.0	1.745	1.125	1.061	.689
7.5	2.118	1.145	1.070	.560
10	2.432	1.158	1.076	.477
15	2.931	1.178	1.085	.382
20	3.312	1.192	1.092	.323
25	3.599	1.203	1.097	.281
30	3.805	1.210	1.100	.248
35	3.938	1.217	1.103	.221
40	3.998	1.222	1.105	.199
45	3.974	1.226	1.107	.178
50	3.857	1.222	1.105	.160
55	3.638	1.193	1.092	.145
60	3.337	1.163	1.078	.128
65	2.971	1.130	1.063	.113
70	2.553	1.094	1.046	.098
75	2.096	1.055	1.027	.084
80	1.617	1.014	1.007	.072
85	1.131	.971	.985	.059
90	.664	.923	.961	.044
95	.252	.873	.934	.031
100	0	.817	.904	0

L. E. radius: 0.434 percent  $c$

NACA 65-009 BASIC THICKNESS FORM

$x$ (percent $c$ )	$y$ (percent $c$ )	$(v/V)^2$	$v/V$	$\Delta v_a/V$
0	0	0	0	3.270
.5	.700	.945	.972	1.962
.75	.845	.985	.992	1.655
1.25	1.058	1.037	1.018	1.315
2.5	1.421	1.089	1.044	.950
5.0	1.961	1.134	1.065	.687
7.5	2.383	1.159	1.077	.560
10	2.736	1.177	1.085	.477
15	3.299	1.200	1.095	.382
20	3.727	1.216	1.103	.323
25	4.050	1.229	1.109	.280
30	4.282	1.238	1.113	.248
35	4.431	1.246	1.116	.220
40	4.496	1.252	1.119	.198
45	4.469	1.258	1.122	.178
50	4.336	1.250	1.118	.160
55	4.086	1.220	1.105	.144
60	3.743	1.185	1.089	.128
65	3.328	1.145	1.070	.111
70	2.856	1.103	1.050	.097
75	2.342	1.059	1.029	.084
80	1.805	1.013	1.006	.071
85	1.260	.963	.981	.059
90	.738	.912	.955	.044
95	.280	.856	.925	.030
100	0	.797	.893	0

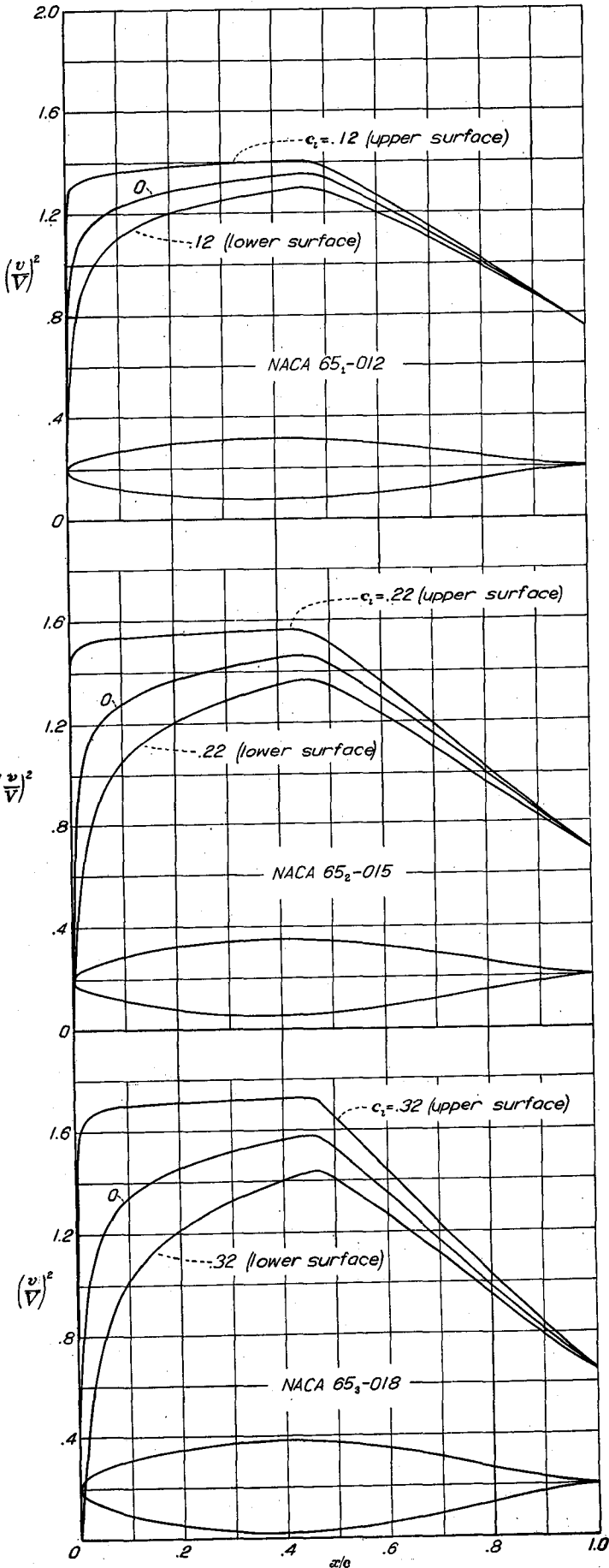
L. E. radius: 0.552 percent  $c$

NACA 65-010 BASIC THICKNESS FORM

$x$ (percent $c$ )	$y$ (percent $c$ )	$(v/V)^2$	$v/V$	$\Delta v_a/V$
0	0	0	0	2.967
.5	.772	.911	.954	1.911
.75	.932	.960	.980	1.614
1.25	1.169	1.025	1.012	1.292
2.5	1.574	1.085	1.042	.932
5.0	2.177	1.143	1.069	.679
7.5	2.647	1.177	1.085	.558
10	3.040	1.197	1.094	.480
15	3.666	1.224	1.106	.383
20	4.143	1.242	1.114	.321
25	4.503	1.257	1.121	.280
30	4.760	1.268	1.126	.248
35	4.924	1.277	1.130	.222
40	4.996	1.284	1.133	.199
45	4.963	1.280	1.136	.179
50	4.812	1.284	1.133	.160
55	4.530	1.244	1.115	.141
60	4.146	1.202	1.096	.126
65	3.682	1.158	1.076	.110
70	3.156	1.112	1.055	.097
75	2.584	1.062	1.031	.082
80	1.987	1.011	1.005	.070
85	1.385	.958	.979	.058
90	.810	.903	.950	.045
95	.306	.844	.919	.030
100	0	.781	.884	0

L. E. radius: 0.687 percent  $c$

NACA 65<sub>1</sub>-012 BASIC THICKNESS FORM



x (percent c)	y (percent c)	(v/V) <sup>2</sup>	v/V	Δv <sub>a</sub> /V
0	0	0	0	2.444
.5	.023	.848	.921	1.776
.75	1.109	.935	.967	1.465
1.25	1.387	1.000	1.000	1.200
2.5	1.875	1.082	1.040	.931
5.0	2.606	1.162	1.078	.702
7.5	3.172	1.201	1.096	.568
10	3.647	1.232	1.110	.480
15	4.402	1.268	1.126	.389
20	4.975	1.295	1.138	.326
25	5.406	1.316	1.147	.282
30	5.716	1.332	1.154	.251
35	5.912	1.343	1.159	.223
40	5.997	1.350	1.162	.204
45	5.949	1.357	1.165	.188
50	5.757	1.343	1.159	.169
55	5.412	1.295	1.138	.145
60	4.943	1.243	1.115	.127
65	4.381	1.188	1.090	.111
70	3.743	1.134	1.065	.094
75	3.059	1.073	1.036	.074
80	2.345	1.010	1.005	.062
85	1.630	.949	.974	.049
90	.947	.884	.940	.038
95	.356	.819	.905	.025
100	0	.748	.865	0

L. E. radius: 1.000 percent c

NACA 65<sub>2</sub>-015 BASIC THICKNESS FORM

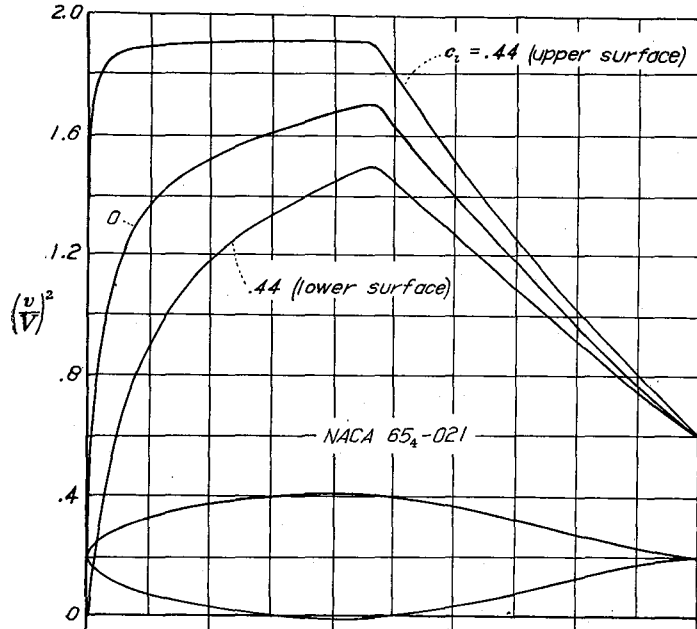
x (percent c)	y (percent c)	(v/V) <sup>2</sup>	v/V	Δv <sub>a</sub> /V
0	0	0	0	2.038
.5	1.124	.654	.809	1.729
.75	1.356	.817	.904	1.390
1.25	1.702	.939	.969	1.156
2.5	2.324	1.063	1.031	.920
5.0	3.245	1.184	1.088	.682
7.5	3.959	1.241	1.114	.563
10	4.555	1.281	1.132	.487
15	5.504	1.336	1.156	.393
20	6.223	1.374	1.172	.334
25	6.764	1.397	1.182	.290
30	7.152	1.418	1.191	.255
35	7.396	1.438	1.199	.227
40	7.498	1.452	1.205	.203
45	7.427	1.464	1.210	.184
50	7.168	1.433	1.197	.160
55	6.720	1.369	1.170	.143
60	6.118	1.297	1.139	.127
65	5.403	1.228	1.108	.109
70	4.600	1.151	1.073	.096
75	3.744	1.077	1.038	.078
80	2.858	1.002	1.001	.068
85	1.977	.924	.961	.052
90	1.144	.846	.920	.038
95	.428	.773	.879	.026
100	0	.697	.835	0

L. E. radius: 1.505 percent c

NACA 65<sub>3</sub>-018 BASIC THICKNESS FORM

x (percent c)	y (percent c)	(v/V) <sup>2</sup>	v/V	Δv <sub>a</sub> /V
0	0	0	0	1.746
.5	1.337	.625	.791	1.437
.75	1.608	.702	.838	1.302
1.25	2.014	.817	.904	1.123
2.5	2.751	1.020	1.010	.858
5.0	3.866	1.192	1.092	.650
7.5	4.733	1.275	1.129	.542
10	5.457	1.329	1.153	.474
15	6.606	1.402	1.184	.385
20	7.476	1.452	1.205	.327
25	8.129	1.488	1.220	.285
30	8.595	1.515	1.231	.251
35	8.886	1.539	1.241	.225
40	8.999	1.561	1.249	.203
45	8.901	1.578	1.256	.182
50	8.568	1.528	1.231	.157
55	8.008	1.440	1.200	.137
60	7.267	1.353	1.163	.118
65	6.395	1.262	1.123	.104
70	5.426	1.170	1.082	.087
75	4.396	1.078	1.037	.074
80	3.358	.985	.992	.062
85	2.295	.896	.947	.050
90	1.319	.813	.902	.039
95	.490	.730	.854	.026
100	0	.657	.811	0

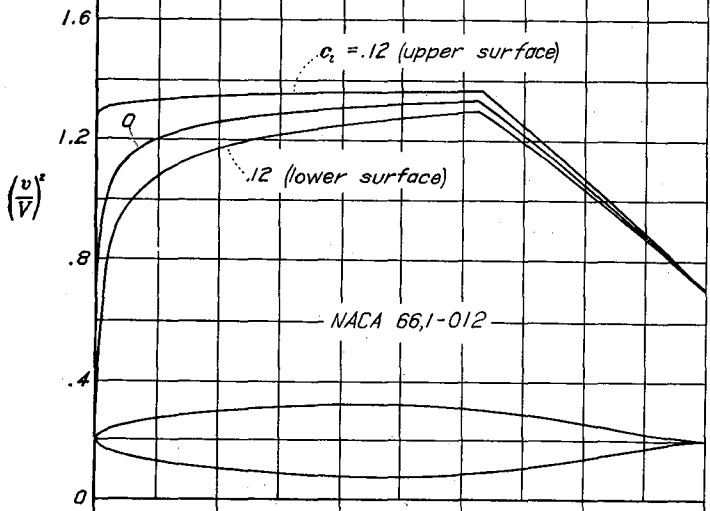
L. E. radius: 1.96 percent c



NACA 65-021 BASIC THICKNESS FORM

$x$ (percent $c$ )	$y$ (percent $c$ )	$(v/V)^2$	$v/V$	$\Delta v_a/V$
0	0	0	0	1.531
.5	1.522	.514	.717	1.333
.75	1.838	.607	.779	1.215
1.25	2.301	.740	.860	1.062
2.5	3.154	.960	.980	.838
5.0	4.472	1.186	1.089	.649
7.5	5.498	1.293	1.137	.544
10	6.352	1.371	1.171	.478
15	7.700	1.469	1.212	.388
20	8.720	1.533	1.238	.330
25	9.487	1.580	1.257	.289
30	10.036	1.621	1.273	.255
35	10.375	1.654	1.286	.229
40	10.499	1.680	1.296	.206
45	10.366	1.700	1.304	.184
50	9.952	1.633	1.278	.158
55	9.277	1.508	1.228	.139
60	8.390	1.397	1.182	.120
65	7.360	1.286	1.134	.101
70	6.224	1.177	1.085	.087
75	5.024	1.073	1.036	.073
80	3.800	.970	.985	.058
85	2.598	.872	.934	.047
90	1.484	.778	.882	.035
95	.546	.694	.833	.020
100		.616	.785	0

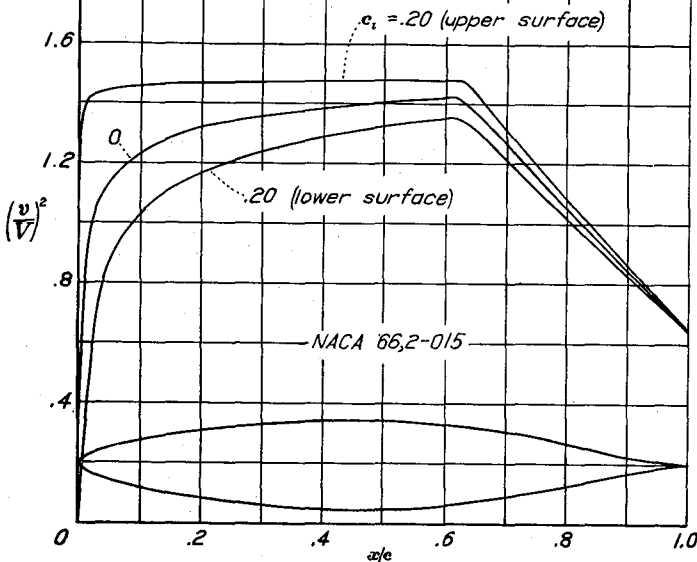
L. E. radius: 2.50 percent  $c$



NACA 66,1-012 BASIC THICKNESS FORM

$x$ (percent $c$ )	$y$ (percent $c$ )	$(v/V)^2$	$v/V$	$\Delta v_a/V$
0	0	0	0	2.555
.5	.900	.854	.924	1.780
.75	1.083	.902	.950	1.540
1.25	1.343	.964	.982	1.247
2.5	1.803	1.069	1.034	.925
5.0	2.484	1.138	1.067	.673
7.5	3.019	1.175	1.084	.552
10	3.482	1.201	1.096	.474
15	4.214	1.237	1.112	.381
20	4.779	1.257	1.121	.319
25	5.218	1.272	1.128	.280
30	5.550	1.284	1.133	.248
35	5.786	1.293	1.137	.220
40	5.934	1.302	1.141	.195
45	5.998	1.309	1.144	.176
50	5.972	1.313	1.146	.161
55	5.844	1.320	1.149	.144
60	5.594	1.327	1.152	.130
65	5.165	1.297	1.139	.117
70	4.555	1.221	1.105	.099
75	3.789	1.143	1.069	.083
80	2.964	1.061	1.030	.069
85	2.098	.974	.987	.053
90	1.244	.885	.941	.041
95	.477	.792	.890	.028
100	0	.701	.837	0

L. E. radius: 0.893 percent  $c$



NACA 66,2-015 BASIC THICKNESS FORM

$x$ (percent $c$ )	$y$ (percent $c$ )	$(v/V)^2$	$v/V$	$\Delta v_a/V$
0	0	0	0	2.085
.5	1.110	.700	.837	1.703
.75	1.329	.870	.933	1.382
1.25	1.645	.940	.970	1.156
2.5	2.229	1.048	1.024	.898
5.0	3.086	1.154	1.074	.656
7.5	3.757	1.210	1.100	.547
10	4.337	1.244	1.115	.473
15	5.255	1.290	1.136	.382
20	5.964	1.323	1.150	.323
25	6.516	1.342	1.158	.283
30	6.933	1.359	1.166	.248
35	7.230	1.374	1.172	.222
40	7.415	1.387	1.178	.199
45	7.495	1.397	1.182	.179
50	7.460	1.407	1.186	.161
55	7.294	1.415	1.190	.145
60	6.961	1.421	1.192	.131
65	6.405	1.372	1.171	.122
70	5.597	1.267	1.126	.102
75	4.652	1.162	1.078	.080
80	3.616	1.057	1.028	.066
85	2.545	.953	.976	.050
90	1.488	.848	.921	.037
95	.560	.743	.862	.025
100	0	.640	.800	0

L. E. radius: 1.384 percent  $c$



NACA 66,2-018 BASIC THICKNESS FORM

$x$ (percent $c$ )	$y$ (percent $c$ )	$(v/V)^2$	$v/V$	$\Delta v_a/V$
0	0	0	0	1.659
.5	1.438	.590	.768	1.317
.75	1.730	.740	.860	1.209
1.25	2.180	.918	.958	1.091
2.5	2.938	1.084	1.041	.867
5.0	3.984	1.217	1.103	.665
7.5	4.804	1.285	1.134	.544
10	5.486	1.325	1.151	.469
15	6.541	1.373	1.172	.379
20	7.342	1.401	1.184	.323
25	7.957	1.422	1.192	.282
30	8.419	1.440	1.200	.251
35	8.741	1.456	1.207	.224
40	8.933	1.468	1.212	.201
45	8.998	1.478	1.216	.181
50	8.934	1.488	1.220	.162
55	8.719	1.497	1.224	.146
60	8.316	1.502	1.226	.134
65	7.629	1.442	1.201	.102
70	6.657	1.314	1.146	.089
75	5.523	1.185	1.089	.078
80	4.296	1.059	1.029	.064
85	3.027	.936	.967	.052
90	1.789	.817	.904	.041
95	.672	.700	.837	.027
100	0	.594	.771	0

L. E. radius: 2.30 percent  $c$

NACA 66-006 BASIC THICKNESS FORM

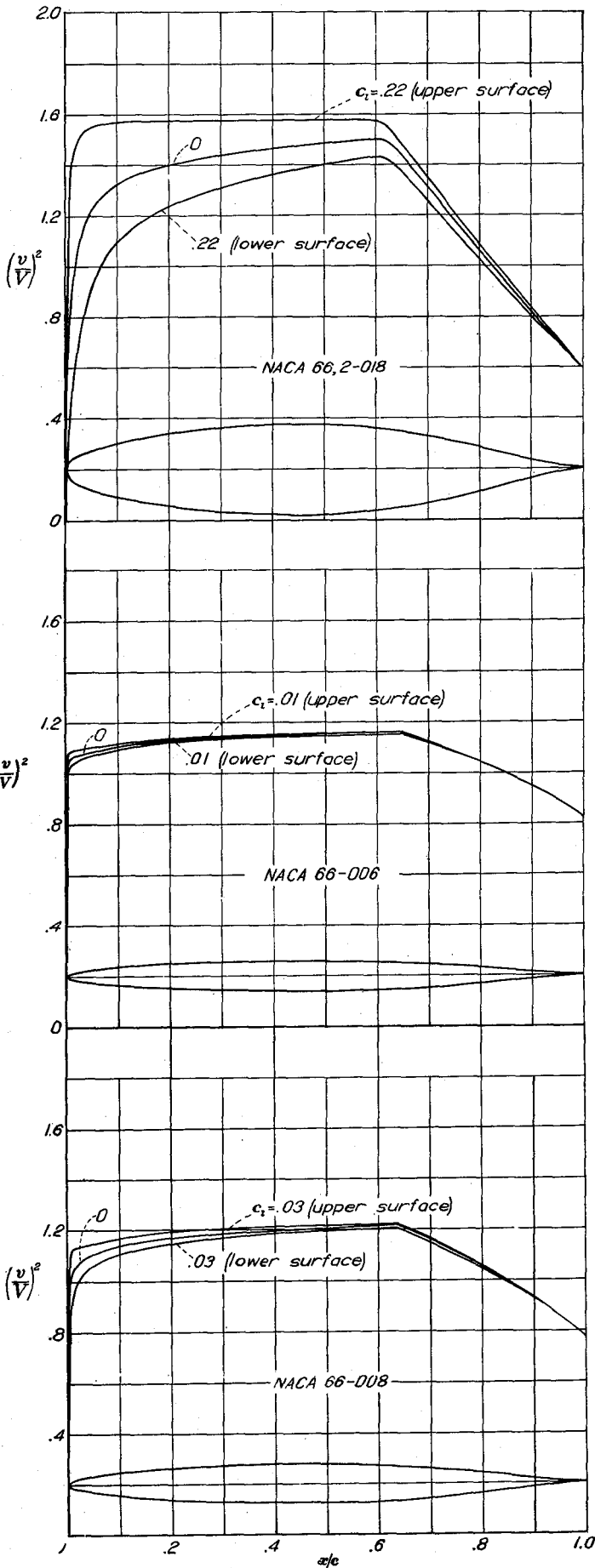
$x$ (percent $c$ )	$y$ (percent $c$ )	$(v/V)^2$	$v/V$	$\Delta v_a/V$
0	0	0	0	4.941
.5	.461	1.052	1.026	2.500
.75	.554	1.057	1.028	2.020
1.25	.693	1.062	1.031	1.500
2.5	.918	1.071	1.035	.967
5.0	1.257	1.086	1.042	.695
7.5	1.524	1.098	1.048	.554
10	1.752	1.107	1.052	.474
15	2.119	1.119	1.058	.379
20	2.401	1.128	1.062	.320
25	2.618	1.133	1.064	.278
30	2.782	1.138	1.067	.245
35	2.899	1.142	1.069	.219
40	2.971	1.145	1.070	.197
45	3.000	1.148	1.071	.178
50	2.985	1.151	1.073	.161
55	2.925	1.153	1.074	.145
60	2.815	1.155	1.075	.130
65	2.611	1.154	1.074	.116
70	2.316	1.118	1.057	.102
75	1.953	1.081	1.040	.089
80	1.543	1.040	1.020	.075
85	1.107	.996	.998	.061
90	.665	.948	.974	.047
95	.262	.890	.943	.030
100	0	.822	.907	0

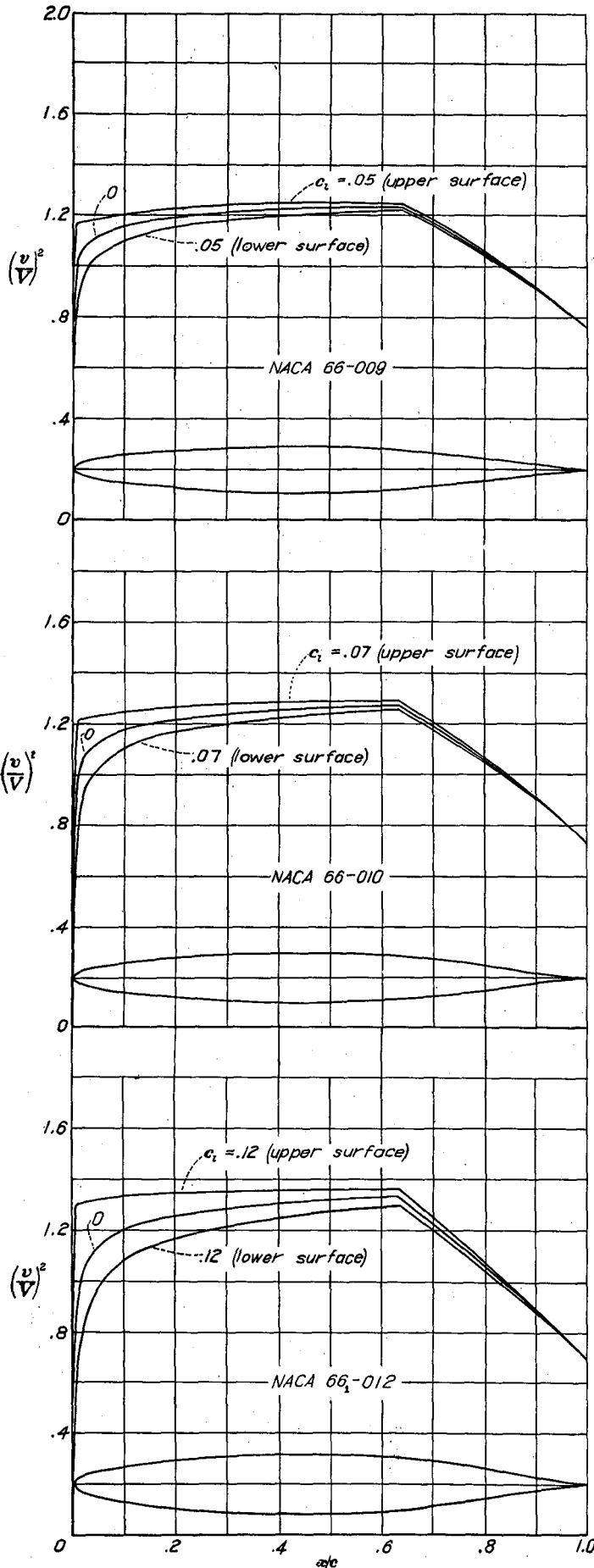
L. E. radius: 0.223 percent  $c$

NACA 66-008 BASIC THICKNESS FORM

$x$ (percent $c$ )	$y$ (percent $c$ )	$(v/V)^2$	$v/V$	$\Delta v_a/V$
0	0	0	0	3.794
.5	.610	.968	1.084	2.220
.75	.735	1.023	1.011	1.825
1.25	.919	1.046	1.023	1.388
2.5	1.219	1.078	1.038	.949
5.0	1.673	1.107	1.052	.689
7.5	2.031	1.128	1.062	.552
10	2.335	1.141	1.068	.474
15	2.826	1.158	1.076	.379
20	3.201	1.171	1.082	.321
25	3.490	1.178	1.085	.278
30	3.709	1.186	1.089	.246
35	3.865	1.191	1.091	.220
40	3.962	1.196	1.094	.198
45	4.000	1.201	1.096	.178
50	3.978	1.205	1.098	.161
55	3.896	1.208	1.099	.145
60	3.740	1.213	1.101	.130
65	3.459	1.202	1.096	.115
70	3.062	1.156	1.075	.101
75	2.574	1.103	1.050	.087
80	2.027	1.048	1.024	.073
85	1.447	.989	.994	.058
90	.864	.926	.962	.045
95	.338	.855	.925	.029
100	0	.768	.876	0

L. E. radius: 0.411 percent  $c$





NACA 66-009 BASIC THICKNESS FORM

$x$ (percent $c$ )	$y$ (percent $c$ )	$(v/V)^2$	$v/V$	$\Delta v_a/V$
0	0	0	0	3.352
.5	.687	.930	.964	2.100
.75	.824	.999	.999	1.750
1.25	1.030	1.036	1.018	1.340
2.5	1.308	1.079	1.039	.940
5.0	1.880	1.119	1.058	.686
7.5	2.283	1.142	1.069	.552
10	2.626	1.159	1.077	.473
15	3.178	1.178	1.085	.379
20	3.601	1.190	1.091	.323
25	3.927	1.201	1.096	.280
30	4.173	1.210	1.100	.246
35	4.348	1.217	1.103	.220
40	4.457	1.221	1.105	.197
45	4.499	1.228	1.108	.178
50	4.475	1.232	1.110	.161
55	4.381	1.237	1.112	.145
60	4.204	1.240	1.114	.130
65	3.882	1.230	1.109	.116
70	3.428	1.172	1.083	.100
75	2.877	1.118	1.055	.085
80	2.293	1.050	1.025	.071
85	1.611	.985	.992	.057
90	.901	.915	.957	.043
95	.374	.839	.916	.028
100	0	.747	.864	0

L. E. radius: 0.530 percent  $c$

NACA 66-010 BASIC THICKNESS FORM

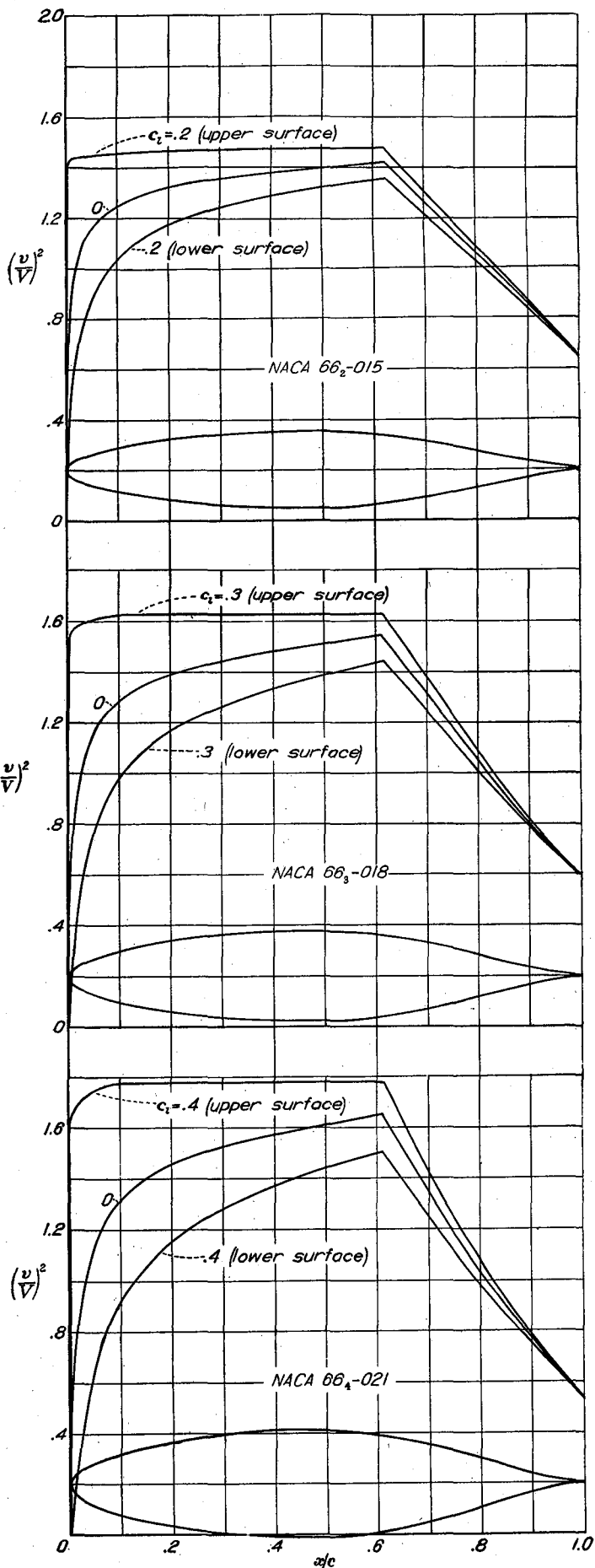
$x$ (percent $c$ )	$y$ (percent $c$ )	$(v/V)^2$	$v/V$	$\Delta v_a/V$
0	0	0	0	3.002
.5	.759	.896	.947	2.012
.75	.913	.972	.986	1.686
1.25	1.141	1.023	1.011	1.296
2.5	1.516	1.078	1.038	.931
5.0	2.087	1.125	1.061	.682
7.5	2.536	1.154	1.074	.551
10	2.917	1.174	1.084	.473
15	3.530	1.198	1.095	.379
20	4.001	1.215	1.102	.322
25	4.383	1.226	1.107	.279
30	4.636	1.236	1.112	.246
35	4.832	1.243	1.115	.220
40	4.983	1.249	1.118	.198
45	5.000	1.255	1.120	.178
50	4.971	1.261	1.123	.161
55	4.865	1.265	1.125	.146
60	4.685	1.270	1.127	.130
65	4.302	1.250	1.116	.114
70	3.787	1.190	1.091	.099
75	3.176	1.121	1.059	.085
80	2.494	1.052	1.026	.070
85	1.773	.979	.989	.056
90	1.054	.904	.951	.043
95	.408	.821	.906	.027
100	0	.729	.854	0

L. E. radius: 0.662 percent  $c$

NACA 66-012 BASIC THICKNESS FORM

$x$ (percent $c$ )	$y$ (percent $c$ )	$(v/V)^2$	$v/V$	$\Delta v_a/V$
0	0	0	0	2.569
.5	.906	.800	.894	1.847
.75	1.087	.915	.957	1.575
1.25	1.358	.980	.990	1.237
2.5	1.808	1.073	1.036	.913
5.0	2.496	1.138	1.067	.674
7.5	3.037	1.177	1.085	.549
10	3.496	1.204	1.097	.473
15	4.234	1.237	1.112	.380
20	4.801	1.259	1.122	.323
25	5.238	1.275	1.129	.280
30	5.568	1.287	1.134	.246
35	5.803	1.297	1.139	.221
40	5.947	1.303	1.142	.197
45	6.000	1.311	1.145	.176
50	5.965	1.318	1.148	.162
55	5.836	1.323	1.150	.147
60	5.588	1.331	1.154	.132
65	5.139	1.302	1.141	.113
70	4.515	1.221	1.105	.098
75	3.767	1.139	1.067	.084
80	2.944	1.053	1.026	.069
85	2.083	.962	.984	.053
90	1.234	.879	.938	.040
95	.474	.788	.888	.031
100	0	.687	.829	0

L. E. radius: 0.952 percent  $c$



NACA 66<sub>2</sub>-015 BASIC THICKNESS FORM

$x$ (percent $c$ )	$y$ (percent $c$ )	$(v/V)^2$	$v/V$	$\Delta v_a/V$
0	0	0	0	2.139
.5	1.122	.760	.872	1.652
.75	1.343	.840	.916	1.431
1.25	1.675	.929	.964	1.172
2.5	2.285	1.055	1.027	.895
5	3.100	1.163	1.078	.663
7.5	3.781	1.208	1.099	.547
10	4.358	1.242	1.114	.473
15	5.286	1.288	1.134	.381
20	5.995	1.317	1.148	.322
25	6.543	1.340	1.158	.280
30	6.956	1.356	1.164	.248
35	7.250	1.370	1.170	.222
40	7.430	1.380	1.175	.200
45	7.495	1.391	1.179	.180
50	7.450	1.401	1.184	.163
55	7.283	1.411	1.188	.146
60	6.959	1.420	1.192	.131
65	6.372	1.367	1.169	.113
70	5.576	1.260	1.122	.096
75	4.632	1.156	1.075	.080
80	3.598	1.053	1.026	.065
85	2.530	.949	.974	.051
90	1.489	.847	.920	.039
95	.566	.744	.863	.025
100	0	.639	.799	0

L. E. radius: 1.435 percent  $c$

NACA 66<sub>3</sub>-018 BASIC THICKNESS FORM

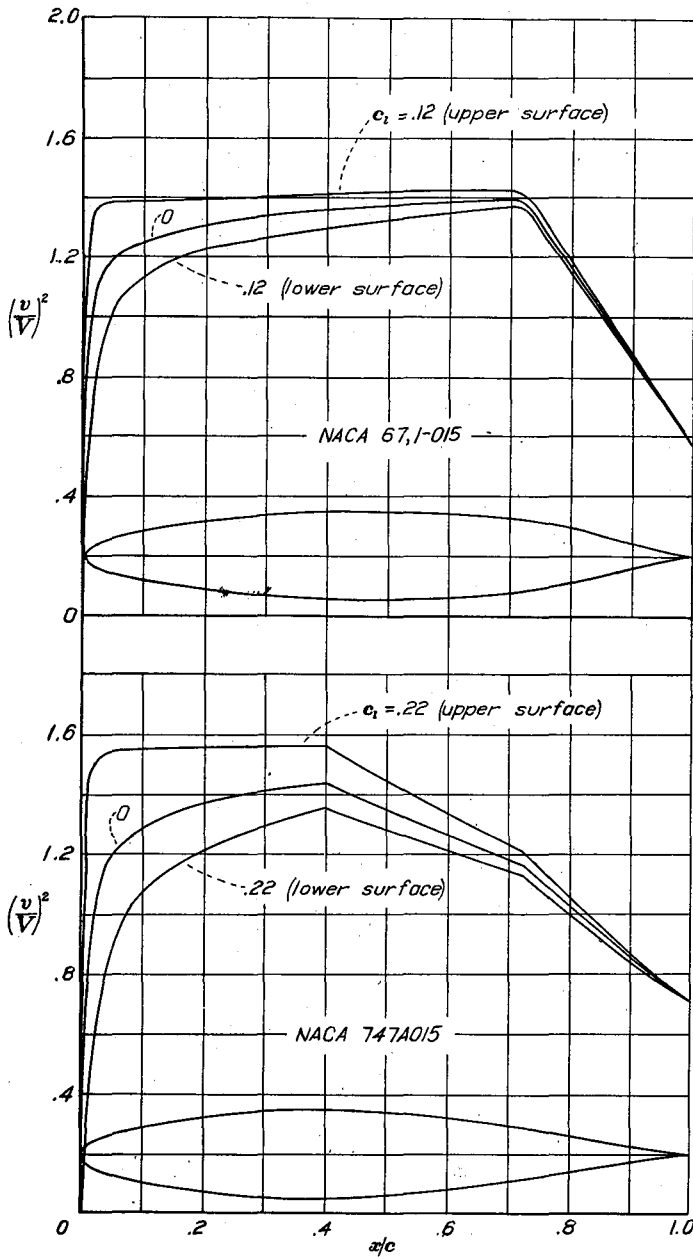
$x$ (percent $c$ )	$y$ (percent $c$ )	$(v/V)^2$	$v/V$	$\Delta v_a/V$
0	0	0	0	1.773
.5	1.323	.650	.806	1.456
.75	1.571	.735	.857	1.312
1.25	1.952	.850	.897	1.121
2.5	2.646	1.005	1.002	.858
5	3.690	1.164	1.074	.649
7.5	4.513	1.234	1.111	.545
10	5.210	1.285	1.134	.472
15	6.393	1.350	1.162	.381
20	7.188	1.393	1.180	.323
25	7.848	1.423	1.193	.282
30	8.346	1.445	1.202	.250
35	8.701	1.464	1.210	.223
40	8.918	1.481	1.217	.201
45	8.998	1.496	1.223	.181
50	8.942	1.509	1.228	.163
55	8.733	1.522	1.234	.147
60	8.323	1.534	1.238	.131
65	7.580	1.438	1.199	.114
70	6.597	1.302	1.141	.095
75	5.451	1.172	1.083	.077
80	4.206	1.045	1.022	.061
85	2.934	.922	.950	.048
90	1.714	.803	.896	.037
95	.646	.692	.832	.022
100	0	.587	.766	0

L. E. radius: 1.955 percent  $c$

NACA 66<sub>4</sub>-021 BASIC THICKNESS FORM

$x$ (percent $c$ )	$y$ (percent $c$ )	$(v/V)^2$	$v/V$	$\Delta v_a/V$
0	0	0	0	1.547
.5	1.525	.580	.761	1.314
.75	1.804	.635	.797	1.218
1.25	2.240	.755	.869	1.054
2.5	3.045	.952	.976	.828
5	4.269	1.143	1.069	.635
7.5	5.233	1.246	1.116	.542
10	6.052	1.318	1.148	.472
15	7.369	1.405	1.185	.381
20	8.376	1.459	1.208	.324
25	9.153	1.499	1.224	.283
30	9.738	1.528	1.236	.251
35	10.154	1.551	1.245	.224
40	10.407	1.574	1.255	.202
45	10.500	1.594	1.263	.183
50	10.434	1.611	1.269	.165
55	10.186	1.629	1.276	.148
60	9.692	1.648	1.284	.132
65	8.793	1.508	1.223	.114
70	7.610	1.335	1.155	.093
75	6.251	1.176	1.084	.073
80	4.796	1.031	1.015	.058
85	3.324	.891	.944	.046
90	1.924	.763	.873	.034
95	.717	.648	.805	.020
100	0	.539	.734	0

L. E. radius: 2.550 percent  $c$



NACA 67,1-015 BASIC THICKNESS FORM

$x$ (percent $c$ )	$y$ (percent $c$ )	$(v/V)^2$	$v/V$	$\Delta v_a/V$
0	0	0	0	2.042
.5	1.167	.650	.806	1.560
.75	1.394	.970	.985	1.370
1.25	1.764	1.059	1.029	1.152
2.5	2.395	1.140	1.068	.906
5.0	3.245	1.209	1.100	.697
7.5	3.900	1.239	1.113	.548
10	4.433	1.259	1.122	.470
15	5.283	1.285	1.134	.370
20	5.940	1.304	1.142	.312
25	6.454	1.318	1.148	.276
30	6.854	1.330	1.153	.248
35	7.155	1.341	1.158	.221
40	7.359	1.351	1.162	.201
45	7.475	1.360	1.166	.180
50	7.497	1.368	1.170	.160
55	7.421	1.375	1.173	.142
60	7.231	1.381	1.175	.124
65	6.905	1.388	1.178	.111
70	6.402	1.390	1.179	.108
75	5.621	1.321	1.149	.094
80	4.540	1.176	1.084	.071
85	3.327	1.018	1.009	.060
90	2.021	.864	.930	.045
95	.788	.712	.844	.025
100	0	.570	.755	0

L. E. radius: 1.523 percent  $c$ .

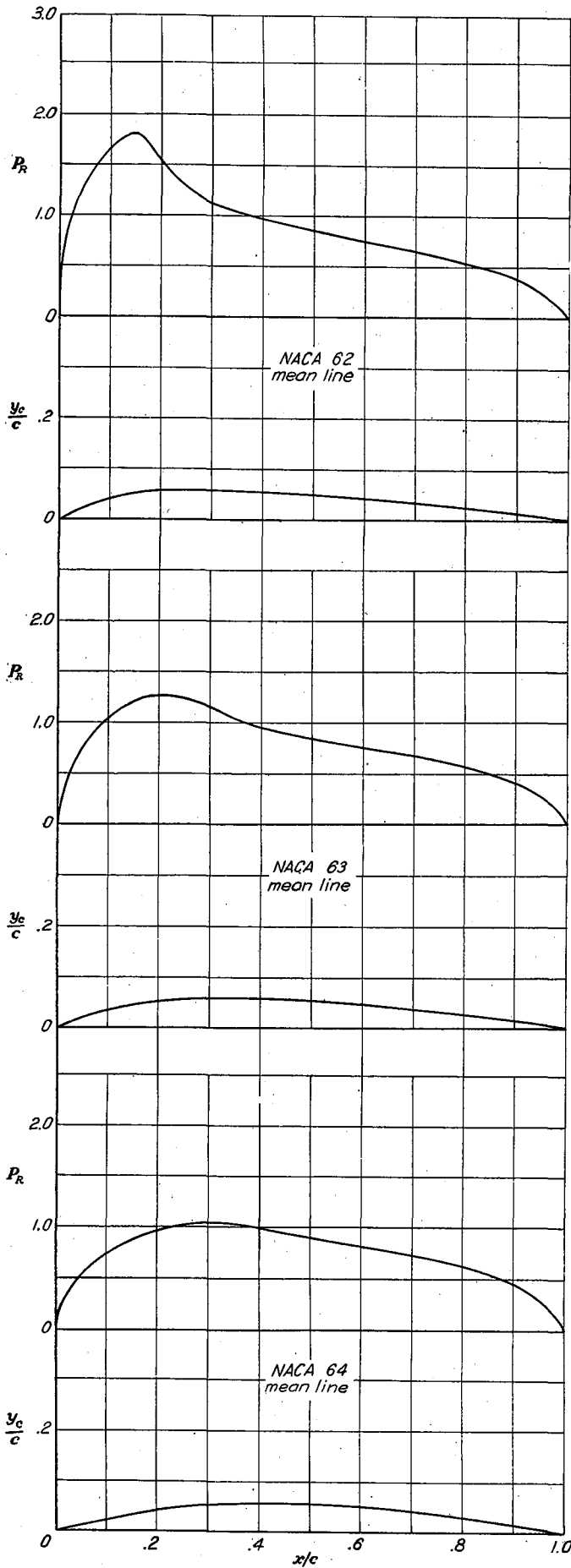
NACA 747A015 BASIC THICKNESS FORM

$x$ (percent $c$ )	$y$ (percent $c$ )	$(v/V)^2$	$v/V$	$\Delta v_a/V$
0	0	0	0	2.028
.5	1.199	.660	.812	1.680
.75	1.435	.799	.894	1.560
1.25	1.801	.942	.971	1.325
2.5	2.462	1.100	1.049	.990
5	3.419	1.201	1.096	.695
7.5	4.143	1.259	1.122	.551
10	4.743	1.295	1.138	.465
15	5.684	1.339	1.156	.383
20	6.384	1.369	1.170	.324
25	6.898	1.390	1.179	.283
30	7.253	1.409	1.187	.252
35	7.454	1.423	1.193	.224
40	7.494	1.435	1.198	.199
45	7.316	1.391	1.179	.176
50	7.003	1.348	1.161	.156
55	6.584	1.306	1.143	.138
60	6.064	1.265	1.125	.122
65	5.449	1.221	1.105	.108
70	4.738	1.178	1.085	.093
75	3.921	1.115	1.056	.079
80	3.020	1.027	1.013	.065
85	2.086	.938	.969	.052
90	1.193	.852	.923	.040
95	.443	.774	.880	.028
100	0	.703	.838	.018

L. E. radius: 1.544 percent  $c$

## II—DATA FOR MEAN LINES

	Page		Page
NACA mean line 62.....	90	NACA mean line $\alpha=0$ .....	93
NACA mean line 63.....	90	NACA mean line $\alpha=0.1$ .....	94
NACA mean line 64.....	90	NACA mean line $\alpha=0.2$ .....	94
NACA mean line 65.....	91	NACA mean line $\alpha=0.3$ .....	94
NACA mean line 66.....	91	NACA mean line $\alpha=0.4$ .....	95
NACA mean line 67.....	91	NACA mean line $\alpha=0.5$ .....	95
NACA mean line 210.....	92	NACA mean line $\alpha=0.6$ .....	95
NACA mean line 220.....	92	NACA mean line $\alpha=0.7$ .....	96
NACA mean line 230.....	92	NACA mean line $\alpha=0.8$ .....	96
NACA mean line 240.....	93	NACA mean line $\alpha=0.9$ .....	96
NACA mean line 250.....	93	NACA mean line $\alpha=1.0$ .....	97



NACA MEAN LINE 62

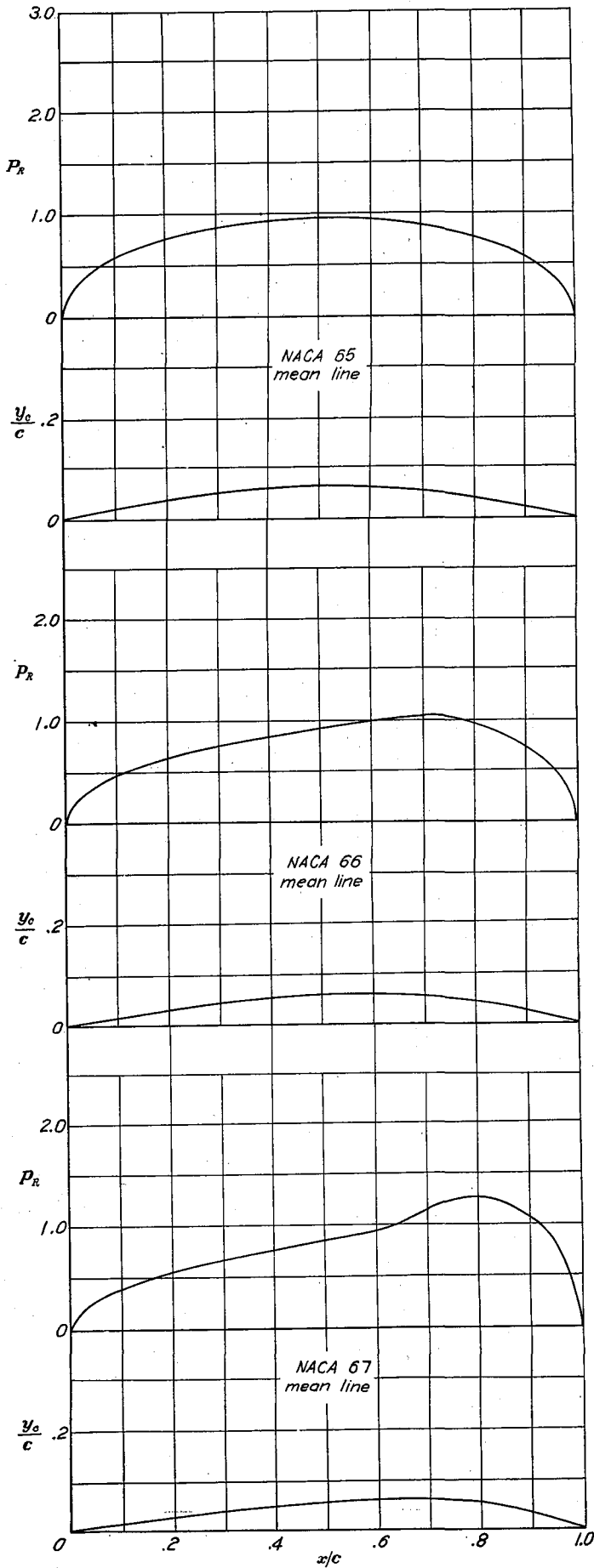
$c_{l_i}=0.90 \quad \alpha_i=2.81^\circ \quad c_{m_{c/4}}=-0.113$				
$x$ (percent $c$ )	$y_c$ (percent $c$ )	$dy_c/dx$	$P_R$	$\Delta v/V = P_R/4$
0	0	0.60000	0	0
1.25	.726	.58250	.682	.171
2.5	1.406	.52500	1.031	.258
5.0	2.625	.45000	1.314	.328
7.5	3.656	.37500	1.503	.376
10	4.500	.30000	1.651	.413
15	5.625	.15000	1.802	.451
20	6.000	0	1.850	.463
25	5.977	-.00938	1.873	.468
30	5.906	-.01875	1.873	.468
40	5.625	-.03750	1.851	.463
50	5.156	-.05625	1.802	.451
60	4.500	-.07500	1.727	.432
70	3.656	-.09375	1.635	.409
80	2.625	-.11250	1.525	.381
90	1.406	-.13125	1.397	.349
95	.727	-.14062	1.261	.315
100	0	-.15000	0	0

NACA MEAN LINE 63

$c_{l_i}=0.80 \quad \alpha_i=1.60^\circ \quad c_{m_{c/4}}=-0.134$				
$x$ (percent $c$ )	$y_c$ (percent $c$ )	$dy_c/dx$	$P_R$	$\Delta v/V = P_R/4$
0	0	0.40000	0	0
1.25	.489	.38333	.389	.097
2.5	.968	.36667	.553	.138
5.0	1.833	.33333	.788	.197
7.5	2.625	.30000	1.040	.260
10	3.333	.26667	1.220	.305
15	4.500	.20000	1.259	.315
20	5.333	.13333	1.233	.308
25	5.833	.06667	1.160	.290
30	6.000	0	.949	.237
40	5.878	-.02449	.850	.213
50	5.510	-.04898	.762	.191
60	4.898	-.07347	.673	.168
70	4.041	-.09796	.580	.145
80	2.939	-.12245	.486	.122
90	1.592	-.14694	.391	.098
95	.827	-.15918	.291	.073
100	0	-.17143	0	0

NACA MEAN LINE 64

$c_{l_i}=0.76 \quad \alpha_i=0.74^\circ \quad c_{m_{c/4}}=-0.157$				
$x$ (percent $c$ )	$y_c$ (percent $c$ )	$dy_c/dx$	$P_R$	$\Delta v/V = P_R/4$
0	0	0.30000	0	0
1.25	.369	.29062	.257	.064
2.5	.728	.28125	.391	.098
5.0	1.406	.26250	.546	.137
7.5	2.039	.24375	.668	.167
10	2.625	.22500	.748	.187
15	3.656	.18750	.871	.218
20	4.500	.15000	1.000	.250
25	5.156	.11250	1.090	.273
30	5.625	.07500	1.040	.260
40	6.000	0	.899	.225
50	5.833	-.03333	.810	.203
60	5.333	-.06667	.750	.188
70	4.500	-.10000	.635	.159
80	3.333	-.13333	.486	.122
90	1.833	-.16667	.334	.084
95	.958	-.18333	.250	.063
100	0	-.20000	0	0



NACA MEAN LINE 65

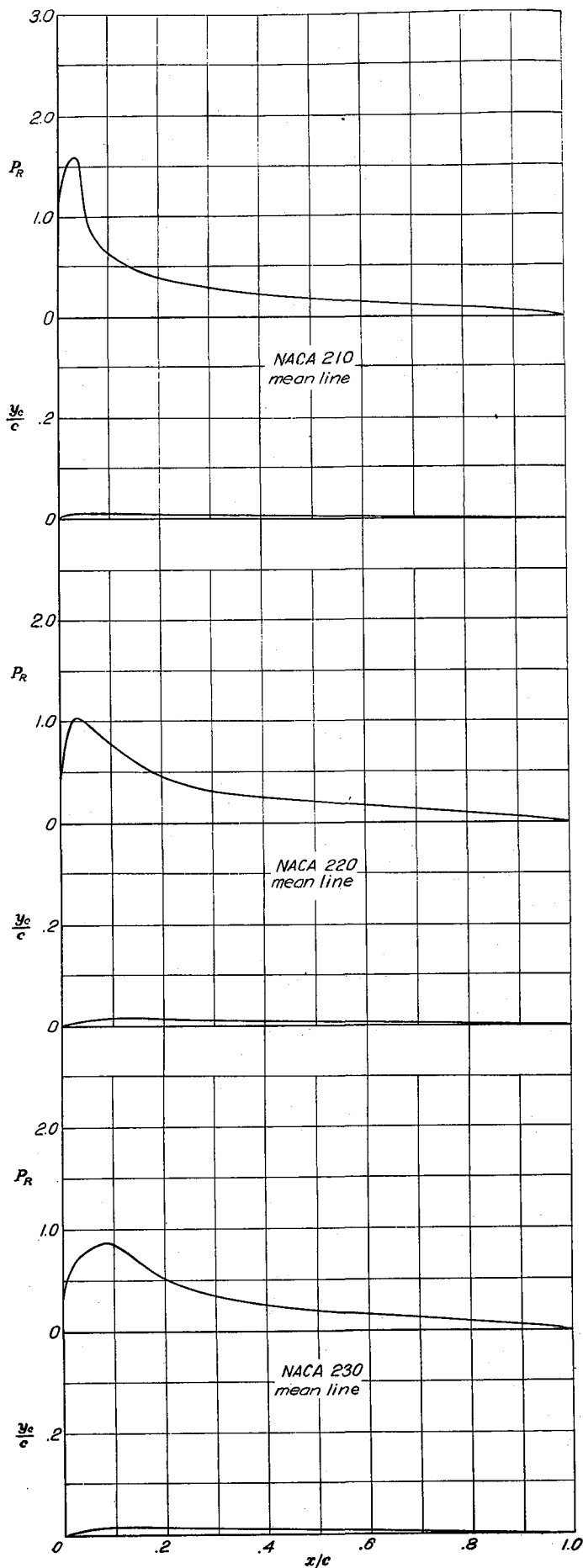
$c_{l_i}=0.75 \quad \alpha_i=0^\circ \quad c_{m_{c/4}}=-0.187$				
$x$ (percent $c$ )	$y_c$ (percent $c$ )	$dy_c/dx$	$P_R$	$\Delta v/V = P_R/4$
0	0	0.24000	0	0
1.25	.206	.23400	.205	.051
2.5	.585	.22800	.294	.074
5.0	1.140	.21600	.413	.103
7.5	1.665	.20400	.502	.126
10	2.160	.19200	.571	.143
15	3.060	.16800	.679	.170
20	3.840	.14400	.760	.190
25	4.500	.12000	.824	.206
30	5.040	.09600	.872	.218
40	5.760	.04800	.932	.233
50	6.000	0	.951	.238
60	5.760	-.04800	.932	.233
70	5.040	-.09600	.872	.218
80	3.840	-.14400	.760	.190
90	2.160	-.19200	.571	.143
95	1.140	-.21600	.413	.103
100	0	-.24000	0	0

NACA MEAN LINE 66

$c_{l_i}=0.76 \quad \alpha_i=-0.74^\circ \quad c_{m_{c/4}}=-0.222$				
$x$ (percent $c$ )	$y_c$ (percent $c$ )	$dy_c/dx$	$P_R$	$\Delta v/V = P_R/4$
0	0	0.20000	0	0
1.25	.247	.19583	.135	.034
2.5	.490	.19167	.244	.061
5.0	.958	.18333	.334	.084
7.5	1.406	.17500	.408	.102
10	1.833	.16667	.466	.117
15	2.625	.15000	.557	.139
20	3.333	.13333	.635	.159
25	3.958	.11667	.700	.175
30	4.500	.10000	.750	.188
40	5.333	.06667	.827	.207
50	5.833	.03333	.910	.228
60	6.000	0	.999	.250
70	5.625	-.07500	1.040	.260
80	4.500	-.15000	.966	.242
90	2.625	-.22500	.748	.187
95	1.406	-.26250	.546	.137
100	0	-.30000	0	0

NACA MEAN LINE 67

$c_{l_i}=0.80 \quad \alpha_i=-1.60^\circ \quad c_{m_{c/4}}=-0.266$				
$x$ (percent $c$ )	$y_c$ (percent $c$ )	$dy_c/dx$	$P_R$	$\Delta v/V = P_R/4$
0	0	0.17143	0	0
1.25	.212	.16837	.137	.034
2.5	.421	.16531	.195	.049
5	.827	.15918	.291	.073
7.5	1.217	.15306	.356	.089
10	1.592	.14694	.406	.102
15	2.296	.13469	.483	.121
20	2.939	.12245	.560	.140
25	3.520	.11020	.616	.154
30	4.041	.09796	.673	.168
40	4.898	.07347	.762	.191
50	5.510	.04898	.850	.213
60	5.878	.02449	.949	.237
70	6.000	0	1.160	.290
80	5.333	-.13333	1.259	.315
90	3.333	-.26667	1.066	.267
95	1.833	-.33333	.788	.197
100	0	-.40000	0	0



NACA MEAN LINE 210

$c_{l_i}=0.30 \quad \alpha_i=2.09^\circ \quad c_{m_{c/4}}=-0.006$				
$x$ (percent $c$ )	$y_c$ (percent $c$ )	$dy_c/dx$	$P_R$	$\Delta v/V = P_R/4$
0	0	0.59613	0	0
1.25	.596	.36236	1.381	.345
2.5	.928	.18504	1.565	.391
5.0	1.114	-.00018	1.221	.305
7.5	1.087		.781	.195
10	1.058		.626	.156
15	.999		.489	.122
20	.940		.408	.102
25	.881		.348	.087
30	.823		.302	.075
40	.705		.242	.061
50	.588	-.01175	.198	.049
60	.470		.160	.040
70	.363		.128	.032
80	.235		.098	.025
90	.118		.065	.016
95	.059		.044	.011
100	0		0	0

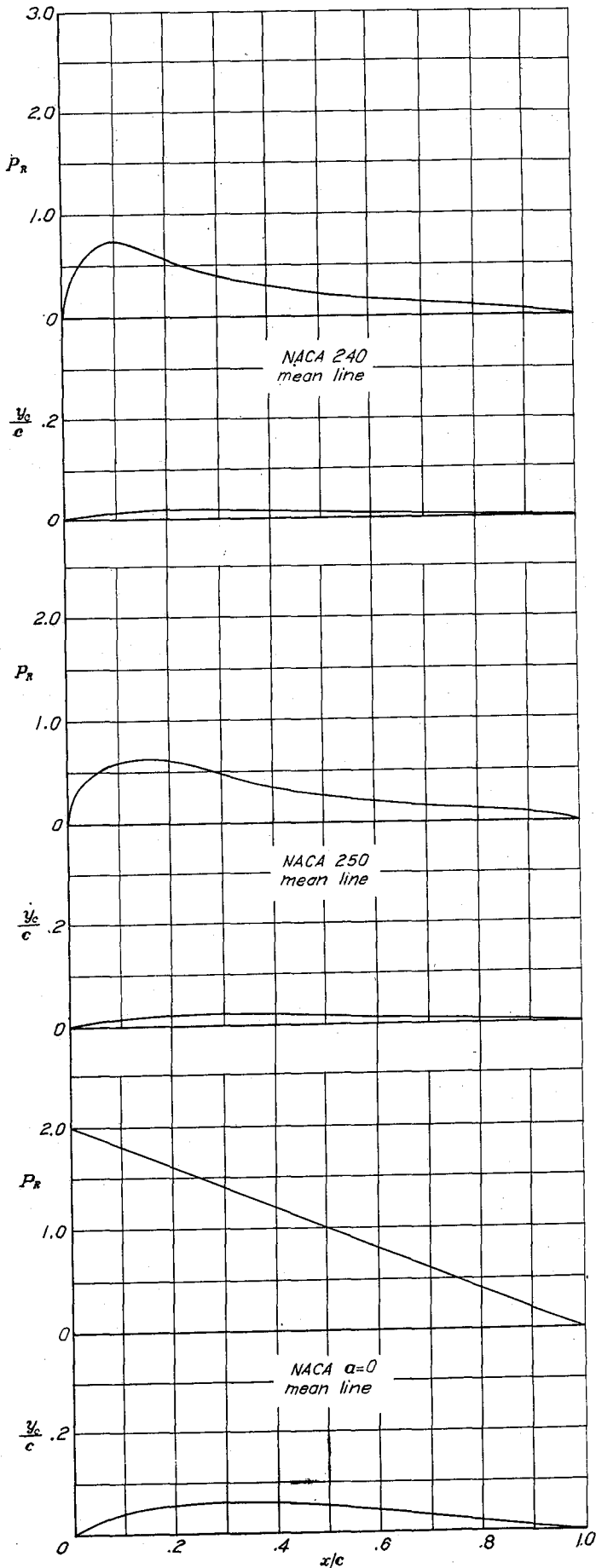
NACA MEAN LINE 220

$c_{l_i}=0.30 \quad \alpha_i=1.86^\circ \quad c_{m_{c/4}}=-0.010$				
$x$ (percent $c$ )	$y_c$ (percent $c$ )	$dy_c/dx$	$P_R$	$\Delta v/V = P_R/4$
0	0	0.39270	0	0
1.25	.442	.31541	.822	.206
2.5	.793	.24618	1.003	.251
5.0	1.257	.13192	.988	.247
7.5	1.479	.04994	.900	.225
10	1.535	.00024	.801	.200
15	1.463		.615	.154
20	1.377		.465	.116
25	1.291		.378	.095
30	1.205		.326	.082
40	1.033		.253	.063
50	.861	-.01722	.205	.051
60	.689		.169	.042
70	.516		.135	.034
80	.344		.100	.025
90	.172		.064	.016
95	.086		.040	.010
100	0		0	0

NACA MEAN LINE 230

$c_{l_i}=0.30 \quad \alpha_i=1.65^\circ \quad c_{m_{c/4}}=-0.014$				
$x$ (percent $c$ )	$y_c$ (percent $c$ )	$dy_c/dx$	$P_R$	$\Delta v/V = P_R/4$
0	0	0.30508	0	0
1.25	.357	.26594	.628	.152
2.5	.666	.22929	.673	.168
5.0	1.155	.16347	.791	.198
7.5	1.492	.10762	.853	.213
10	1.701	.06174	.859	.215
15	1.838	-.00009	.678	.170
20	1.787	-.02203	.519	.130
25	1.656		.419	.105
30	1.546		.361	.090
40	1.325		.274	.069
50	1.104		.217	.054
60	.883	-.02208	.177	.044
70	.662		.144	.036
80	.442		.105	.026
90	.221		.069	.017
95	.110		.042	.011
100	0		0	0





NACA MEAN LINE 240

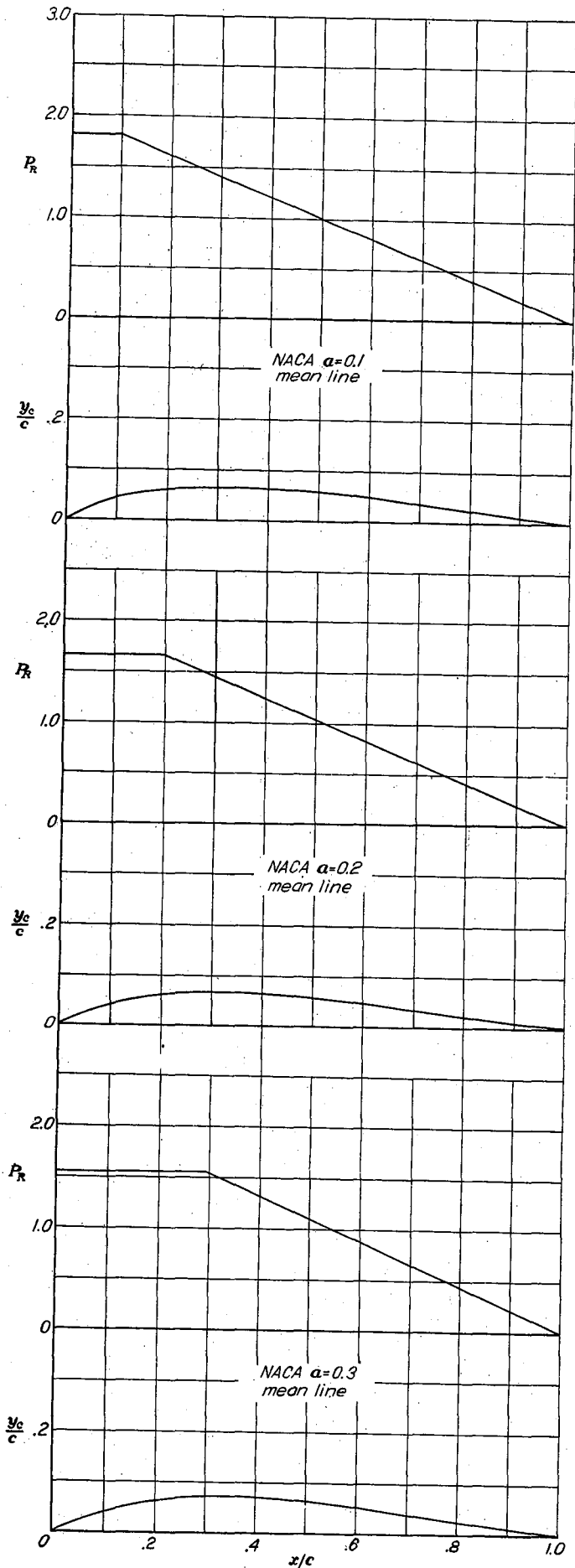
$c_{l_i}=0.30 \quad \alpha_i=1.45^\circ \quad c_{m_{c/4}}=-0.019$				
$x$ (percent $c$ )	$y_c$ (percent $c$ )	$dy_c/dx$	$P_R$	$\Delta v/V=P_R/4$
0	0	0.25233	0	0
1.25	.301	.22877	.377	.094
2.5	.572	.20625	.491	.123
5.0	1.035	.16432	.625	.156
7.5	1.397	.12653	.718	.180
10	1.671	.09290	.750	.188
15	1.991	.03810	.677	.169
20	2.079	-.00010	.566	.142
25	2.018	-.02169	.477	.119
30	1.890		.410	.103
40	1.620		.304	.076
50	1.350		.234	.059
60	1.080		.186	.047
70	.810	-.02700	.150	.038
80	.540		.110	.028
90	.270		.071	.018
95	.135		.047	.012
100	0		0	0

NACA MEAN LINE 250

$c_{l_i}=0.30 \quad \alpha_i=1.26^\circ \quad c_{m_{c/4}}=-0.026$				
$x$ (percent $c$ )	$y_c$ (percent $c$ )	$dy_c/dx$	$P_R$	$\Delta v/V=P_R/4$
0	0	0.21472	0	0
1.25	.258	.19920	.281	.070
2.5	.498	.18416	.369	.092
5.0	.922	.15582	.477	.119
7.5	1.277	.12909	.552	.138
10	1.570	.10458	.592	.148
15	1.982	.06182	.624	.156
20	2.199	.02674	.610	.153
25	2.263	-.00007	.547	.137
30	2.212	-.01880	.470	.117
40	1.931		.346	.087
50	1.609		.255	.064
60	1.287		.197	.049
70	.965	-.03218	.154	.038
80	.644		.119	.030
90	.322		.076	.019
95	.161		.051	.013
100	0		0	0

NACA MEAN LINE  $\alpha=0$

$c_{l_i}=1.0 \quad \alpha_i=4.56^\circ \quad c_{m_{c/4}}=-0.083$				
$x$ (percent $c$ )	$y_c$ (percent $c$ )	$dy_c/dx$	$P_R$	$\Delta v/V=P_R/4$
0	0			
.5	.460	0.75867	1.990	0.498
.75	.641	.69212	1.985	.496
1.25	.964	.60715	1.975	.494
2.5	1.641	.48892	1.950	.488
5.0	2.693	.36561	1.900	.475
7.5	3.507	.29028	1.850	.463
10	4.161	.23515	1.800	.450
15	5.124	.15508	1.700	.425
20	5.747	.09693	1.600	.400
25	6.114	.05156	1.500	.375
30	6.277	.01482	1.400	.350
35	6.273	-.01554	1.300	.325
40	6.130	-.04086	1.200	.300
45	5.871	-.06201	1.100	.275
50	5.516	-.07958	1.000	.250
55	5.081	-.09395	.900	.225
60	4.581	-.10539	.800	.200
65	4.032	-.11406	.700	.175
70	3.445	-.12003	.600	.150
75	2.836	-.12329	.500	.125
80	2.217	-.12371	.400	.100
85	1.604	-.12099	.300	.075
90	1.013	-.11455	.200	.050
95	.467	-.10301	.100	.025
100	0	-.07958	0	0



NACA MEAN LINE  $\alpha=0.1$

$c_{l_i}=1.0 \quad \alpha_i=4.43^\circ \quad c_{m_{c/4}}=-0.086$				
$x$ (percent $c$ )	$y_c$ (percent $c$ )	$dy_c/dx$	$P_R$	$\Delta v/V = P_R/4$
0	0	0.73441		
.5	.440	0.67479	1.818	0.455
.75	.616	.59896		
1.25	.933	.49366		
2.5	1.608	.38235		
5.0	2.689	.31067		
7.5	3.551	.26057		
10	4.253	.16087		
15	5.261	.09981	1.616	.404
20	5.905	.05281	1.515	.379
25	6.282	.01498	1.414	.354
30	6.449	-.01617	1.313	.328
35	6.443	-.04210	1.212	.303
40	6.296	-.06373	1.111	.278
45	6.029	-.08168	1.010	.253
50	5.664	-.09637	.909	.227
55	5.218	-.10806	.808	.202
60	4.706	-.11694	.707	.177
65	4.142	-.12307	.606	.152
70	3.541	-.12644	.505	.126
75	2.916	-.12893	.404	.101
80	2.281	-.12425	.303	.076
85	1.652	-.11781	.202	.050
90	1.045	-.10820	.101	.025
95	.482			
100	0	-.08258	0	0

NACA MEAN LINE  $\alpha=0.2$

$c_{l_i}=1.0 \quad \alpha_i=4.17^\circ \quad c_{m_{c/4}}=-0.094$				
$x$ (percent $c$ )	$y_c$ (percent $c$ )	$dy_c/dx$	$P_R$	$\Delta v/V = P_R/4$
0	0	0.69492		
.5	.414	.64047	1.667	0.417
.75	.581	.57135		
1.25	.882	.47592		
2.5	1.530	.37661		
5.0	2.583	.31487		
7.5	3.443	.26803		
10	4.169	.19373		
15	5.317	.12405	1.459	.365
20	6.117	.06345	1.355	.339
25	6.572	-.01418	1.250	.313
30	6.777	-.04246	1.146	.287
35	6.789	-.06588	1.042	.260
40	6.646	-.08522	.938	.234
45	6.373	-.10101	.834	.208
50	5.994	-.11359	.729	.182
55	5.527	-.12317	.625	.156
60	4.989	-.12985	.521	.130
65	4.396	-.13363	.417	.104
70	3.762	-.13440	.313	.078
75	3.102	-.13186	.208	.052
80	2.431	-.12541	.104	.026
85	1.764	-.11361		
90	1.119	-.08941	0	0
95	.518			
100	0			

NACA MEAN LINE  $\alpha=0.3$

$c_{l_i}=1.0 \quad \alpha_i=3.84^\circ \quad c_{m_{c/4}}=-0.106$				
$x$ (percent $c$ )	$y_c$ (percent $c$ )	$dy_c/dx$	$P_R$	$\Delta v/V = P_R/4$
0	0	0.65536		
.5	.389	.60524	1.538	0.385
.75	.546	.54158		
1.25	.832	.45399		
2.5	1.448	.36344		
5.0	2.458	.30780		
7.5	3.293	.26621		
10	4.008	.20246		
15	5.172	.15068	1.319	.330
20	6.052	.10278	1.209	.302
25	6.685	.04833	1.099	.275
30	7.072	-.00205	.989	.247
35	7.175	-.03710	.879	.220
40	7.074	-.06492	.769	.192
45	6.816	-.08746	.659	.165
50	6.433	-.10567	.549	.137
55	5.949	-.12014	.440	.110
60	5.383	-.13119	.330	.082
65	4.753	-.13901	.220	.055
70	4.076	-.14365	.110	.028
75	3.368	-.14500		
80	2.645	-.14279		
85	1.924	-.13638		
90	1.224	-.12430		
95	.570	-.09907	0	0
100	0			

NACA MEAN LINE  $\alpha=0.4$

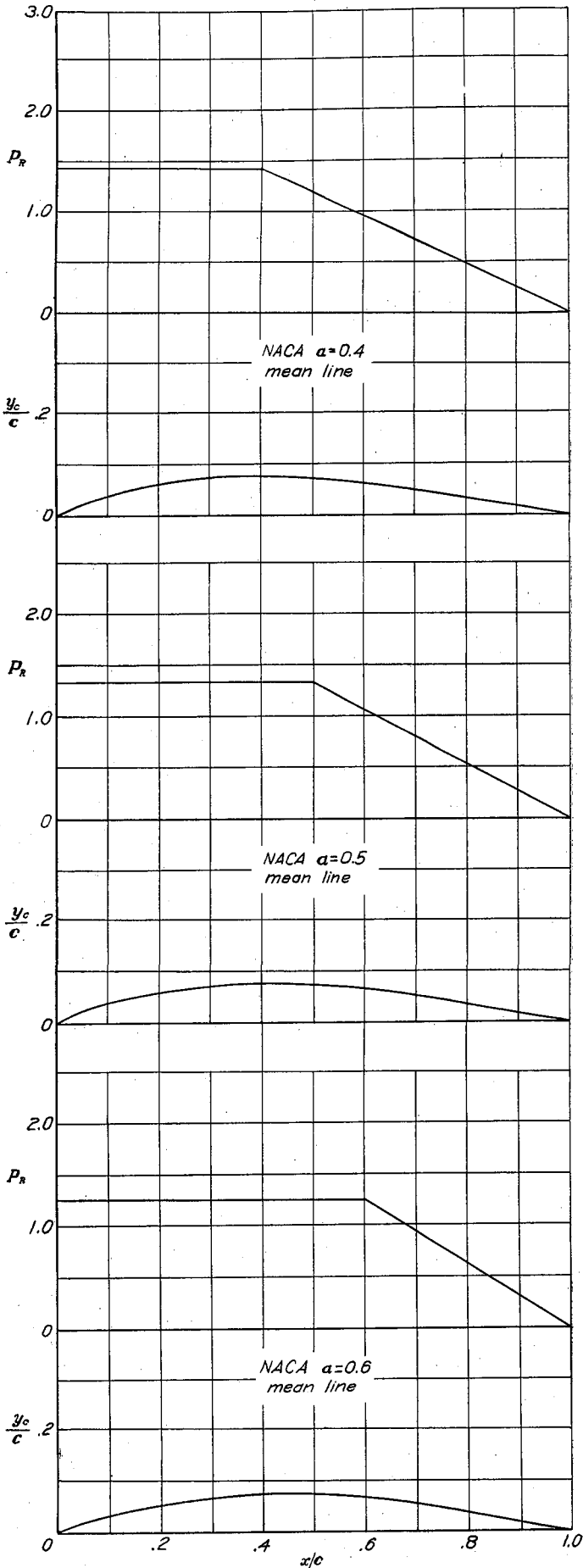
$c_{l_i}=1.0$ $\alpha_i=3.46^\circ$ $c_{m_{c/4}}=-0.121$				
$x$ (percent $c$ )	$y_c$ (percent $c$ )	$dy_c/dx$	$P_R$	$\Delta v/V = P_R/4$
0	0	0.61759	-----	-----
.5	.366	0.61759	1.429	0.357
.75	.514	.57105		
1.25	.784	.51210		
2.5	1.367	.43106		
5.0	2.330	.34764		
7.5	3.131	.29671		
10	3.824	.25892		
15	4.968	.20185		
20	5.862	.16682		
25	6.546	.11733		
30	7.039	.07988		
35	7.343	.04136		
40	7.439	-.00721		
45	7.275	-.05321	1.310	.327
50	6.929	-.08380	1.190	.298
55	6.449	-.10734	1.071	.268
60	5.864	-.12567	.952	.238
65	5.199	-.13962	.833	.208
70	4.475	-.14963	.714	.179
75	3.709	-.15589	.595	.149
80	2.922	-.15857	.476	.119
85	2.132	-.15685	.357	.089
90	1.361	-.15062	.238	.060
95	.636	-.13816	.119	.030
100	0	-.11138	0	0

NACA MEAN LINE  $\alpha=0.5$

$c_{l_i}=1.0$ $\alpha_i=3.04^\circ$ $c_{m_{c/4}}=-0.139$				
$x$ (percent $c$ )	$y_c$ (percent $c$ )	$dy_c/dx$	$P_R$	$\Delta v/V = P_R/4$
0	0	0.58195	-----	-----
.5	.345	0.58195	1.333	0.333
.75	.485	.53855		
1.25	.735	.43360		
2.5	1.295	.40815		
5.0	2.205	.33070		
7.5	2.970	.28355		
10	3.630	.24890		
15	4.740	.19690		
20	5.620	.15650		
25	6.310	.12180		
30	6.840	.09000		
35	7.215	.05930		
40	7.430	.02800		
45	7.490	-.00630		
50	7.350	-.05305	1.200	.300
55	6.965	-.08765	1.067	.267
60	6.405	-.12550	.933	.233
65	5.725	-.14570	.800	.200
70	4.955	-.16015	.667	.167
75	4.130	-.16960	.533	.133
80	3.265	-.17435	.400	.100
85	2.395	-.17415	.267	.067
90	1.535	-.16850	.133	.033
95	.720	-.15565	0	0
100	0	-.12660	0	0

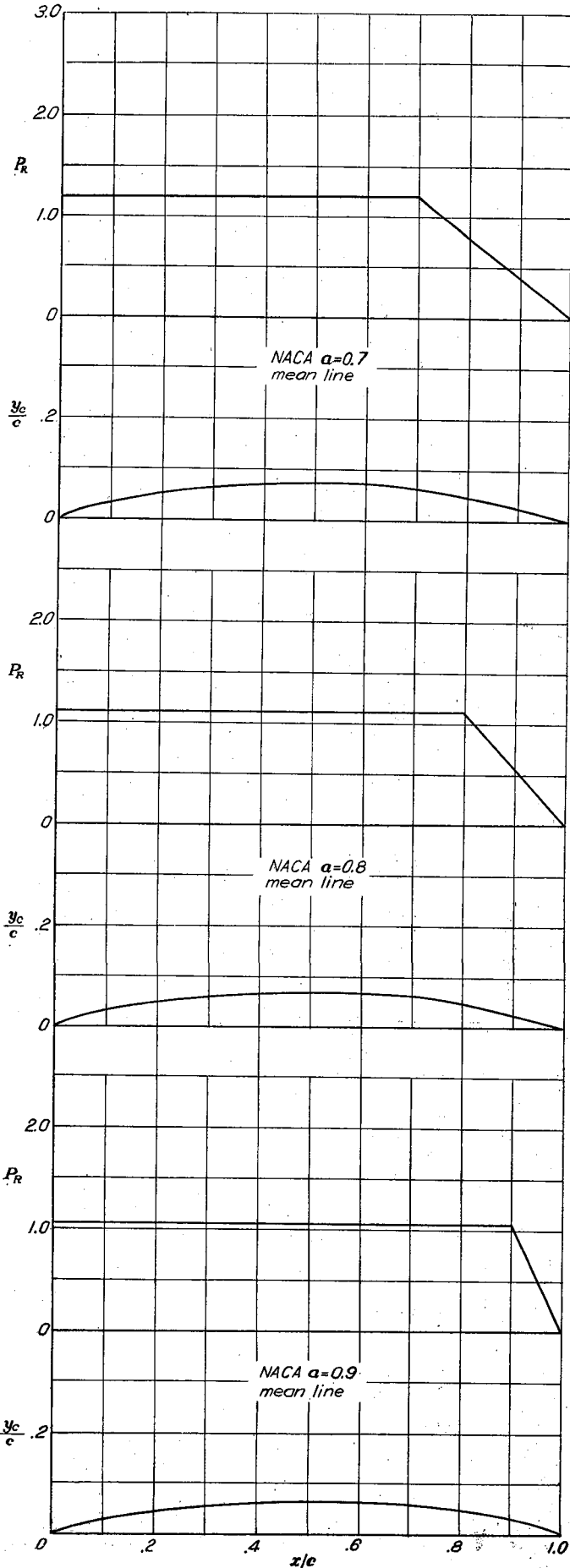
NACA MEAN LINE  $\alpha=0.6$

$c_{l_i}=1.0$ $\alpha_i=2.58^\circ$ $c_{m_{c/4}}=-0.158$				
$x$ (percent $c$ )	$y_c$ (percent $c$ )	$dy_c/dx$	$P_R$	$\Delta v/V = P_R/4$
0	0	0.54825	-----	-----
.5	.325	0.54825	1.250	0.312
.75	.455	.50760		
1.25	.695	.45615		
2.5	1.220	.38555		
5.0	2.080	.31325		
7.5	2.805	.26950		
10	3.435	.23730		
15	4.495	.18935		
20	5.345	.15250		
25	6.035	.12125		
30	6.570	.09310		
35	6.965	.06660		
40	7.235	.04060		
45	7.370	.01405		
50	7.370	-.01435	1.094	.273
55	7.220	-.04700	.938	.234
60	6.880	-.09470	.781	.195
65	6.275	-.14015	.625	.156
70	5.505	-.16595	.469	.117
75	4.630	-.18270	.312	.078
80	3.695	-.19225	.156	.039
85	2.720	-.19515	0	0
90	1.755	-.19095	0	0
95	.825	-.17790	0	0
100	0	-.14550	0	0



NACA MEAN LINE  $\alpha=0.7$

$c_{l_i}=1.0$		$\alpha_i=2.09^\circ$	$c_{m_{c/4}}=-0.179$	
$x$ (percent $c$ )	$y_c$ (percent $c$ )	$dy_c/dx$	$P_R$	$\Delta v/V = P_R/4$
0	0	---	---	---
.5	.305	0.51620	1.176	0.294
.75	.425	.47795		
1.25	.655	.42960		
2.5	1.100	.36325		
5.0	1.955	.29545		
7.5	2.645	.25450		
10	3.240	.22445		
15	4.245	.17995		
20	5.060	.14595		
25	5.715	.11740		
30	6.240	.09200		
35	6.635	.06840		
40	6.925	.04570		
45	7.095	.02315		
50	7.155	0		
55	7.090	-.02455		
60	6.900	-.05185		
65	6.565	-.08475		
70	6.030	-.13650		
75	5.205	-.18510		
80	4.215	-.20855		
85	3.140	-.21955		
90	2.035	-.21060		
95	.965	-.20725		
100	0	-.16985	0	0

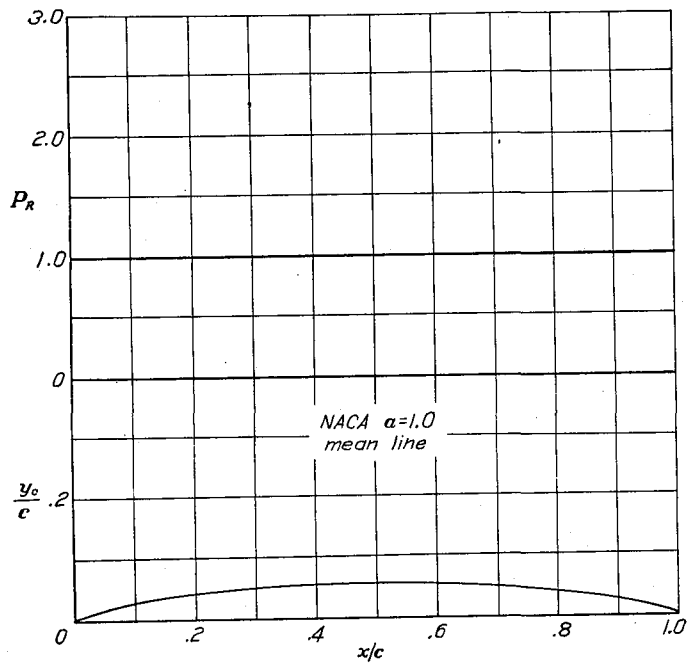


NACA MEAN LINE  $\alpha=0.8$

$c_{l_i}=1.0$		$\alpha_i=1.54^\circ$	$c_{m_{c/4}}=-0.202$	
$x$ (percent $c$ )	$y_c$ (percent $c$ )	$dy_c/dx$	$P_R$	$\Delta v/V = P_R/4$
0	0	---	---	---
.5	.287	0.48535	1.111	0.278
.75	.404	.44925		
1.25	.616	.40359		
2.5	1.077	.34104		
5.0	1.841	.27718		
7.5	2.483	.23868		
10	3.043	.21050		
15	3.985	.16892		
20	4.748	.13734		
25	5.367	.11101		
30	5.863	.08775		
35	6.248	.06634		
40	6.528	.04601		
45	6.709	.02613		
50	6.790	.00620		
55	6.770	-.01433		
60	6.644	-.03611		
65	6.405	-.06010		
70	6.037	-.08790		
75	5.514	-.12311		
80	4.771	-.18412		
85	3.683	-.23921		
90	2.435	-.25583		
95	1.163	-.24904		
100	0	-.20385	0	0

NACA MEAN LINE  $\alpha=0.9$

$c_{l_i}=1.0$		$\alpha_i=0.90^\circ$	$c_{m_{c/4}}=-0.225$	
$x$ (percent $c$ )	$y_c$ (percent $c$ )	$dy_c/dx$	$P_R$	$\Delta v/V = P_R/4$
0	0	---	---	---
.5	.269	0.45482	1.053	0.263
.75	.379	.42064		
1.25	.677	.37740		
2.5	1.008	.31821		
5.0	1.720	.25786		
7.5	2.316	.22153		
10	2.835	.19500		
15	3.707	.15595		
20	4.410	.12644		
25	4.980	.10196		
30	5.435	.08047		
35	5.787	.06084		
40	6.045	.04234		
45	6.212	.02447		
50	6.290	.00678		
55	6.279	-.01111		
60	6.173	-.02865		
65	5.981	-.04938		
70	5.681	-.07103		
75	5.265	-.09583		
80	4.714	-.12305		
85	3.987	-.16727		
90	2.984	-.22204		
95	1.503	-.28463		
100	0	-.26086	0	0



NACA MEAN LINE  $\alpha=1.0$

$c_{l_i}=1.0 \quad \alpha_i=0^\circ \quad c_{m_{c/4}}=-0.250$				
$x$ (percent $c$ )	$y_e$ (percent $c$ )	$dy_e/dx$	$P_R$	$\Delta v/V = P_R/4$
0	0			
.5	.250	0.42120	1.000	0.250
.75	.350	.38875		
1.25	.535	.34770		
2.5	.930	.29155		
5.0	1.580	.23430		
7.5	2.120	.19995		
10	2.585	.17485		
15	3.365	.13805		
20	3.980	.11030		
25	4.475	.08745		
30	4.860	.06745		
35	5.150	.04925		
40	5.355	.03225		
45	5.475	.01595		
50	5.515	0		
55	5.475	-.01595		
60	5.355	-.03225		
65	5.150	-.04925		
70	4.860	-.06745		
75	4.475	-.08745		
80	3.980	-.11030		
85	3.365	-.13805		
90	2.585	-.17485		
95	1.580	-.23430		
100	0			

## III—AIRFOIL ORDINATES

	Page		Page
NACA 0006	100	NACA 64 <sub>3</sub> -218	105
NACA 0009	100	NACA 64 <sub>3</sub> -418	106
NACA 1408	100	NACA 64 <sub>3</sub> -618	106
NACA 1410	100	NACA 64 <sub>4</sub> -021	106
NACA 1412	100	NACA 64 <sub>4</sub> -221	106
NACA 2412	100	NACA 64 <sub>4</sub> -421	196
NACA 2415	100	NACA 65, 3-018	106
NACA 2418	100	NACA 65, 3-418, $\alpha=0.8$	106
NACA 2421	100	NACA 65, 3-618	106
NACA 2424	100	NACA 65(216)-415, $\alpha=0.5$	106
NACA 4412	101	NACA 65-006	106
NACA 4415	101	NACA 65-009	107
NACA 4418	101	NACA 65-206	107
NACA 4421	101	NACA 65-209	107
NACA 4424	101	NACA 65-210	107
NACA 23012	101	NACA 65-410	107
NACA 23015	101	NACA 65 <sub>1</sub> -012	107
NACA 23018	101	NACA 65 <sub>1</sub> -212	107
NACA 23021	101	NACA 65 <sub>1</sub> -212, $\alpha=0.6$	107
NACA 23024	101	NACA 65 <sub>1</sub> -412	107
NACA 63, 4-420	102	NACA 65 <sub>2</sub> -015	107
NACA 63, 4-420, $\alpha=0.3$	102	NACA 65 <sub>2</sub> -215	108
NACA 63(420)-422	102	NACA 65 <sub>2</sub> -415	108
NACA 63(420)-517	102	NACA 65 <sub>2</sub> -415, $\alpha=0.5$	108
NACA 63-006	102	NACA 65 <sub>3</sub> -018	108
NACA 63-009	102	NACA 65 <sub>3</sub> -218	108
NACA 63-206	102	NACA 65 <sub>3</sub> -418	108
NACA 63-209	102	NACA 65 <sub>3</sub> -418, $\alpha=0.5$	108
NACA 63-210	102	NACA 65 <sub>3</sub> -618	108
NACA 63 <sub>1</sub> -012	102	NACA 65 <sub>3</sub> -618, $\alpha=0.5$	108
NACA 63 <sub>1</sub> -212	103	NACA 65 <sub>4</sub> -021	109
NACA 63 <sub>1</sub> -412	103	NACA 65 <sub>4</sub> -221	109
NACA 63 <sub>2</sub> -015	103	NACA 65 <sub>4</sub> -421	109
NACA 63 <sub>2</sub> -215	103	NACA 65 <sub>4</sub> -421, $\alpha=0.5$	109
NACA 63 <sub>2</sub> -415	103	NACA 65(215)-114	109
NACA 63 <sub>2</sub> -615	103	NACA 65(420)-420	109
NACA 63 <sub>3</sub> -018	103	NACA 66, 1-212	109
NACA 63 <sub>3</sub> -218	103	NACA 66(215)-016	109
NACA 63 <sub>3</sub> -418	103	NACA 66(215)-216	109
NACA 63 <sub>3</sub> -618	103	NACA 66(215)-216, $\alpha=0.6$	109
NACA 63 <sub>4</sub> -021	104	NACA 66(215)-416	109
NACA 63 <sub>4</sub> -221	104	NACA 66-006	110
NACA 63 <sub>4</sub> -421	104	NACA 66-009	110
NACA 64-006	104	NACA 66-206	110
NACA 64-009	104	NACA 66-209	110
NACA 64-108	104	NACA 66-210	110
NACA 64-110	104	NACA 66 <sub>1</sub> -012	110
NACA 64-206	104	NACA 66 <sub>1</sub> -212	110
NACA 64-208	104	NACA 66 <sub>2</sub> -015	110
NACA 64-209	104	NACA 66 <sub>2</sub> -215	110
NACA 64-210	105	NACA 66 <sub>2</sub> -415	110
NACA 64 <sub>1</sub> -012	105	NACA 66 <sub>3</sub> -018	111
NACA 64 <sub>1</sub> -112	105	NACA 66 <sub>3</sub> -218	111
NACA 64 <sub>1</sub> -212	105	NACA 66 <sub>3</sub> -418	111
NACA 64 <sub>1</sub> -412	105	NACA 66 <sub>4</sub> -021	111
NACA 64 <sub>2</sub> -015	105	NACA 66 <sub>4</sub> -221	111
NACA 64 <sub>2</sub> -215	105	NACA 67, 1-215	111
NACA 64 <sub>2</sub> -415	105	NACA 747A315	111
NACA 64 <sub>3</sub> -018	105	NACA 747A415	111







NACA 63,4-420

[Stations and ordinates given in percent of airfoil chord]

Table with 4 columns: Station, Ordinate, Station, Ordinate. Rows include station numbers from 0 to 100 and corresponding ordinates for upper and lower surfaces. L. E. radius: 3.16, Slope of radius through L. E.: 0.168

NACA 63,4-420

a = 0.3 [Stations and ordinates given in percent of airfoil chord]

Table with 4 columns: Station, Ordinate, Station, Ordinate. Rows include station numbers from 0 to 100 and corresponding ordinates for upper and lower surfaces. L. E. radius: 3.16, Slope of radius through L. E.: 0.262

NACA 63(420)-422

[Stations and ordinates given in percent of airfoil chord]

Table with 4 columns: Station, Ordinate, Station, Ordinate. Rows include station numbers from 0 to 100 and corresponding ordinates for upper and lower surfaces. L. E. radius: 3.82, Slope of radius through L. E.: 0.168

NACA 63(420)-517

[Stations and ordinates given in percent of airfoil chord]

Table with 4 columns: Station, Ordinate, Station, Ordinate. Rows include station numbers from 0 to 100 and corresponding ordinates for upper and lower surfaces. L. E. radius: 2.283, Slope of radius through L. E.: 0.211

NACA 63-006

[Stations and ordinates given in percent of airfoil chord]

Table with 4 columns: Station, Ordinate, Station, Ordinate. Rows include station numbers from 0 to 100 and corresponding ordinates for upper and lower surfaces. L. E. radius: 0.297

NACA 63-009

[Stations and ordinates given in percent of airfoil chord]

Table with 4 columns: Station, Ordinate, Station, Ordinate. Rows include station numbers from 0 to 100 and corresponding ordinates for upper and lower surfaces. L. E. radius: 0.631

NACA 63-206

[Stations and ordinates given in percent of airfoil chord]

Table with 4 columns: Station, Ordinate, Station, Ordinate. Rows include station numbers from 0 to 100 and corresponding ordinates for upper and lower surfaces. L. E. radius: 0.297, Slope of radius through L. E.: 0.0842

NACA 63-209

[Stations and ordinates given in percent of airfoil chord]

Table with 4 columns: Station, Ordinate, Station, Ordinate. Rows include station numbers from 0 to 100 and corresponding ordinates for upper and lower surfaces. L. E. radius: 0.631, Slope of radius through L. E.: 0.0842

NACA 63-210

[Stations and ordinates given in percent of airfoil chord]

Table with 4 columns: Station, Ordinate, Station, Ordinate. Rows include station numbers from 0 to 100 and corresponding ordinates for upper and lower surfaces. L. E. radius: 0.770, Slope of radius through L. E.: 0.0842

NACA 631-012

[Stations and ordinates given in percent of airfoil chord]

Table with 4 columns: Station, Ordinate, Station, Ordinate. Rows include station numbers from 0 to 100 and corresponding ordinates for upper and lower surfaces. L. E. radius: 1.087



NACA 634-021

[Stations and ordinates given in percent of airfoil chord]

Table with 4 columns: Station, Ordinate, Station, Ordinate. Rows 0 to 100. L. E. radius: 2.650

NACA 634-221

[Stations and ordinates given in percent of airfoil chord]

Table with 4 columns: Station, Ordinate, Station, Ordinate. Rows 0 to 100. L. E. radius: 2.650, Slope of radius through L. E.: 0.0842

NACA 634-421

[Stations and ordinates given in percent of airfoil chord]

Table with 4 columns: Station, Ordinate, Station, Ordinate. Rows 0 to 100. L. E. radius: 2.650, Slope of radius through L. E.: 0.1685

NACA 64-006

[Stations and ordinates given in percent of airfoil chord]

Table with 4 columns: Station, Ordinate, Station, Ordinate. Rows 0 to 100. L. E. radius: 0.256

NACA 64-009

[Stations and ordinates given in percent of airfoil chord]

Table with 4 columns: Station, Ordinate, Station, Ordinate. Rows 0 to 100. L. E. radius: 0.579

NACA 64-108

[Stations and ordinates given in percent of airfoil chord]

Table with 4 columns: Station, Ordinate, Station, Ordinate. Rows 0 to 100. L. E. radius: 0.455, Slope of radius through L. E.: 0.042

NACA 64-110

[Stations and ordinates given in percent of airfoil chord]

Table with 4 columns: Station, Ordinate, Station, Ordinate. Rows 0 to 100. L. E. radius: 0.720, Slope of radius through L. E.: 0.042

NACA 64-206

[Stations and ordinates given in percent of airfoil chord]

Table with 4 columns: Station, Ordinate, Station, Ordinate. Rows 0 to 100. L. E. radius: 0.256, Slope of radius through L. E.: 0.084

NACA 64-208

[Stations and ordinates given in percent of airfoil chord]

Table with 4 columns: Station, Ordinate, Station, Ordinate. Rows 0 to 100. L. E. radius: 0.455, Slope of radius through L. E.: 0.084

NACA 64-209

[Stations and ordinates given in percent of airfoil chord]

Table with 4 columns: Station, Ordinate, Station, Ordinate. Rows 0 to 100. L. E. radius: 0.579, Slope of radius through L. E.: 0.084



NACA 643-418

[Stations and ordinates given in percent of airfoil chord]

Table with 4 columns: Station, Ordinate, Station, Ordinate. Rows 0 to 100.000. L. E. radius: 2.208, Slope of radius through L. E.: 0.168

NACA 643-618

[Stations and ordinates given in percent of airfoil chord]

Table with 4 columns: Station, Ordinate, Station, Ordinate. Rows 0 to 100.000. L. E. radius: 2.208, Slope of radius through L. E.: 0.253

NACA 644-021

[Stations and ordinates given in percent of airfoil chord]

Table with 4 columns: Station, Ordinate, Station, Ordinate. Rows 0 to 100. L. E. radius: 2.884

NACA 644-221

[Stations and ordinates given in percent of airfoil chord]

Table with 4 columns: Station, Ordinate, Station, Ordinate. Rows 0 to 100.000. L. E. radius: 2.884, Slope of radius through L. E.: 0.084

NACA 644-421

[Stations and ordinates given in percent of airfoil chord]

Table with 4 columns: Station, Ordinate, Station, Ordinate. Rows 0 to 100.000. L. E. radius: 2.884, Slope of radius through L. E.: 0.168

NACA 65,3-018

[Stations and ordinates given in percent of airfoil chord]

Table with 4 columns: Station, Ordinate, Station, Ordinate. Rows 0 to 100. L. E. radius: 1.92

NACA 65,3-418  
a=0.8

[Stations and ordinates given in percent of airfoil chord]

Table with 4 columns: Station, Ordinate, Station, Ordinate. Rows 0 to 100.000. L. E. radius: 1.92, Slope of radius through L. E.: 0.194

NACA 65,3-618

[Stations and ordinates given in percent of airfoil chord]

Table with 4 columns: Station, Ordinate, Station, Ordinate. Rows 0 to 100.000. L. E. radius: 1.92, Slope of radius through L. F.: 0.253

NACA 65(216)-415  
a=0.5

[Stations and ordinates given in percent of airfoil chord]

Table with 4 columns: Station, Ordinate, Station, Ordinate. Rows 0 to 100.000. L. E. radius: 1.498, Slope of radius through L. E.: 0.233

NACA 65-006

[Stations and ordinates given in percent of airfoil chord]

Table with 4 columns: Station, Ordinate, Station, Ordinate. Rows 0 to 100. L. E. radius: 0.240



NACA 652-215

[Stations and ordinates given in percent of airfoil chord]

Table with 4 columns: Station, Ordinate, Station, Ordinate. Rows 0 to 100.000. Includes L. E. radius: 1.505 and Slope of radius through L. E.: 0.084.

NACA 652-415

[Stations and ordinates given in percent of airfoil chord]

Table with 4 columns: Station, Ordinate, Station, Ordinate. Rows 0 to 100.000. Includes L. E. radius: 1.505 and Slope of radius through L. E.: 0.168.

NACA 652-415 a=0.5

[Stations and ordinates given in percent of airfoil chord]

Table with 4 columns: Station, Ordinate, Station, Ordinate. Rows 0 to 100.000. Includes L. E. radius: 1.505 and Slope of radius through L. E.: 0.233.

NACA 653-018

[Stations and ordinates given in percent of airfoil chord]

Table with 4 columns: Station, Ordinate, Station, Ordinate. Rows 0 to 100. Includes L. E. radius: 1.96.

NACA 653-218

[Stations and ordinates given in percent of airfoil chord]

Table with 4 columns: Station, Ordinate, Station, Ordinate. Rows 0 to 100.000. Includes L. E. radius: 1.96 and Slope of radius through L. E.: 0.084.

NACA 653-418

[Stations and ordinates given in percent of airfoil chord]

Table with 4 columns: Station, Ordinate, Station, Ordinate. Rows 0 to 100.000. Includes L. E. radius: 1.96 and Slope of radius through L. E.: 0.168.

NACA 653-418 a=0.5

[Stations and ordinates given in percent of airfoil chord]

Table with 4 columns: Station, Ordinate, Station, Ordinate. Rows 0 to 100.000. Includes L. E. radius: 1.96 and Slope of radius through L. E.: 0.233.

NACA 653-618

[Stations and ordinates given in percent of airfoil chord]

Table with 4 columns: Station, Ordinate, Station, Ordinate. Rows 0 to 100.000. Includes L. E. radius: 1.96 and Slope of radius through L. E.: 0.253.

NACA 653-618 a=0.5

[Stations and ordinates given in percent of airfoil chord]

Table with 4 columns: Station, Ordinate, Station, Ordinate. Rows 0 to 100.000. Includes L. E. radius: 1.96 and Slope of radius through L. E.: 0.349.

NACA 654-021

[Stations and ordinates given in percent of airfoil chord]

Table with 4 columns: Station, Ordinate, Station, Ordinate. Rows 0 to 100. Includes L. E. radius: 2.50.





NACA 66-006

[Stations and ordinates given in percent of airfoil chord]

Table with 4 columns: Station, Ordinate, Station, Ordinate. Rows for upper and lower surfaces from 0 to 100. L. E. radius: 0.223

NACA 66-009

[Stations and ordinates given in percent of airfoil chord]

Table with 4 columns: Station, Ordinate, Station, Ordinate. Rows for upper and lower surfaces from 0 to 100. L. E. radius: 0.530

NACA 66-206

[Stations and ordinates given in percent of airfoil chord]

Table with 4 columns: Station, Ordinate, Station, Ordinate. Rows for upper and lower surfaces from 0 to 100. L. E. radius: 0.223, Slope of radius through L. E.: 0.084

NACA 66-209

[Stations and ordinates given in percent of airfoil chord]

Table with 4 columns: Station, Ordinate, Station, Ordinate. Rows for upper and lower surfaces from 0 to 100. L. E. radius: 0.530, Slope of radius through L. E.: 0.084

NACA 66-210

[Stations and ordinates given in percent of airfoil chord]

Table with 4 columns: Station, Ordinate, Station, Ordinate. Rows for upper and lower surfaces from 0 to 100. L. E. radius: 0.662, Slope of radius through L. E.: 0.094

NACA 661-012

[Stations and ordinates given in percent of airfoil chord]

Table with 4 columns: Station, Ordinate, Station, Ordinate. Rows for upper and lower surfaces from 0 to 100. L. E. radius: 0.952

NACA 661-212

[Stations and ordinates given in percent of airfoil chord]

Table with 4 columns: Station, Ordinate, Station, Ordinate. Rows for upper and lower surfaces from 0 to 100. L. E. radius: 0.952, Slope of radius through L. E.: 0.084

NACA 662-015

[Stations and ordinates given in percent of airfoil chord]

Table with 4 columns: Station, Ordinate, Station, Ordinate. Rows for upper and lower surfaces from 0 to 100. L. E. radius: 1.435

NACA 662-215

[Stations and ordinates given in percent of airfoil chord]

Table with 4 columns: Station, Ordinate, Station, Ordinate. Rows for upper and lower surfaces from 0 to 100. L. E. radius: 1.435, Slope of radius through L. E.: 0.084

NACA 662-415

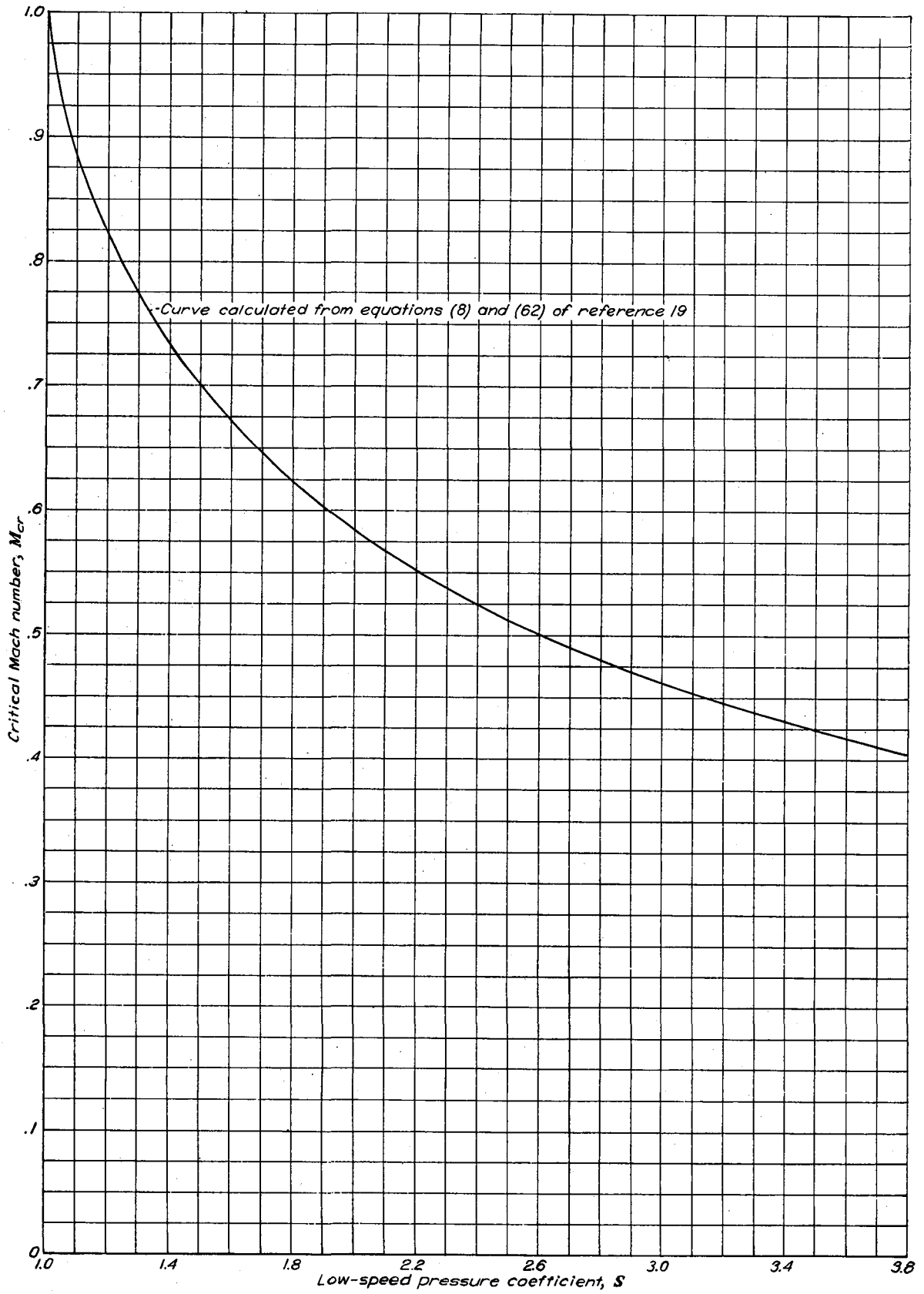
[Stations and ordinates given in percent of airfoil chord]

Table with 4 columns: Station, Ordinate, Station, Ordinate. Rows for upper and lower surfaces from 0 to 100. L. E. radius: 1.435, Slope of radius through L. E.: 0.168

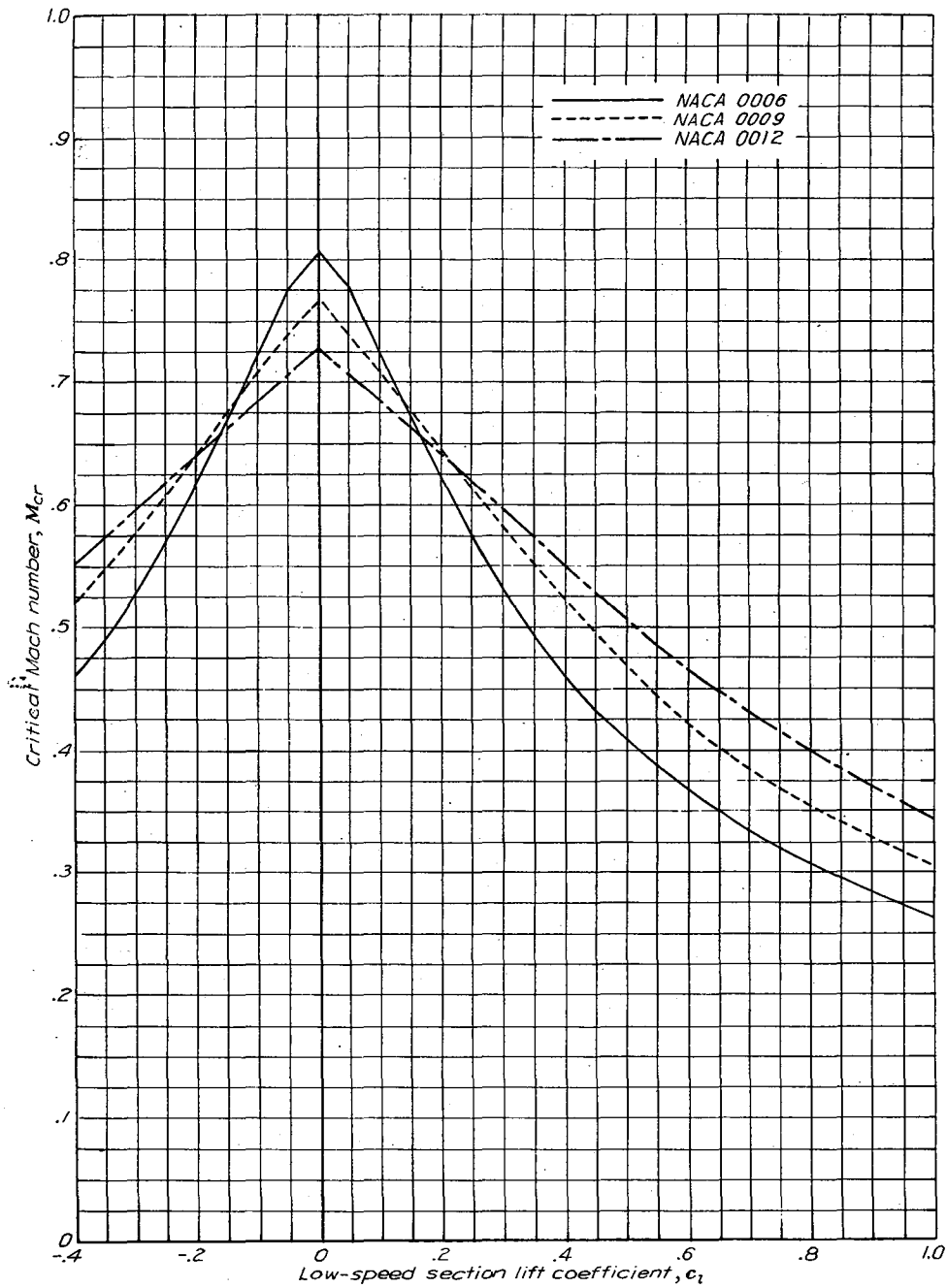


## IV—PREDICTED CRITICAL MACH NUMBERS

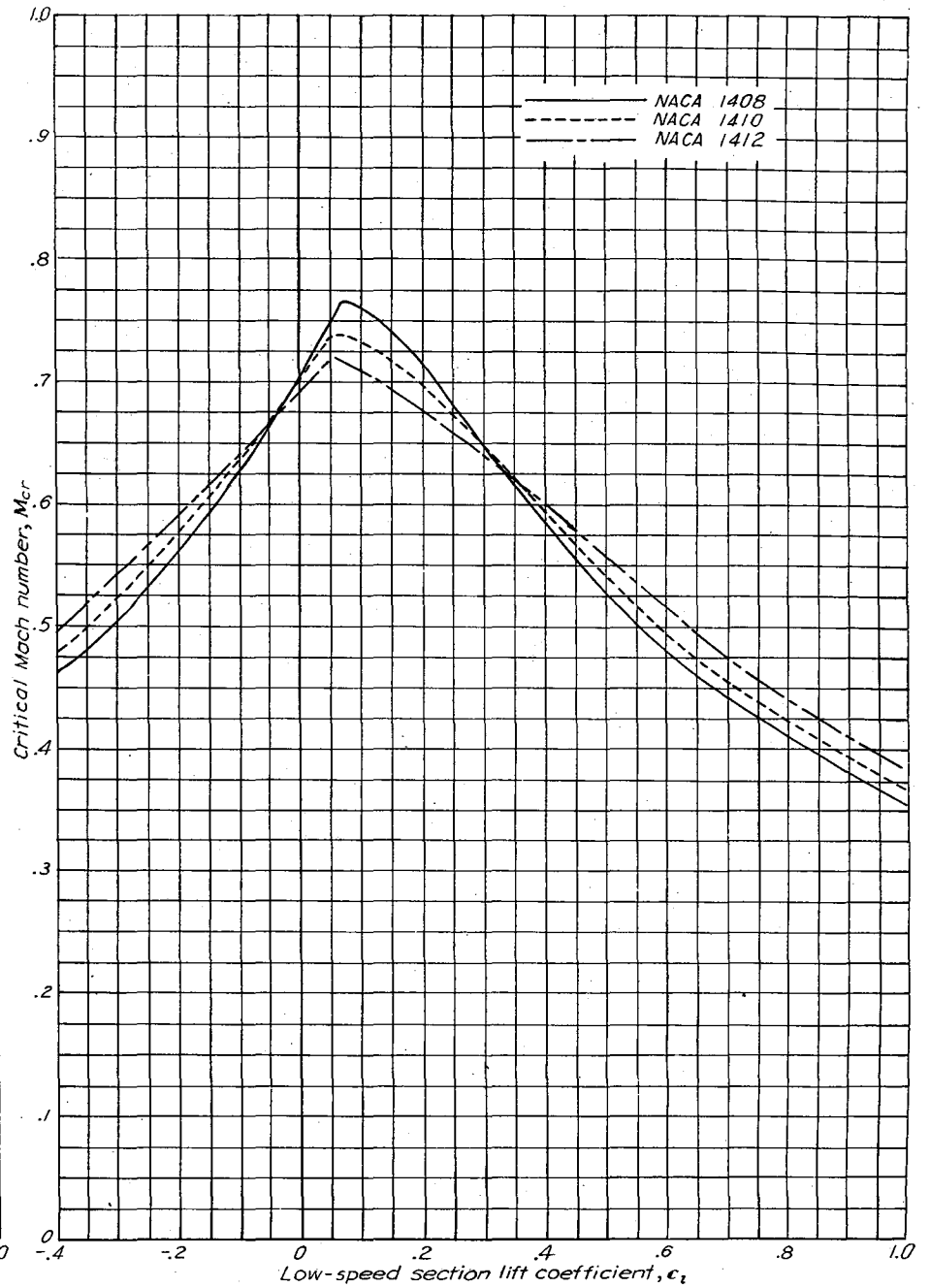
	Page		Page
Critical Mach number chart.....	114	Variation of critical Mach number with low-speed section lift coefficient—Continued	
Variation of critical Mach number with low-speed section lift coefficient:		For several NACA 65-series symmetrical airfoil sections of various thicknesses.....	122
For the NACA 0006, 0009, and 0012 airfoil sections.....	115	For several NACA 65-series airfoil sections with a thickness ratio of 0.18 and cambered for various design lift coefficients.....	123
For several NACA 14-series airfoil sections of various thicknesses.....	115	For several NACA 65-series airfoil sections of various thicknesses, cambered for a design lift coefficient of 0.2.....	123
For several NACA 24-series airfoil sections of various thicknesses.....	116	For several NACA 65-series airfoil sections of various thicknesses, cambered for a design lift coefficient of 0.4.....	124
For several NACA 44-series airfoil sections of various thicknesses.....	116	For several NACA 65-series airfoil sections with mean line of the type $a=0.5$ and cambered for a design lift coefficient of 0.4.....	124
For several NACA 230-series airfoil sections of various thicknesses.....	117	For two NACA 65-series airfoil sections of different thicknesses, cambered for a design lift coefficient of 0.6.....	125
For several NACA 63-series airfoil sections of various thicknesses, cambered for various design lift coefficients..	117	For two NACA 65-series airfoil sections with mean line of the type $a=0.5$ , with different thicknesses, and cambered for a design lift coefficient of 0.6.....	125
For several NACA 63-series symmetrical airfoil sections of various thicknesses.....	118	For several NACA 66-series symmetrical airfoil sections of various thicknesses.....	126
For several NACA 63-series airfoil sections of various thicknesses, cambered for a design lift coefficient of 0.2.....	118	For several NACA 66-series airfoil sections of various thicknesses, cambered for a design lift coefficient of 0.2.....	126
For several NACA 63-series airfoil sections of various thicknesses, cambered for a design lift coefficient of 0.4.....	119	For two NACA 66-series airfoil sections of different thicknesses, cambered for a design lift coefficient of 0.4.....	127
For two NACA 63-series airfoil sections of different thicknesses, cambered for a design lift coefficient of 0.6.....	119	For several NACA 66-series airfoil sections with a thickness ratio of 0.16 and cambered for various design lift coefficients.....	127
For several NACA 64-series symmetrical airfoil sections of various thicknesses.....	120	For several NACA 6-series airfoil sections with different positions of minimum pressure and various thicknesses, cambered for various design lift coefficients.....	128
For several NACA 64-series airfoil sections of various thicknesses, cambered for a design lift coefficient of 0.1.....	120	For two NACA 7-series airfoil sections with a thickness ratio of 0.15 and cambered for different design lift coefficients..	128
For several NACA 64-series airfoil sections of various thicknesses, cambered for a design lift coefficient of 0.2.....	121		
For several NACA 64-series airfoil sections of various thicknesses, cambered for a design lift coefficient of 0.4.....	121		
For two NACA 64-series airfoil sections of different thicknesses, cambered for a design lift coefficient of 0.6.....	122		



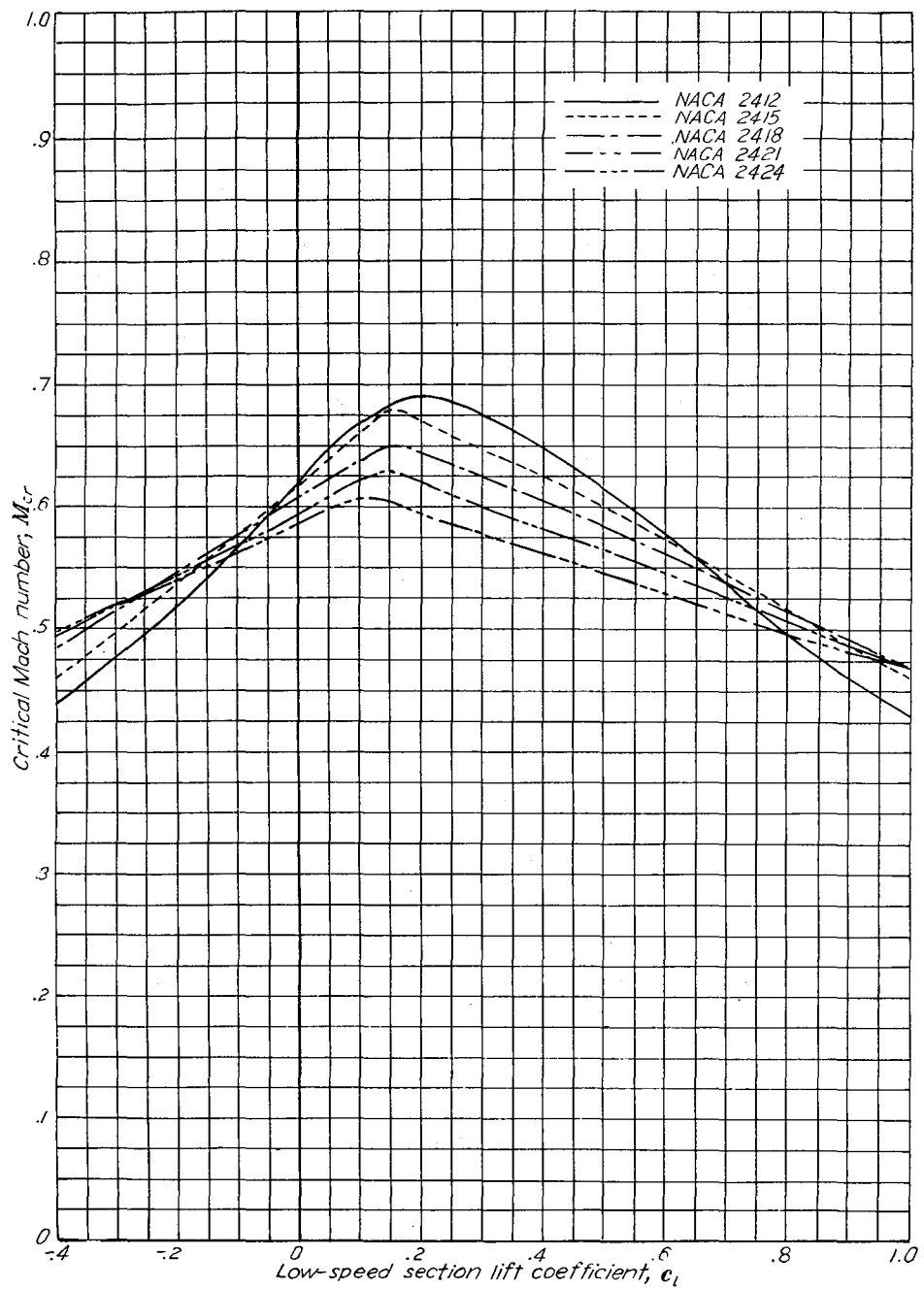
Critical Mach number chart.



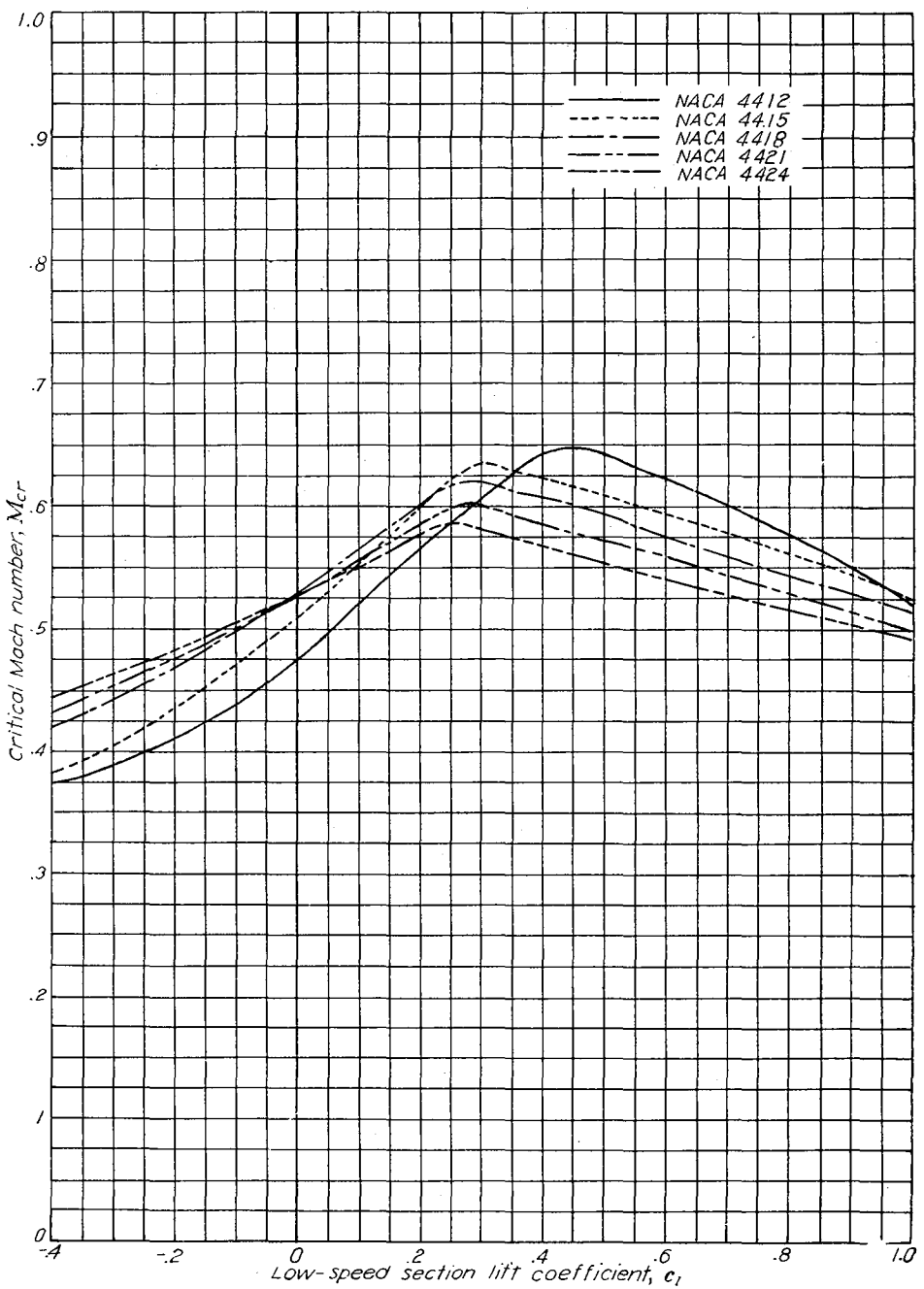
Variation of critical Mach number with low-speed section lift coefficient for the NACA 0006, 0009, and 0012 airfoil sections.



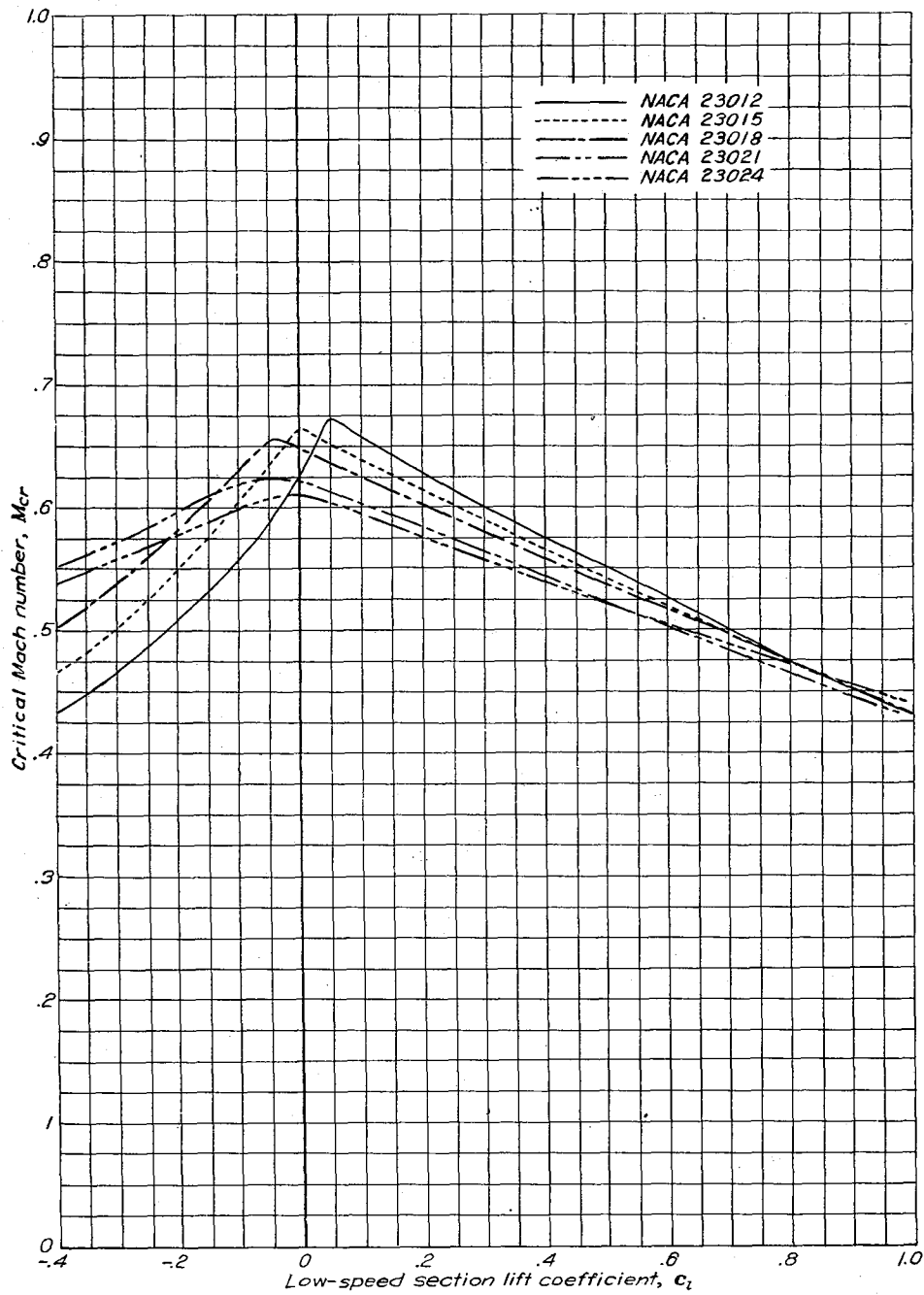
Variation of critical Mach number with low-speed section lift coefficient for several NACA 14-series airfoil sections of various thicknesses.



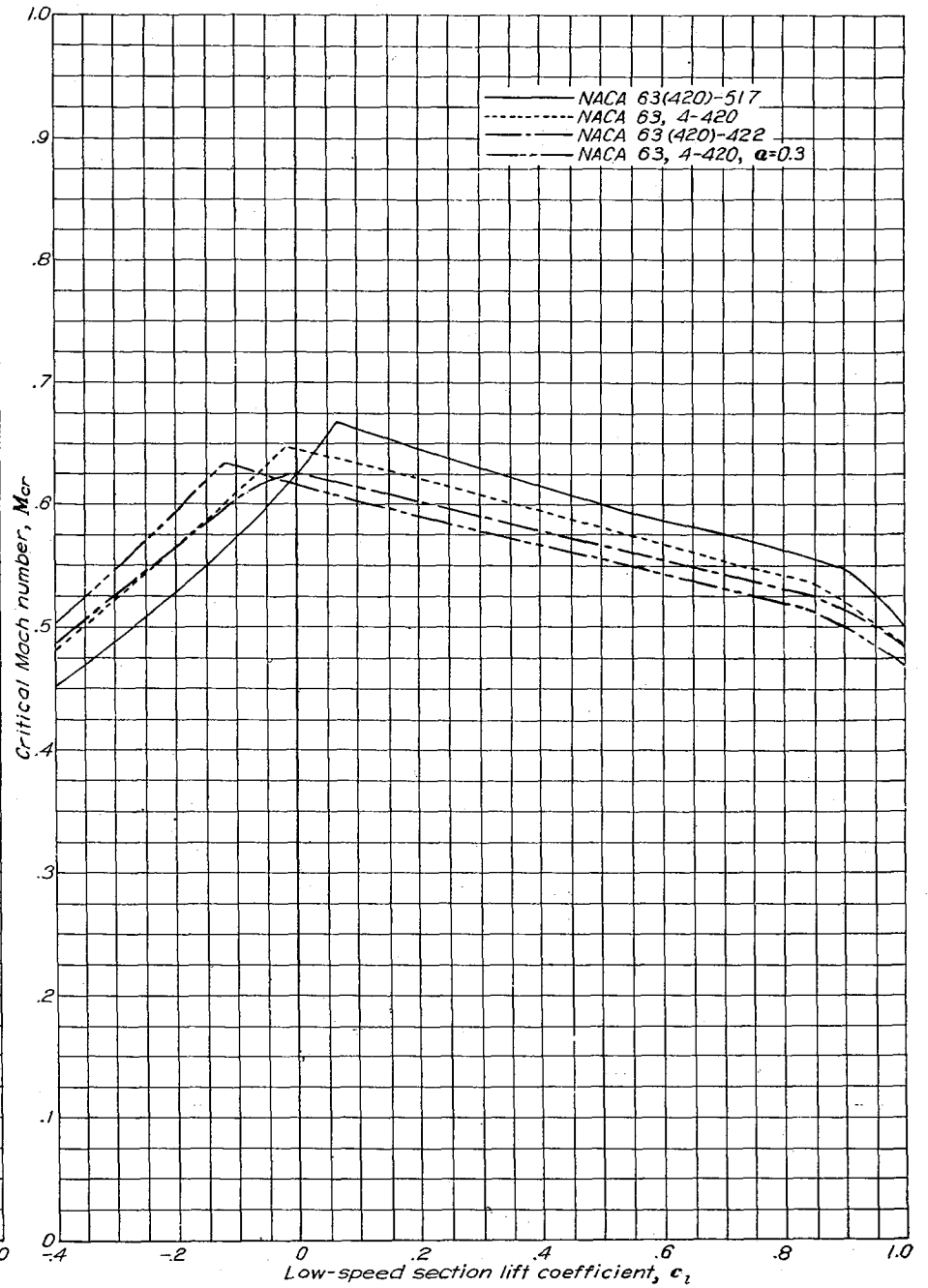
Variation of critical Mach number with low speed section lift coefficient for several NACA 24 series airfoil sections of various thicknesses.



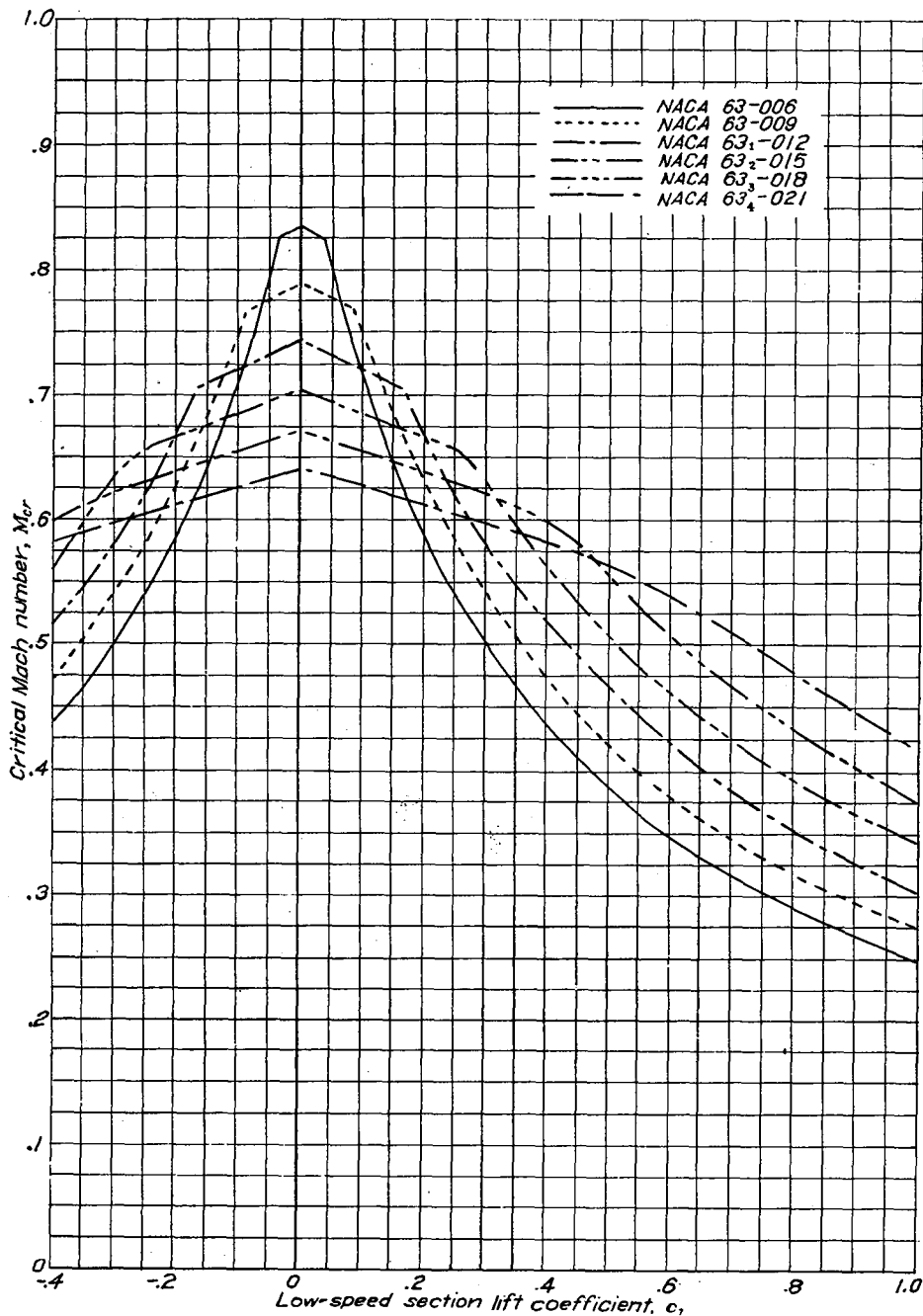
Variation of critical Mach number with low-speed section lift coefficient for several NACA 44-series airfoil sections of various thicknesses.



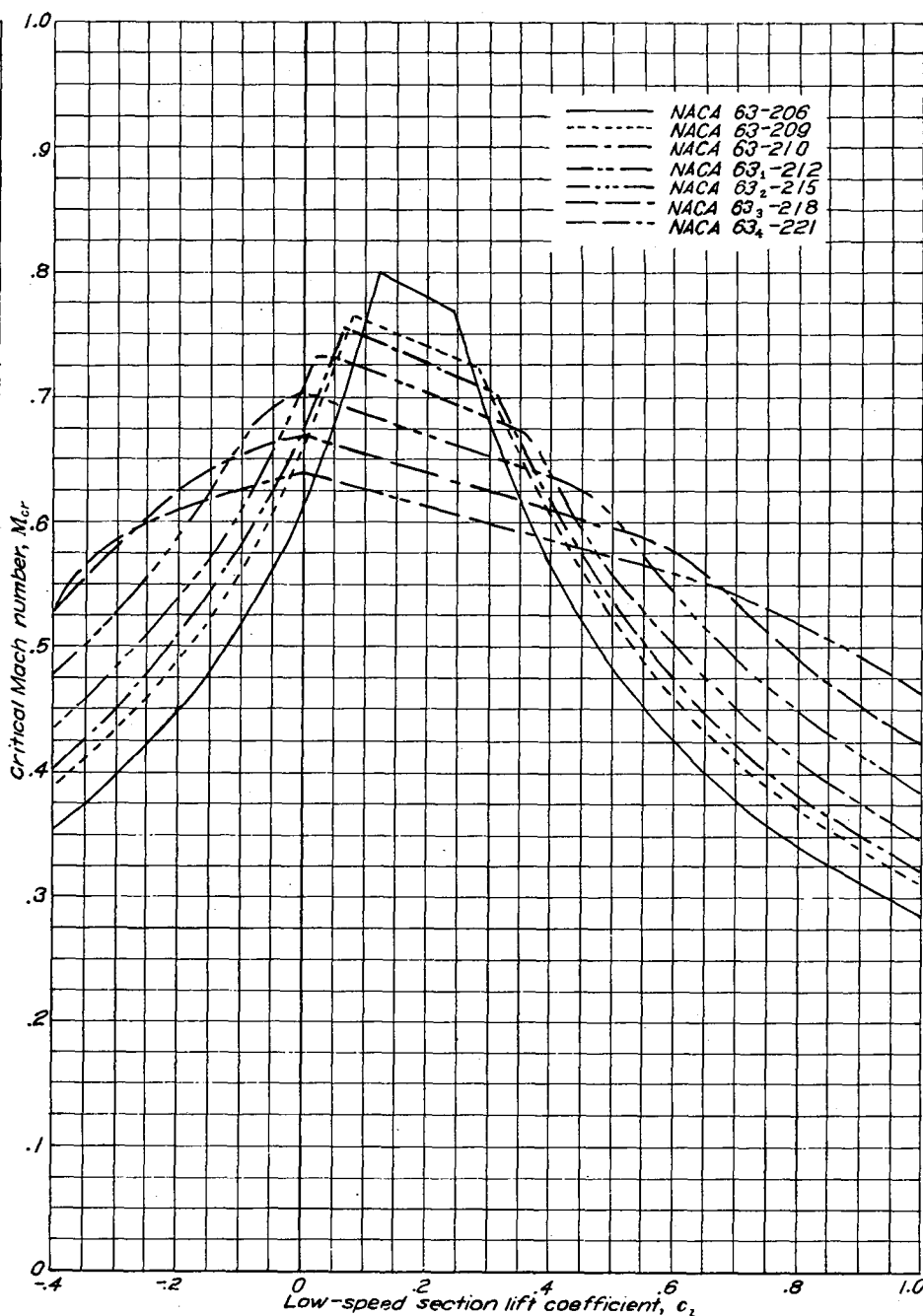
Variation of critical Mach number with low-speed section lift coefficient for several NACA 230-series airfoil sections of various thicknesses.



Variation of critical Mach number with low-speed section lift coefficient for several NACA 63-series airfoil sections of various thicknesses, cambered for various design lift coefficients.

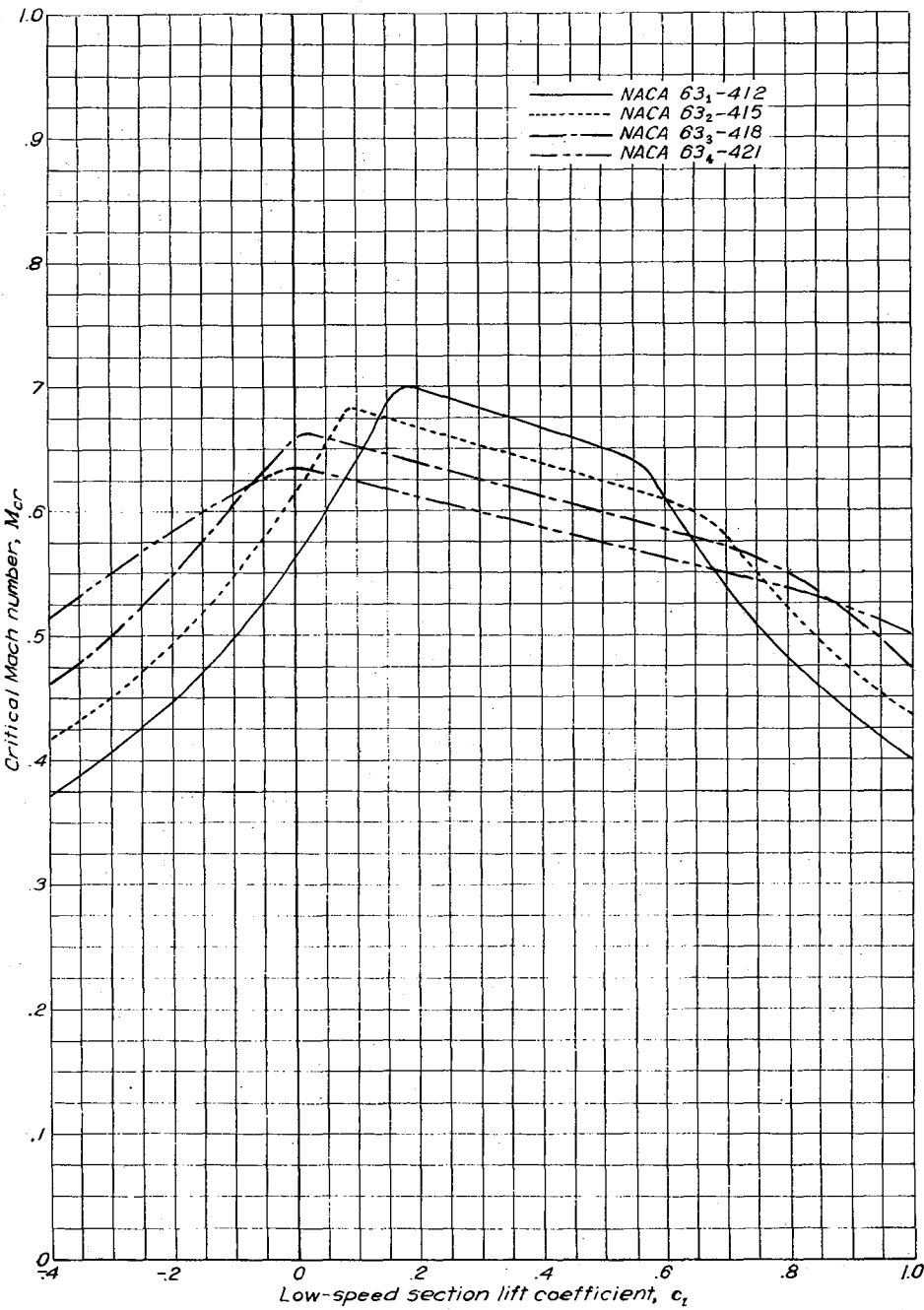


Variation of critical Mach number with low-speed section lift coefficient for several NACA 63-series symmetrical airfoil sections of various thicknesses.

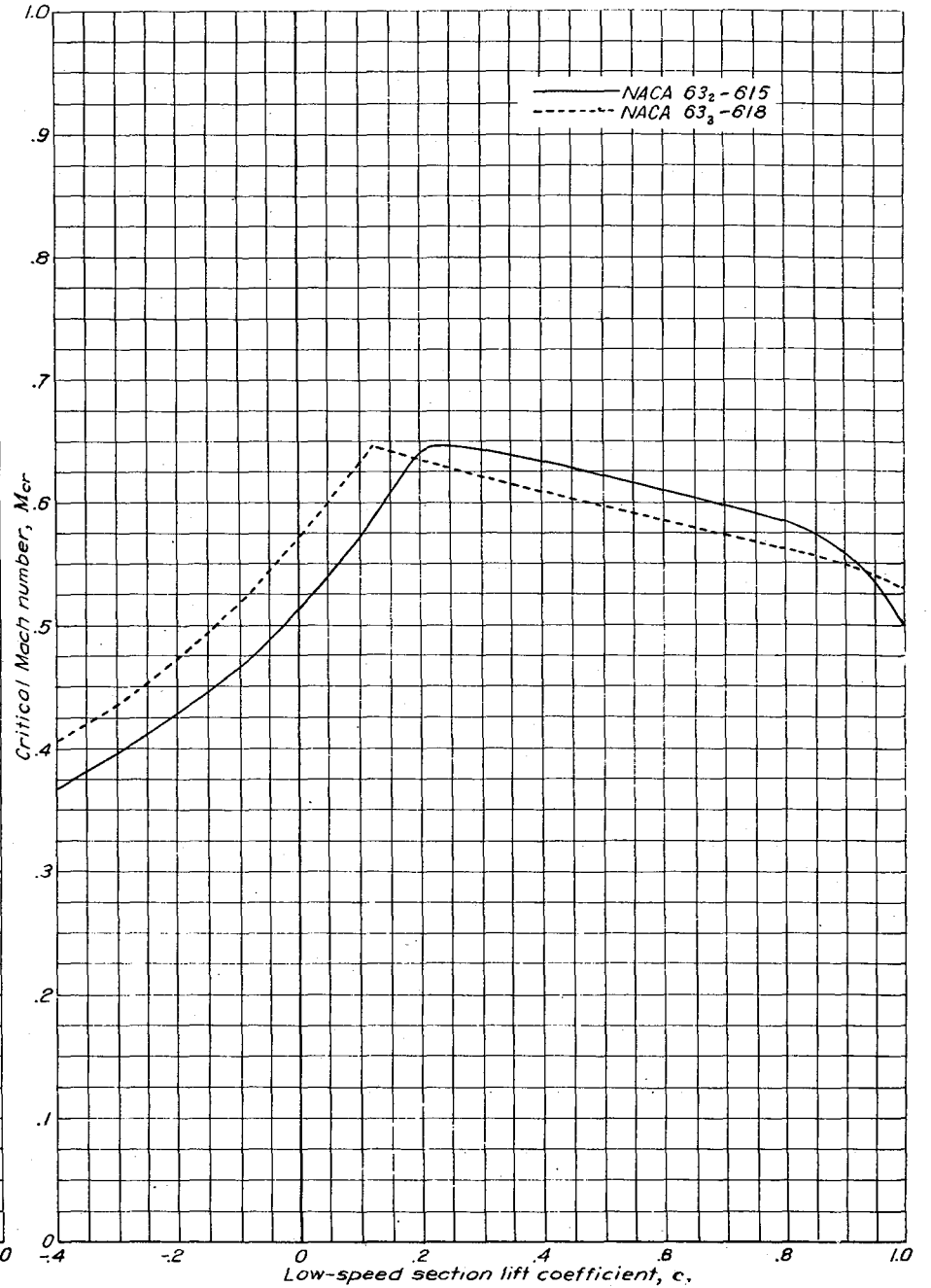


Variation of critical Mach number with low-speed section lift coefficient for several NACA 63-series airfoil sections of various thicknesses, cambered for a design lift coefficient of 0.2.

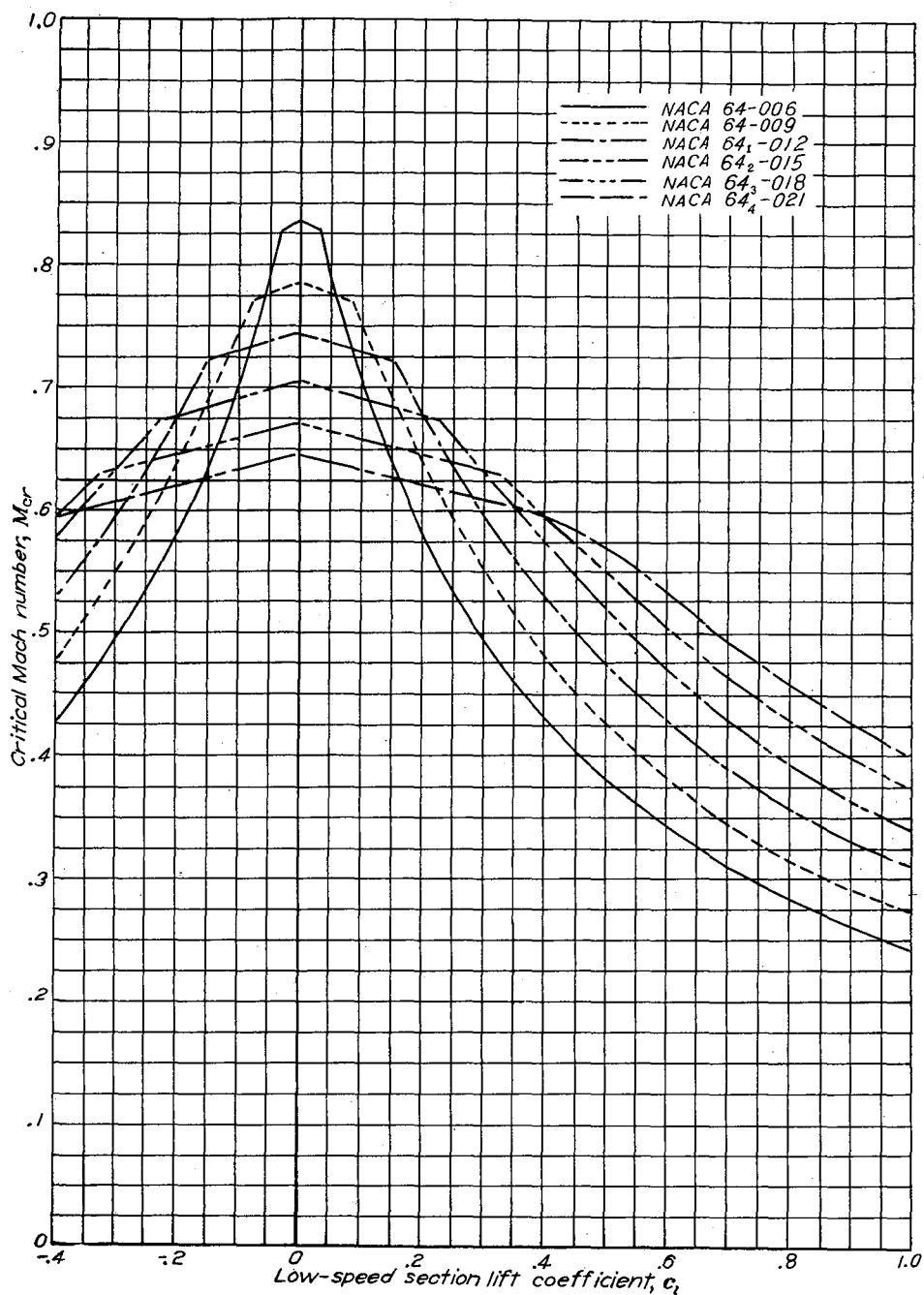




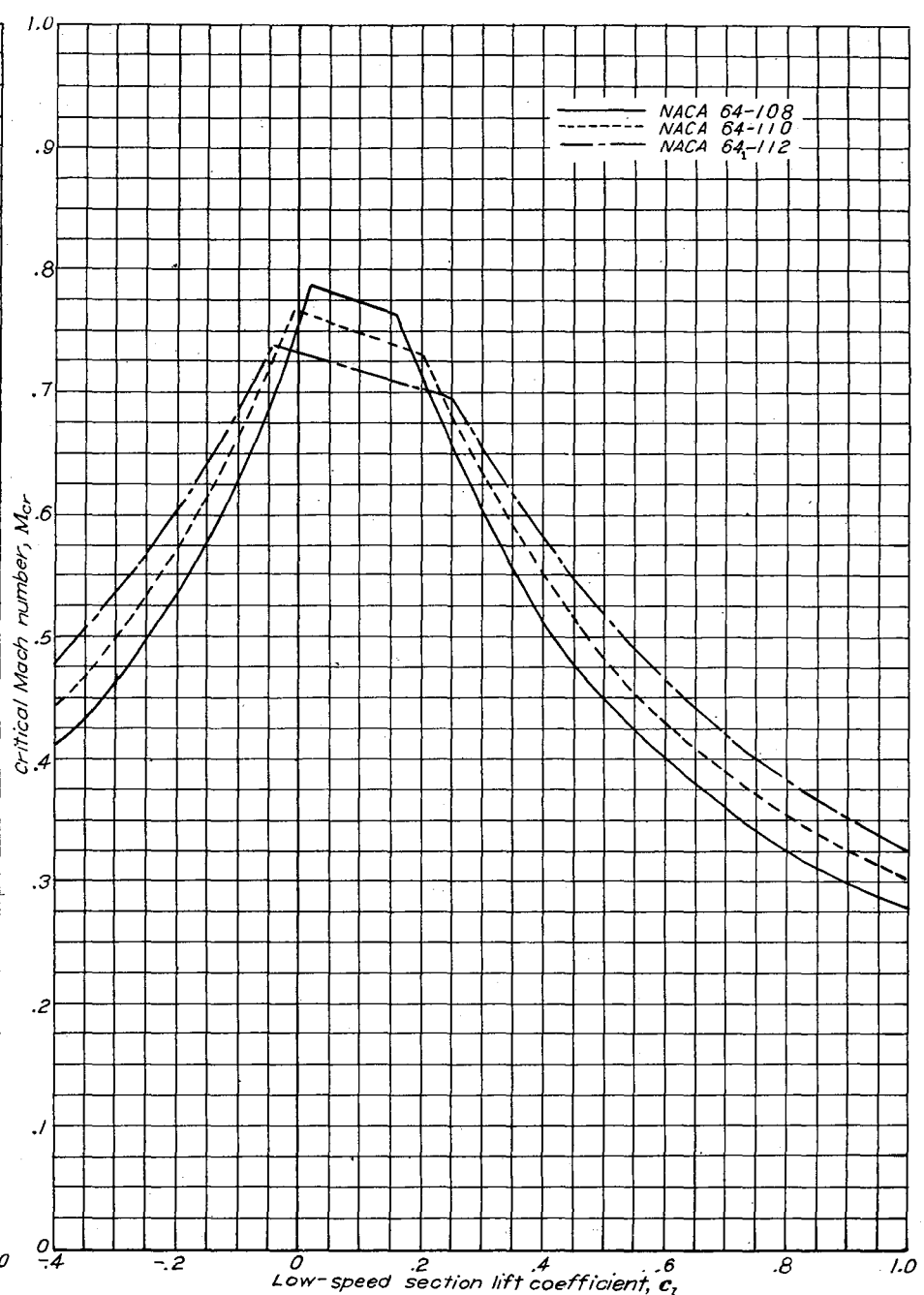
Variation of critical Mach number with low-speed section lift coefficient for several NACA 63-series airfoil sections of various thicknesses, cambered for a design lift coefficient of 0.4.



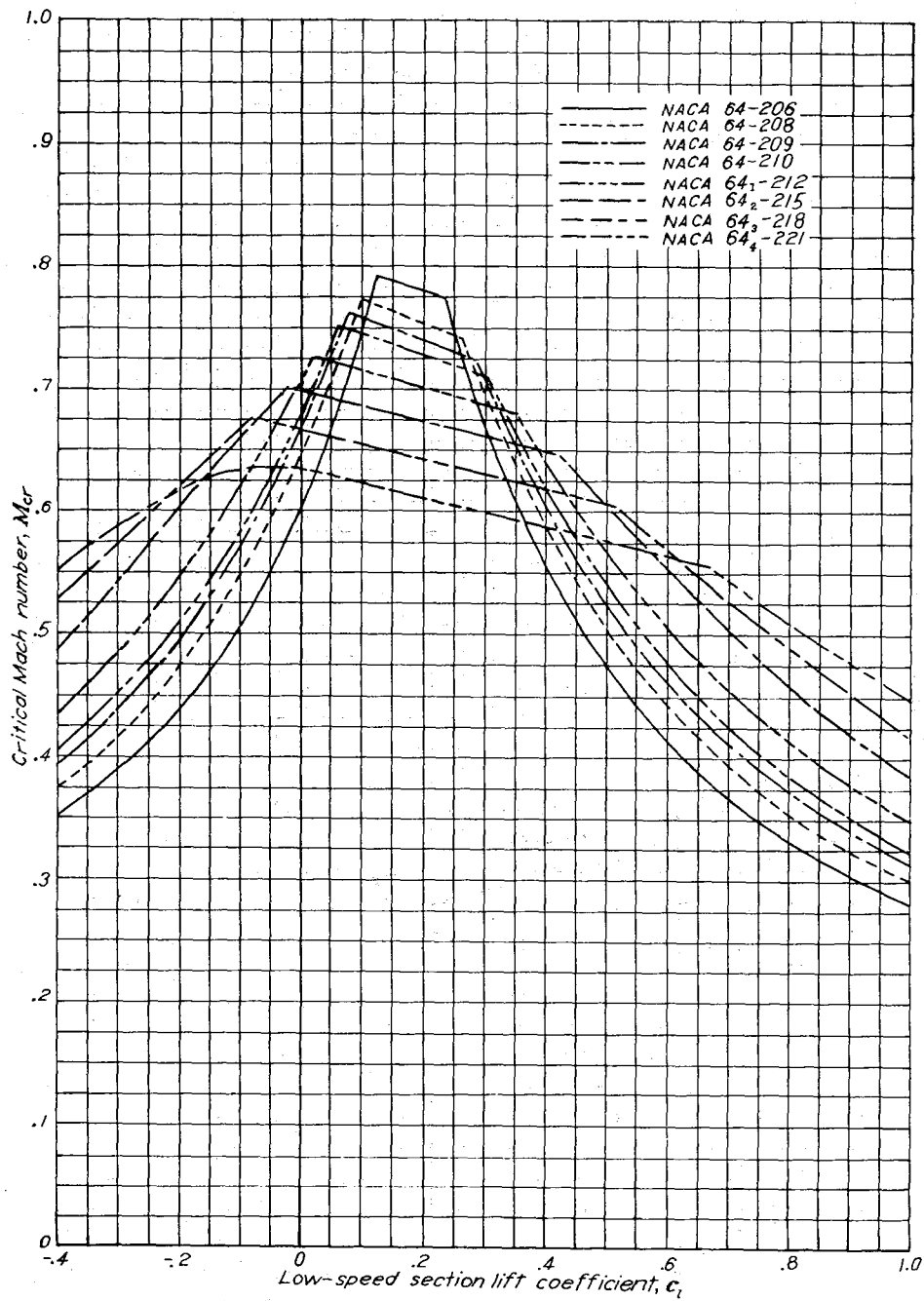
Variation of critical Mach number with low-speed section lift coefficient for two NACA 63-series airfoil sections of different thicknesses, cambered for a design lift coefficient of 0.6.



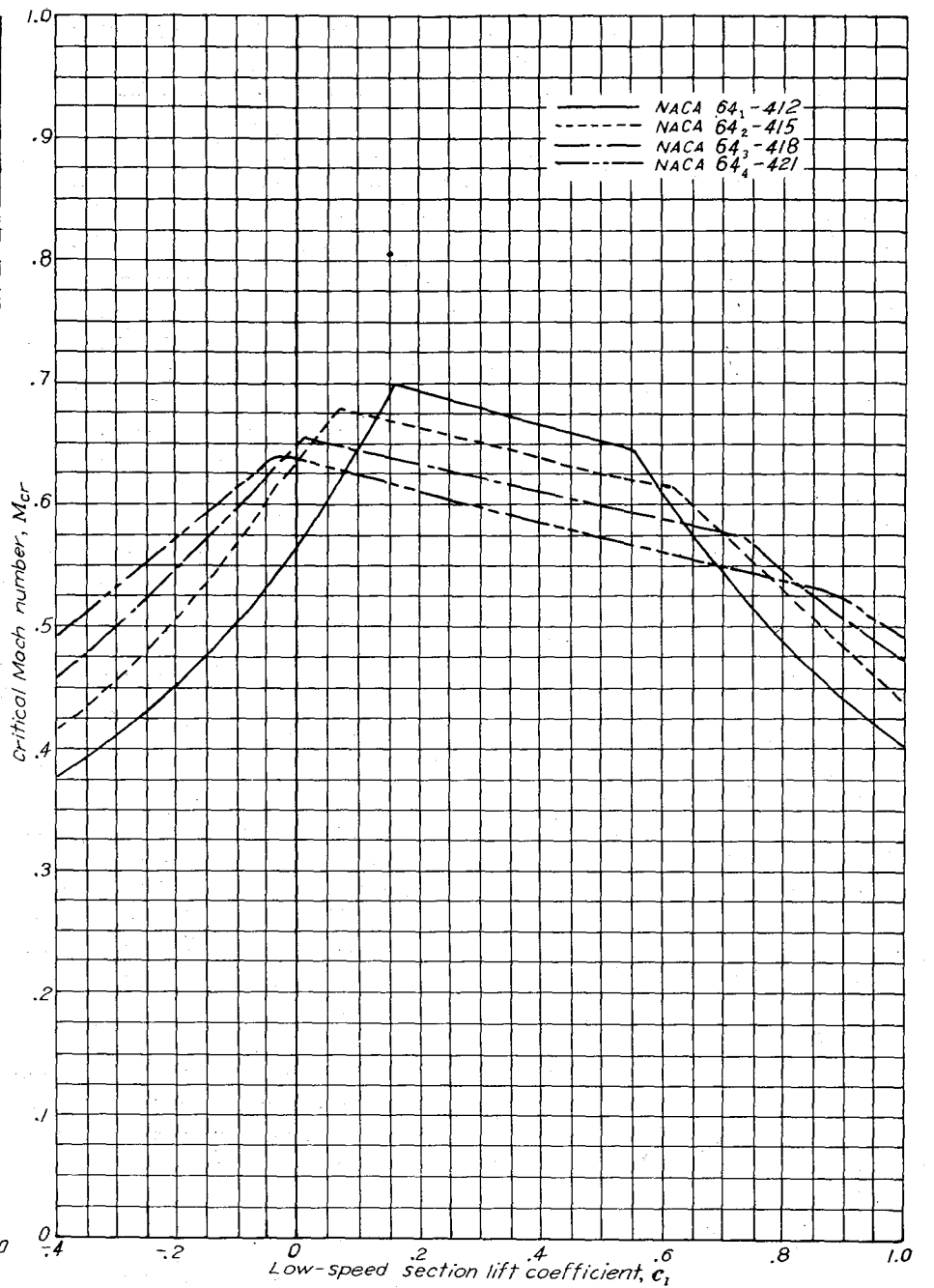
Variation of critical Mach number with low-speed section lift coefficient for several NACA 64-series symmetrical airfoil sections of various thicknesses.



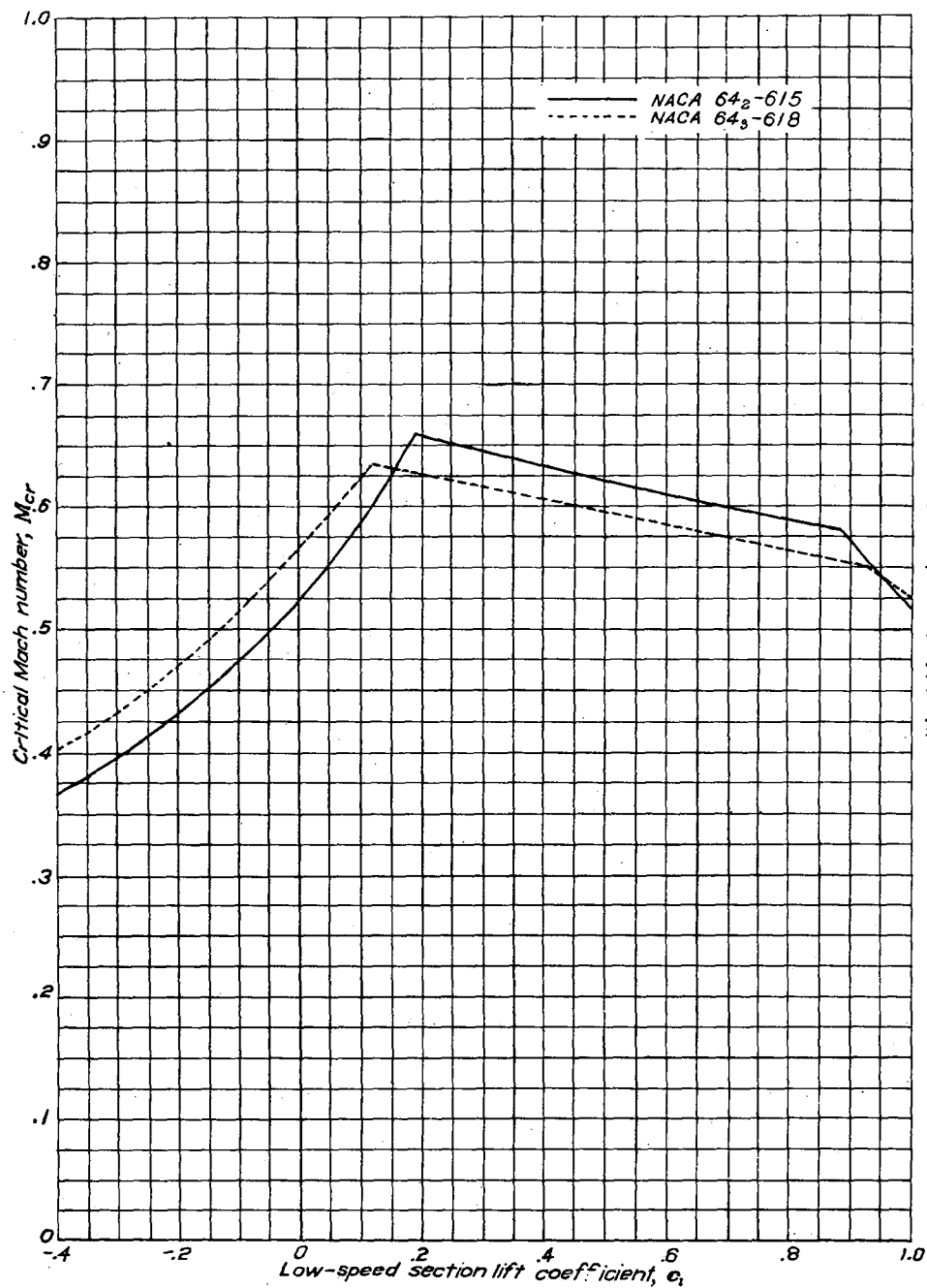
Variation of critical Mach number with low-speed section lift coefficient for several NACA 64-series airfoil sections of various thicknesses, cambered for a design lift coefficient of 0.1.



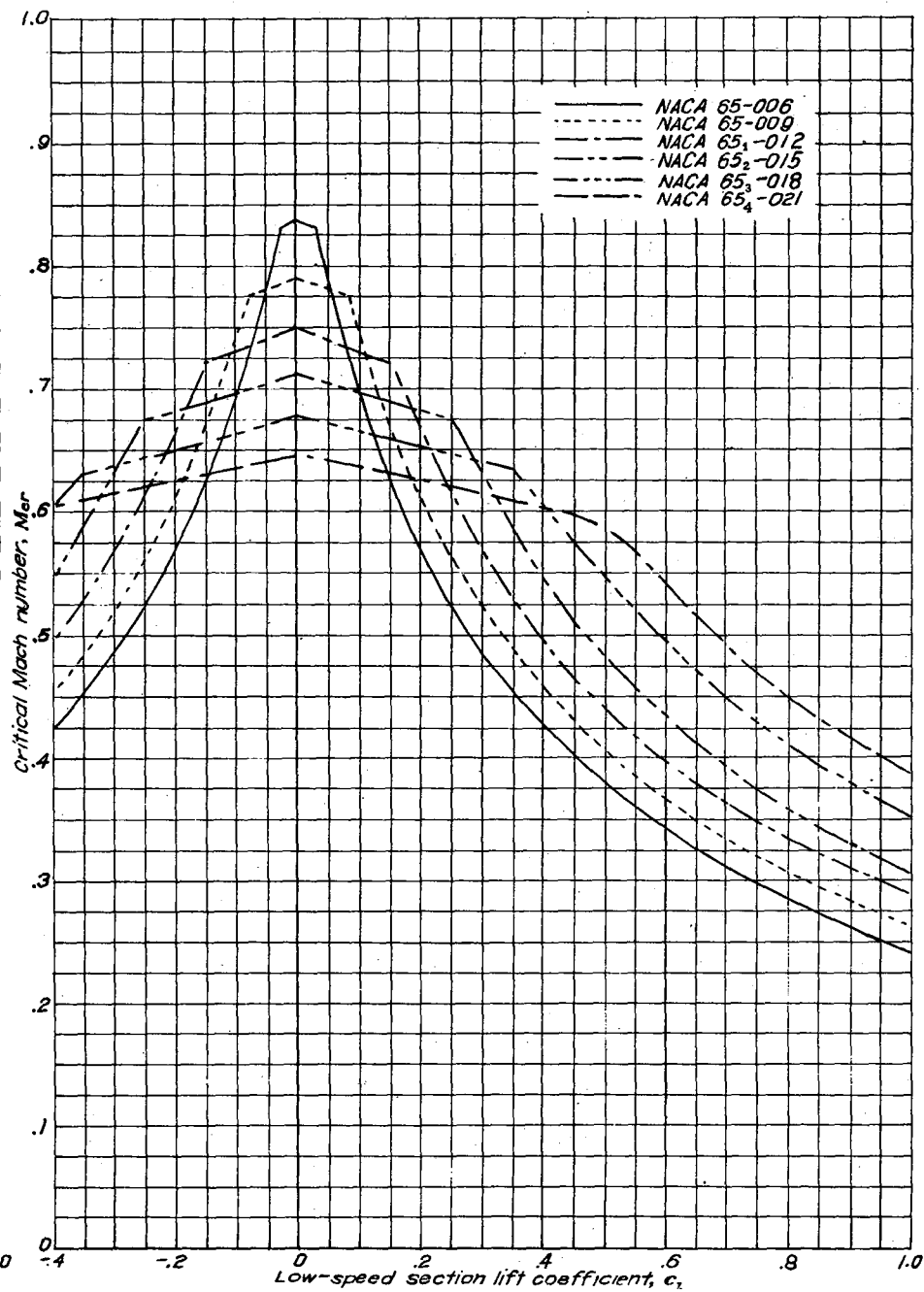
Variation of critical Mach number with low-speed section lift coefficient for several NACA 64-series airfoil sections of various thicknesses, cambered for a design lift coefficient of 0.2.



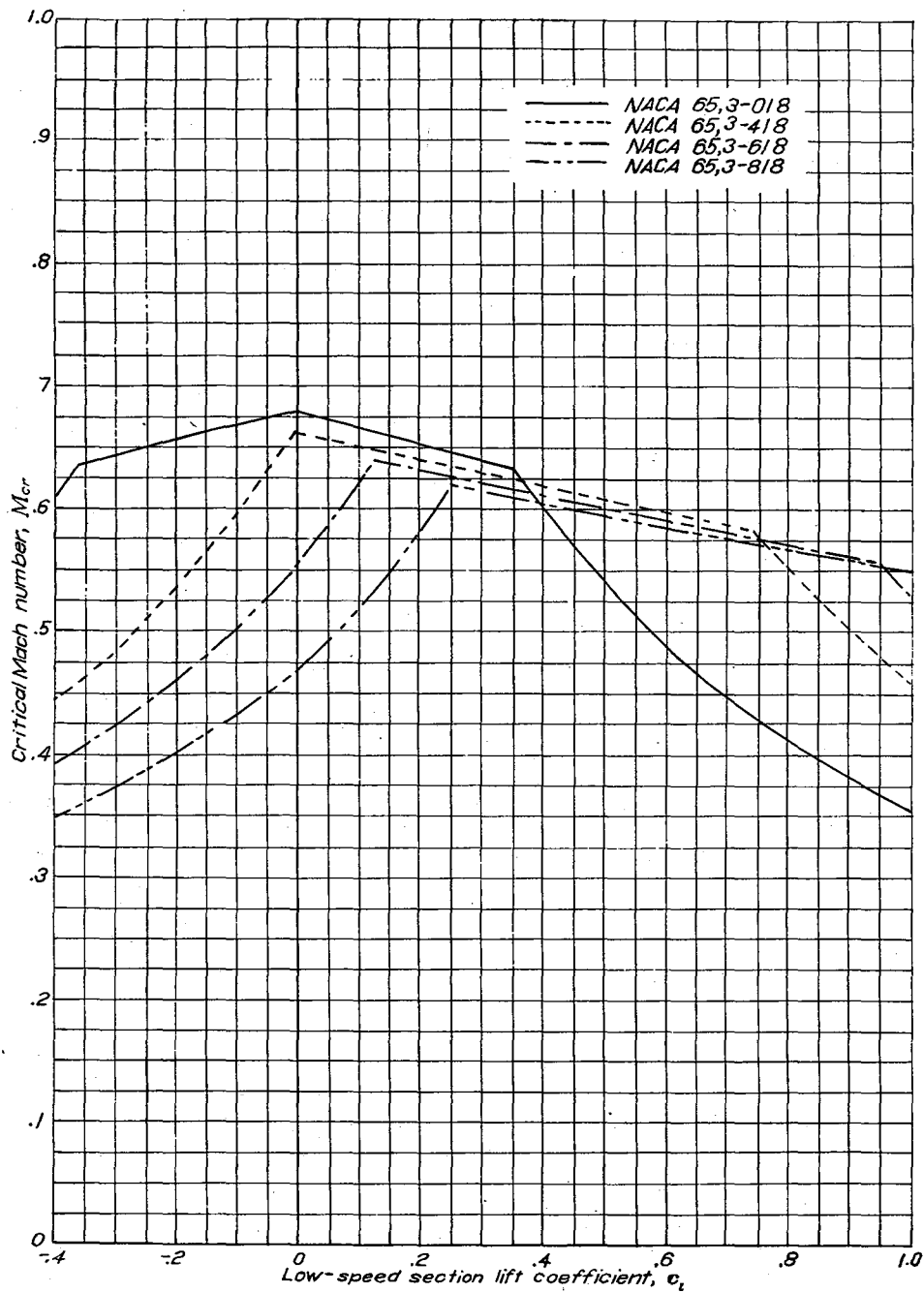
Variation of critical Mach number with low-speed section lift coefficient for several NACA 64-series airfoil sections of various thicknesses, cambered for a design lift coefficient of 0.4.



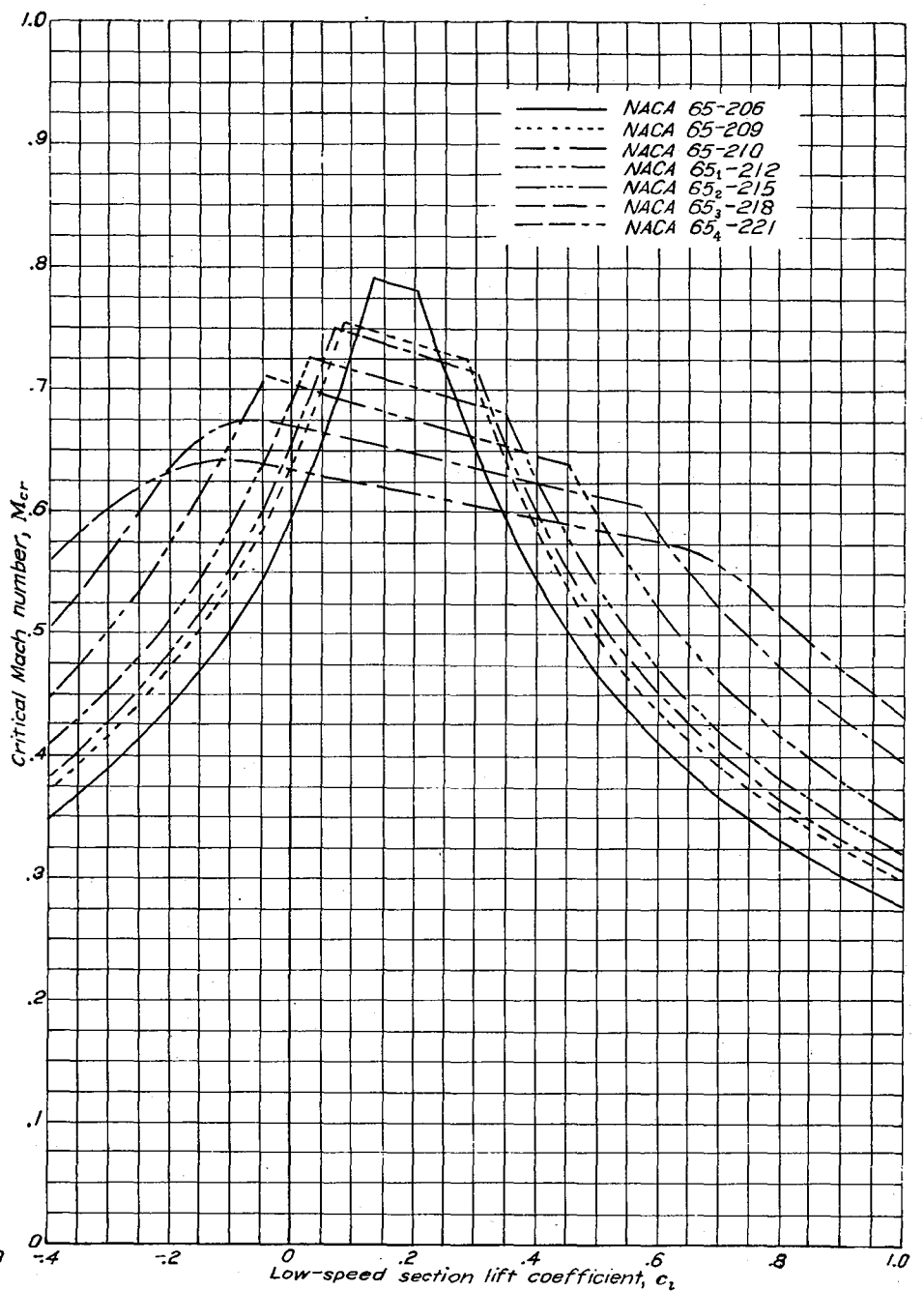
Variation of critical Mach number with low-speed section lift coefficient for two NACA 64-series airfoil sections of different thicknesses, cambered for a design lift coefficient of 0.6.



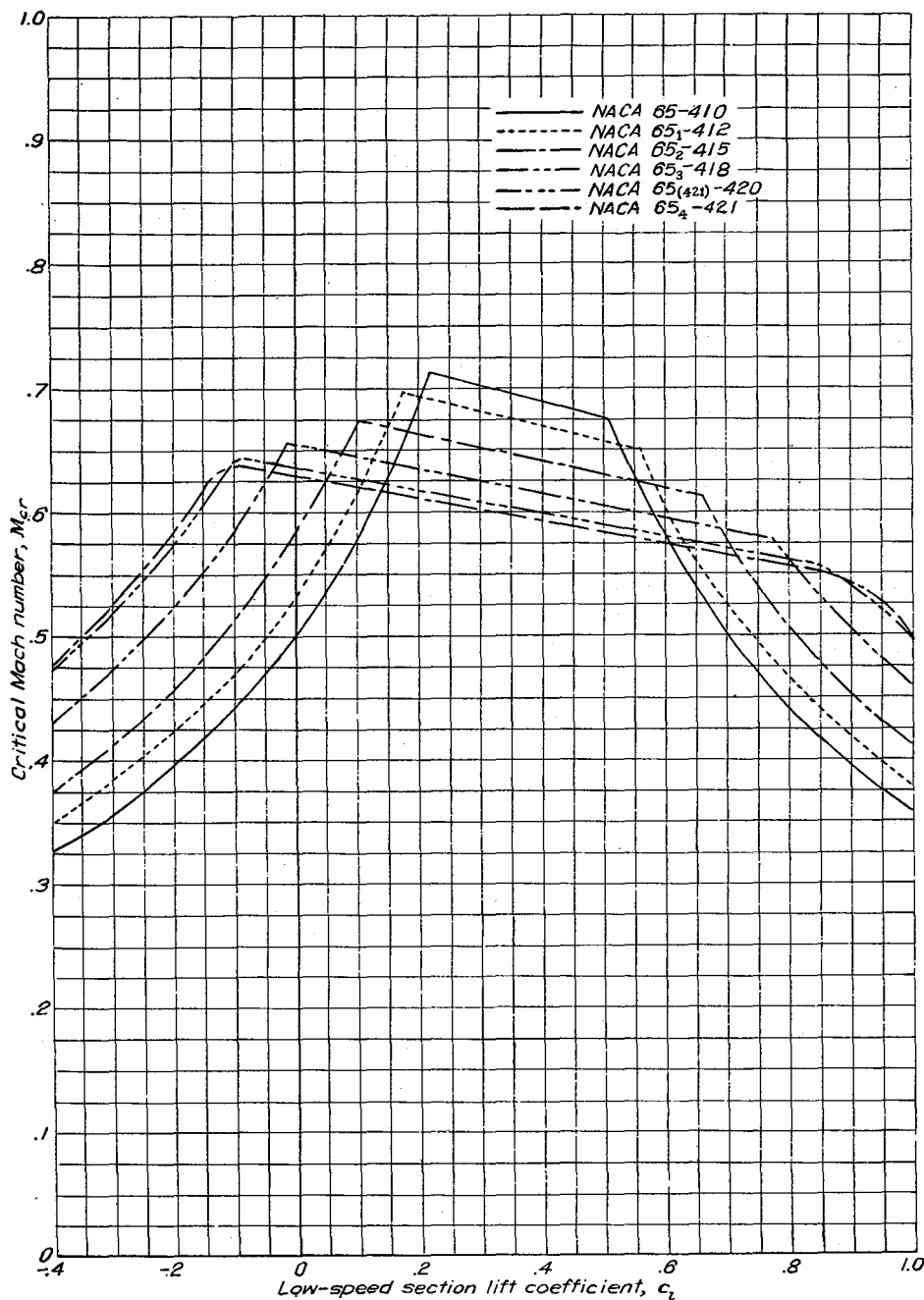
Variation of critical Mach number with low-speed section lift coefficient for several NACA 65-series symmetrical airfoil sections of various thicknesses.



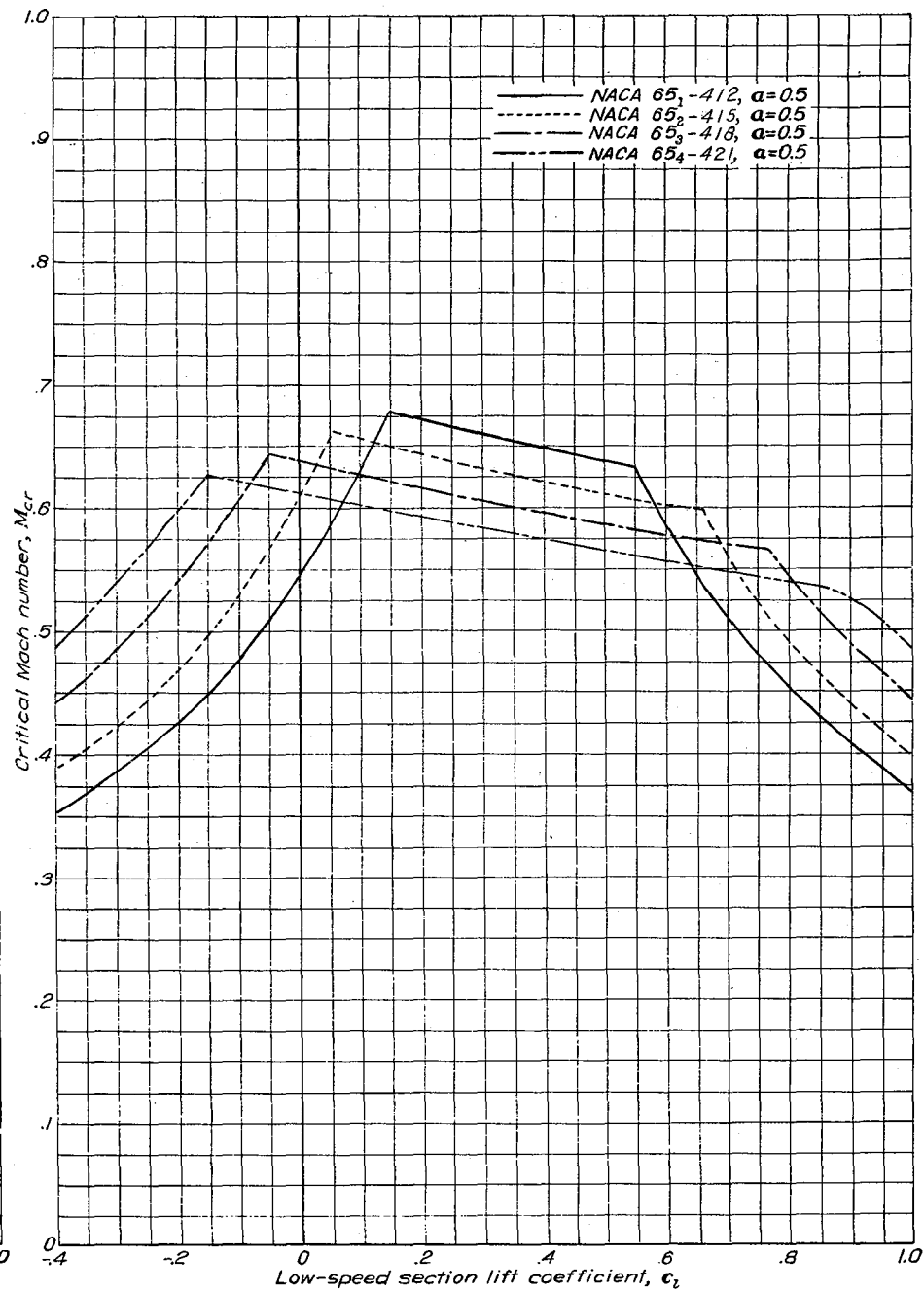
Variation of critical Mach number with low-speed section lift coefficient for several NACA 65-series airfoil sections with a thickness ratio of 0.18 and cambered for various design lift coefficients.



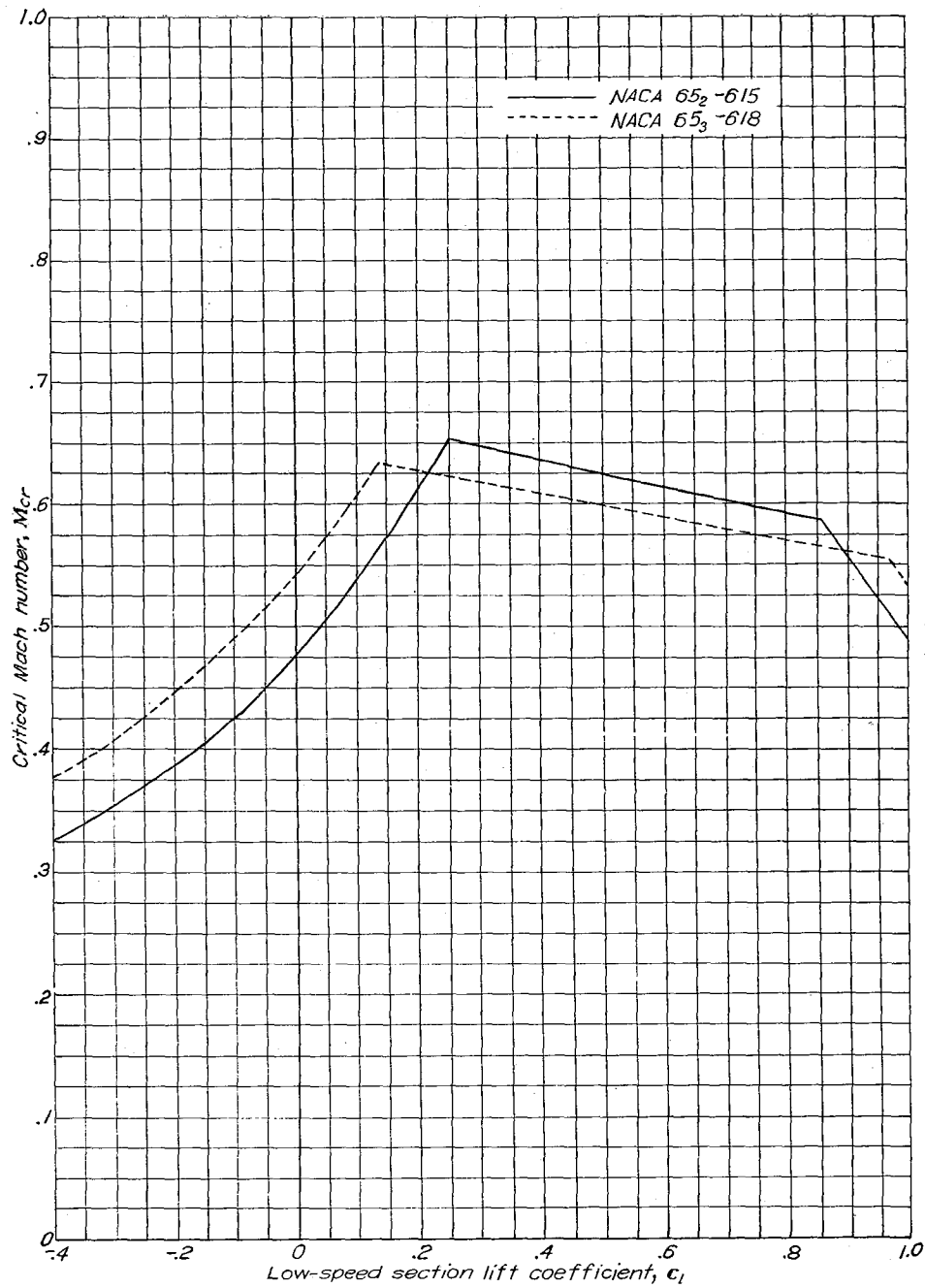
Variation of critical Mach number with low-speed section lift coefficient for several NACA 65-series airfoil sections of various thicknesses, cambered for a design lift coefficient of 0.2.



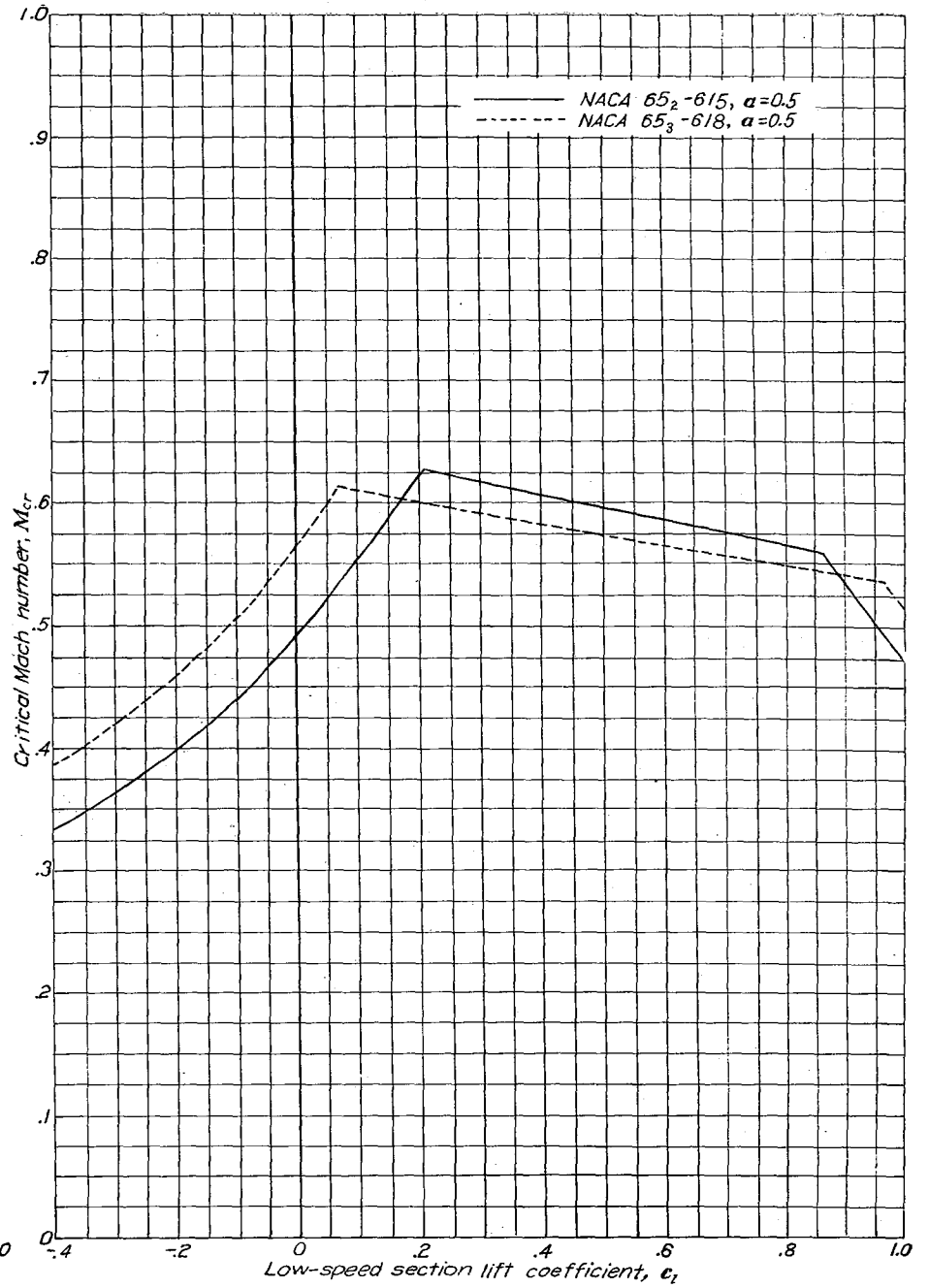
Variation of critical Mach number with low-speed section lift coefficient for several NACA 65-series airfoil sections of various thicknesses, cambered for a design lift coefficient of 0.4.



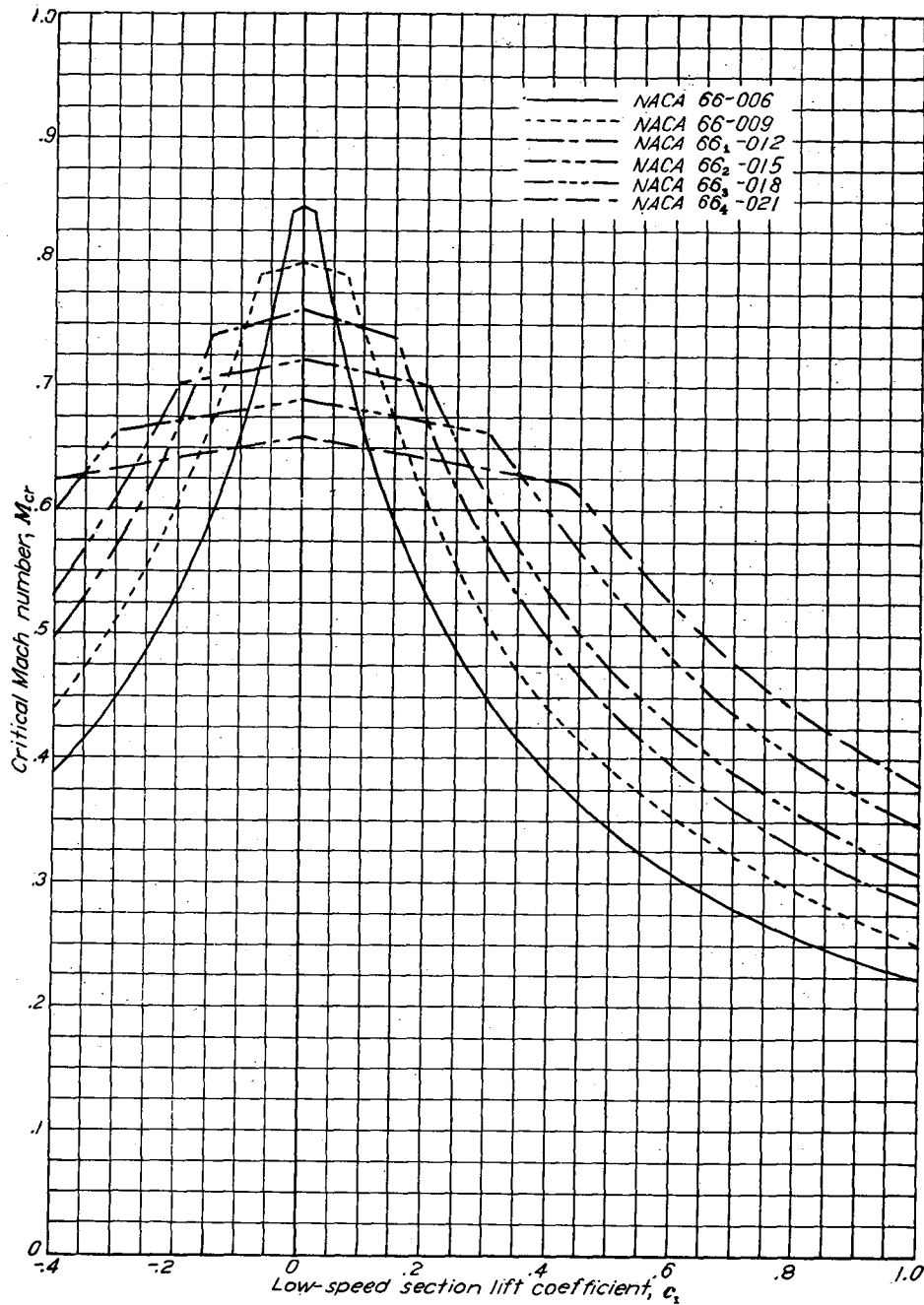
Variation of critical Mach number with low-speed section lift coefficient for several NACA 65-series airfoil sections with mean line of the type  $\alpha=0.5$  and cambered for a design lift coefficient of 0.4.



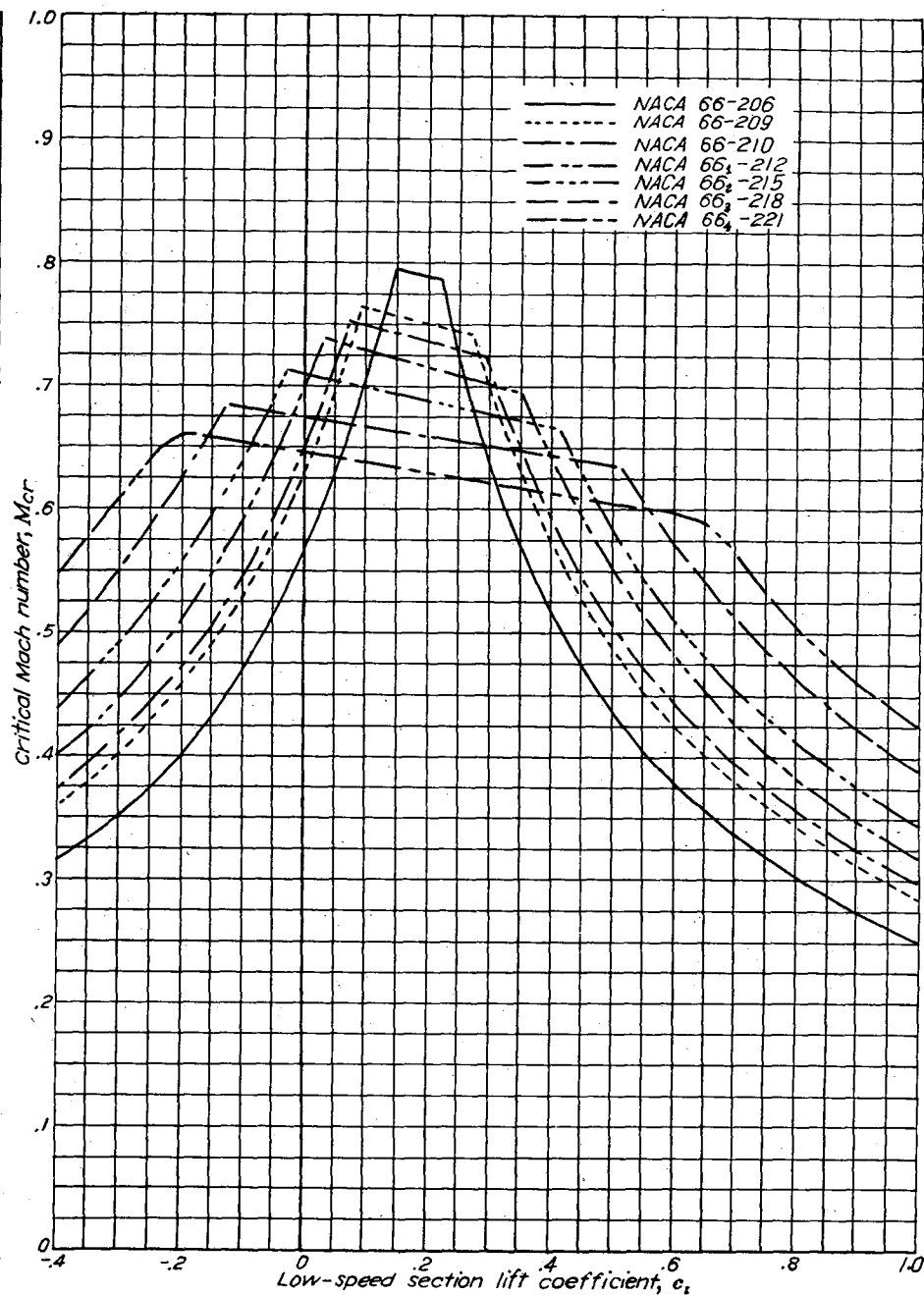
Variation of critical Mach number with low-speed section lift coefficient for two NACA 65-series airfoil sections of different thicknesses, cambered for a design lift coefficient of 0.6.



Variation of critical Mach number with low-speed section lift coefficient for two NACA 65-series airfoil sections with mean line of the type  $\alpha=0.5$ , with different thicknesses, and cambered for a design lift coefficient of 0.6.

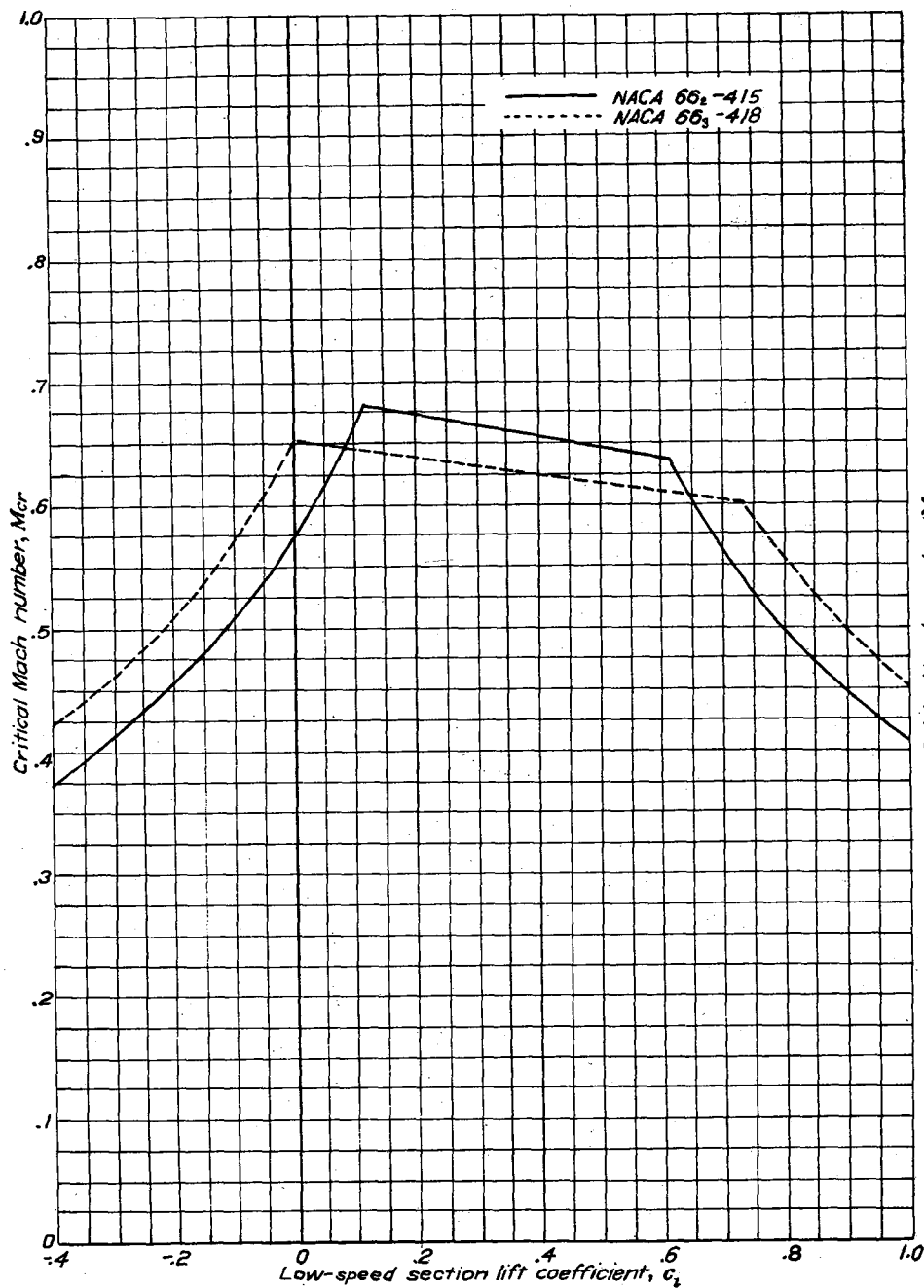


Variation of critical Mach number with low-speed section lift coefficient for several NACA 66-series symmetrical airfoil sections of various thicknesses.

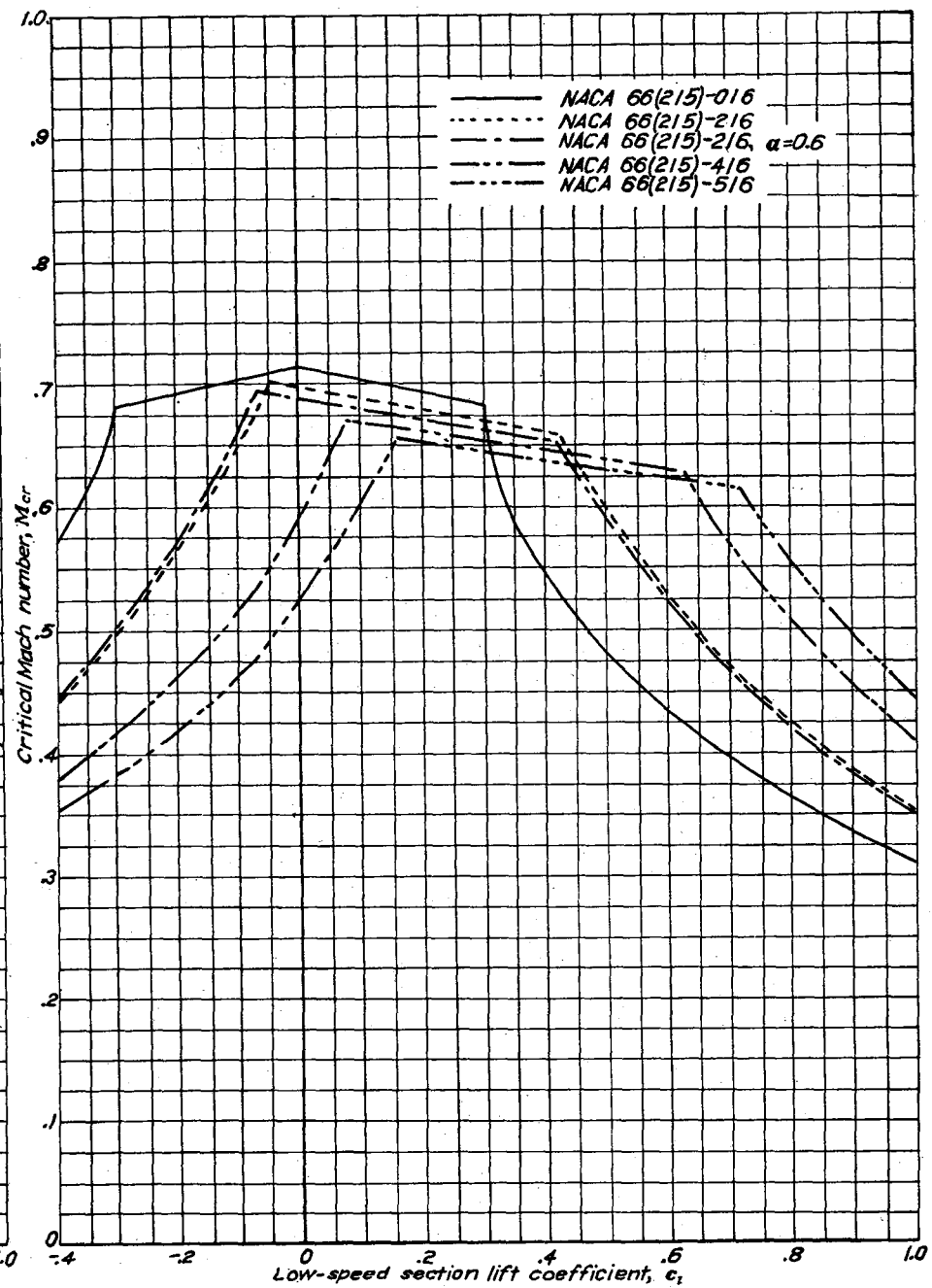


Variation of critical Mach number with low-speed section lift coefficient for several NACA 66-series airfoil sections of various thicknesses, cambered for a design lift coefficient of 0.2.

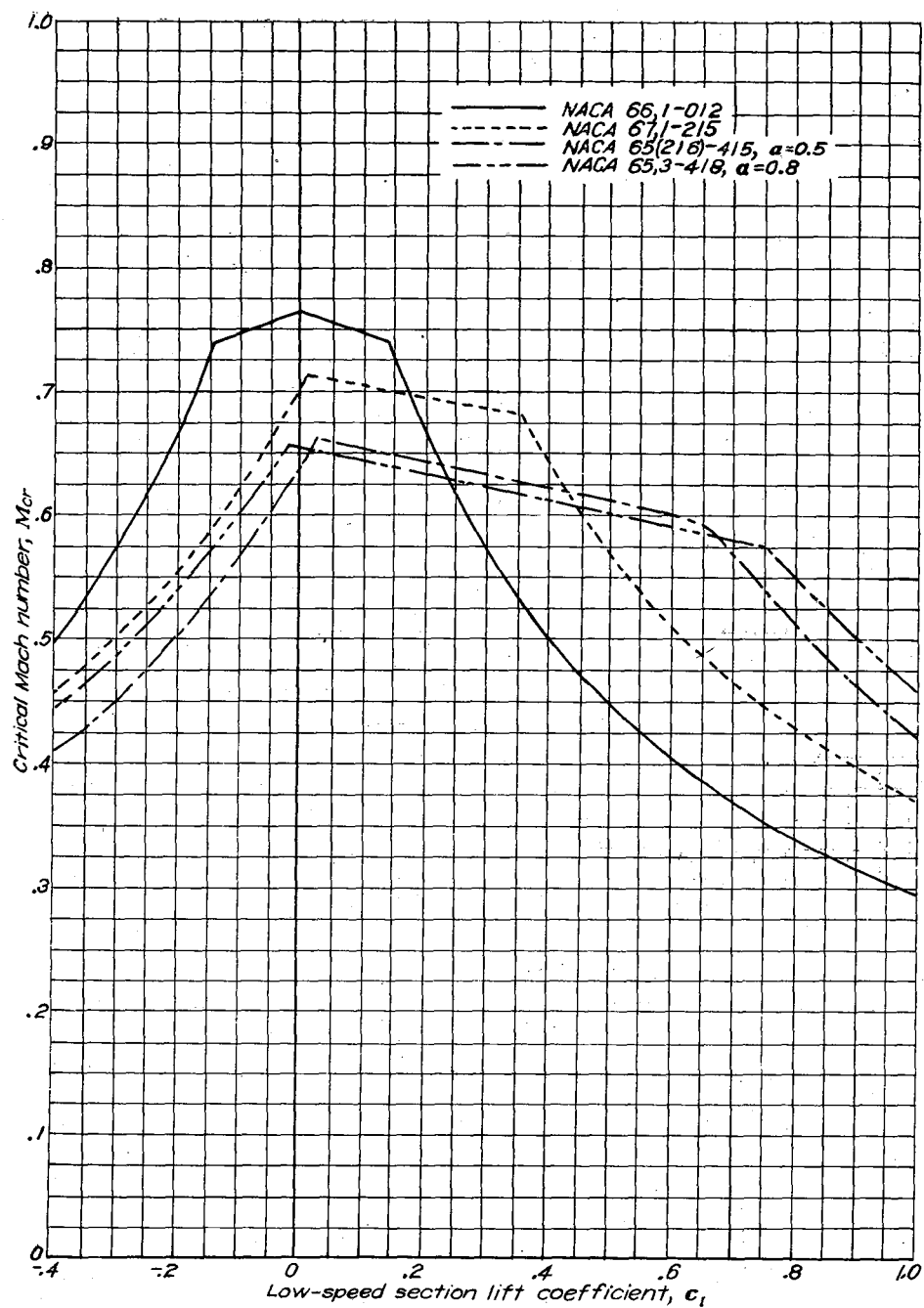




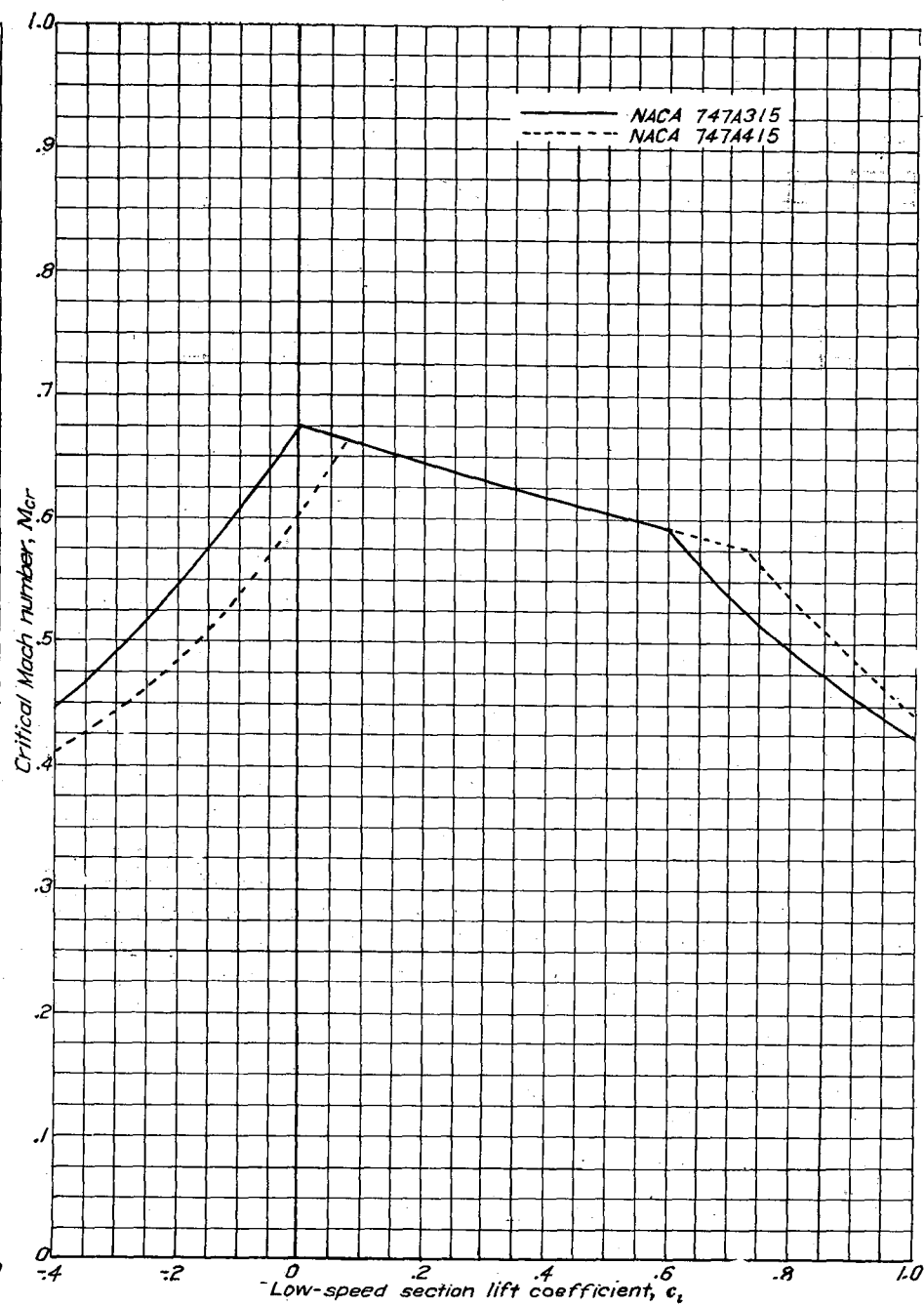
Variation of critical Mach number with low-speed section lift coefficient for two NACA 66-series airfoil sections of different thicknesses, cambered for a design lift coefficient of 0.4.



Variation of critical Mach number with low-speed section lift coefficient for several NACA 66-series airfoil sections with a thickness ratio of 0.16 and cambered for various design lift coefficients.



Variation of critical Mach number with low-speed section lift coefficient for several NACA 6-series airfoil sections with different positions of minimum pressure and various thicknesses, cambered for various design lift coefficients.

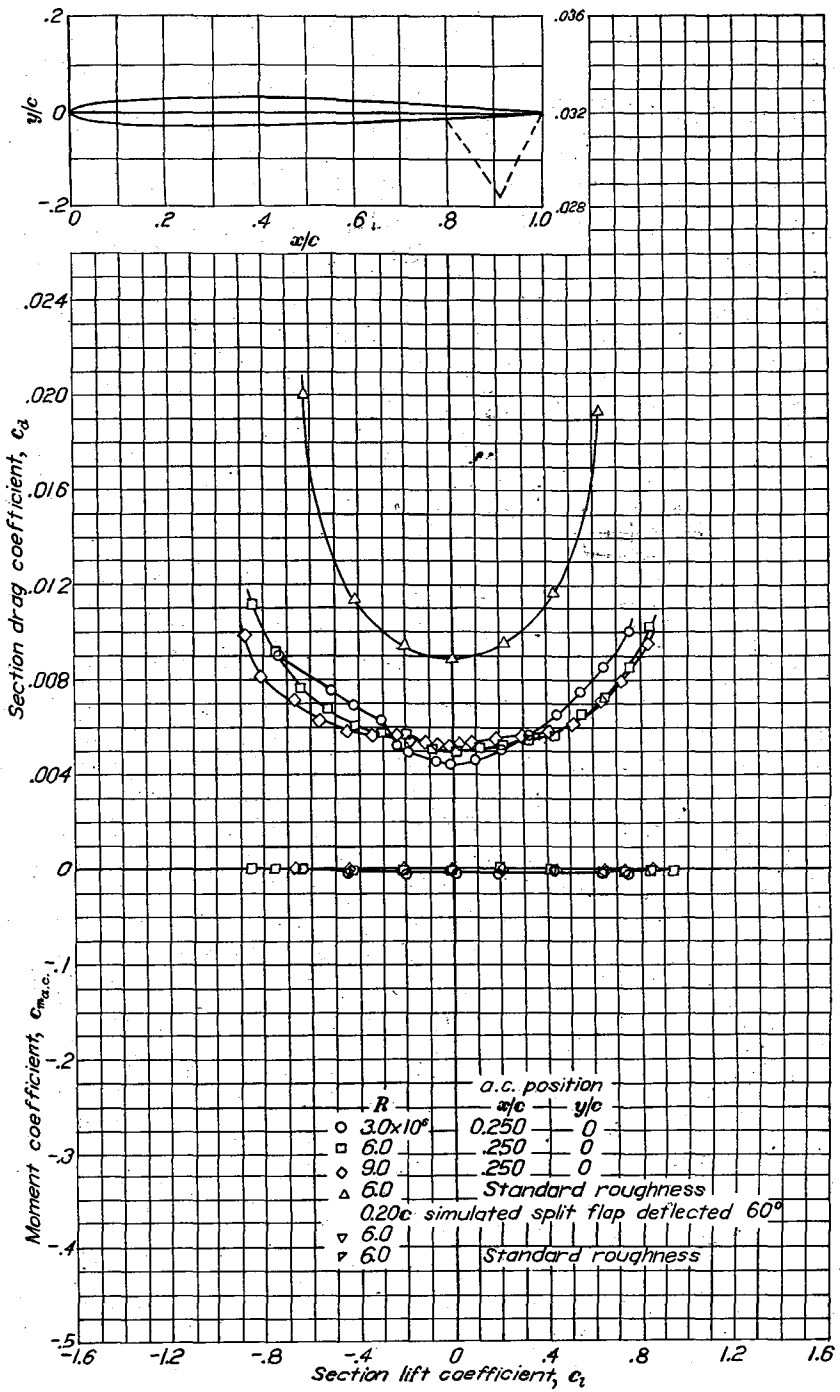
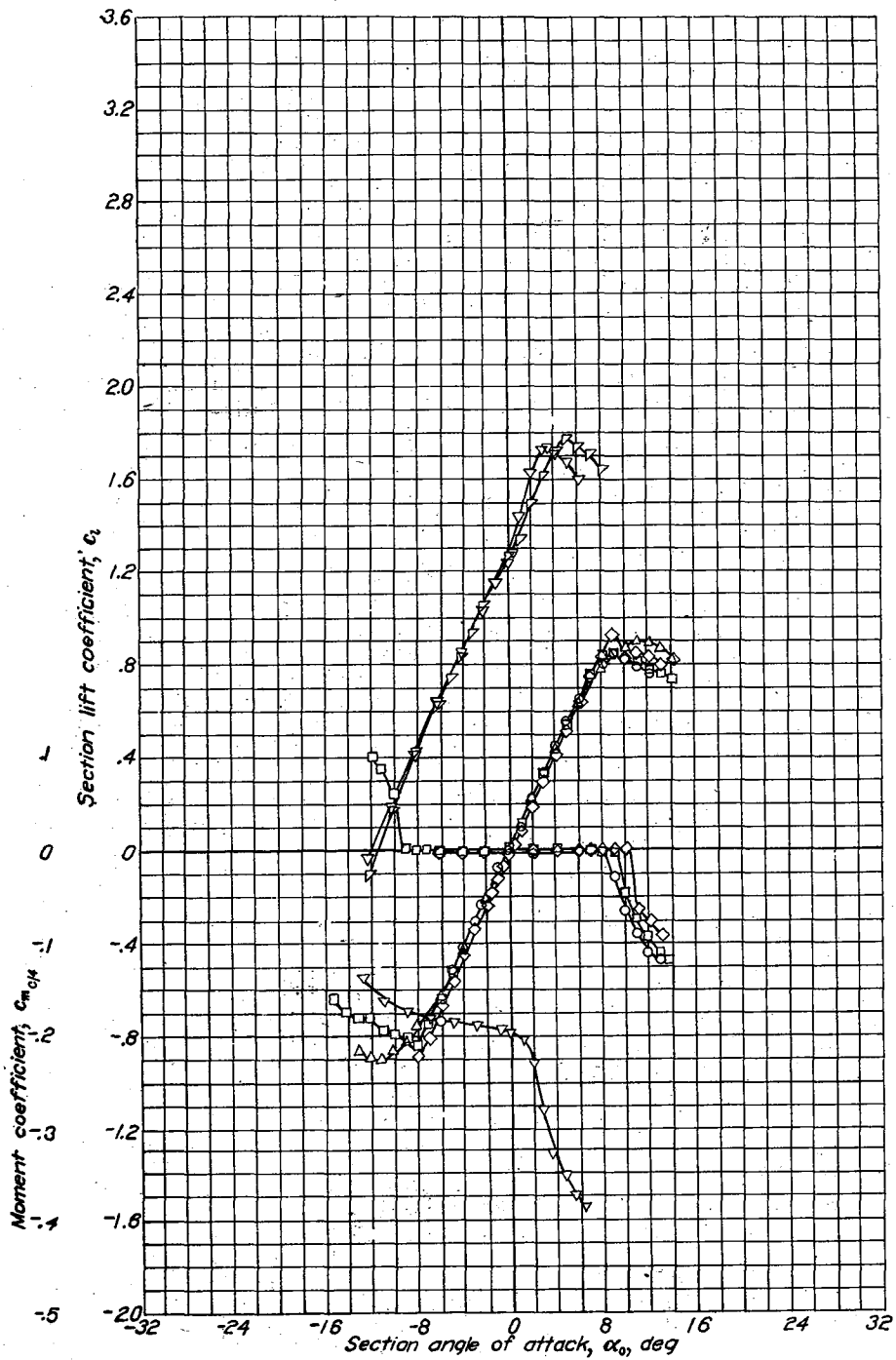


Variation of critical Mach number with low-speed section lift coefficient for two NACA 7-series airfoil sections with a thickness ratio of 0.15 and cambered for different design lift coefficients.

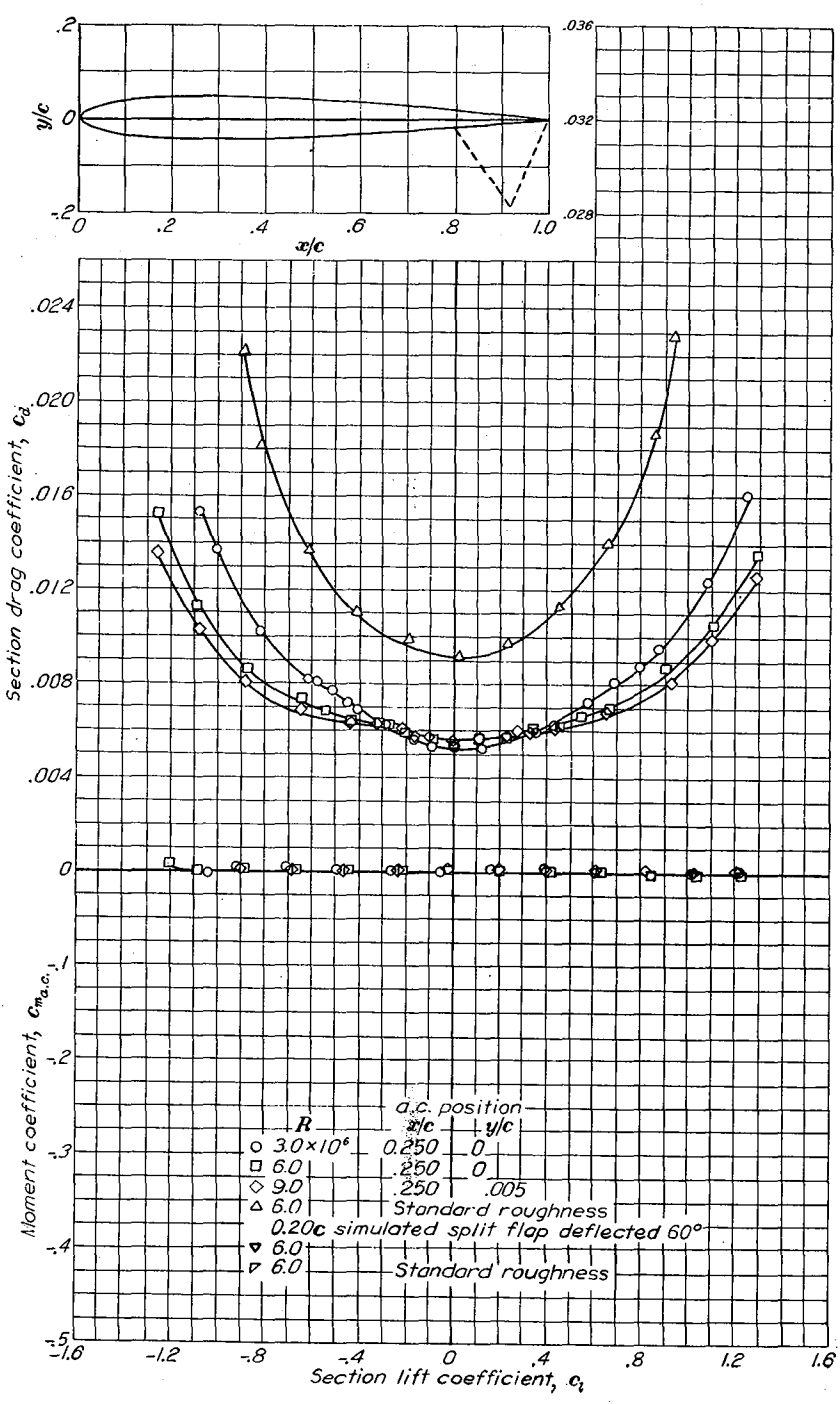
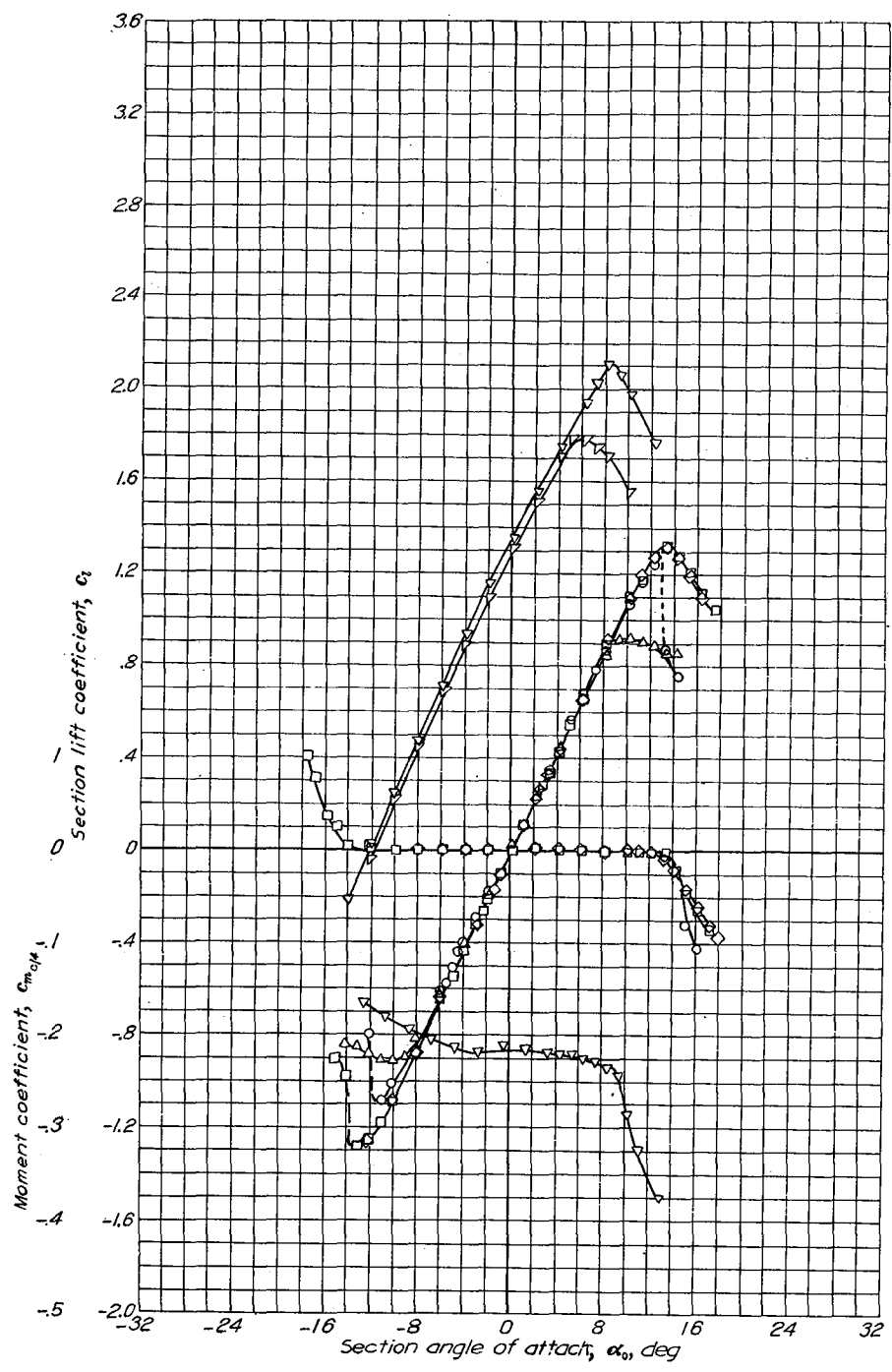
## V—AERODYNAMIC CHARACTERISTICS OF VARIOUS AIRFOIL SECTIONS

	Page		Page
NACA 0006	131	NACA 64 <sub>3</sub> -418	194
NACA 0009	132	NACA 64 <sub>3</sub> -618	195
NACA 1408	133	NACA 64 <sub>4</sub> -021	196
NACA 1410	134	NACA 64 <sub>4</sub> -221	197
NACA 1412	135	NACA 64 <sub>4</sub> -421	198
NACA 2412	136	NACA 65 <sub>3</sub> -018	199
NACA 2415	137	NACA 65 <sub>3</sub> -418, $\alpha=0.8$	200
NACA 2418	138	NACA 65 <sub>3</sub> -618	201
NACA 2421	139	NACA 65 <sub>3</sub> -618 with 0.20c sealed plain flap	202
NACA 2424	140	NACA 65(216)-415, $\alpha=0.5$	203
NACA 4412	141	NACA 65-006	204
NACA 4415	142	NACA 65-009	205
NACA 4418	143	NACA 65-206	206
NACA 4421	144	NACA 65-209	207
NACA 4424	145	NACA 65-210	208
NACA 23012	146	NACA 65-410	209
NACA 23015	147	NACA 65 <sub>1</sub> -012	210
NACA 23018	148	NACA 65 <sub>1</sub> -212	211
NACA 23021	149	NACA 65 <sub>1</sub> -212 with 0.20c split flap (lift and moment characteristics)	212
NACA 23024	150	NACA 65 <sub>1</sub> -212, $\alpha=0.6$	213
NACA 63,4-420	151	NACA 65 <sub>1</sub> -412	214
NACA 63,4-420 with 0.25c slotted flap		NACA 65 <sub>2</sub> -015	215
(a) Configuration	152	NACA 65 <sub>2</sub> -215	216
(b) Aerodynamic characteristics with hinge location 1	153	NACA 65 <sub>2</sub> -415	217
(c) Aerodynamic characteristics with hinge location 2	154	NACA 65 <sub>2</sub> -415, $\alpha=0.5$	218
NACA 63,4-420, $\alpha=0.3$	155	NACA 65 <sub>3</sub> -018	219
NACA 63(420)-422	156	NACA 65 <sub>3</sub> -118 with 0.309c double slotted flap	
NACA 63(420)-517	157	(a) Configuration	220
NACA 63-006	158	(b) Aerodynamic characteristics	221
NACA 63-009	159	NACA 65 <sub>3</sub> -218	222
NACA 63-206	160	NACA 65 <sub>3</sub> -418	223
NACA 63-209	161	NACA 65 <sub>3</sub> -418, $\alpha=0.5$	224
NACA 63-210	162	NACA 65 <sub>3</sub> -618	225
NACA 63 <sub>1</sub> -012	163	NACA 65 <sub>3</sub> -618, $\alpha=0.5$	226
NACA 63 <sub>1</sub> -212	164	NACA 65 <sub>4</sub> -021	227
NACA 63 <sub>1</sub> -412	165	NACA 65 <sub>4</sub> -221	228
NACA 63 <sub>2</sub> -015	166	NACA 65 <sub>4</sub> -421	229
NACA 63 <sub>2</sub> -215	167	NACA 65 <sub>4</sub> -421, $\alpha=0.5$	230
NACA 63 <sub>2</sub> -415	168	NACA 65(215)-114	231
NACA 63 <sub>2</sub> -615	169	NACA 65(421)-420	232
NACA 63 <sub>3</sub> -018	170	NACA 66,1-212	233
NACA 63 <sub>3</sub> -218	171	NACA 66,1-212 with 0.20c split flap (lift and moment characteristics)	234
NACA 63 <sub>3</sub> -418	172	NACA 66(215)-016	235
NACA 63 <sub>3</sub> -618	173	NACA 66(215)-216	236
NACA 63 <sub>4</sub> -021	174	NACA 66(215)-216 with 0.20c sealed plain flap	237
NACA 63 <sub>4</sub> -221	175	NACA 66(125)-216 with 0.20c split flap (lift and moment characteristics)	238
NACA 63 <sub>4</sub> -421	176	NACA 66(215)-216, $\alpha=0.6$	239
NACA 64-006	177	NACA 66(215)-216, $\alpha=0.6$ with 0.30c slotted and 0.10c plain flap	
NACA 64-009	178	(a) Airfoil-flap configuration	240
NACA 64-108	179	(b) Flap configuration	240
NACA 64-110	180	(c) Aerodynamic characteristics. Slotted flap retracted	241
NACA 64-206	181	(d) Lift and moment characteristics. Slotted flap deflected 22°	242
NACA 64-208	182	(e) Lift and moment characteristics. Slotted flap deflected 27°	243
NACA 64-209	183	(f) Lift and moment characteristics. Slotted flap deflected 32°	244
NACA 64-210	184	(g) Lift and moment characteristics. Slotted flap deflected 37°	245
NACA 64 <sub>1</sub> -012	185	NACA 66(215)-416	246
NACA 64 <sub>1</sub> -112	186		
NACA 64 <sub>1</sub> -212	187		
NACA 64 <sub>1</sub> -412	188		
NACA 64 <sub>2</sub> -015	189		
NACA 64 <sub>2</sub> -215	190		
NACA 64 <sub>2</sub> -415	191		
NACA 64 <sub>3</sub> -018	192		
NACA 64 <sub>3</sub> -218	193		

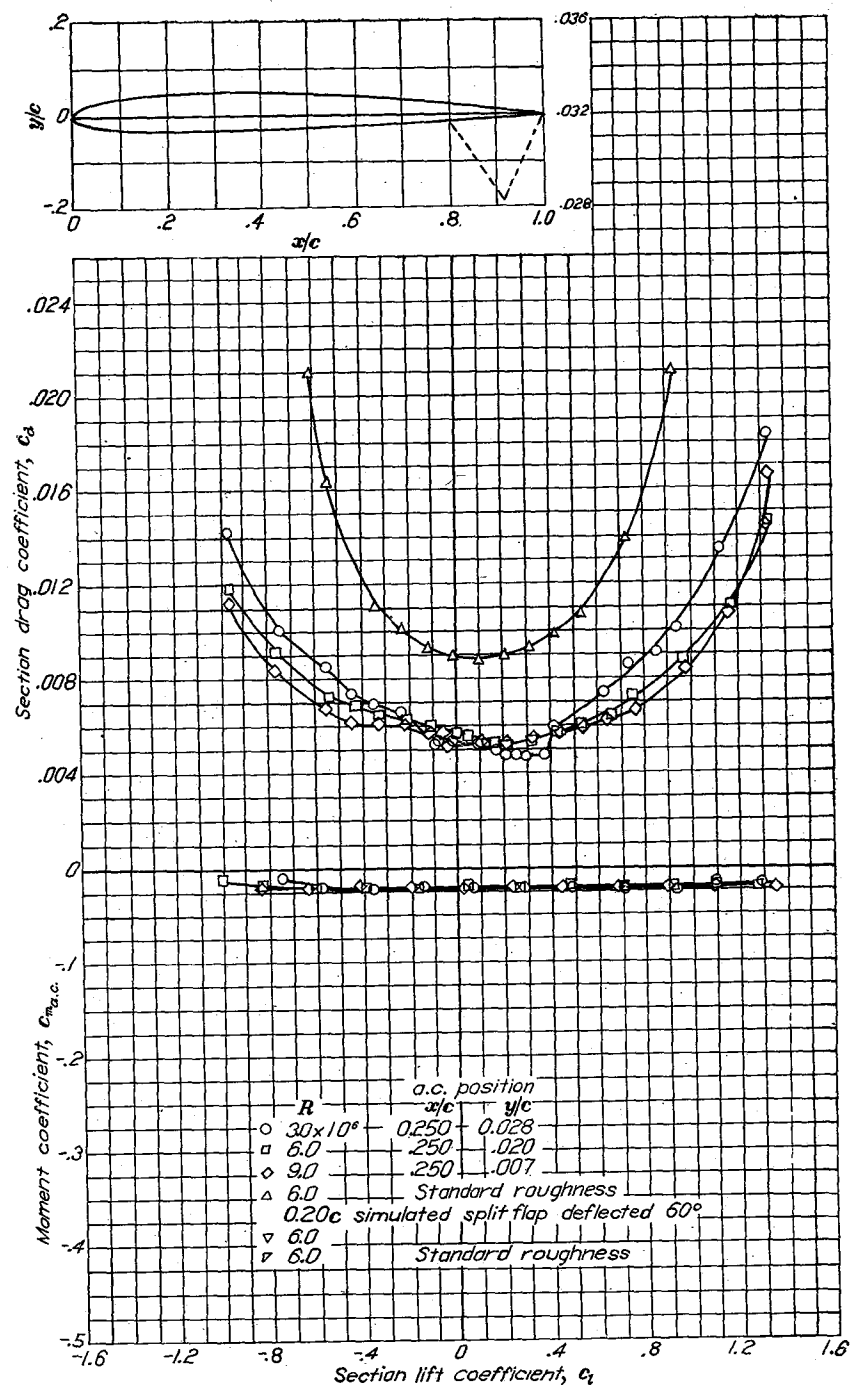
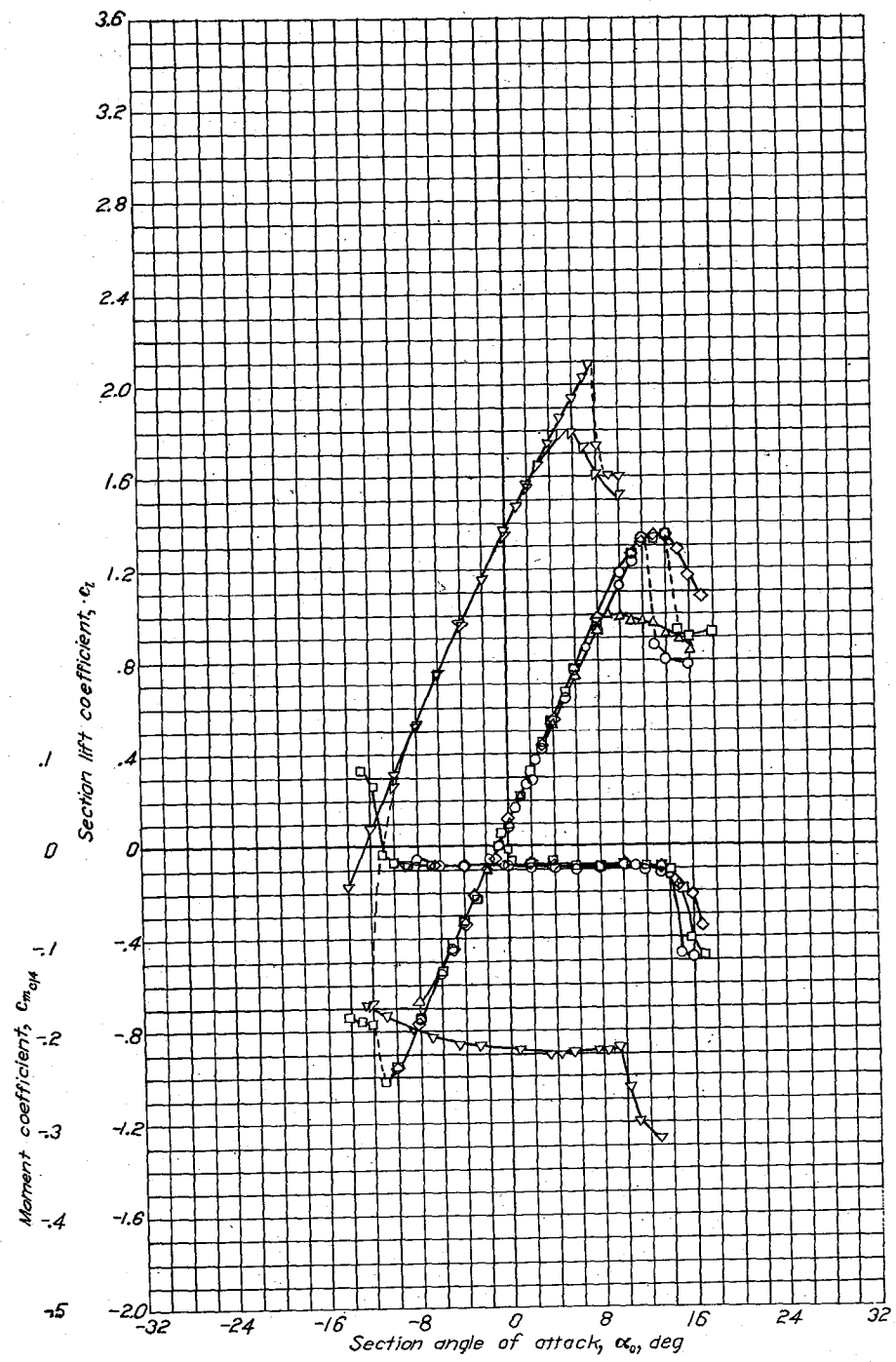
	Page		Page
NACA 66-006.....	247	NACA 66 <sub>2</sub> -415.....	256
NACA 66-009.....	248	NACA 66 <sub>3</sub> -018.....	257
NACA 66-206.....	249	NACA 66 <sub>3</sub> -218.....	258
NACA 66-209.....	250	NACA 66 <sub>3</sub> -418.....	259
NACA 66-210.....	251	NACA 66 <sub>4</sub> -021.....	260
NACA 66 <sub>1</sub> -012.....	252	NACA 66 <sub>4</sub> -221.....	261
NACA 66 <sub>1</sub> -212.....	253	NACA 67,1-215.....	262
NACA 66 <sub>2</sub> -015.....	254	NACA 747A315.....	263
NACA 66 <sub>2</sub> -215.....	255	NACA 747A415.....	264



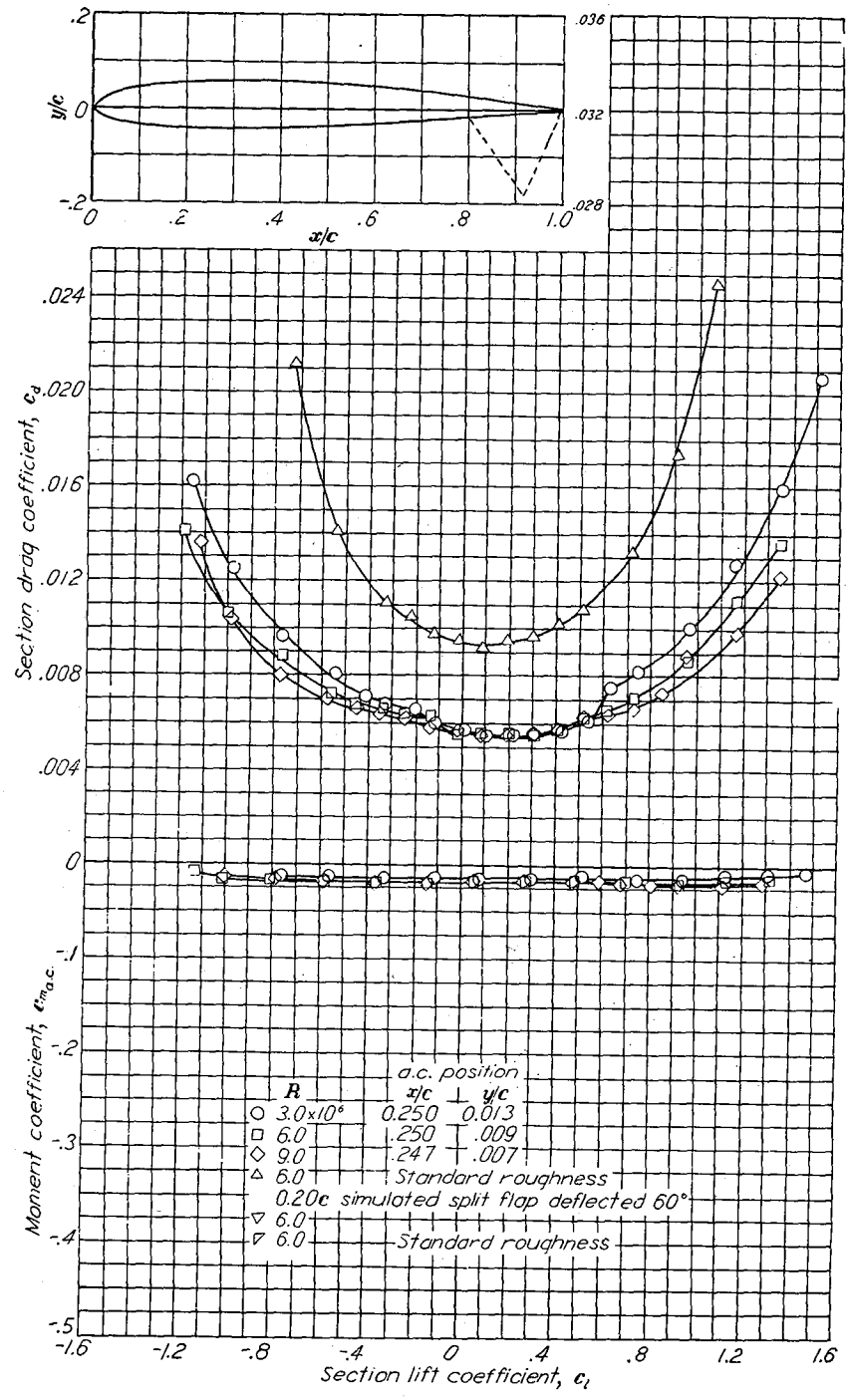
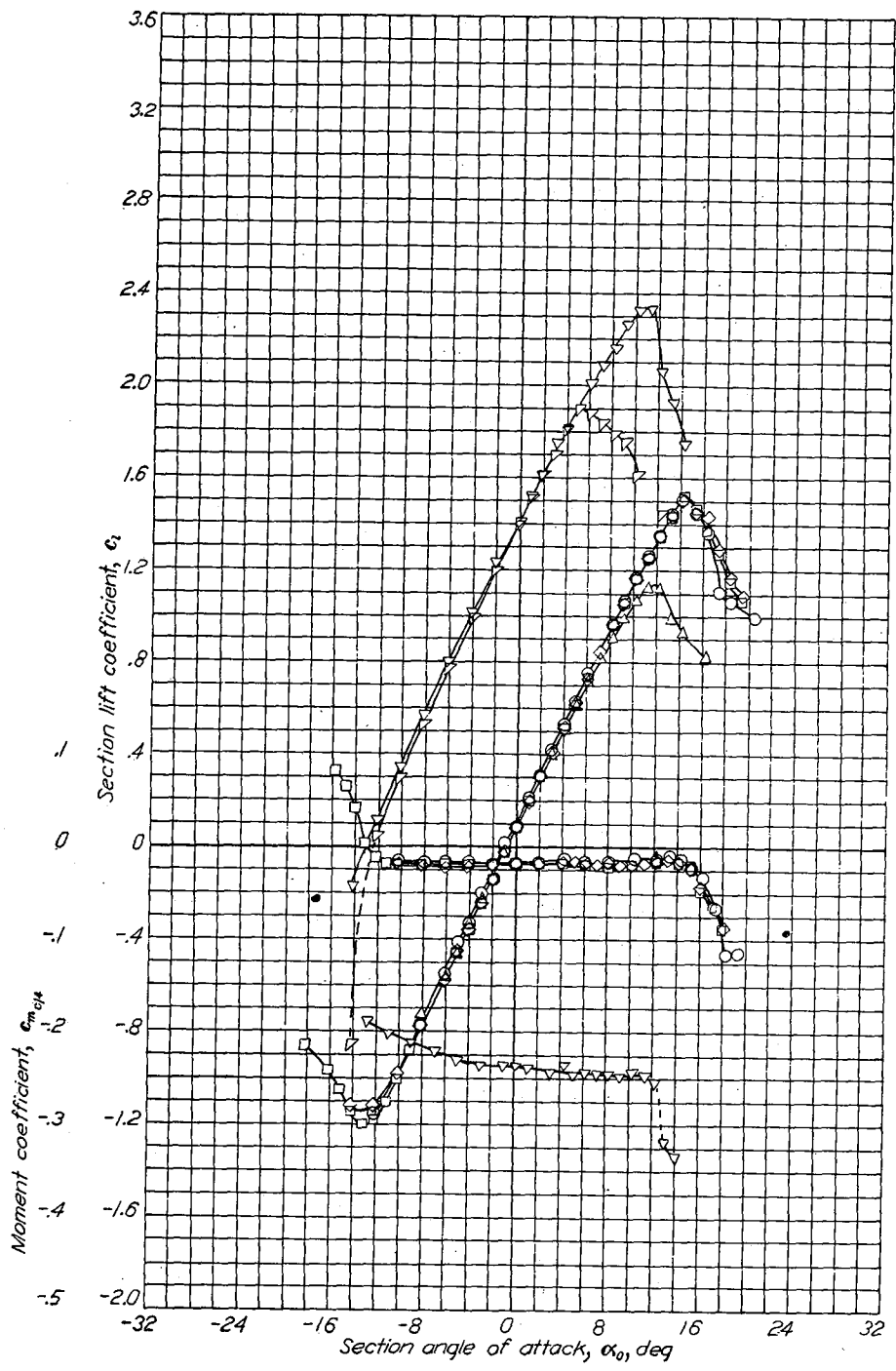
Aerodynamic characteristics of the NACA 0006 airfoil section, 24-inch chord.



Aerodynamic characteristics of the NACA 0009 airfoil section, 24-inch chord.

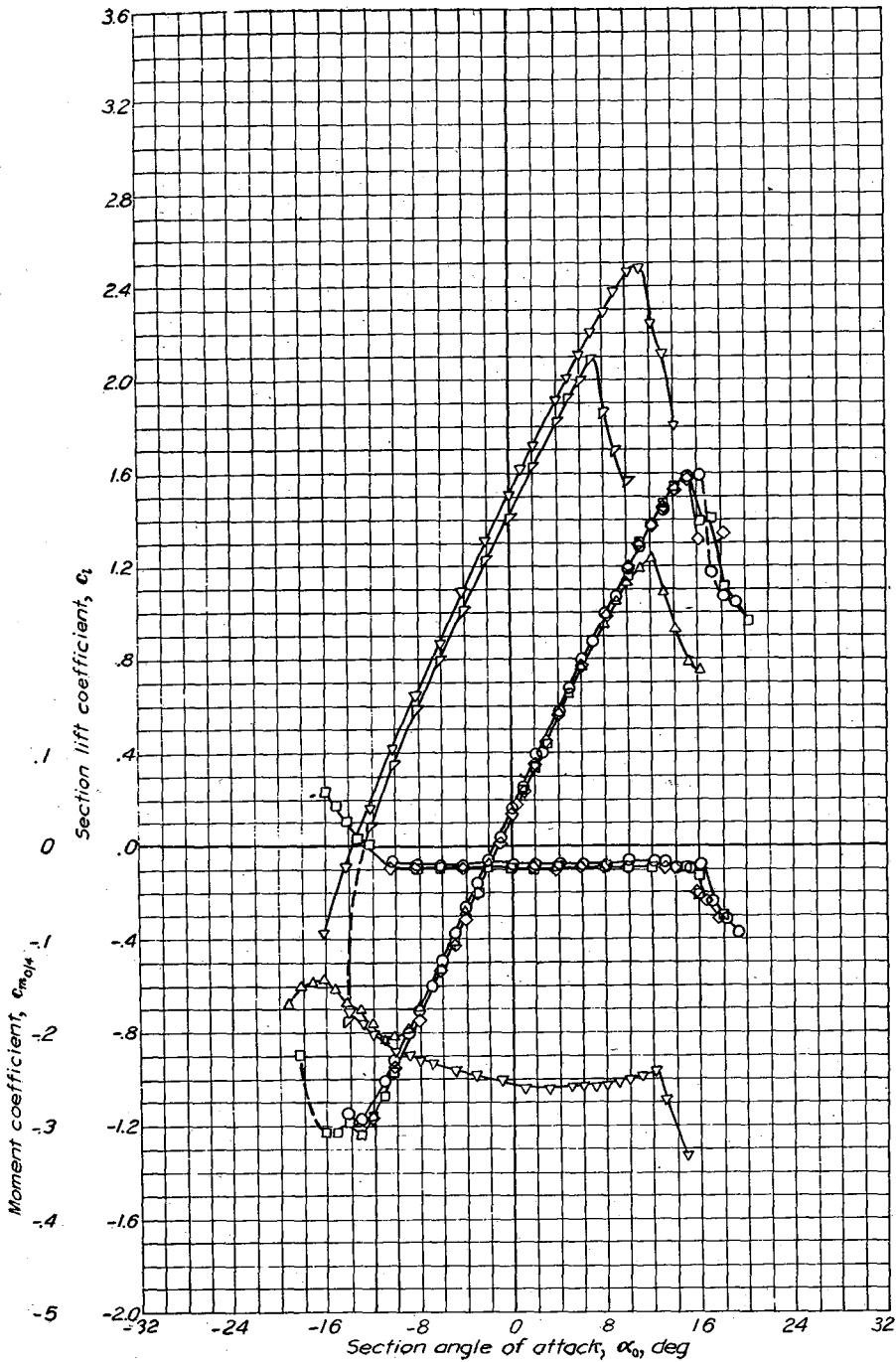


Aerodynamic characteristics of the NACA 1408 airfoil section, 24-inch chord.

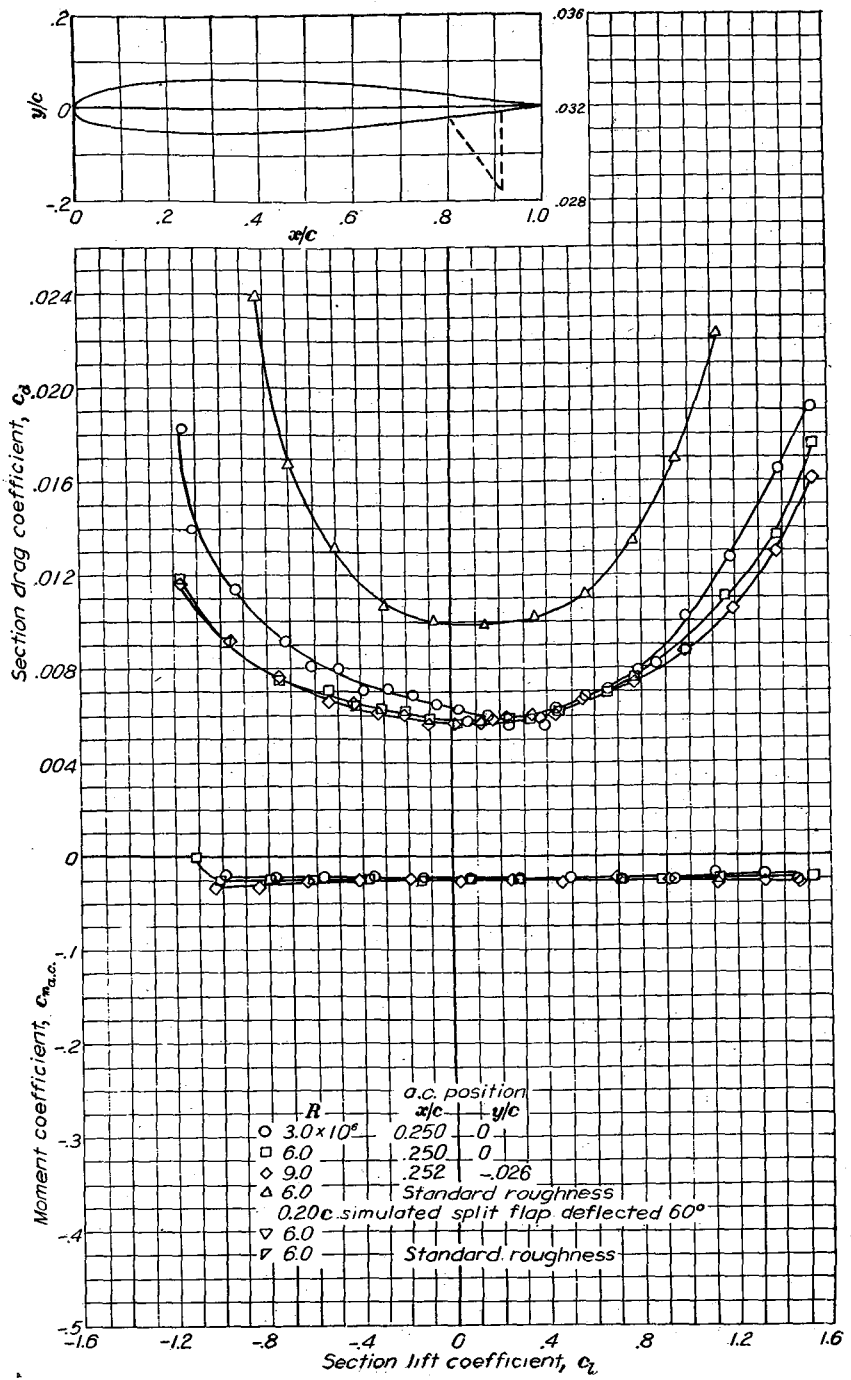


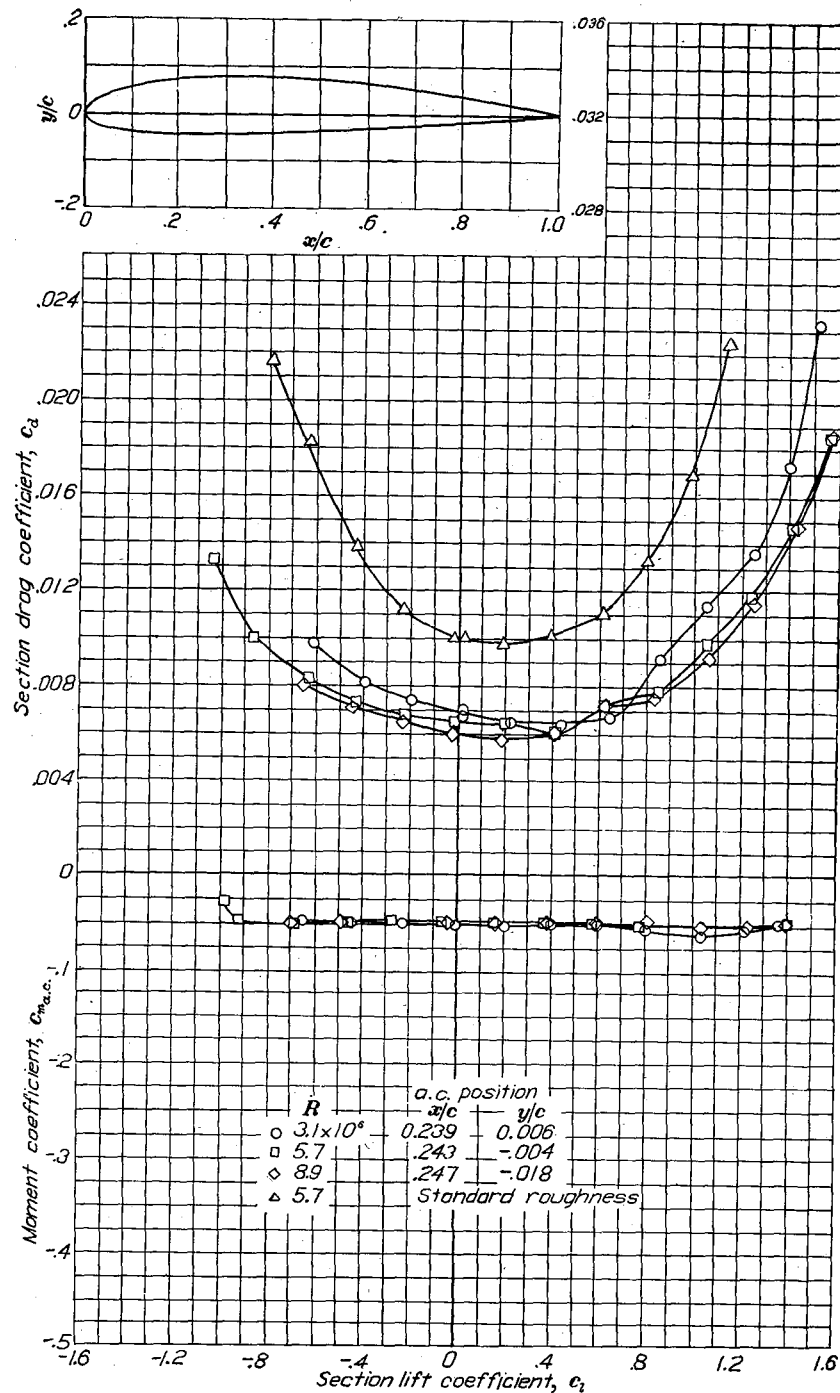
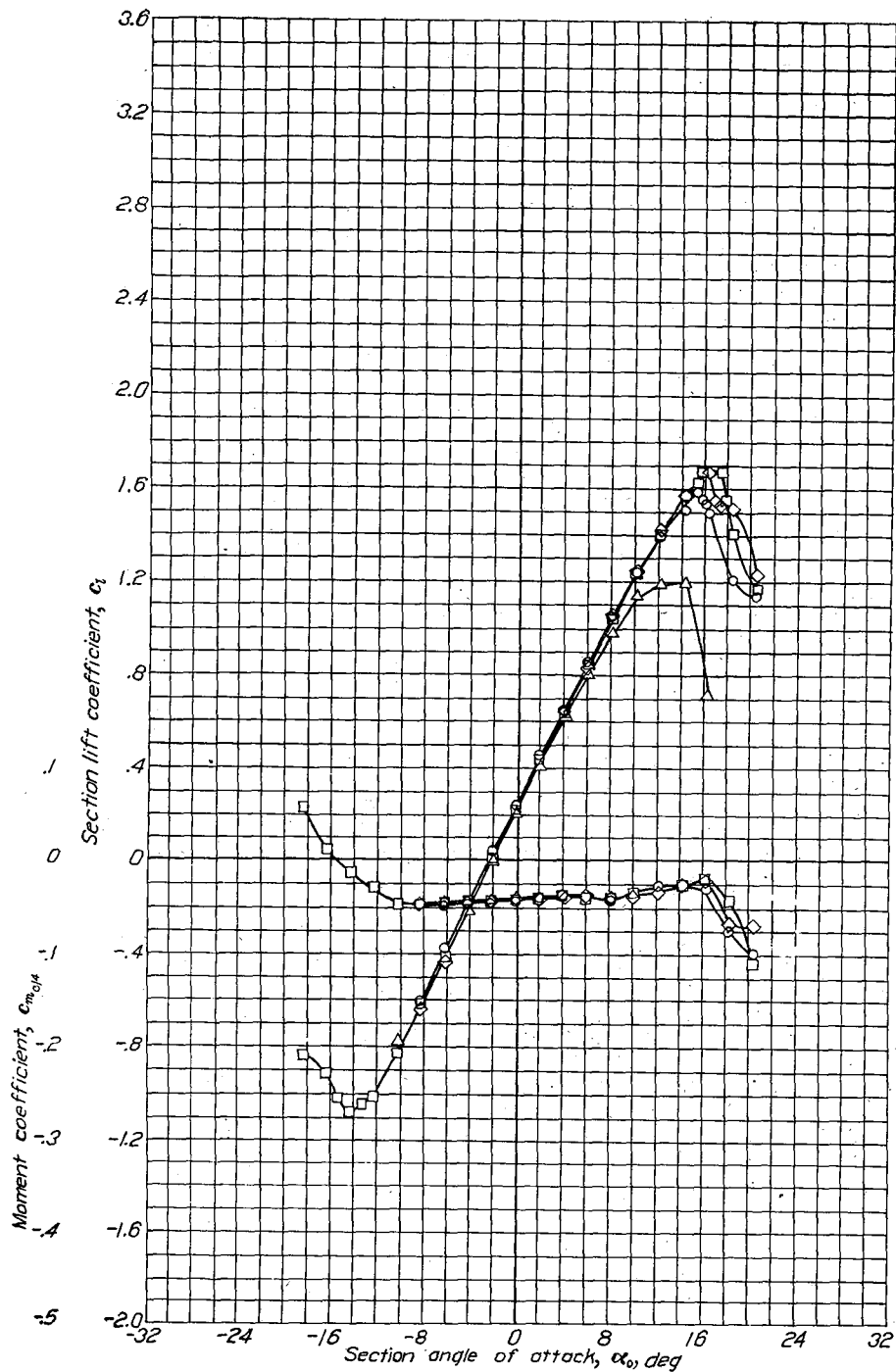
Aerodynamic characteristics of the NACA 1410 airfoil section, 24-inch chord.



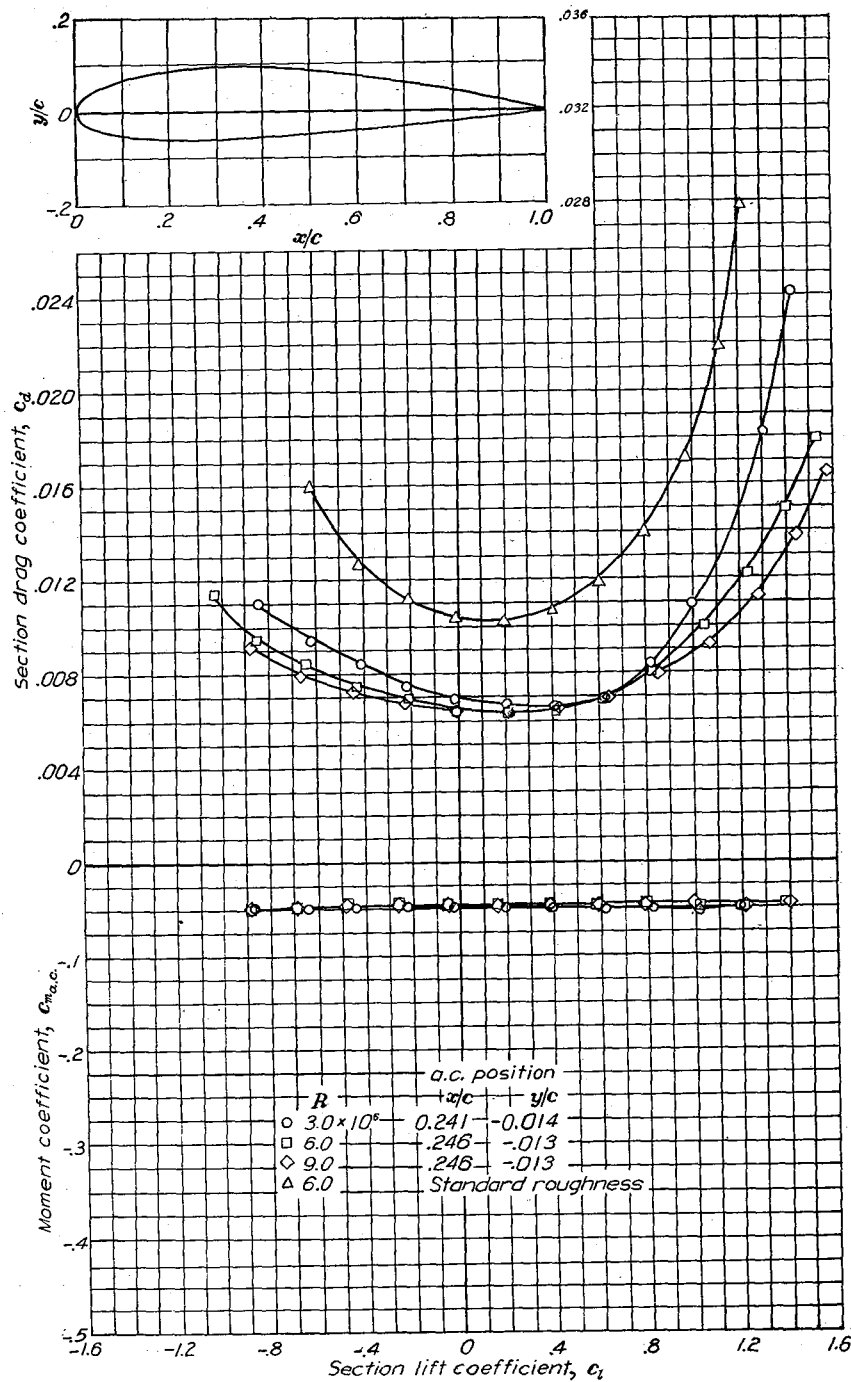
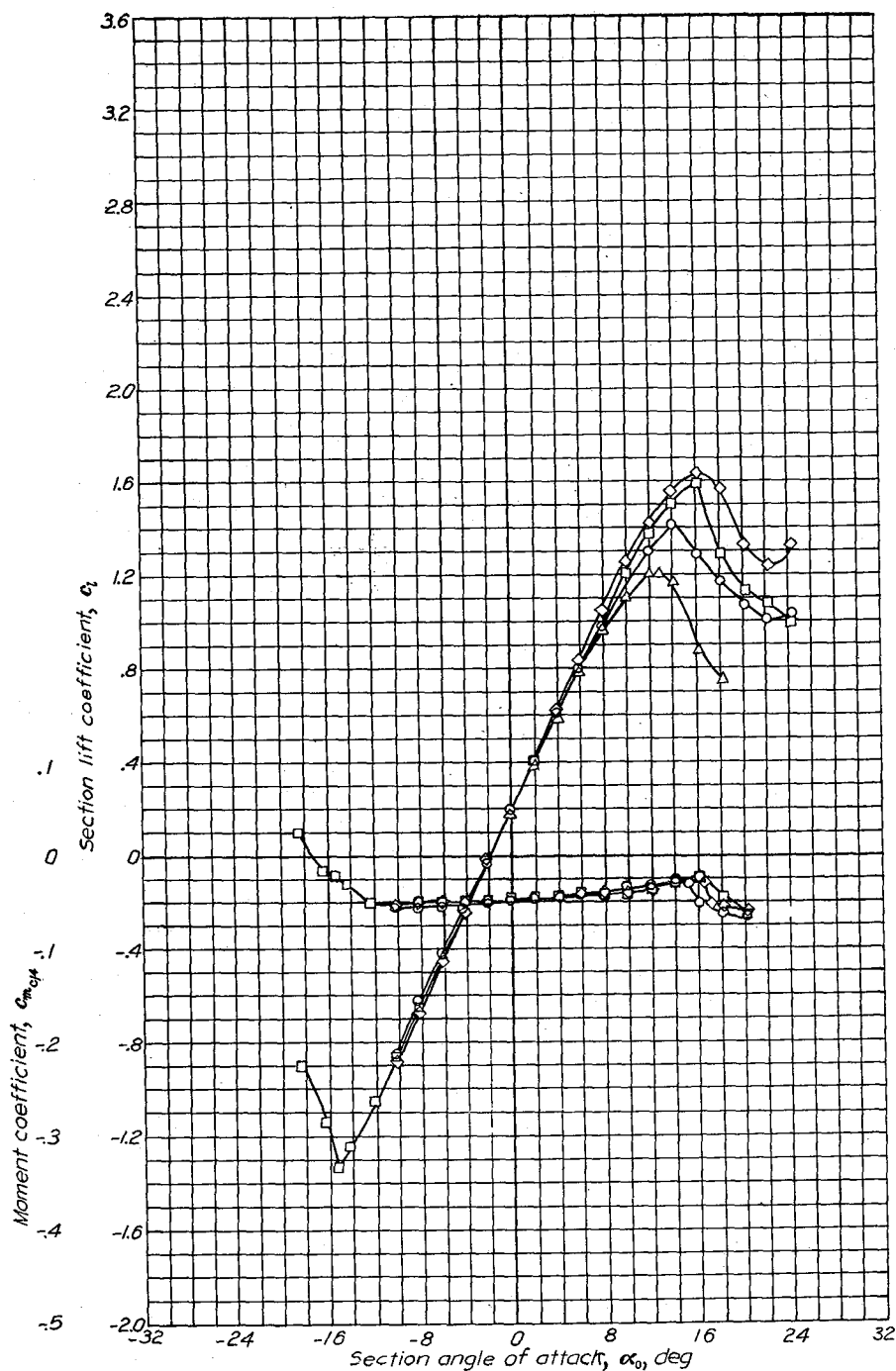


Aerodynamic characteristics of the NACA 1412 airfoil section, 24-inch chord.

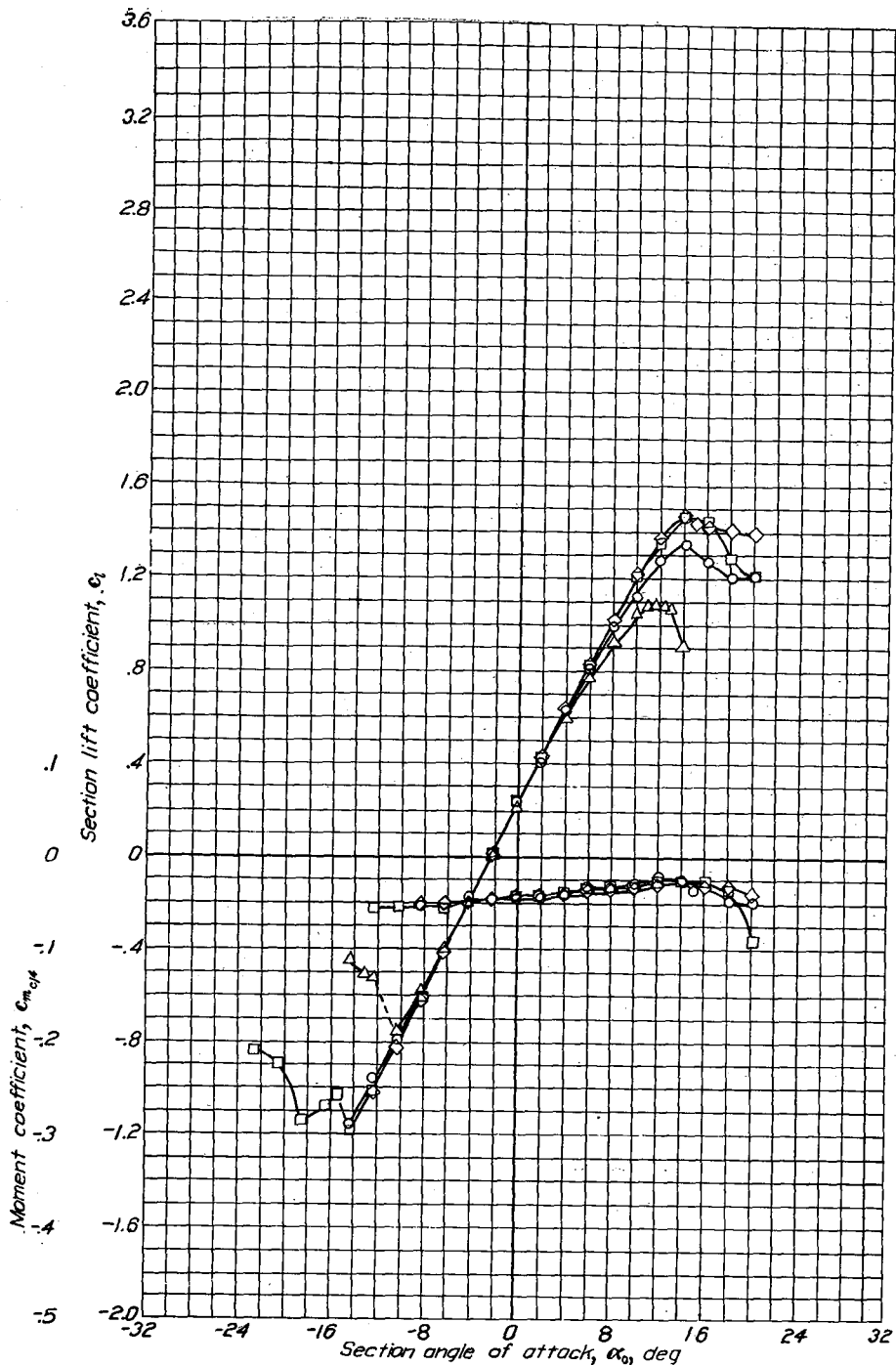




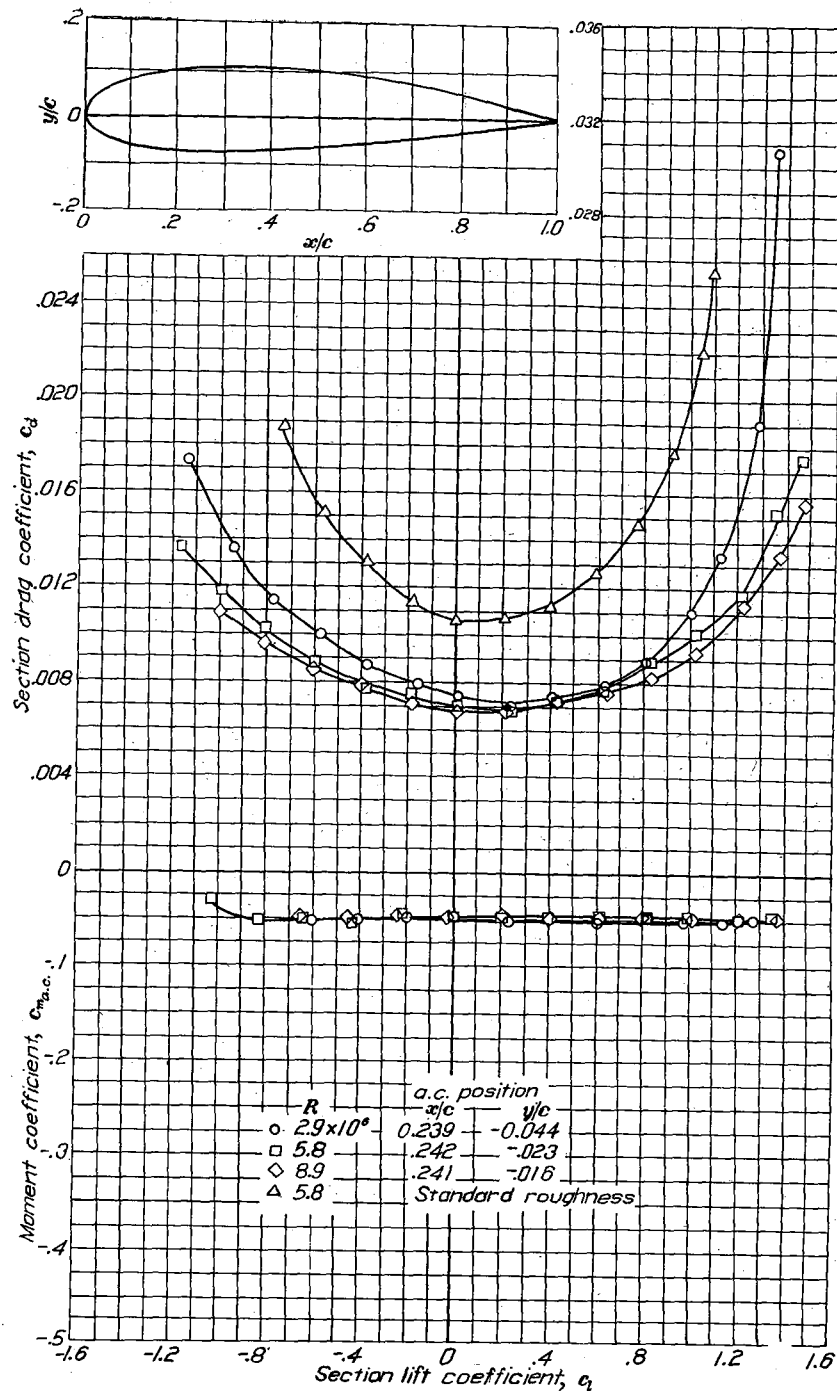
Aerodynamic characteristics of the NACA 2412 airfoil section, 24-inch chord.

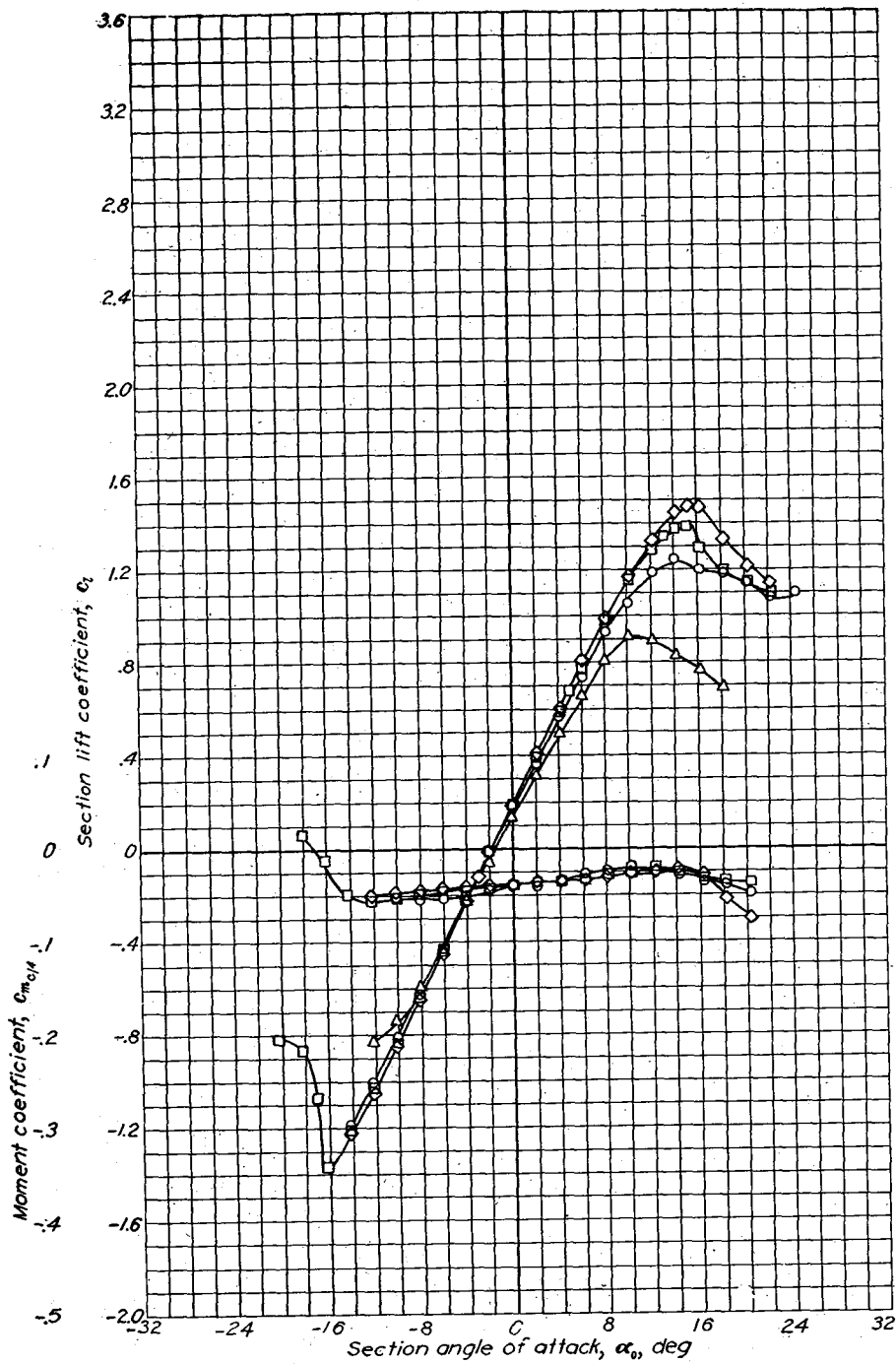


Aerodynamic characteristics of the NACA 2415 airfoil section, 24-inch chord.

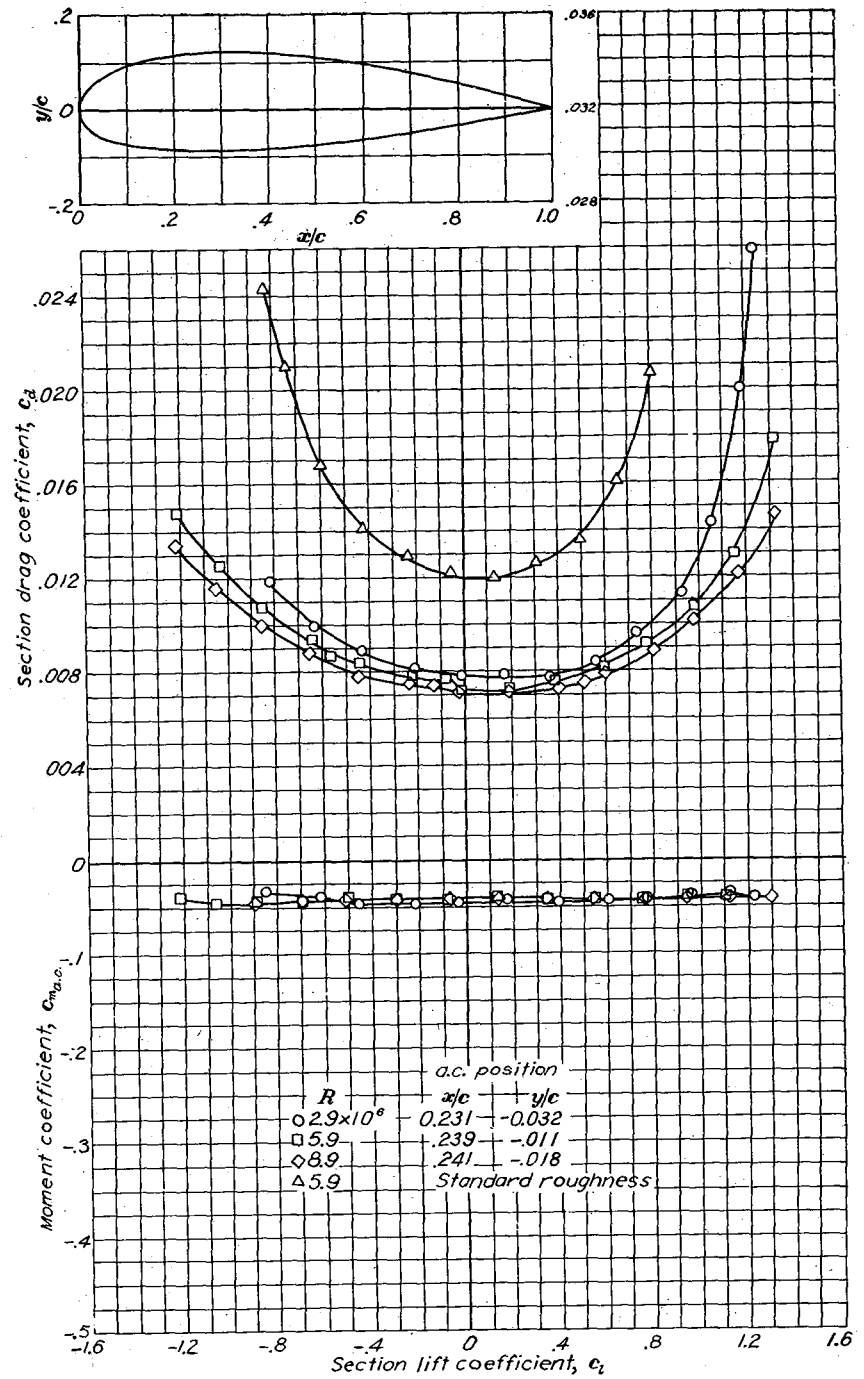


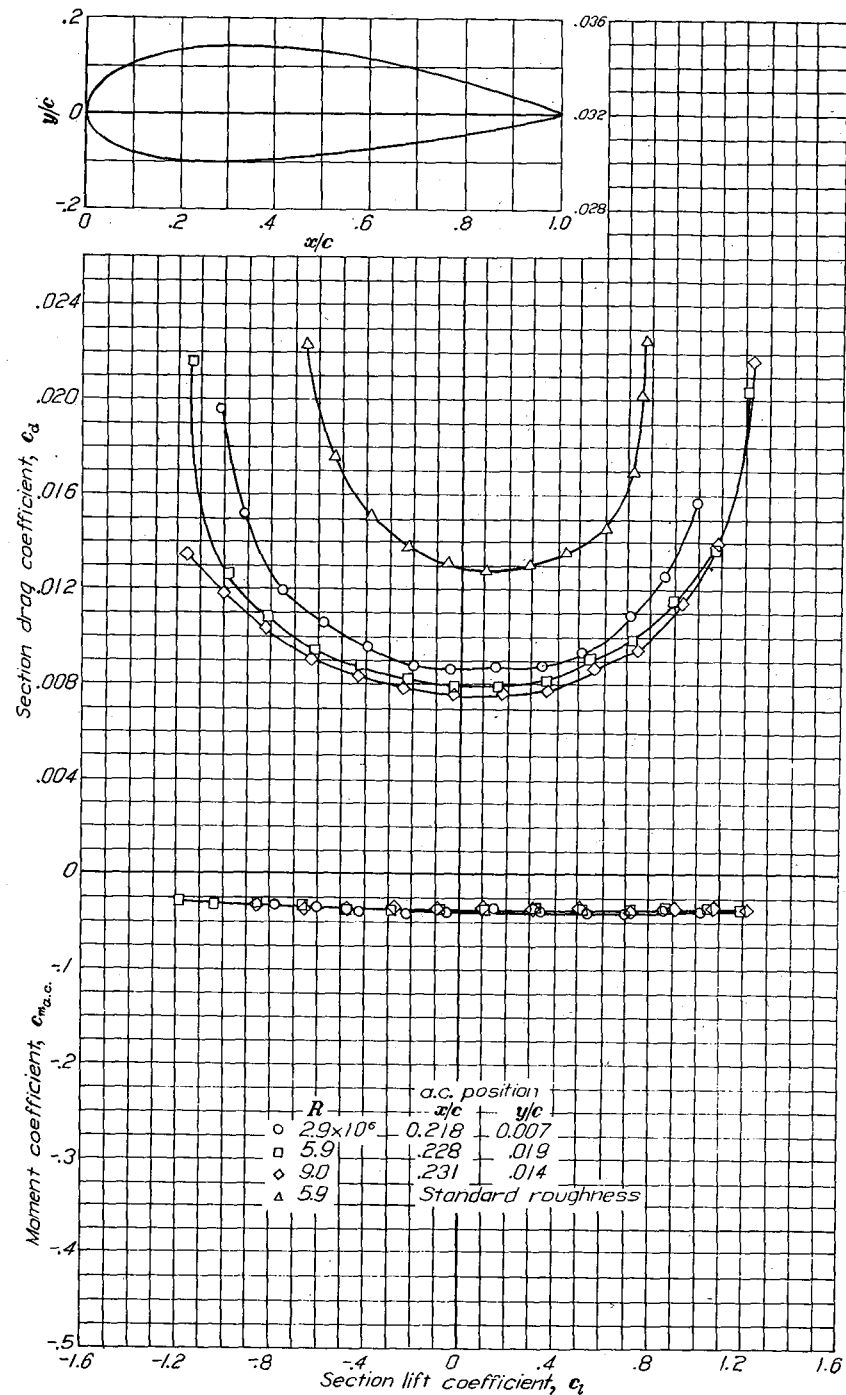
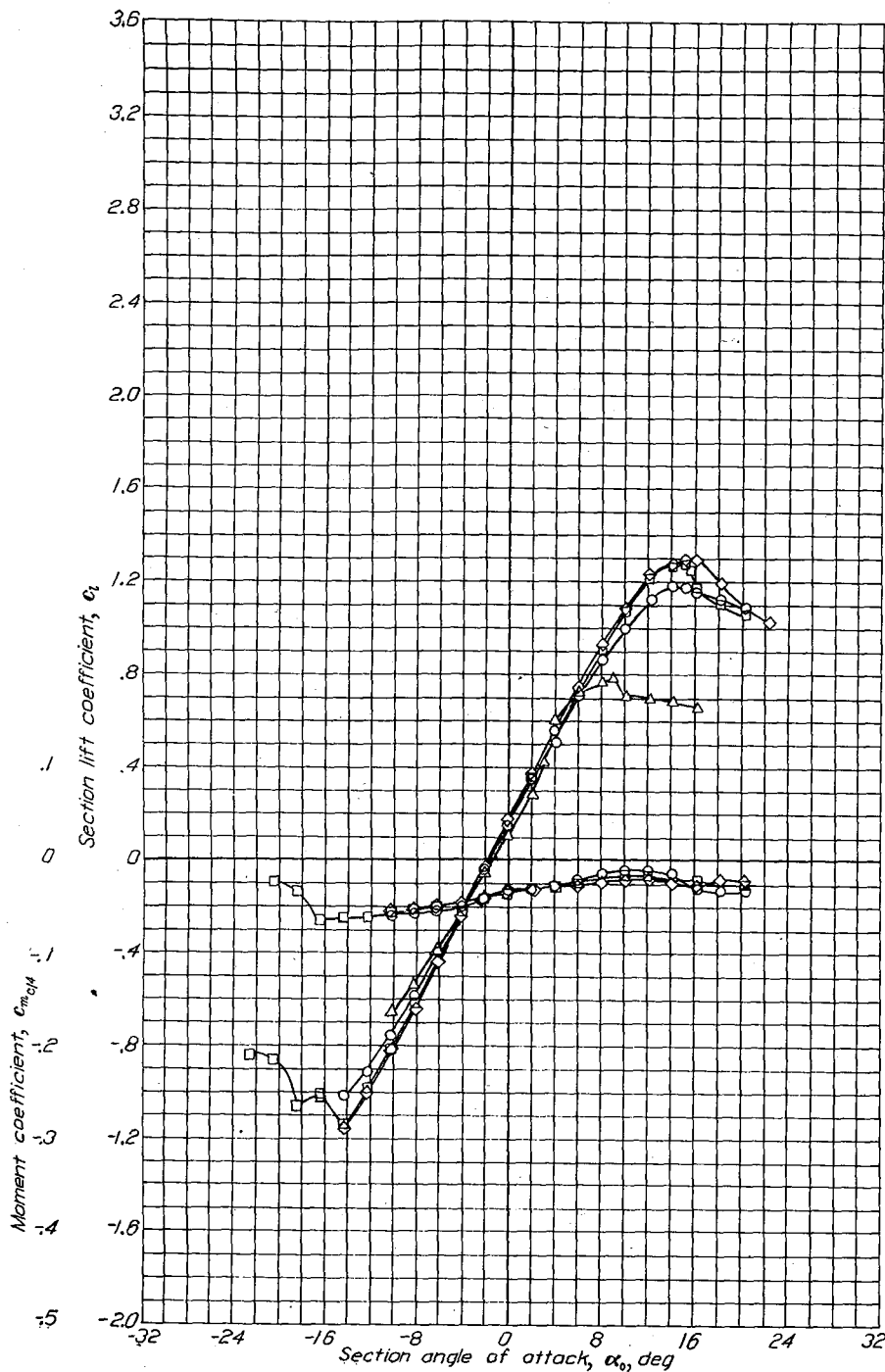
Aerodynamic characteristics of the NACA 2418 airfoil section, 24-inch chord,



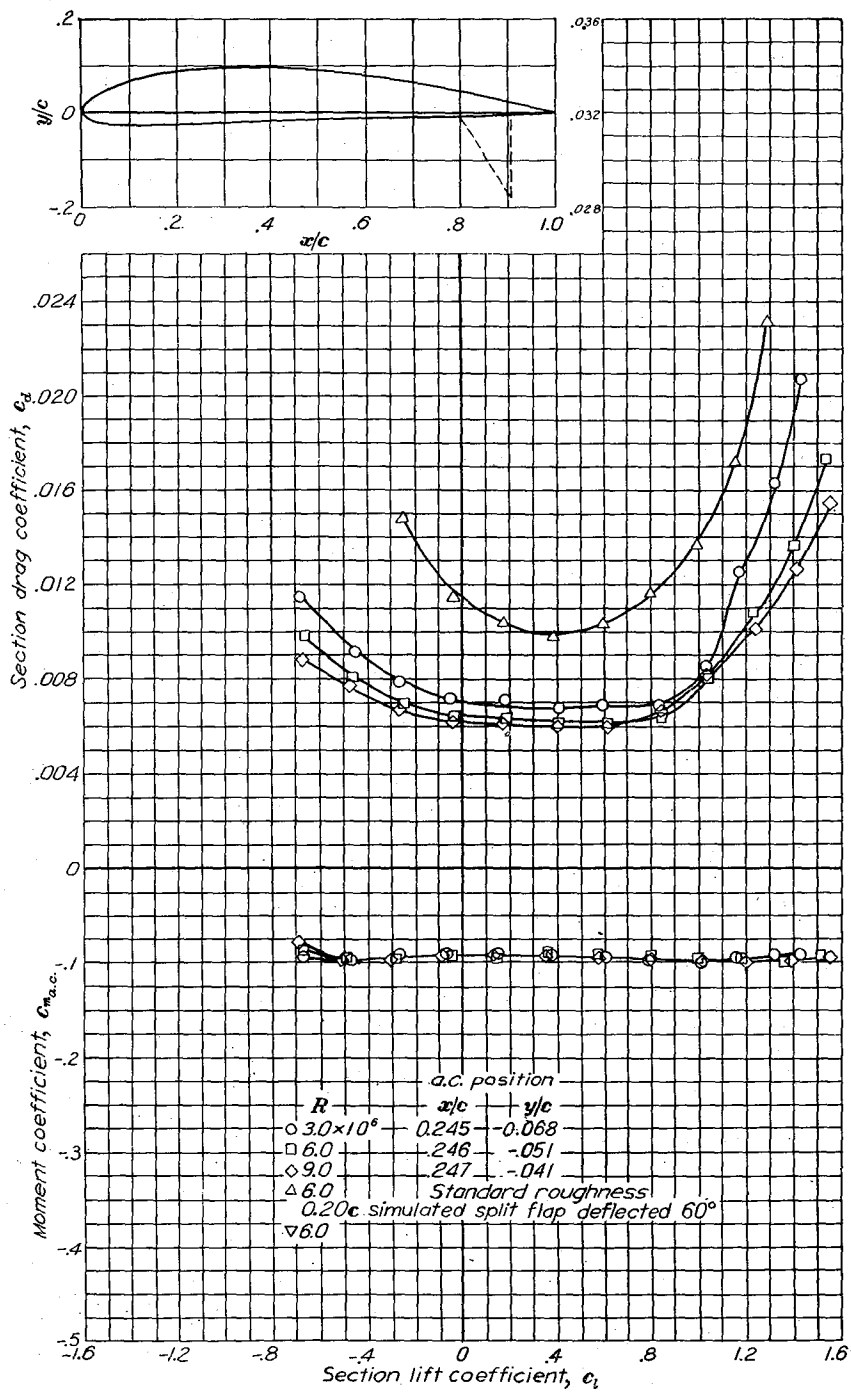
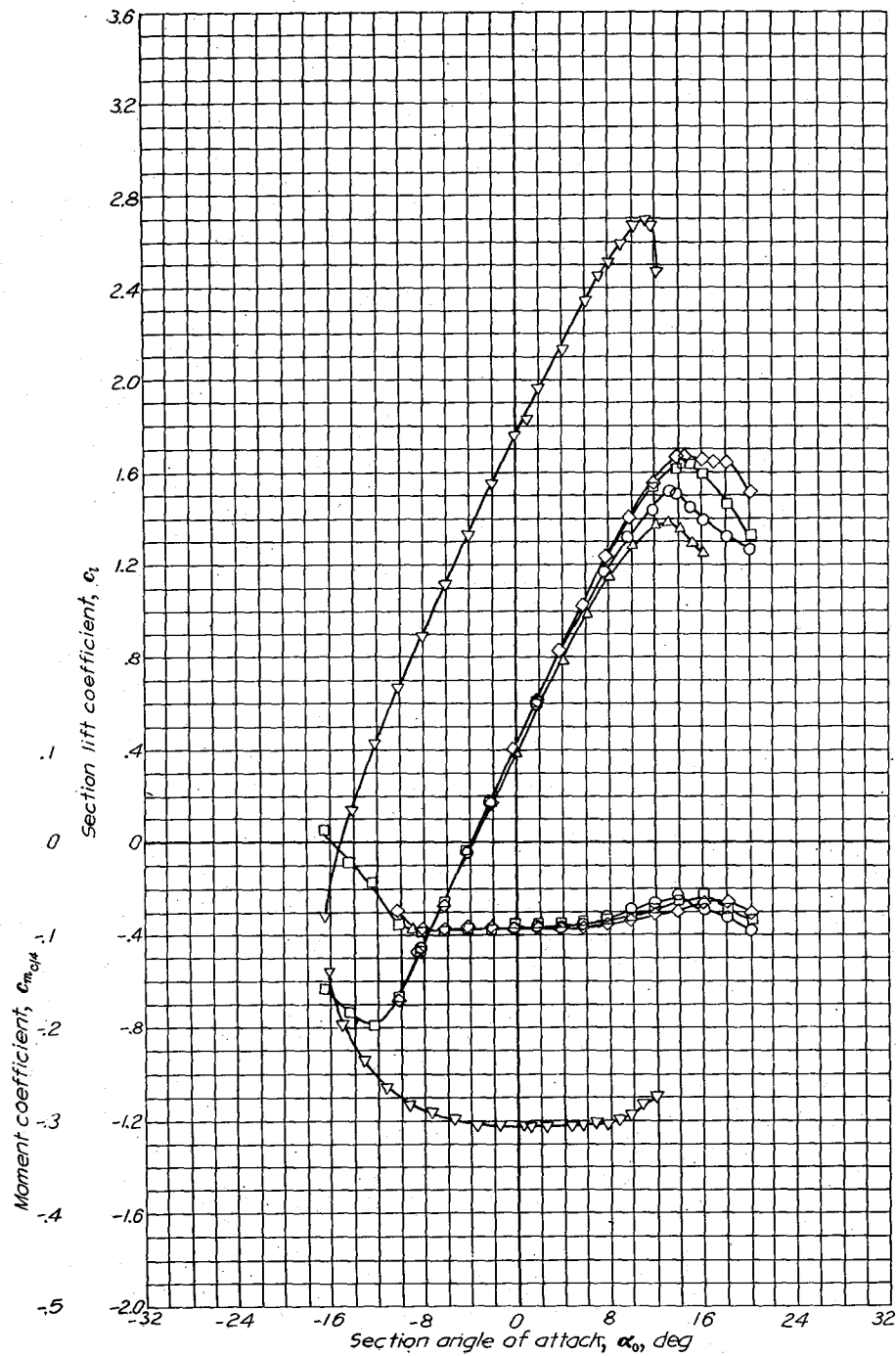


Aerodynamic characteristics of the NACA 2421 airfoil section, 24-inch chord.

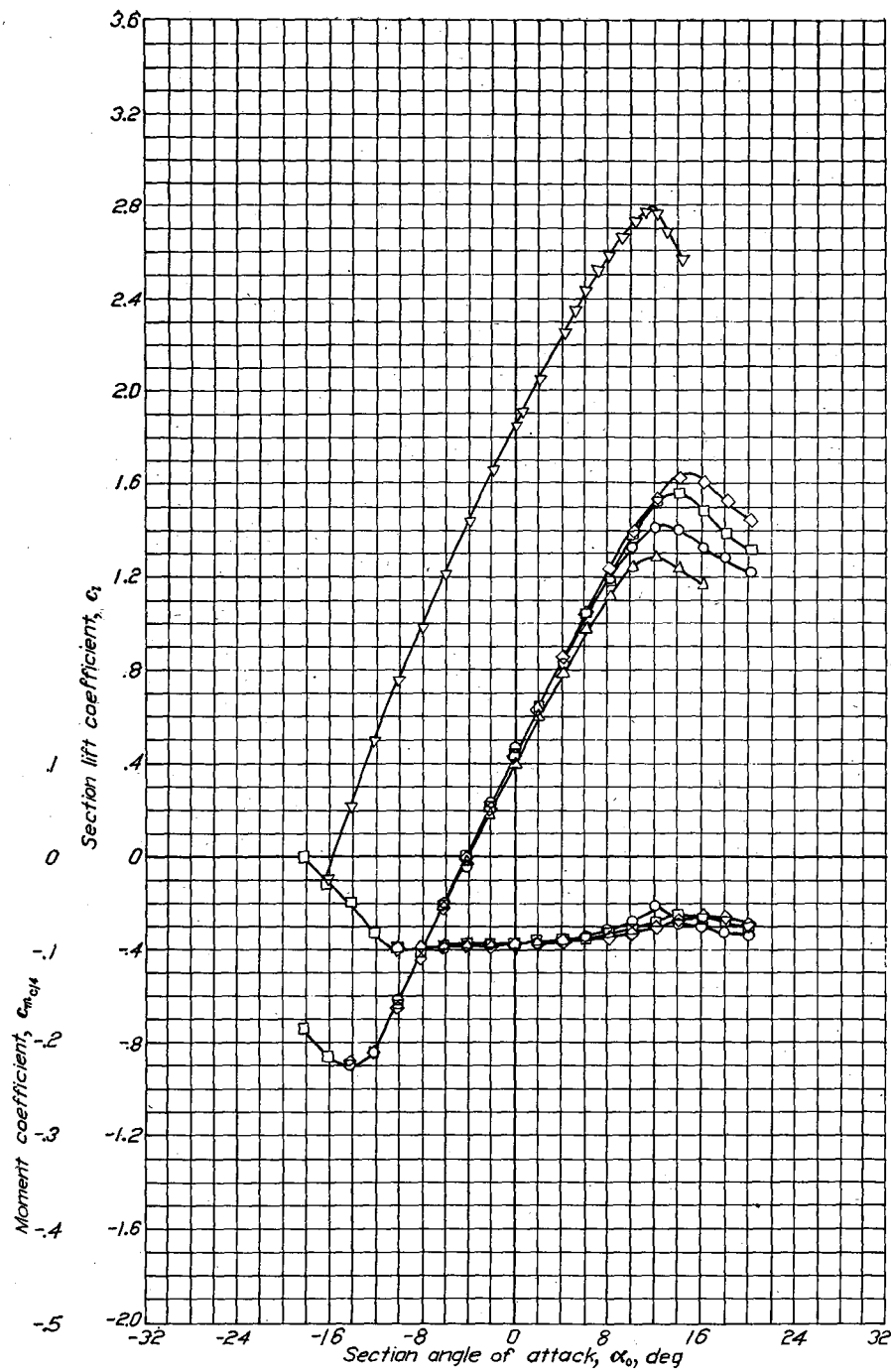




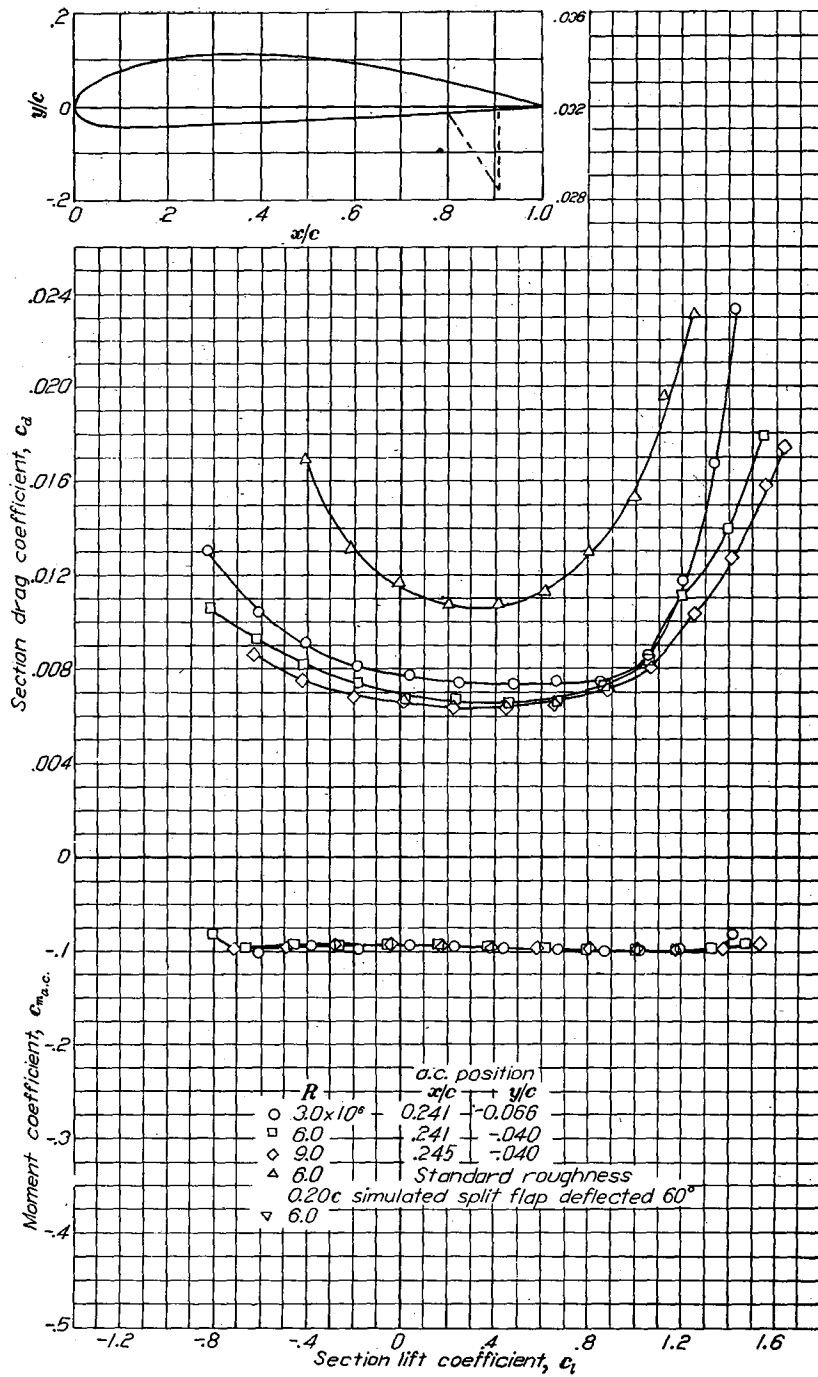
Aerodynamic characteristics of the NACA 2424 airfoil section. 24-inch chord.



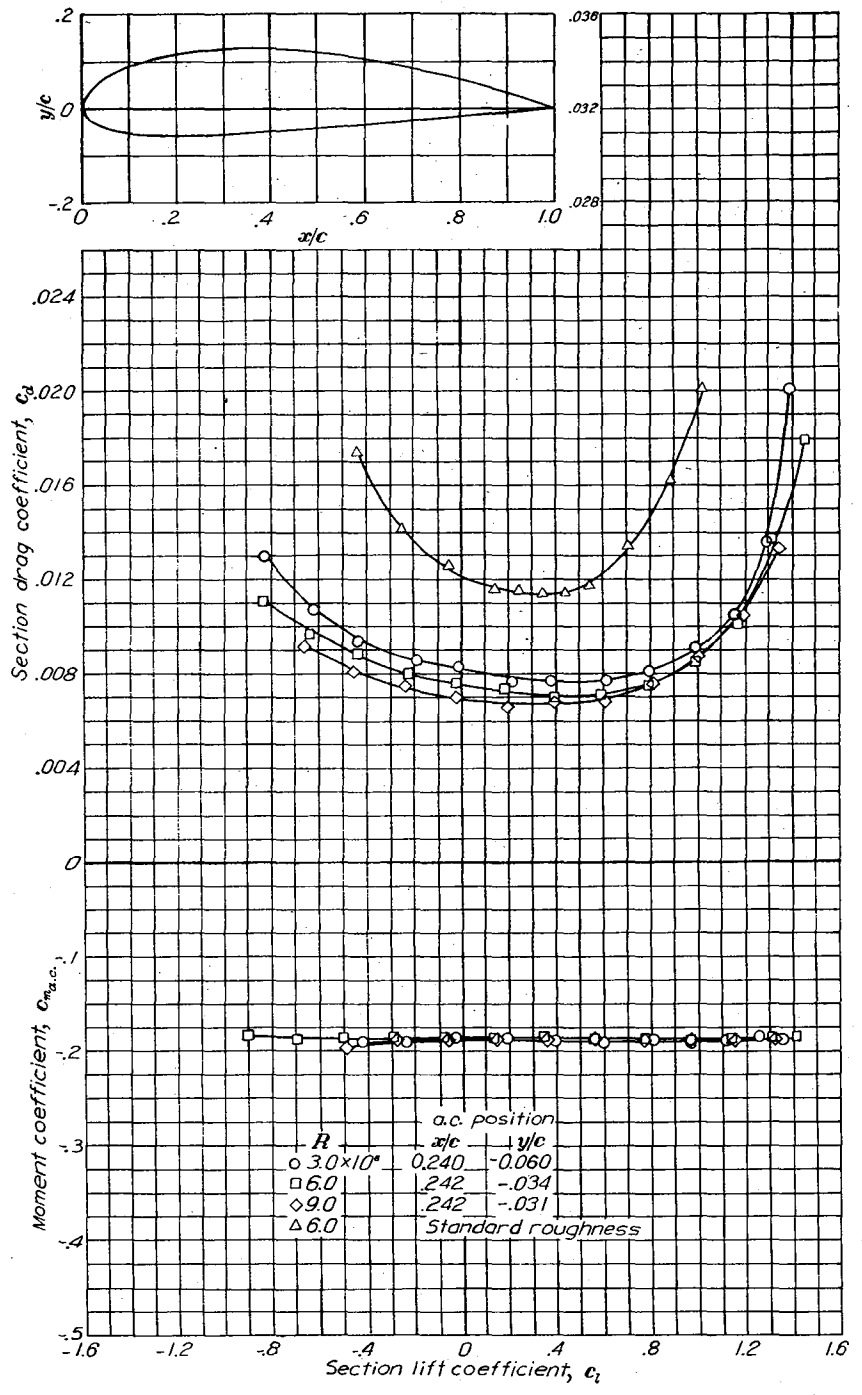
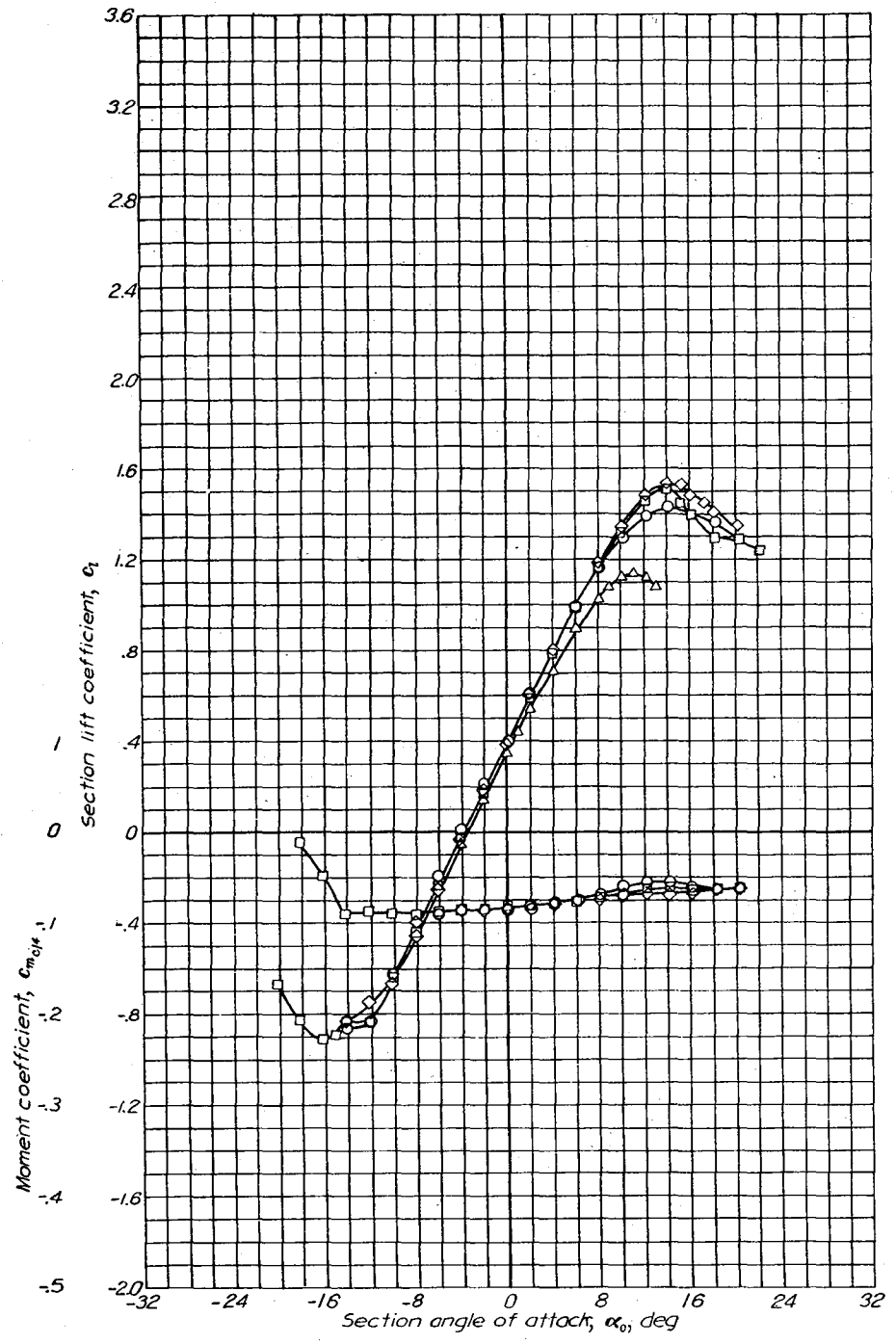
Aerodynamic characteristics of the NACA 4412 airfoil section, 24-inch chord.



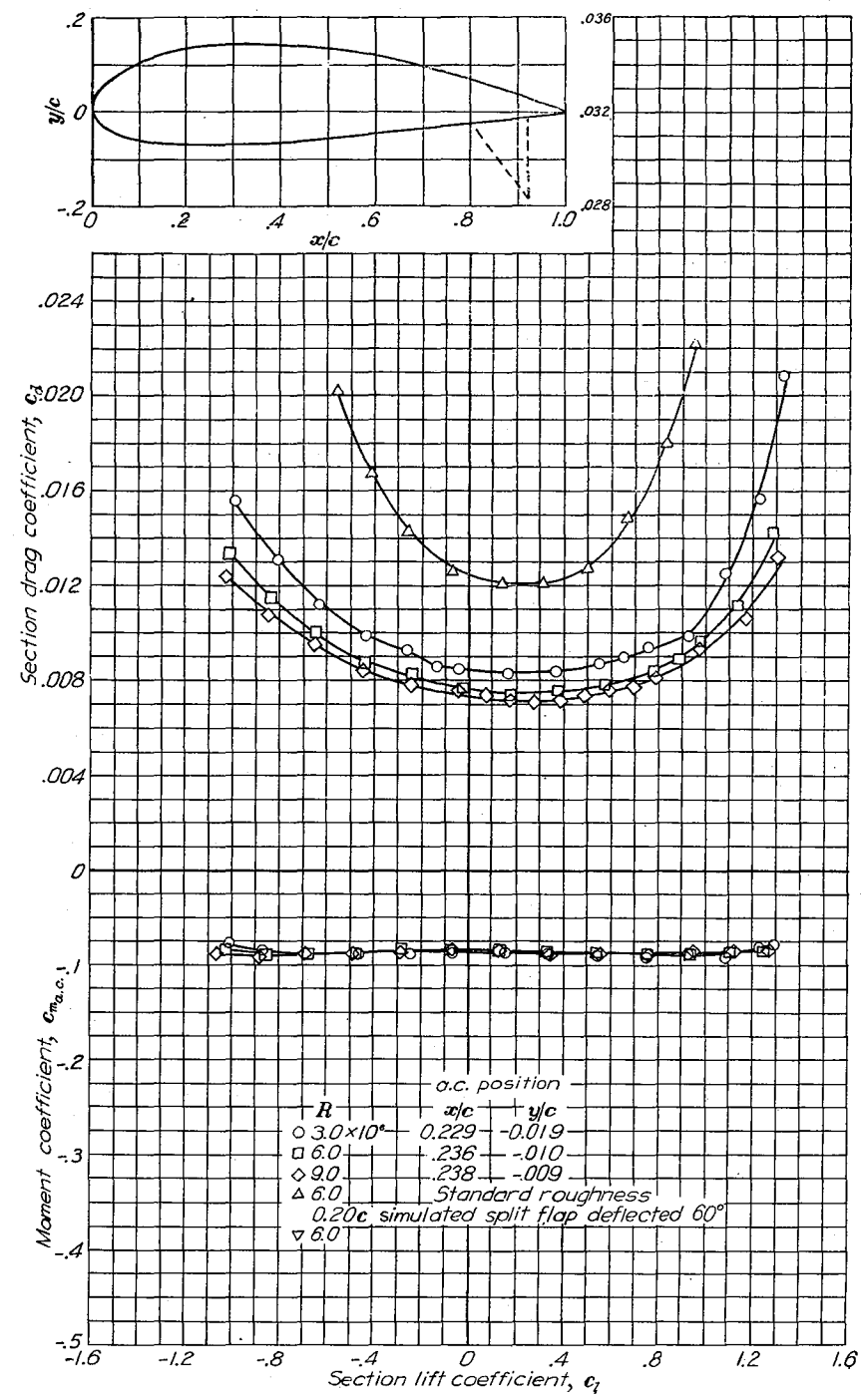
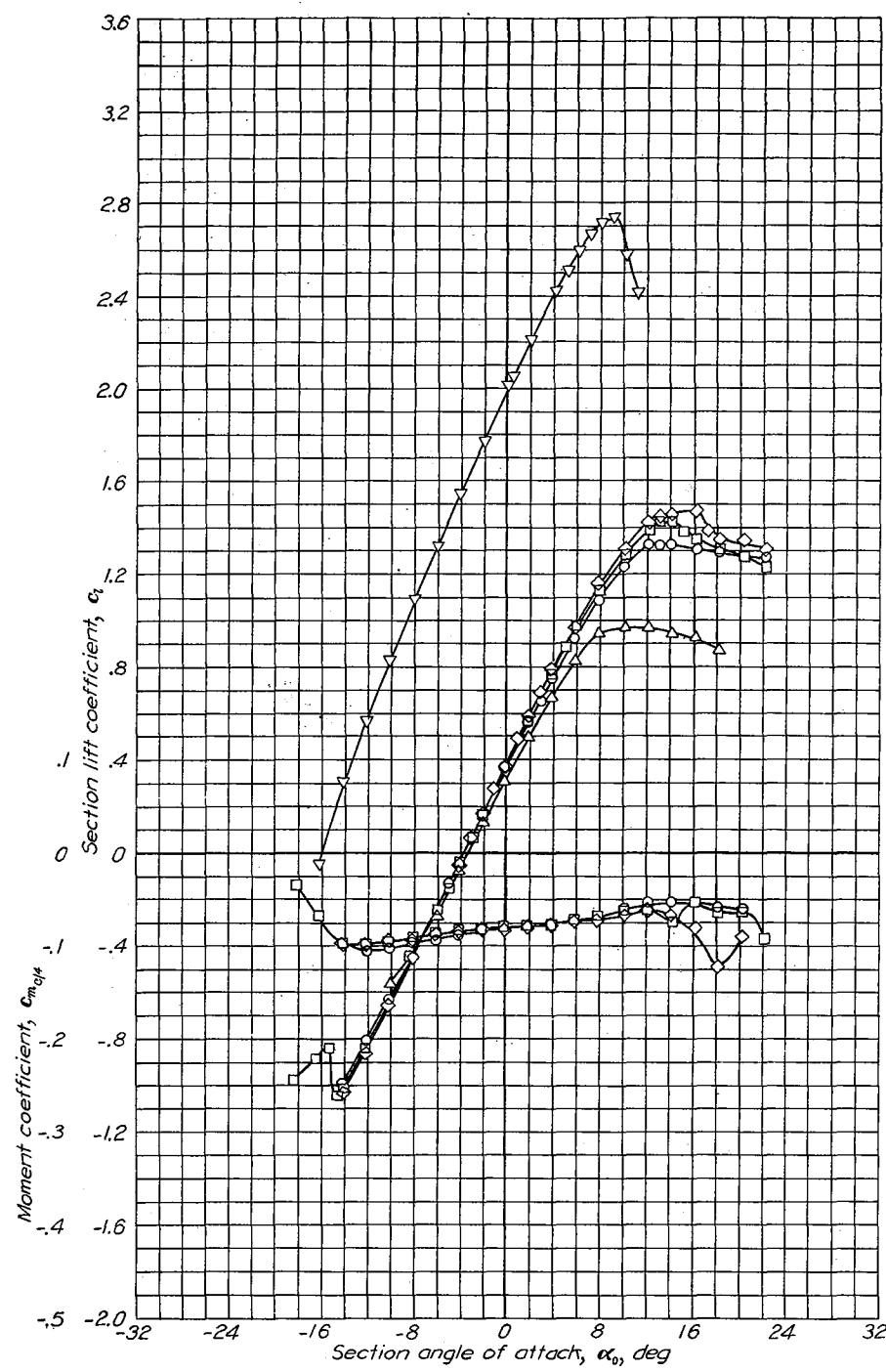
Aerodynamic characteristics of the NACA 4415 airfoil section, 24-inch chord.





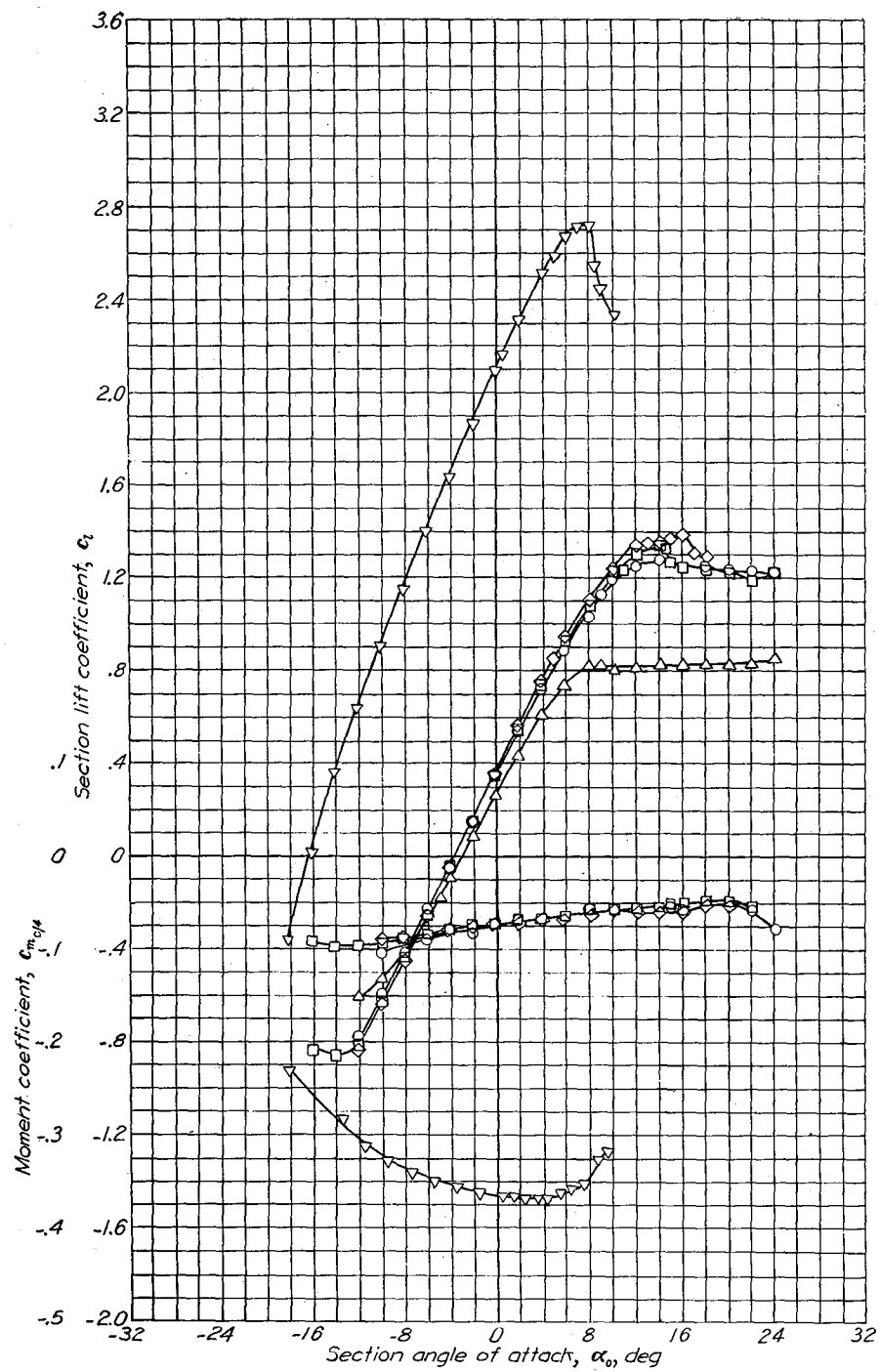


Aerodynamic characteristics of the NACA 4418 airfoil section, 24-inch chord.

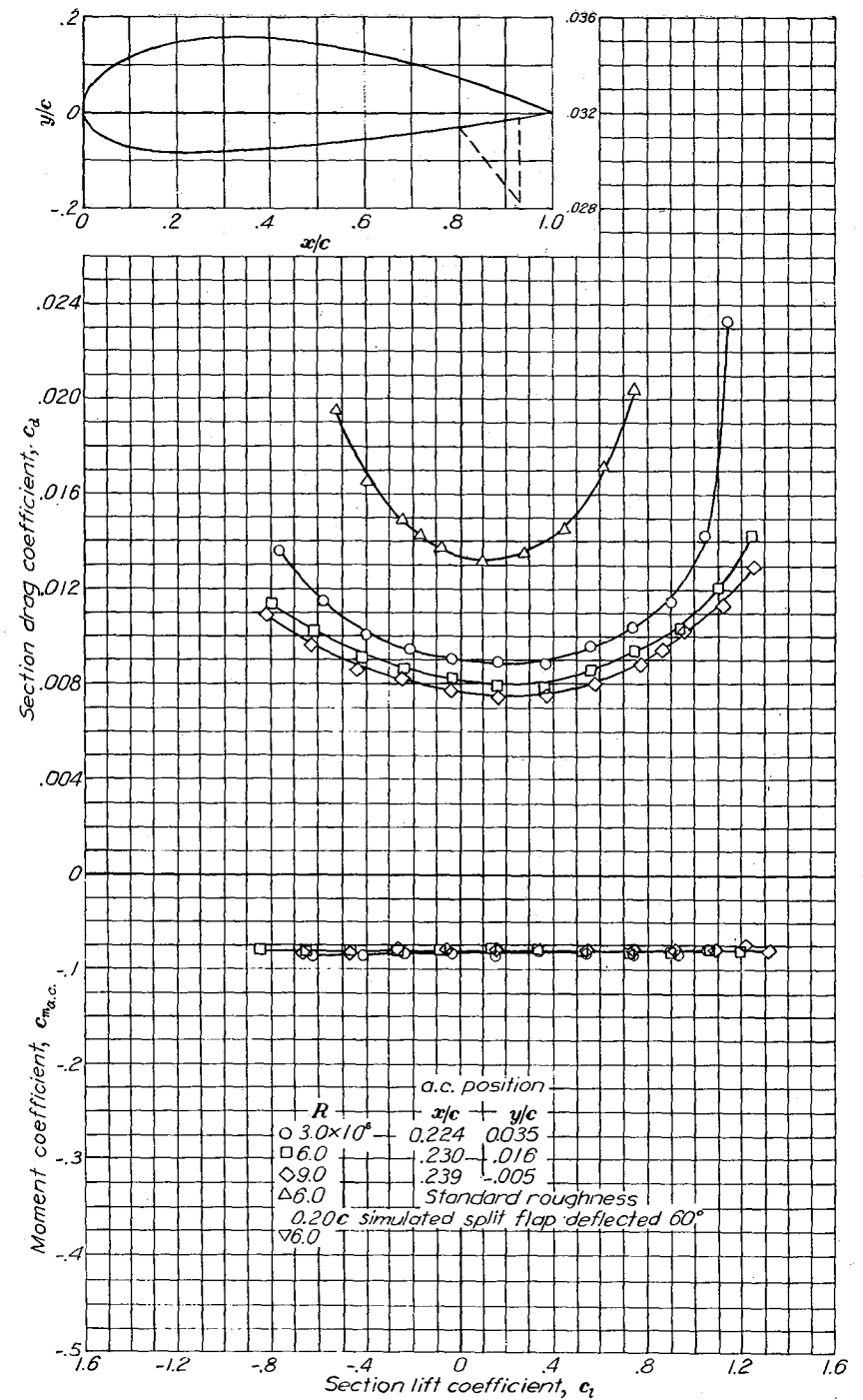


Aerodynamic characteristics of the NACA 4421 airfoil section, 24-inch chord.

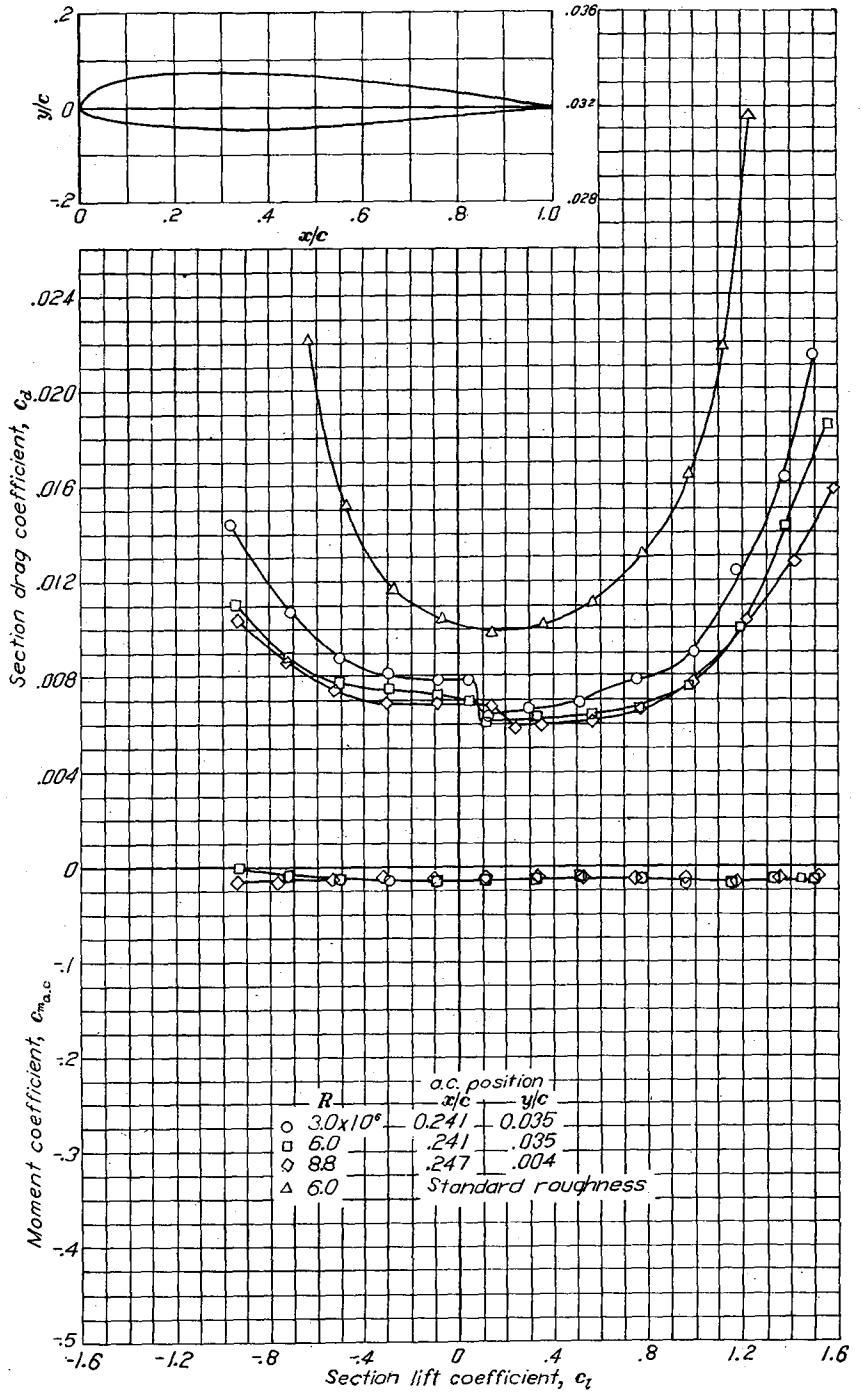
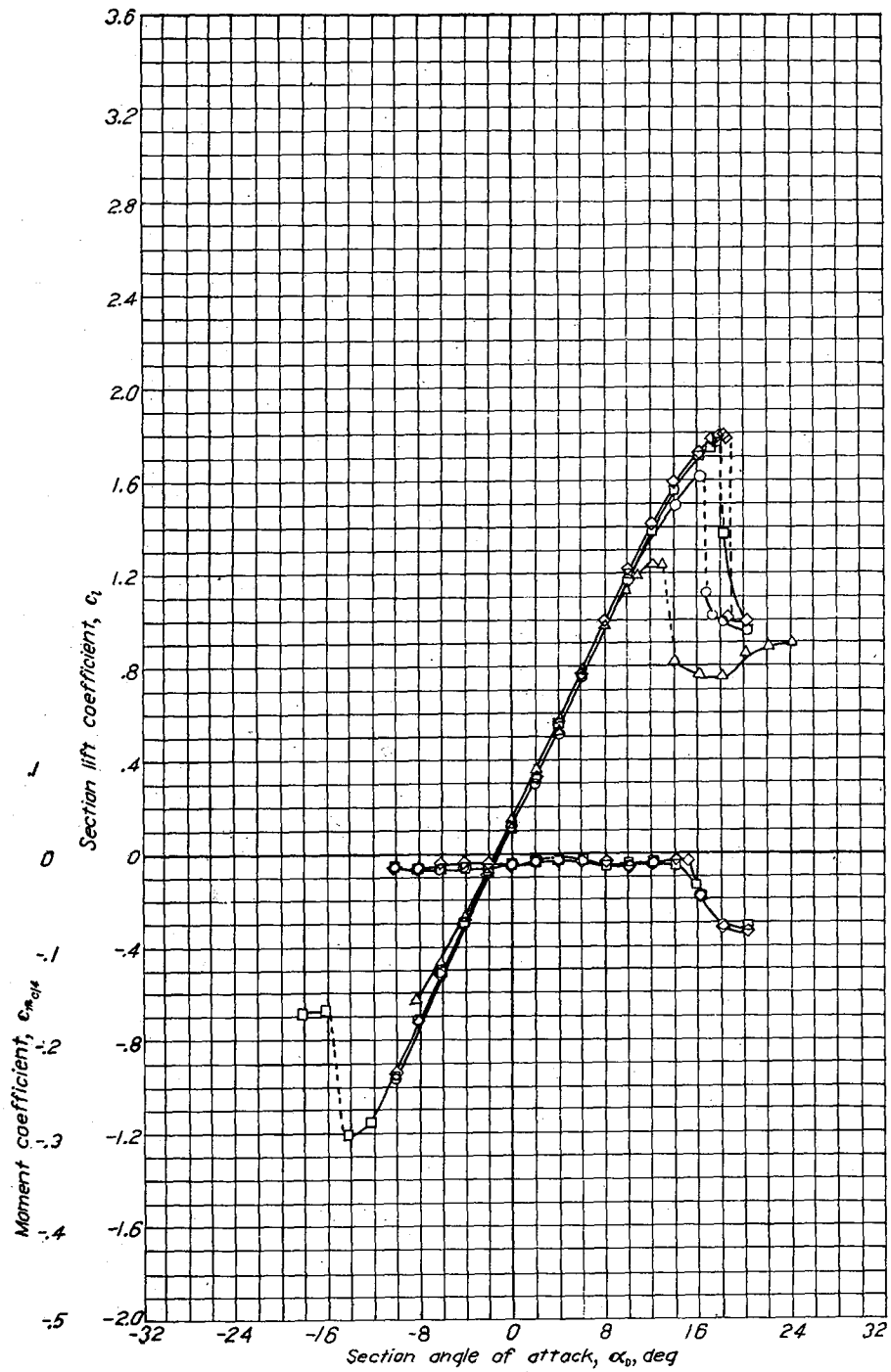
a.c. position		
R	x/c	y/c
○	3.0 × 10 <sup>-4</sup>	-0.229 - -0.019
□	6.0	.236 - -0.010
◇	9.0	.238 - -0.009
△	6.0	Standard roughness
▽	6.0	0.20c simulated split flap deflected 60°



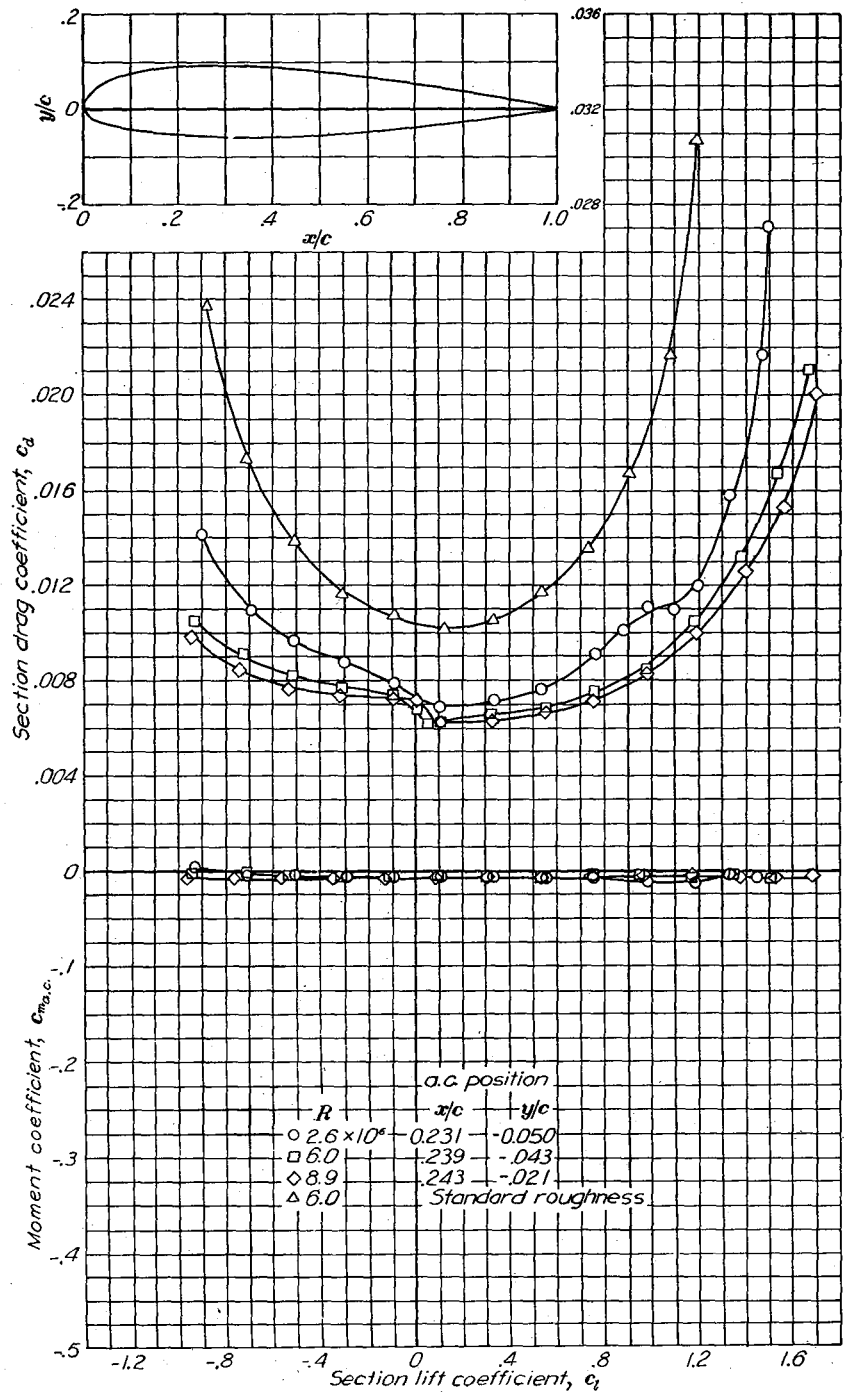
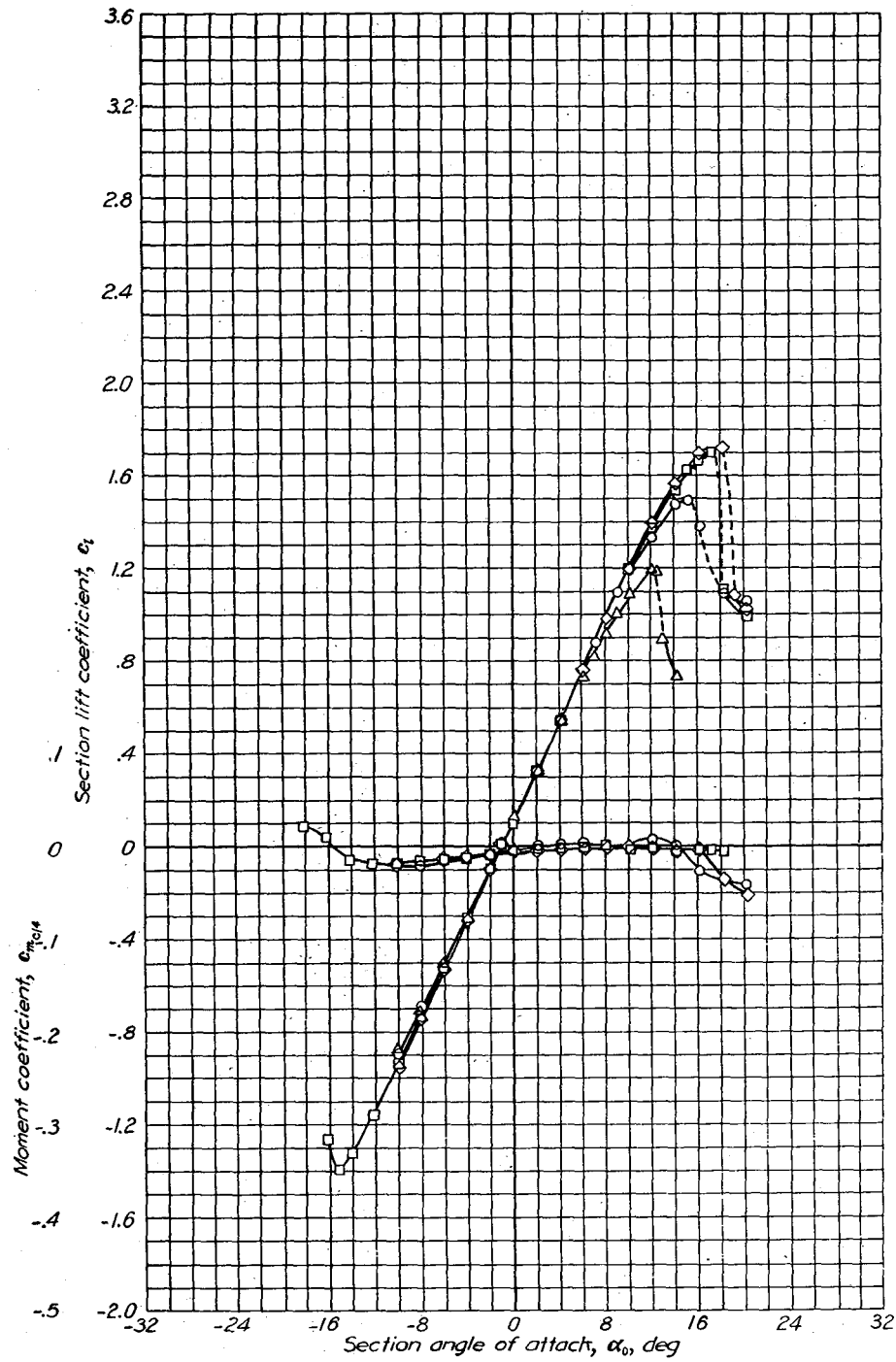
Aerodynamic characteristics of the NACA 4424 airfoil section, 24-inch chord.



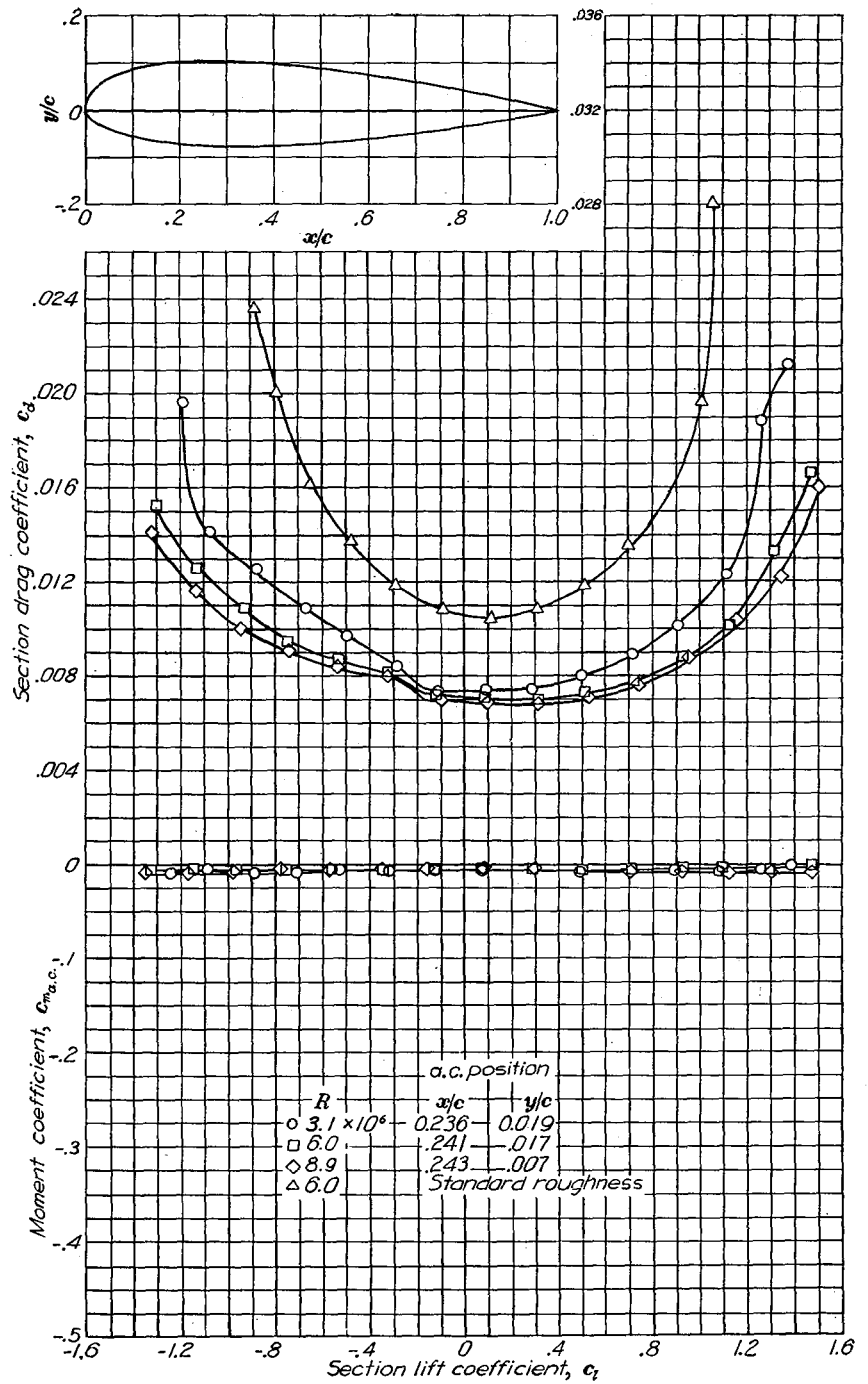
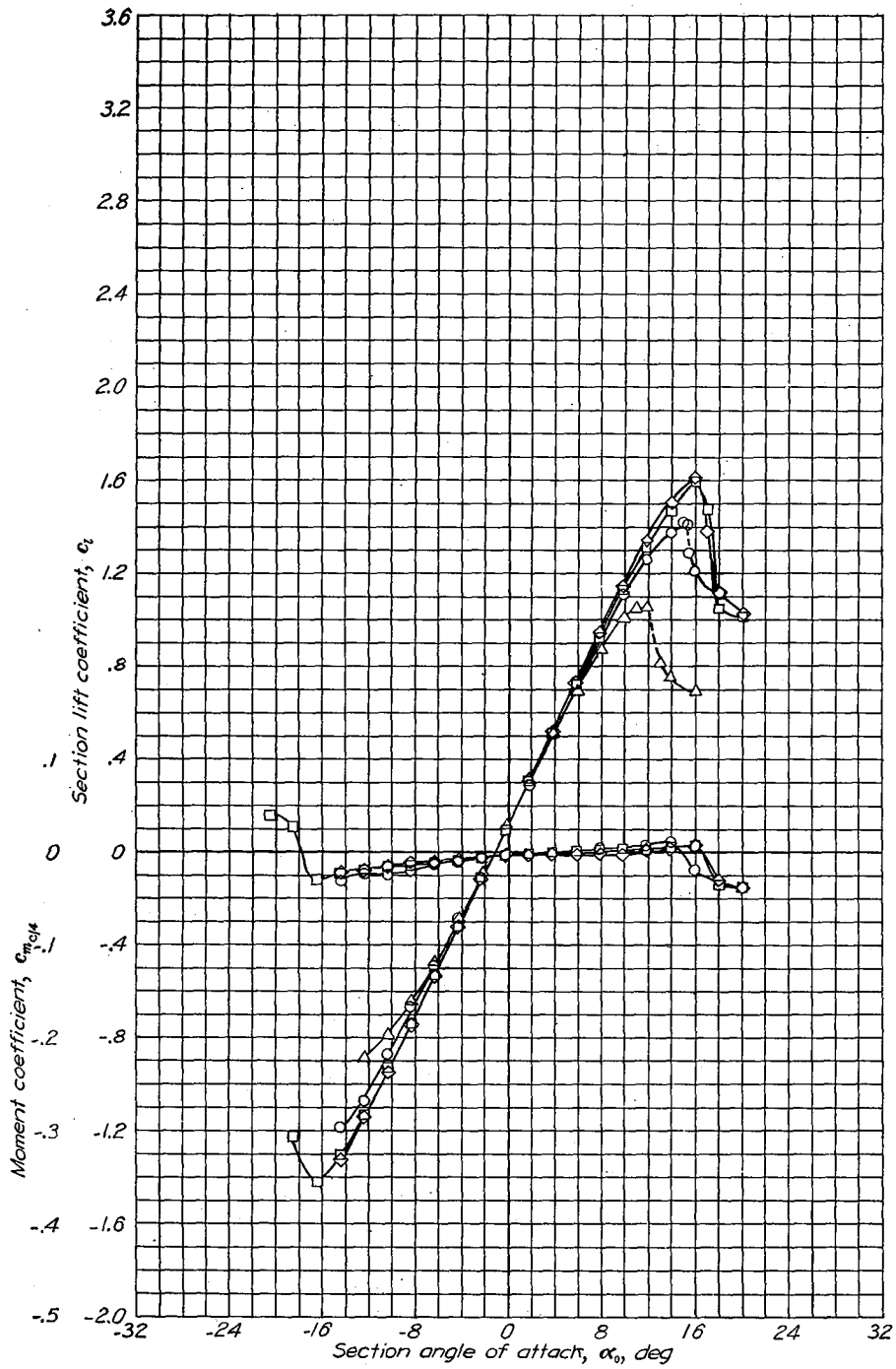
NACA 4424



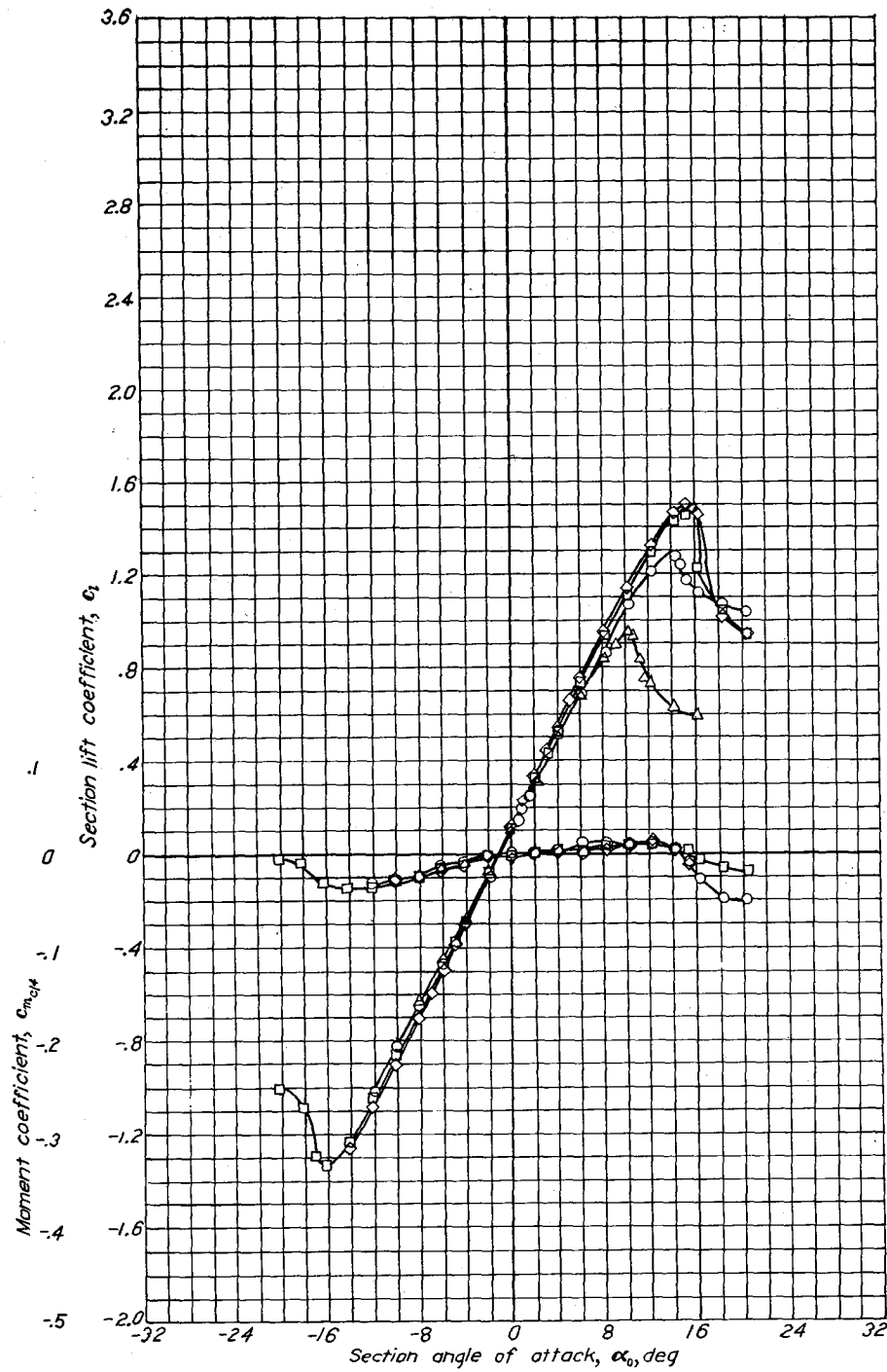
Aerodynamic characteristics of the NACA 23012 airfoil section, 24-inch chord.



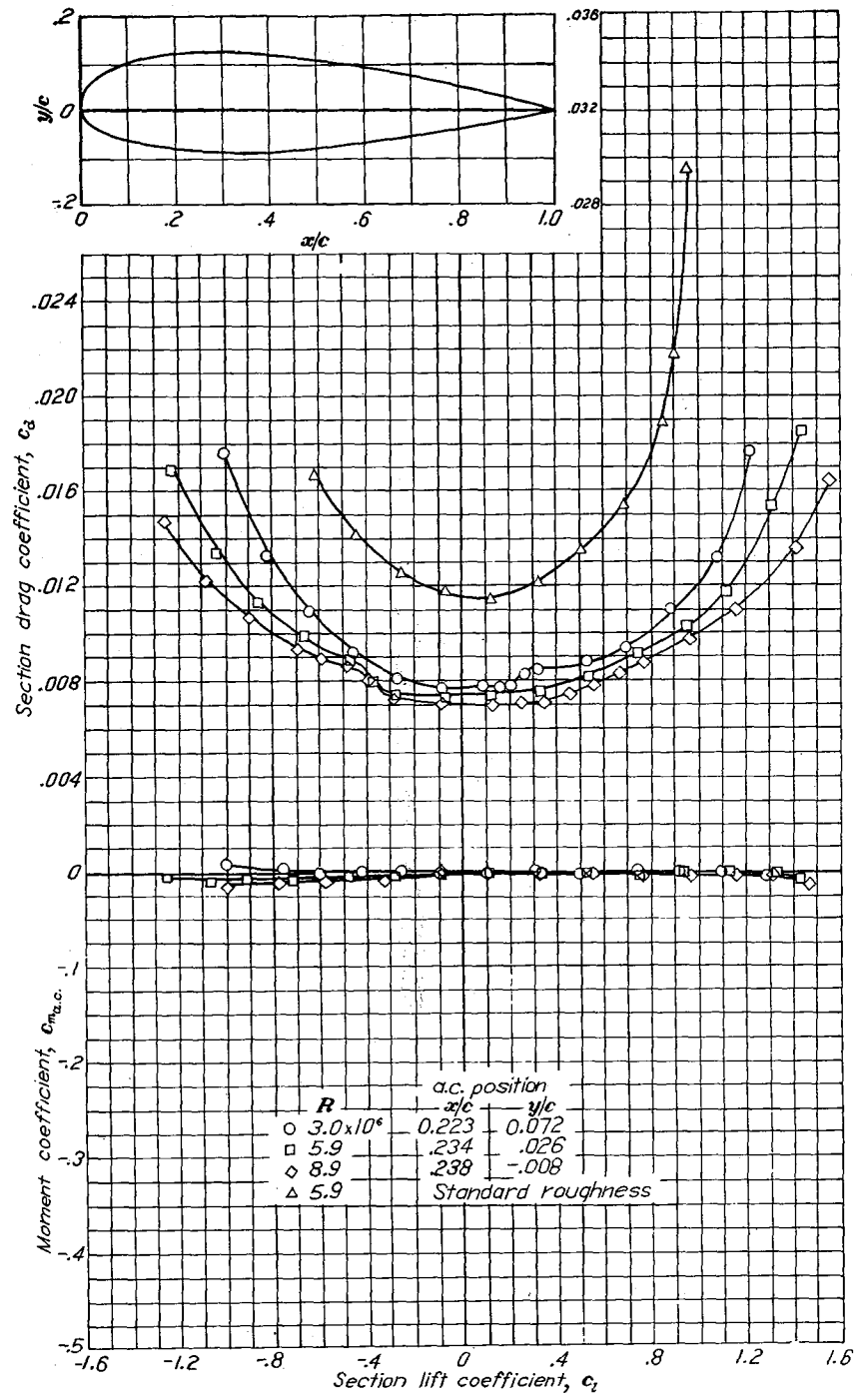
Aerodynamic characteristics of the NACA 23015 airfoil section, 24-inch chord.

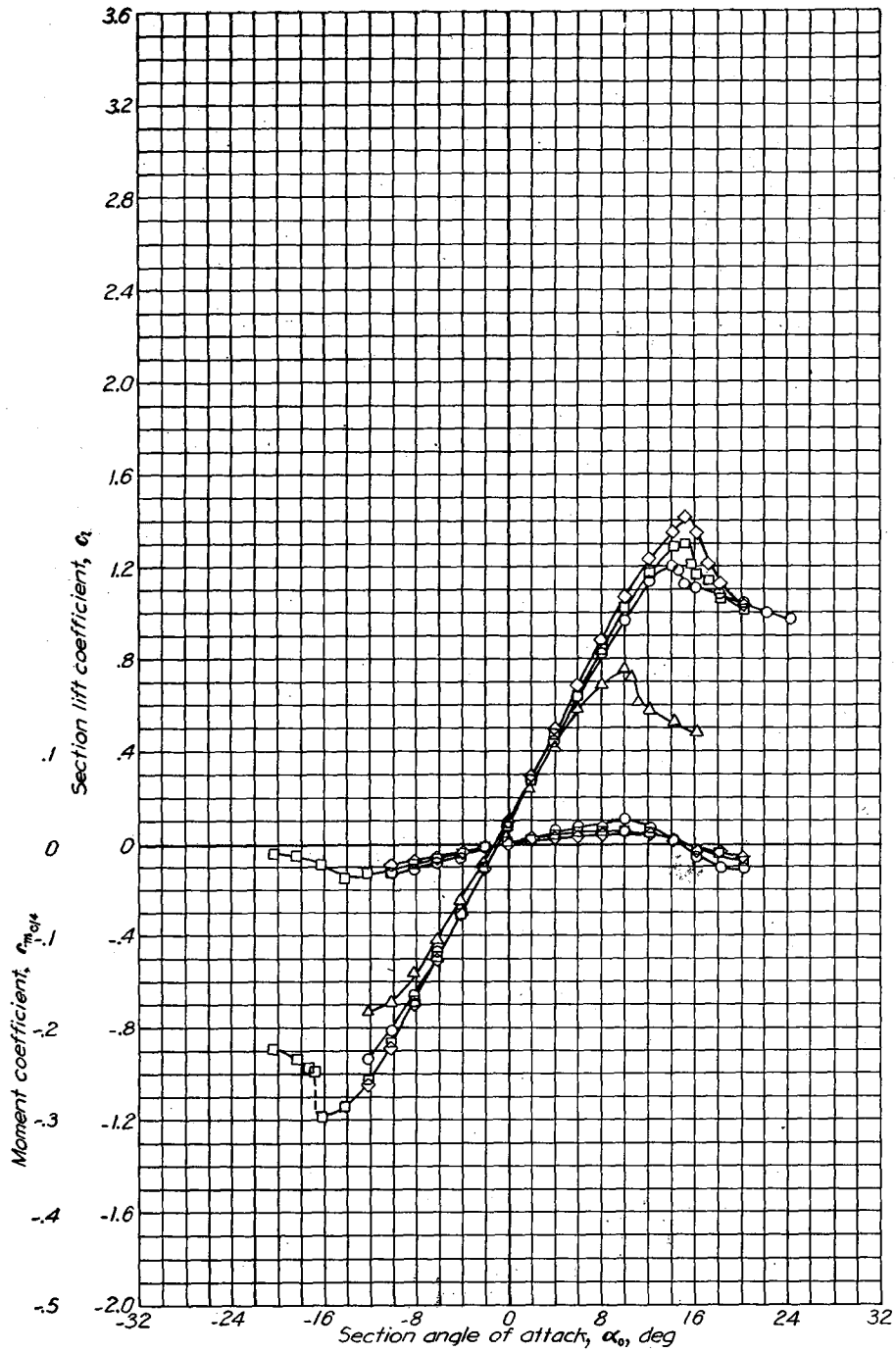


Aerodynamic characteristics of the NACA 23018 airfoil section, 24-inch chord.

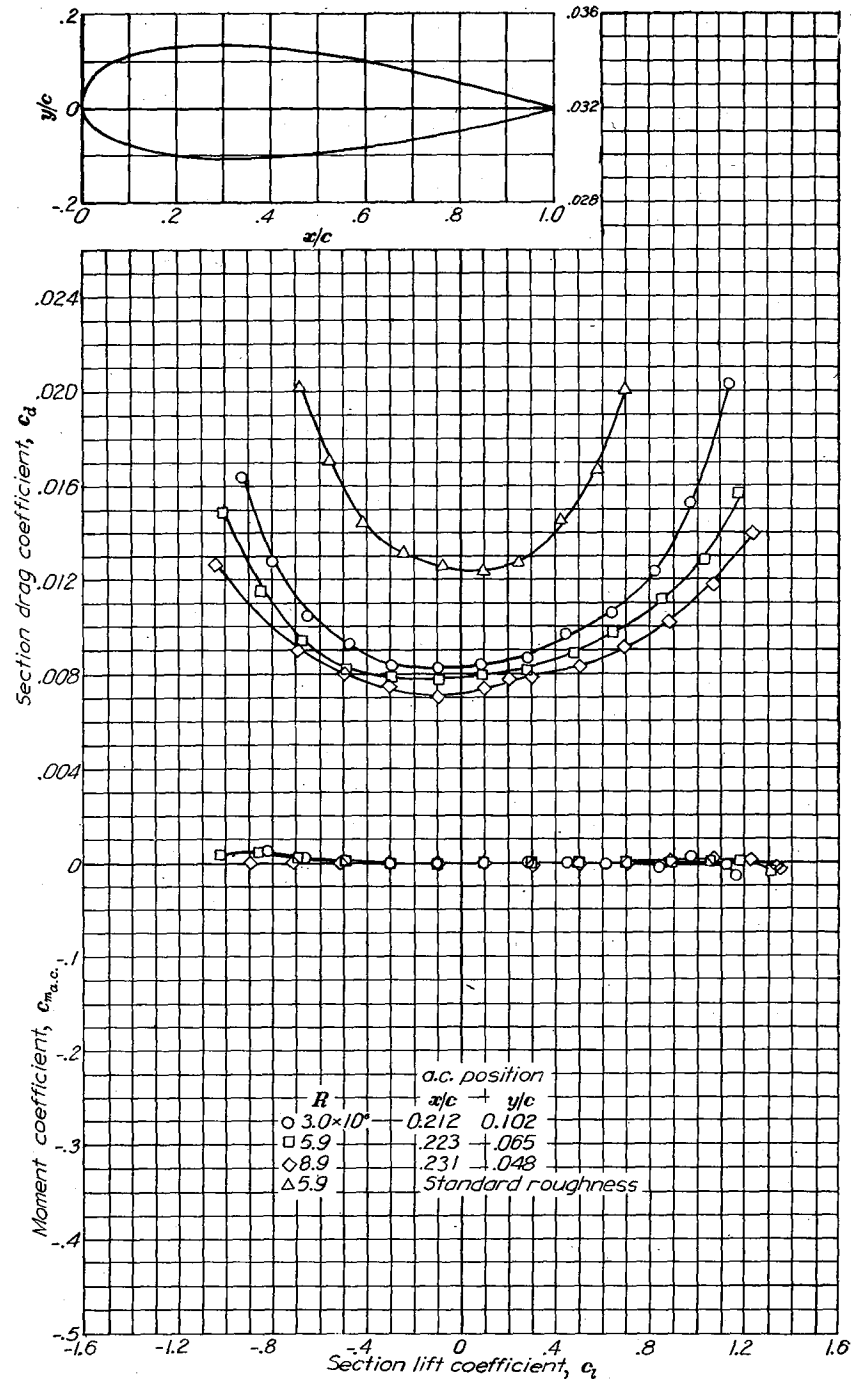


Aerodynamic characteristics of the NACA 23021 airfoil section, 24-inch chord.

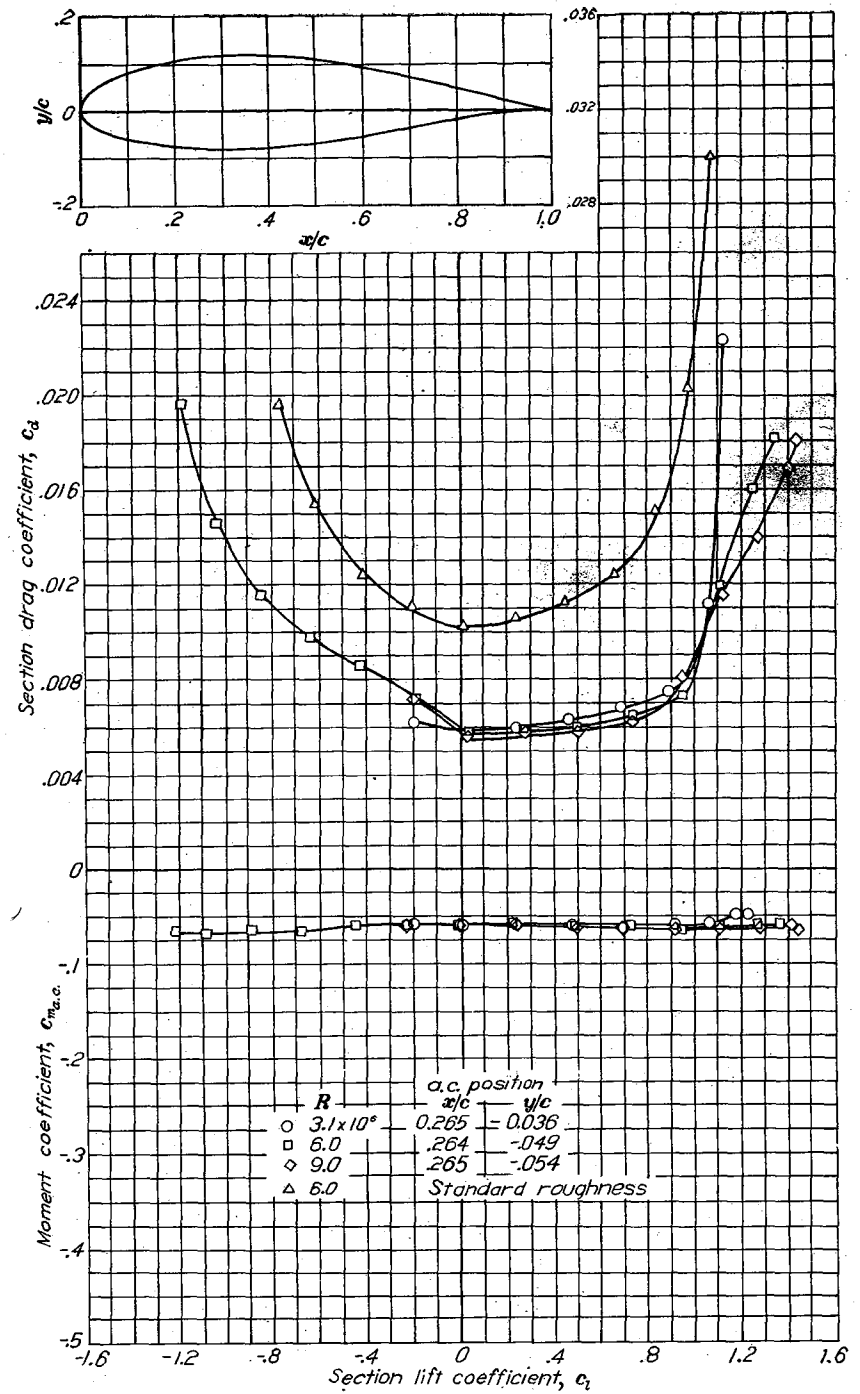
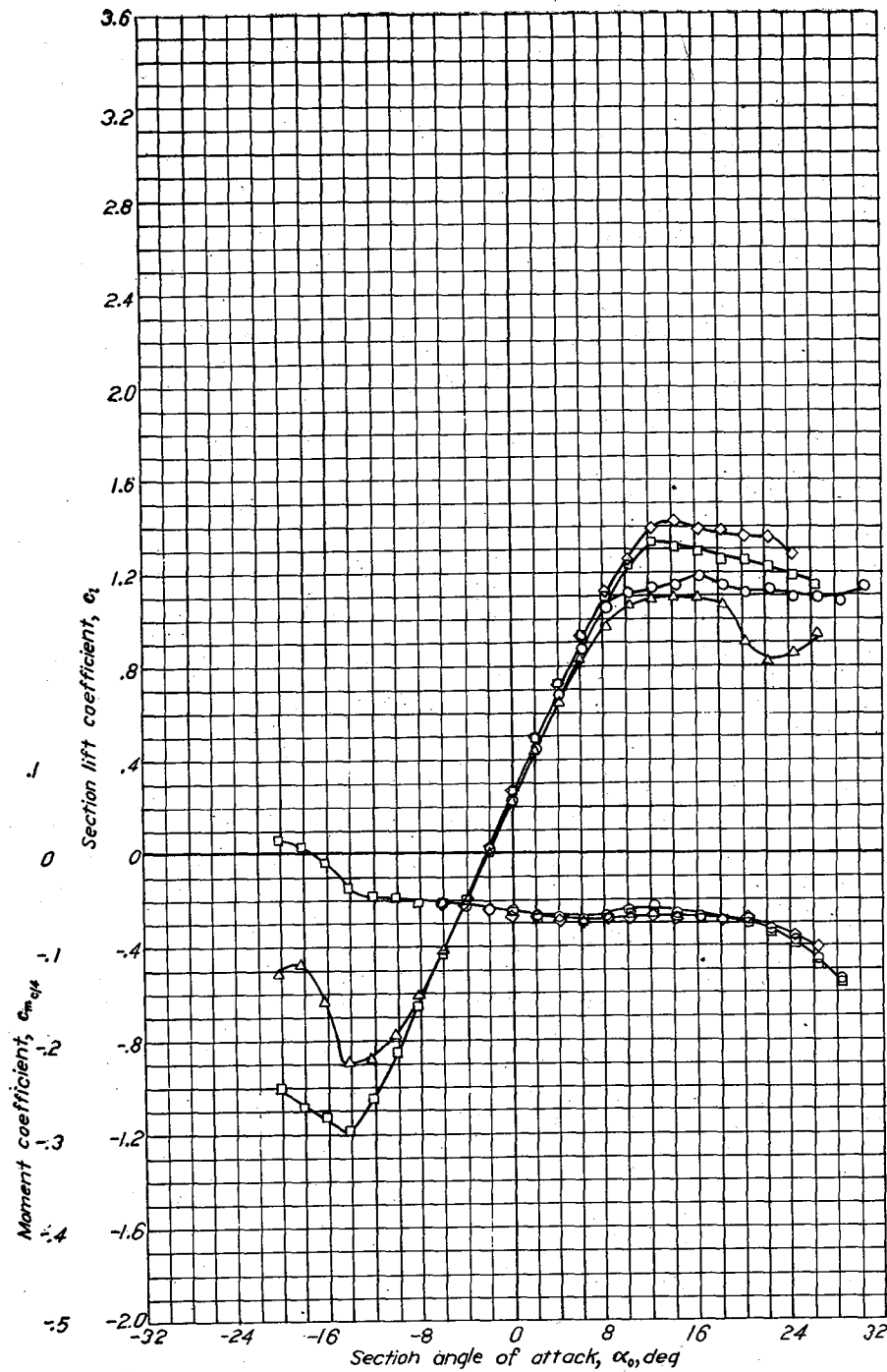




Aerodynamic characteristics of the NACA 23024 airfoil section, 24-inch chord.

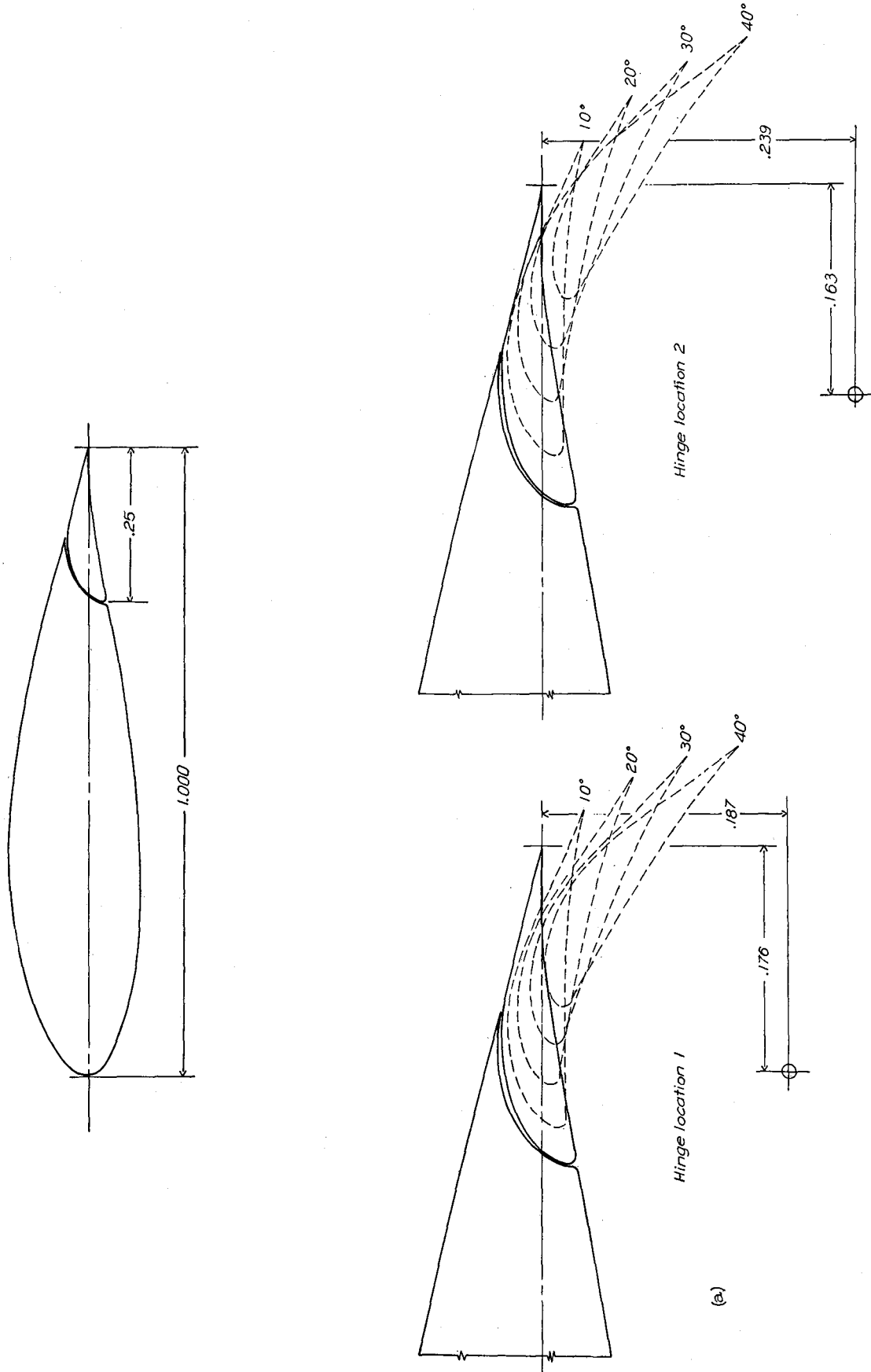




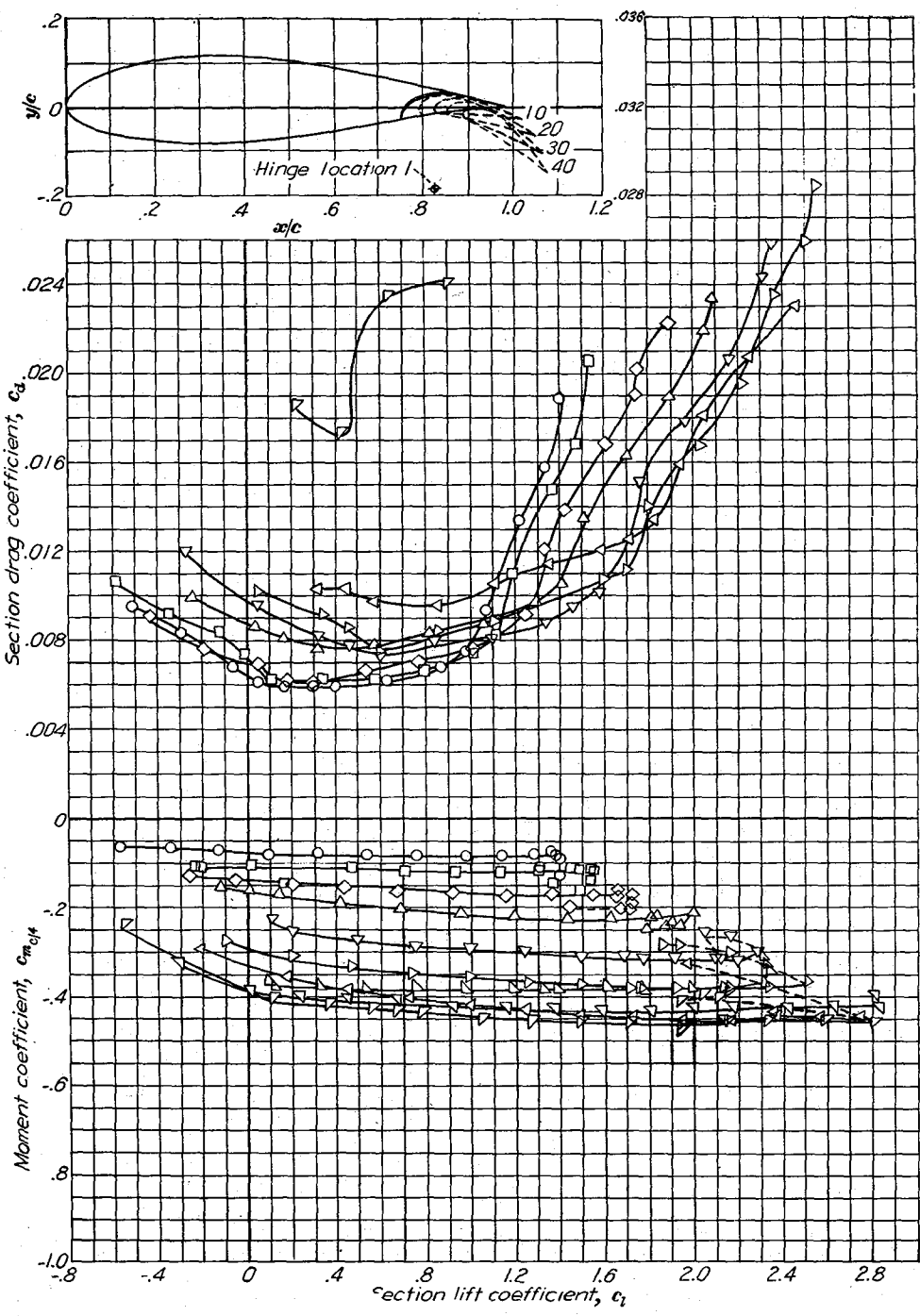
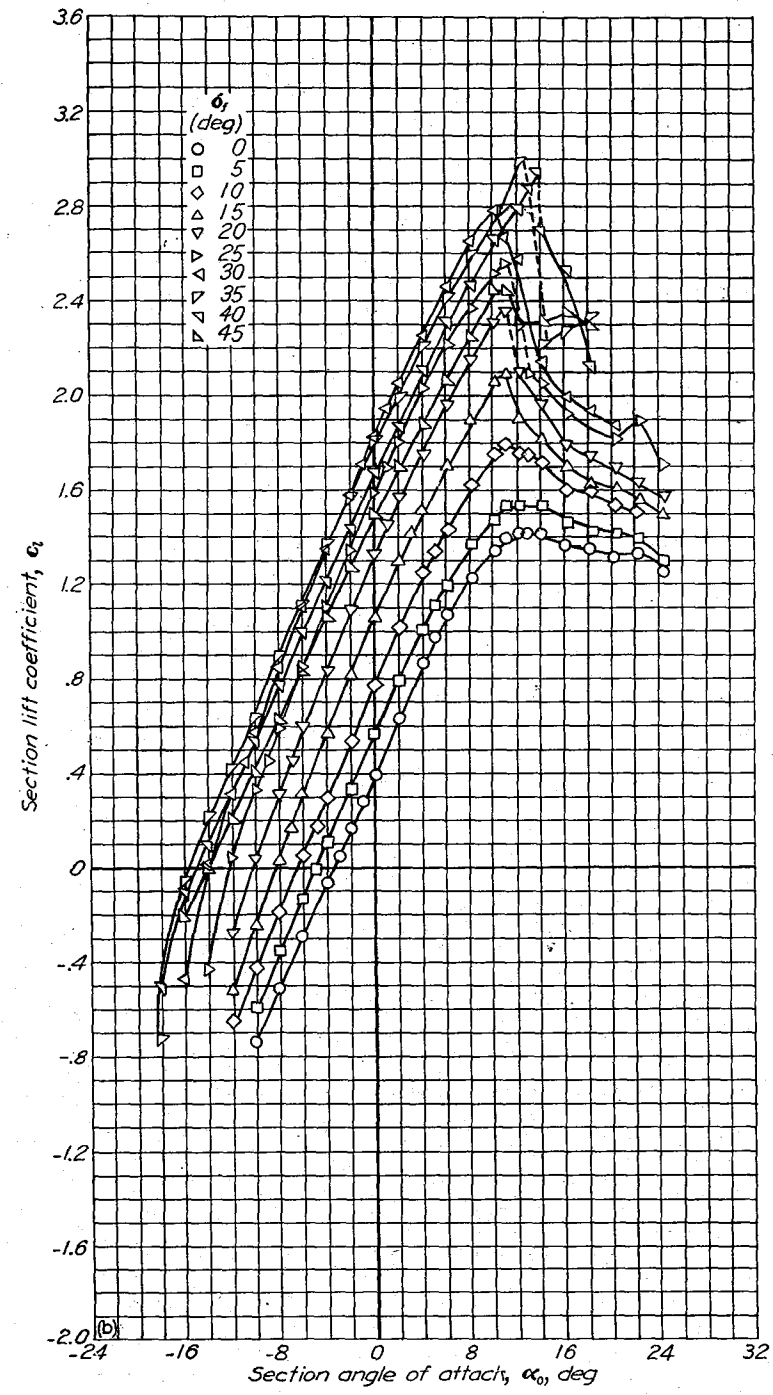


Aerodynamic characteristics of the NACA 63,4-420 airfoil section, 24-inch chord.

NACA 63,4-420 with flap

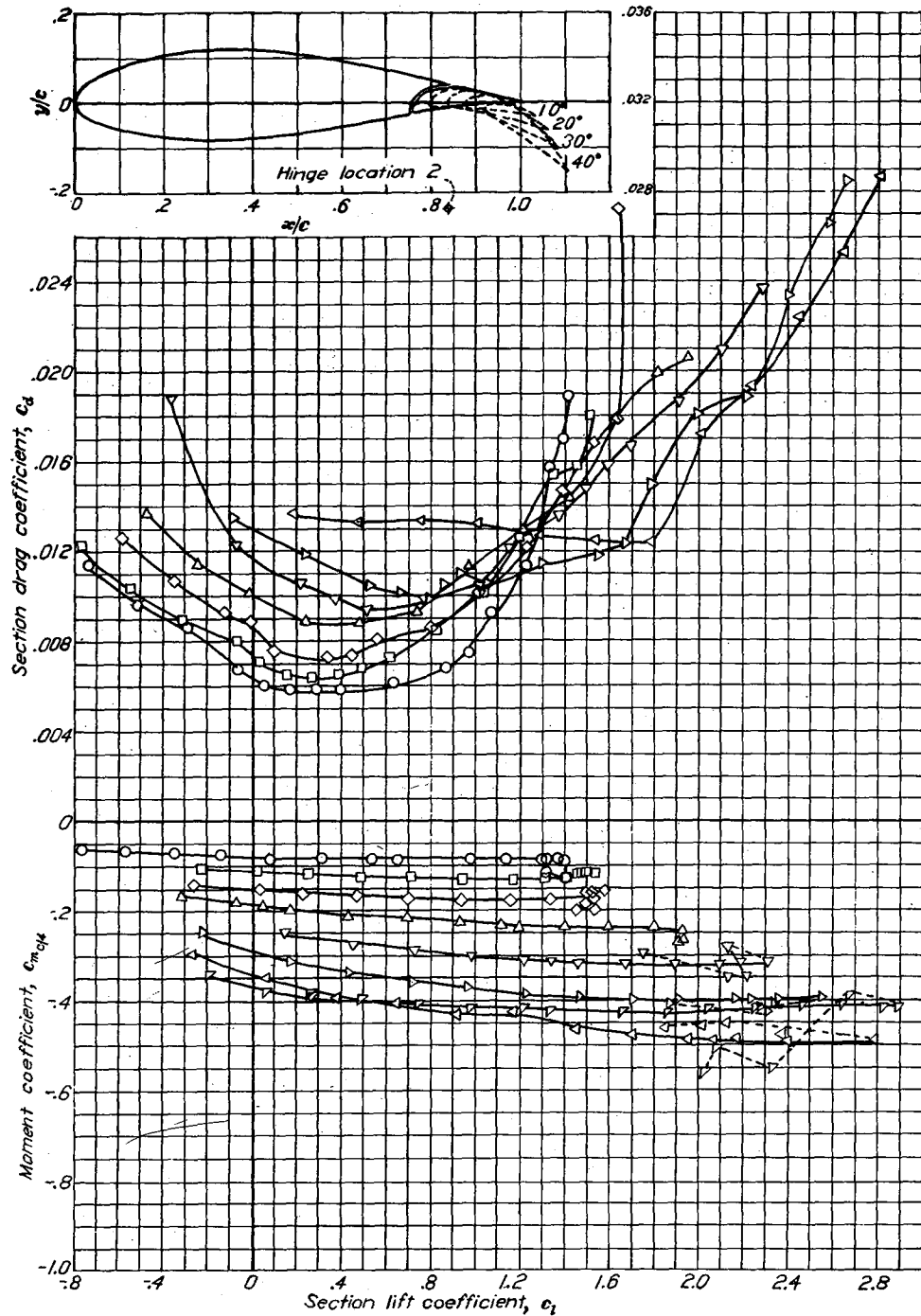
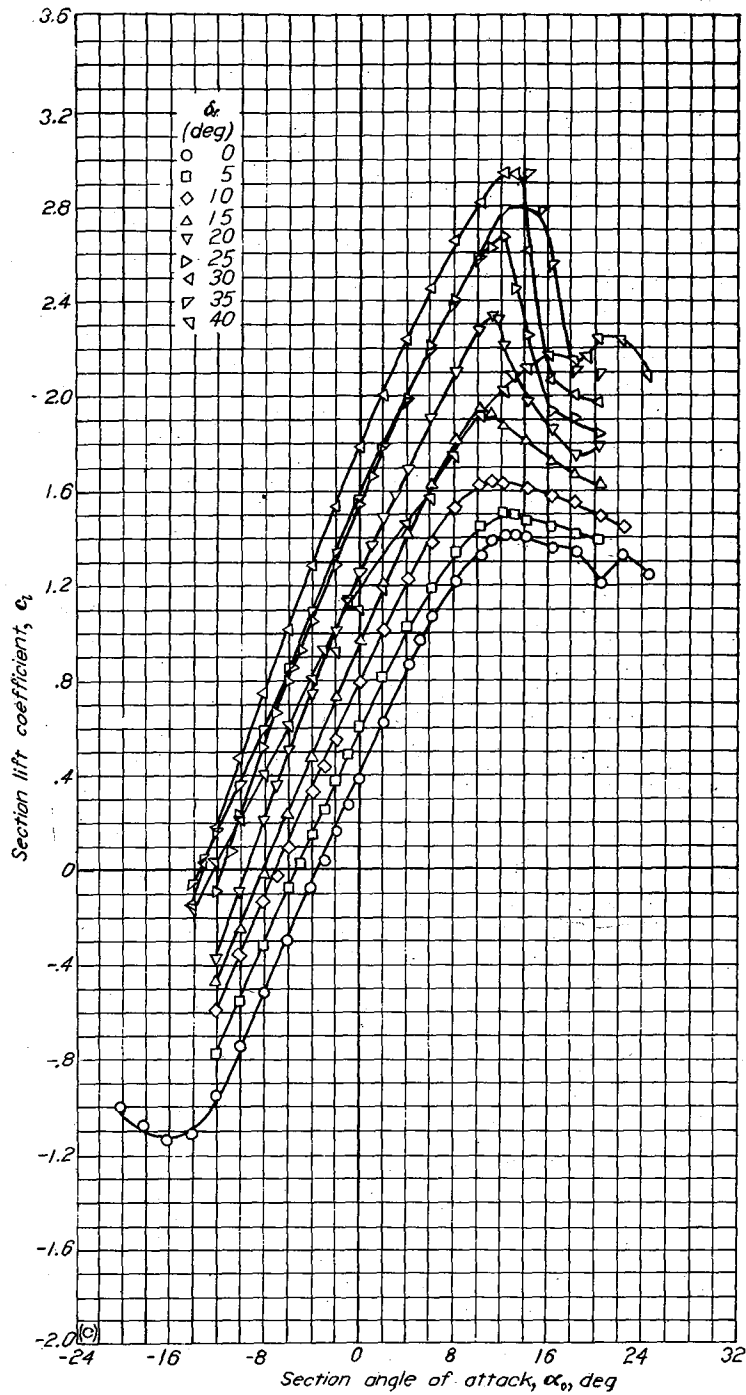


(a) Configuration.  
NACA 63,4-420 airfoil section with 0.25c slotted flap.

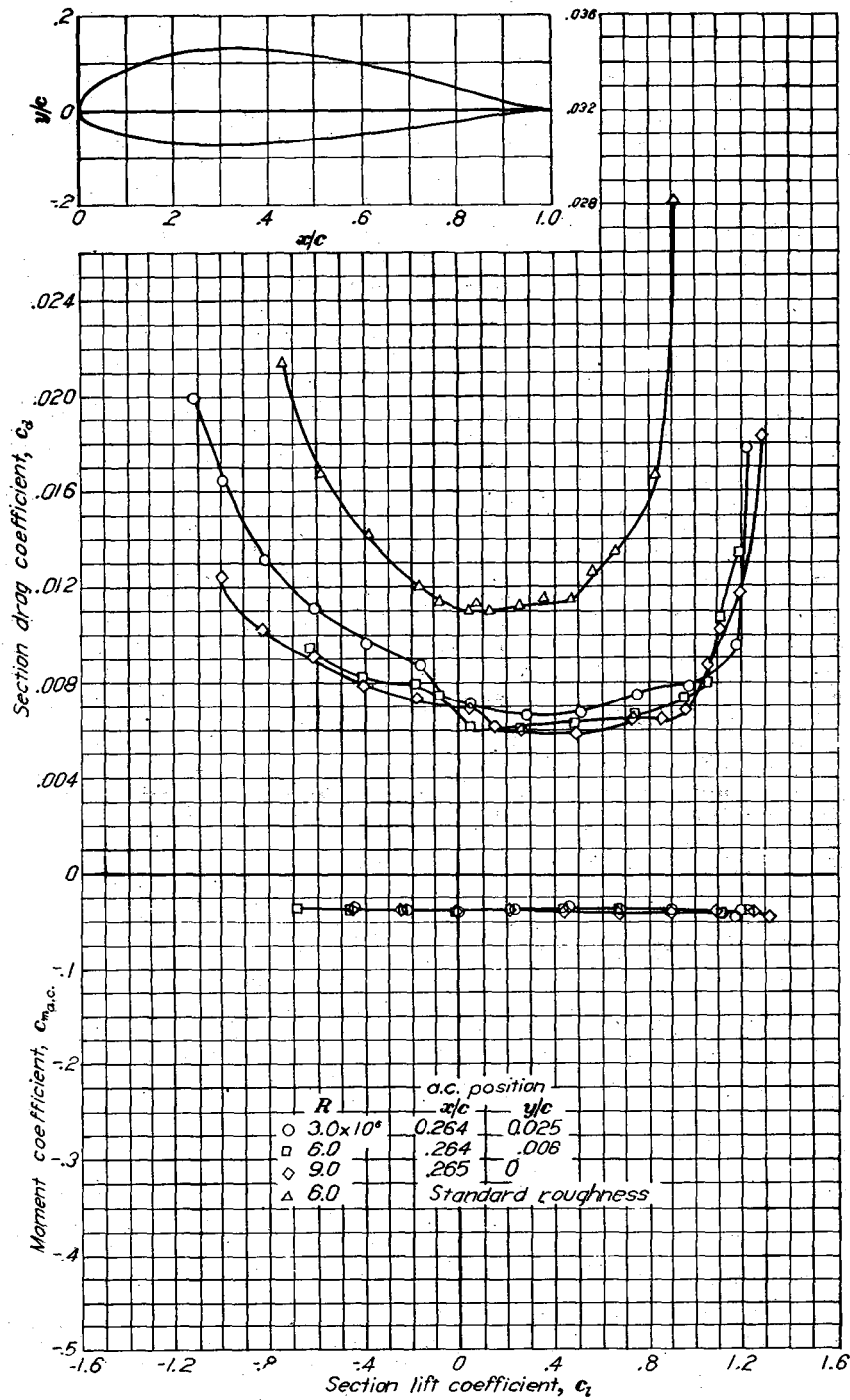
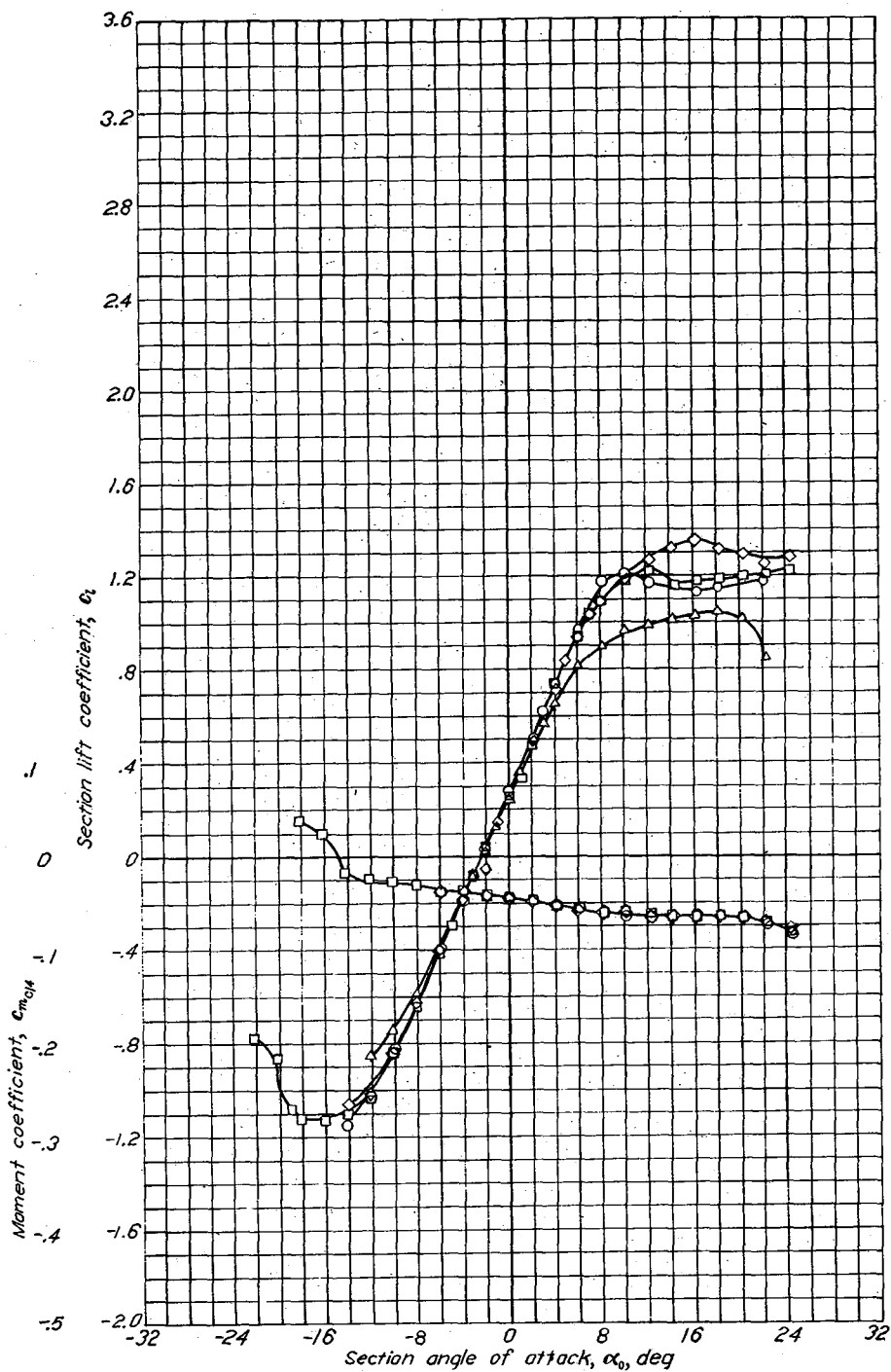


(b) Aerodynamic characteristics with hinge location 1.  $R = 6 \times 10^6$ .  
 NACA 63,4-420 airfoil section with 0.25c slotted flap.

NACA 63,4-420 with flap

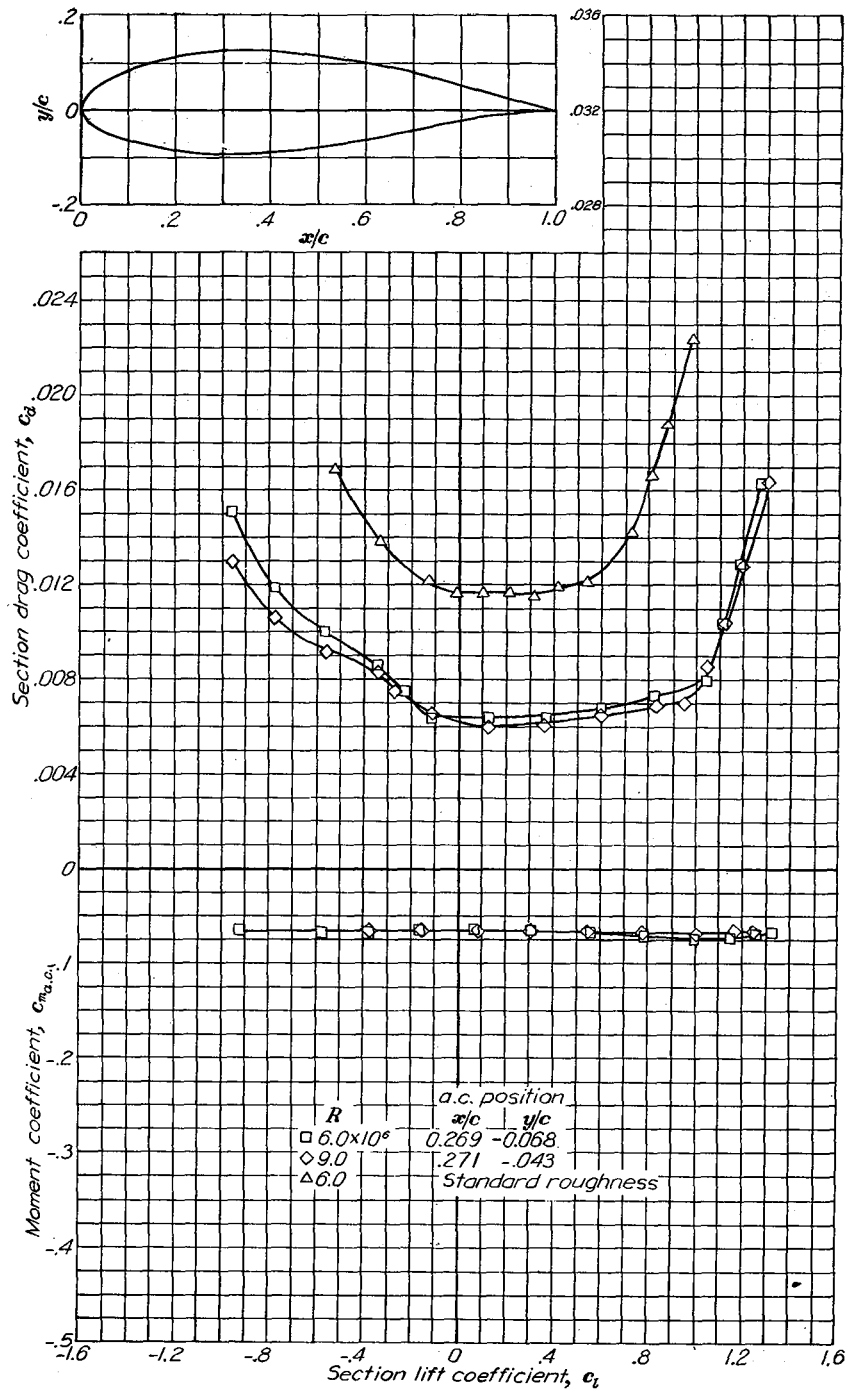
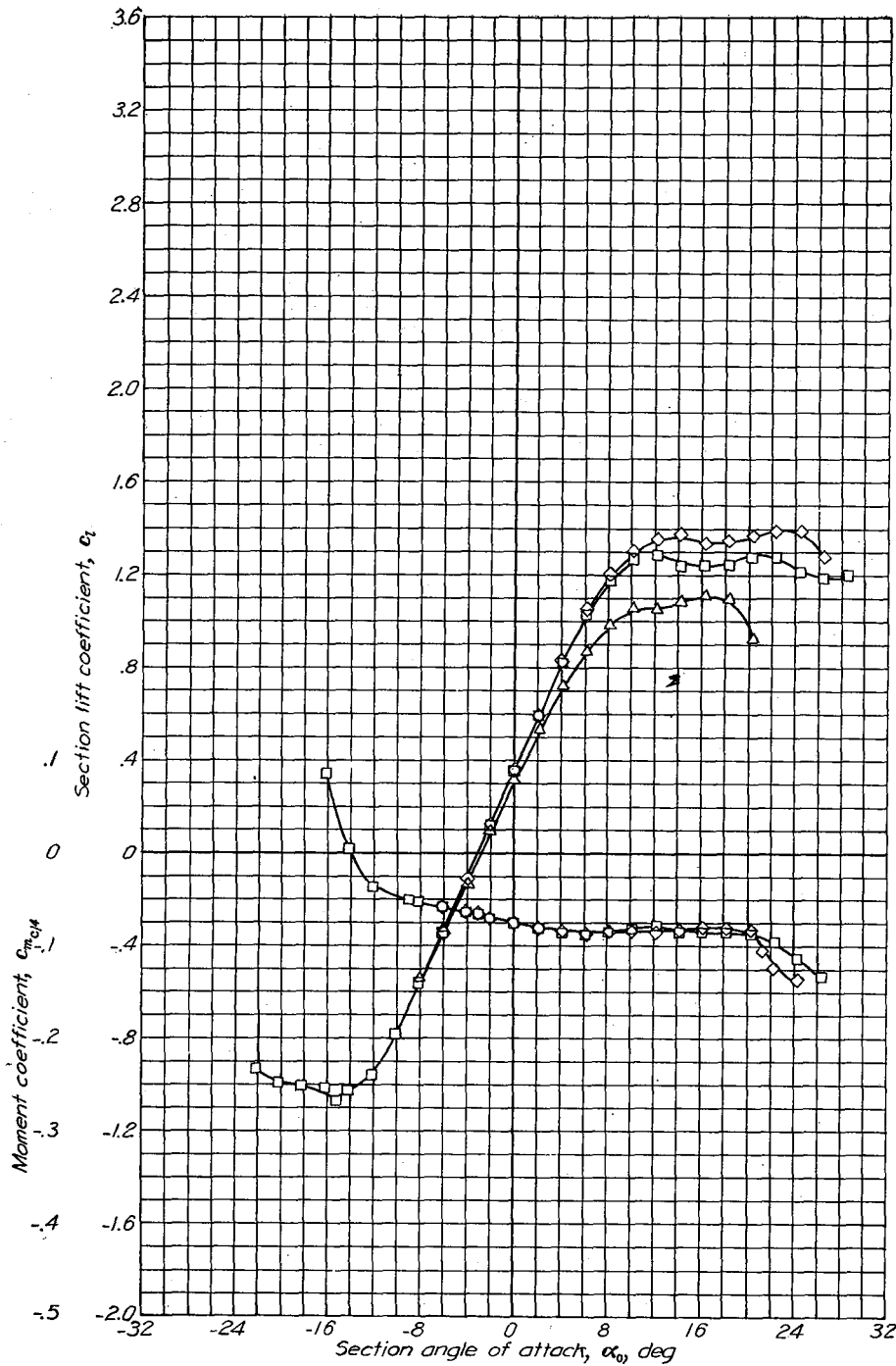


(c) Aerodynamic characteristics with hinge location 2.  $R = 6 \times 10^6$ .  
NACA 63,4-420 airfoil section with 0.25c slotted flap.

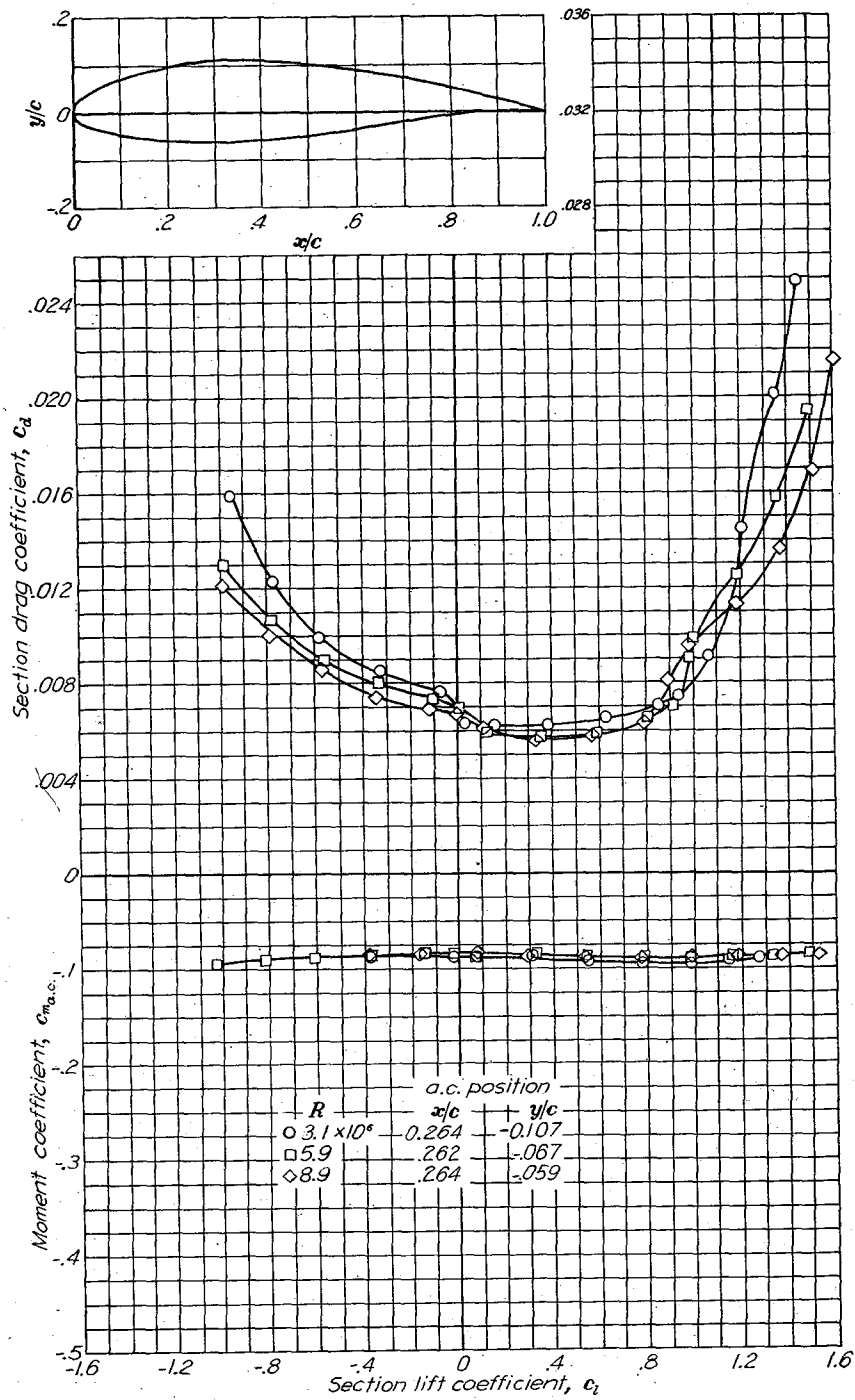
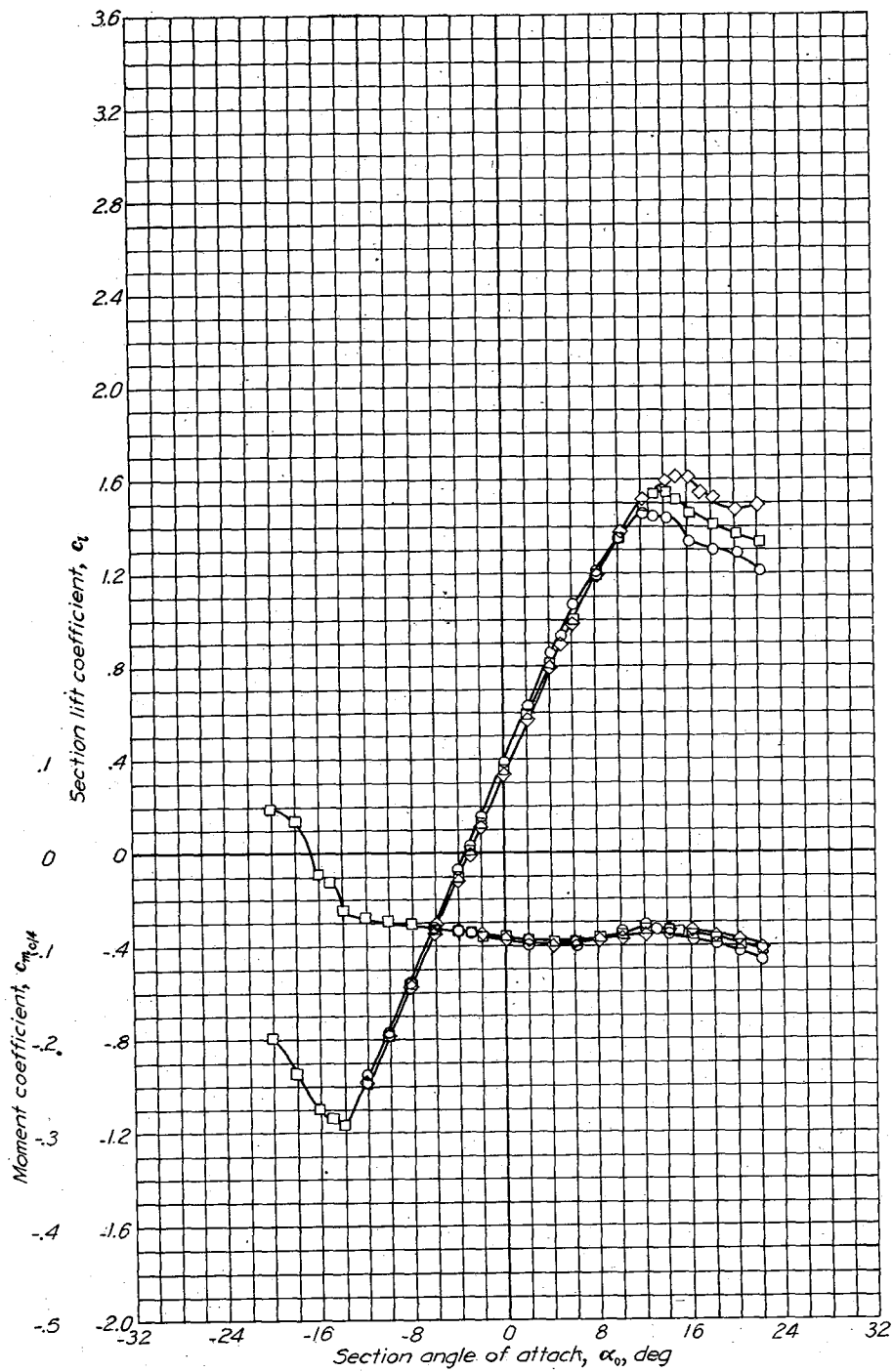


Aerodynamic characteristics of the NACA 63,4-420,  $\alpha = 0.3$  airfoil section, 24-inch chord.

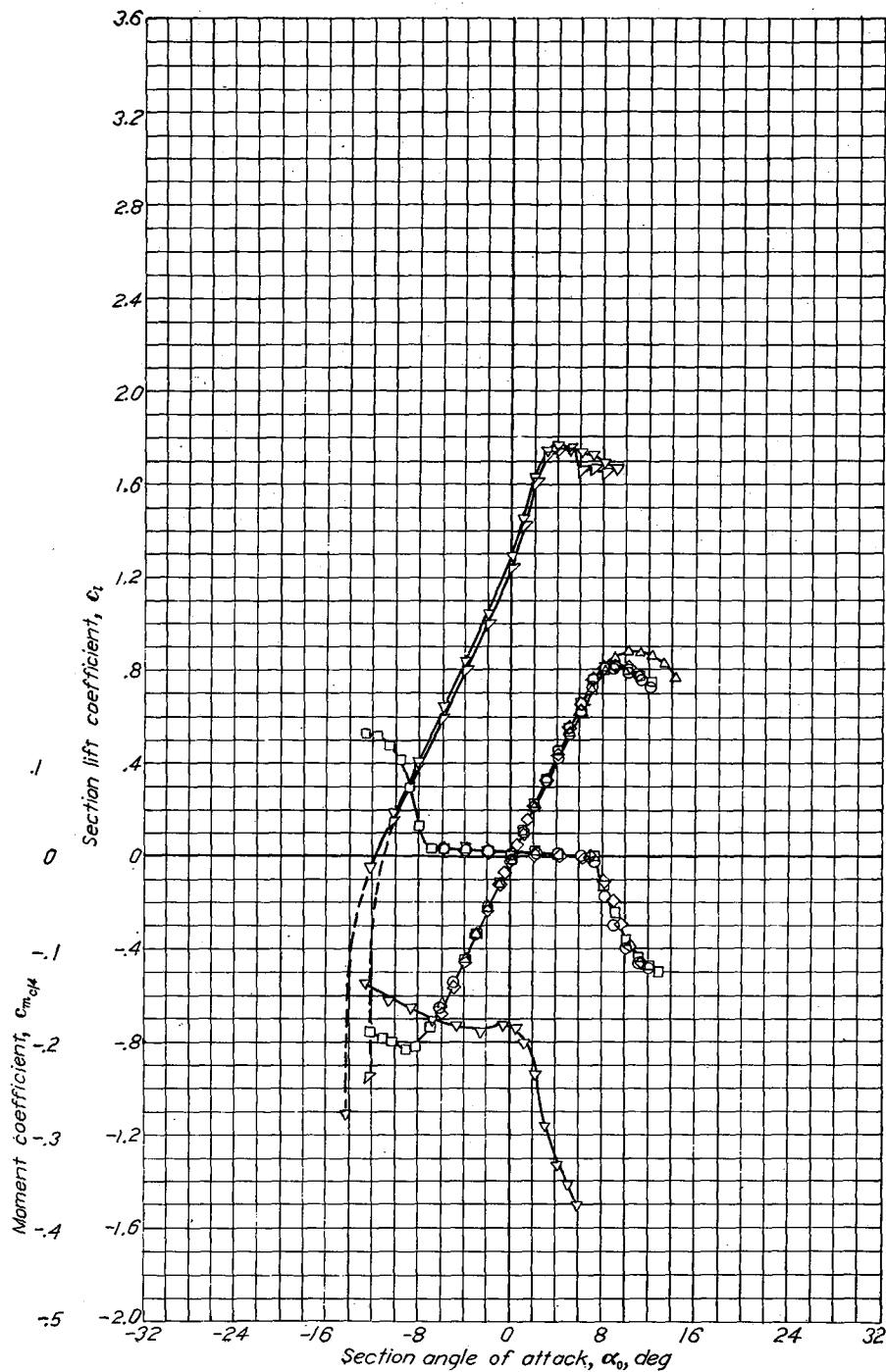
NACA 63(420)-422



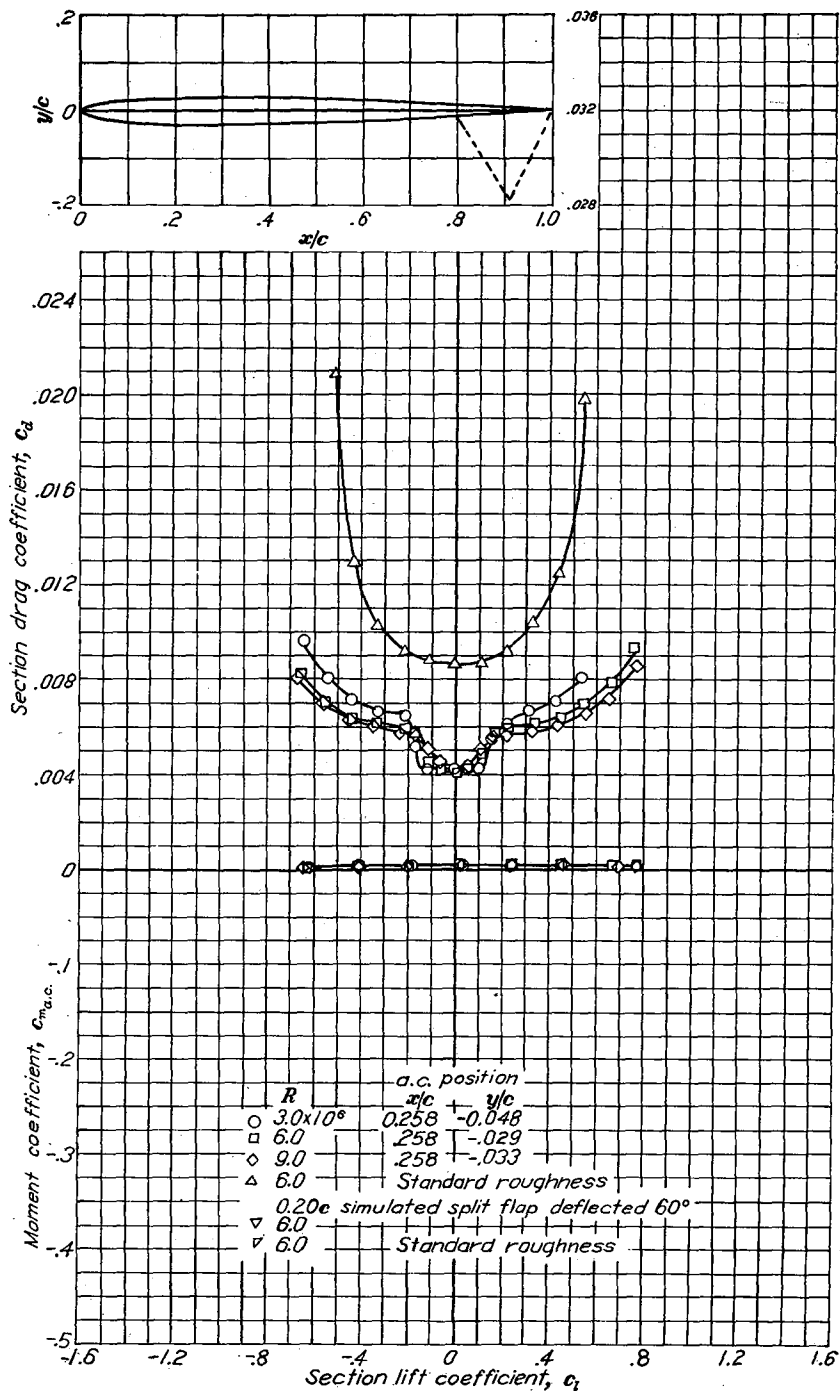
Aerodynamic characteristics of the NACA 63(420)-422 airfoil section, 24-inch chord.



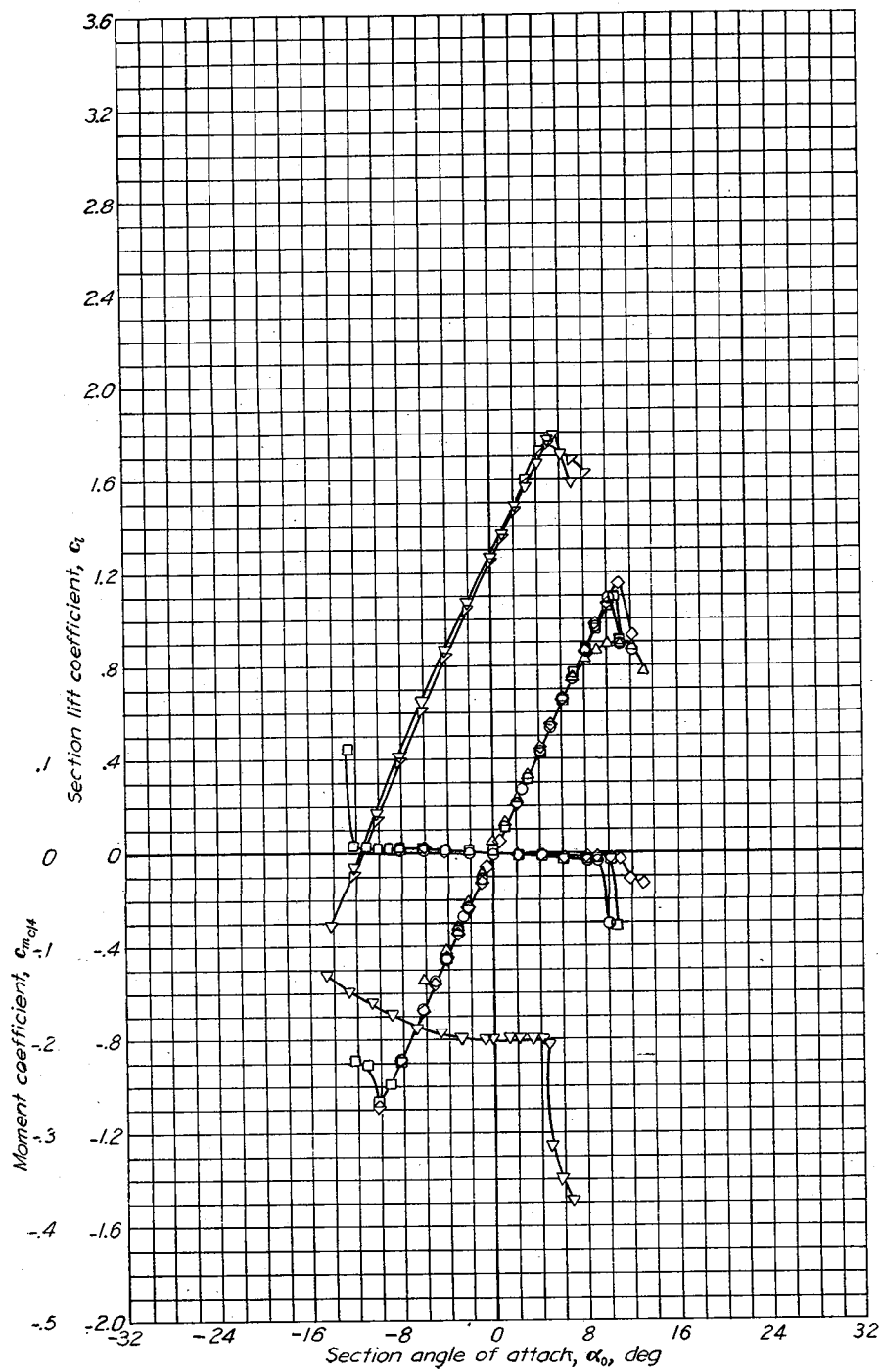
Aerodynamic characteristics of the NACA 63(420)-517 airfoil section, 24-inch chord.



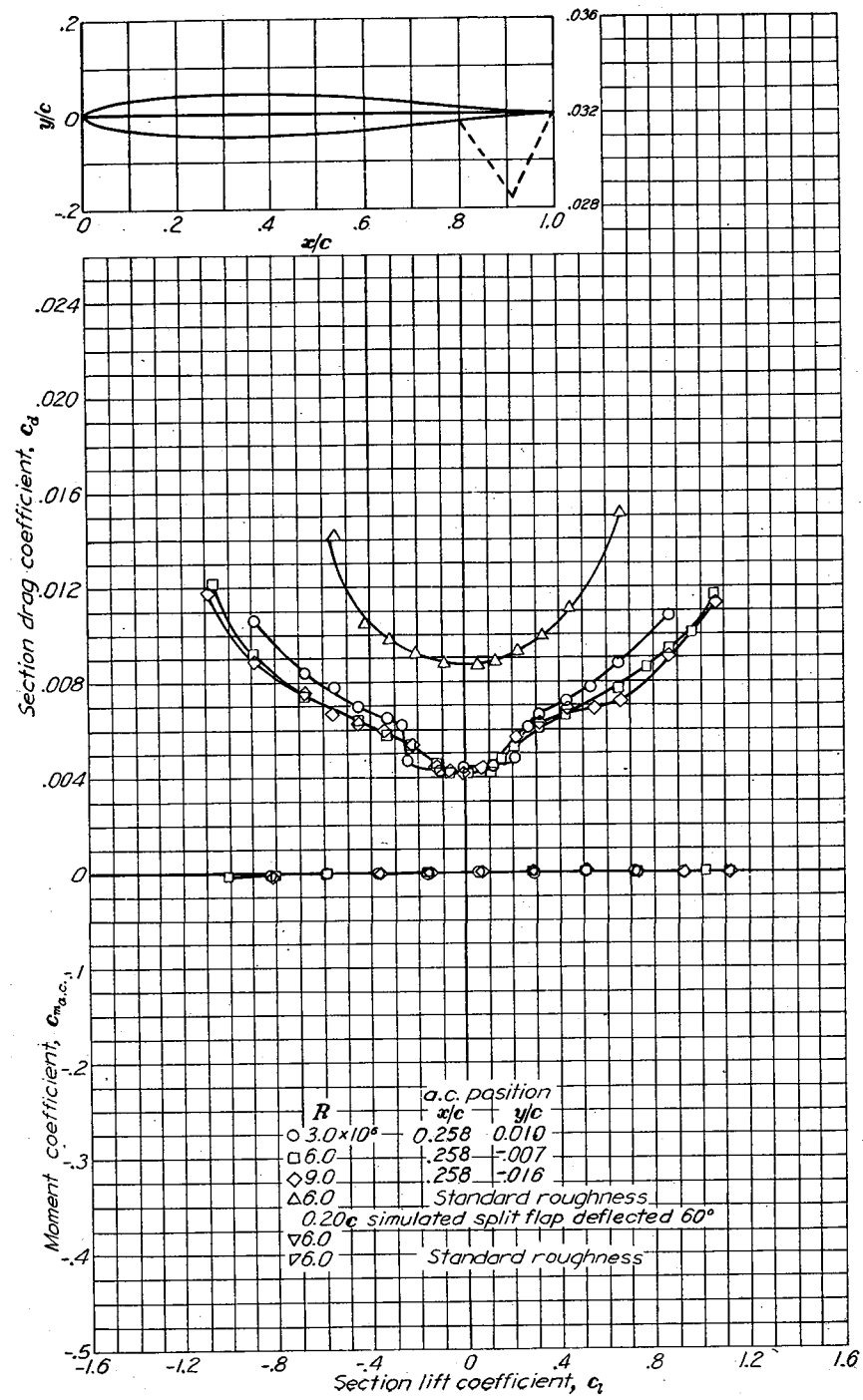
Aerodynamic characteristics of the NACA 63-006 airfoil section, 24-inch chord.

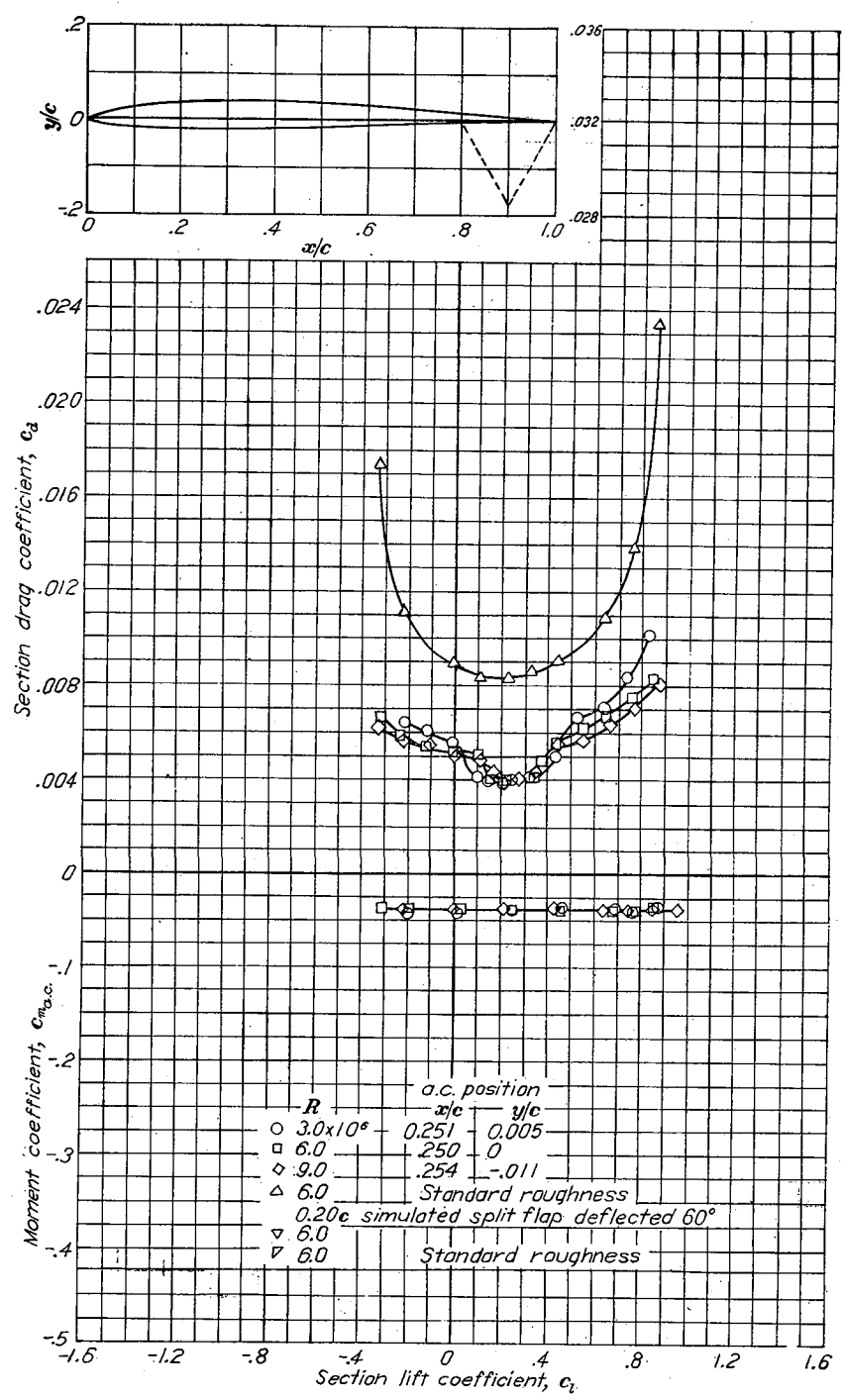
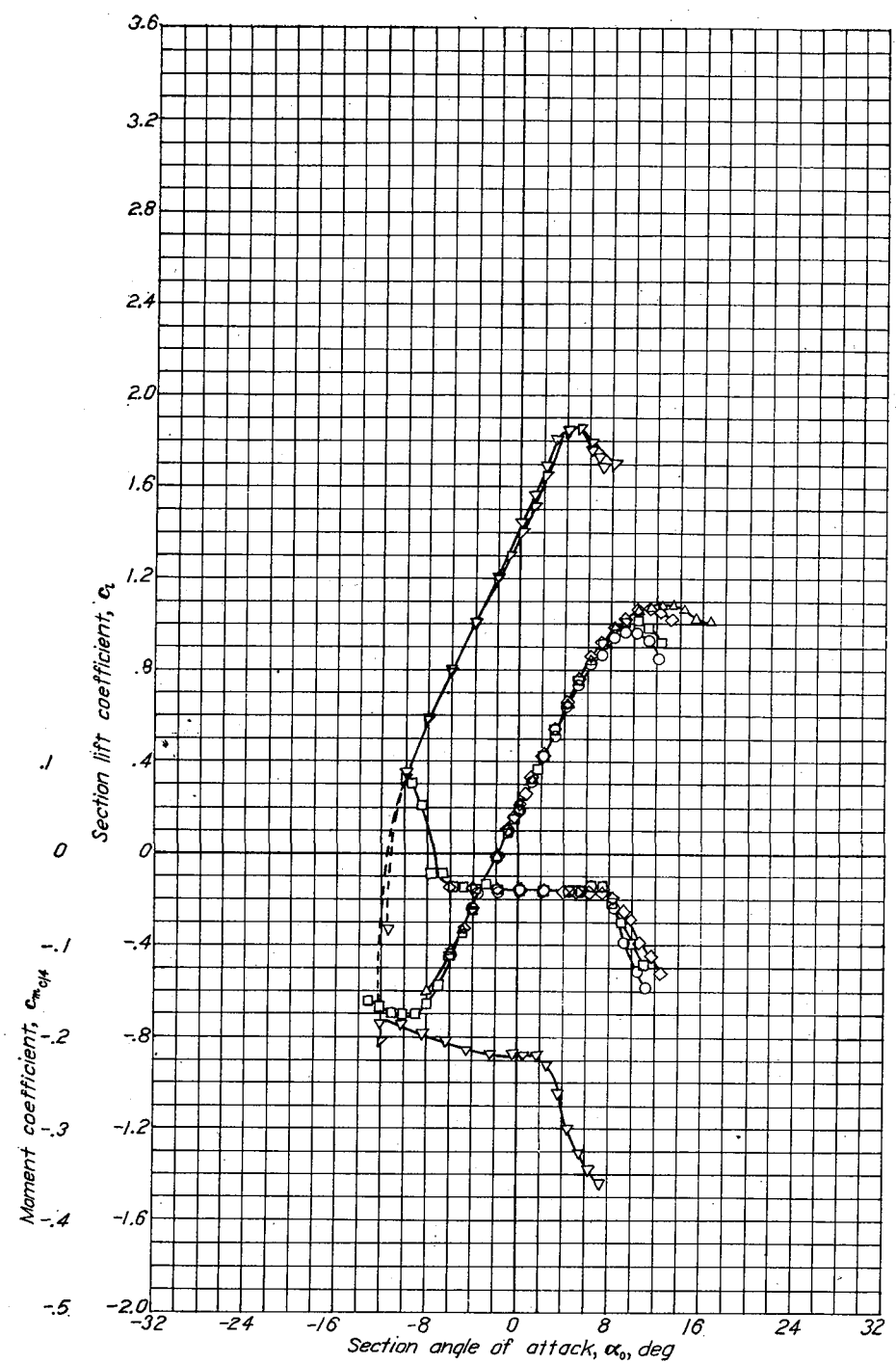




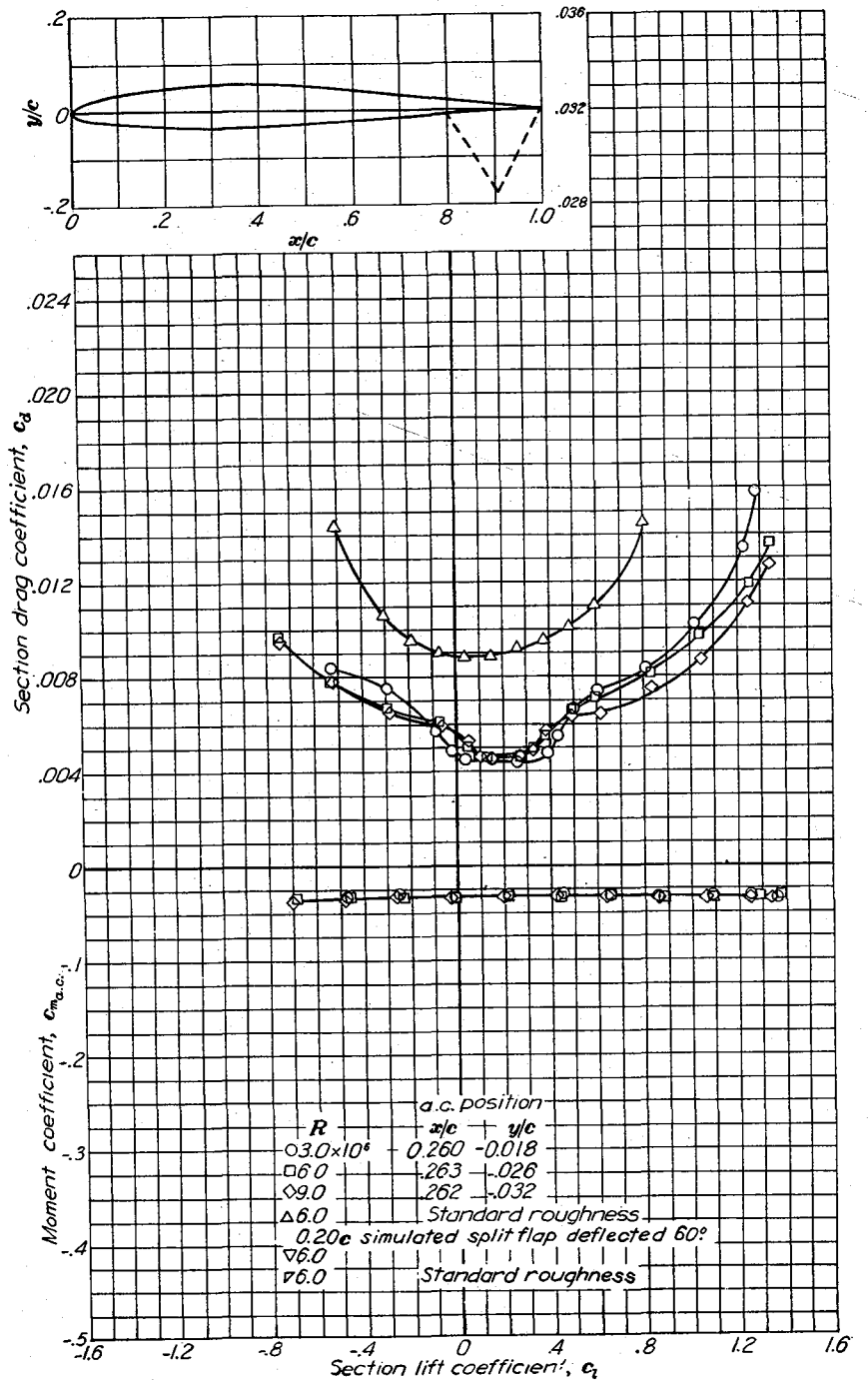
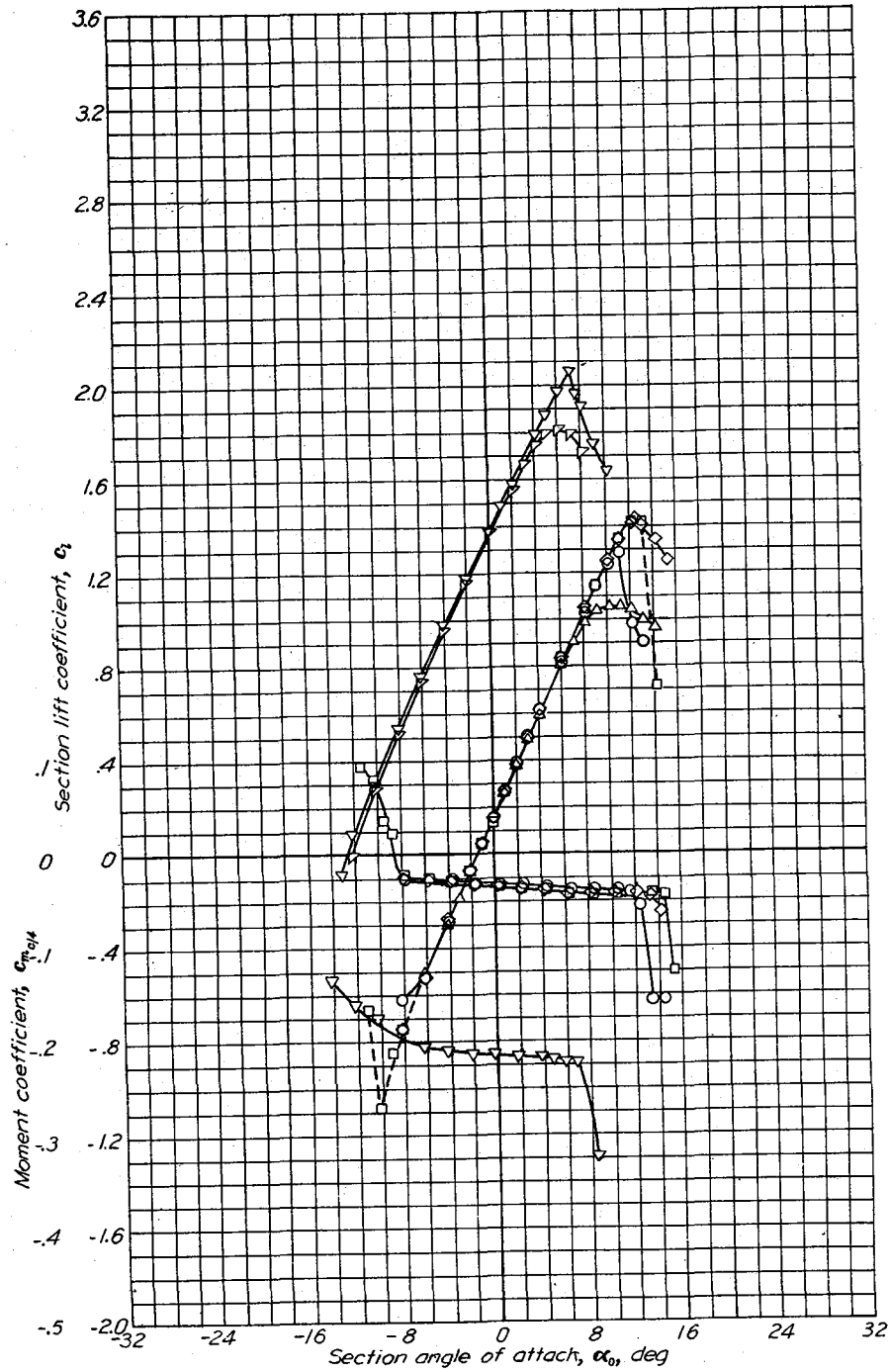


Aerodynamic characteristics of the NACA 63-009 airfoil section, 24-inch chord.

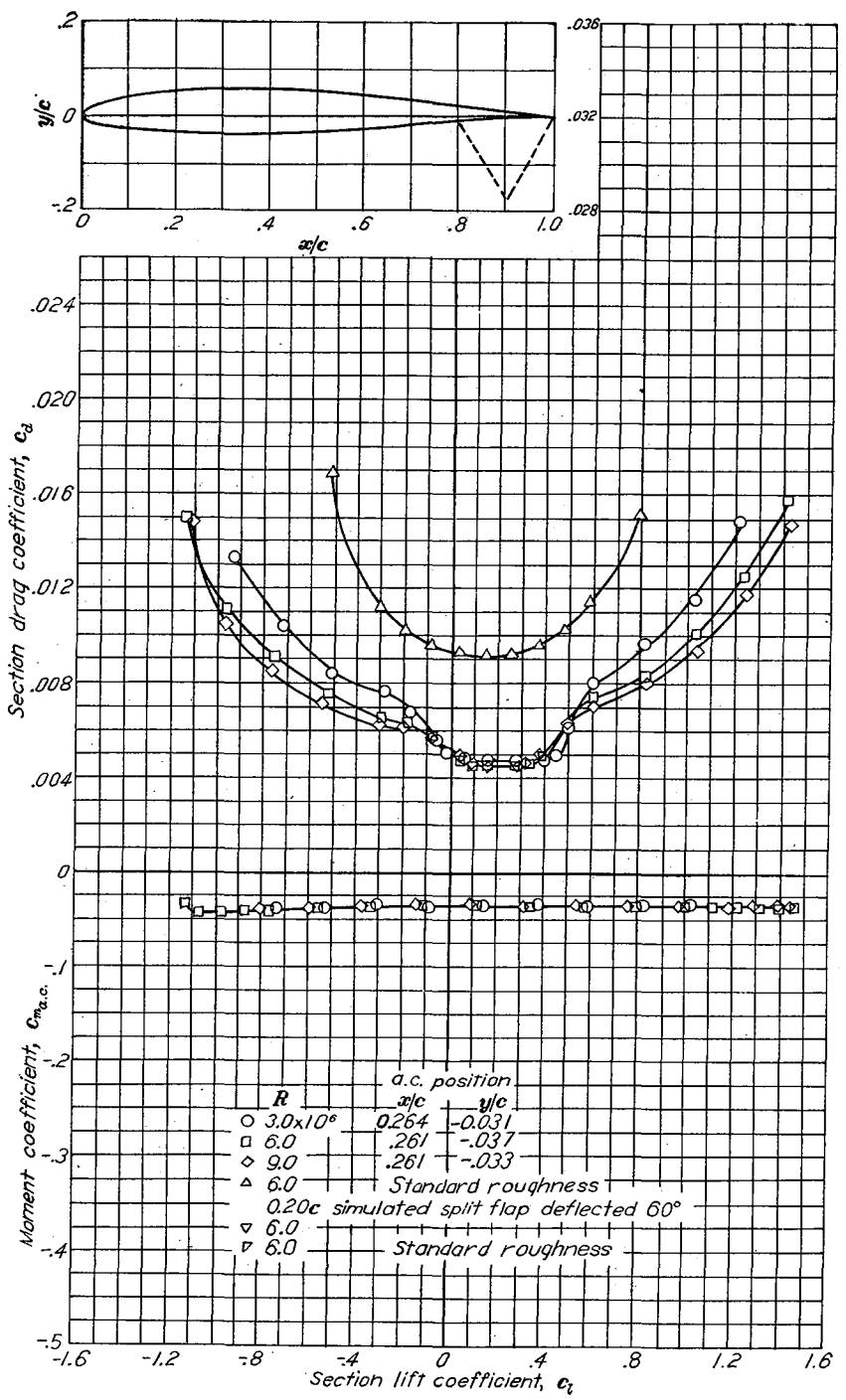
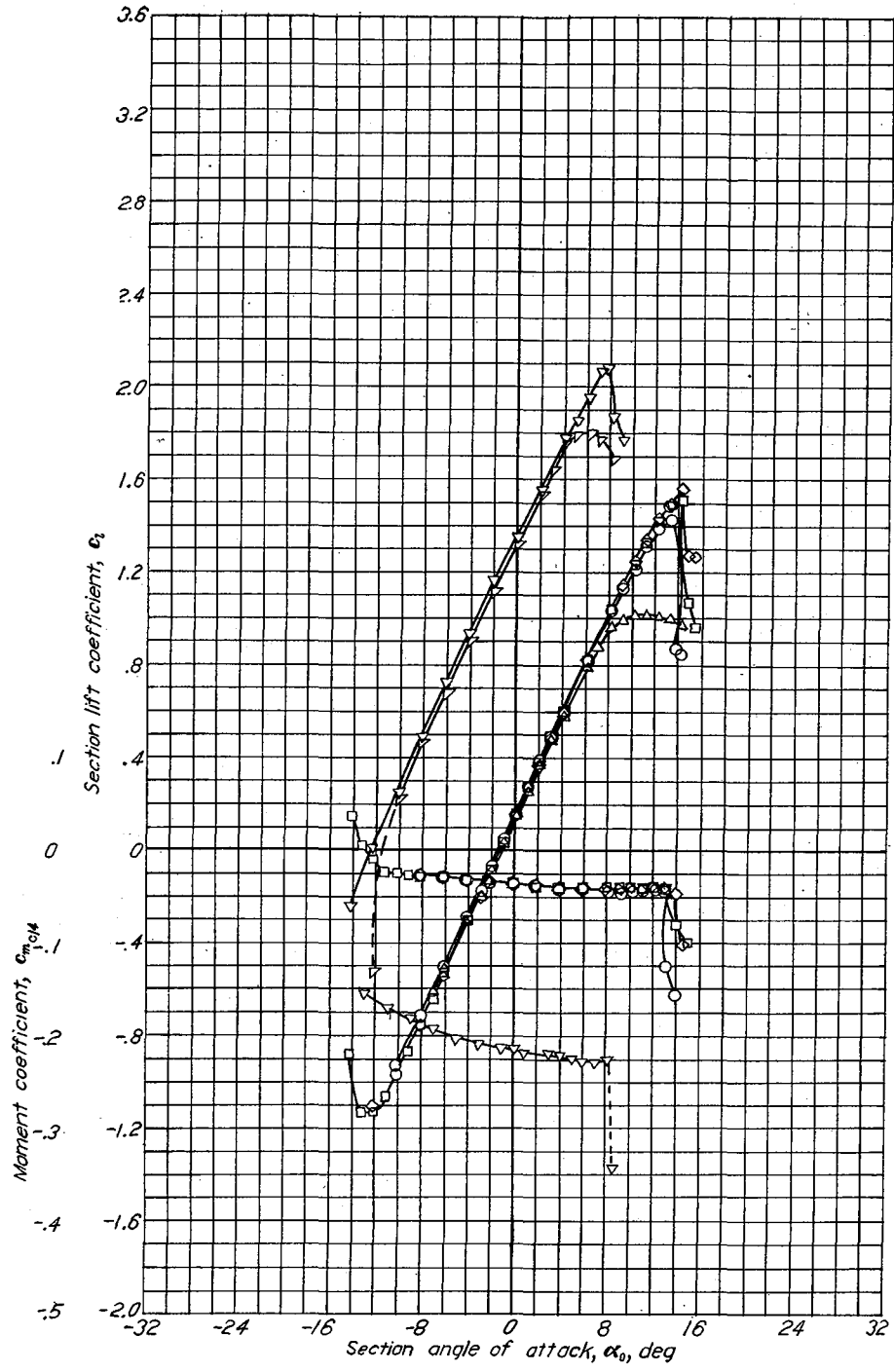




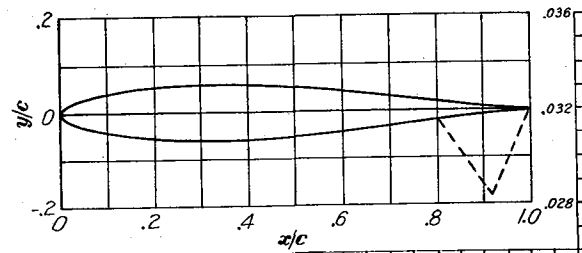
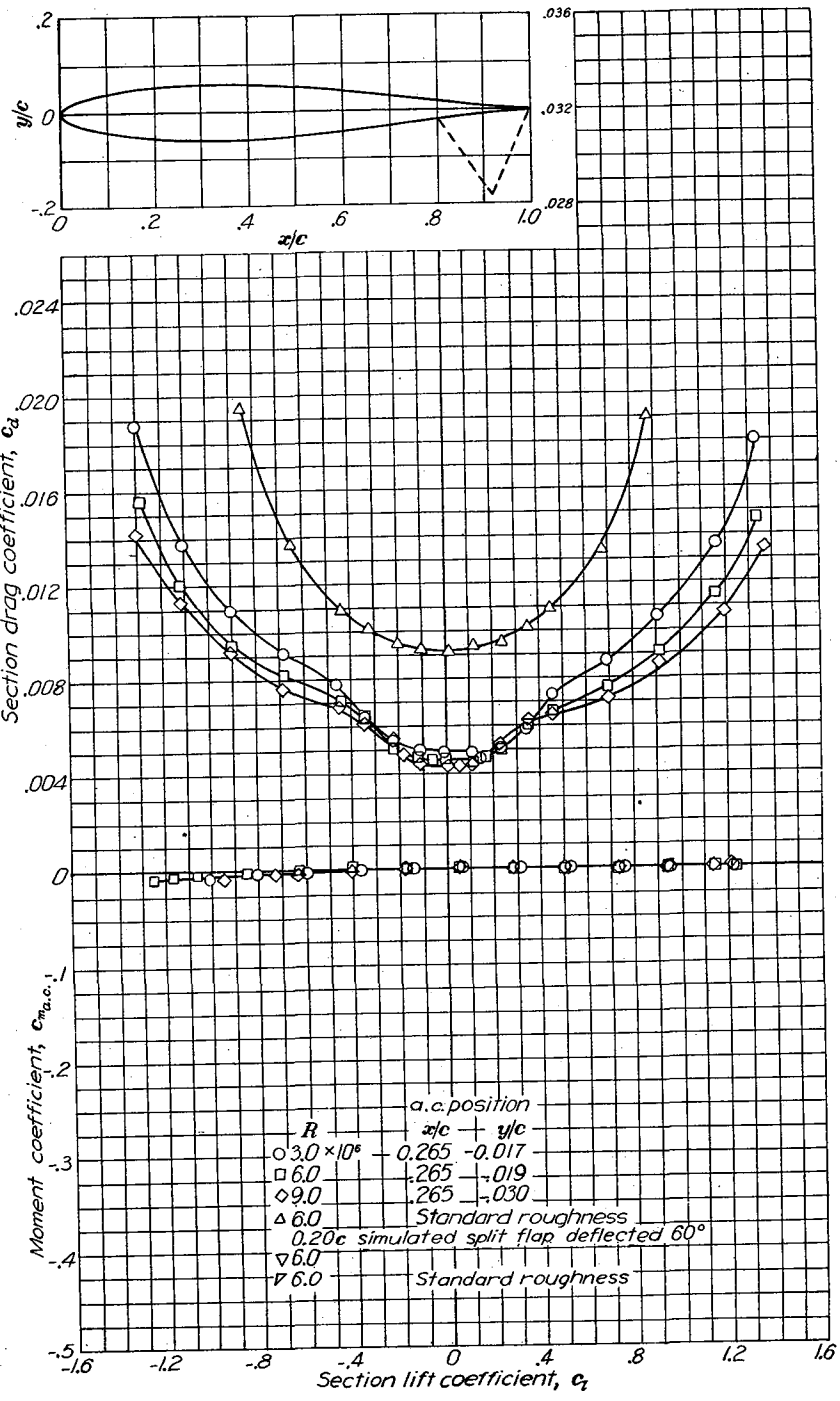
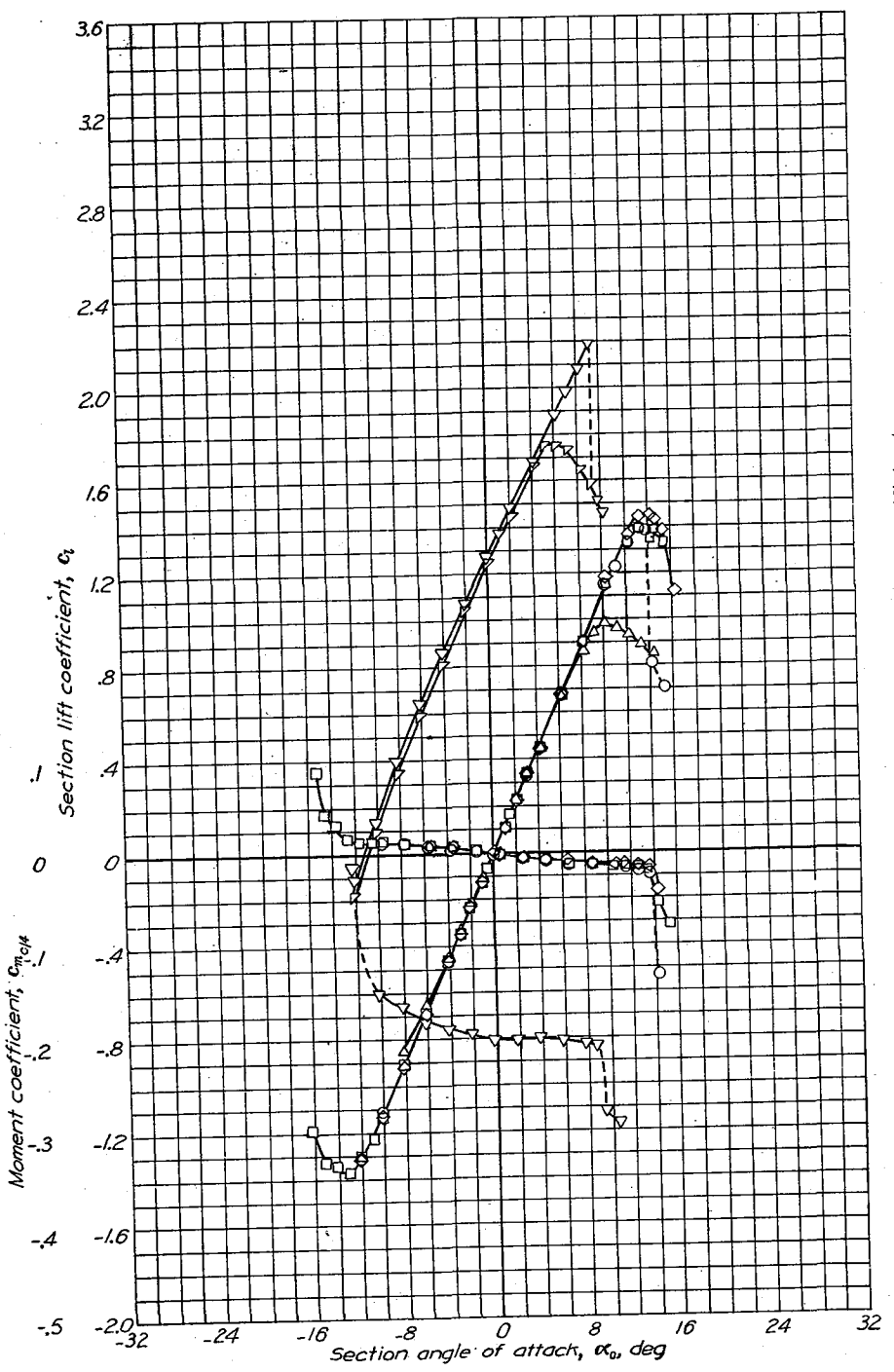
Aerodynamic characteristics of the NACA 63-206 airfoil section, 24-inch chord.



Aerodynamic characteristics of the NACA 63-209 airfoil section, 24-inch chord.

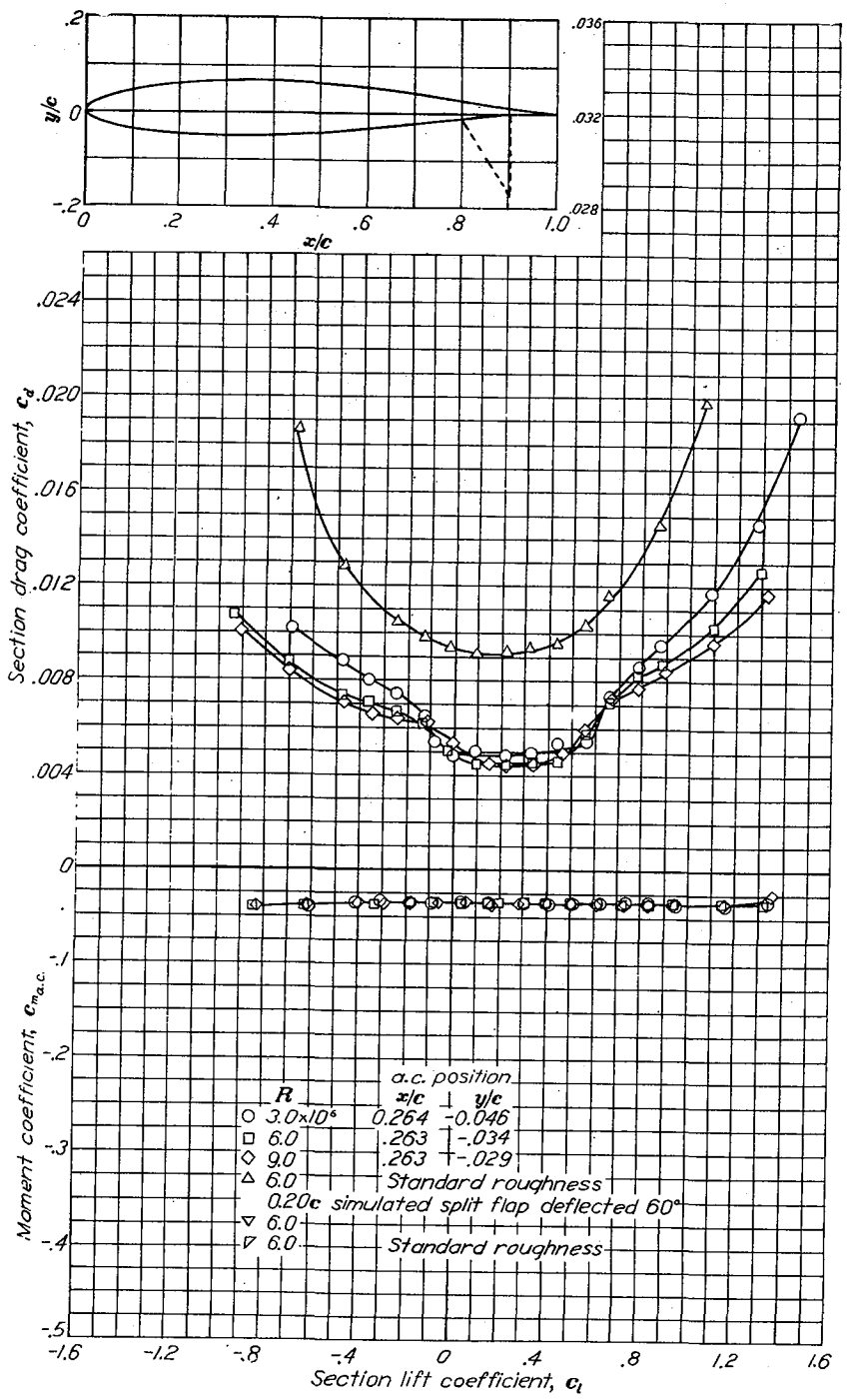
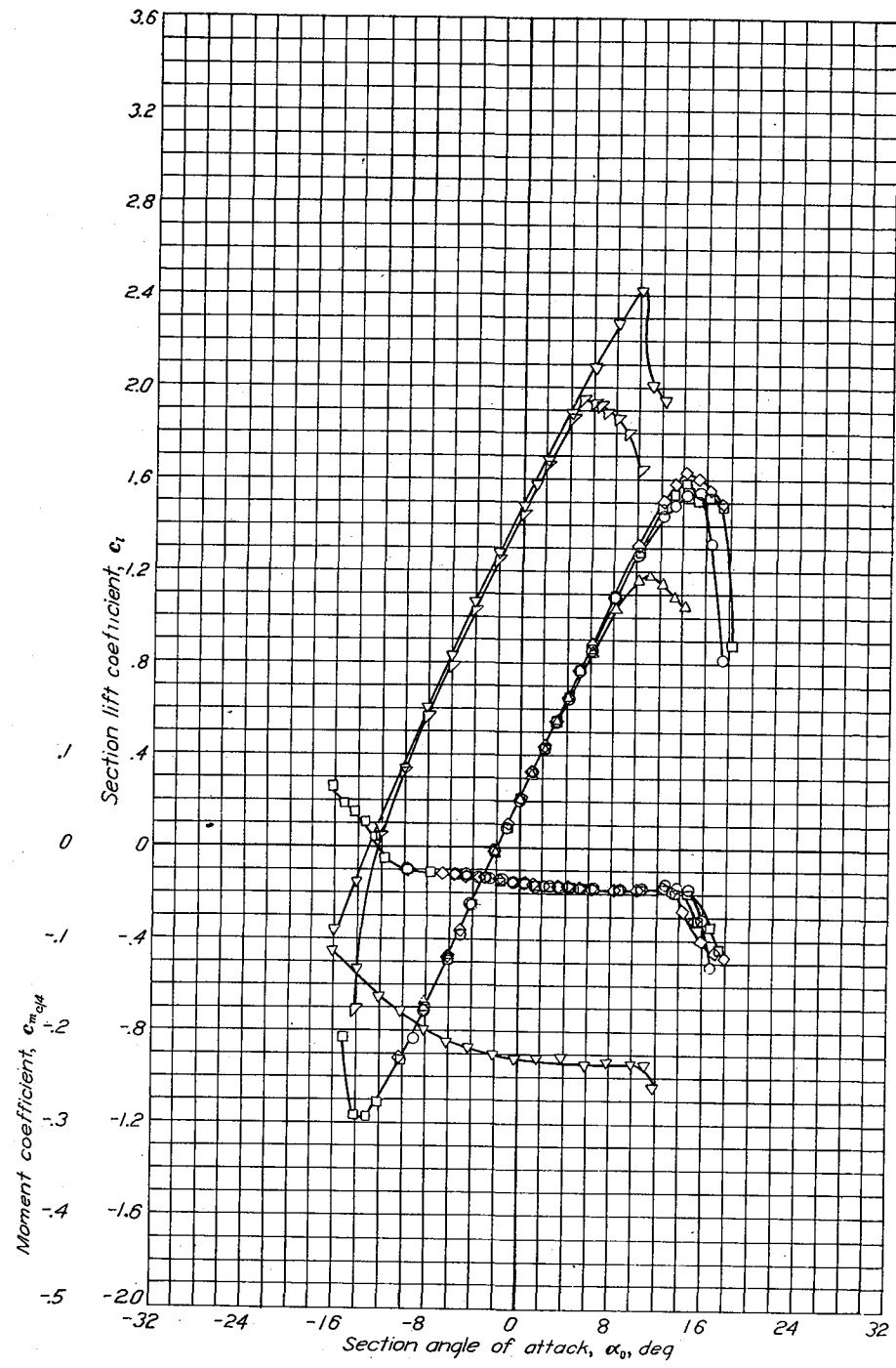


Aerodynamic characteristics of the NACA 63-210 airfoil section, 24-inch chord.

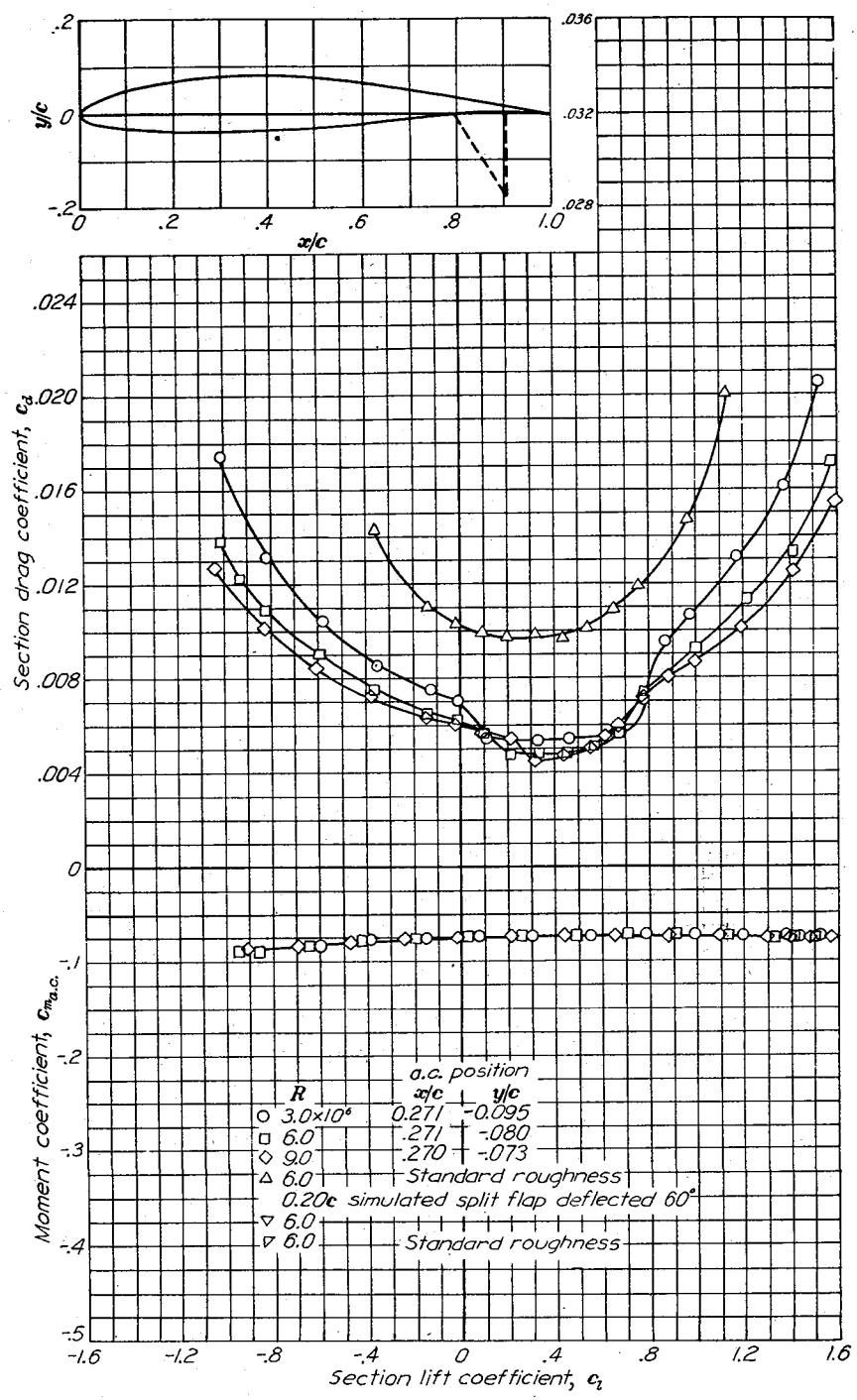
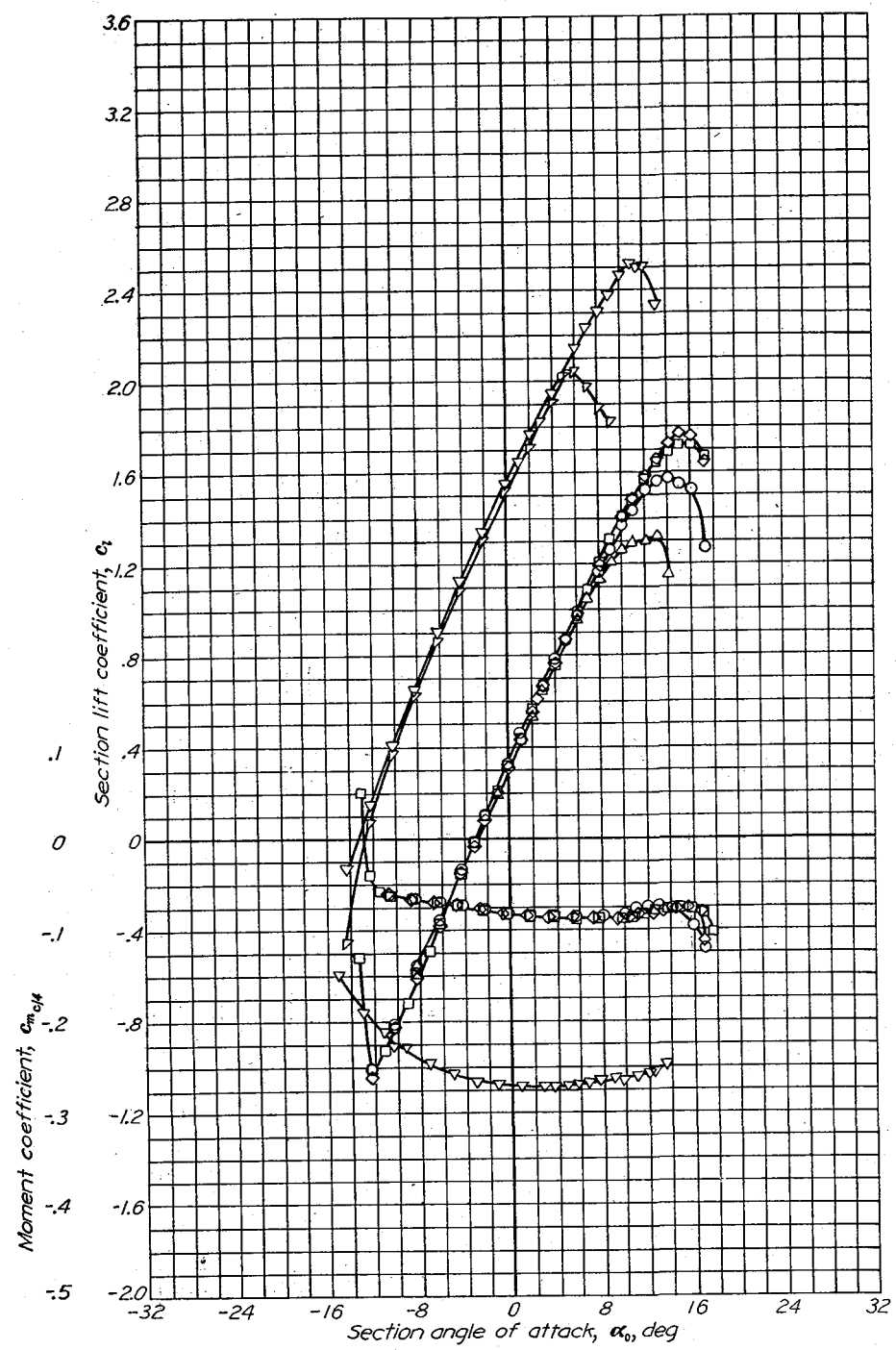


a.c. position	
$R$	$x/c \quad y/c$
$\circ$ $3.0 \times 10^6$	0.265 -0.017
$\square$ 6.0	0.265 -0.019
$\diamond$ 9.0	0.265 -0.030
$\triangle$ 6.0	Standard roughness
$\nabla$ 6.0	0.20c simulated split flap deflected 60°
$\nabla$ 6.0	Standard roughness

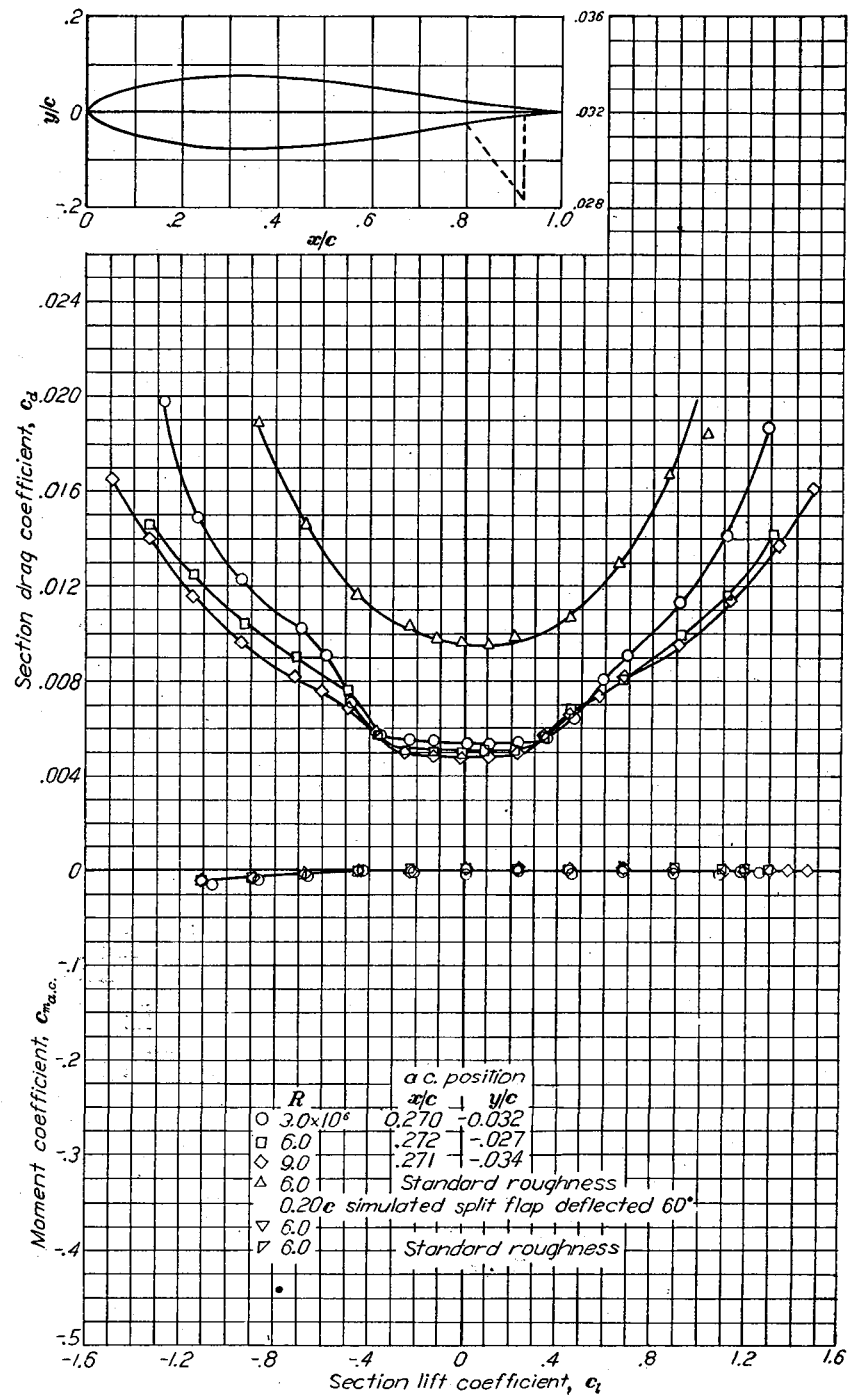
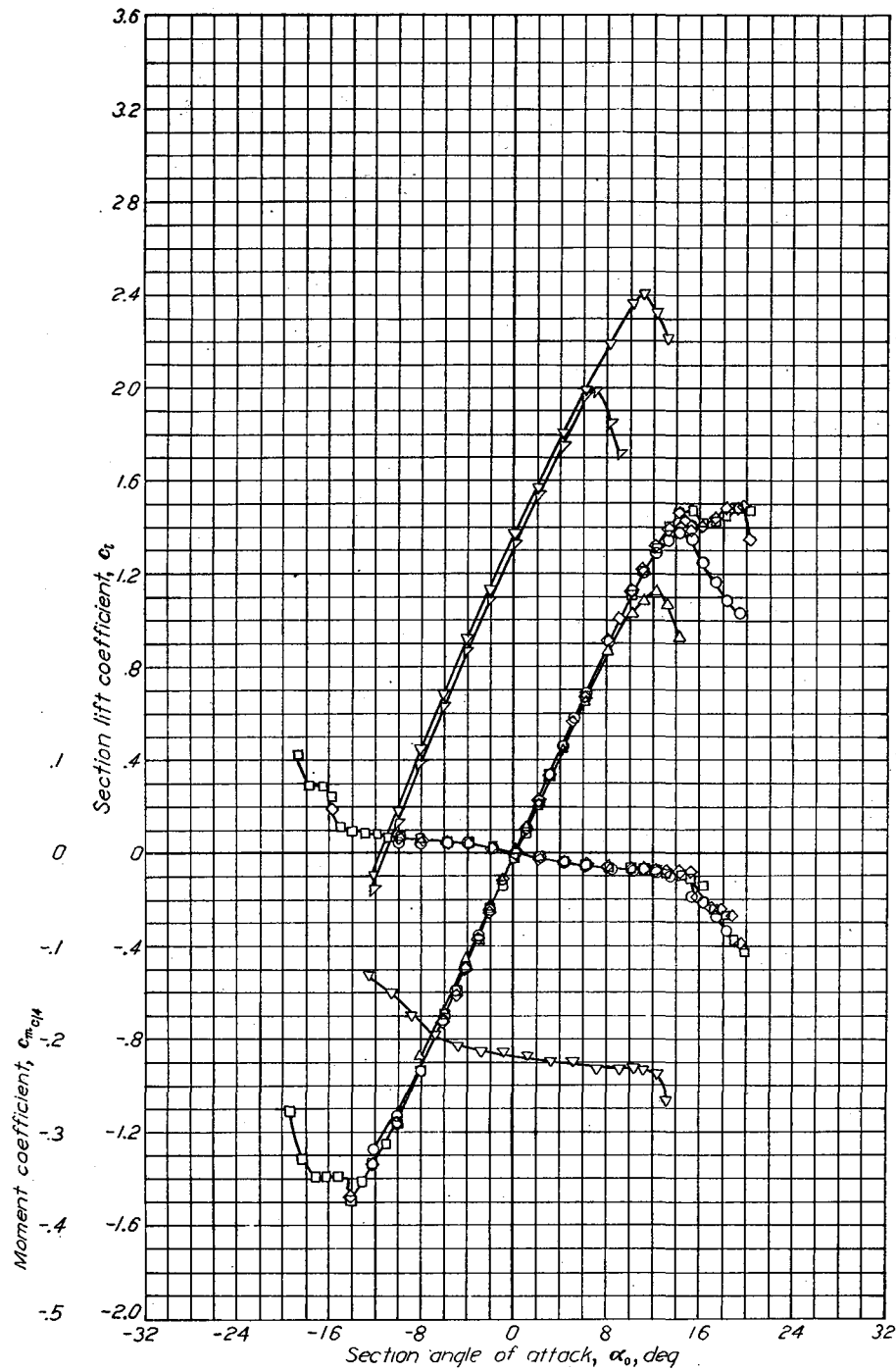
Aerodynamic characteristics of the NACA 631-012 airfoil section, 24-inch chord.



Aerodynamic characteristics of the NACA 631-212 airfoil section, 24-inch chord.

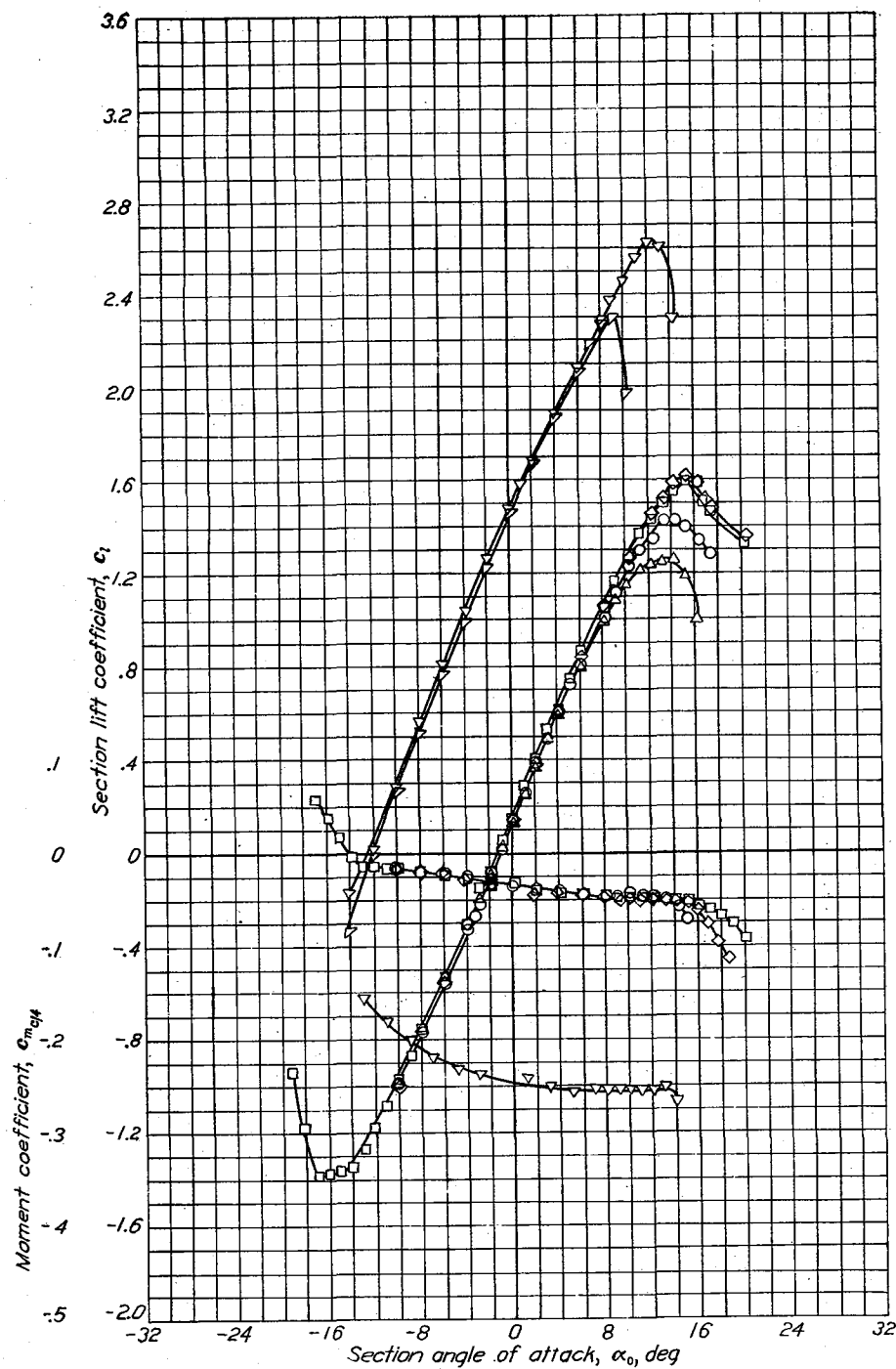


Aerodynamic characteristics of the NACA 631-412 airfoil section, 24-inch chord.

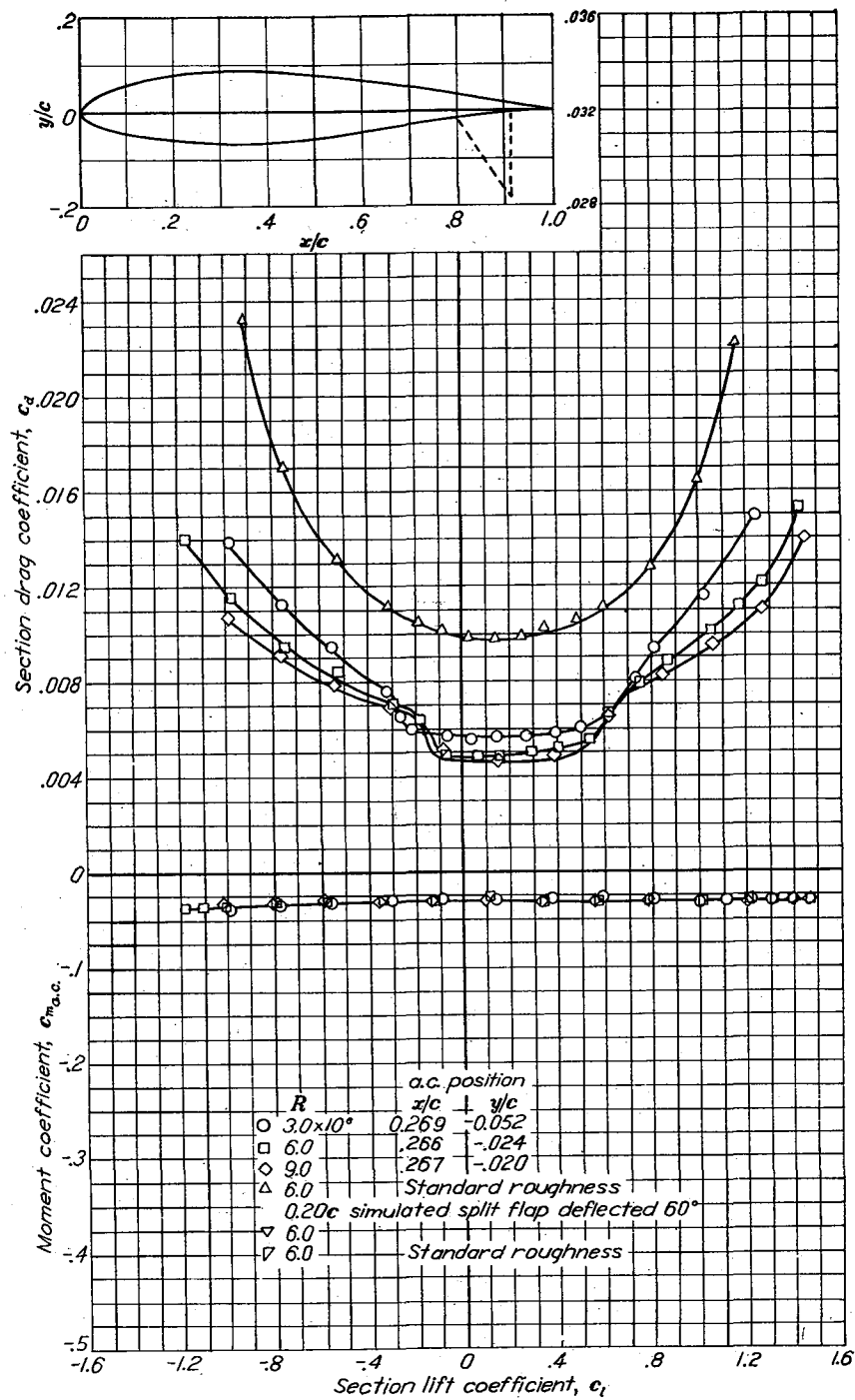


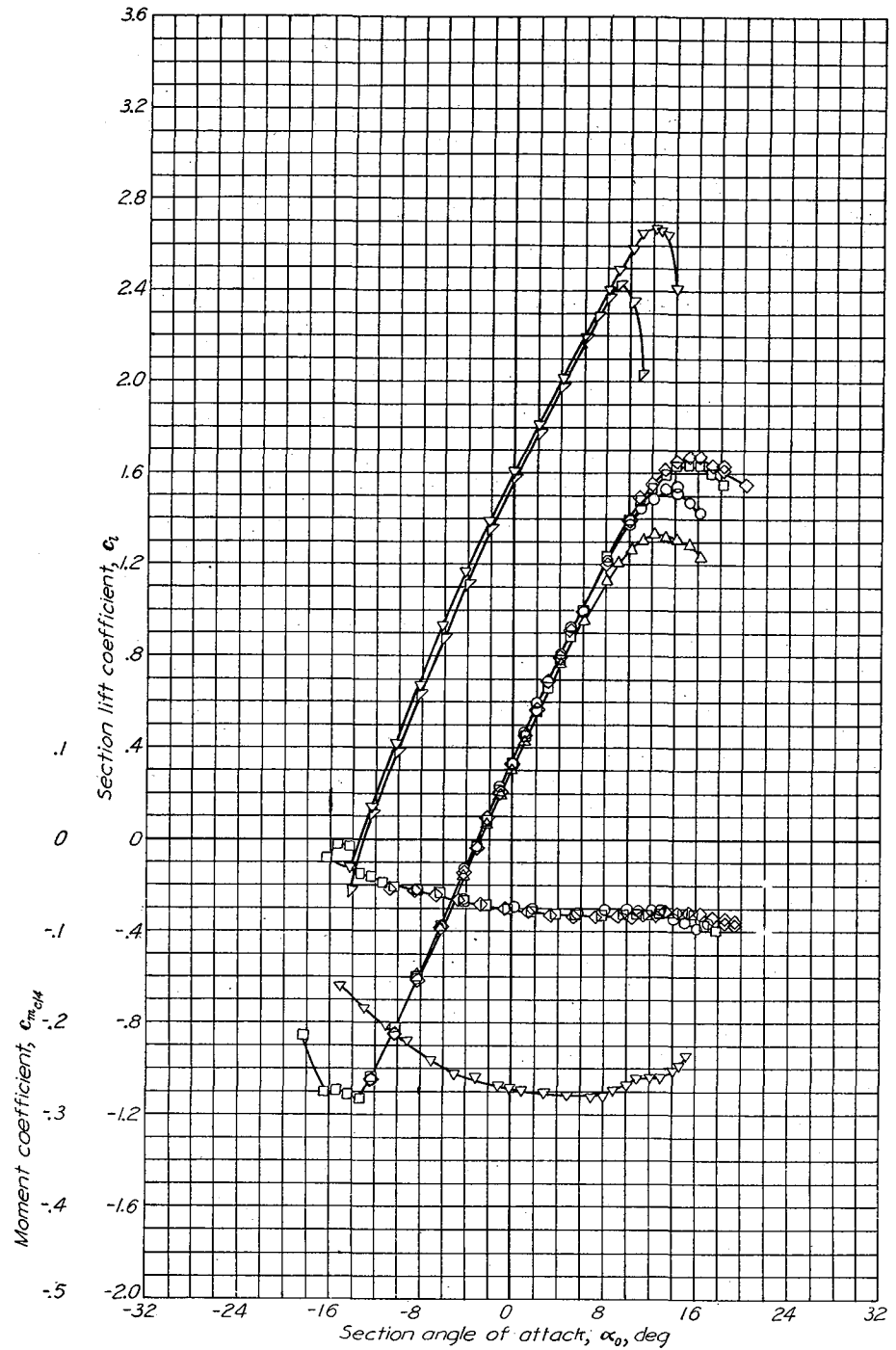
Aerodynamic characteristics of the NACA 632-015 airfoil section, 24-inch chord.



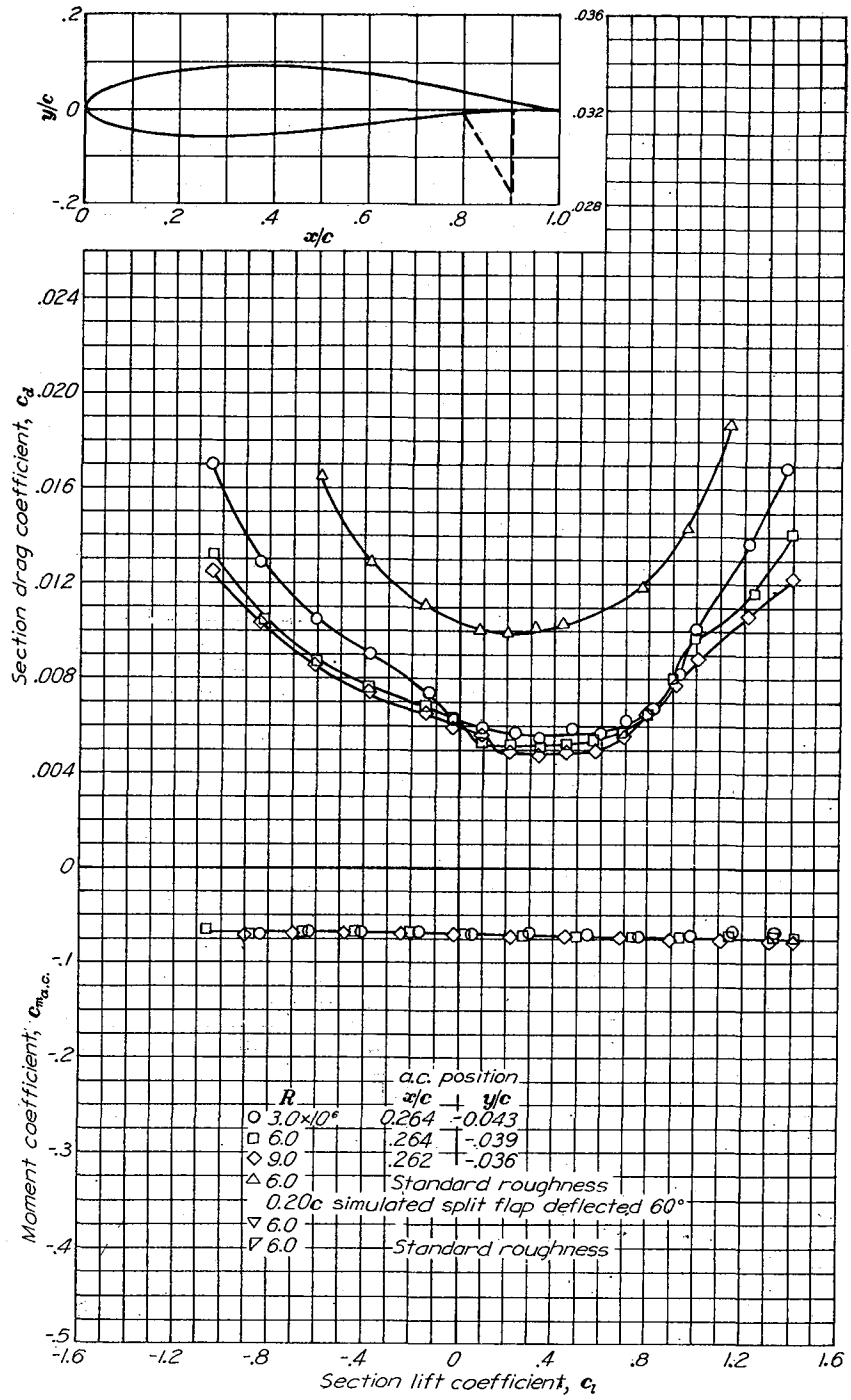


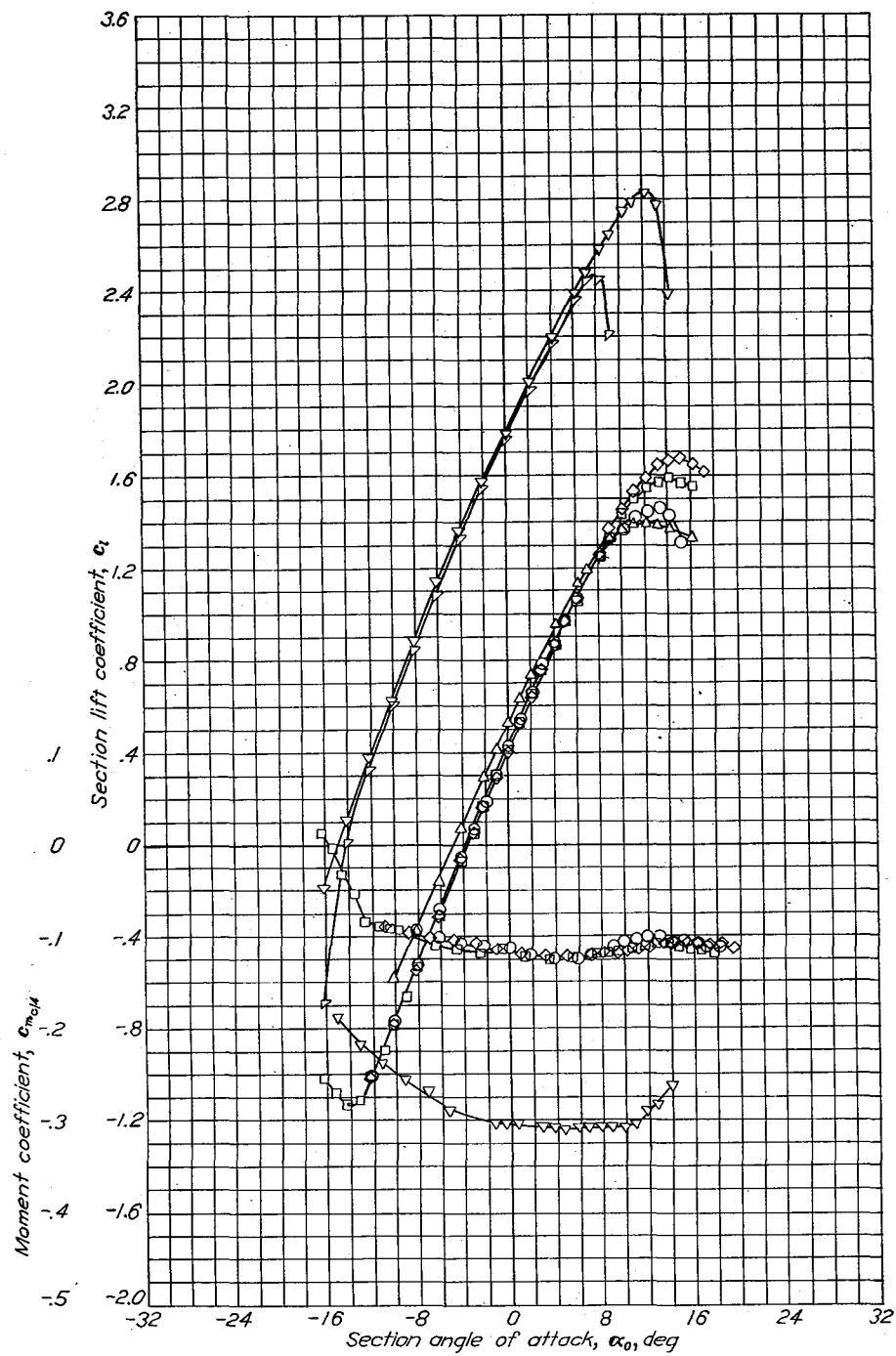
Aerodynamic characteristics of the NACA 632-215 airfoil section, 24-inch chord.



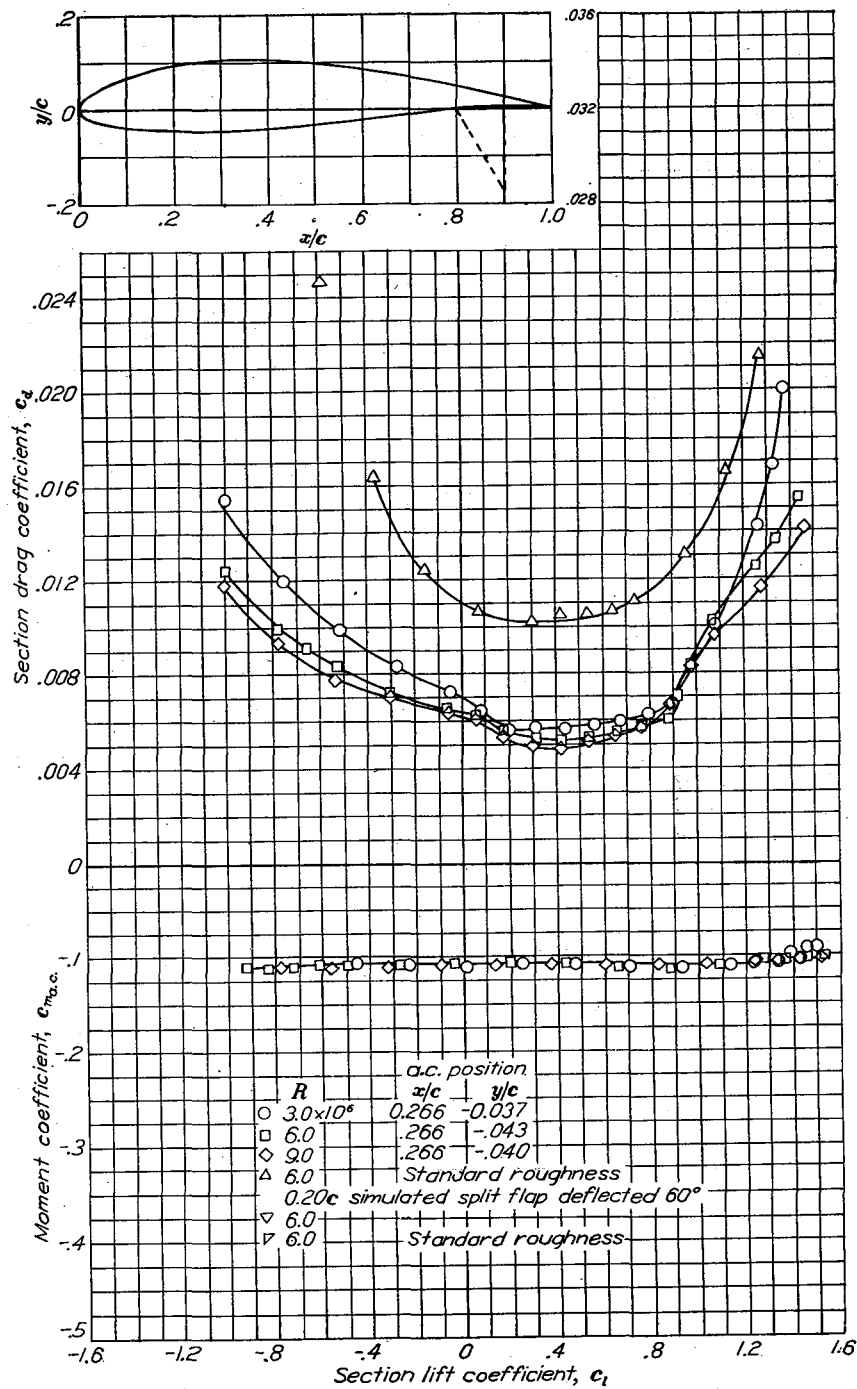


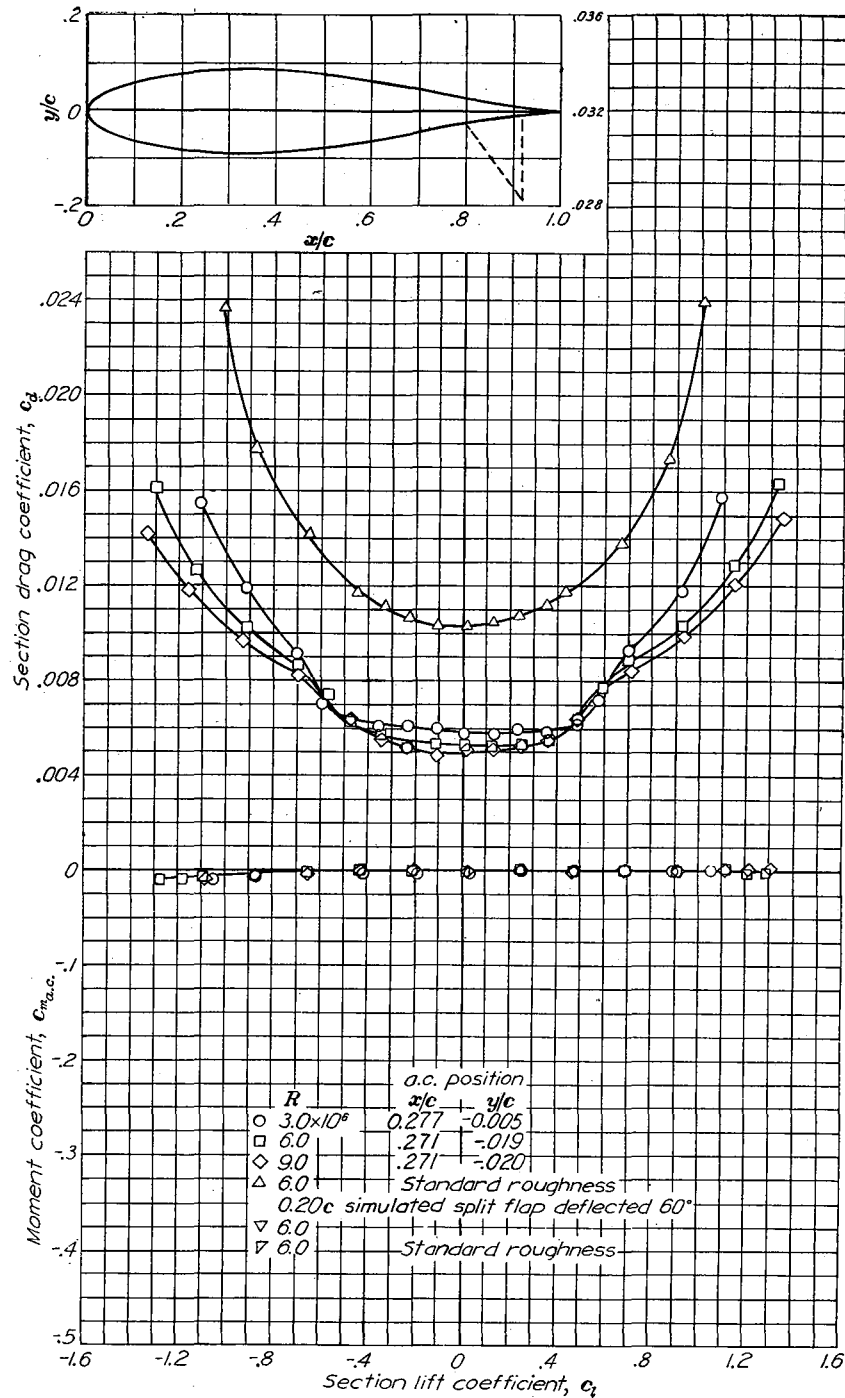
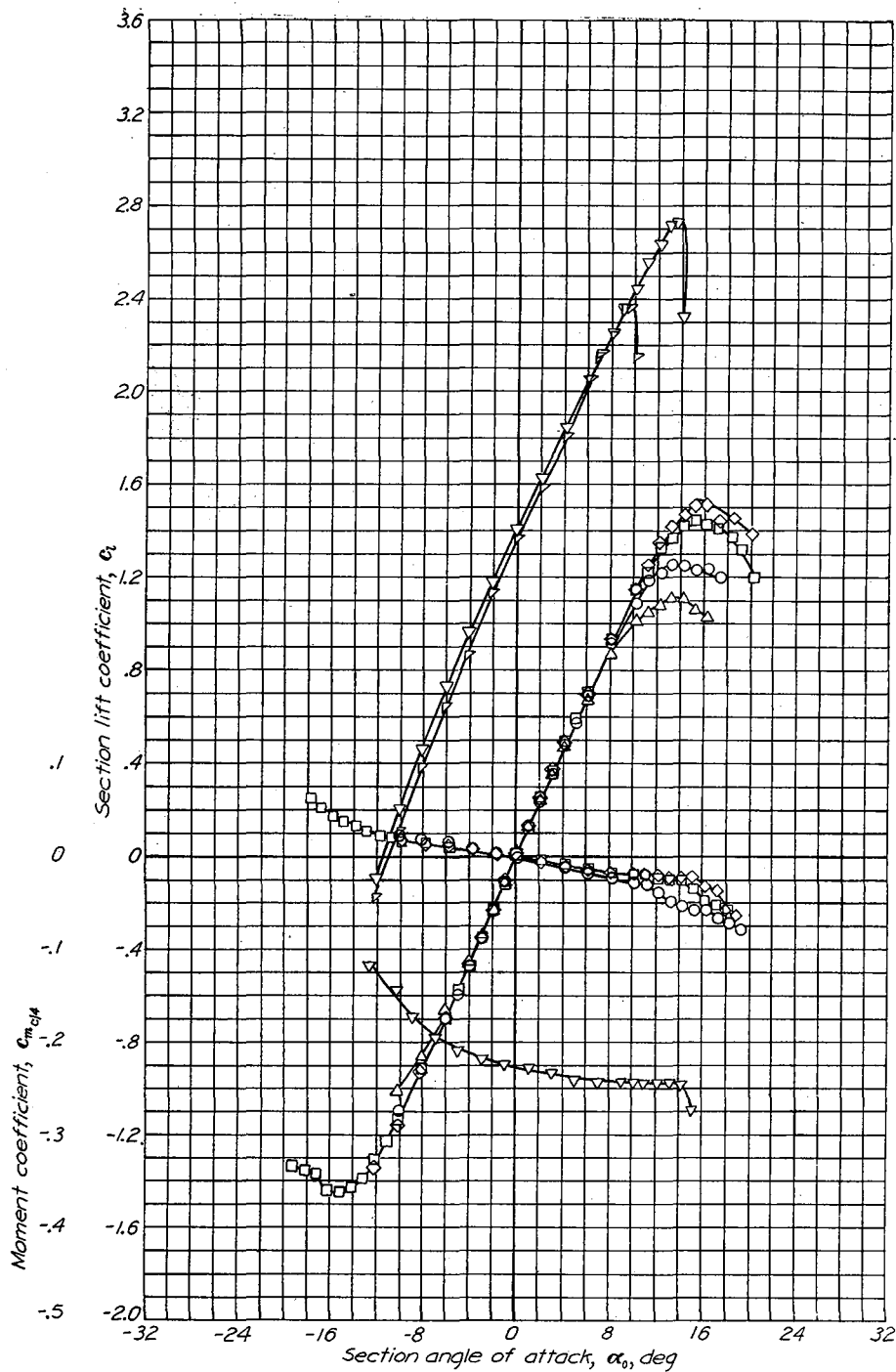
Aerodynamic characteristics of the NACA 632-415 airfoil section, 24-inch chord.



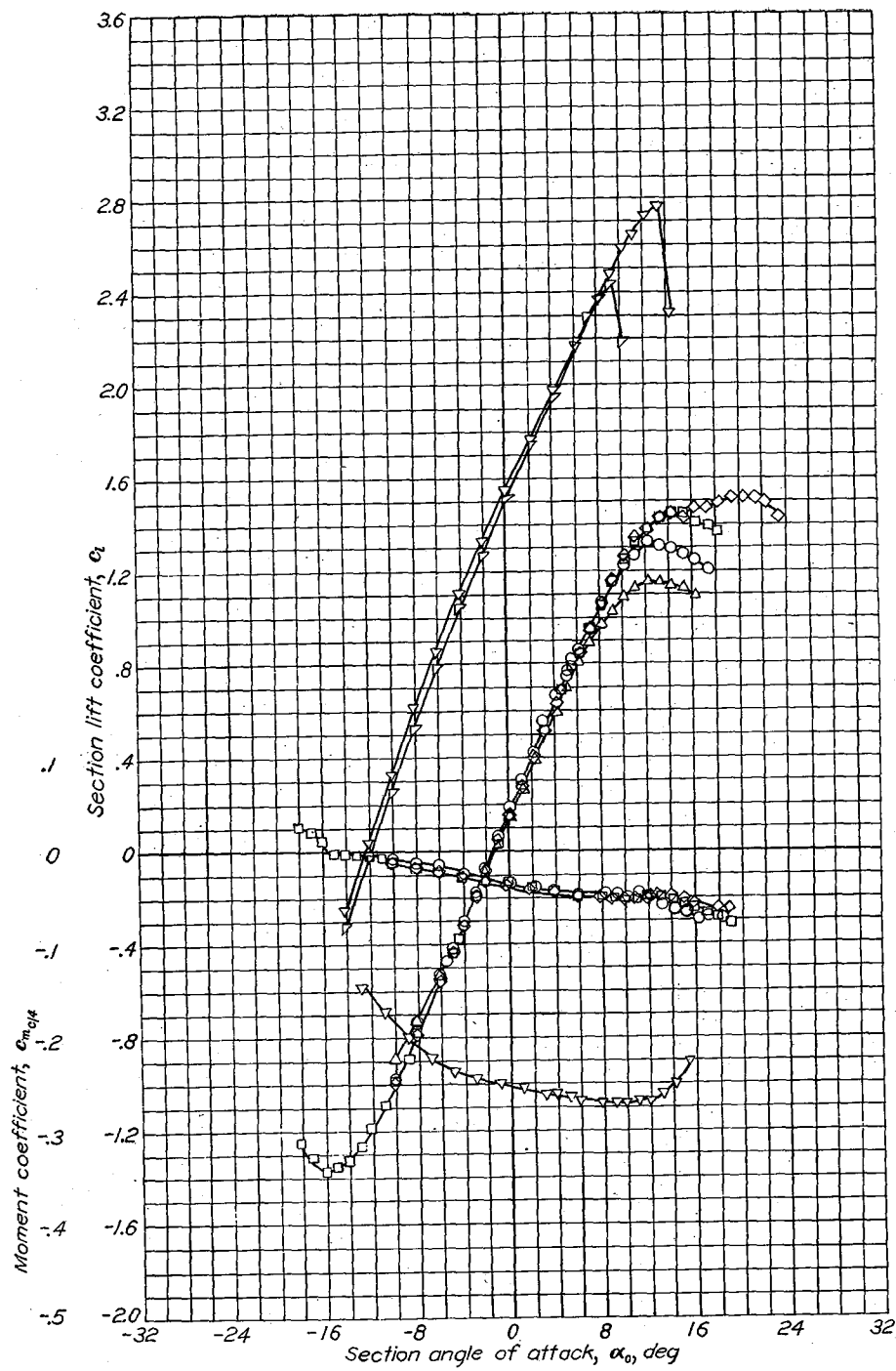


Aerodynamic characteristics of the NACA 632-615 airfoil section, 24-inch chord.

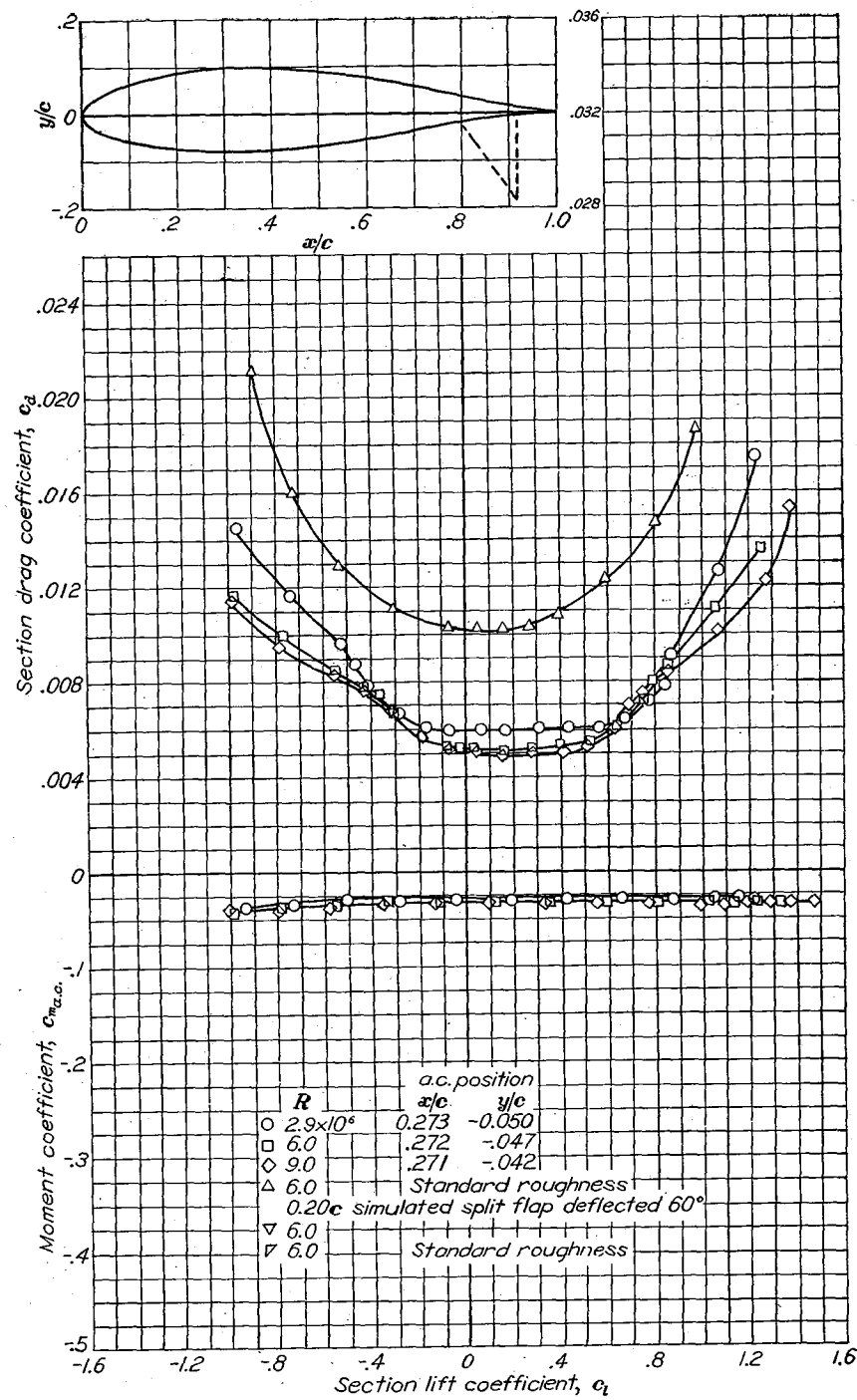


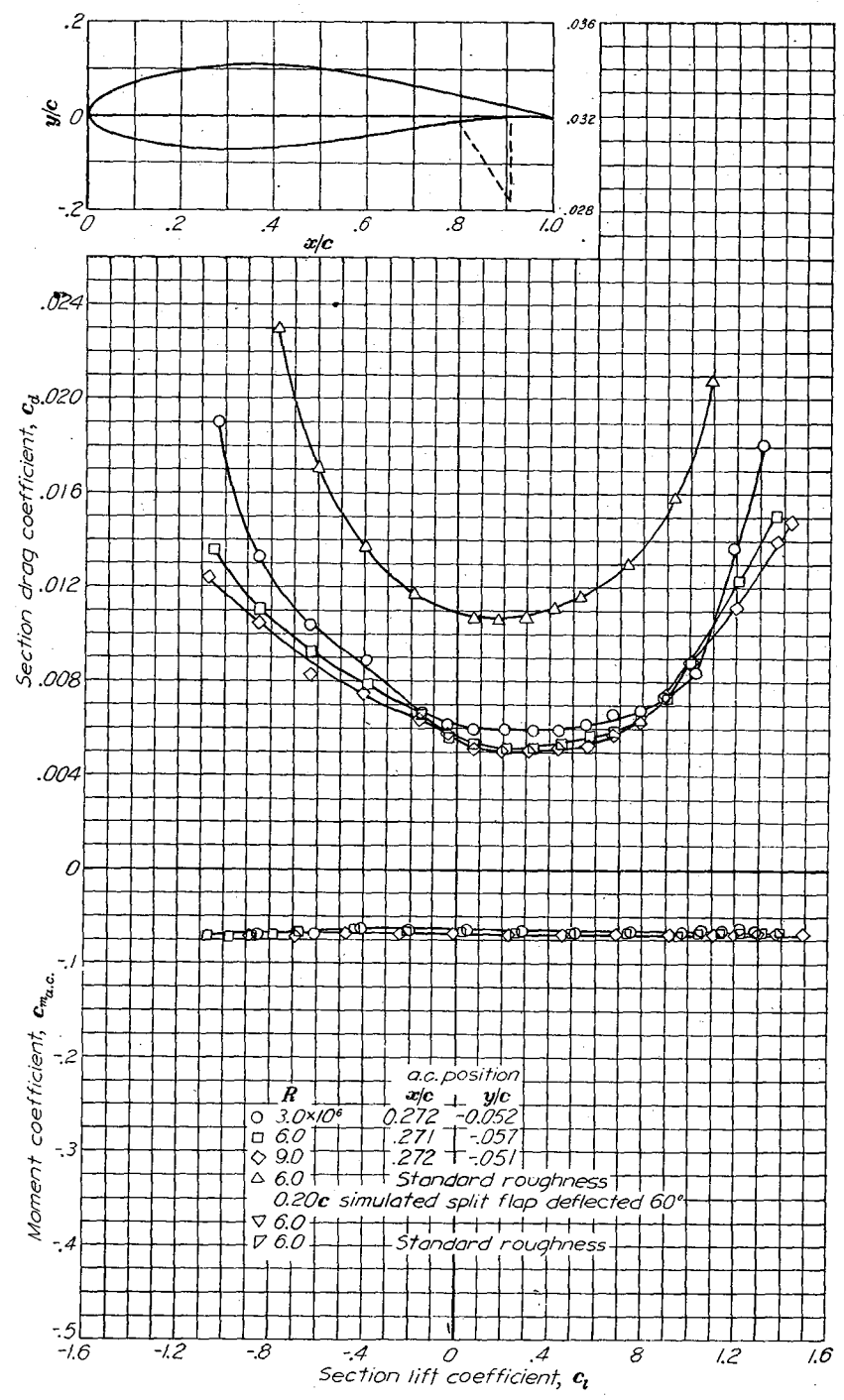
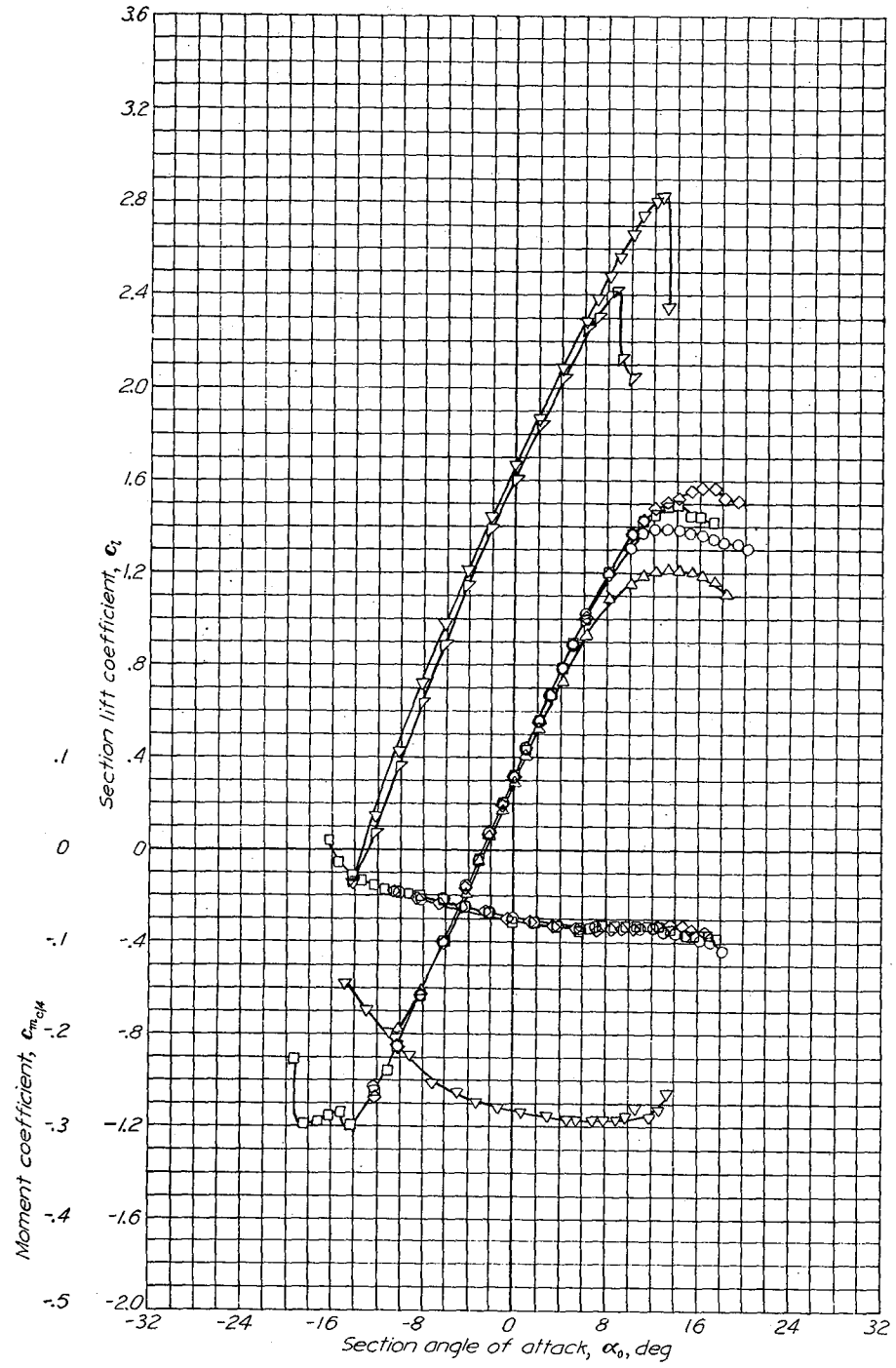


Aerodynamic characteristics of the NACA 633-018 airfoil section, 24-inch chord,

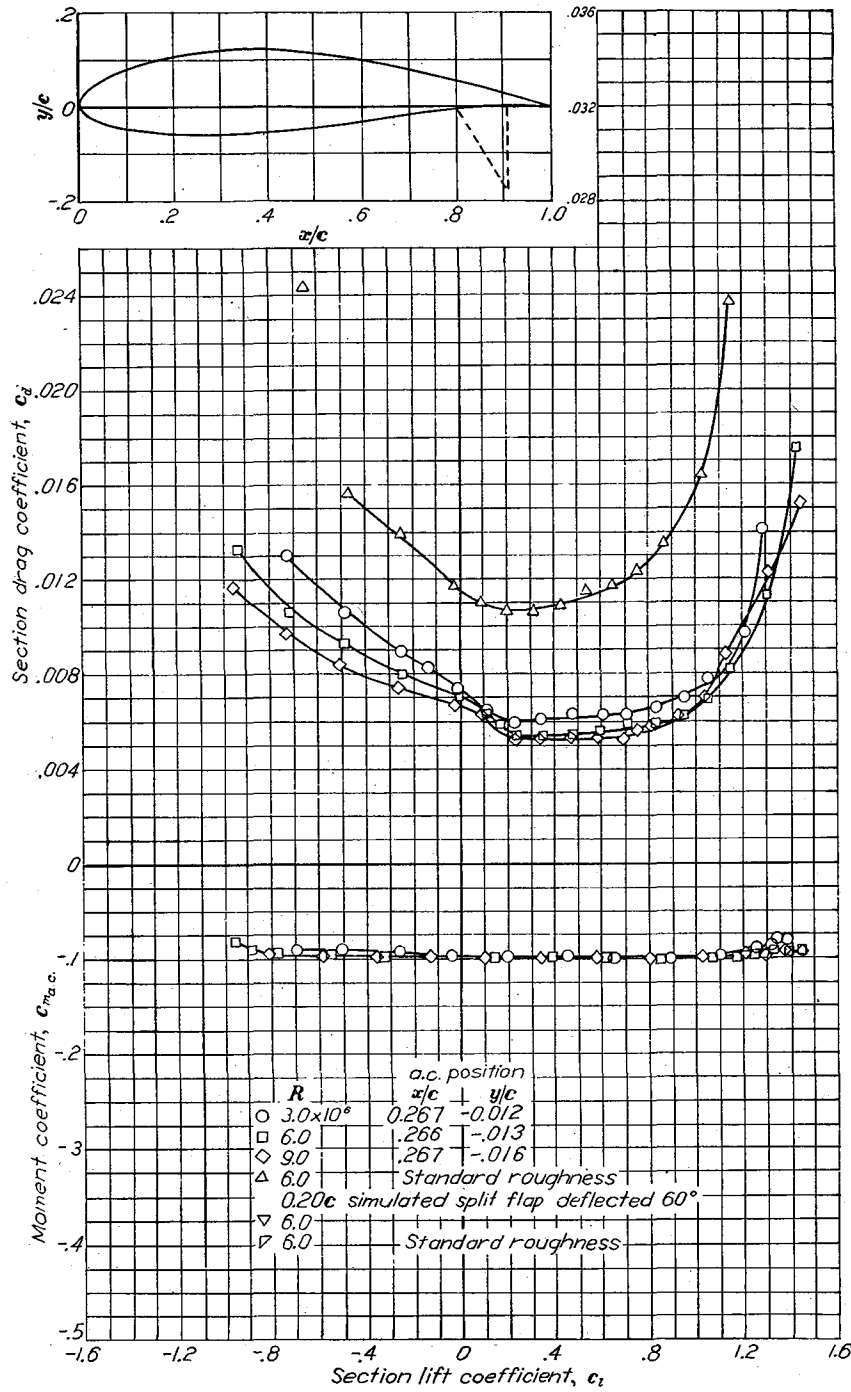
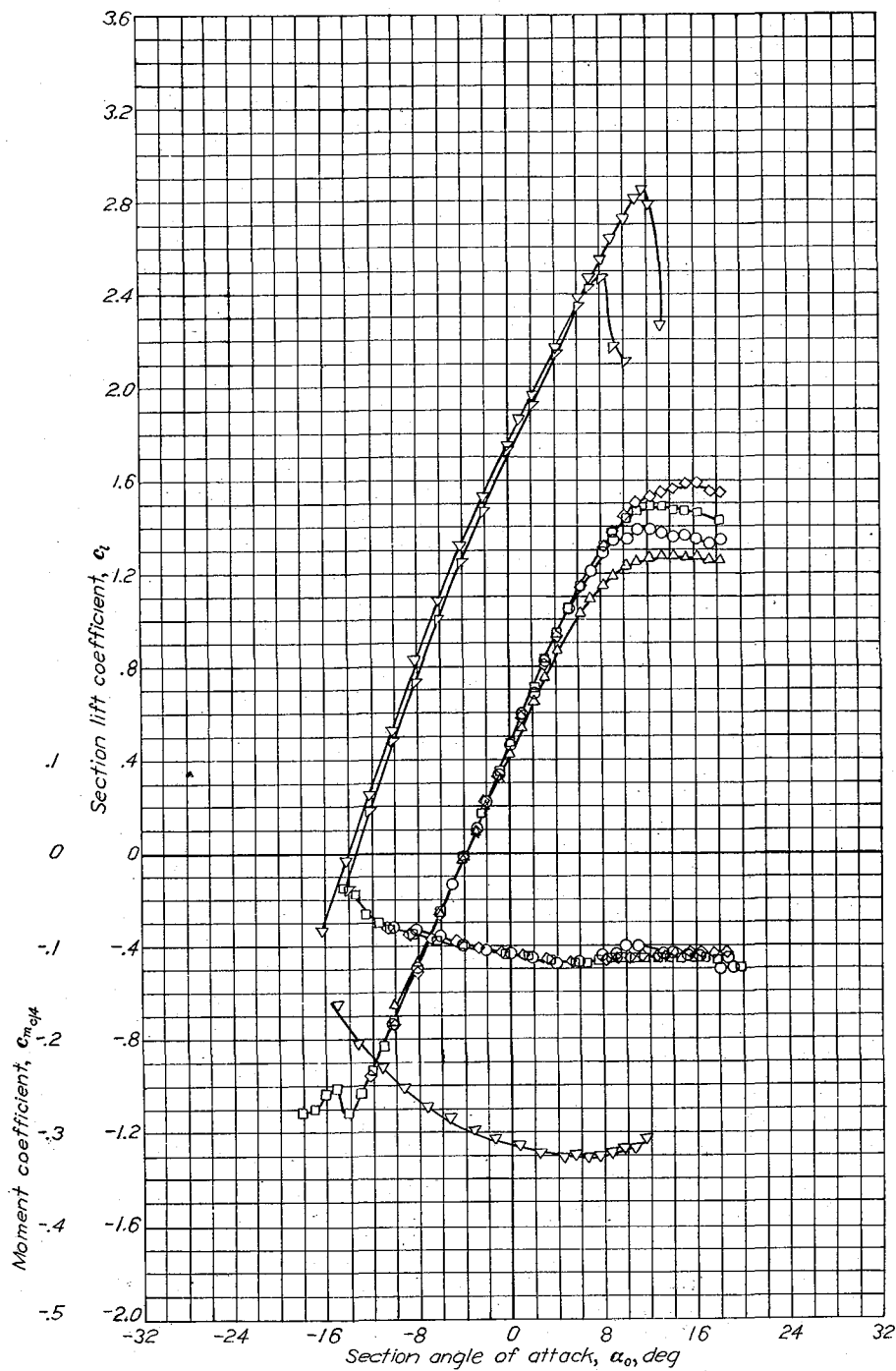


Aerodynamic characteristics of the NACA 633-218 airfoil section, 24-inch chord.

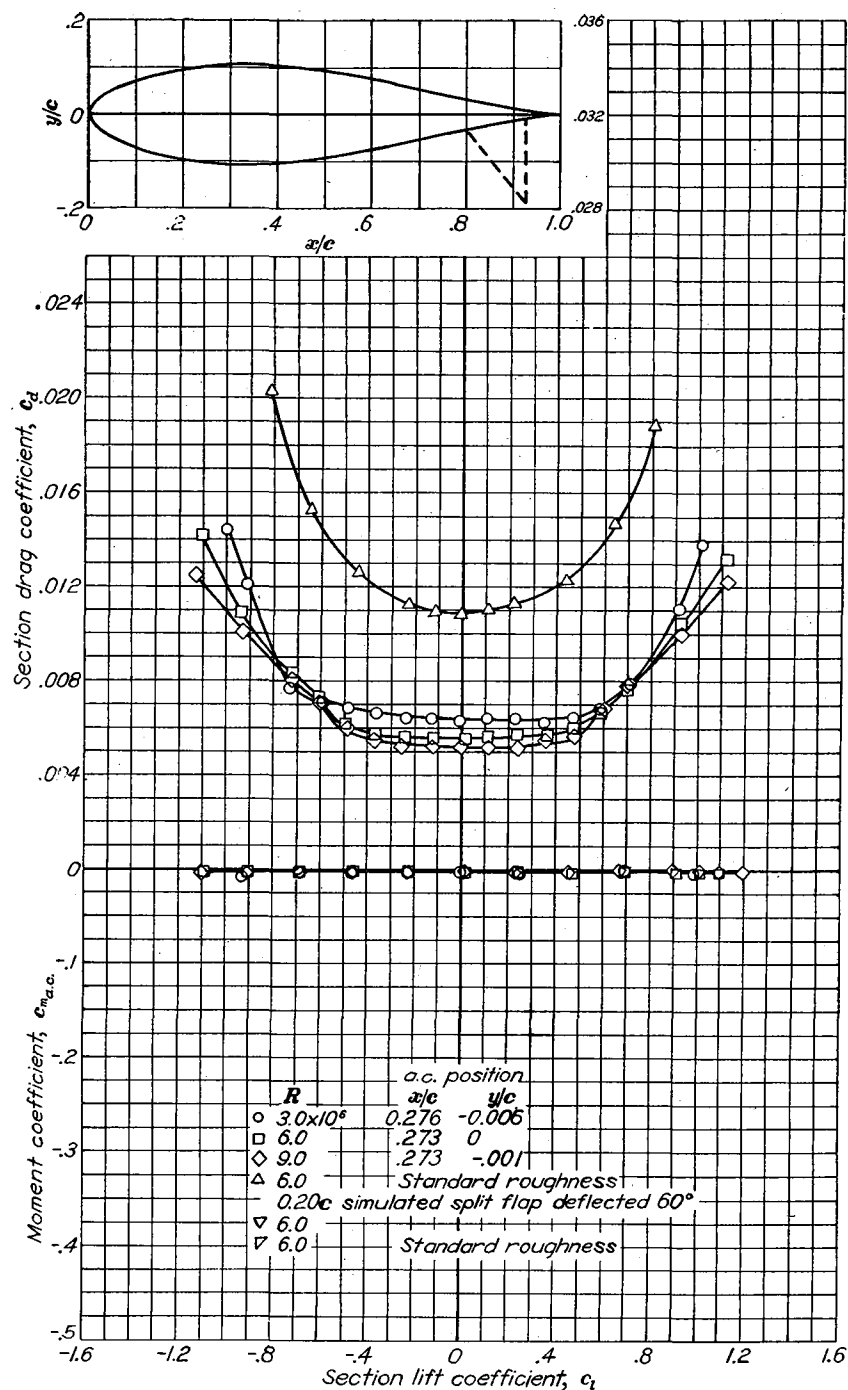
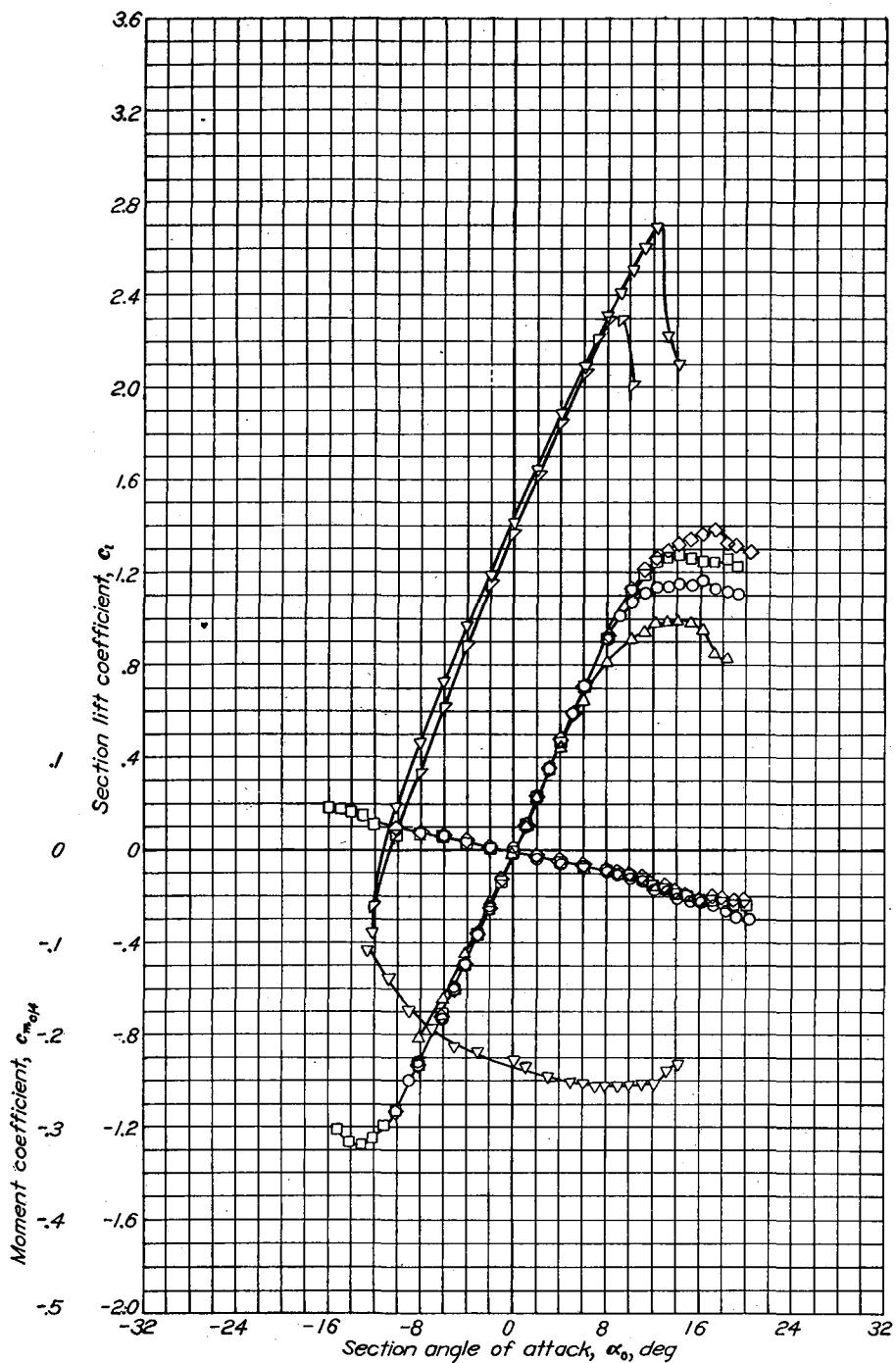




Aerodynamic characteristics of the NACA 633-418 airfoil section, 24-inch chord.

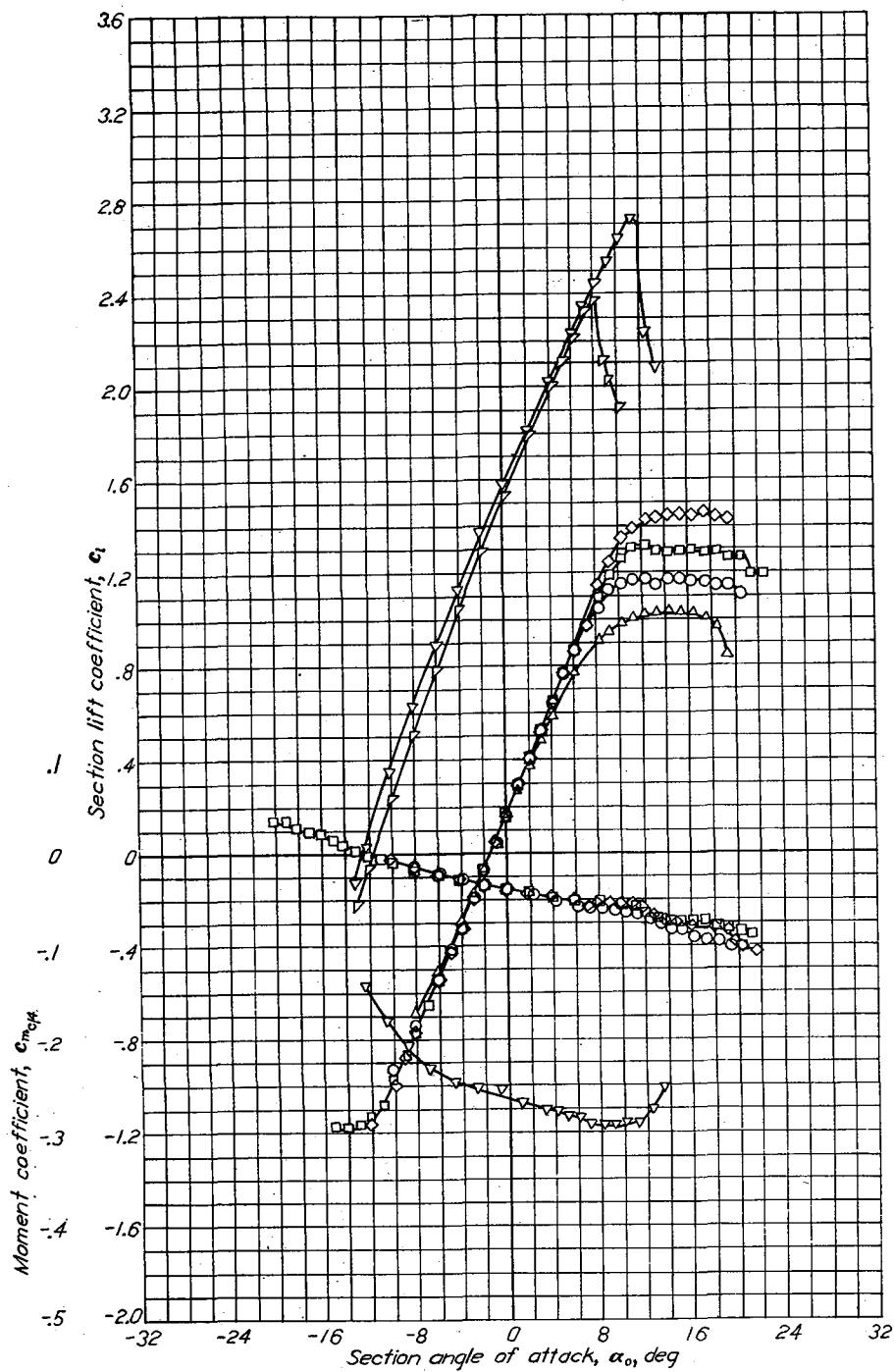


Aerodynamic characteristics of the NACA 63-618 airfoil section, 24-inch chord.

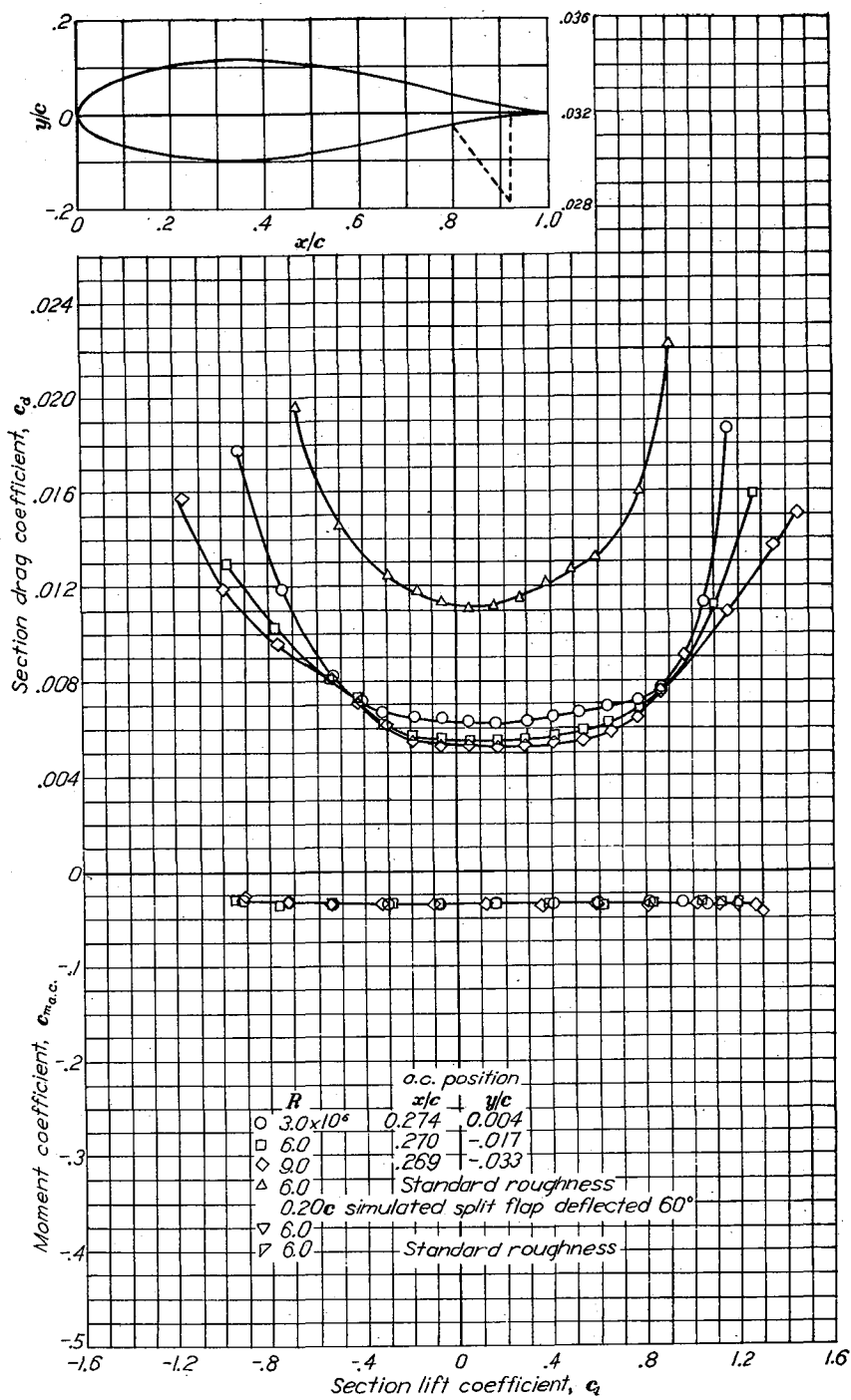


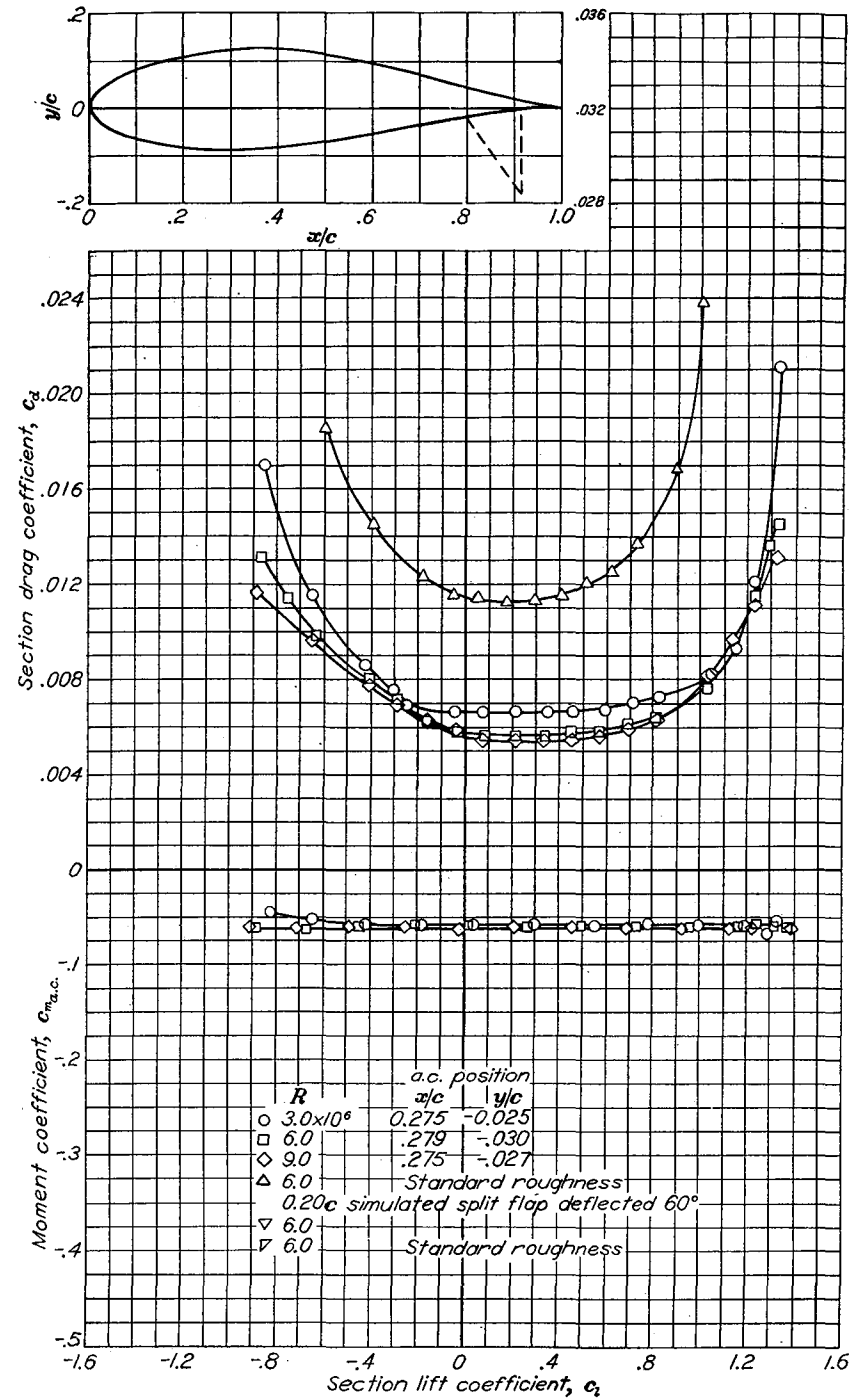
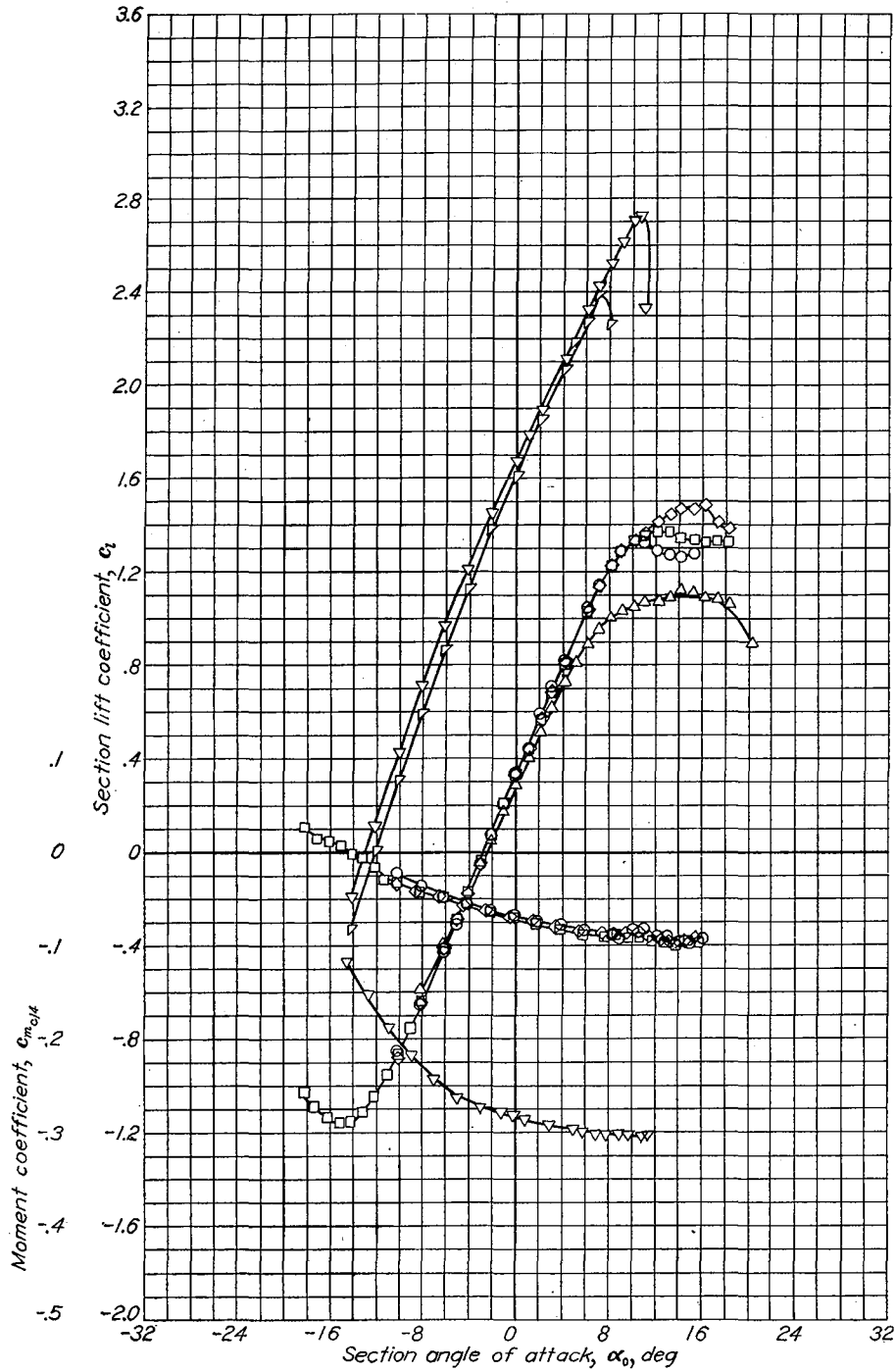
Aerodynamic characteristics of the NACA 634-021 airfoil section, 24-inch chord.



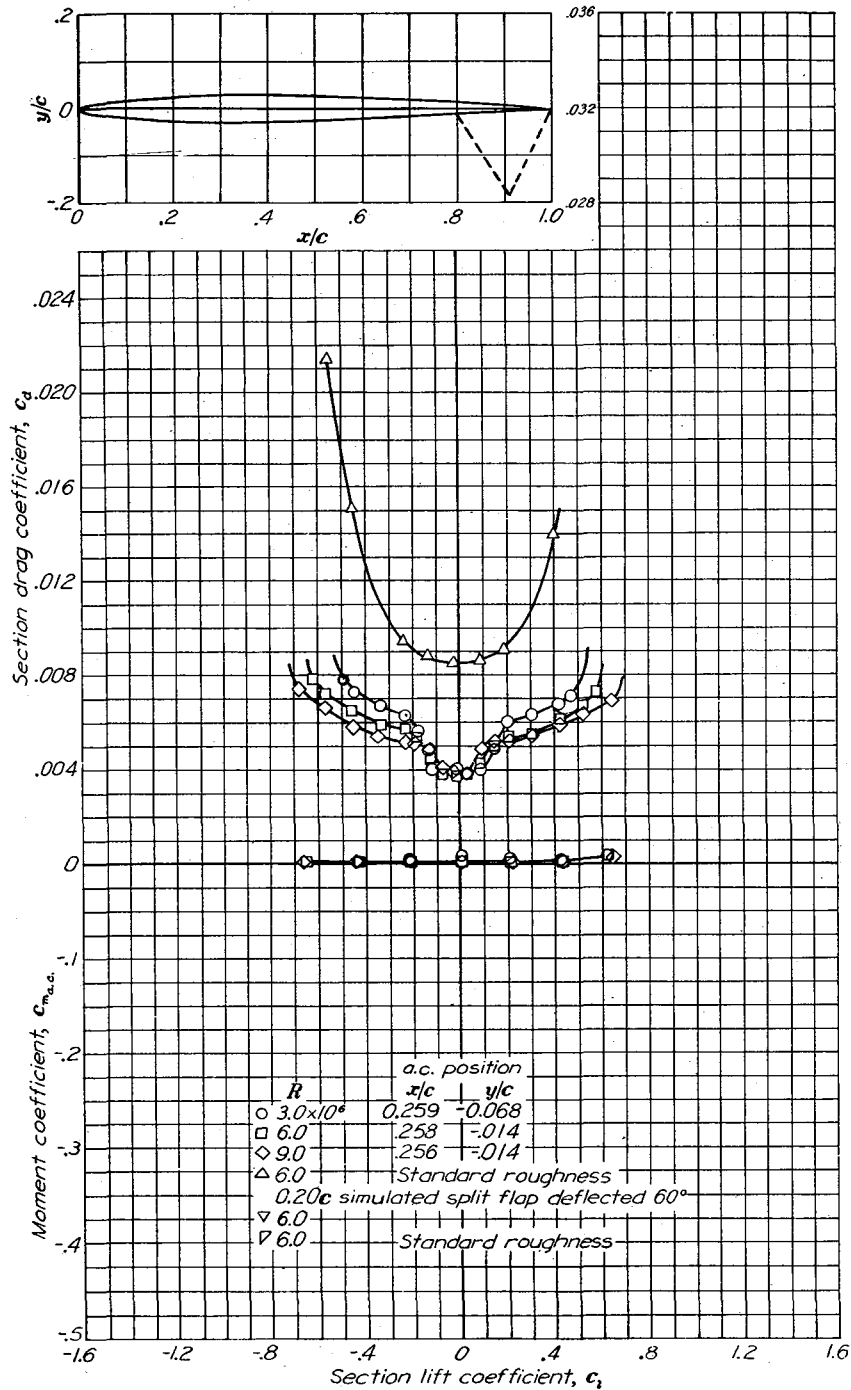
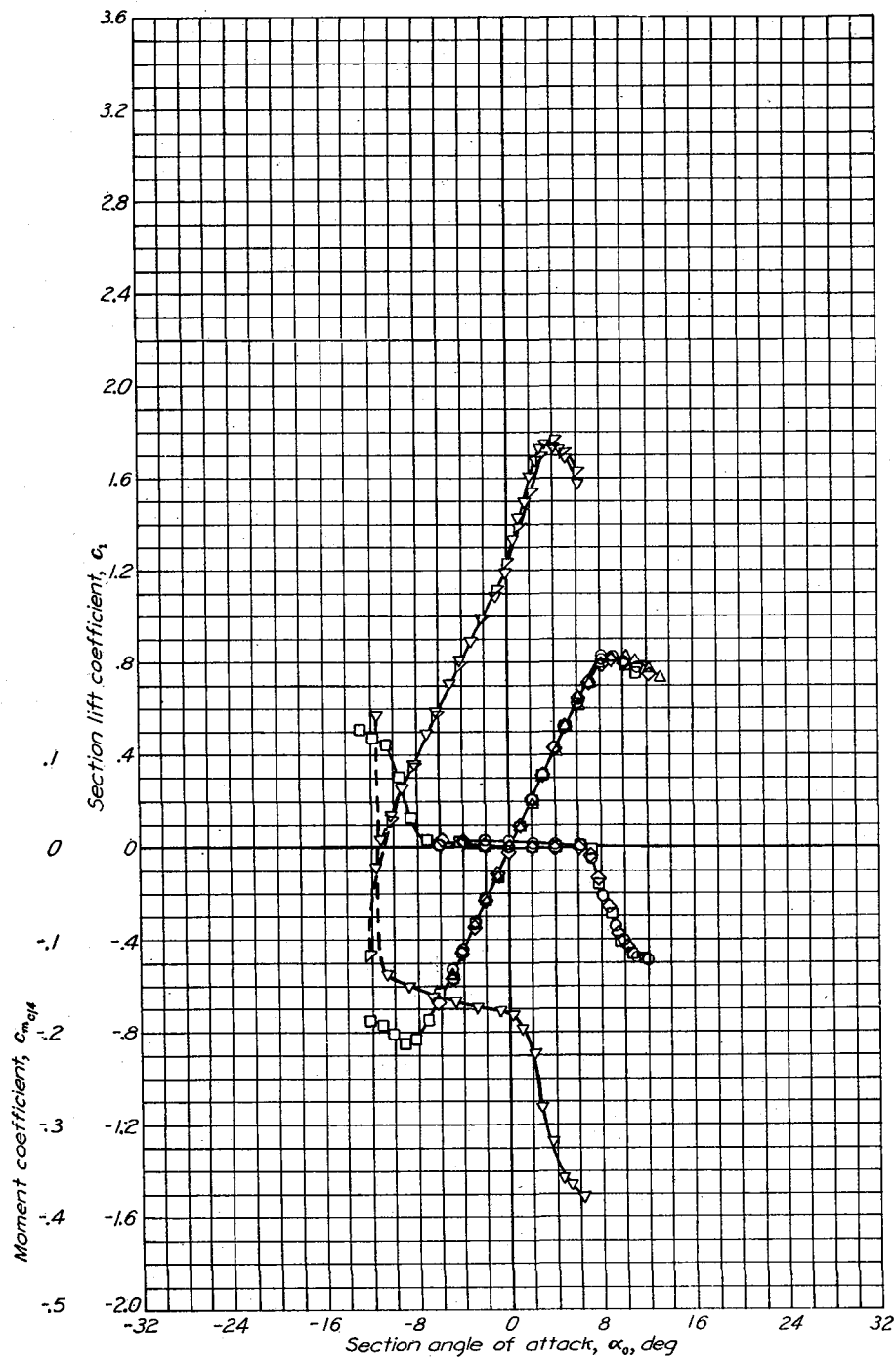


Aerodynamic characteristics of the NACA 634-221 airfoil section, 24-inch chord.

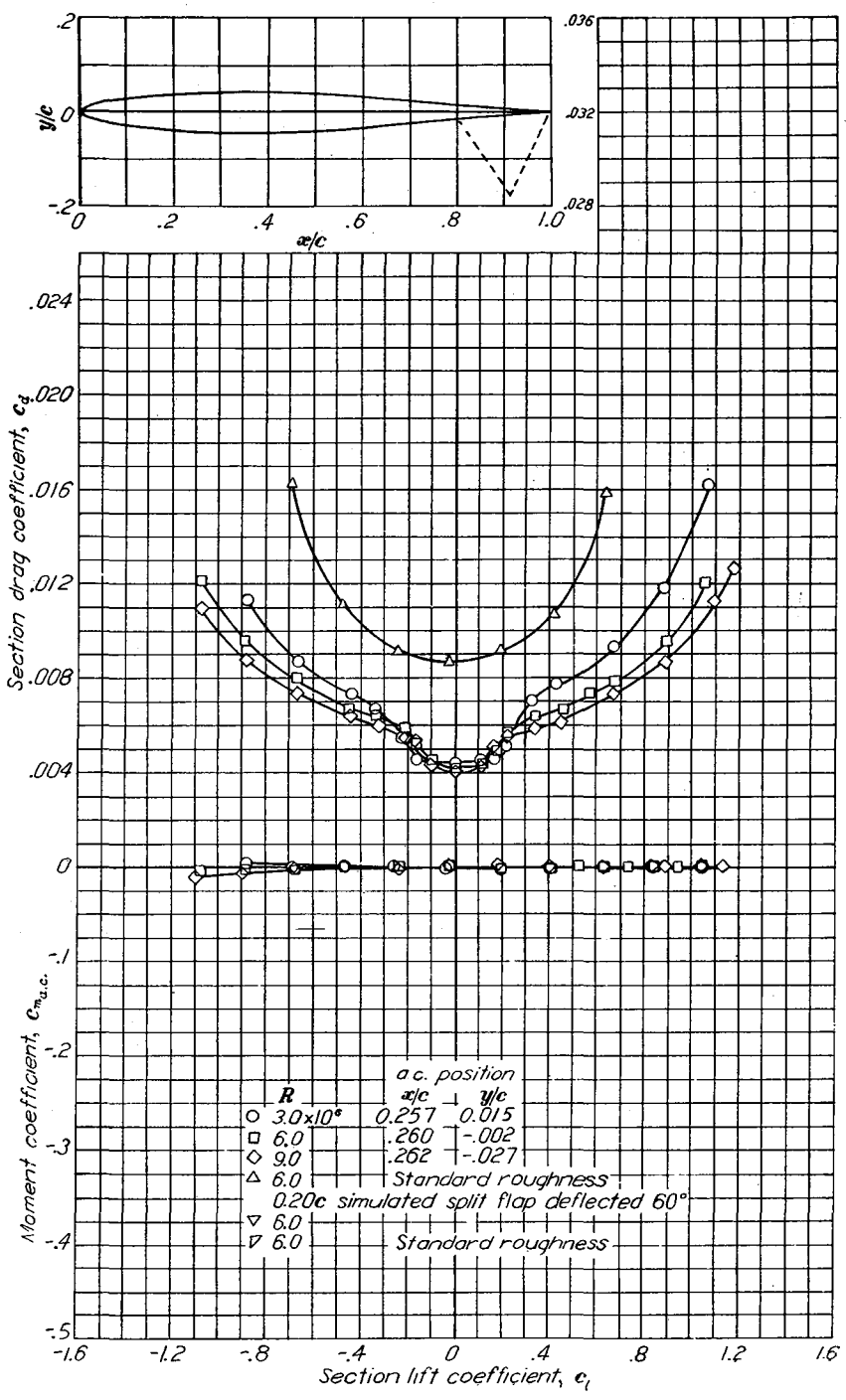
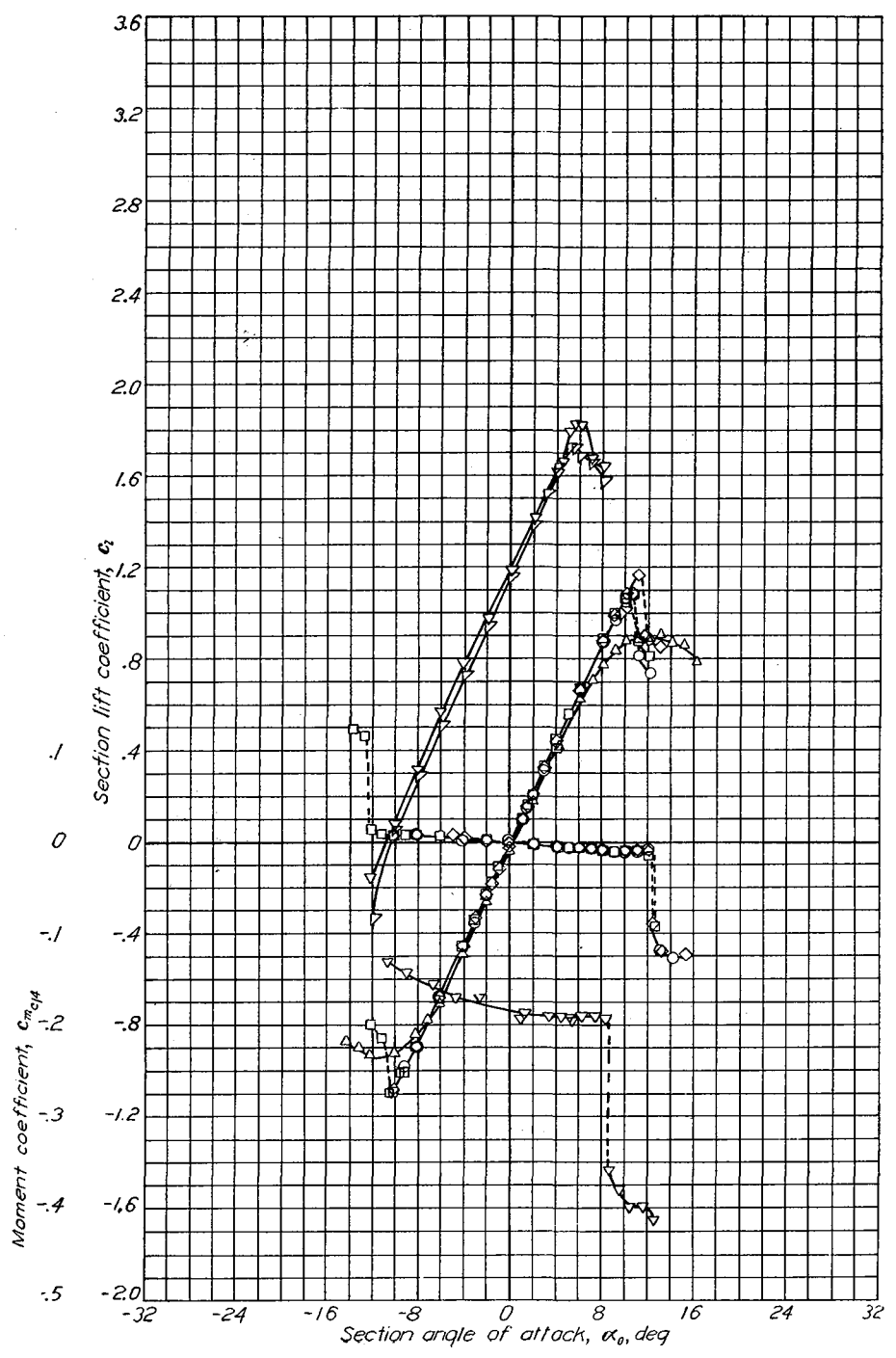




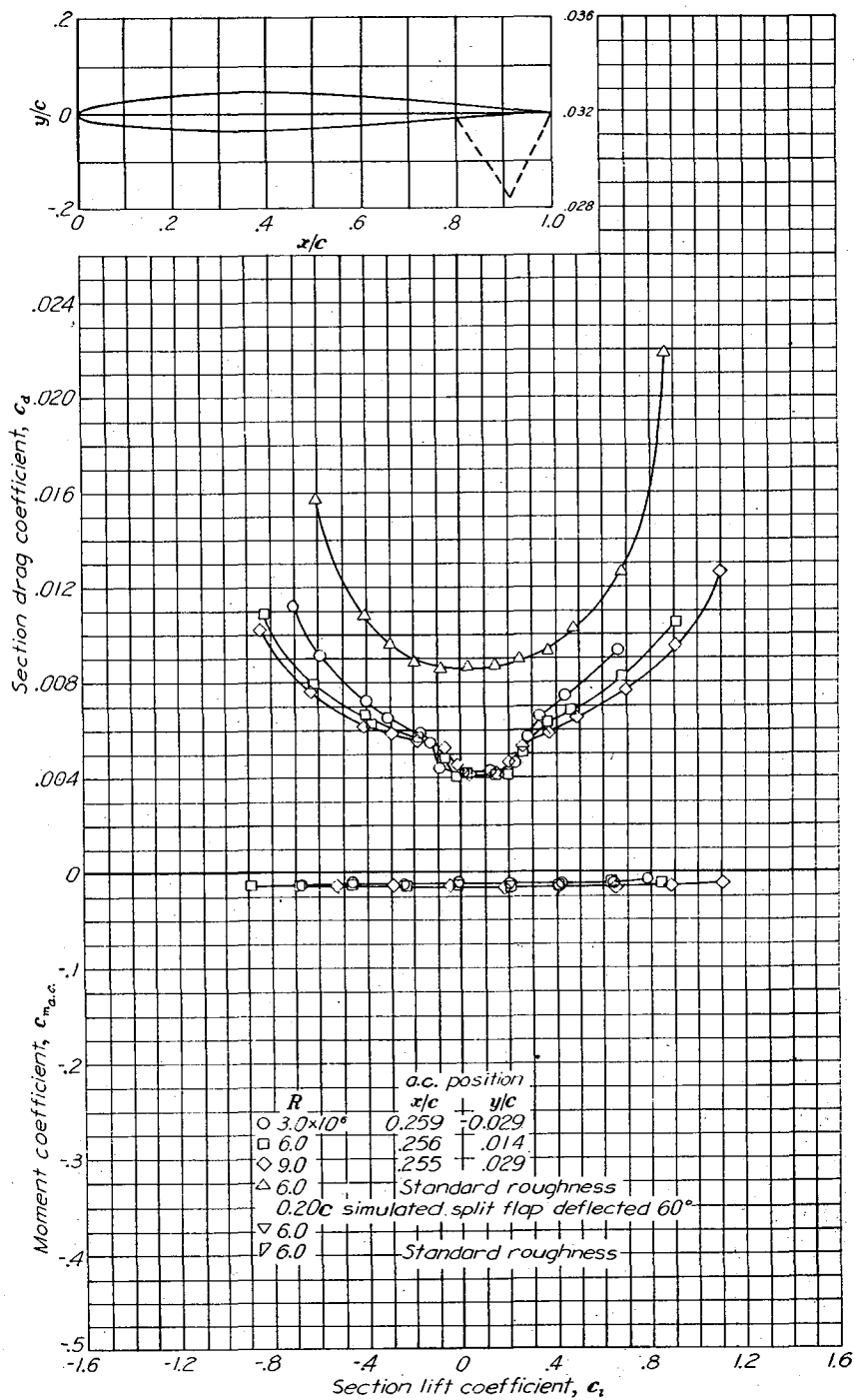
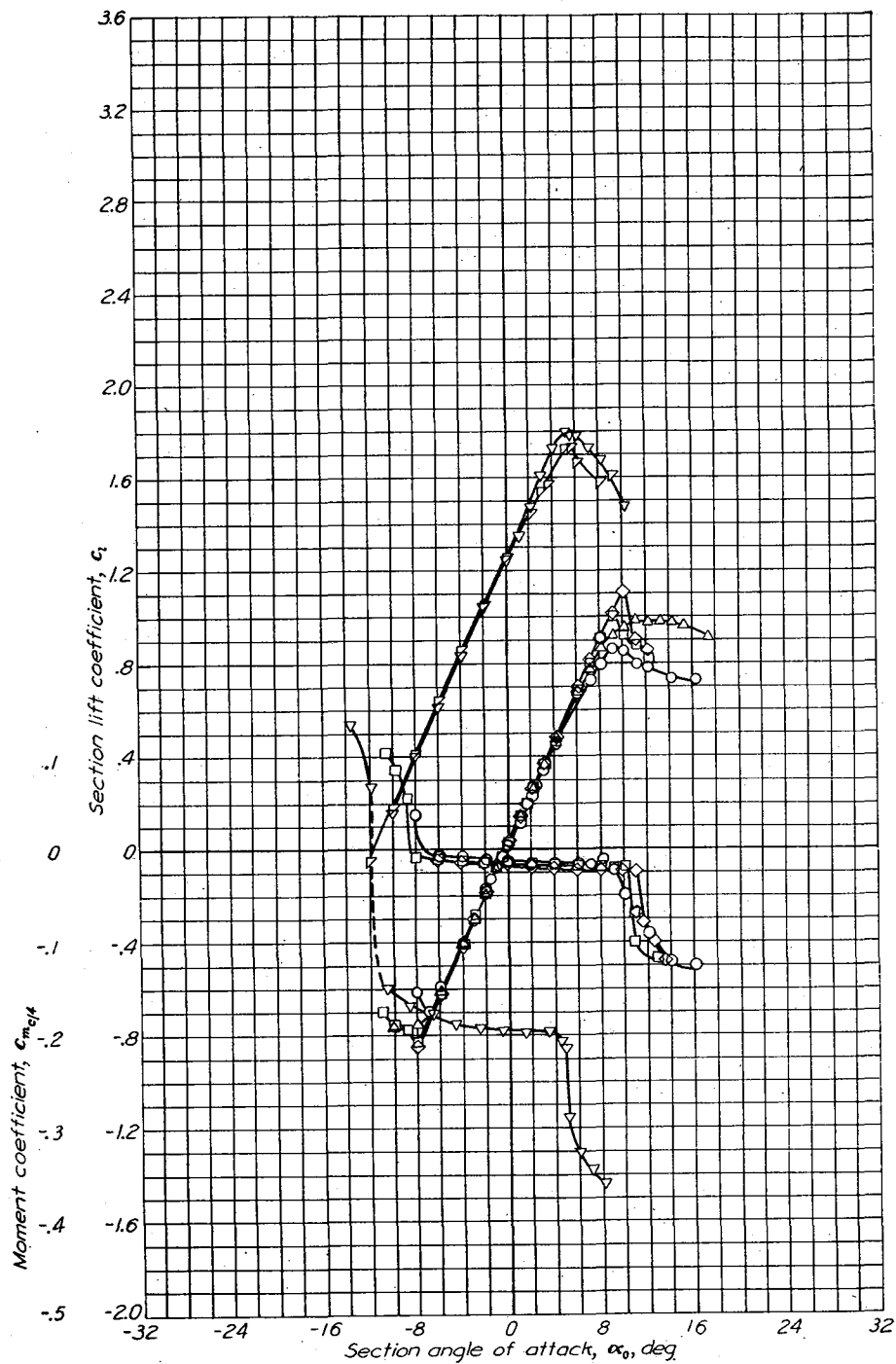
Aerodynamic characteristics of the NACA 634-421 airfoil section, 24-inch chord.



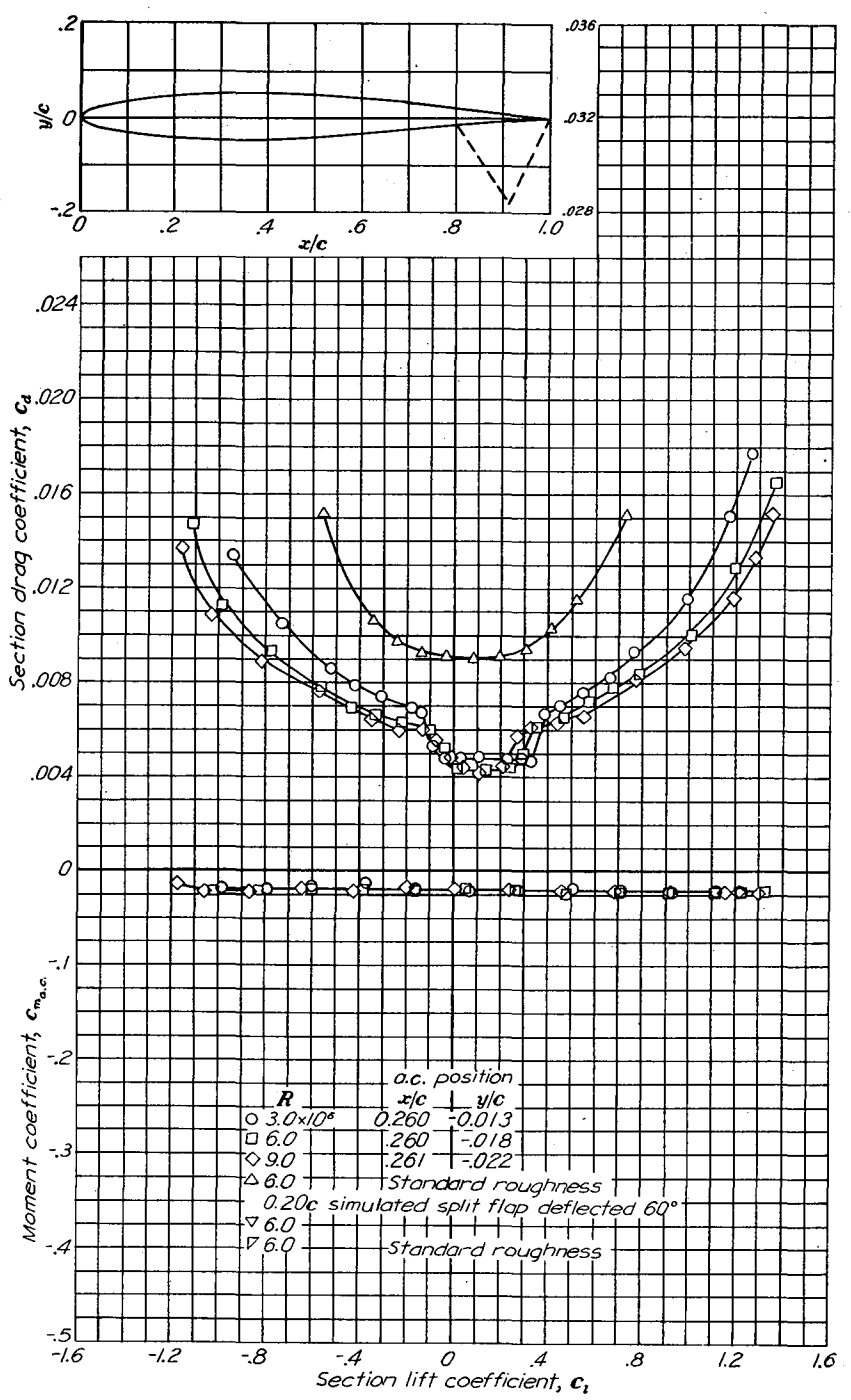
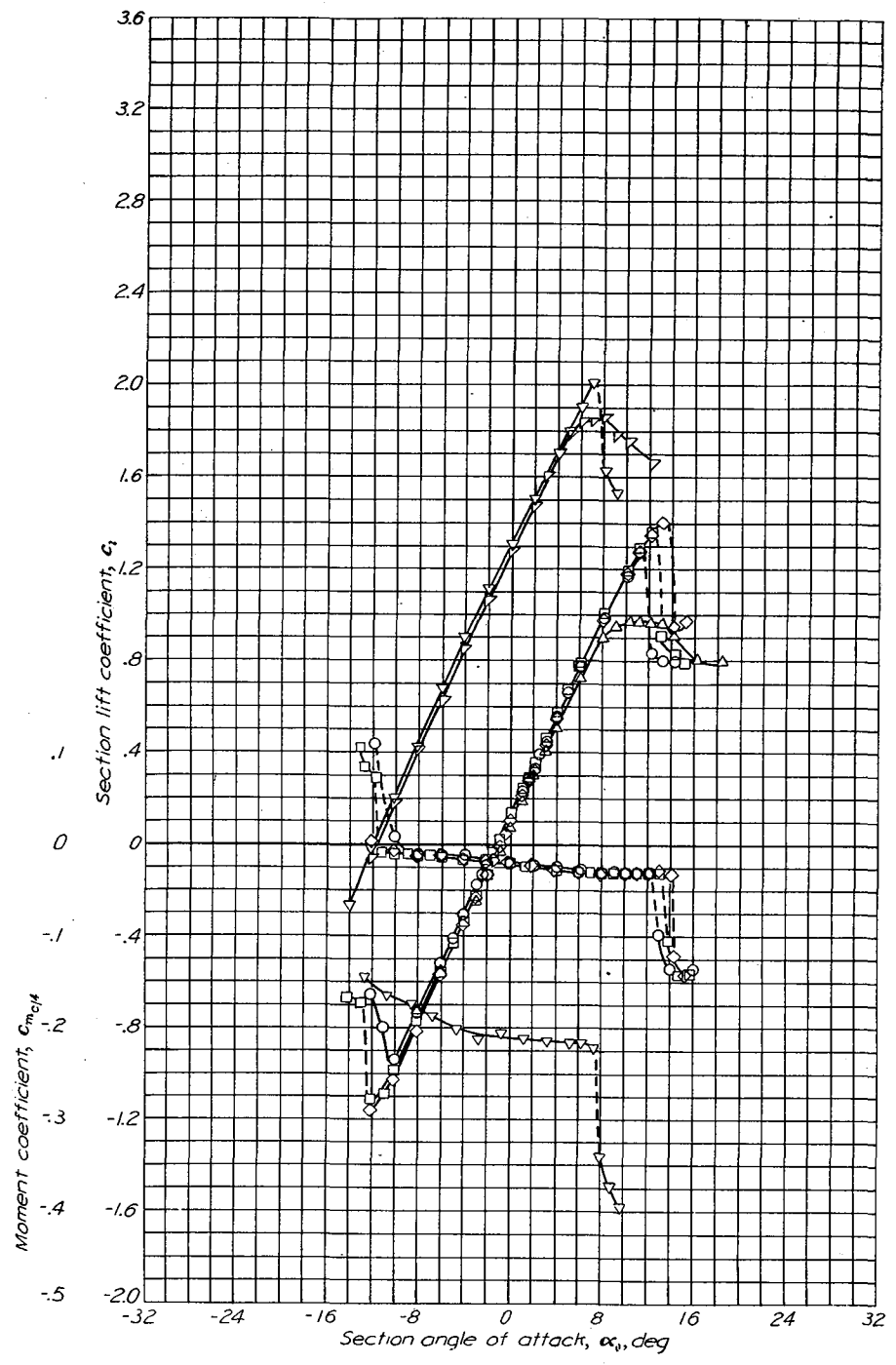
Aerodynamic characteristics of the NACA 64-006 airfoil section, 24-inch chord.



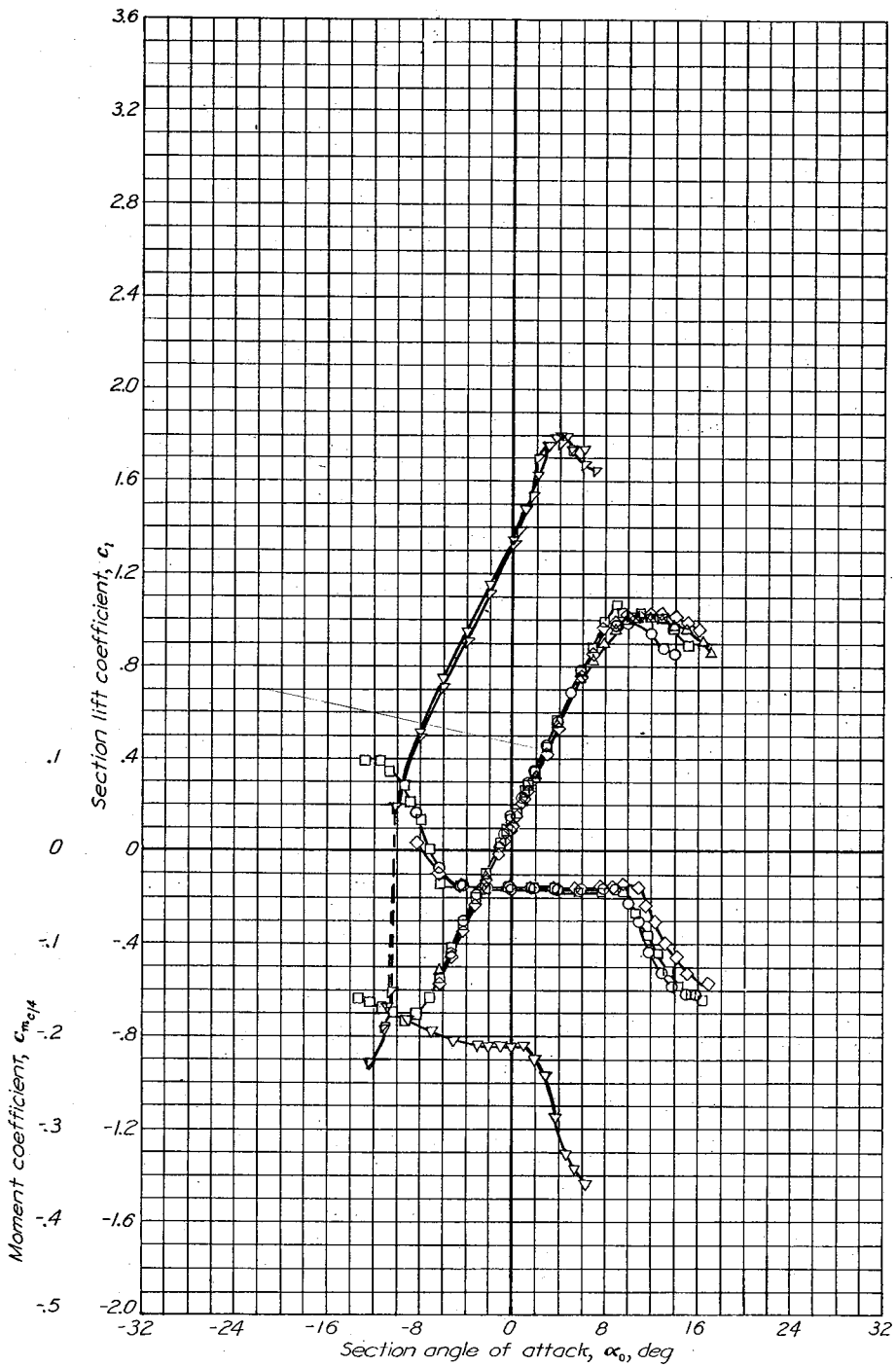
Aerodynamic characteristics of the NACA 64-009 airfoil section, 24-inch chord.



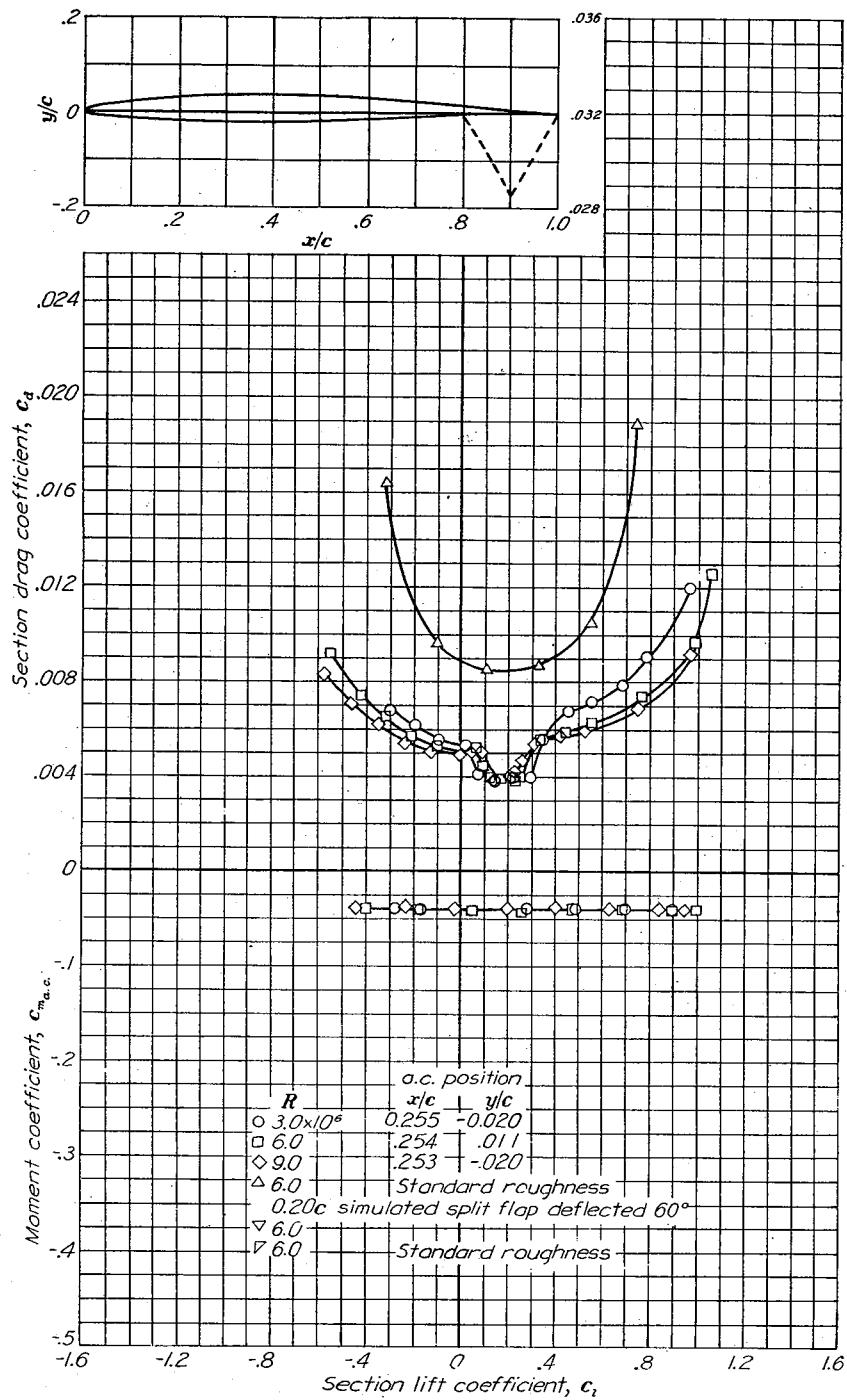
Aerodynamic characteristics of the NACA 64-108 airfoil section, 24-inch chord.

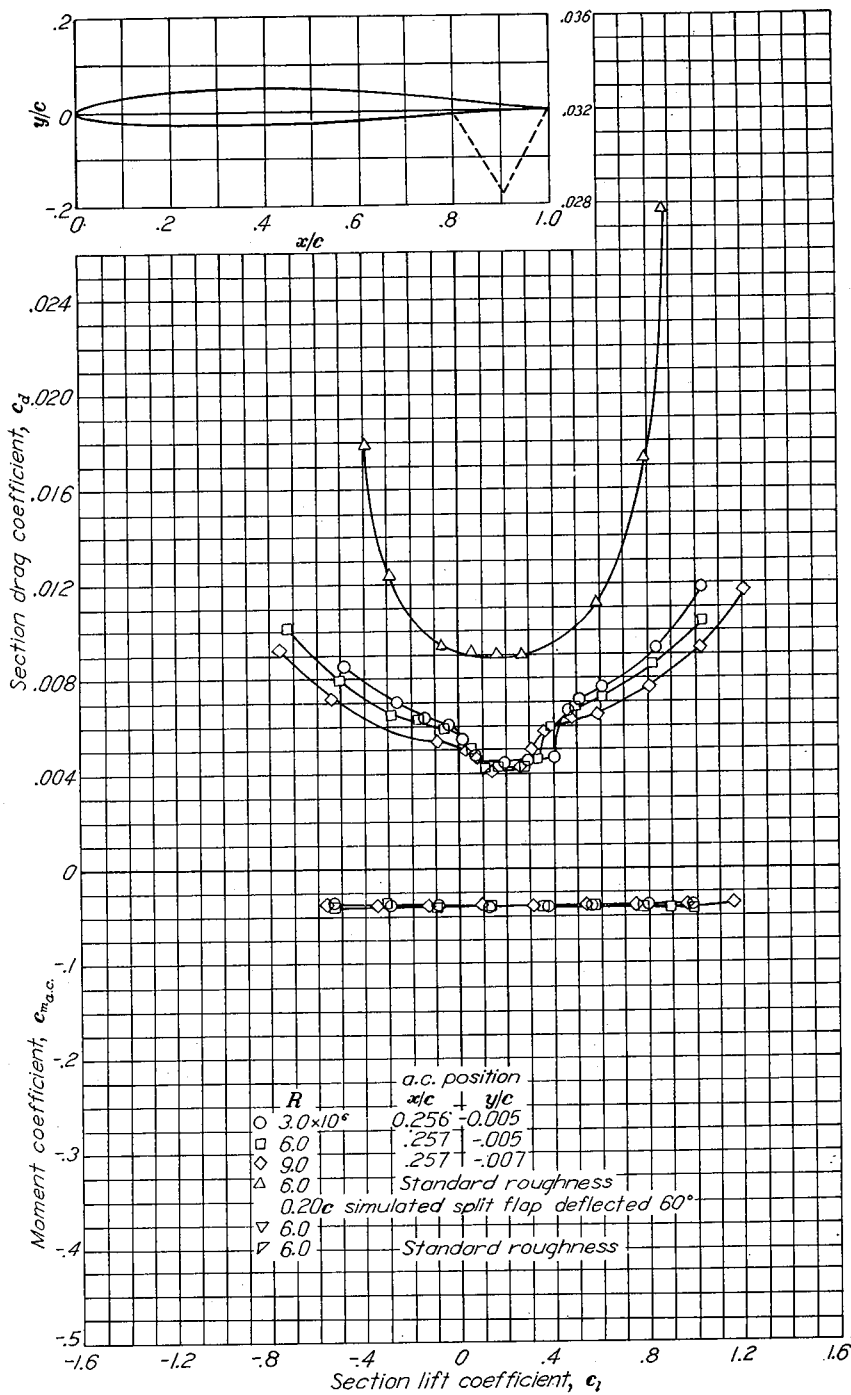
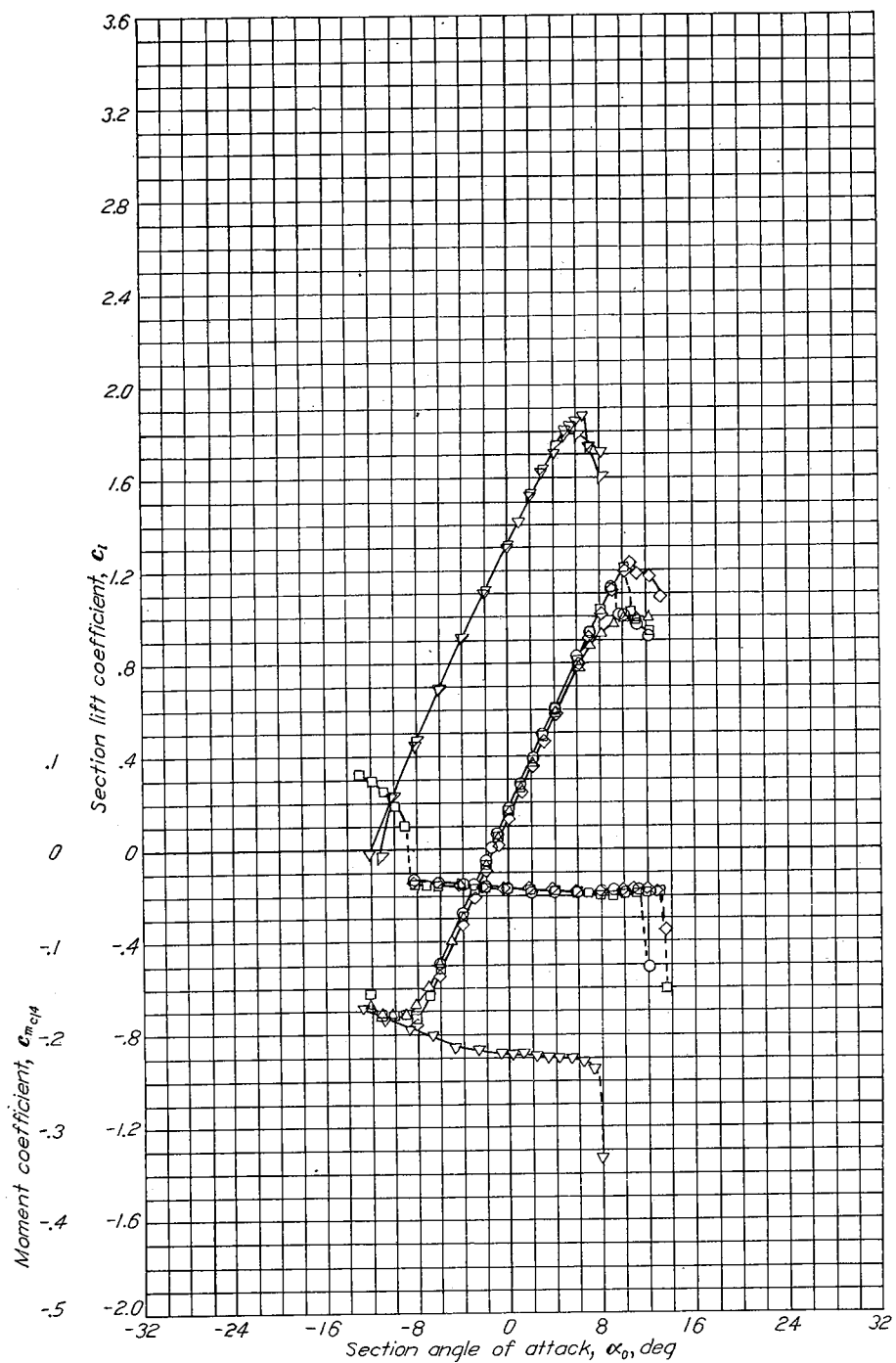


Aerodynamic characteristics of the NACA 64-110 airfoil section, 24-inch chord.



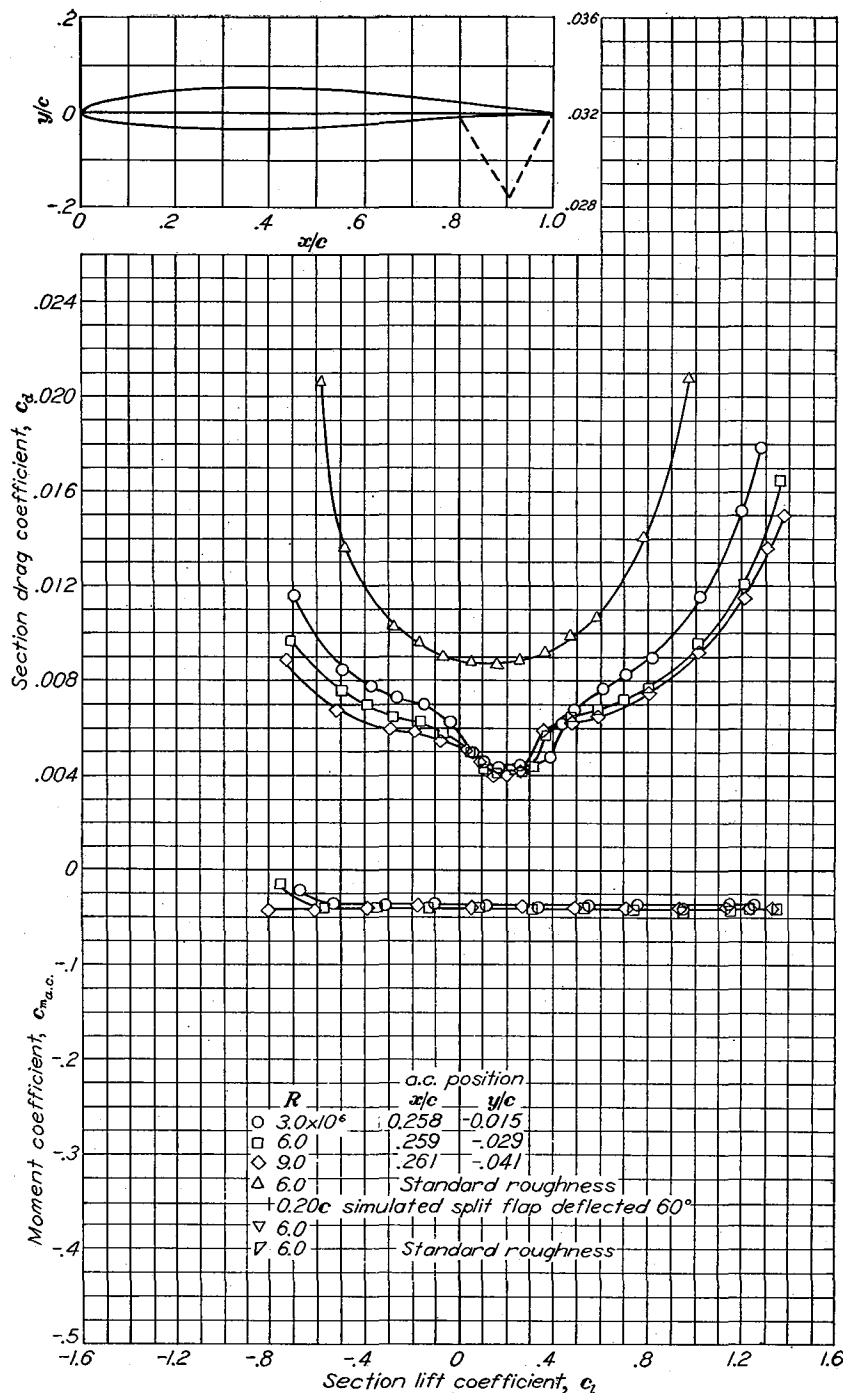
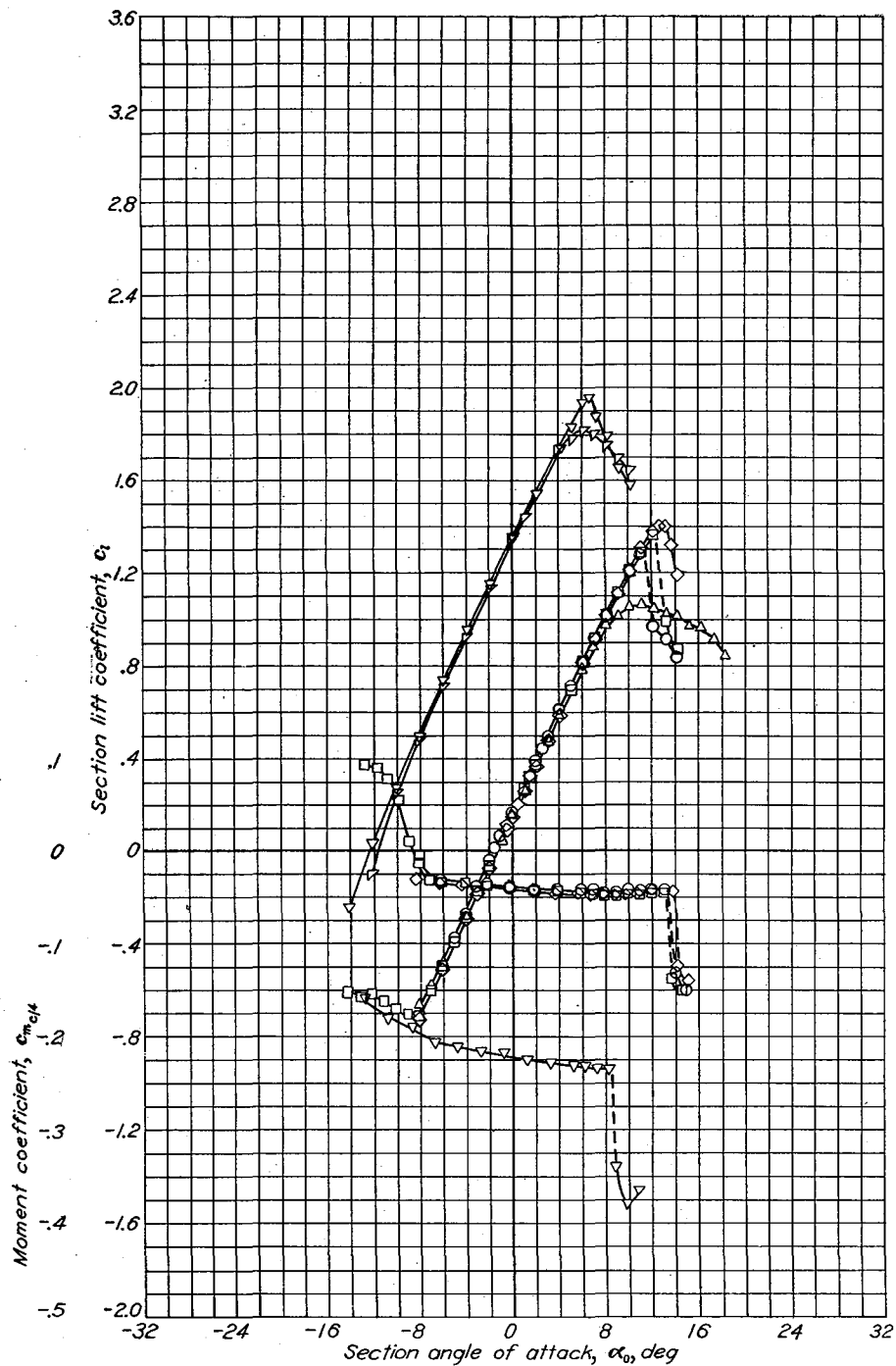
Aerodynamic characteristics of the NACA 64-206 airfoil section, 24-inch chord.



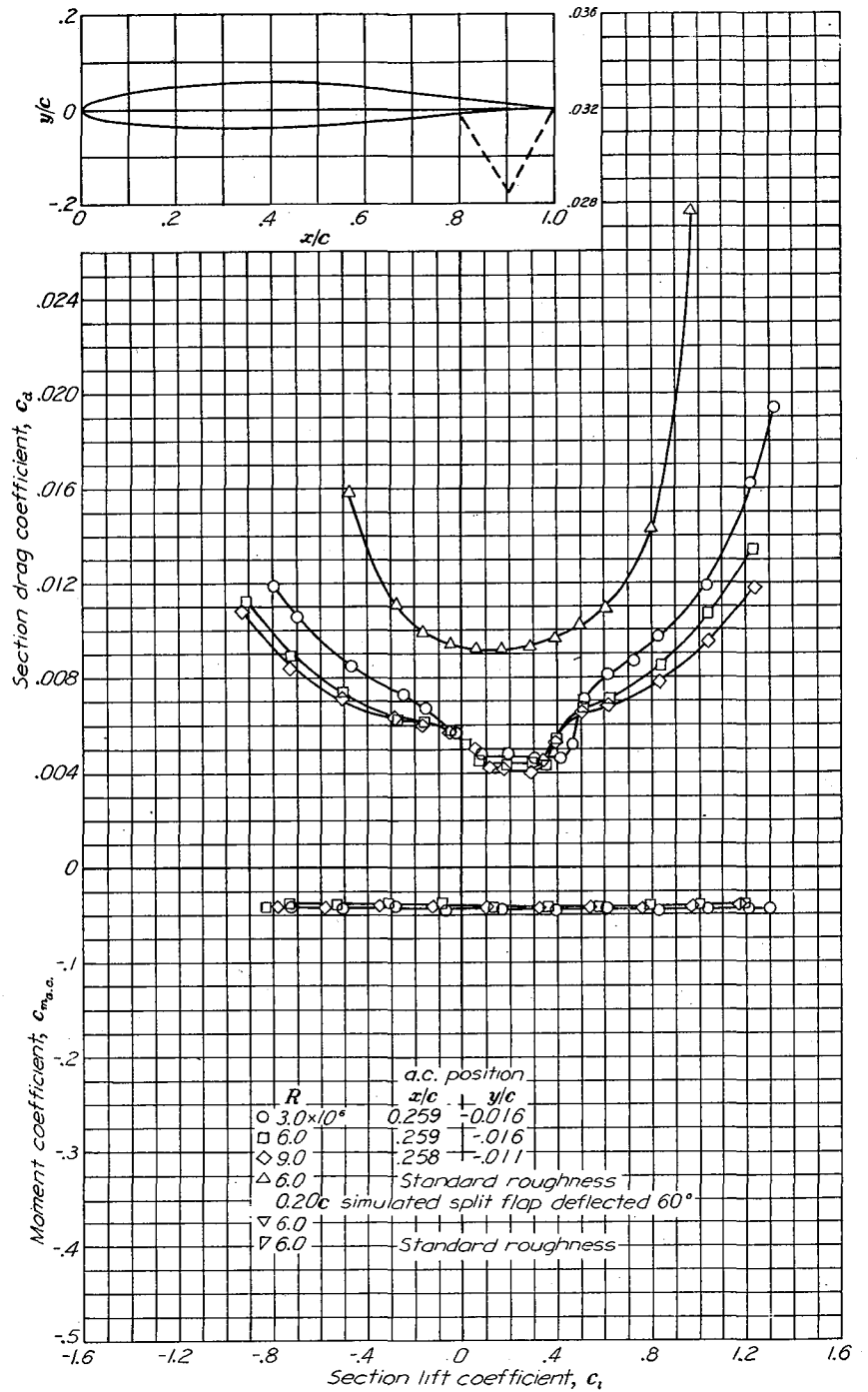
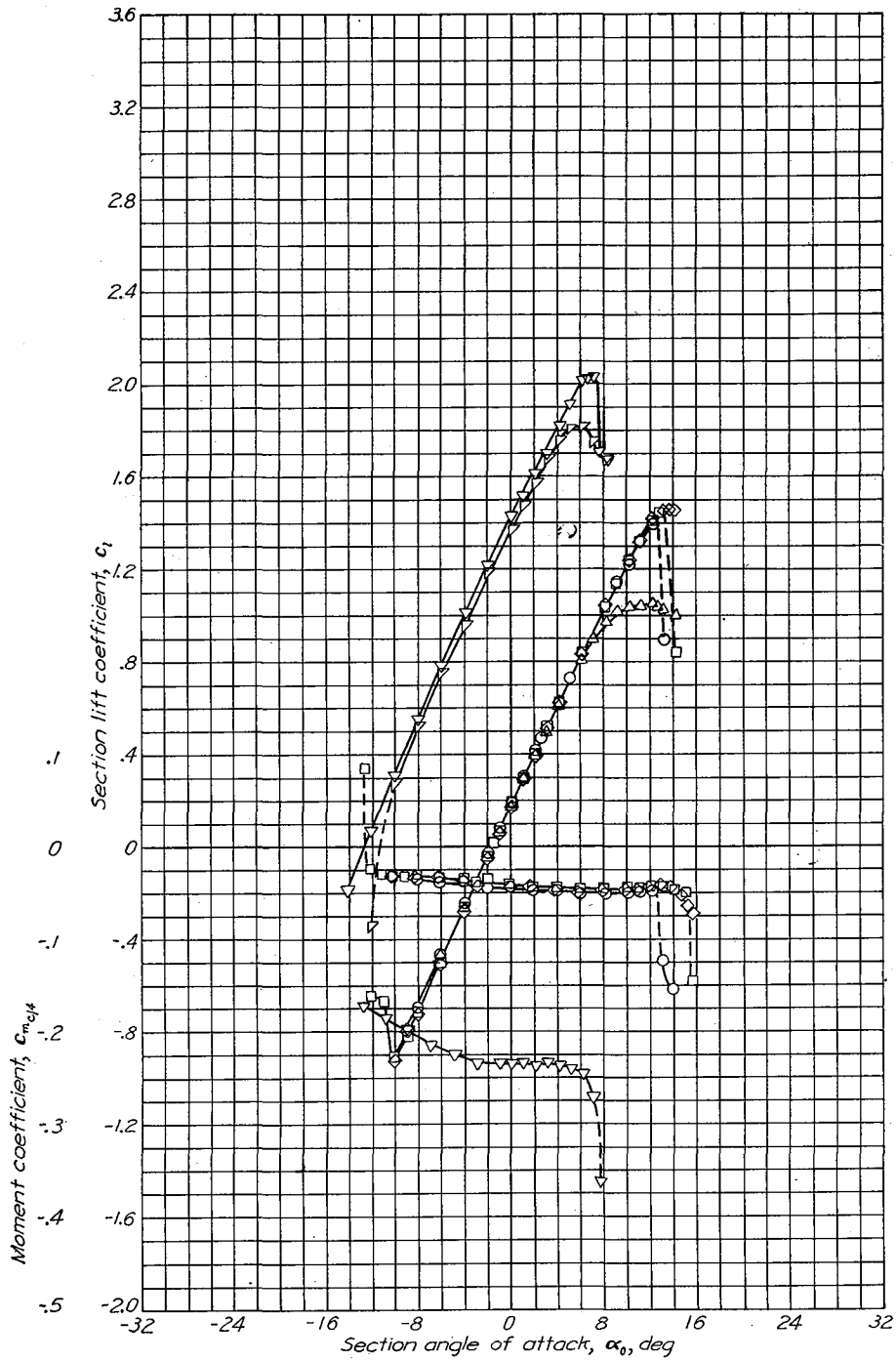


Aerodynamic characteristics of the NACA 64-208 airfoil section, 24-inch chord.

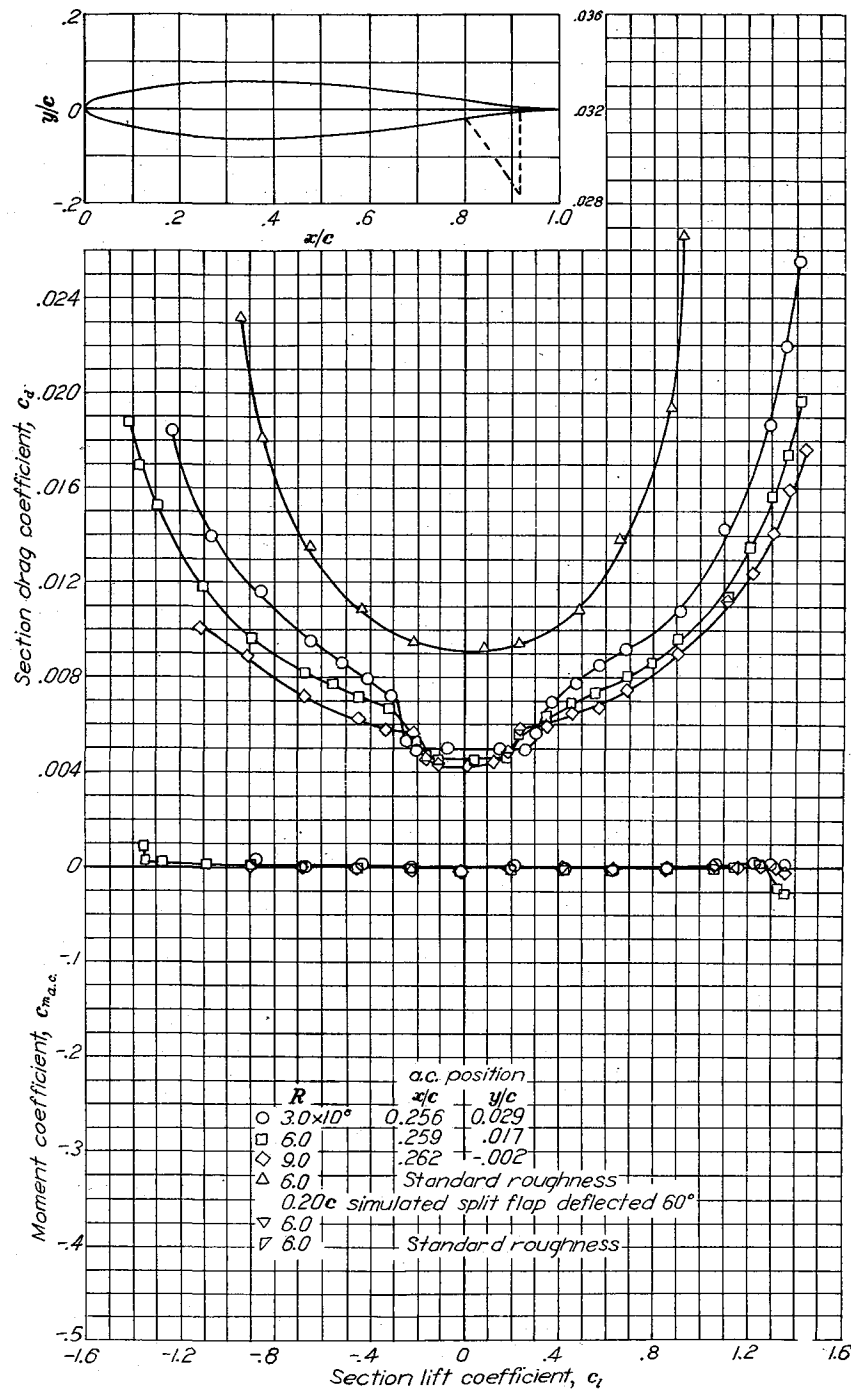
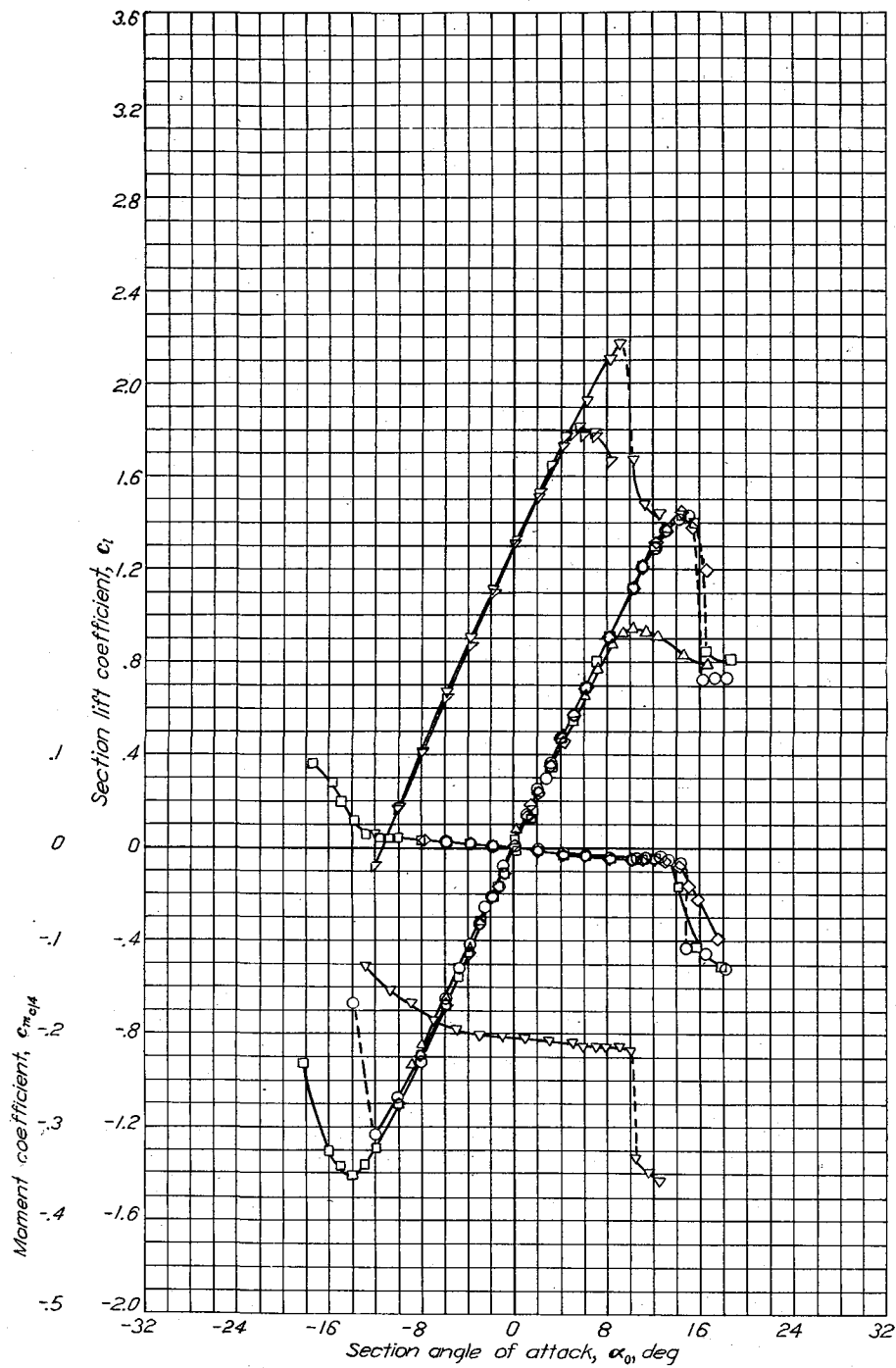




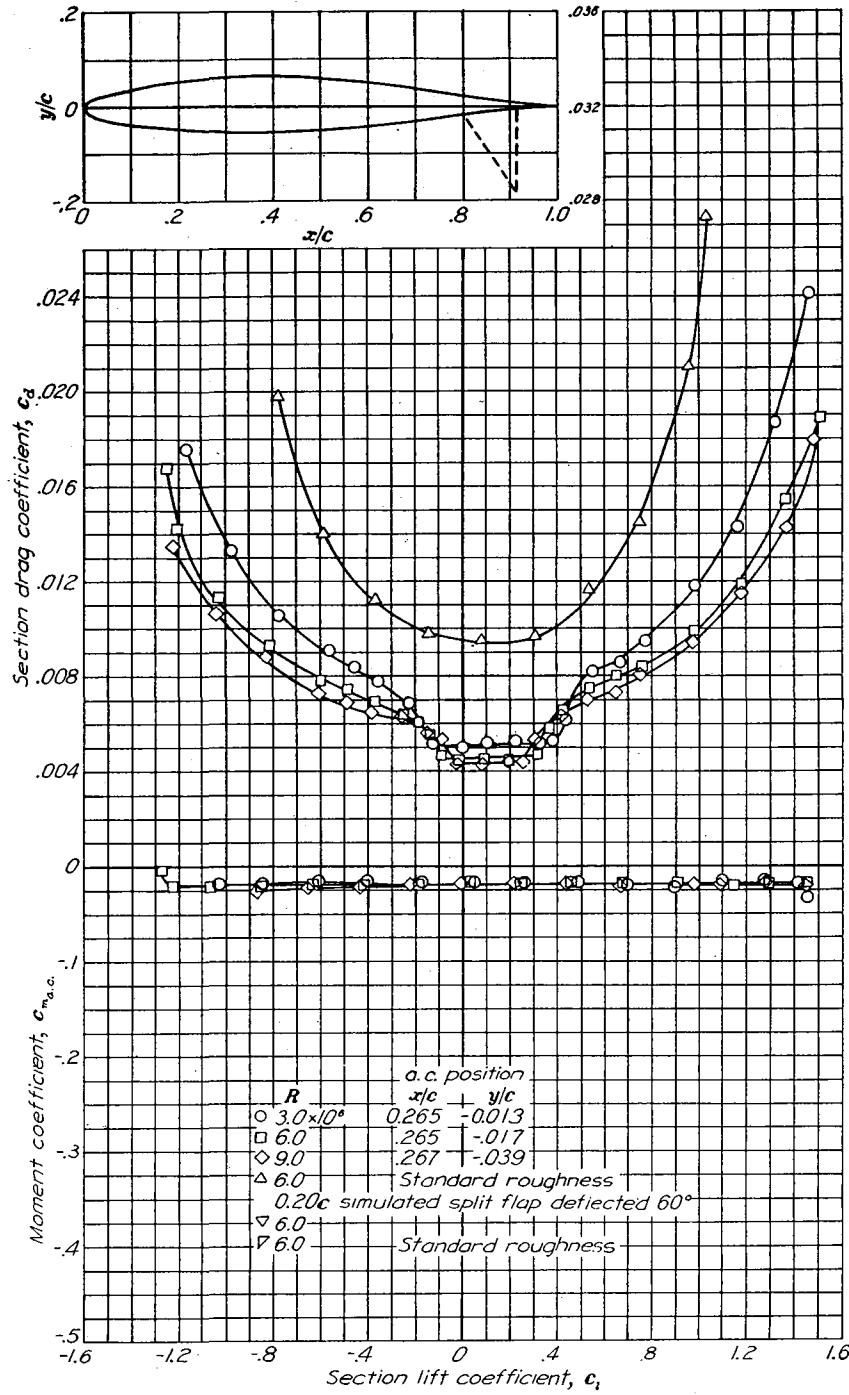
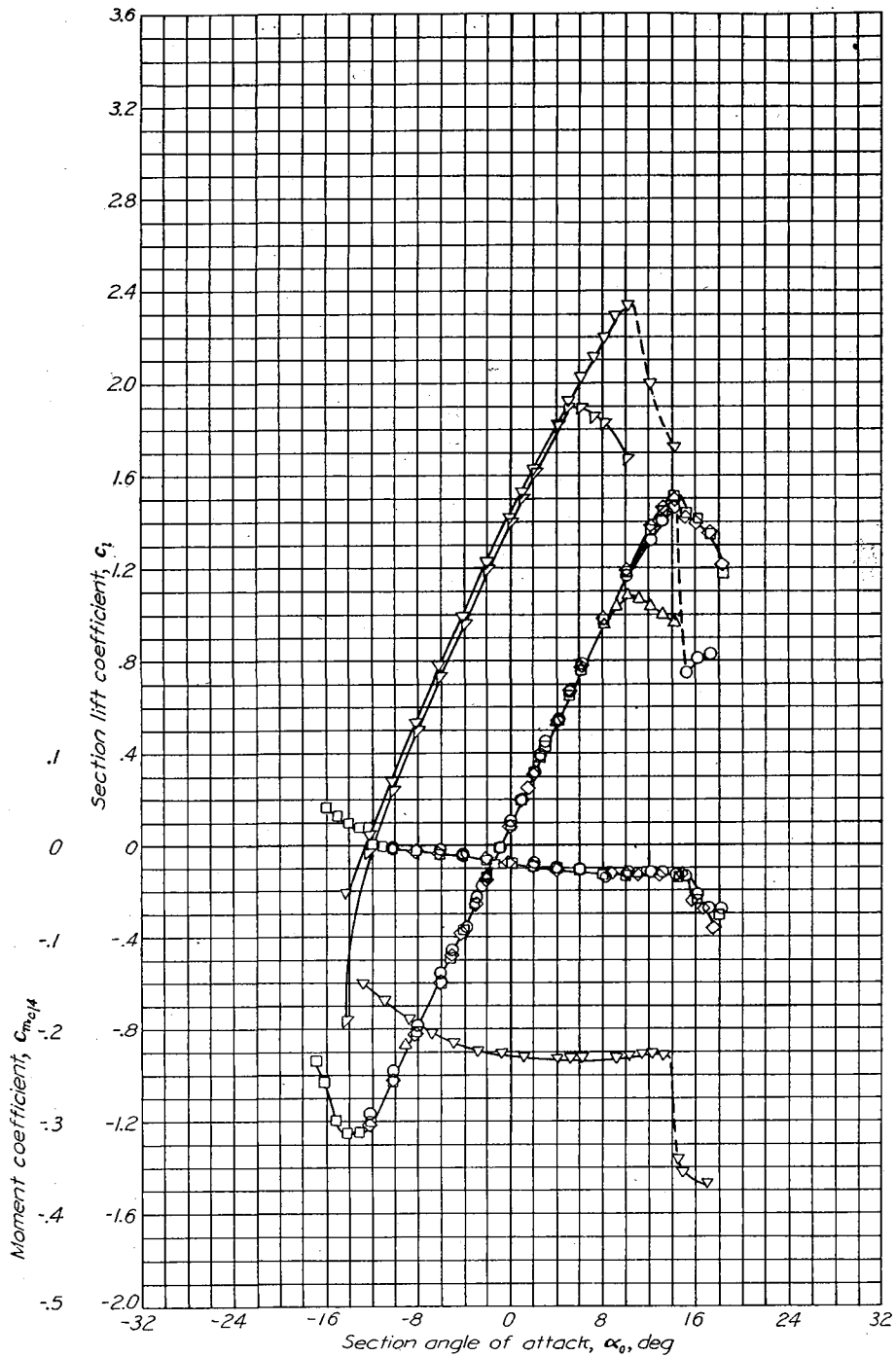
Aerodynamic characteristics of the NACA 64-209 airfoil section, 24-inch chord.



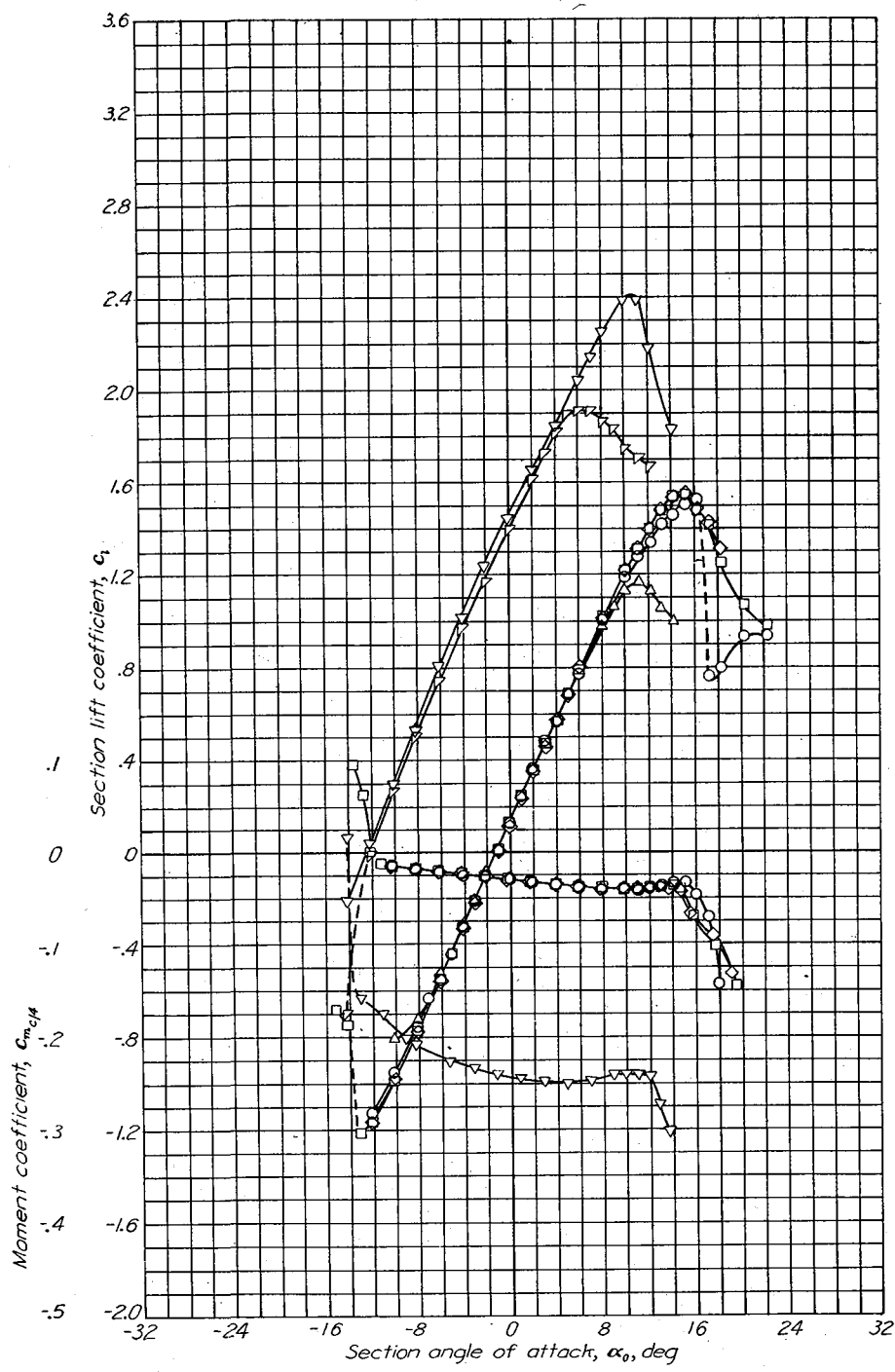
Aerodynamic characteristics of the NACA 64-210 airfoil section, 24-inch chord.



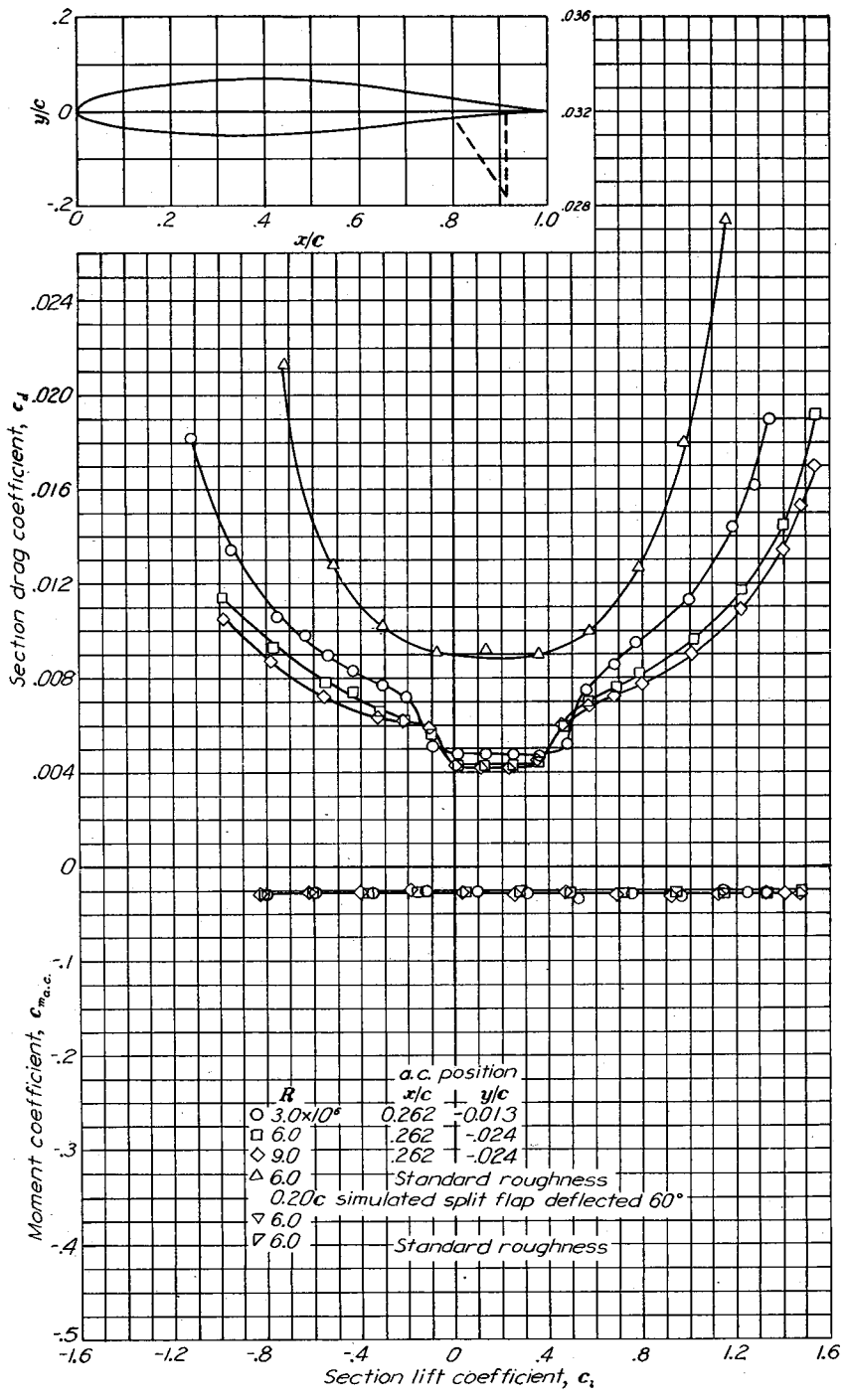
Aerodynamic characteristics of the NACA 64-1-012 airfoil section, 24-inch chord.

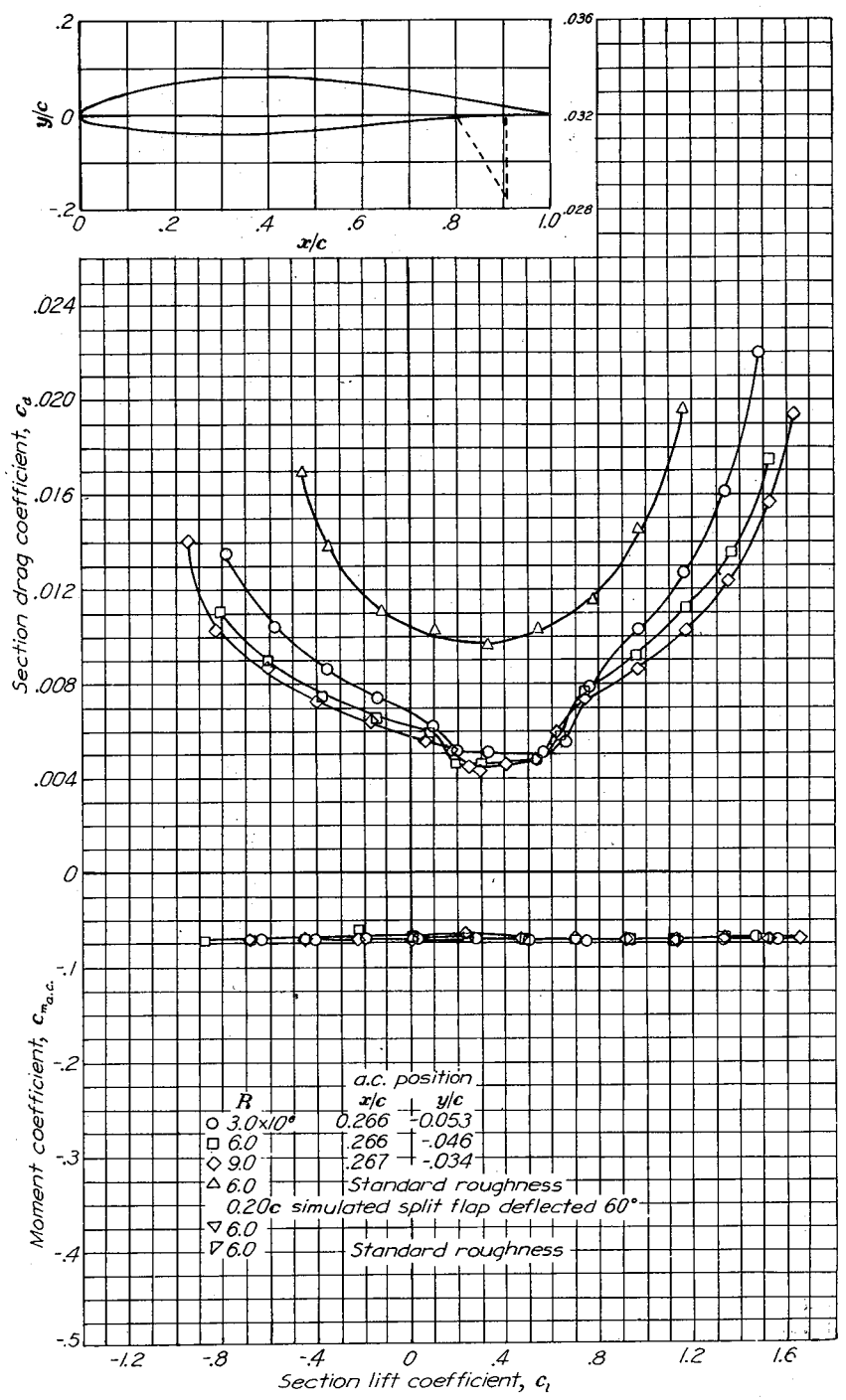
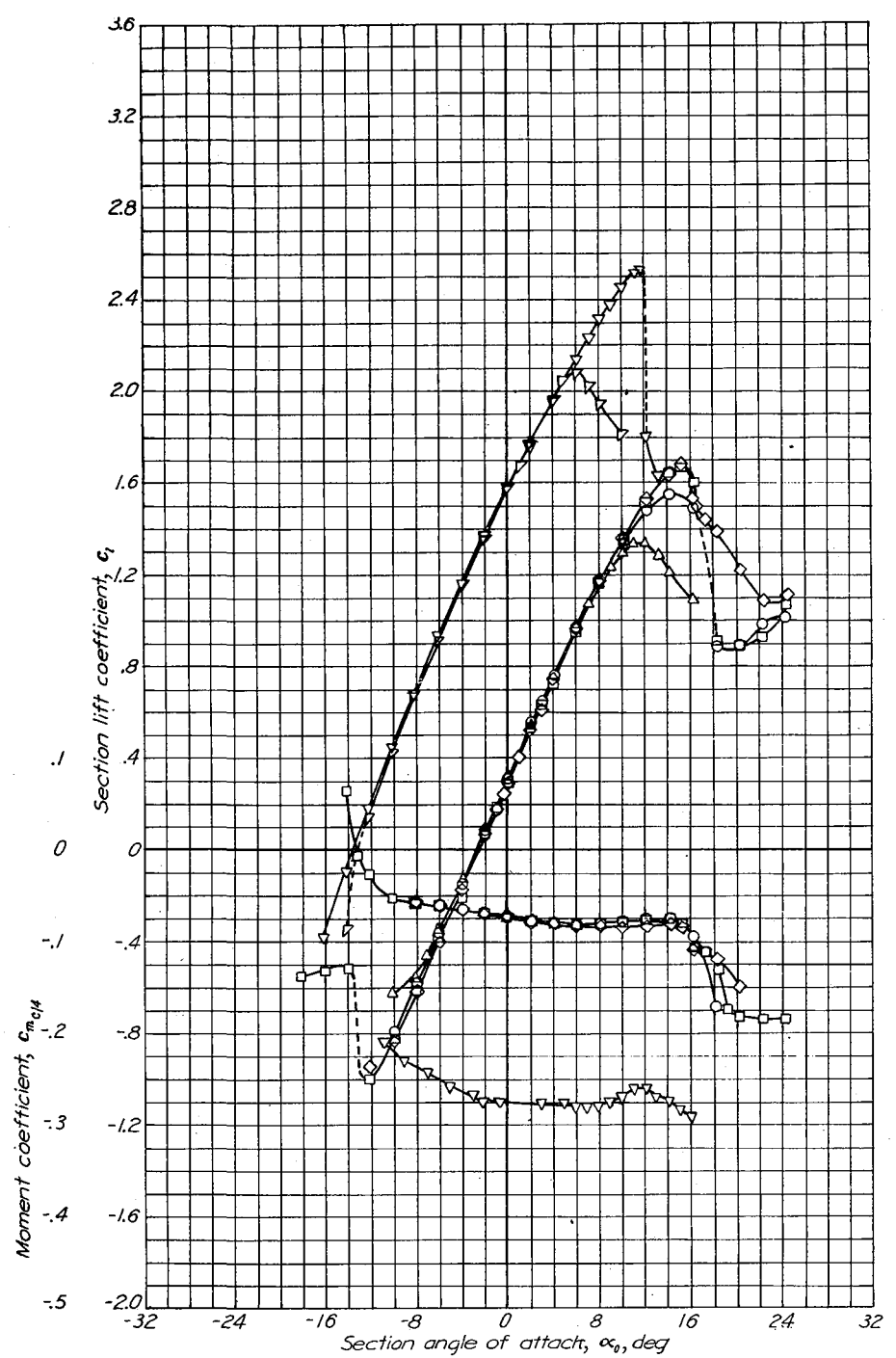


Aerodynamic characteristics of the NACA 64-1-112 airfoil section, 24-inch chord.

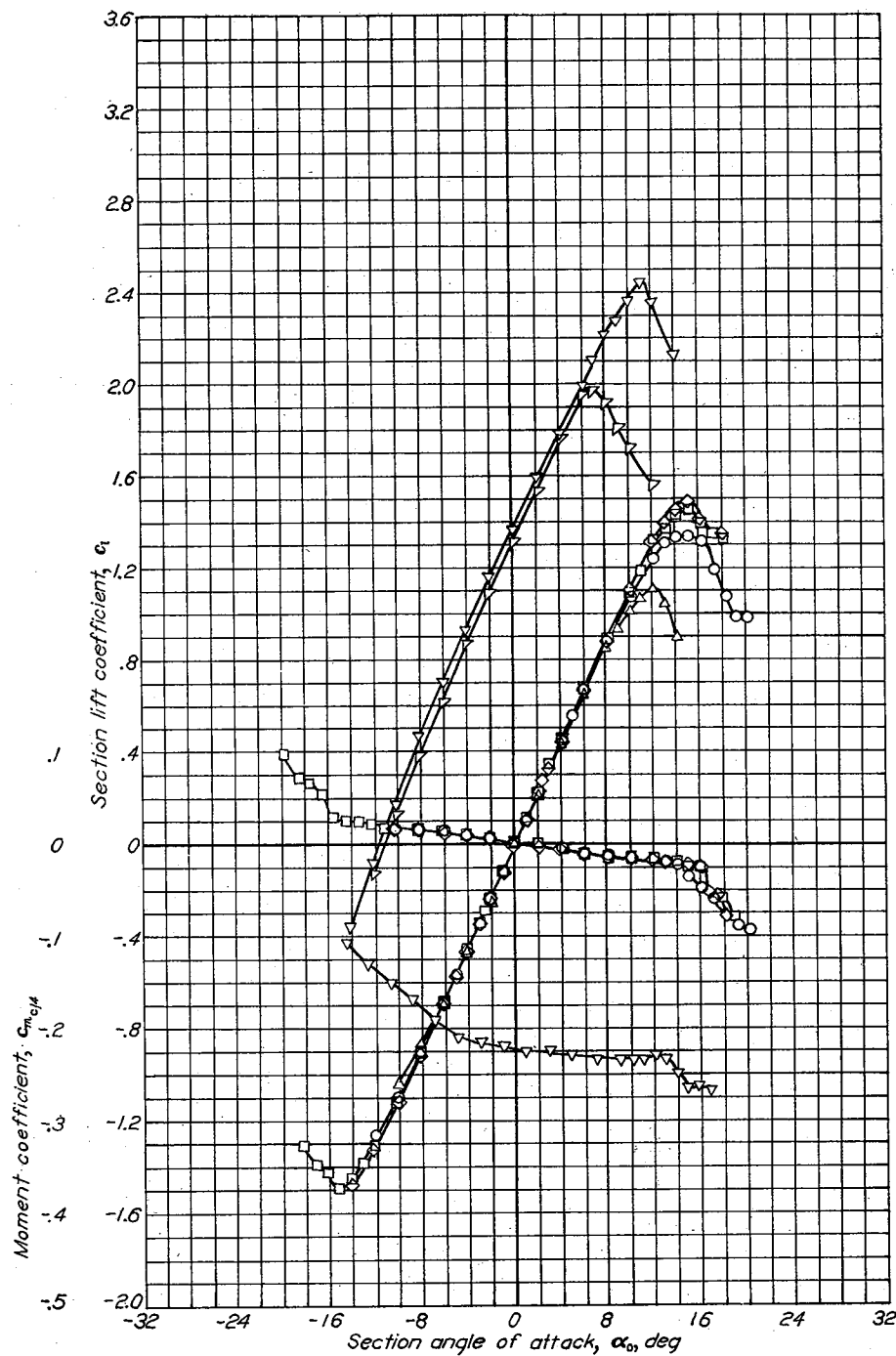


Aerodynamic characteristics of the NACA 641-212 airfoil section, 24-inch chord.

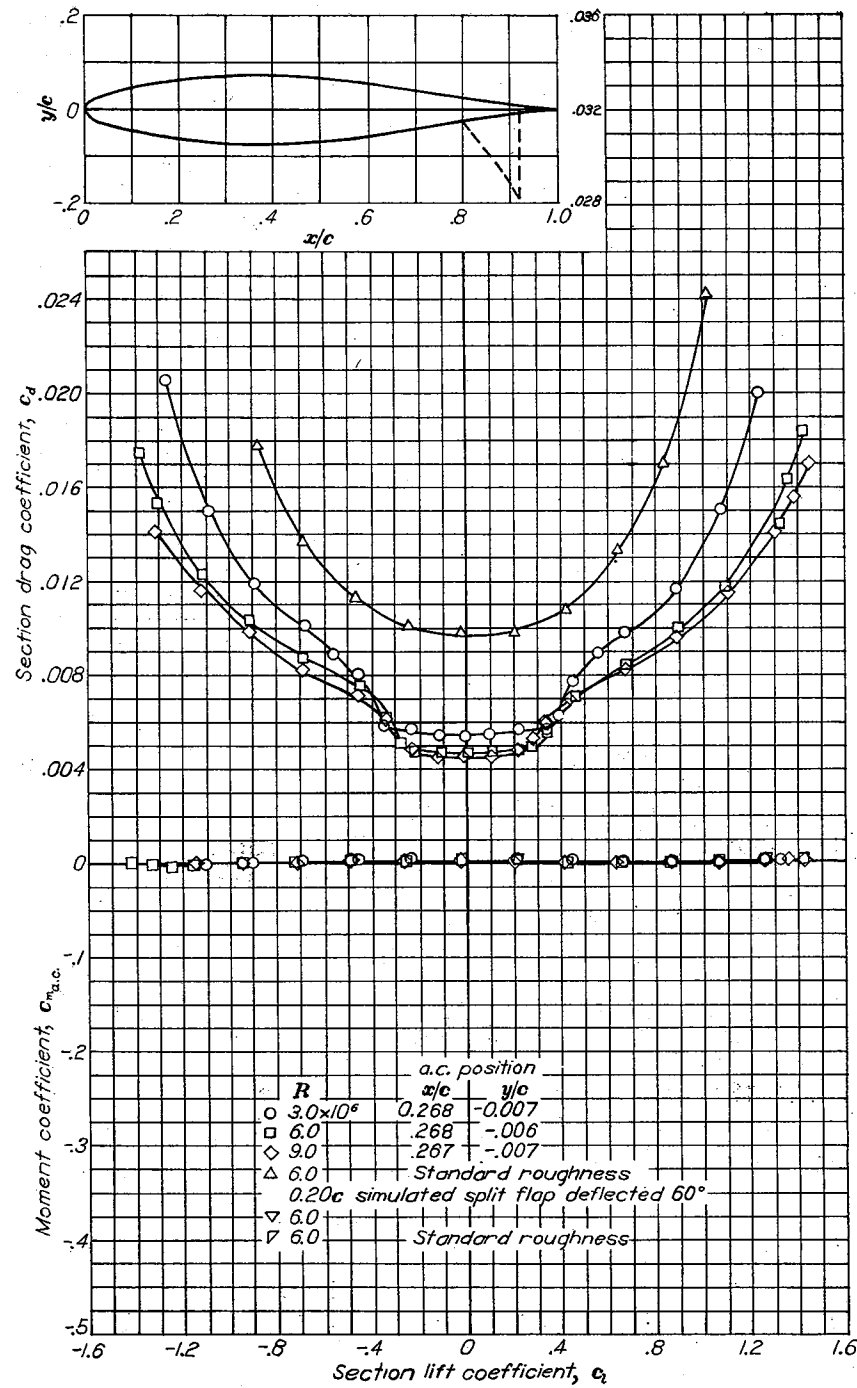


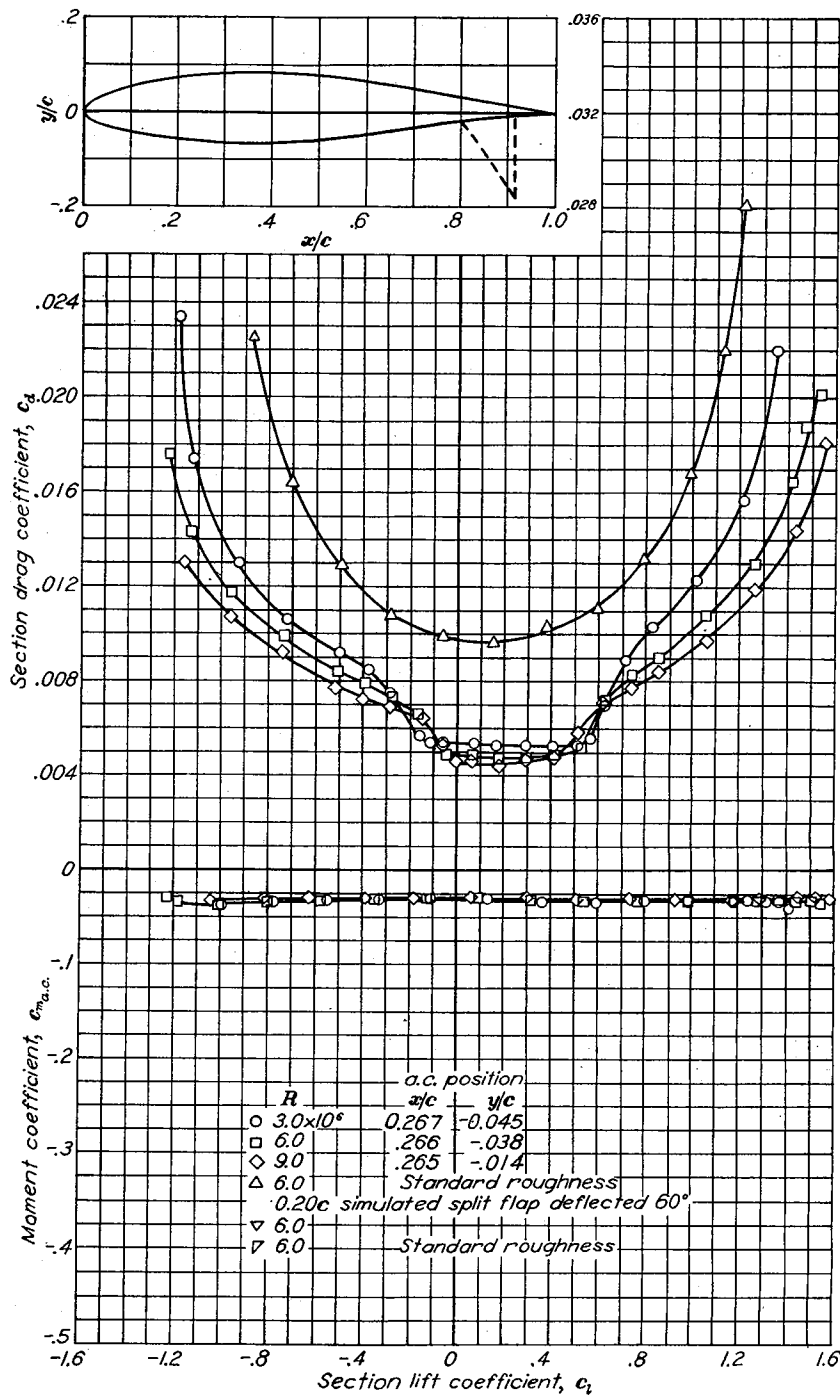
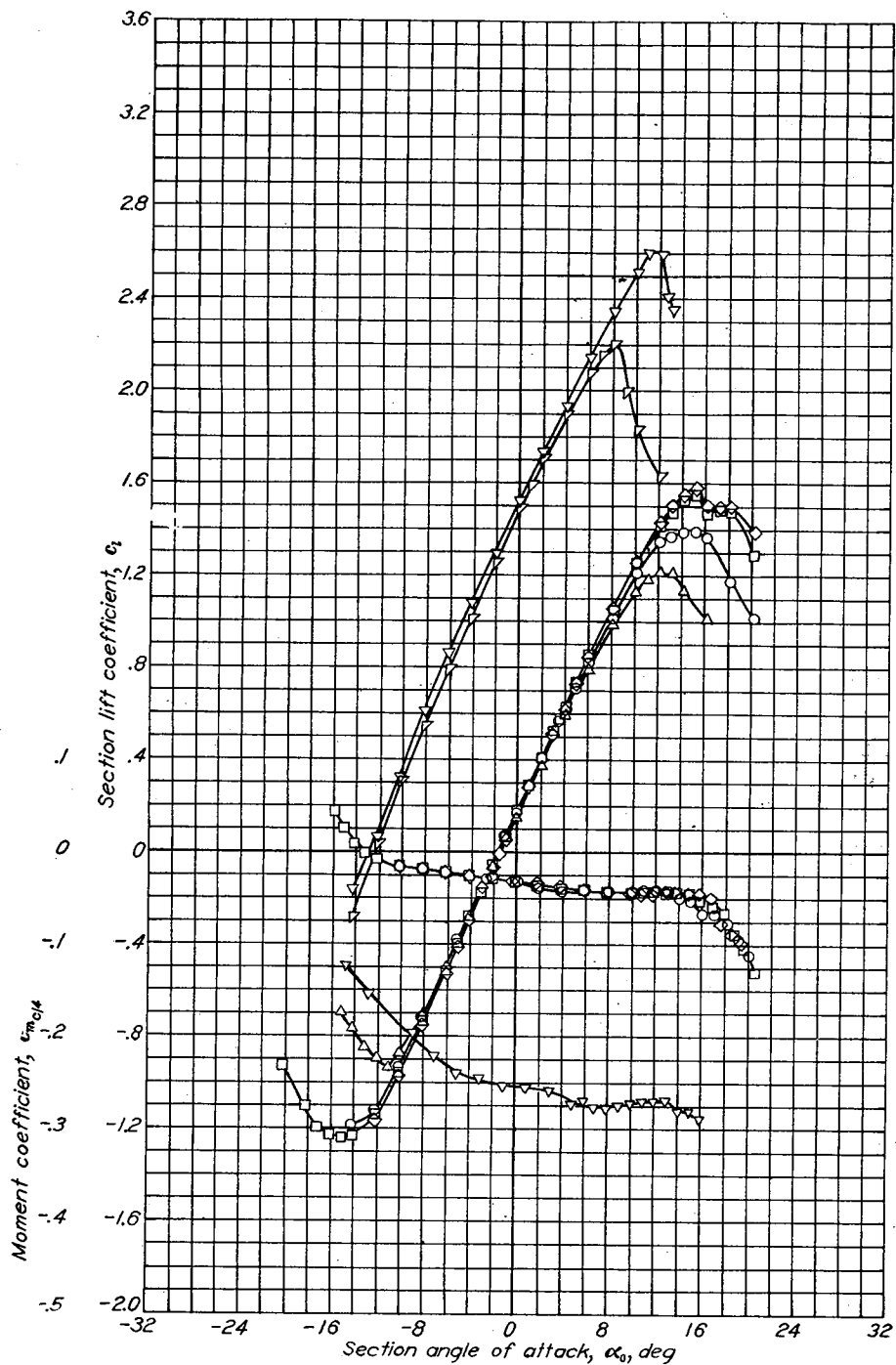


Aerodynamic characteristics of the NACA 641-412 airfoil section, 24-inch chord.



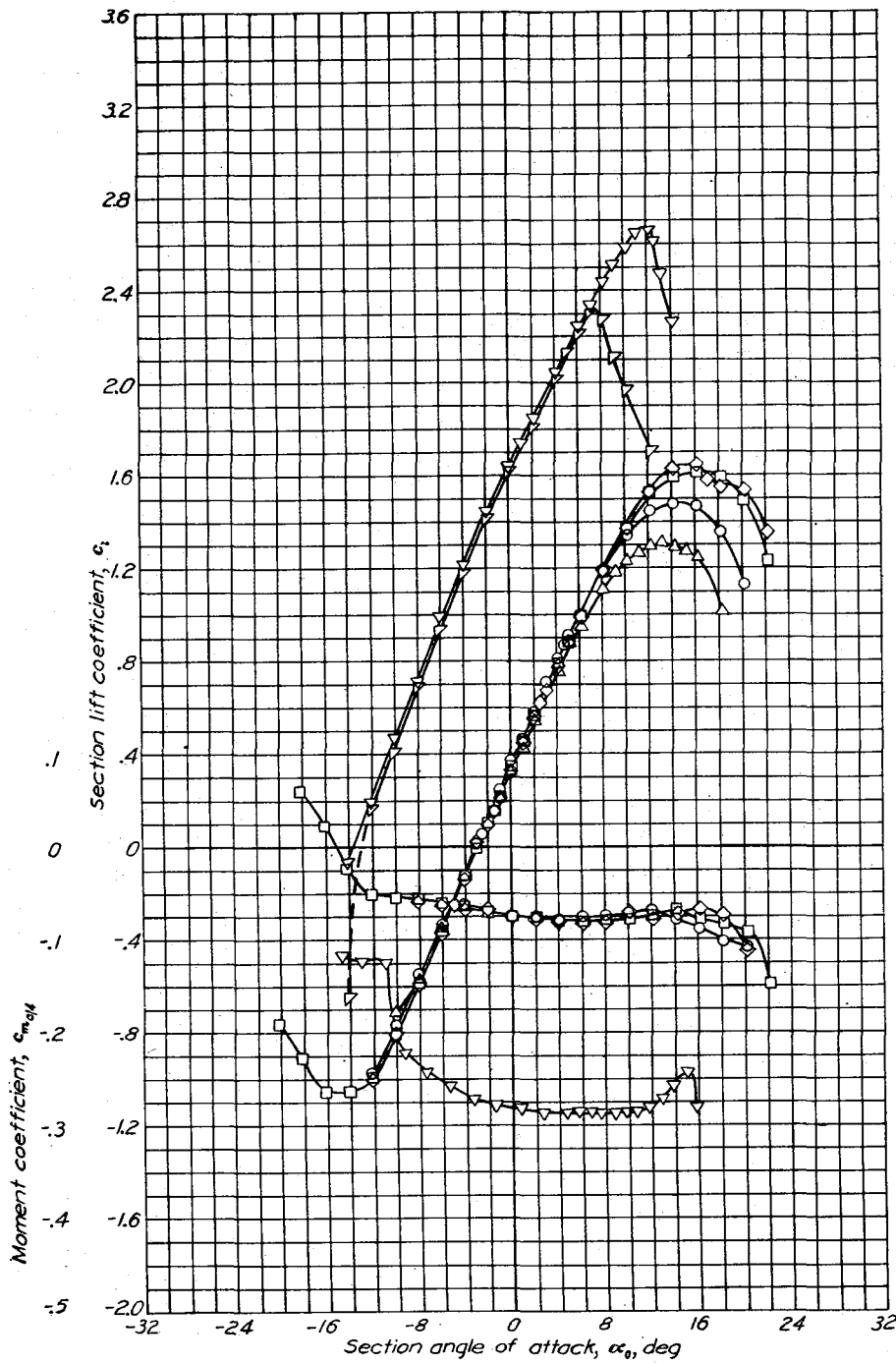
Aerodynamic characteristics of the NACA 642-015 airfoil section, 24-inch chord.



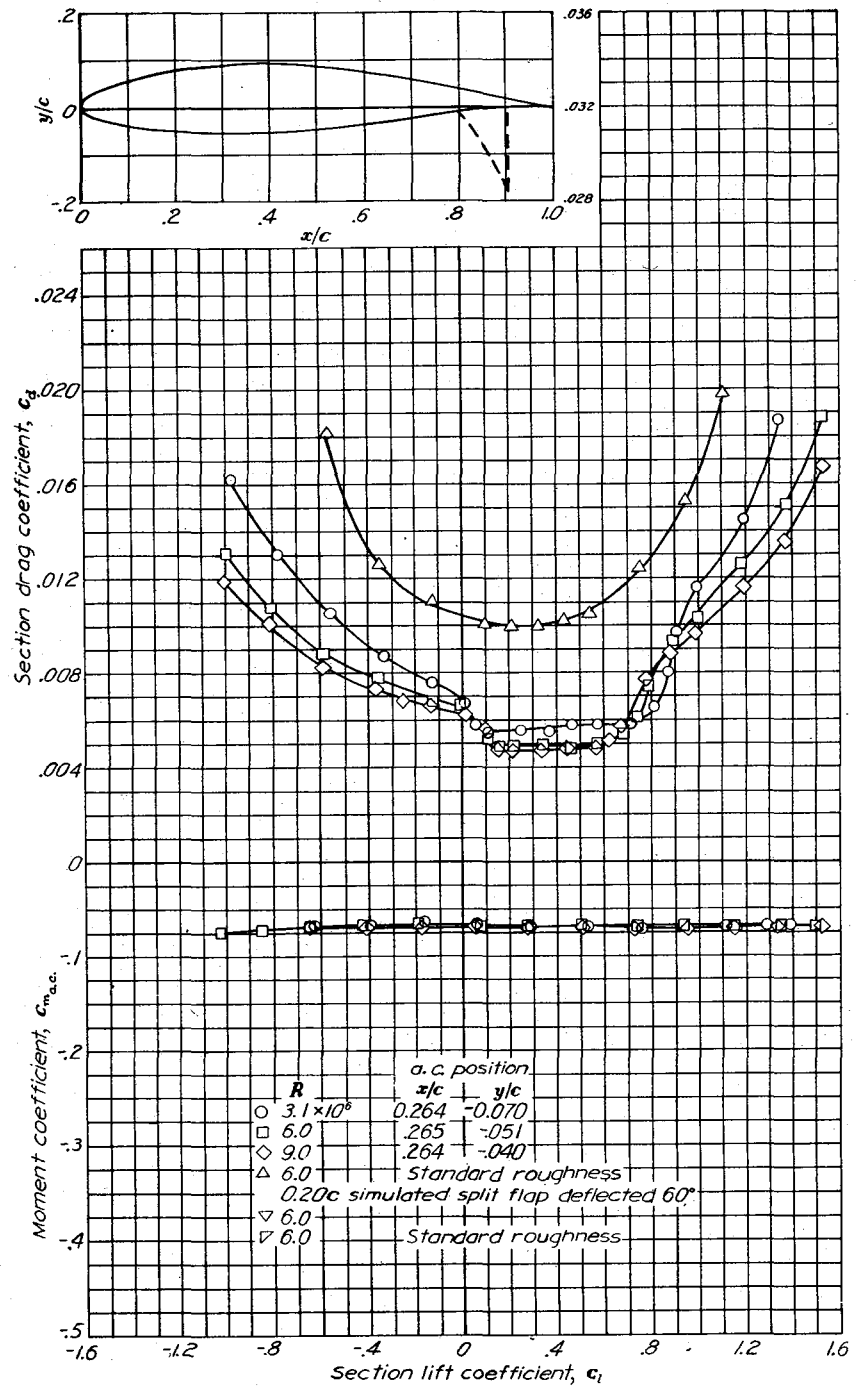


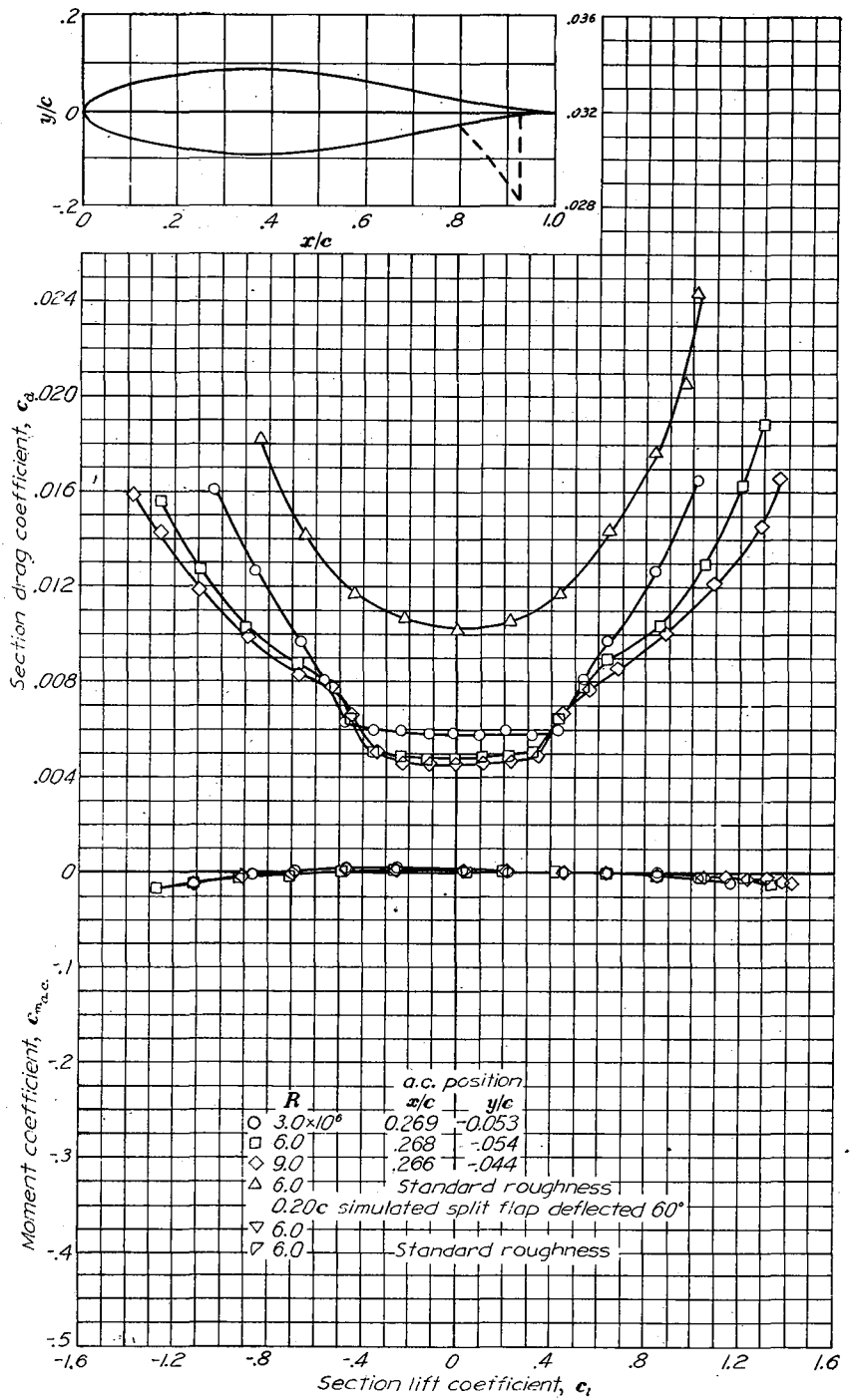
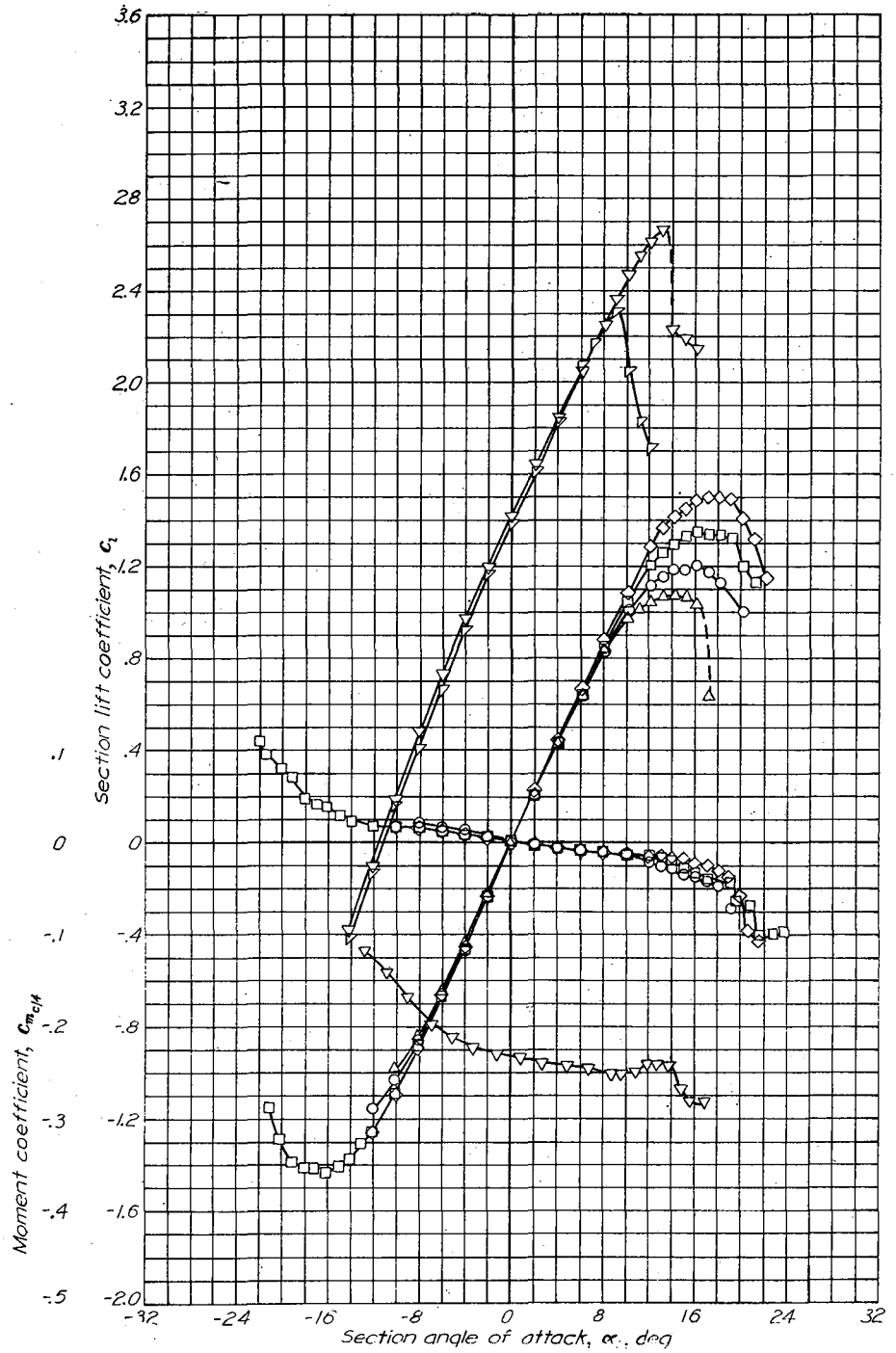
Aerodynamic characteristics of the NACA 642-215 airfoil section, 24-inch chord.



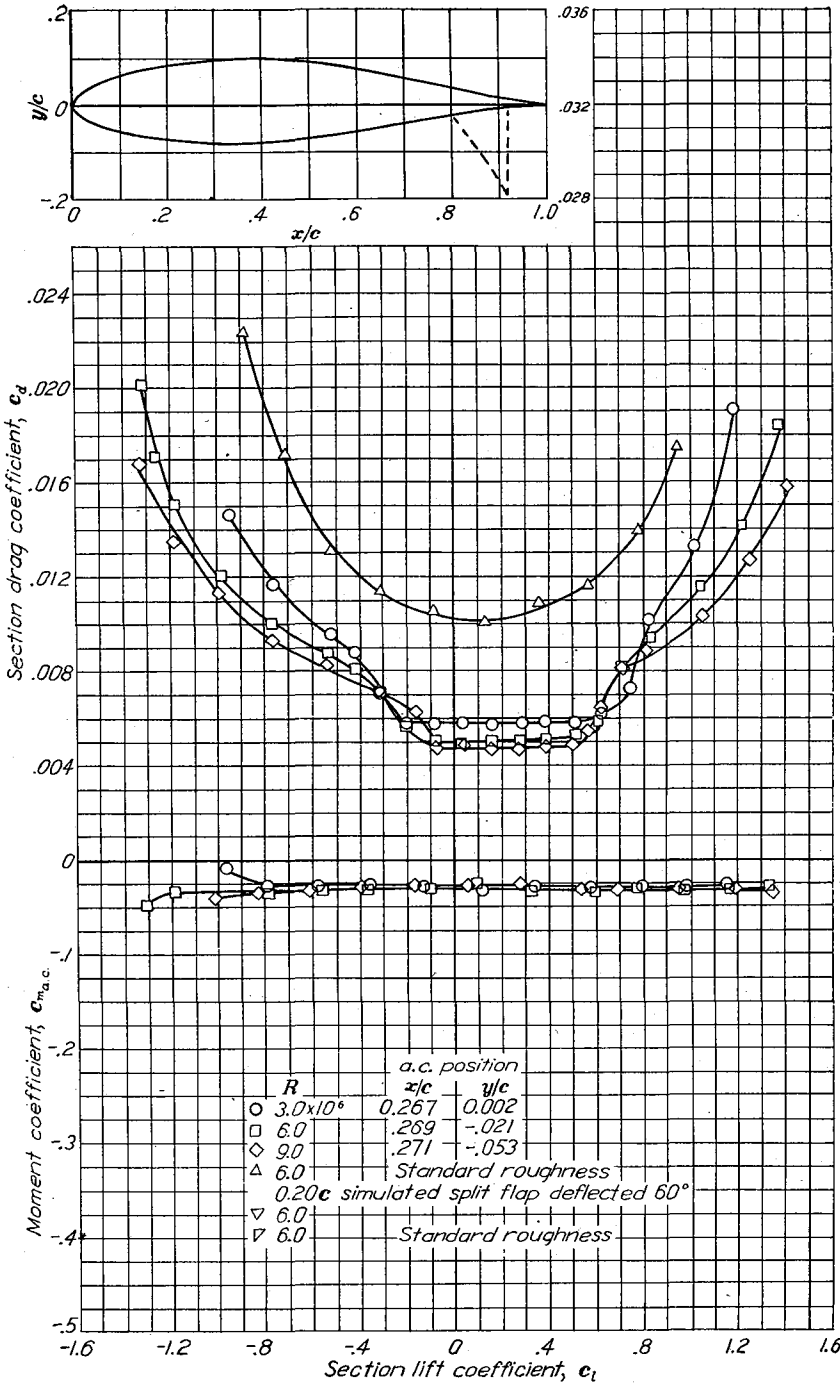
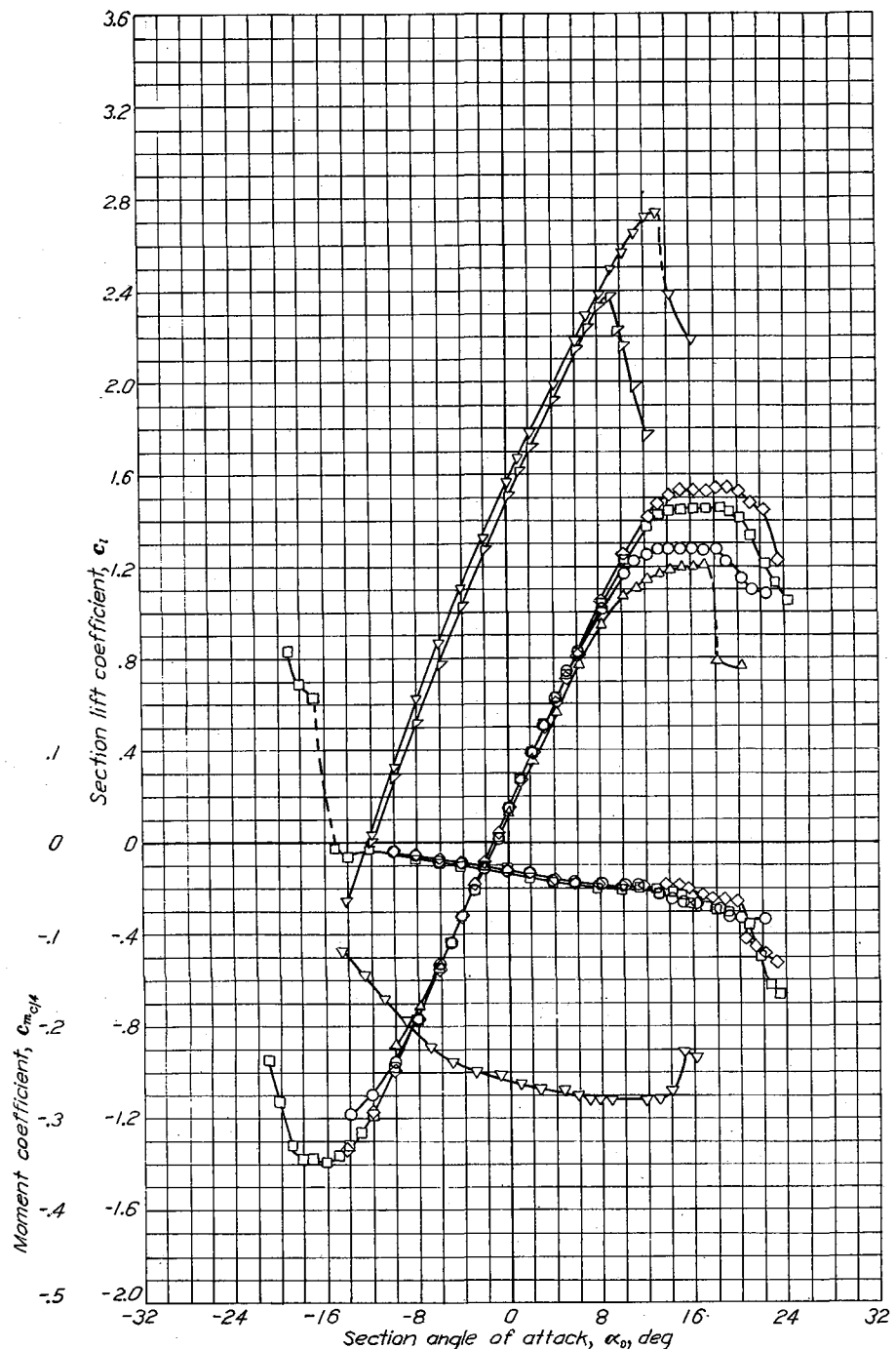


Aerodynamic characteristics of the NACA 64-415 airfoil section, 24-inch chord.

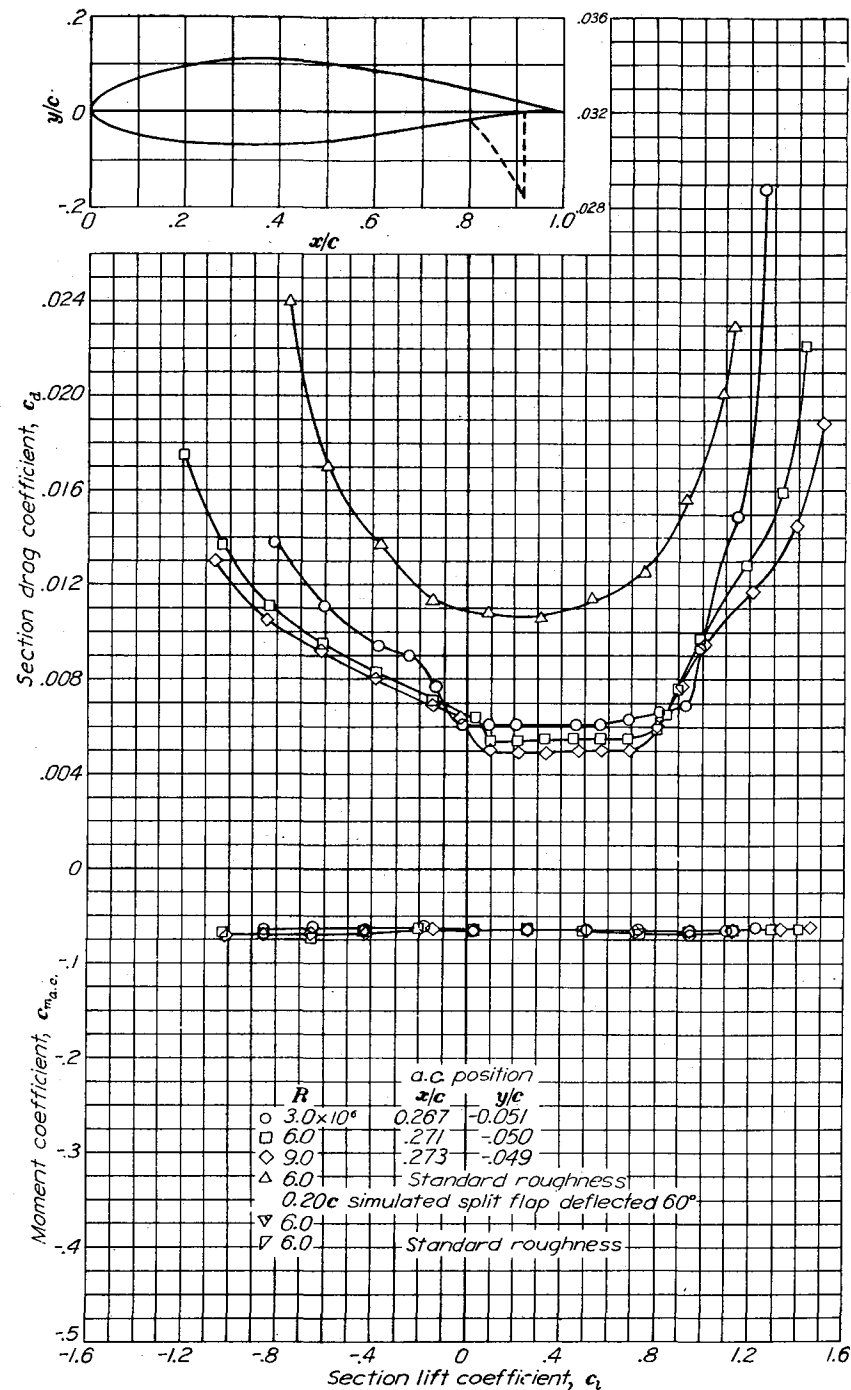
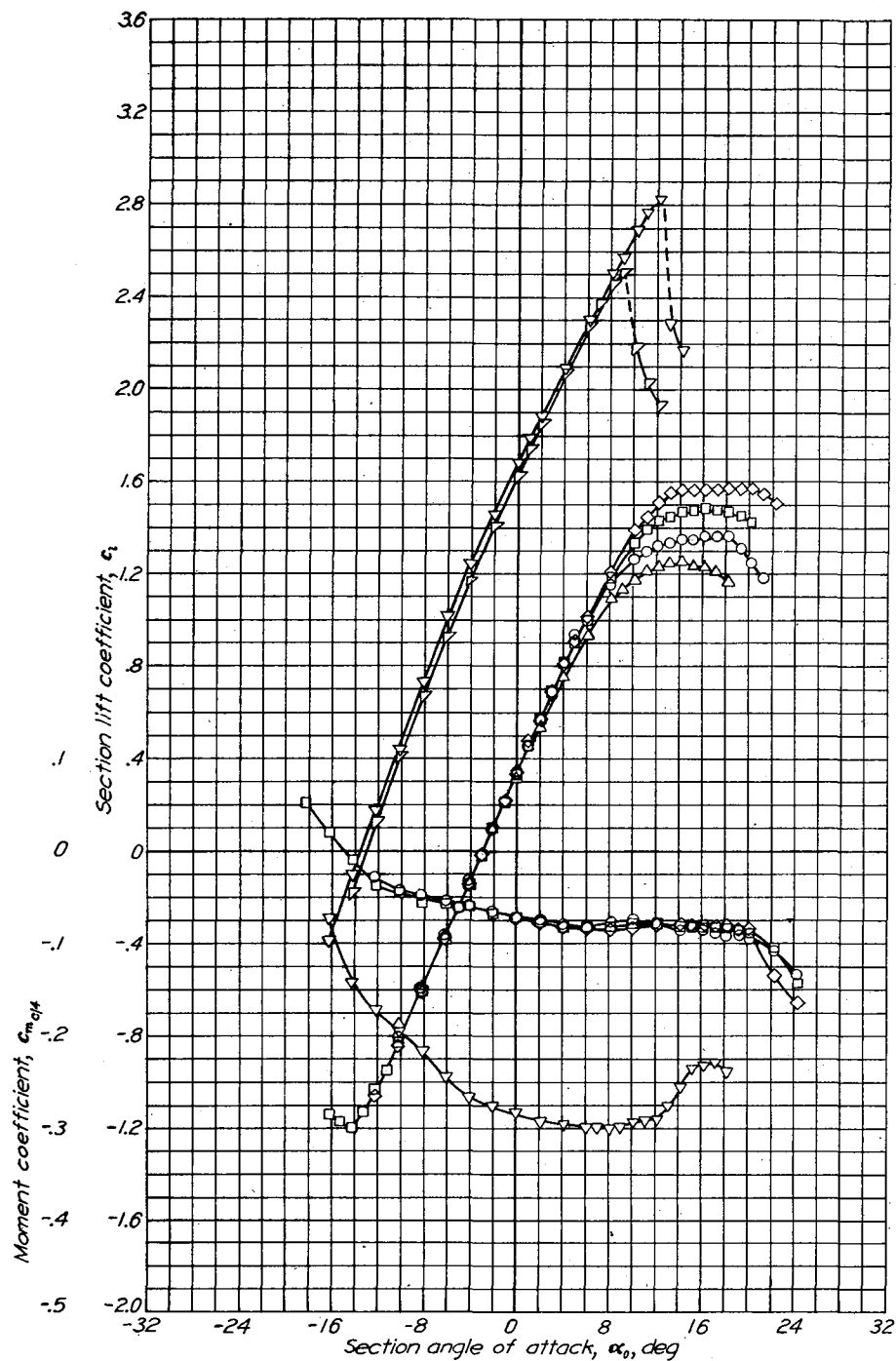




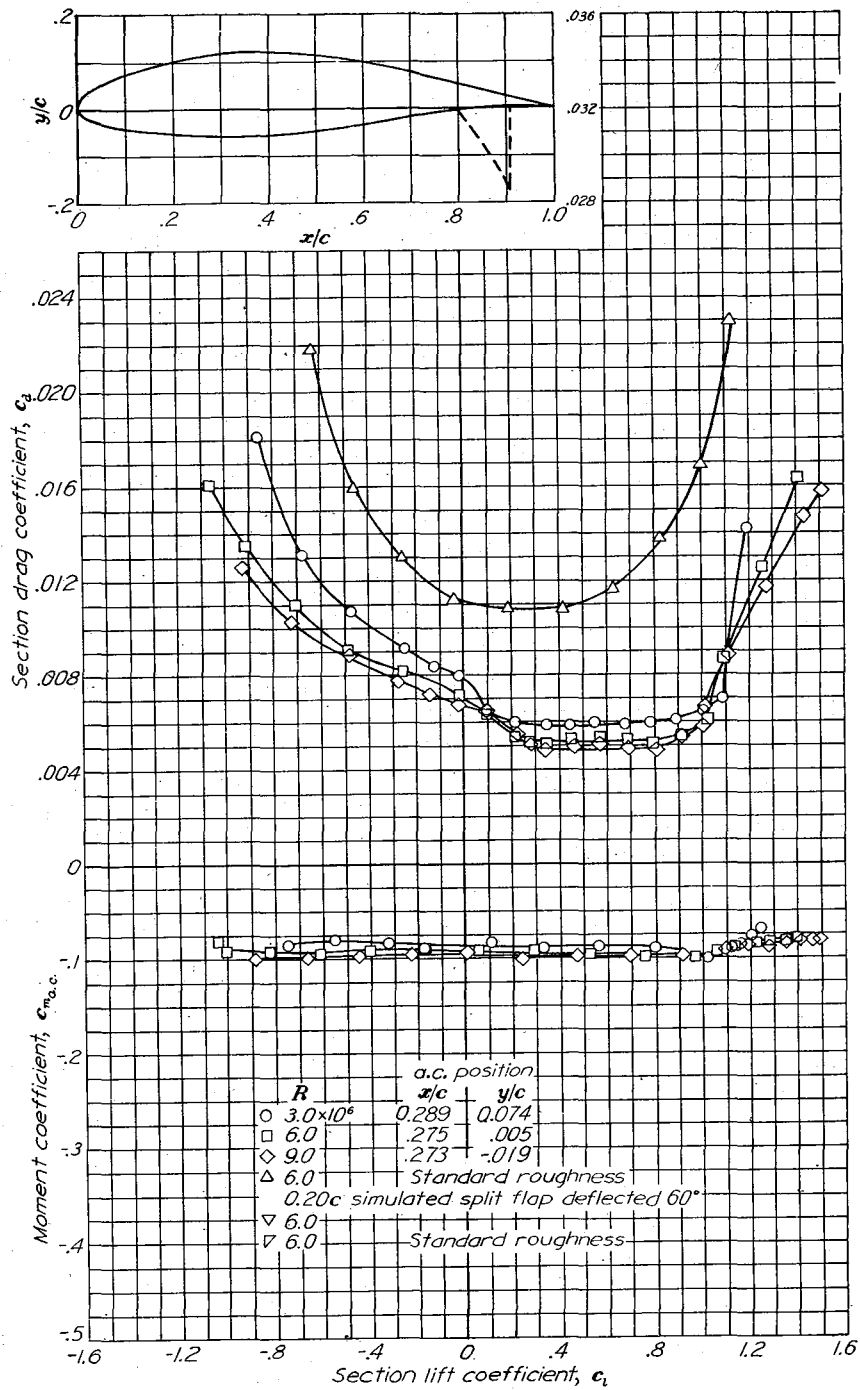
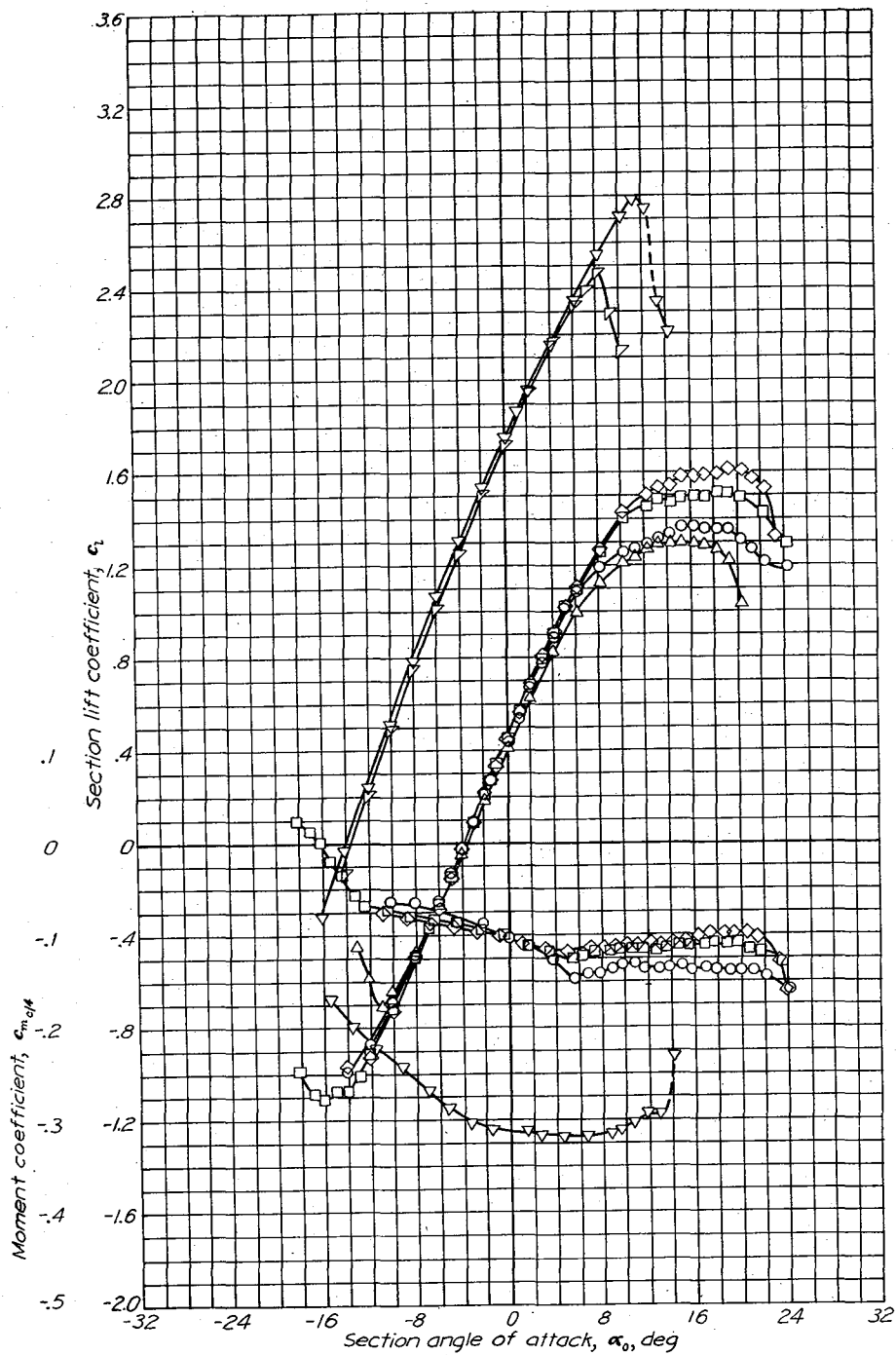
Aerodynamic characteristics of the NACA 643-018 airfoil section, 24-inch chord.



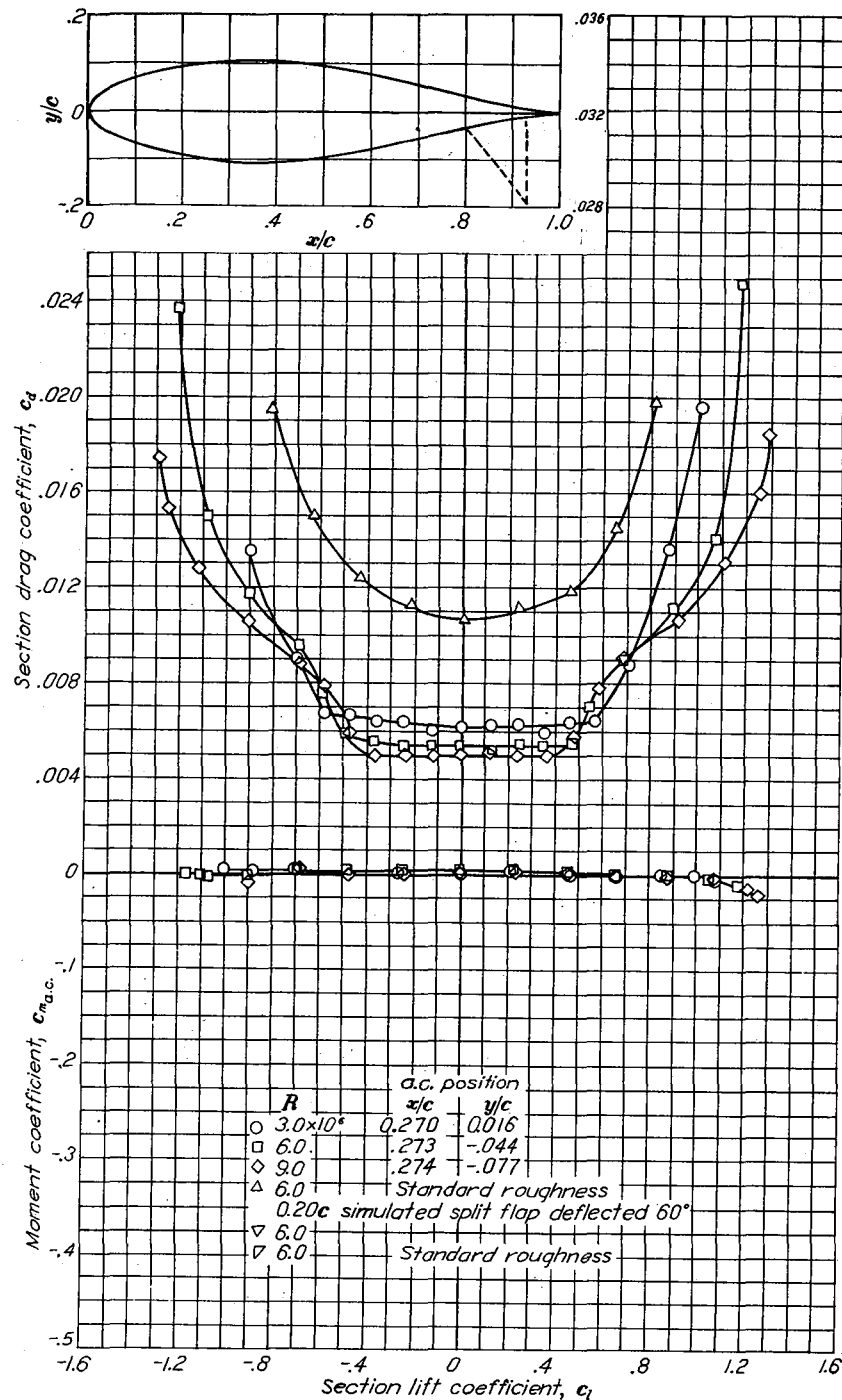
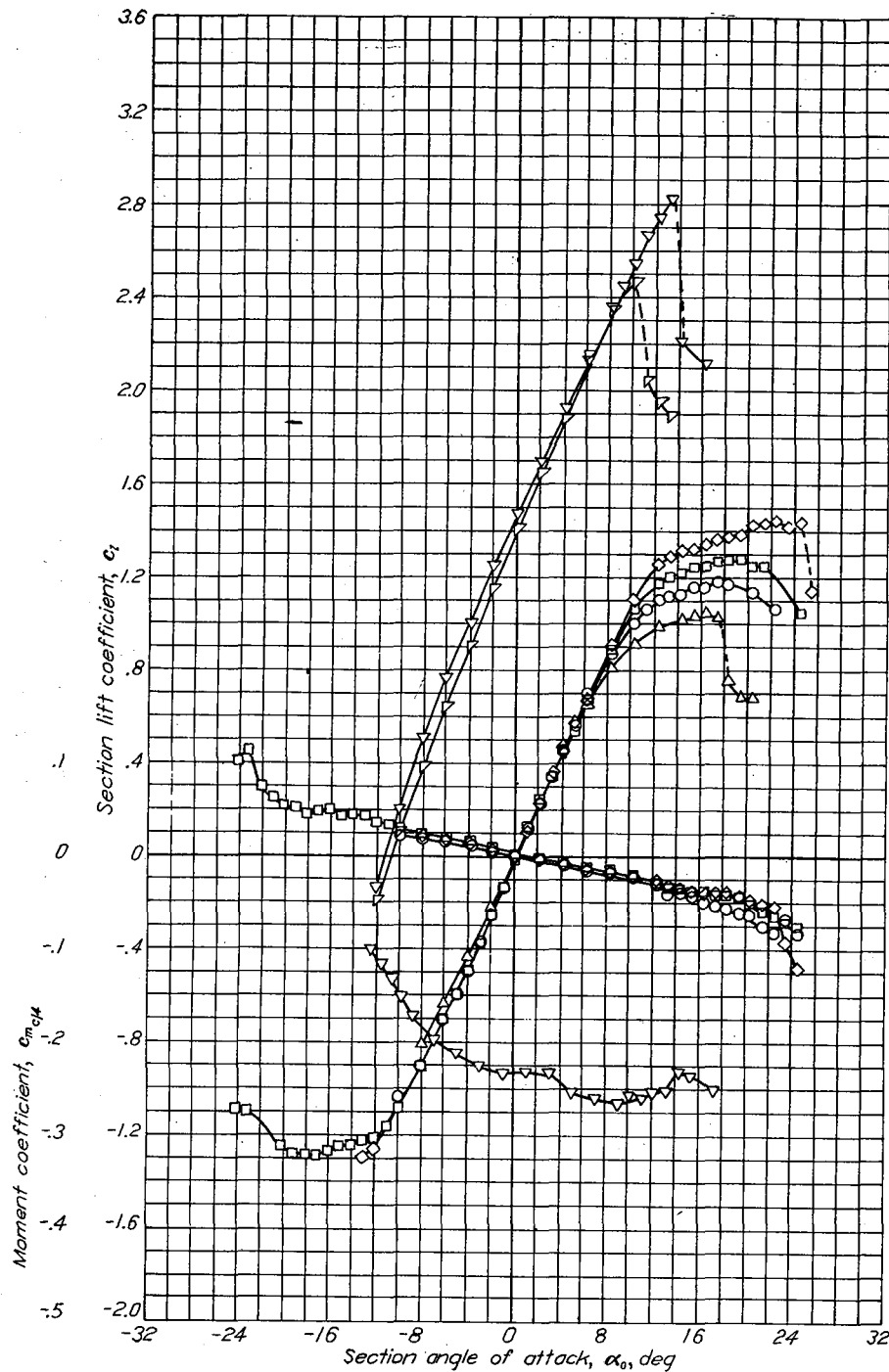
Aerodynamic characteristics of the NACA 64-3-218 airfoil section, 24-inch chord.



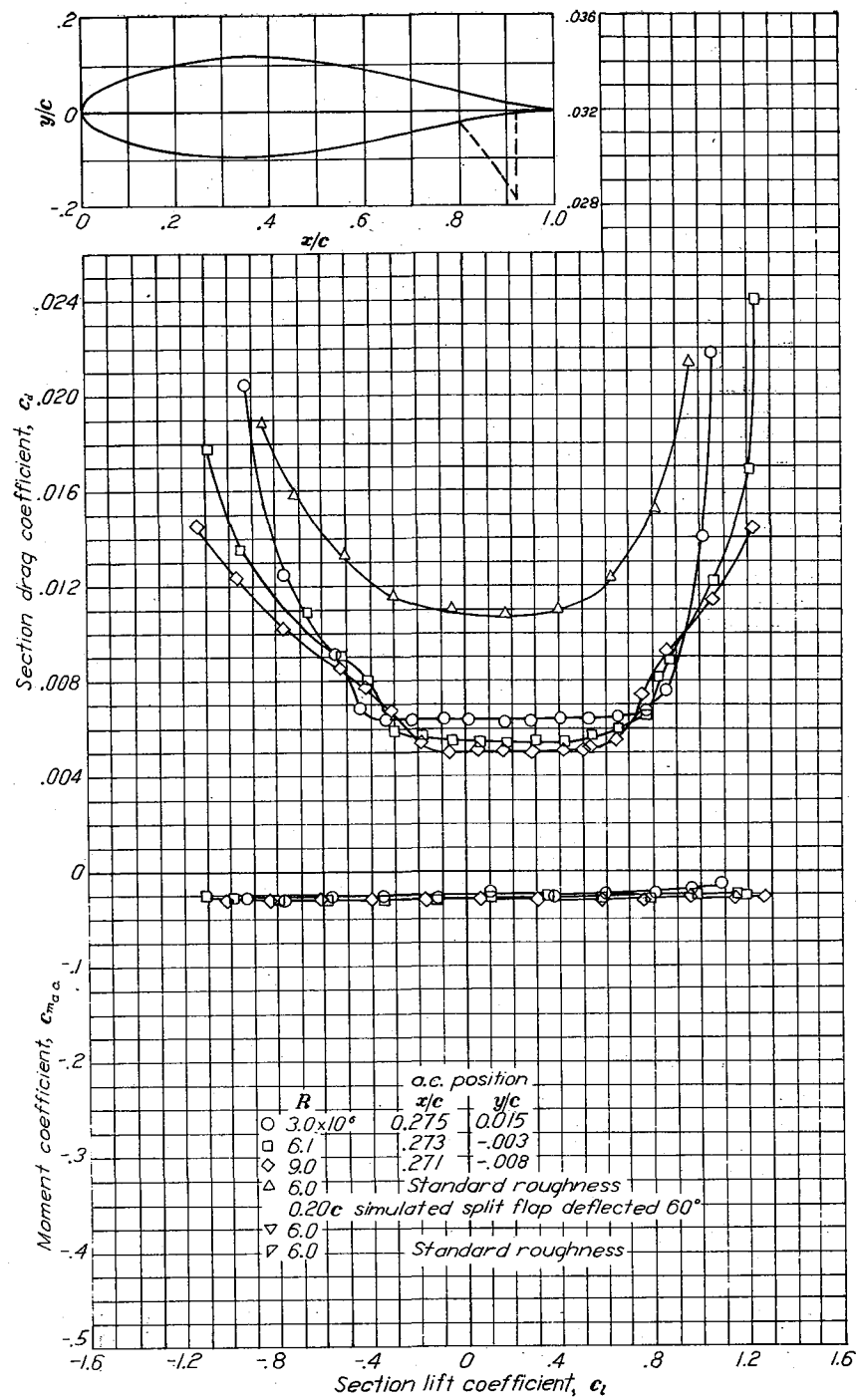
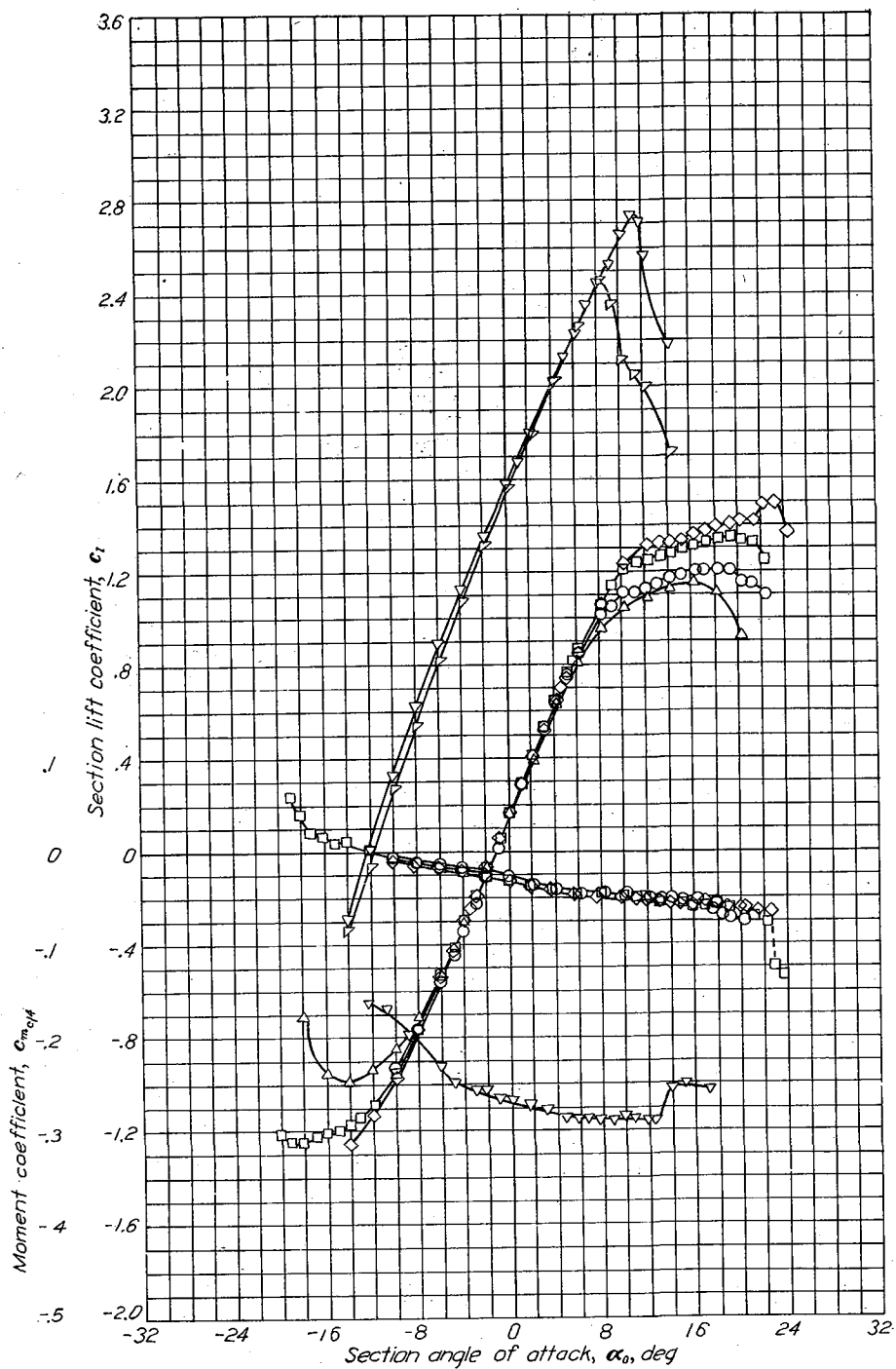
Aerodynamic characteristics of the NACA 643-418 airfoil section, 24-inch chord.



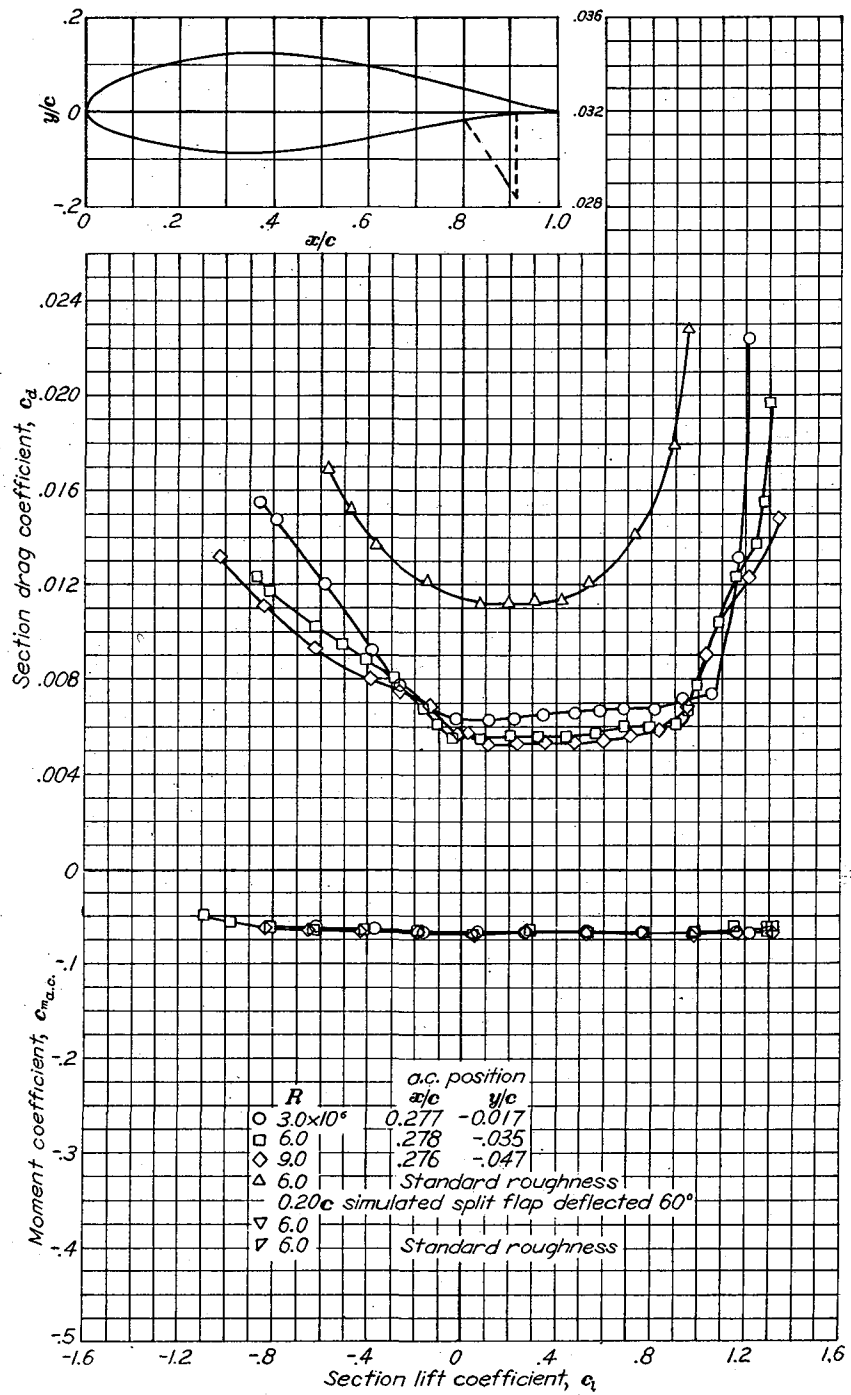
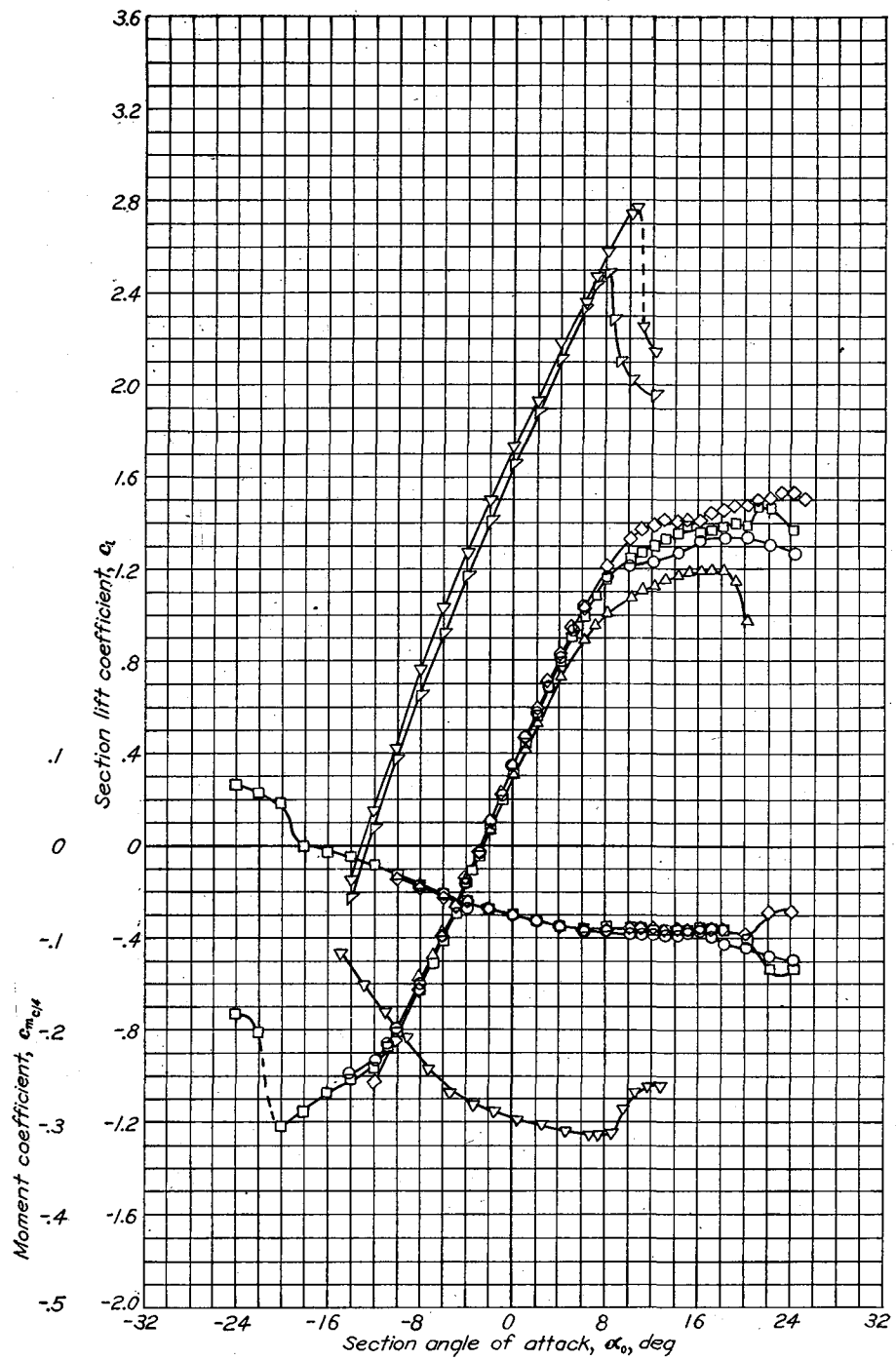
Aerodynamic characteristics of the NACA 643-618 airfoil section, 24-inch chord.



Aerodynamic characteristics of the NACA 644-021 airfoil section, 24-inch chord.

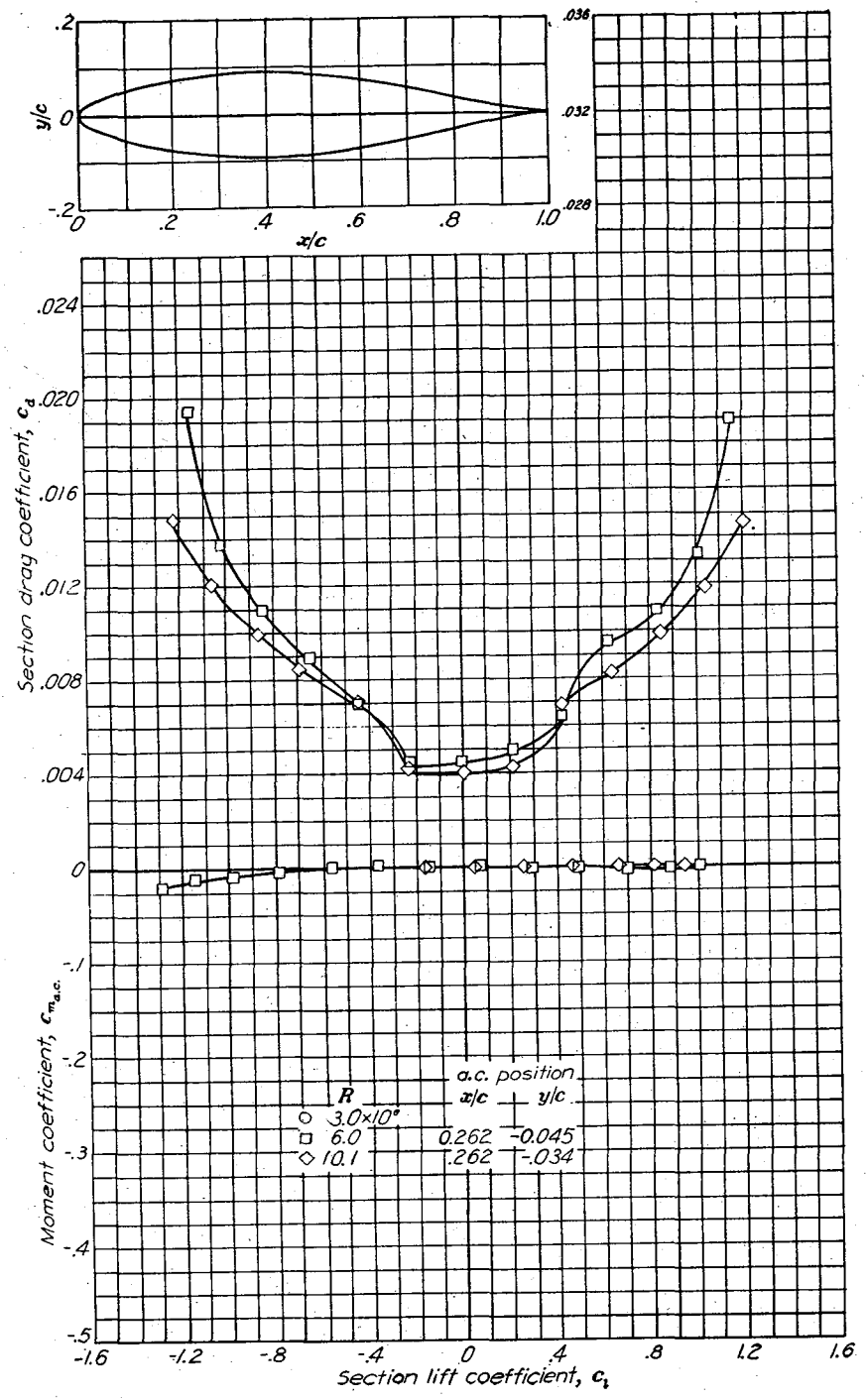
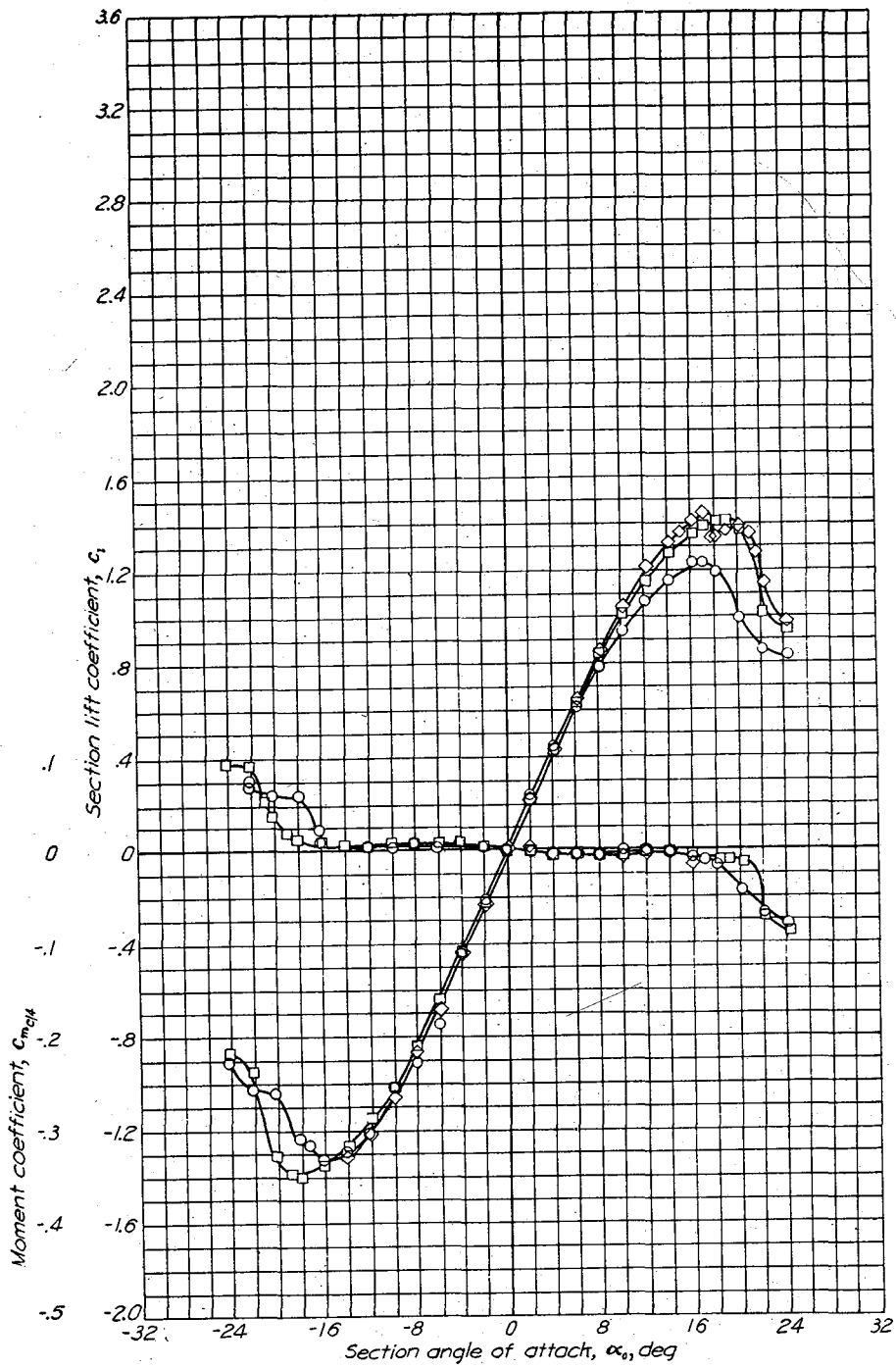


Aerodynamic characteristics of the NACA 64-221 airfoil section, 24-inch chord.

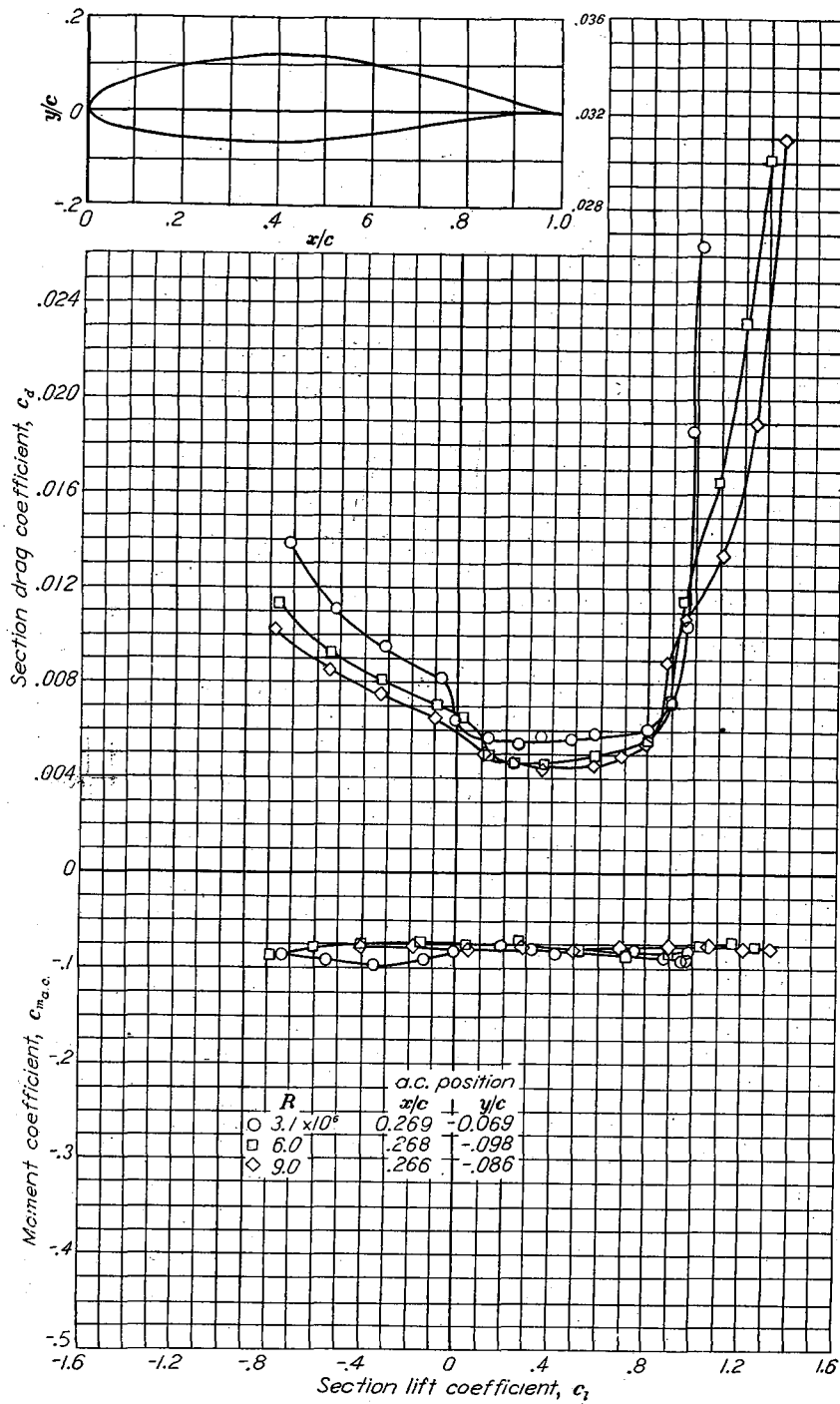
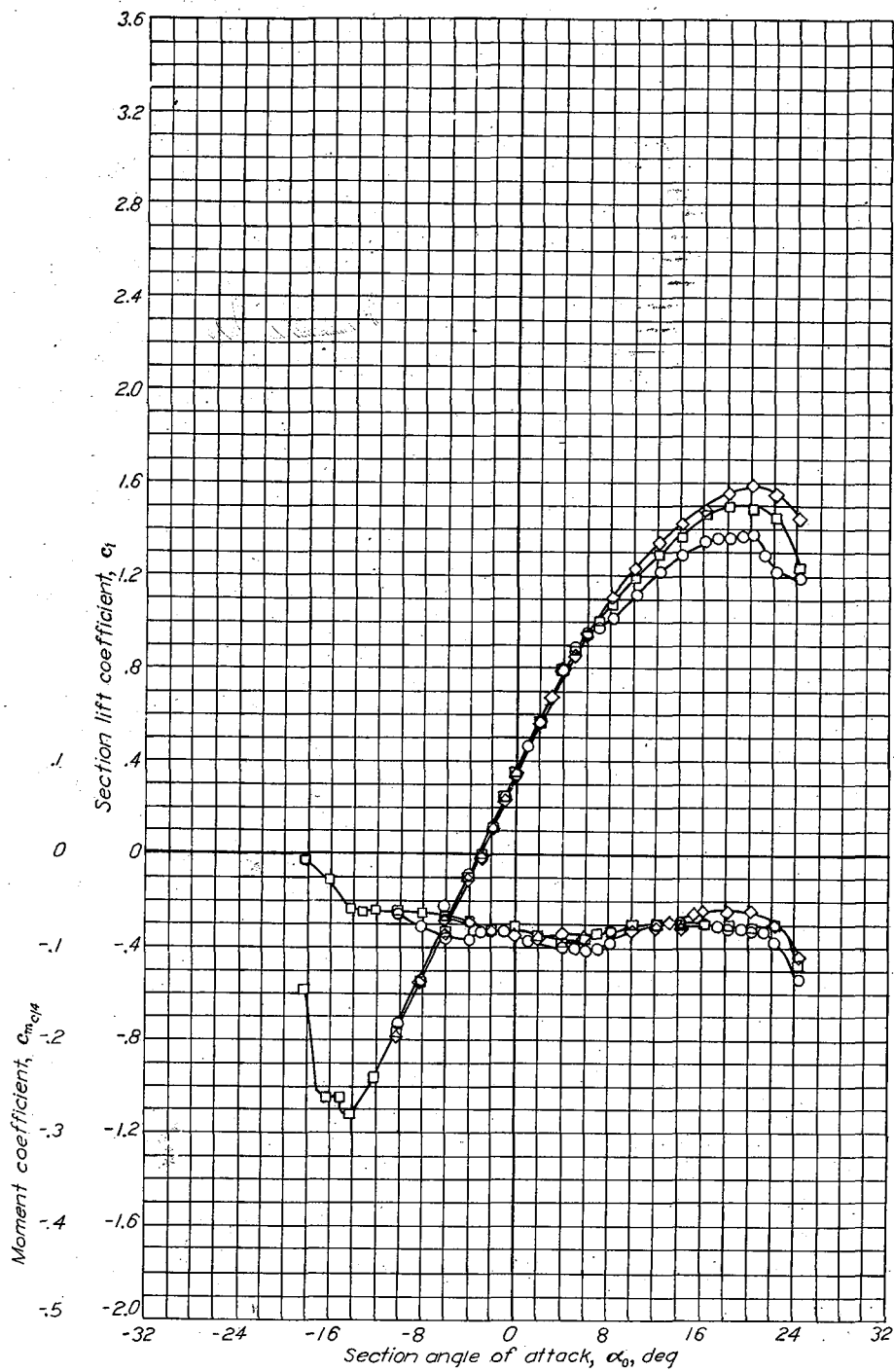


Aerodynamic characteristics of the NACA 64-421 airfoil section, 24-inch chord.

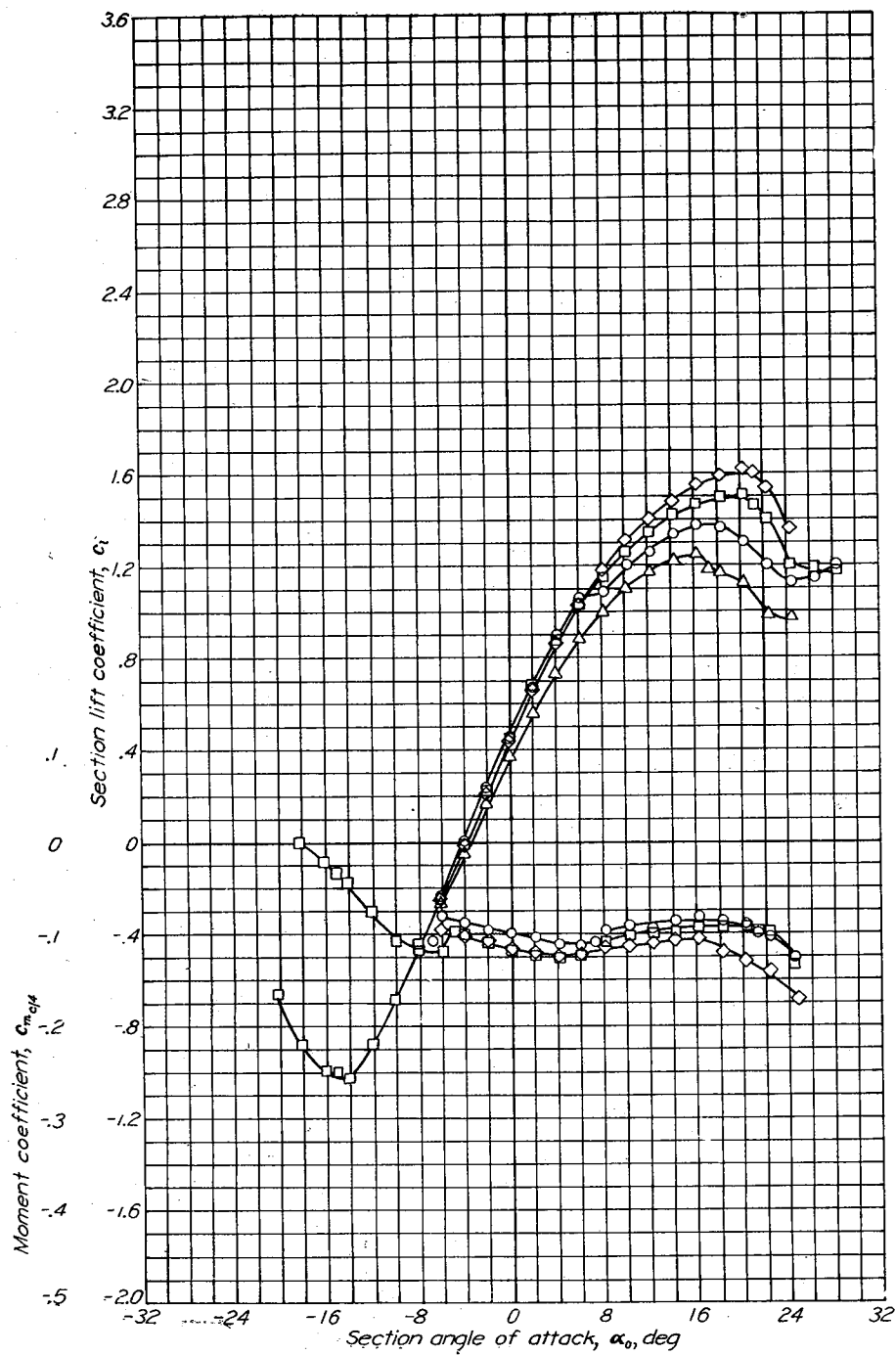




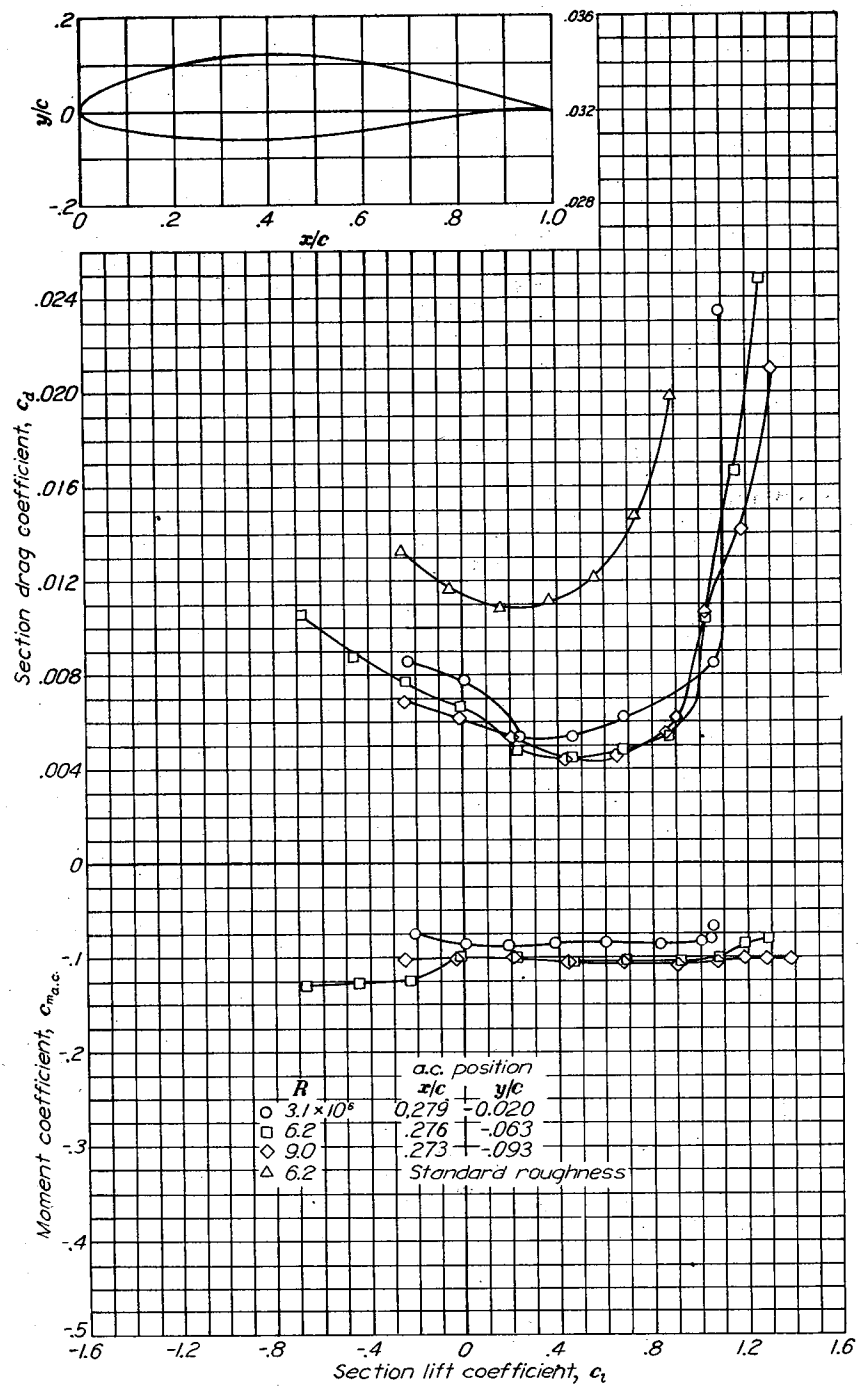
Aerodynamic characteristics of the NACA 65,3-018 airfoil section, 24-inch chord.



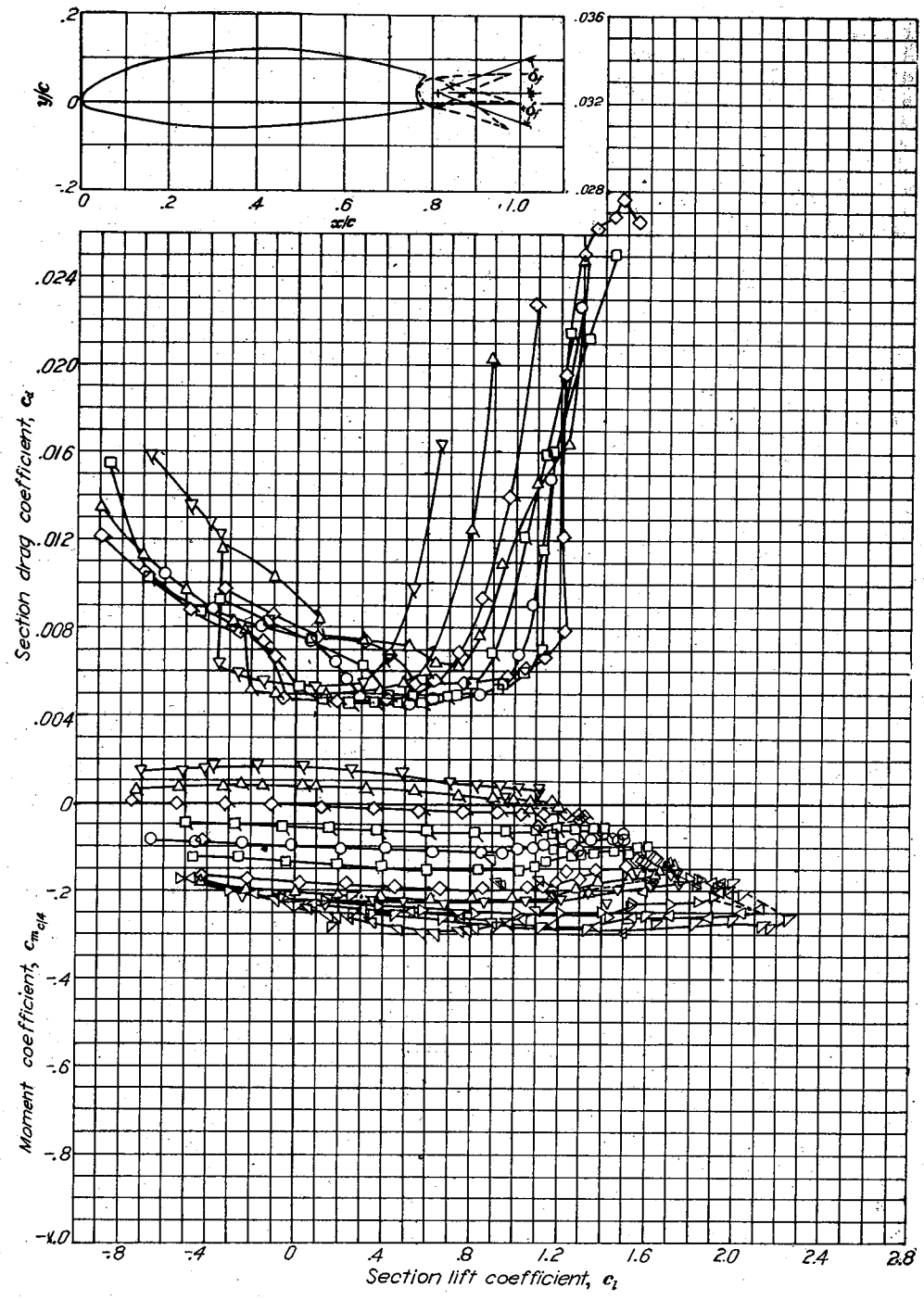
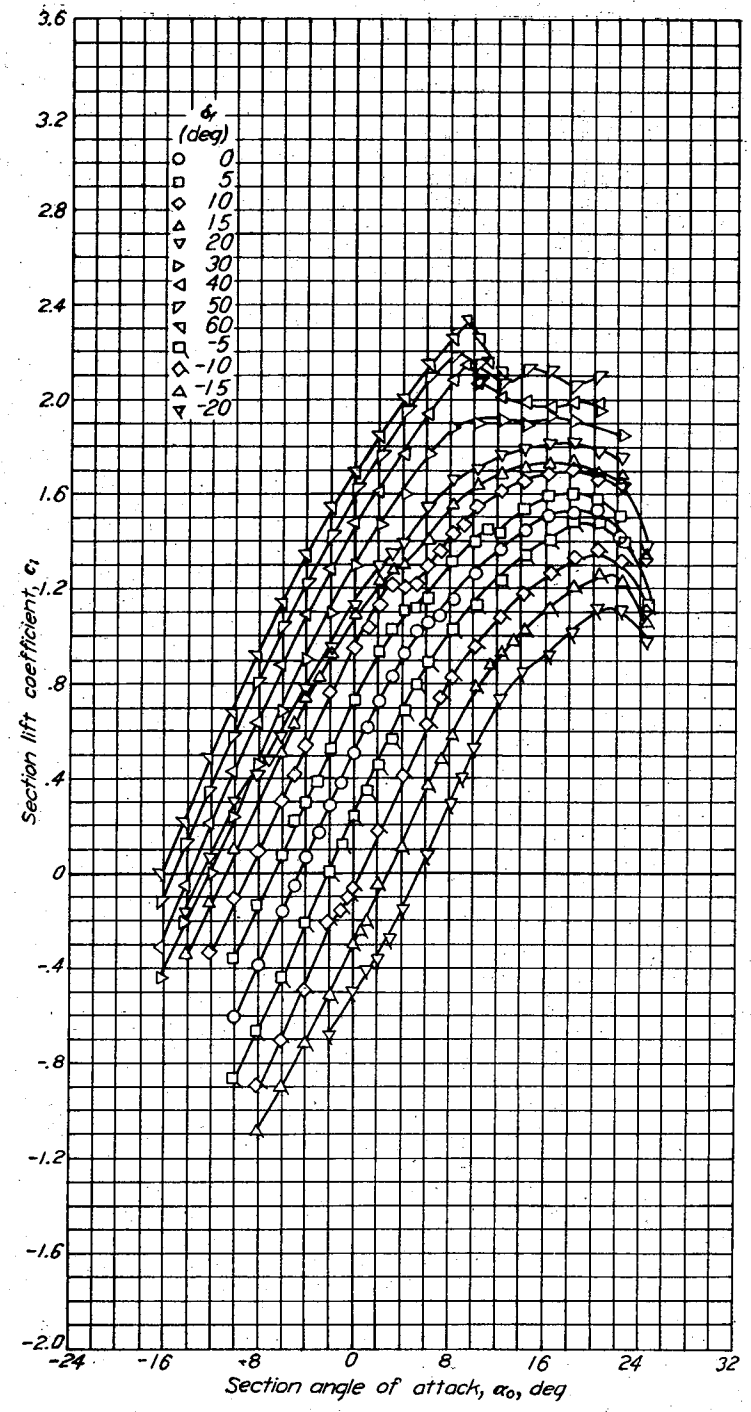
Aerodynamic characteristics of the NACA 65,3-418,  $\alpha = 0.8$  airfoil section, 24-inch chord.



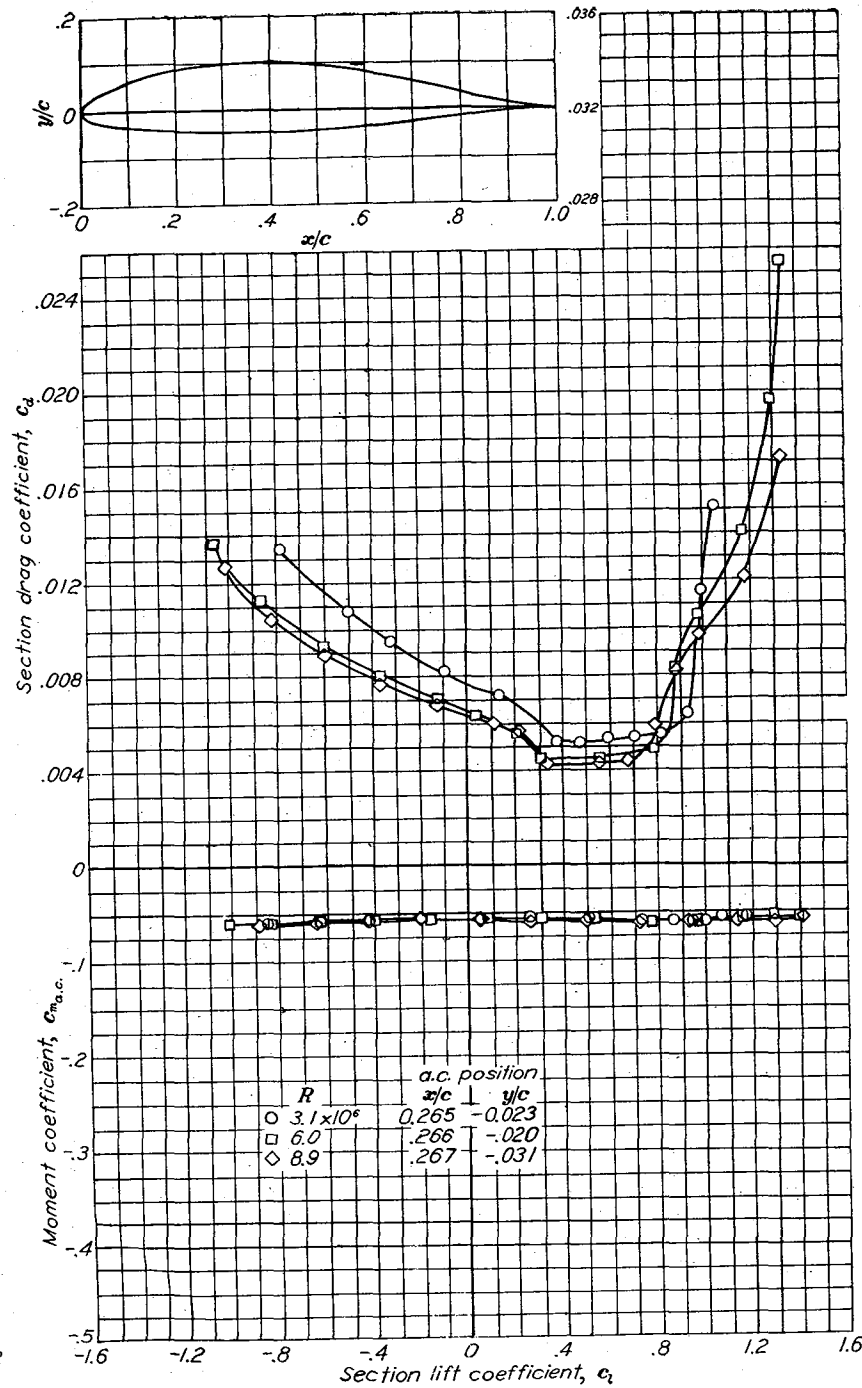
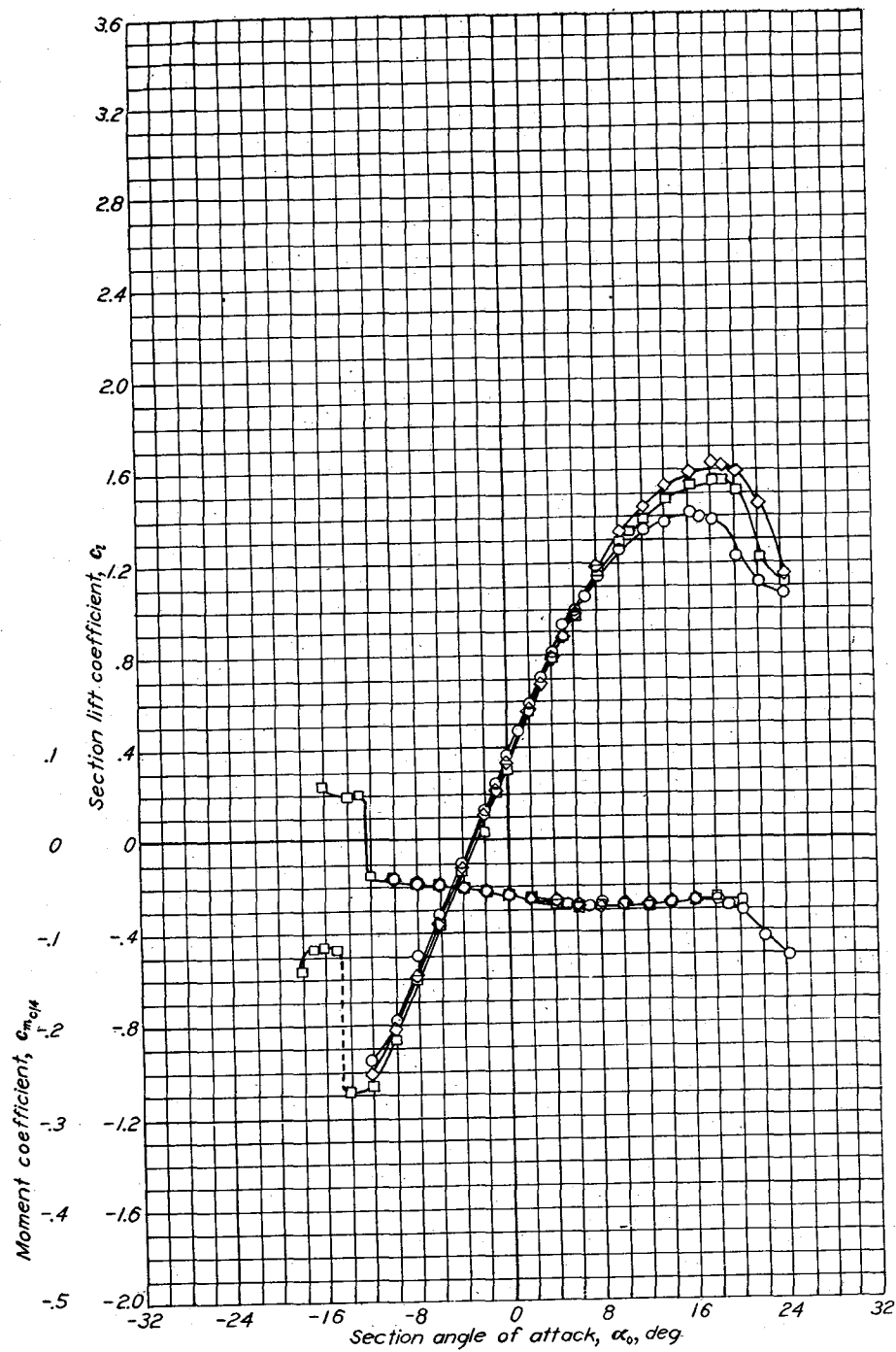
Aerodynamic characteristics of the NACA 65,3-618 airfoil section, 24-inch chord.



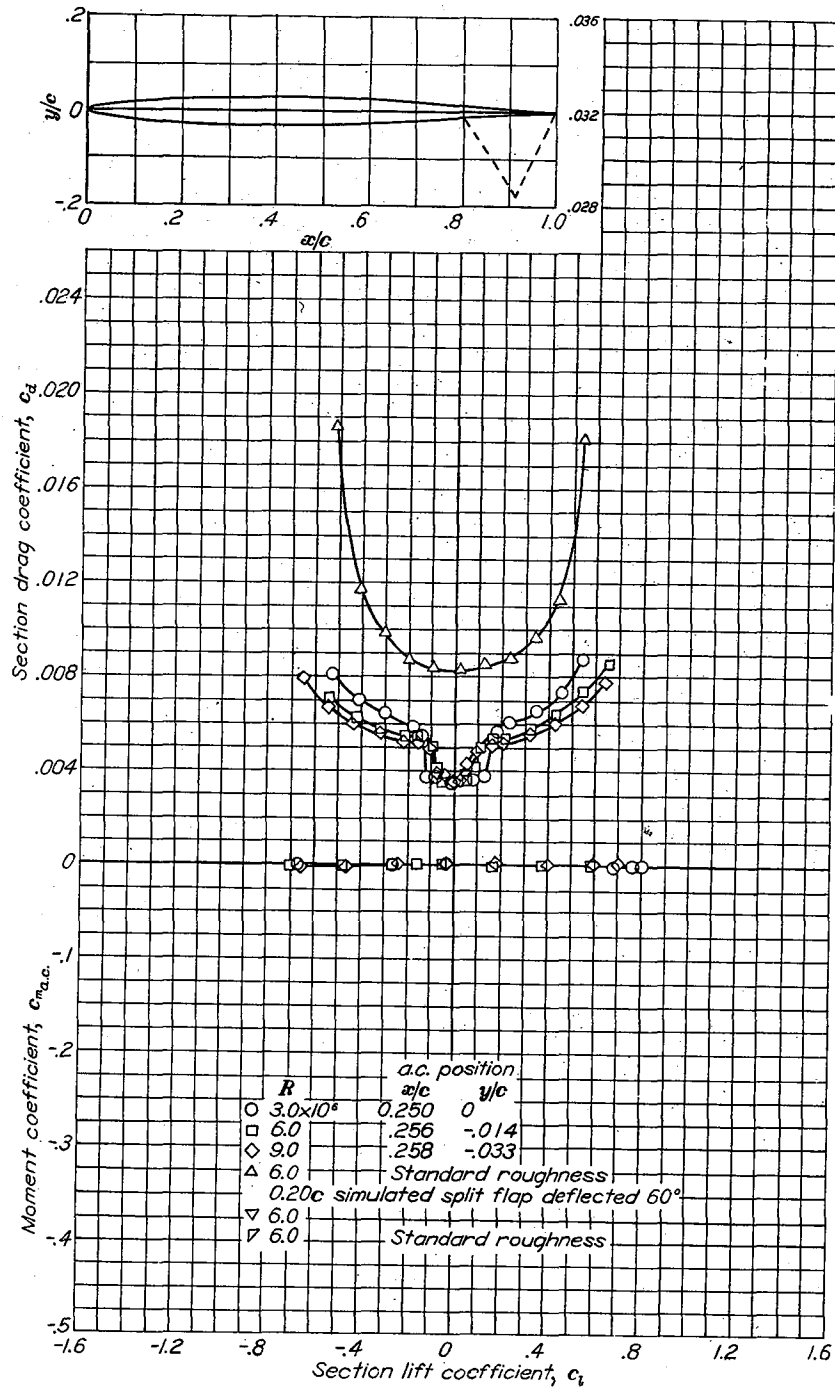
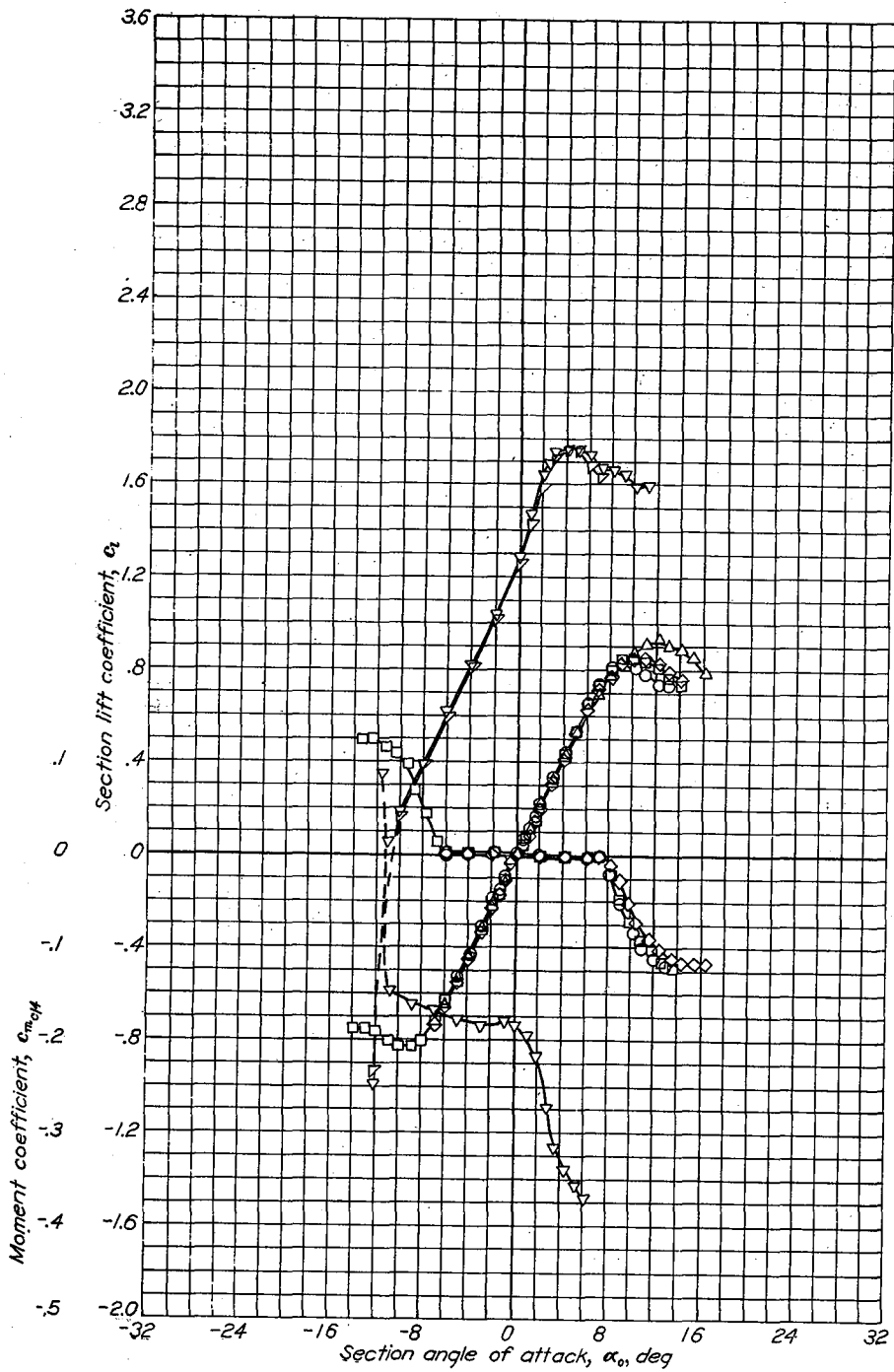
NACA 65,3-618 with flap



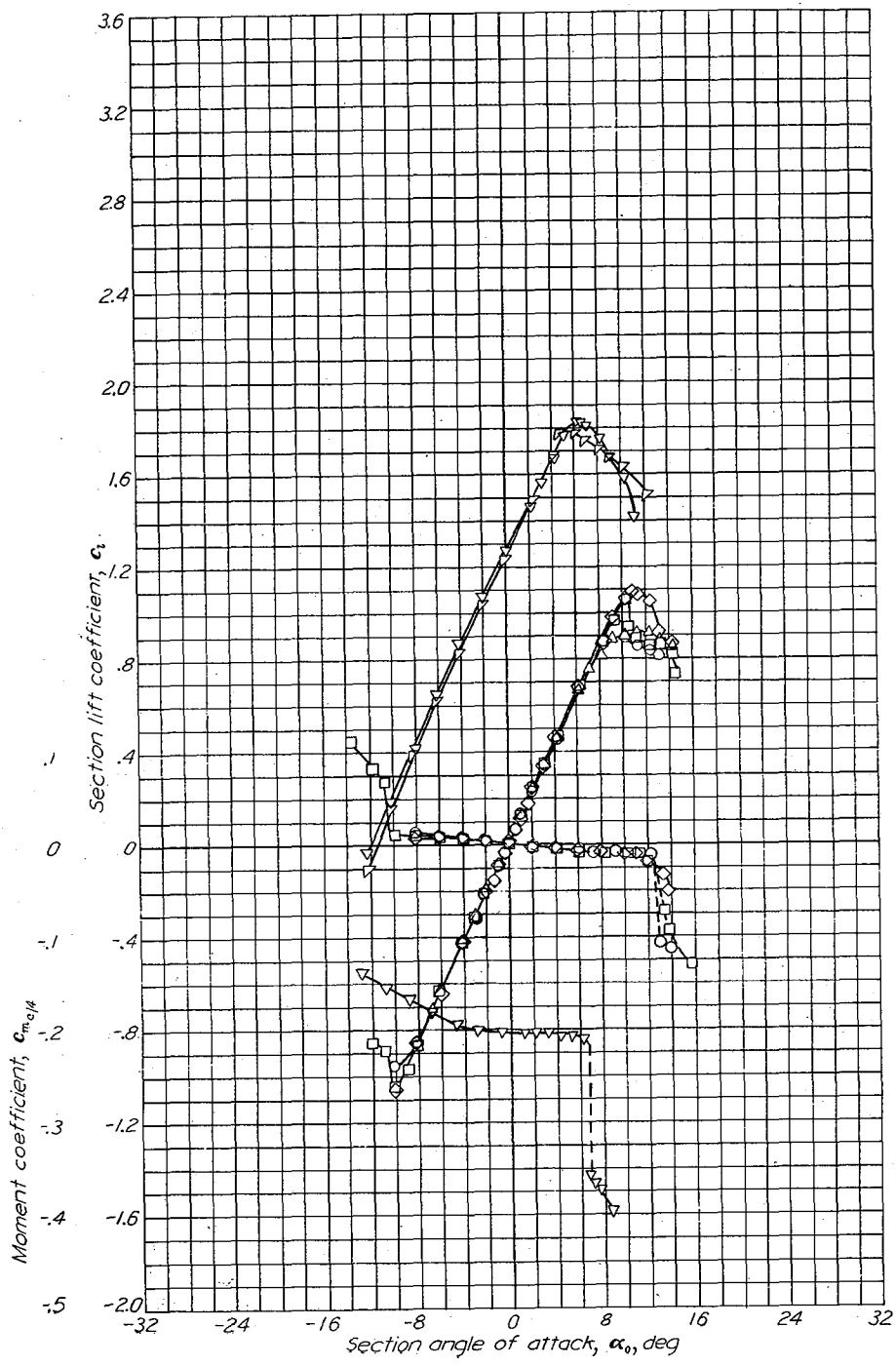
Aerodynamic characteristics of the NACA 65,3-618 airfoil section with 0.20c sealed plain flap.  $R=6 \times 10^6$ .



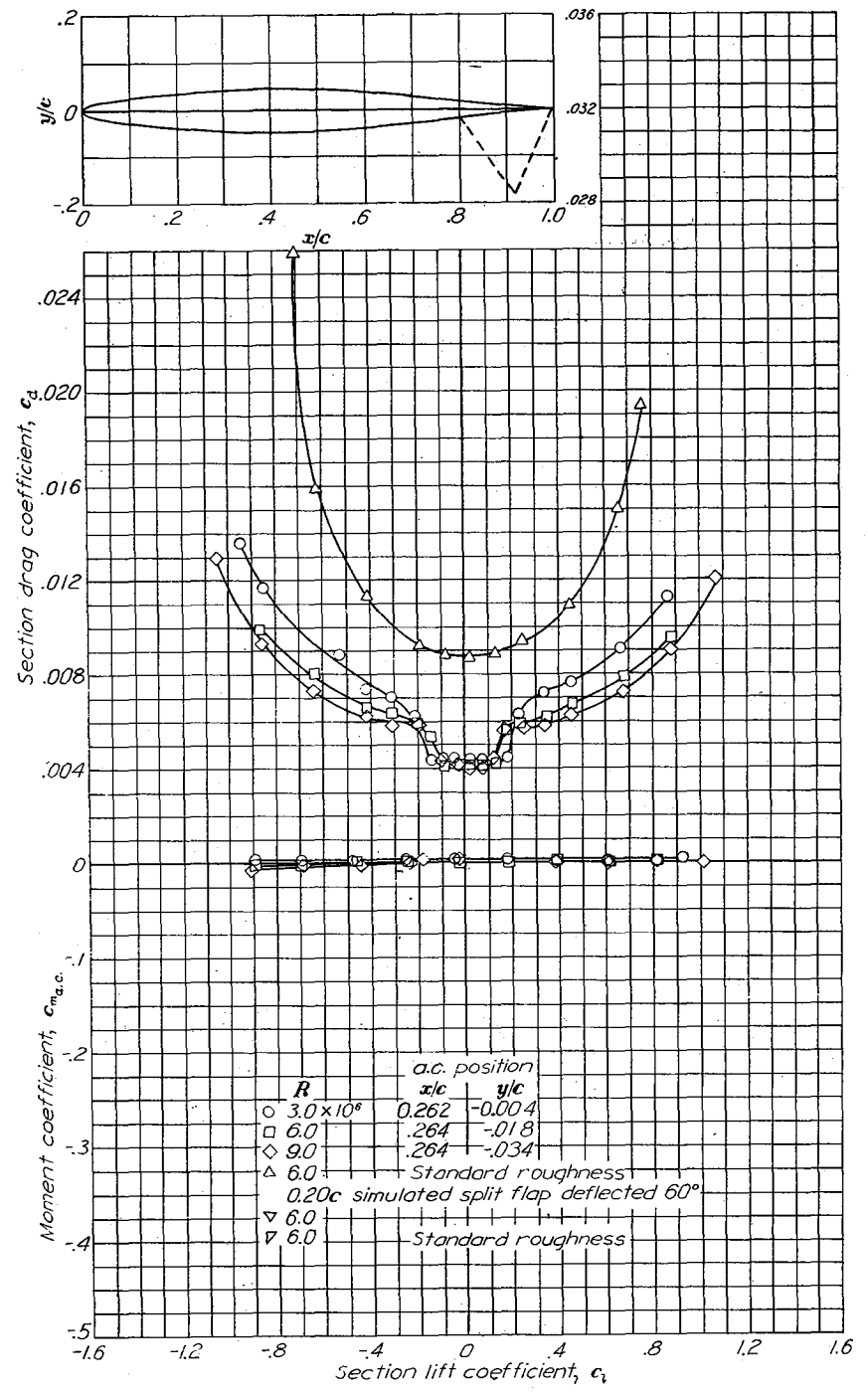
Aerodynamic characteristics of the NACA 65(216)-415,  $\alpha=0.5$  airfoil section, 24-inch chord.



Aerodynamic characteristics of the NACA 65-006 airfoil section, 24-inch chord.

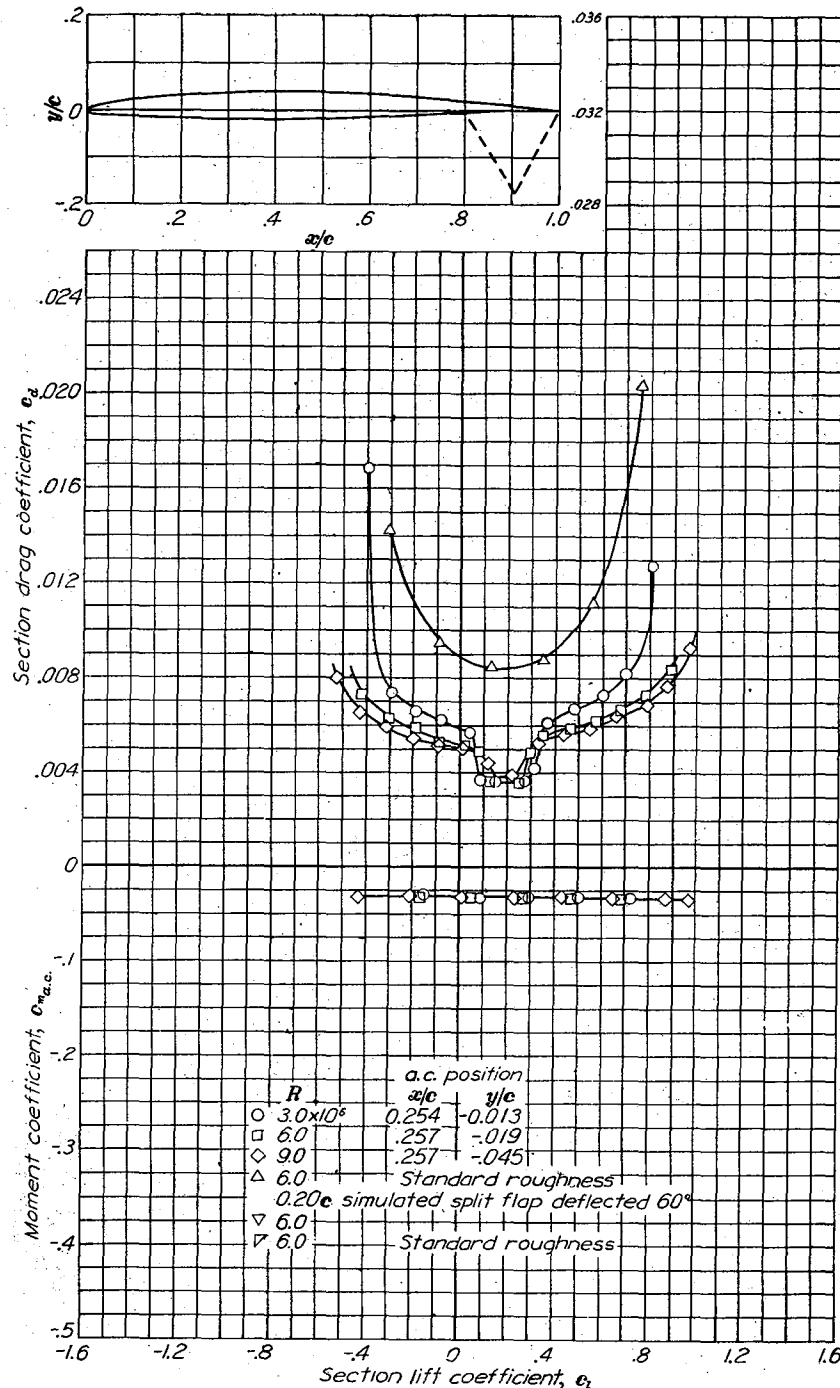
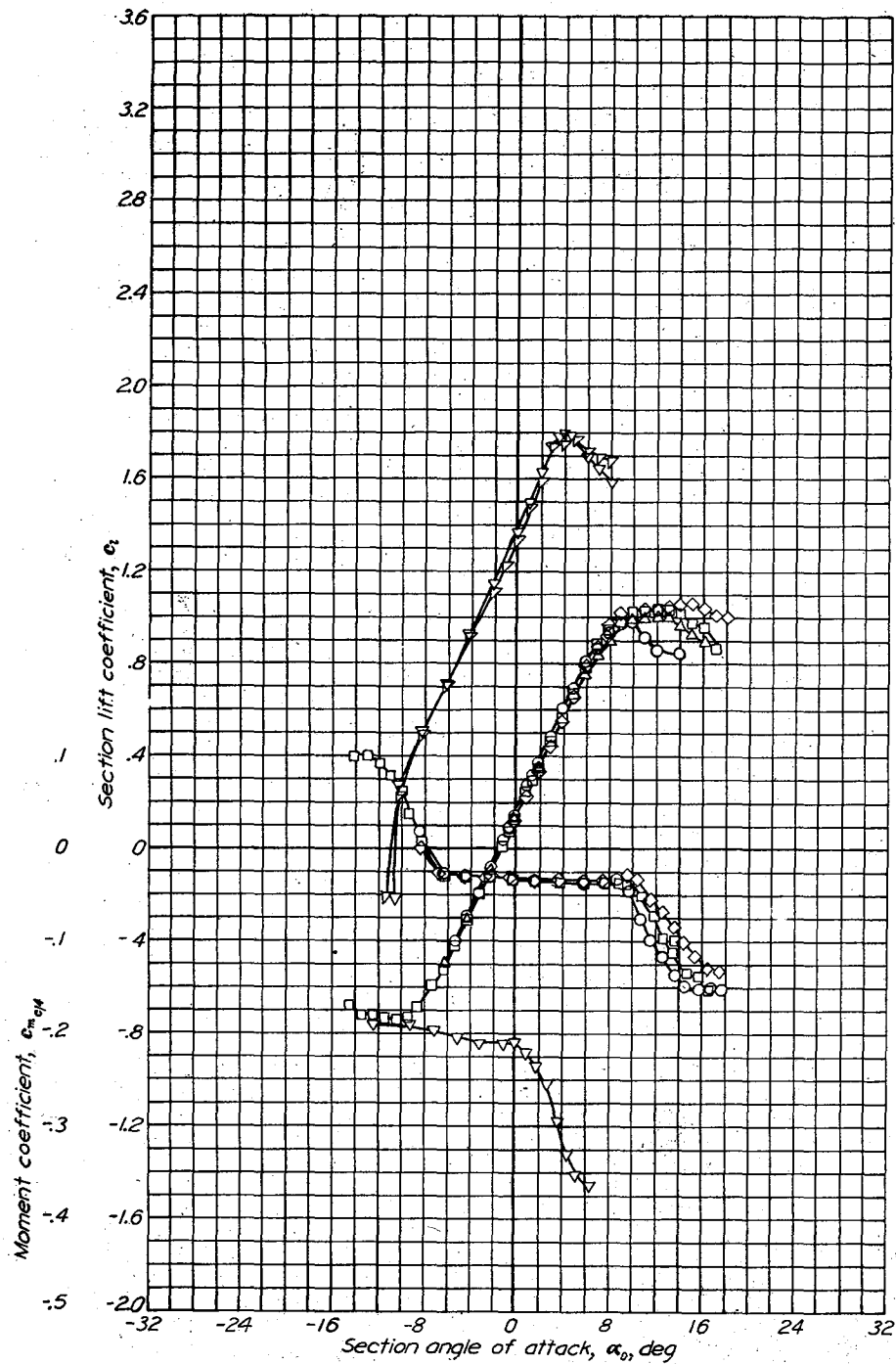


Aerodynamic characteristics of the NACA 65-009 airfoil section, 24-inch chord.



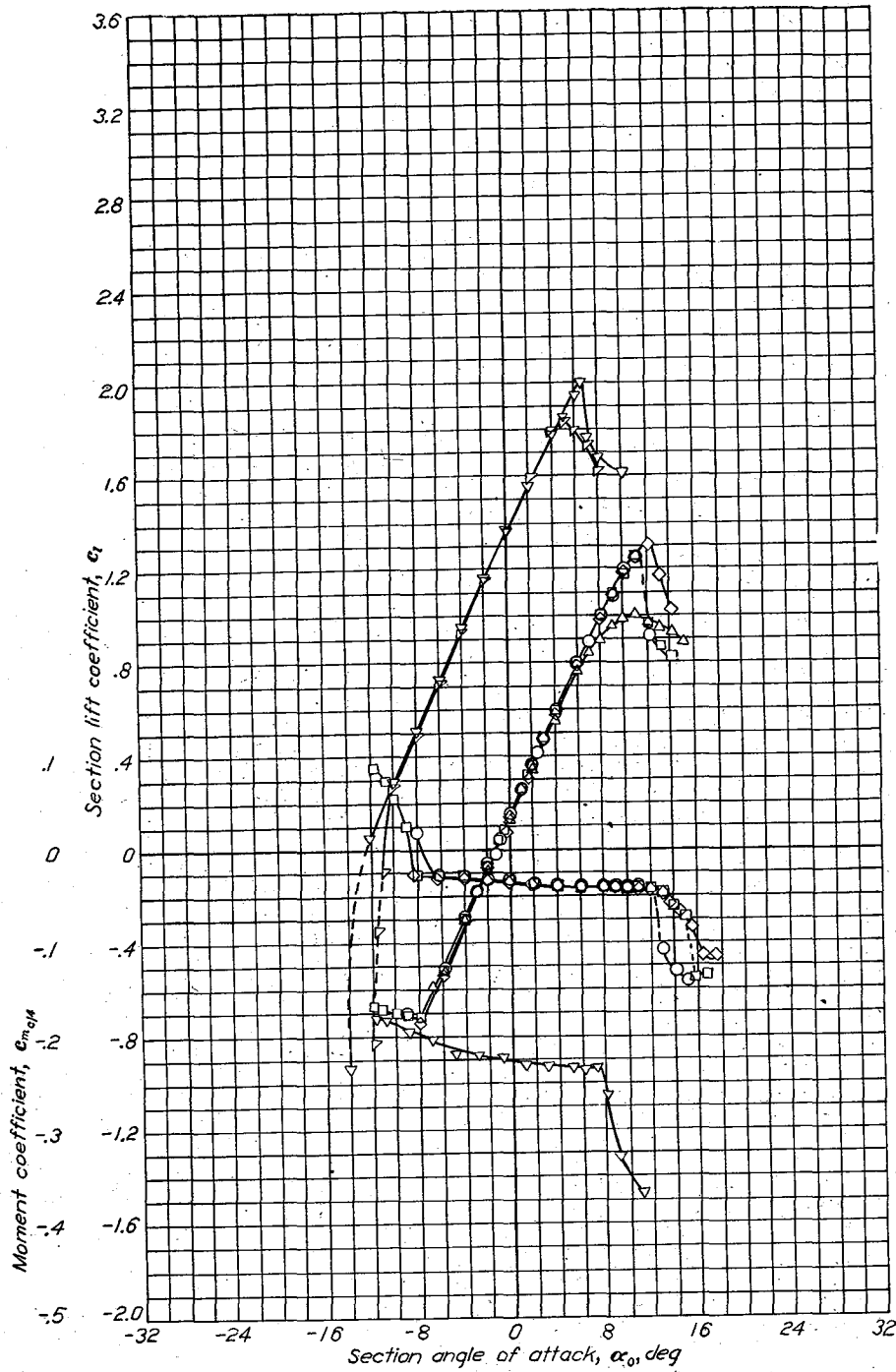
NACA 65-009

SUMMARY OF AIRFOIL DATA

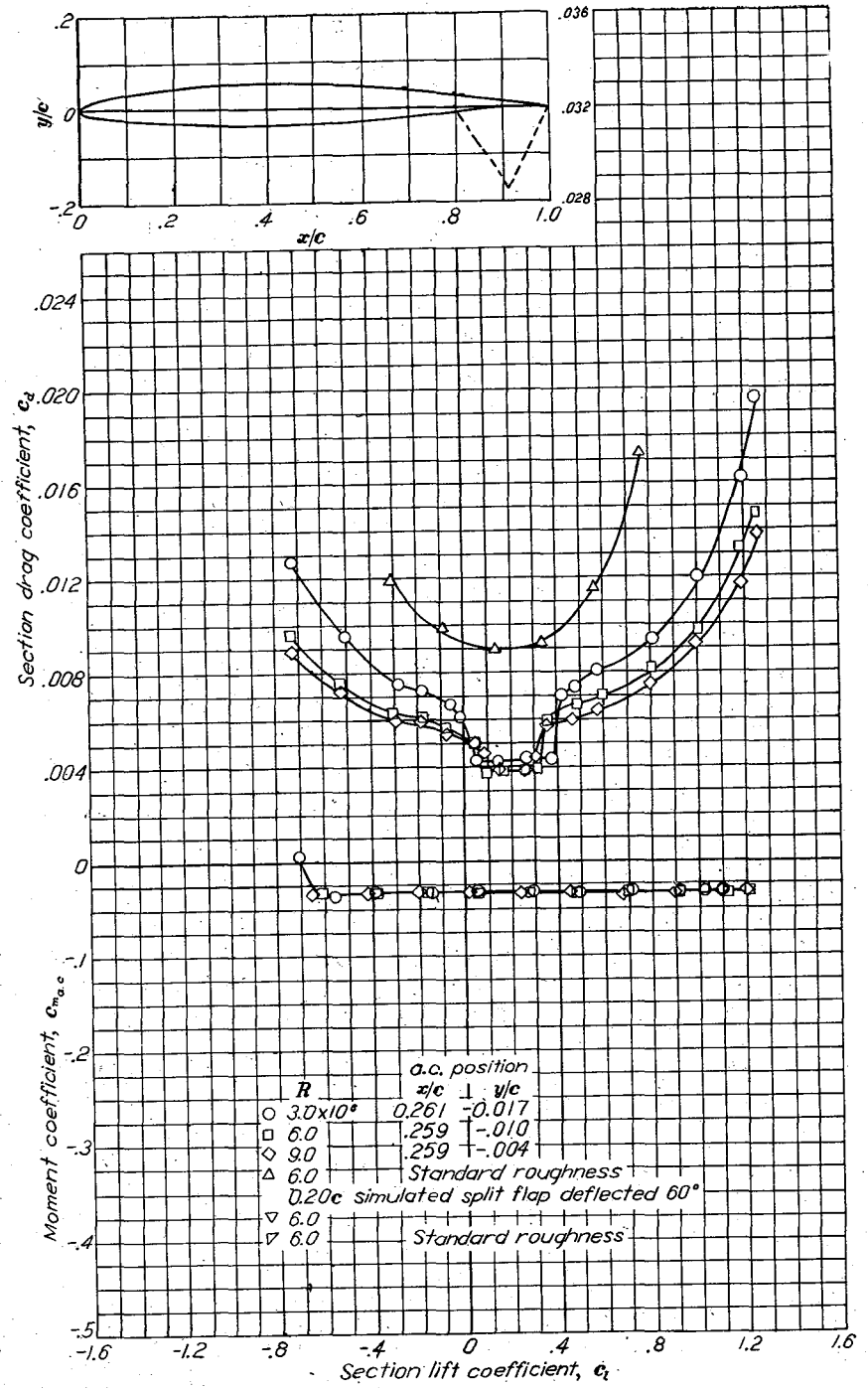


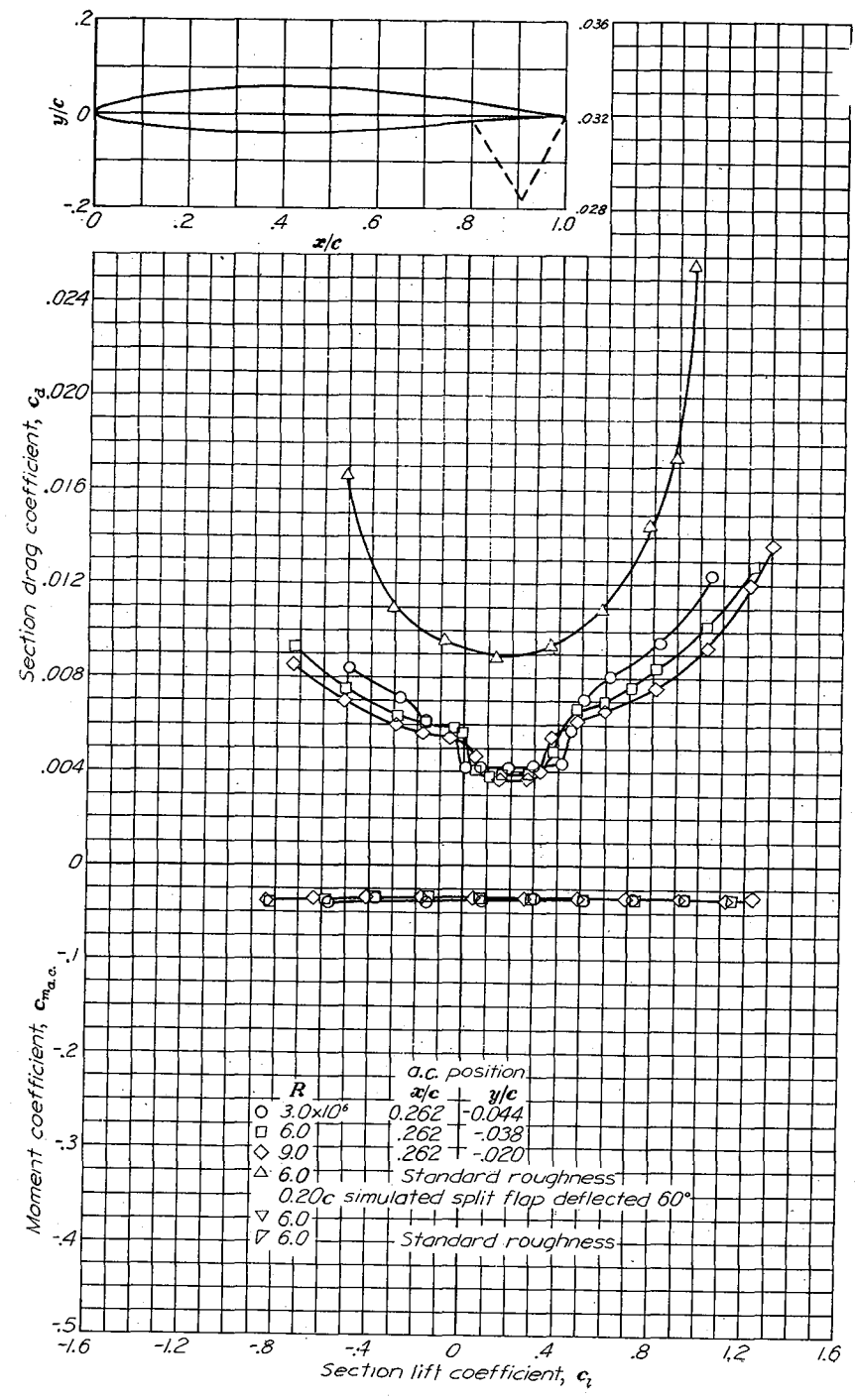
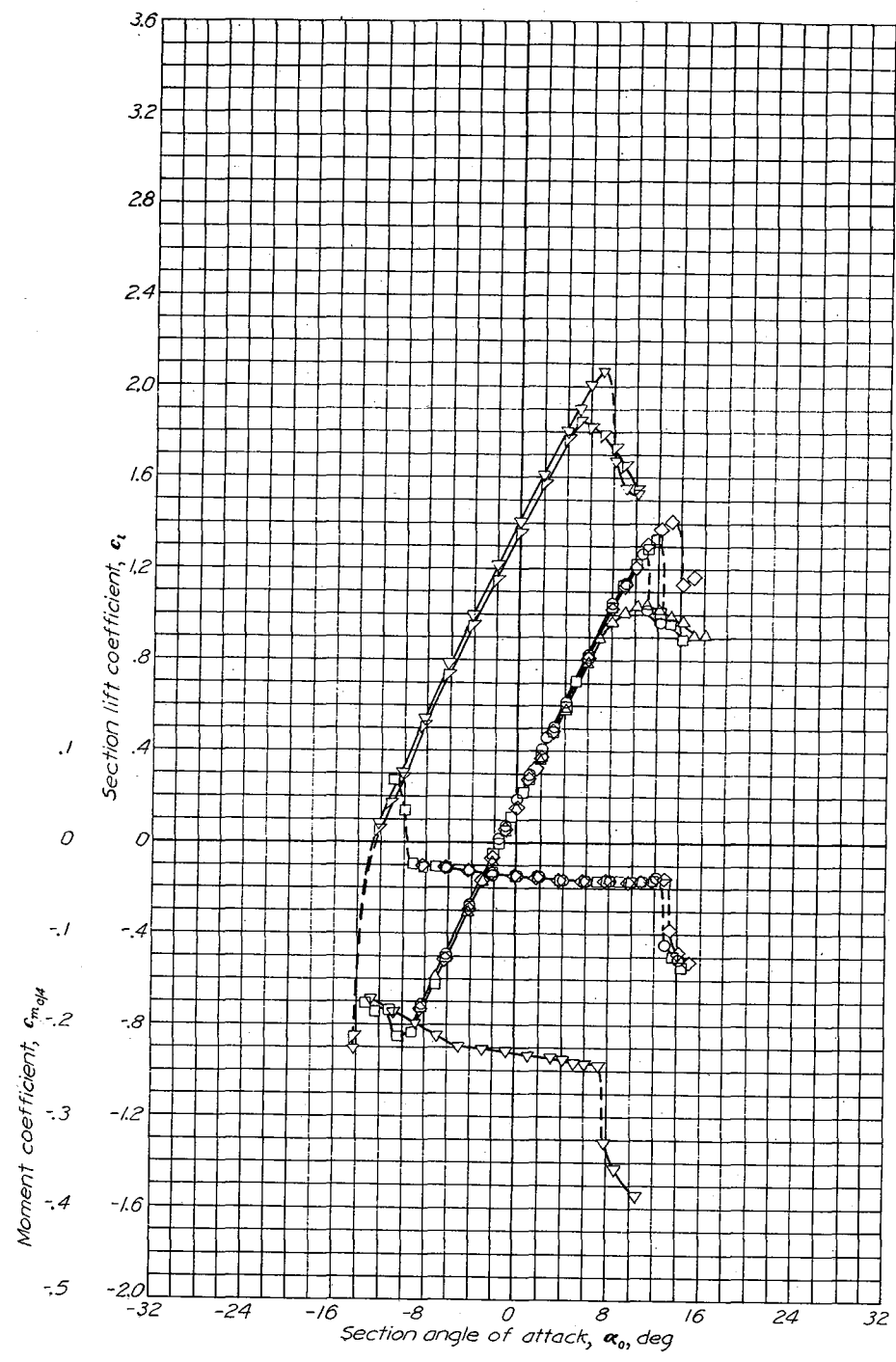
Aerodynamic characteristics of the NACA 65-206 airfoil section, 24-inch chord.



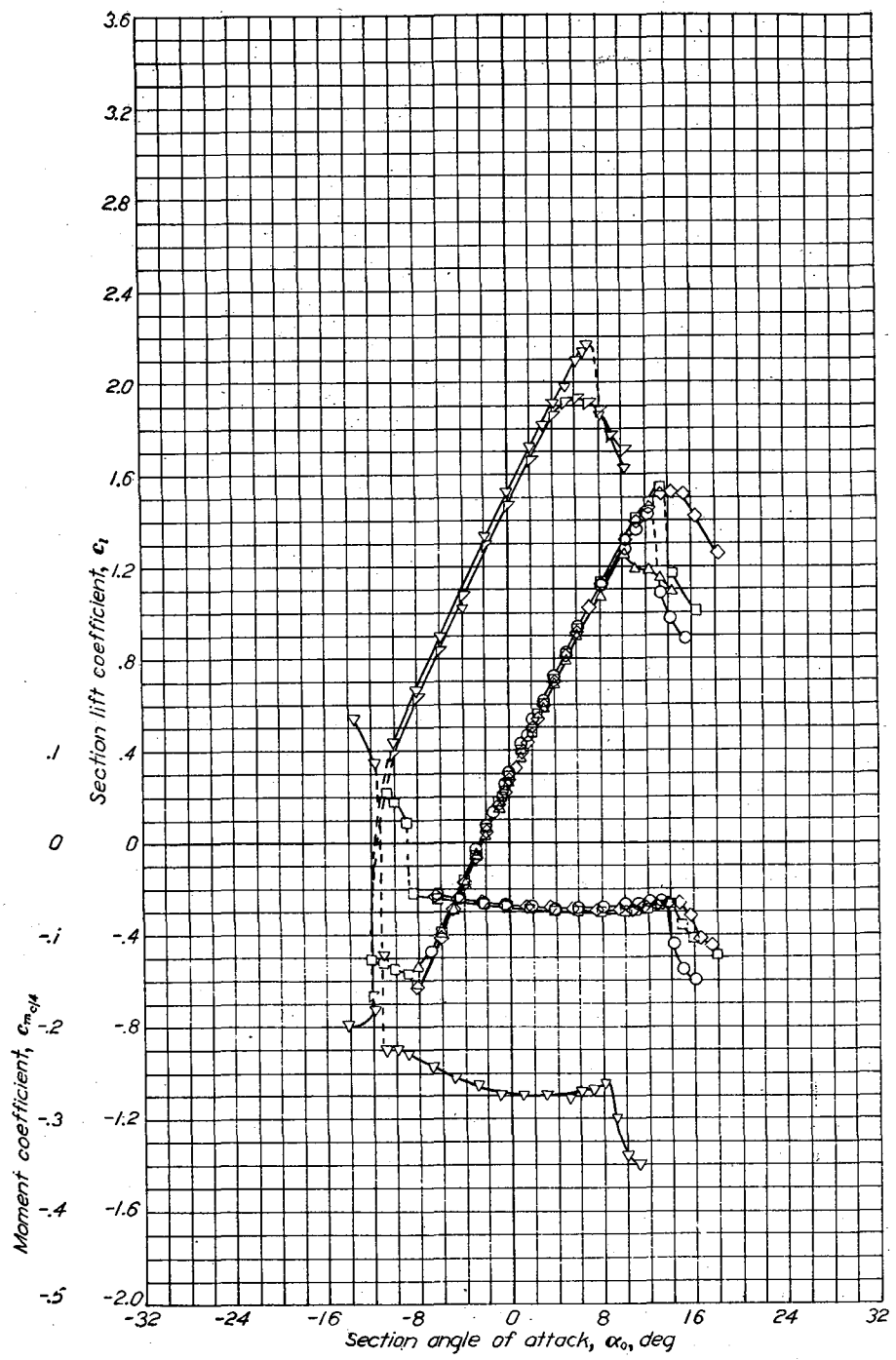


Aerodynamic characteristics of the NACA 65-209 airfoil section, 24 inch chord.

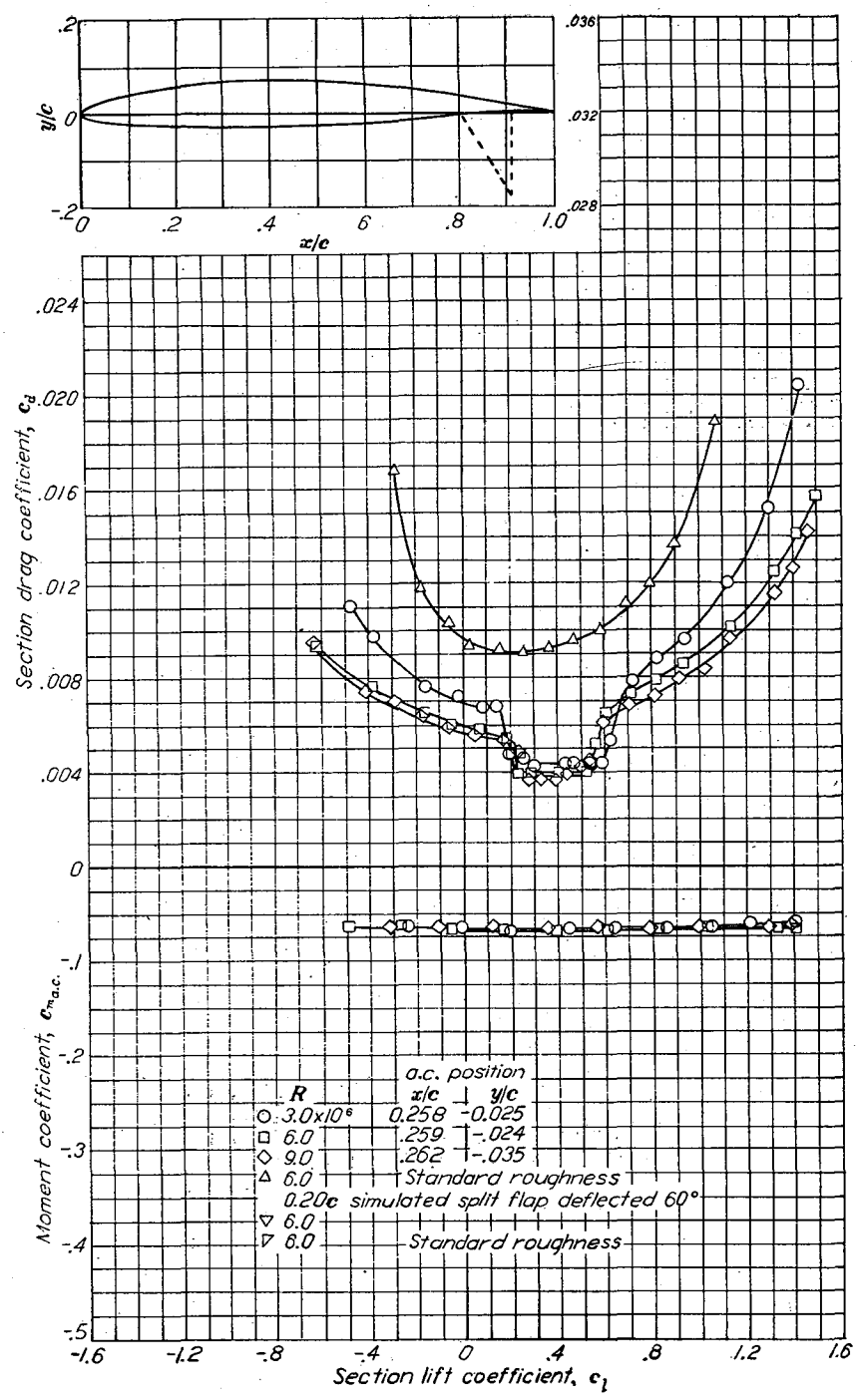


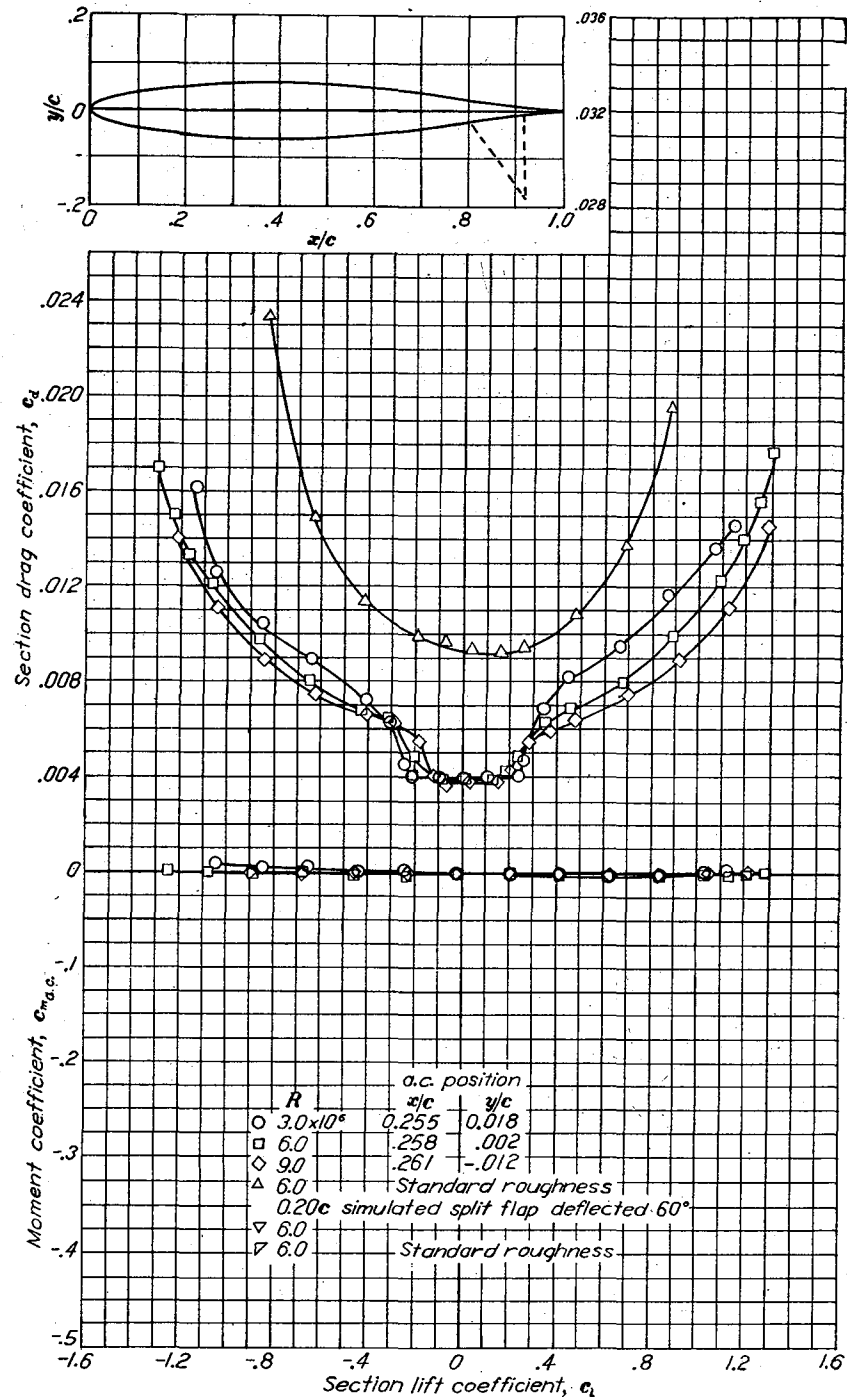
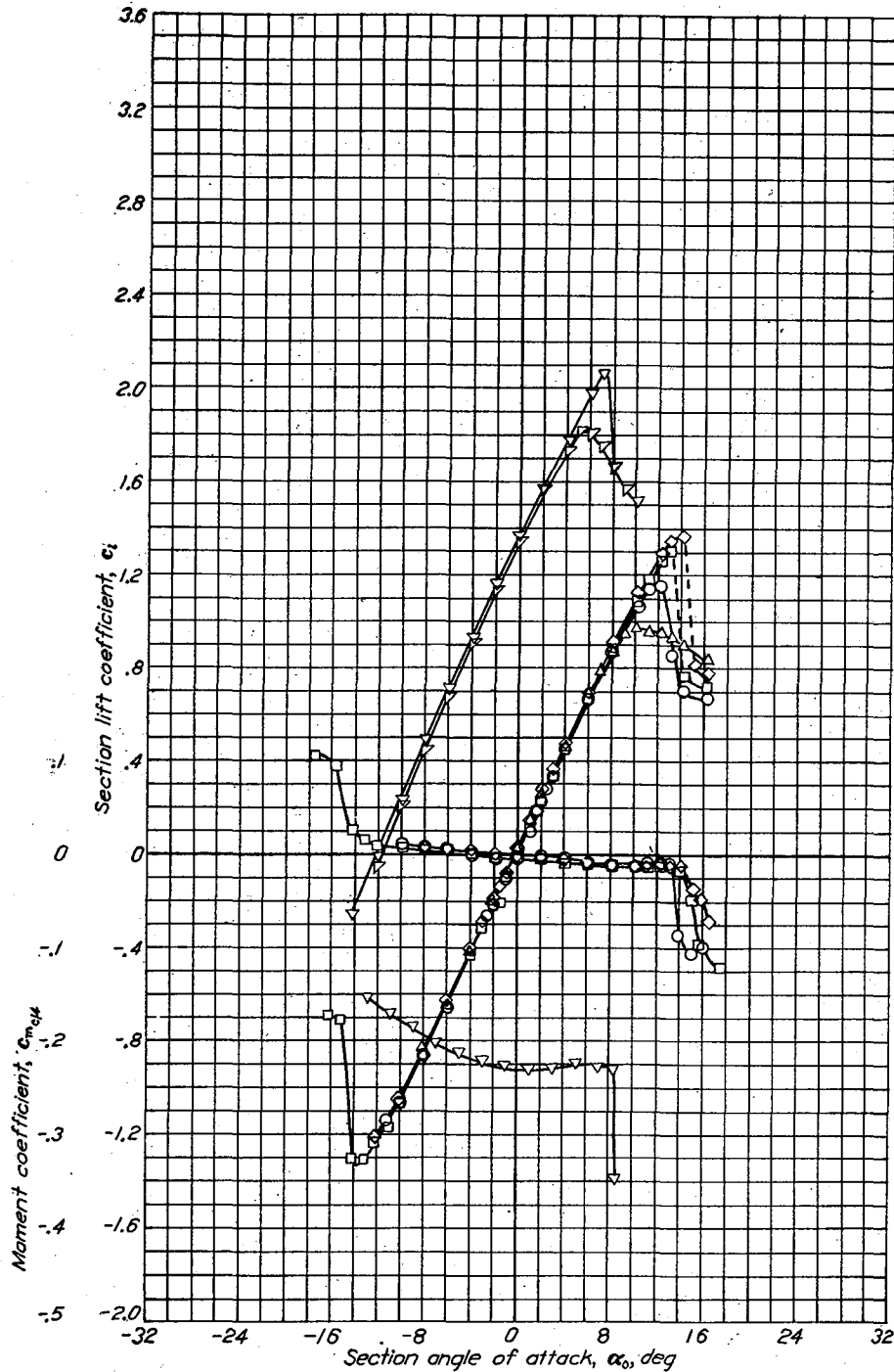


Aerodynamic characteristics of the NACA 65-210 airfoil section, 24-inch chord.

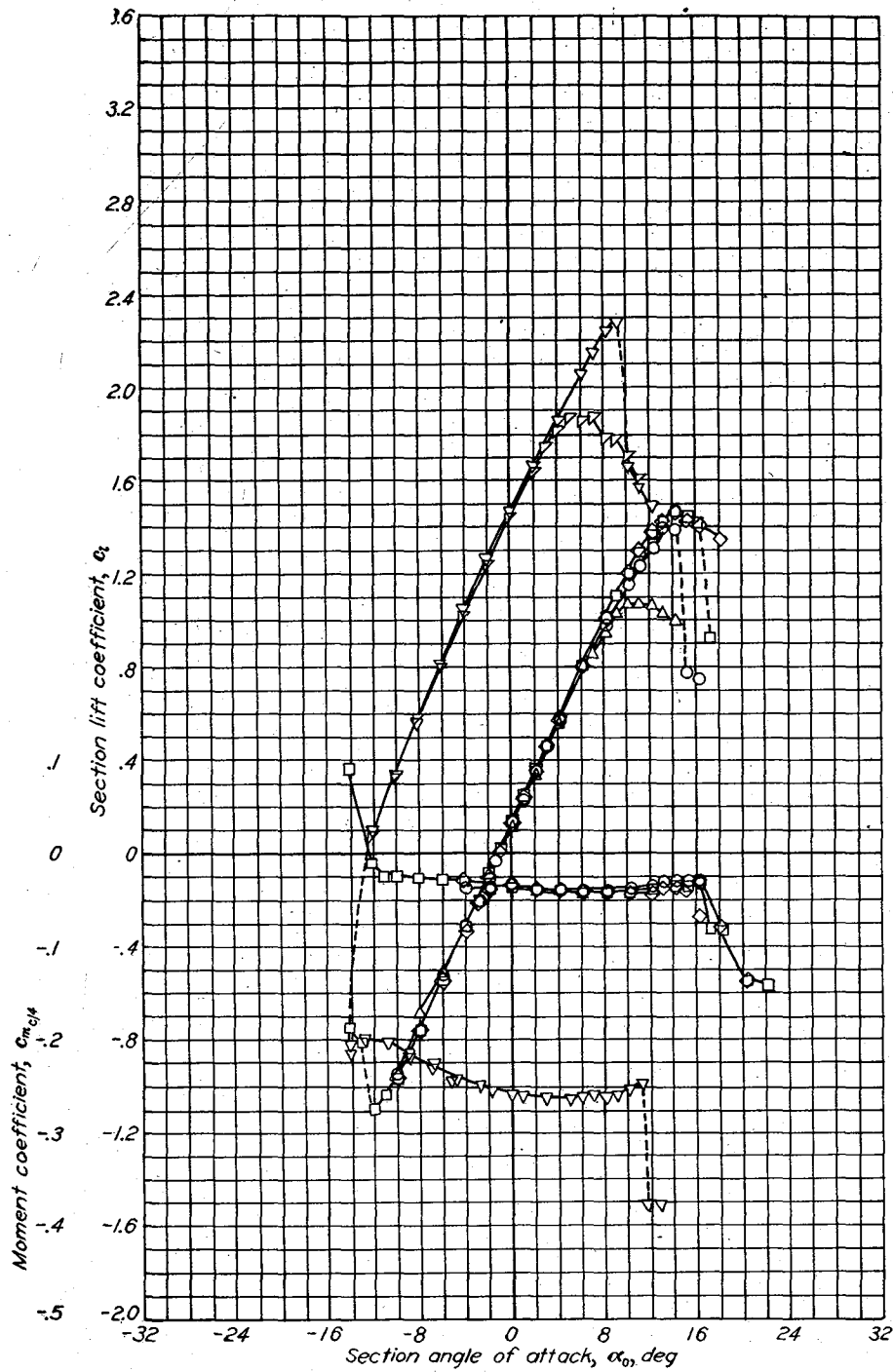


Aerodynamic characteristics of the NACA 65-410 airfoil section, 24-inch chord.

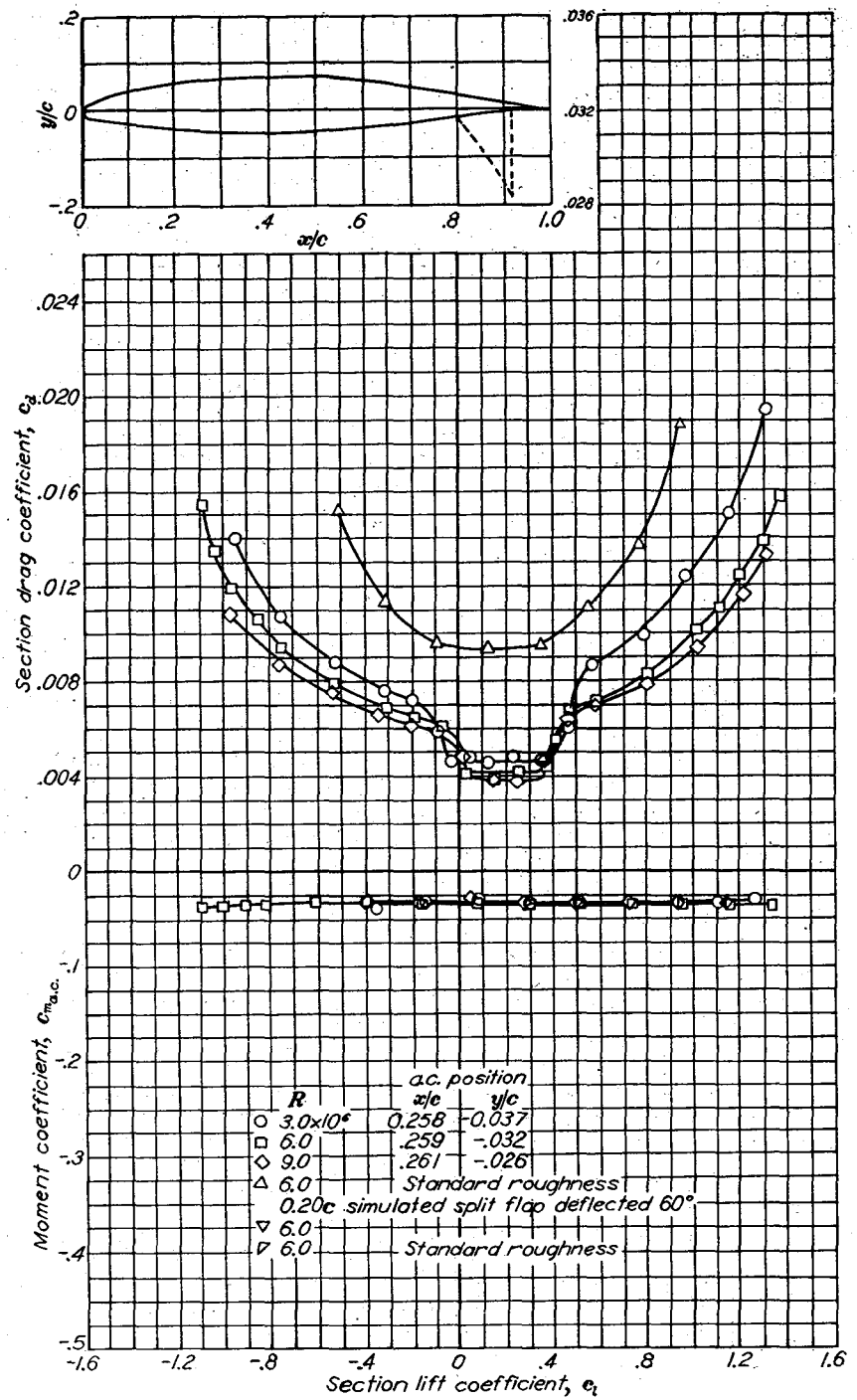




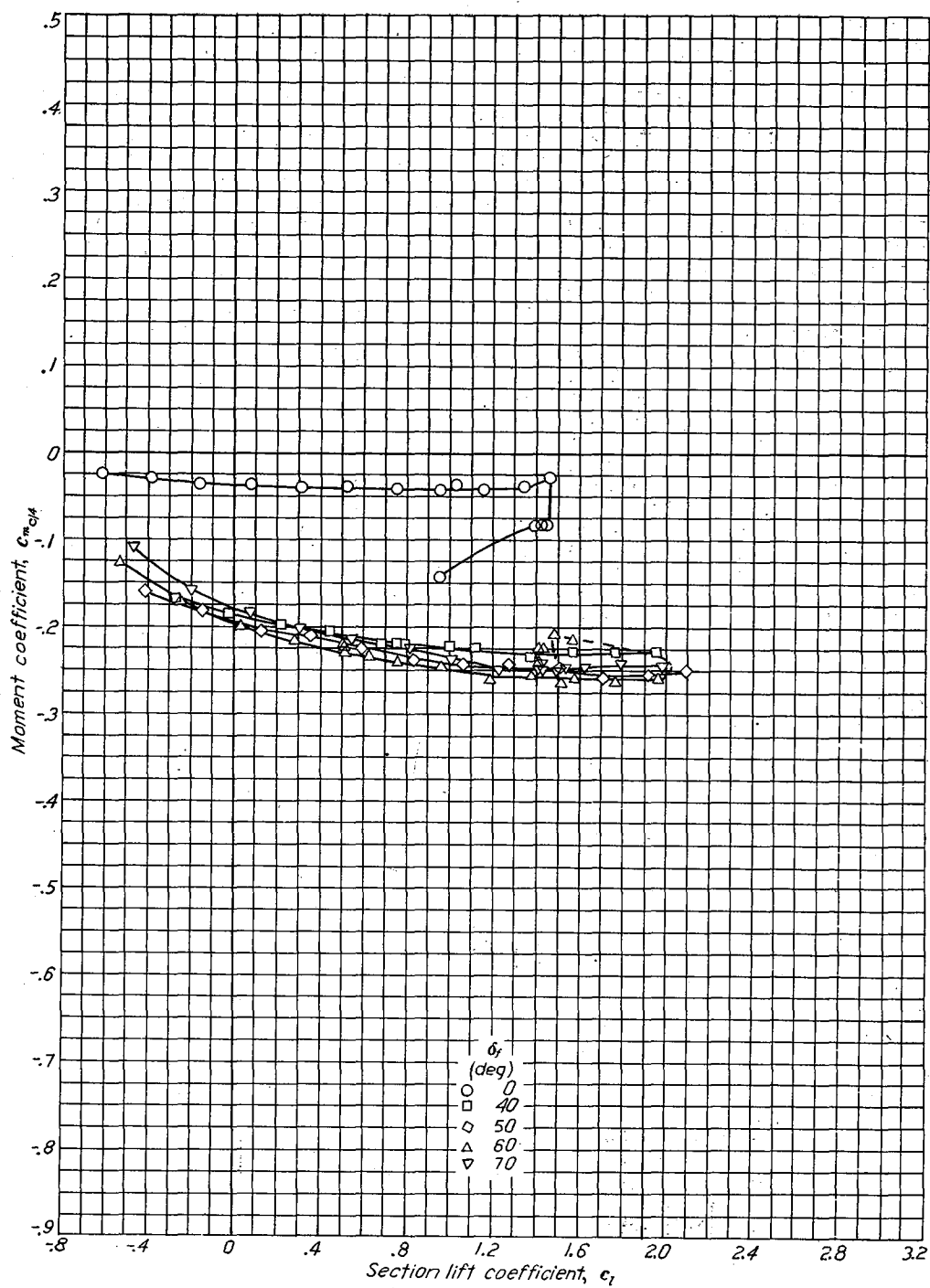
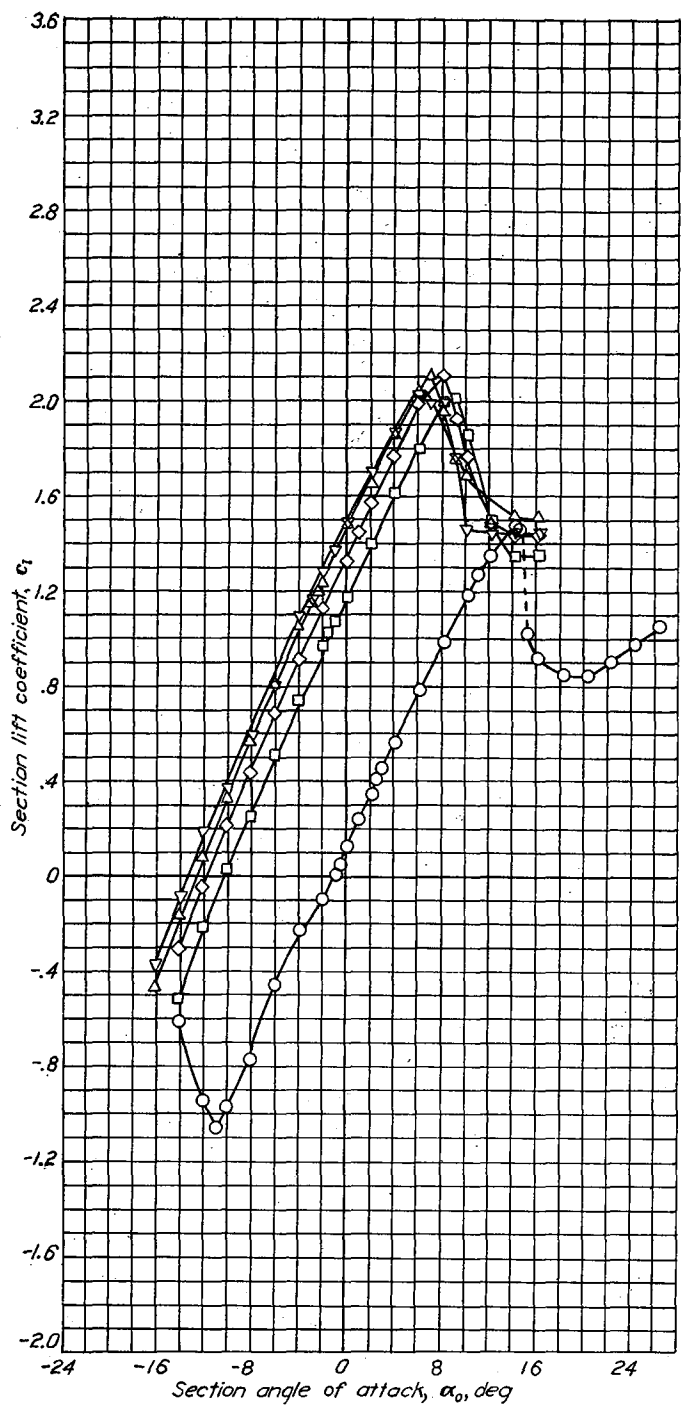
Aerodynamic characteristics of the NACA 65-012 airfoil section, 24-inch chord.

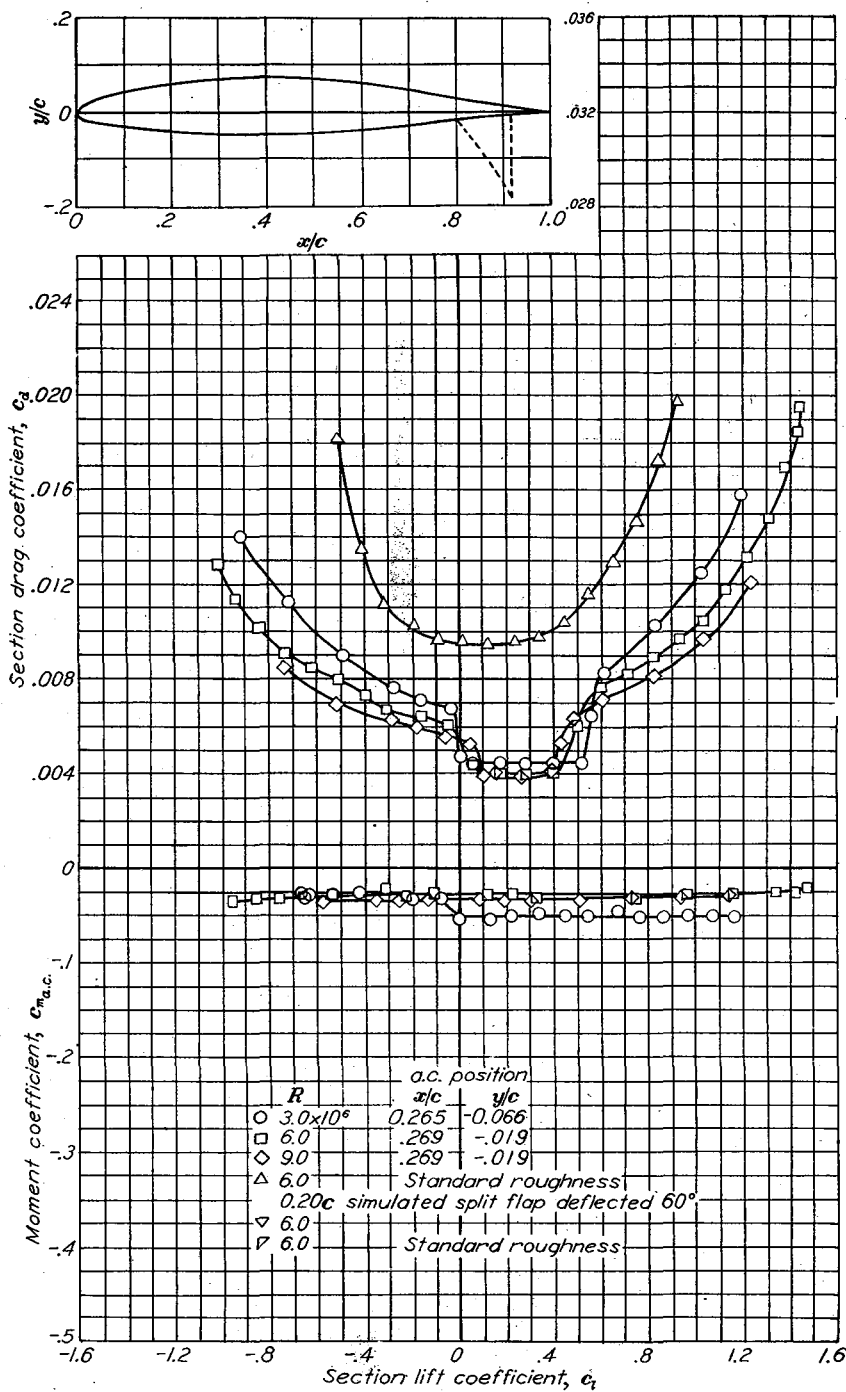
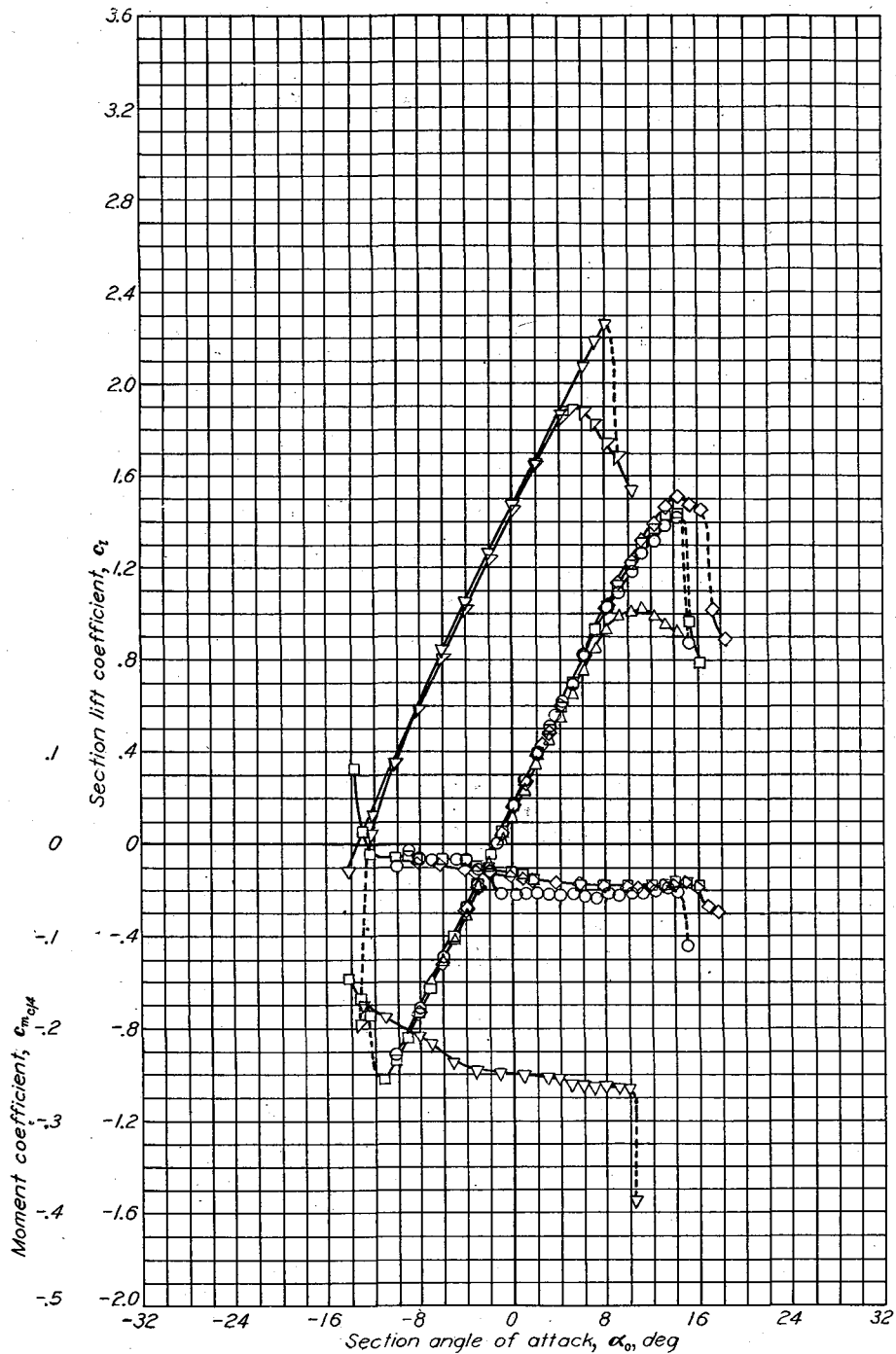


Aerodynamic characteristics of the NACA 65-212 airfoil section, 24-inch chord.

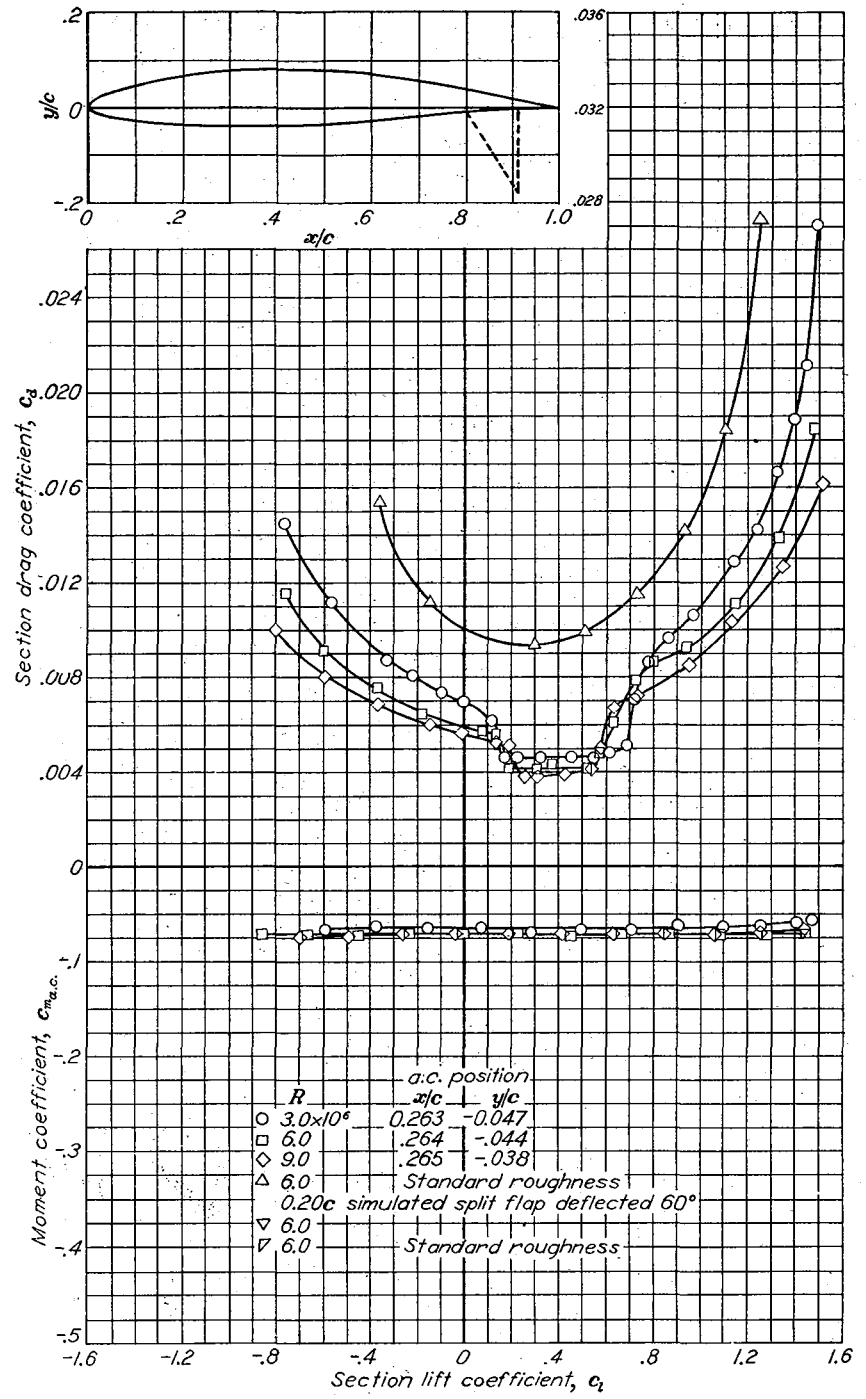
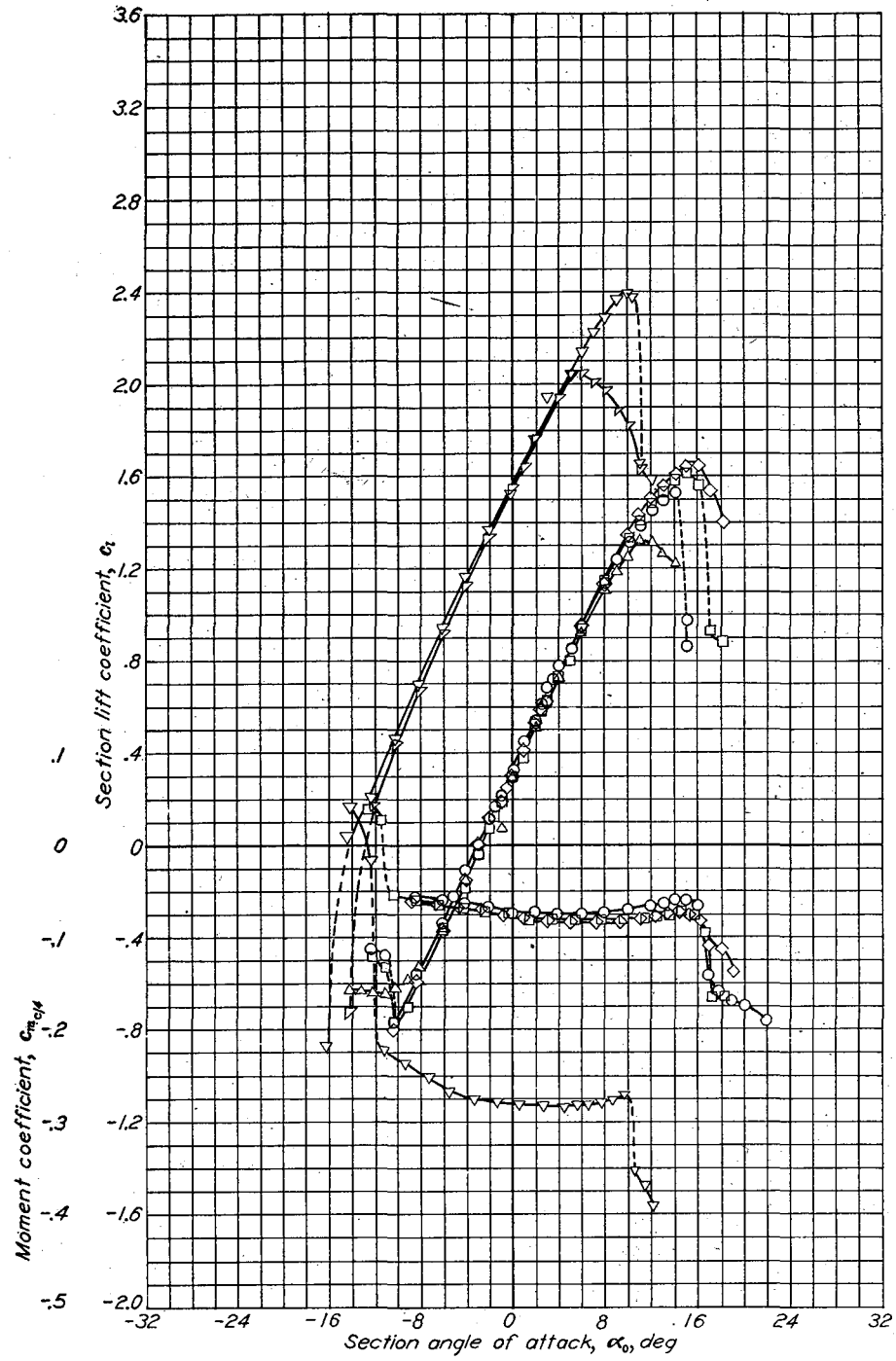


## NACA 651-212 with flap

Lift and moment characteristics of the NACA 651-212 airfoil section with 0.20c split flap.  $R=6 \times 10^5$ .

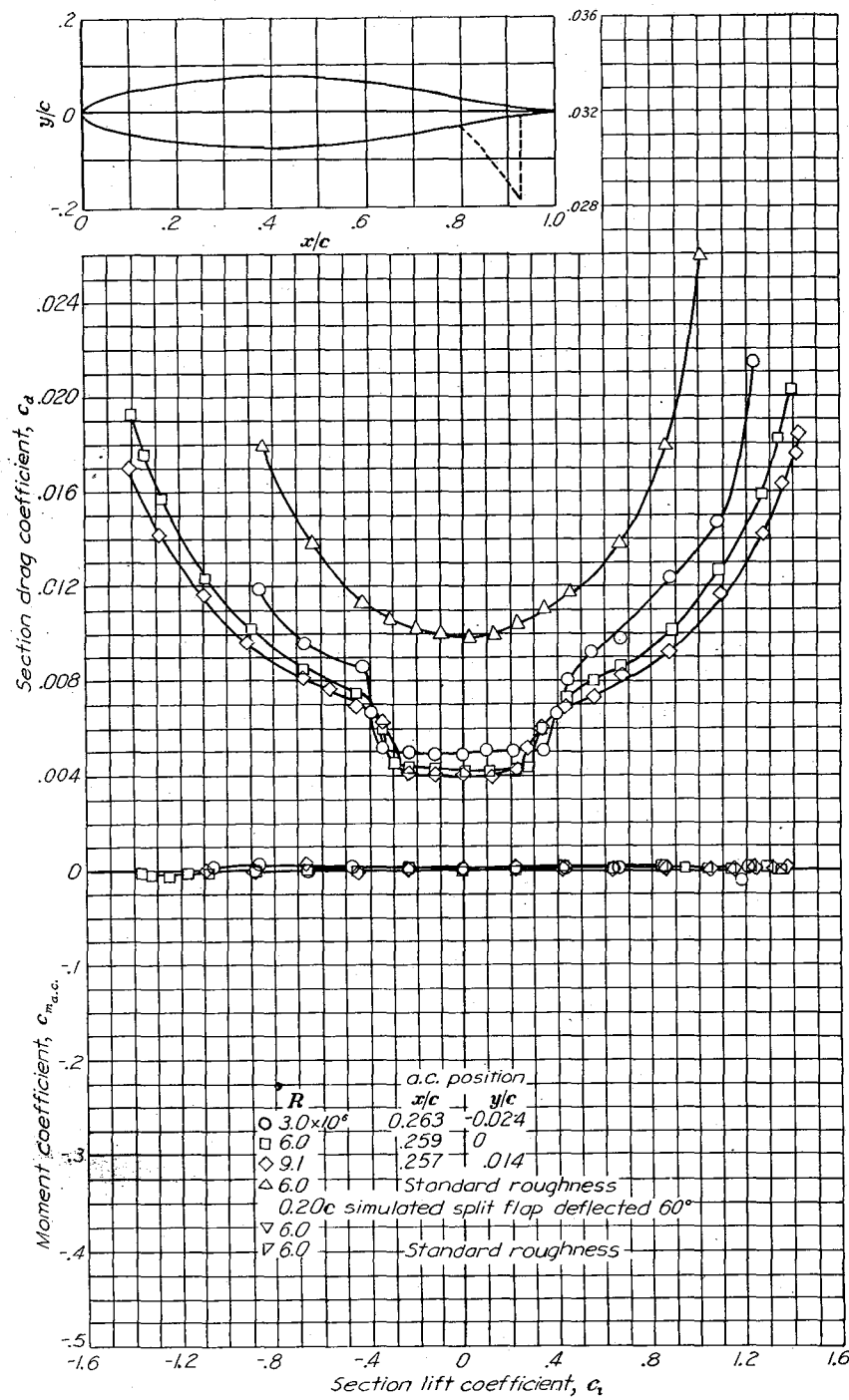
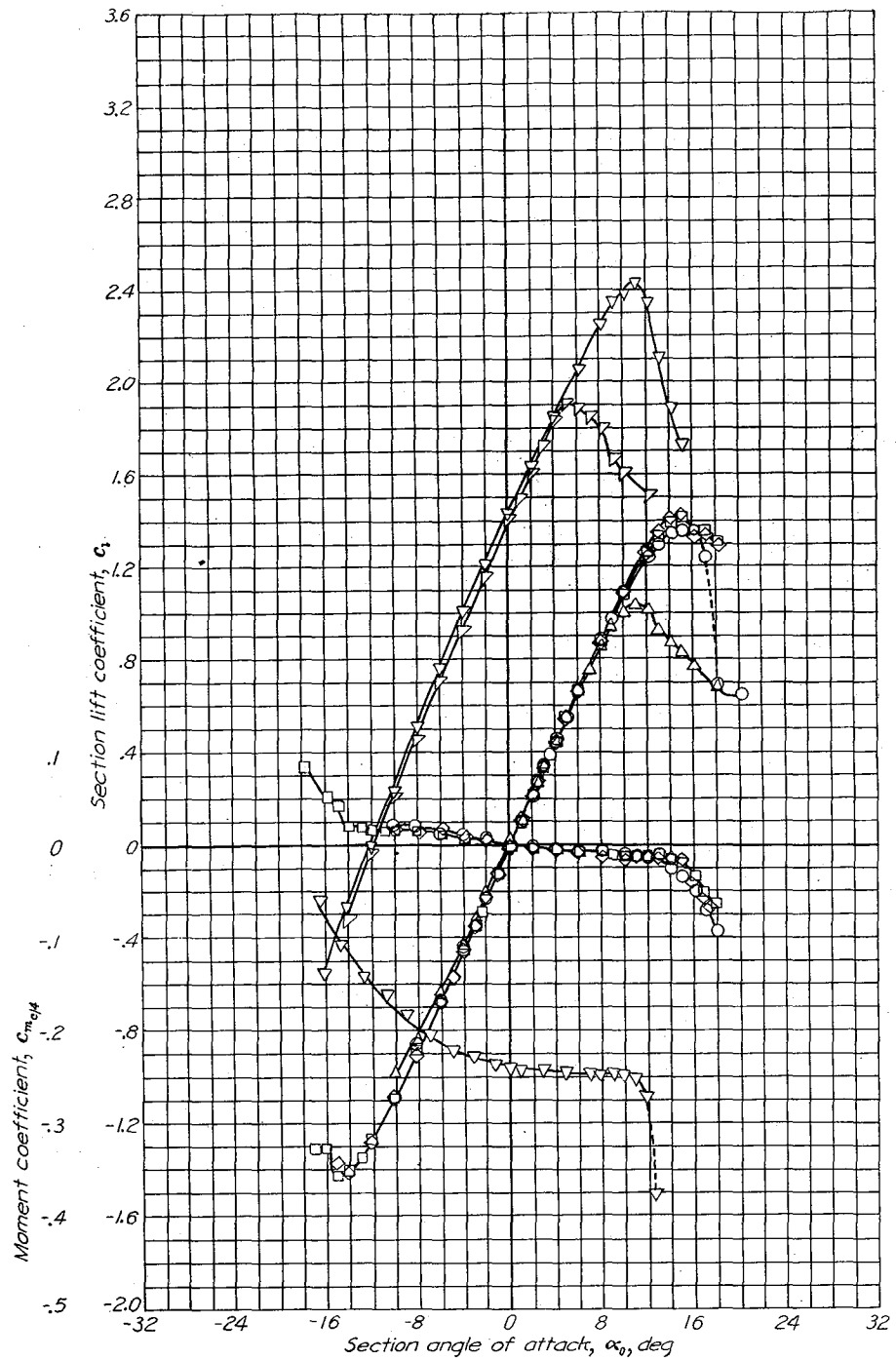


Aerodynamic characteristics of the NACA 651-212,  $\alpha=0.6$  airfoil section, 24-inch chord.

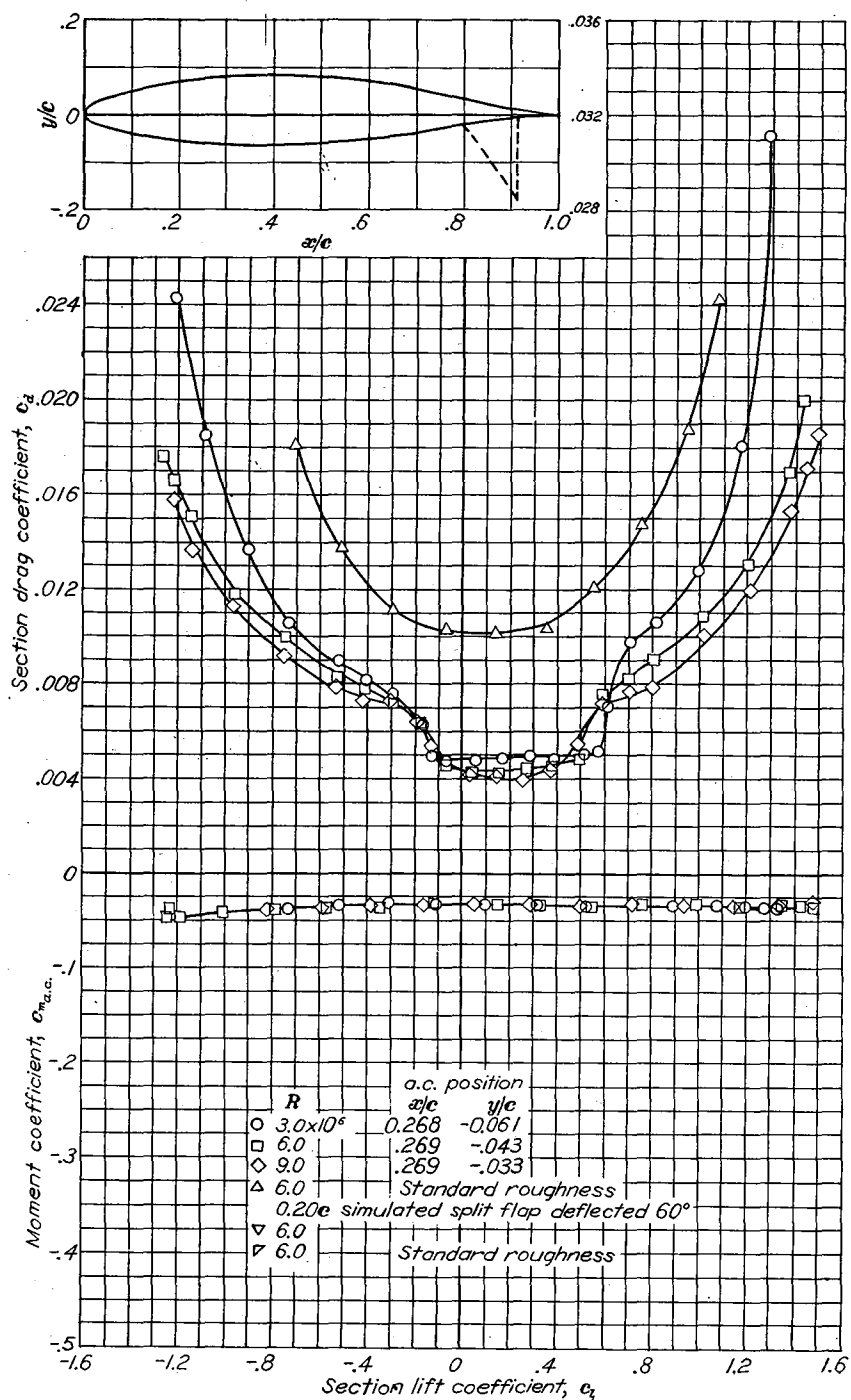
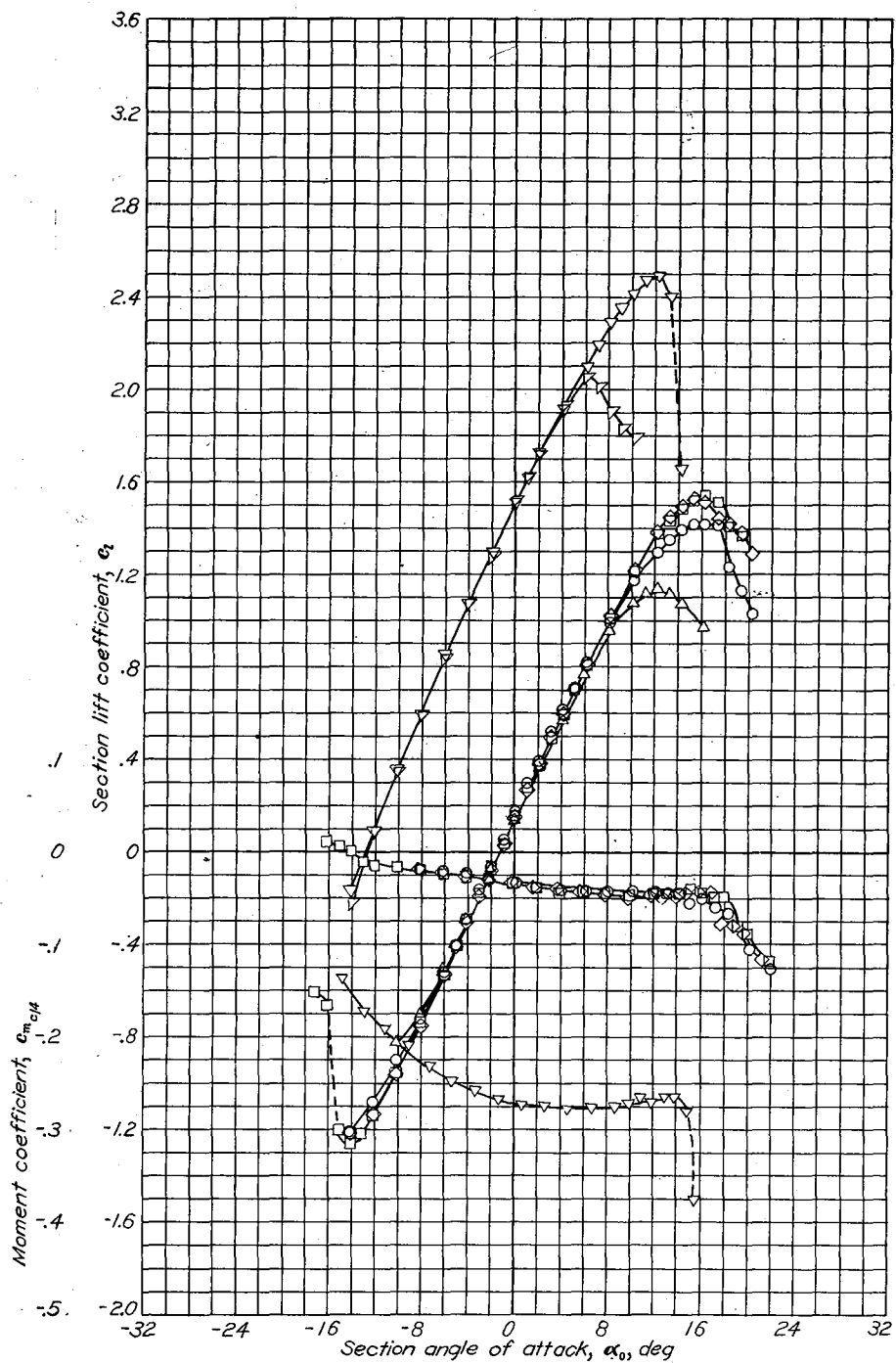


Aerodynamic characteristics of the NACA 651-412 airfoil section, 24 inch chord.

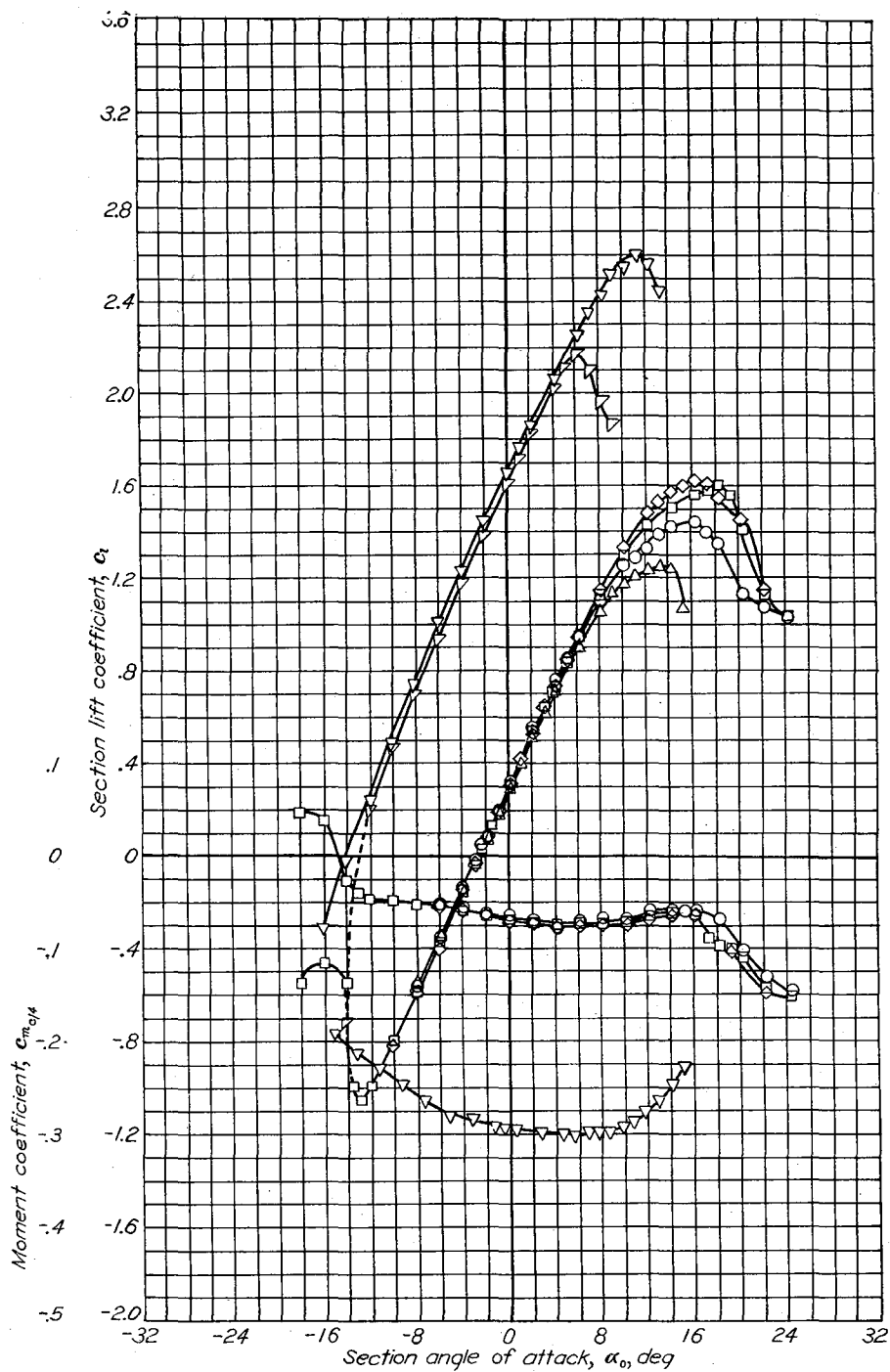




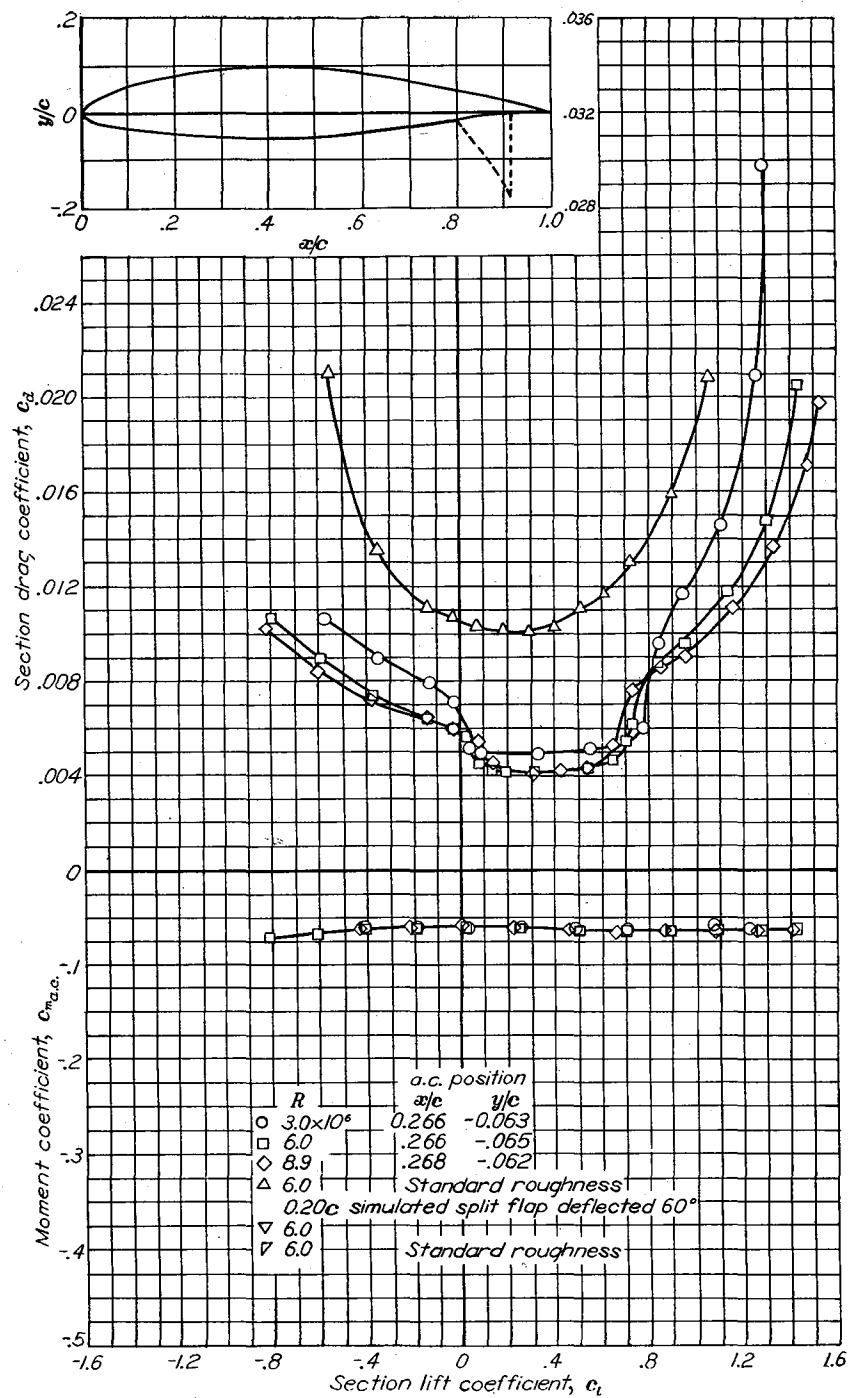
Aerodynamic characteristics of the NACA 652-015 airfoil section, 24-inch chord.



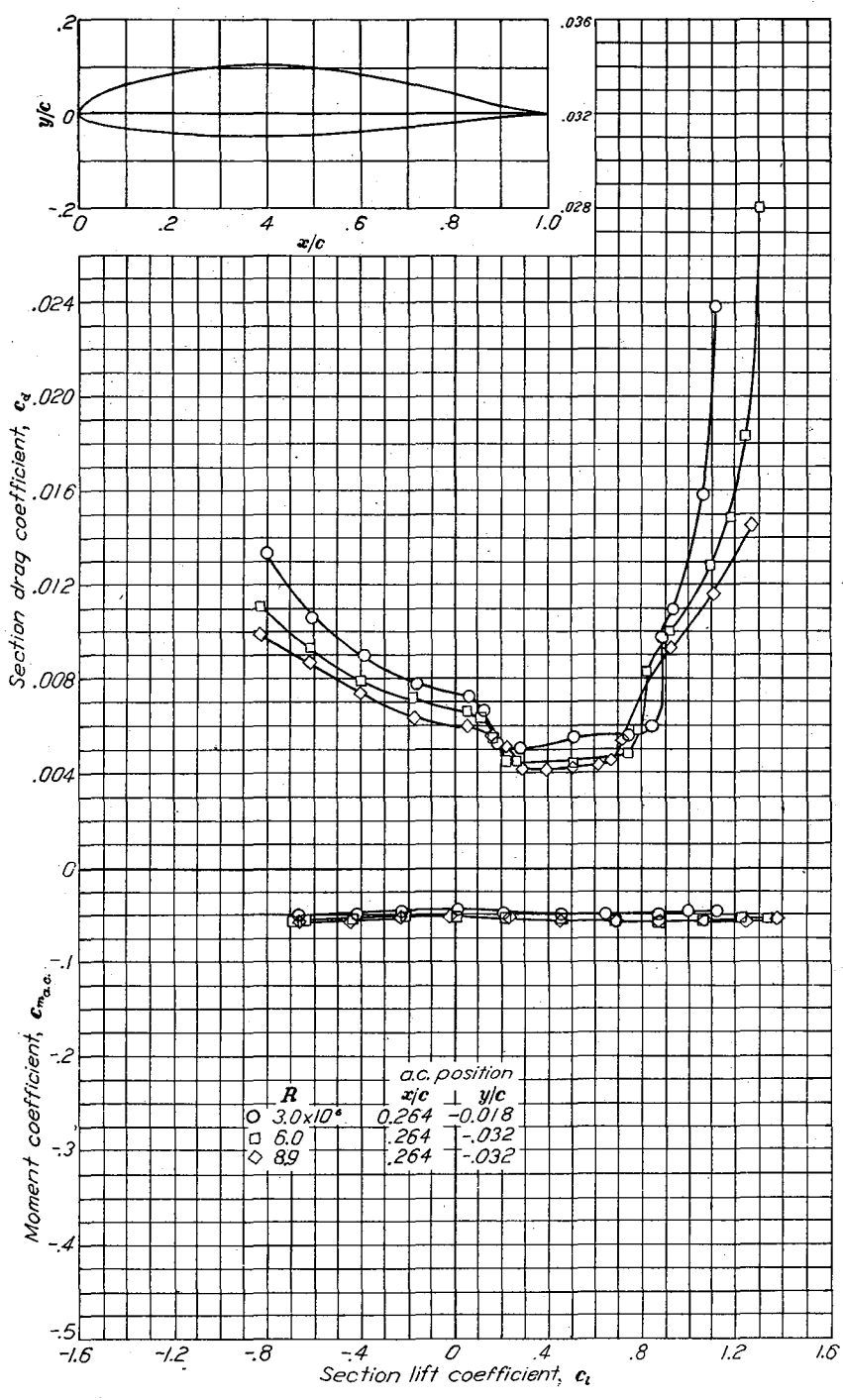
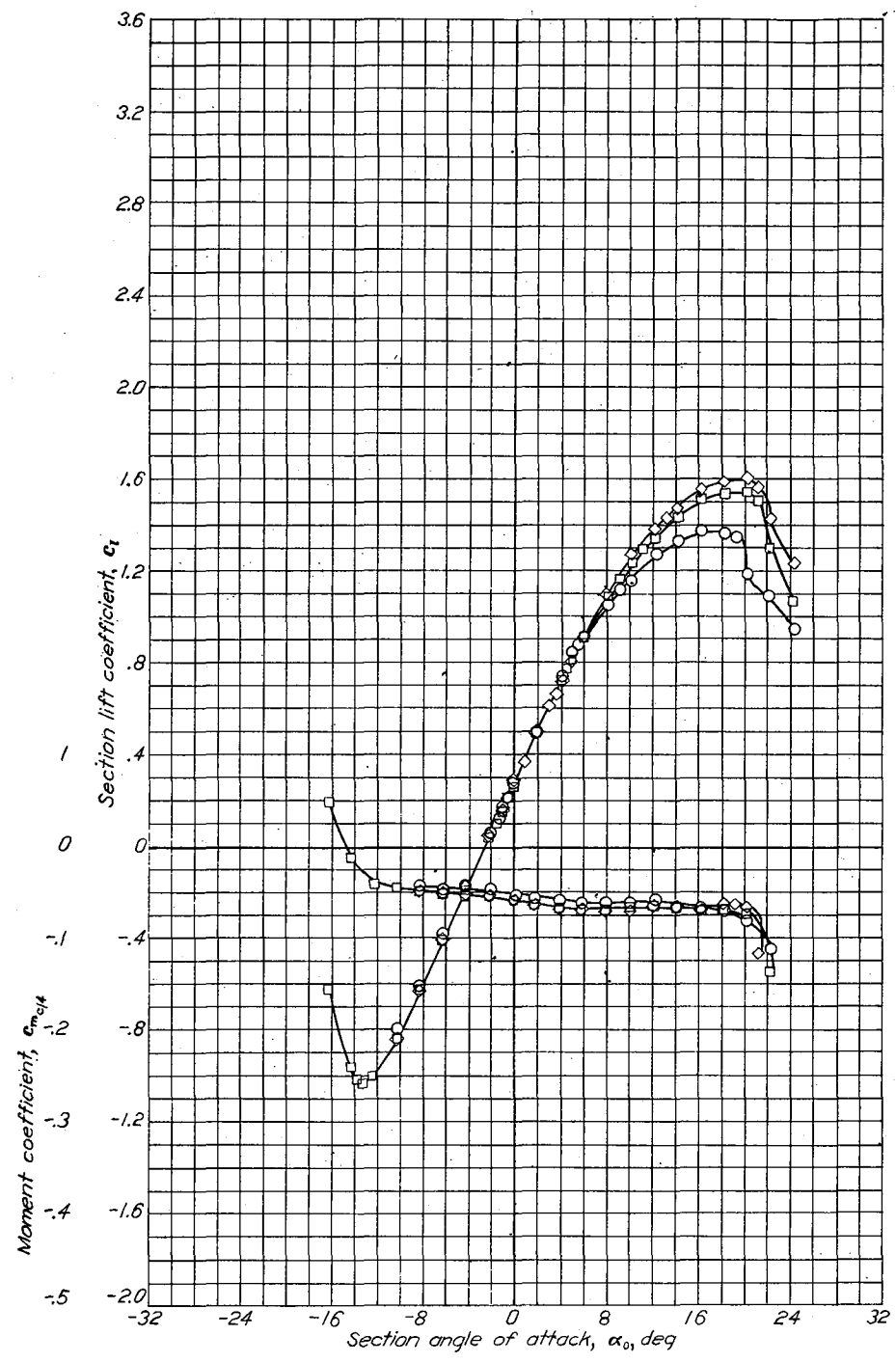
Aerodynamic characteristics of the NACA 65-2-215 airfoil section, 24-inch chord.



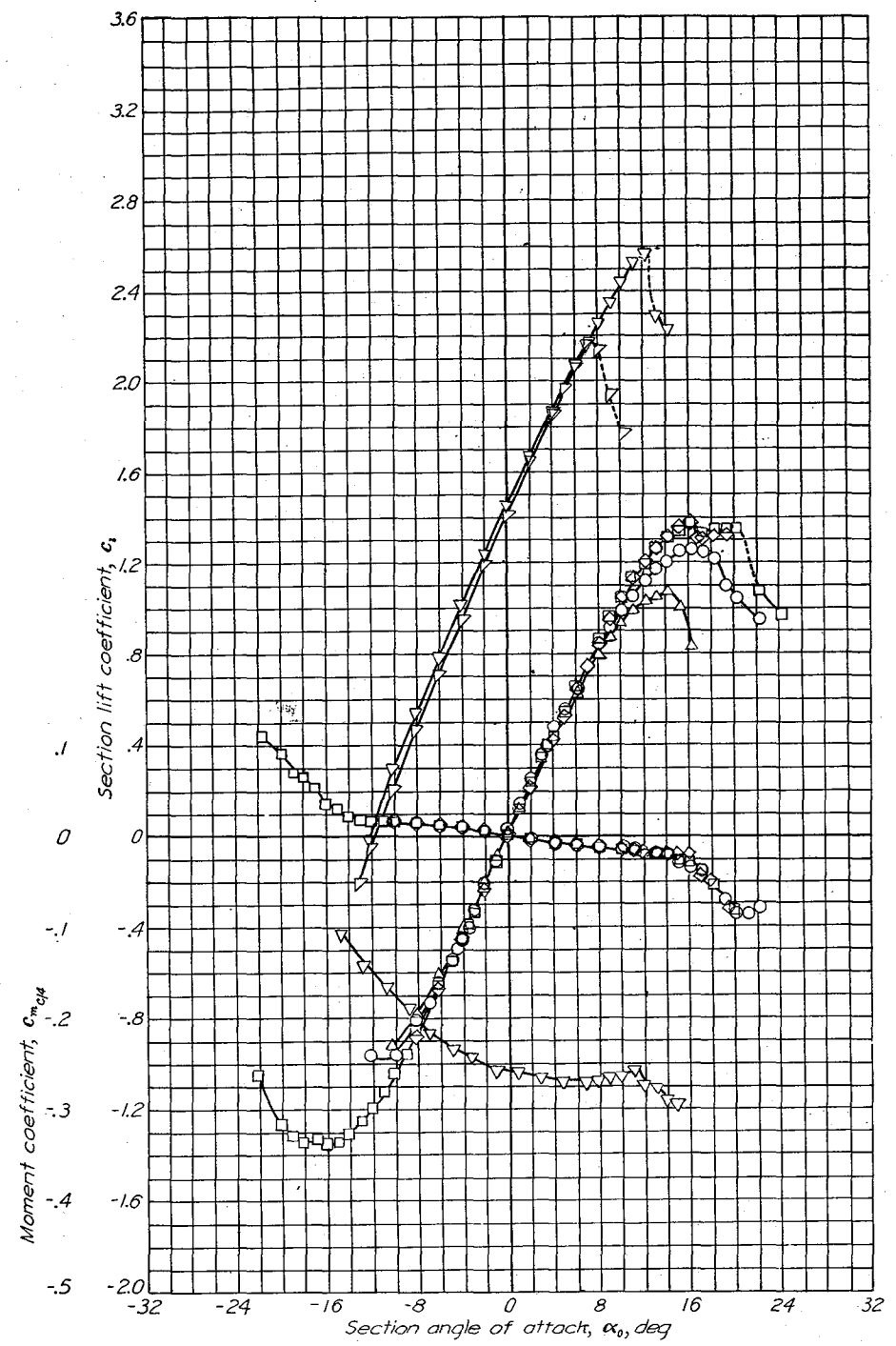
Aerodynamic characteristics of the NACA 65-415 airfoil section, 24-inch chord.



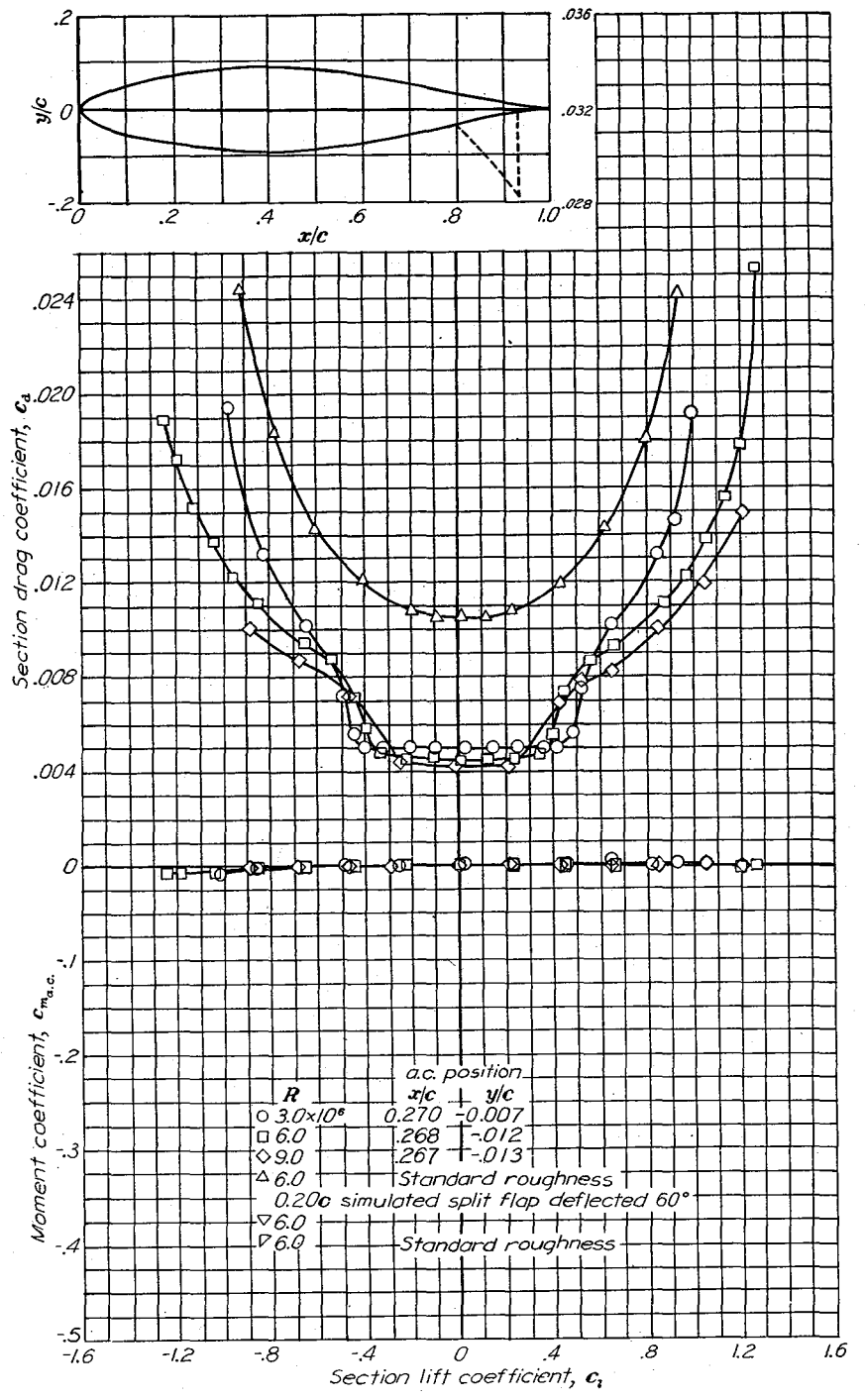
NACA 652-415,  $\alpha = 0.5$



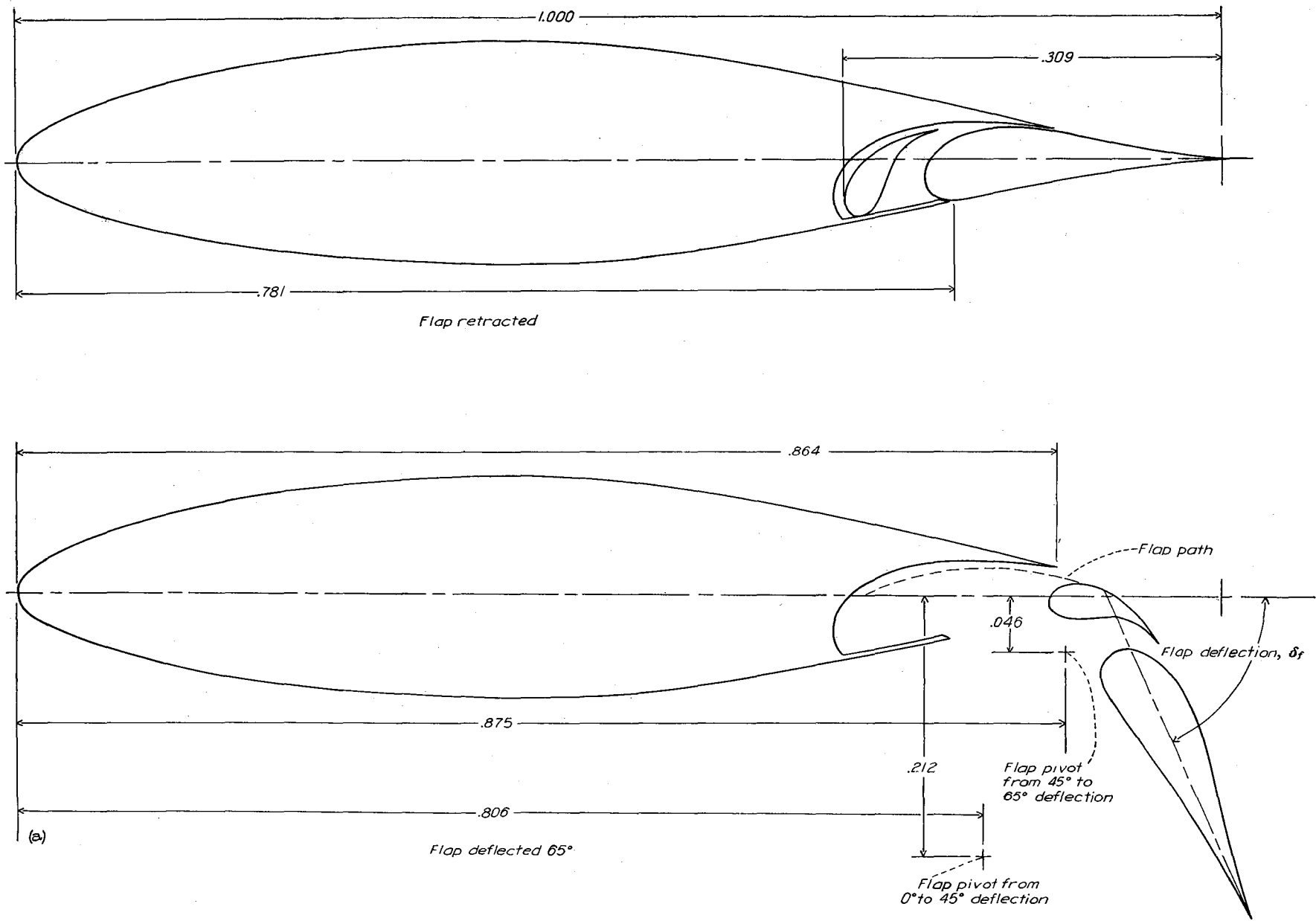
Aerodynamic characteristics of the NACA 652-415,  $\alpha=0.5$  airfoil section, 24-inch chord.



Aerodynamic characteristics of the NACA 653-018 airfoil section, 24-inch chord.

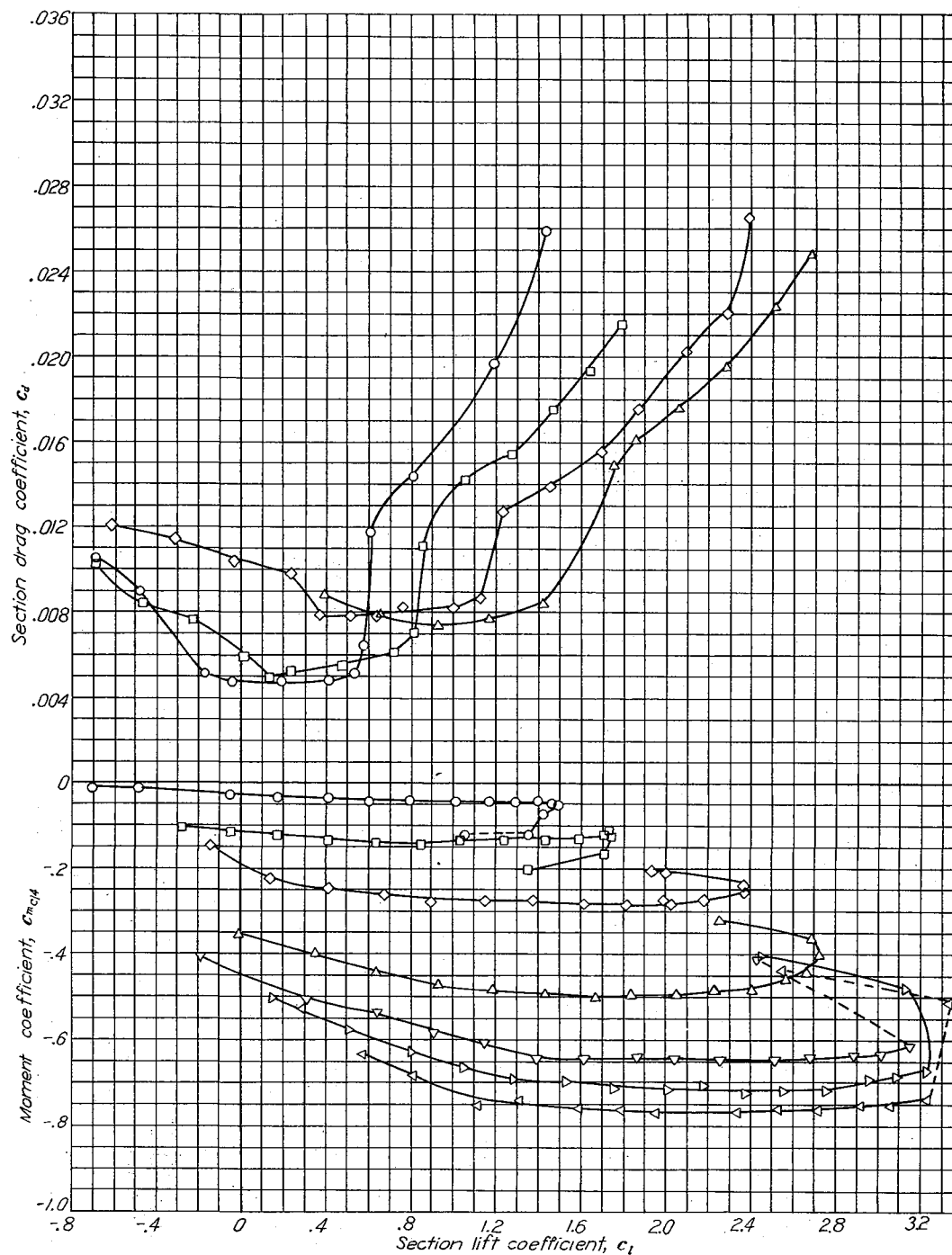
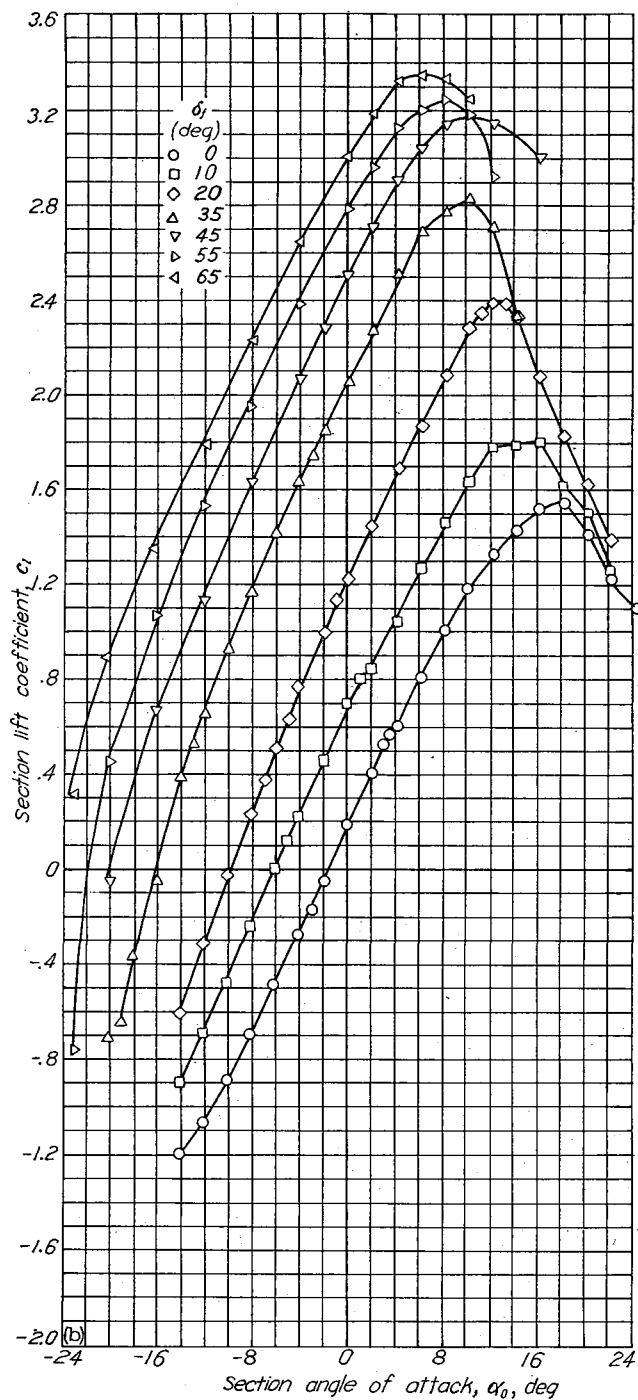


NACA 65<sub>3</sub>-118 with flap

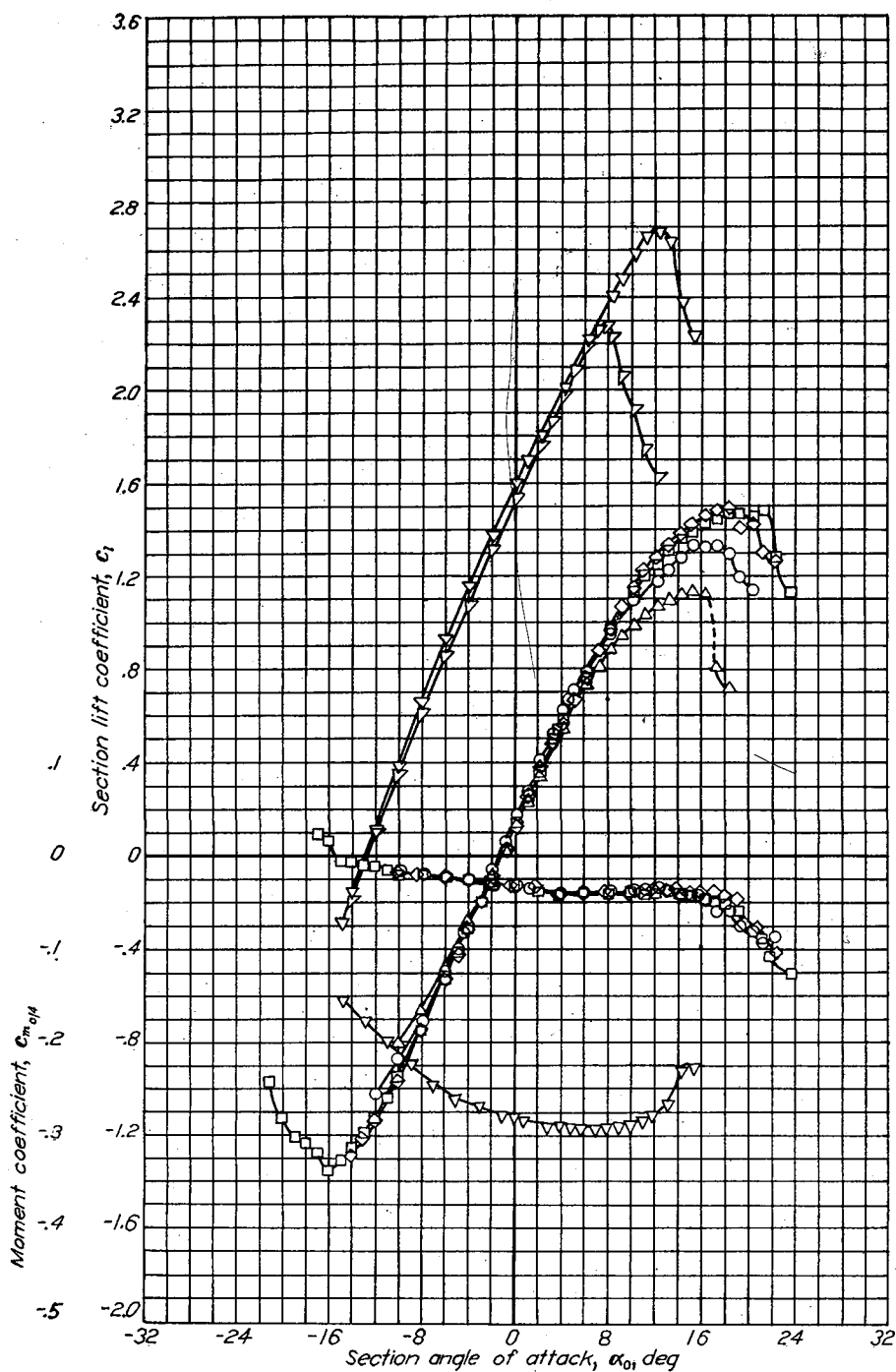


(a) Configuration.  
NACA 65<sub>3</sub>-118 airfoil section with 0.309c double slotted flap.

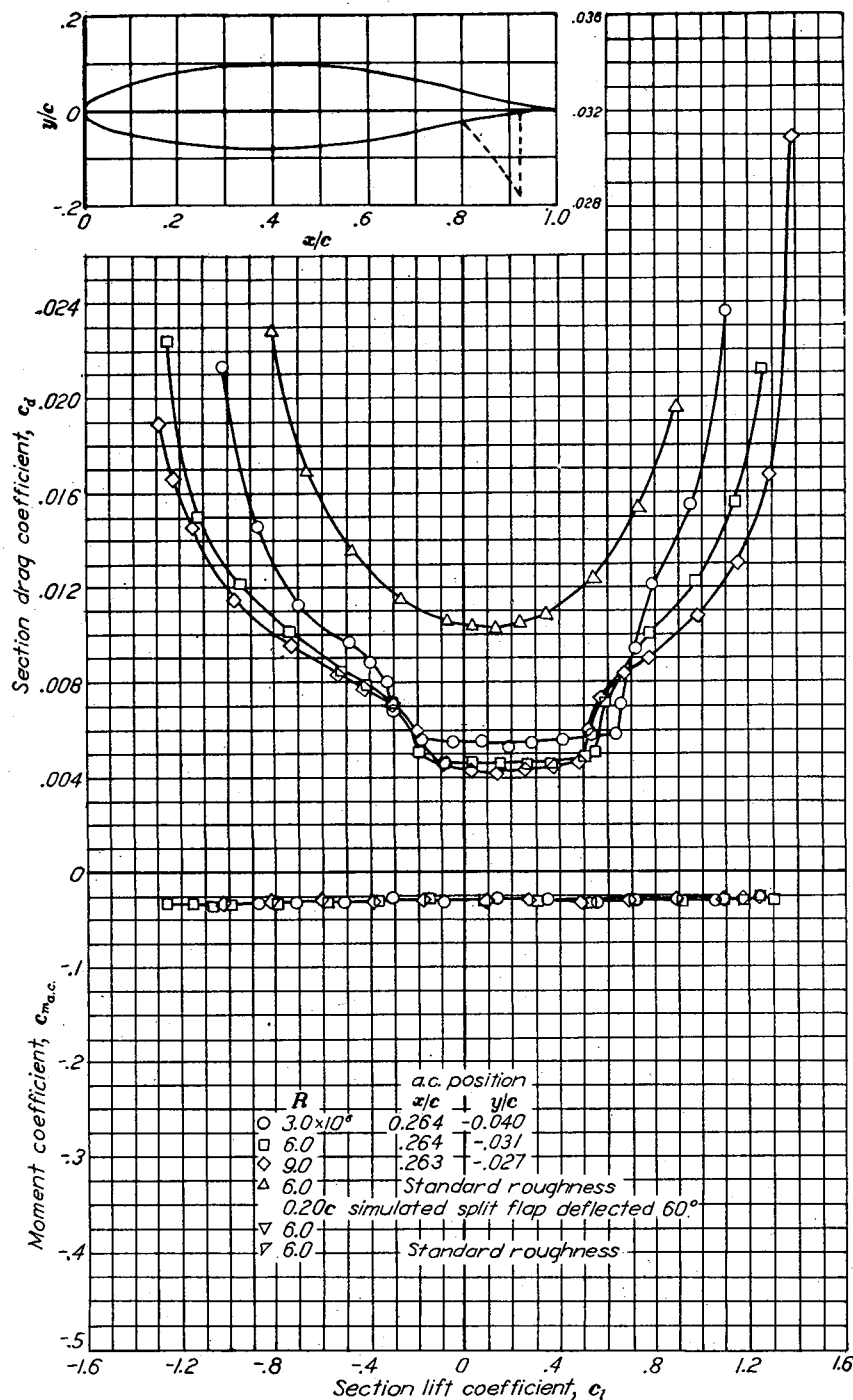
NACA 65s-118 with flap



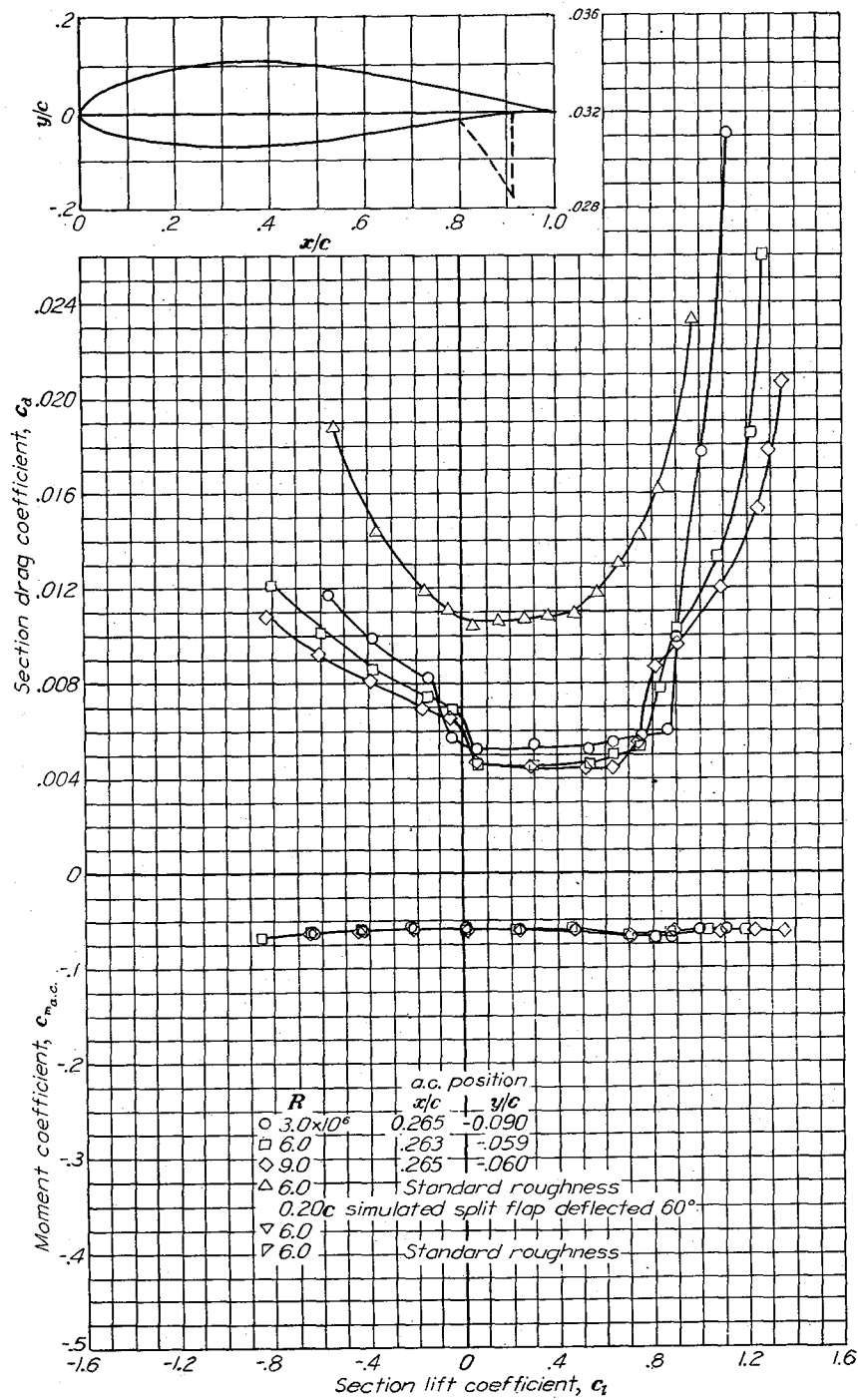
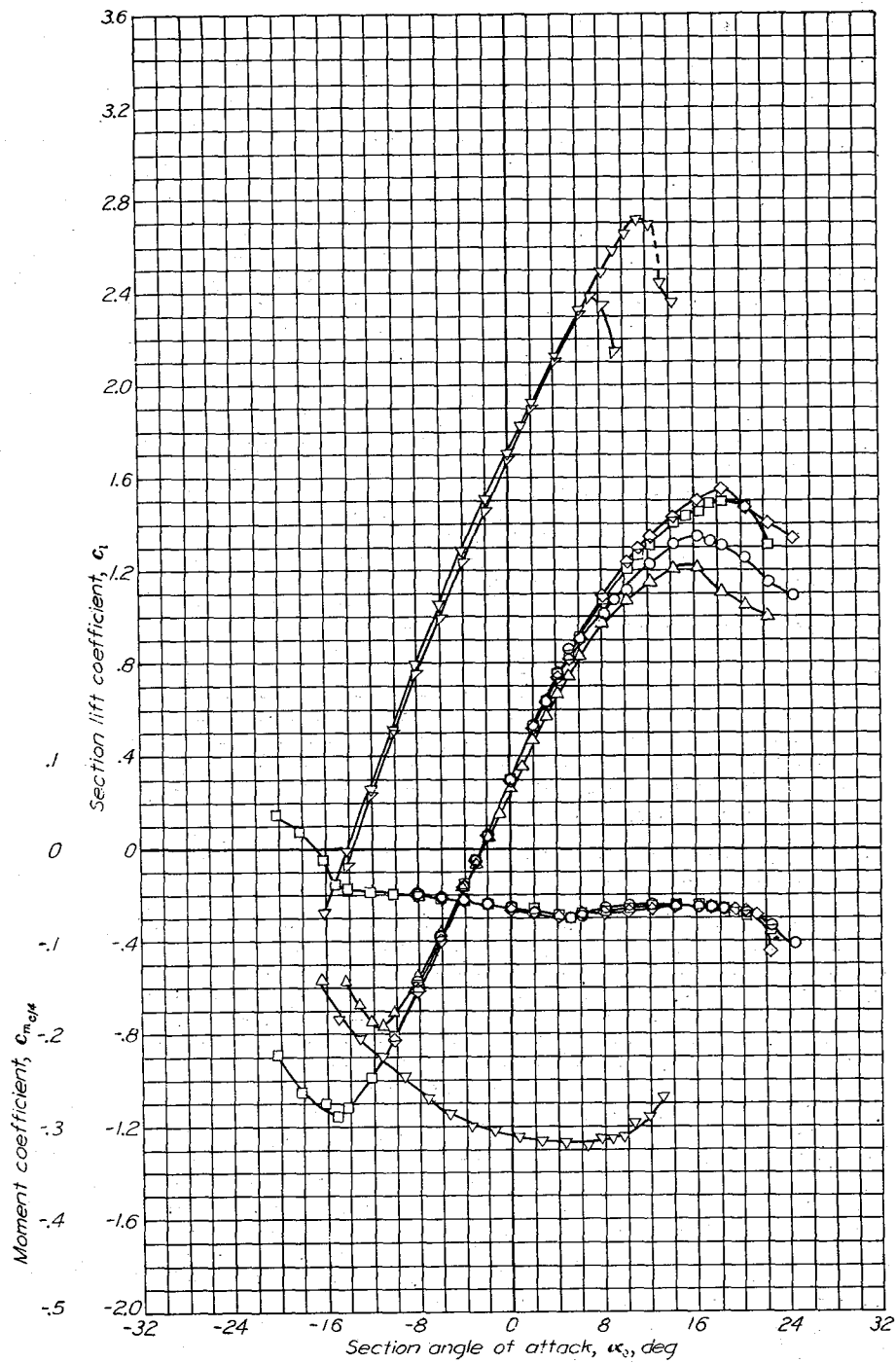
(b) Aerodynamic characteristics.  $R=6 \times 10^6$ .  
NACA 65s-118 airfoil section with 0.309c double slotted flap.



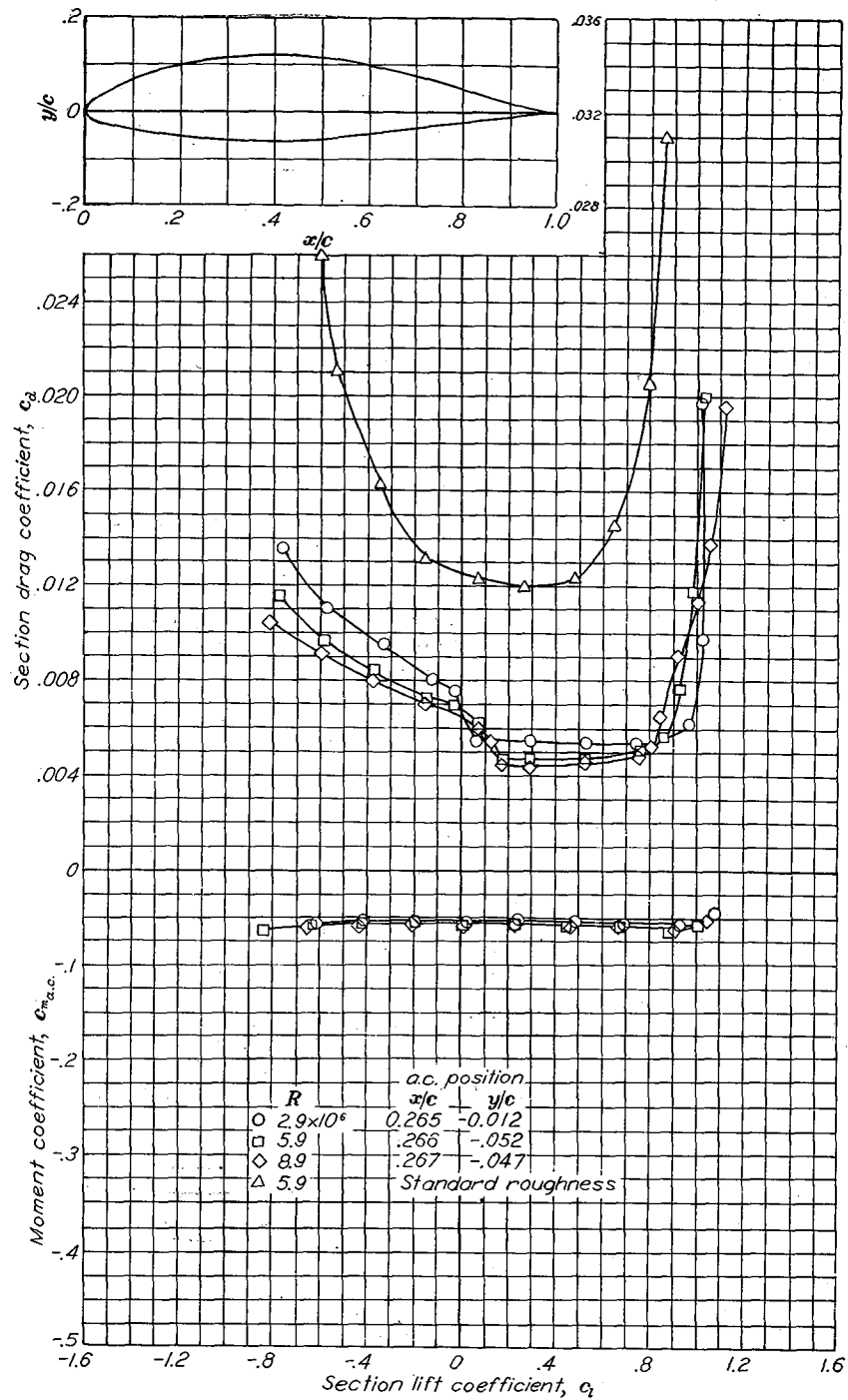
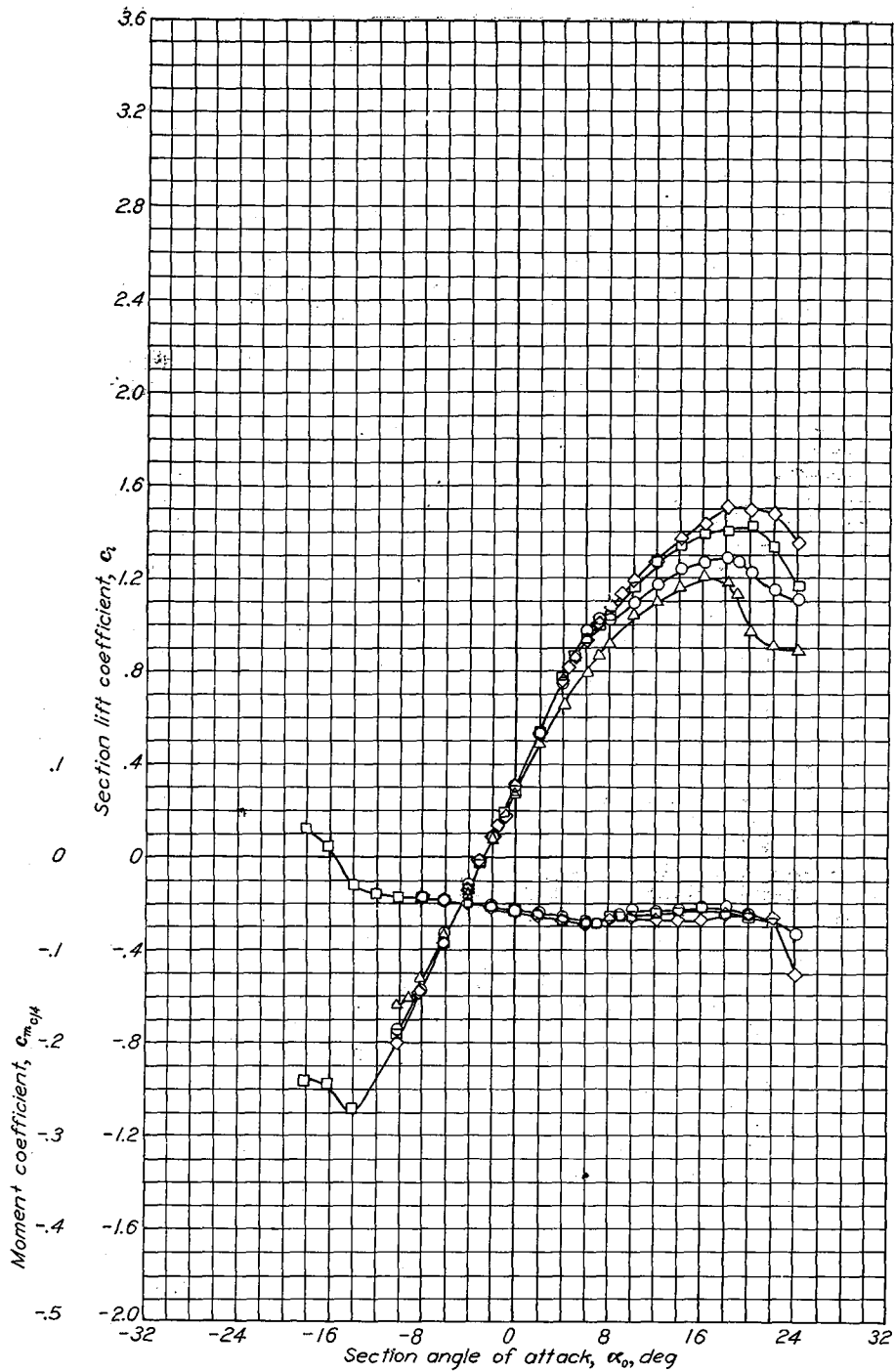
Aerodynamic characteristics of the NACA 65-218 airfoil section, 24-inch chord.



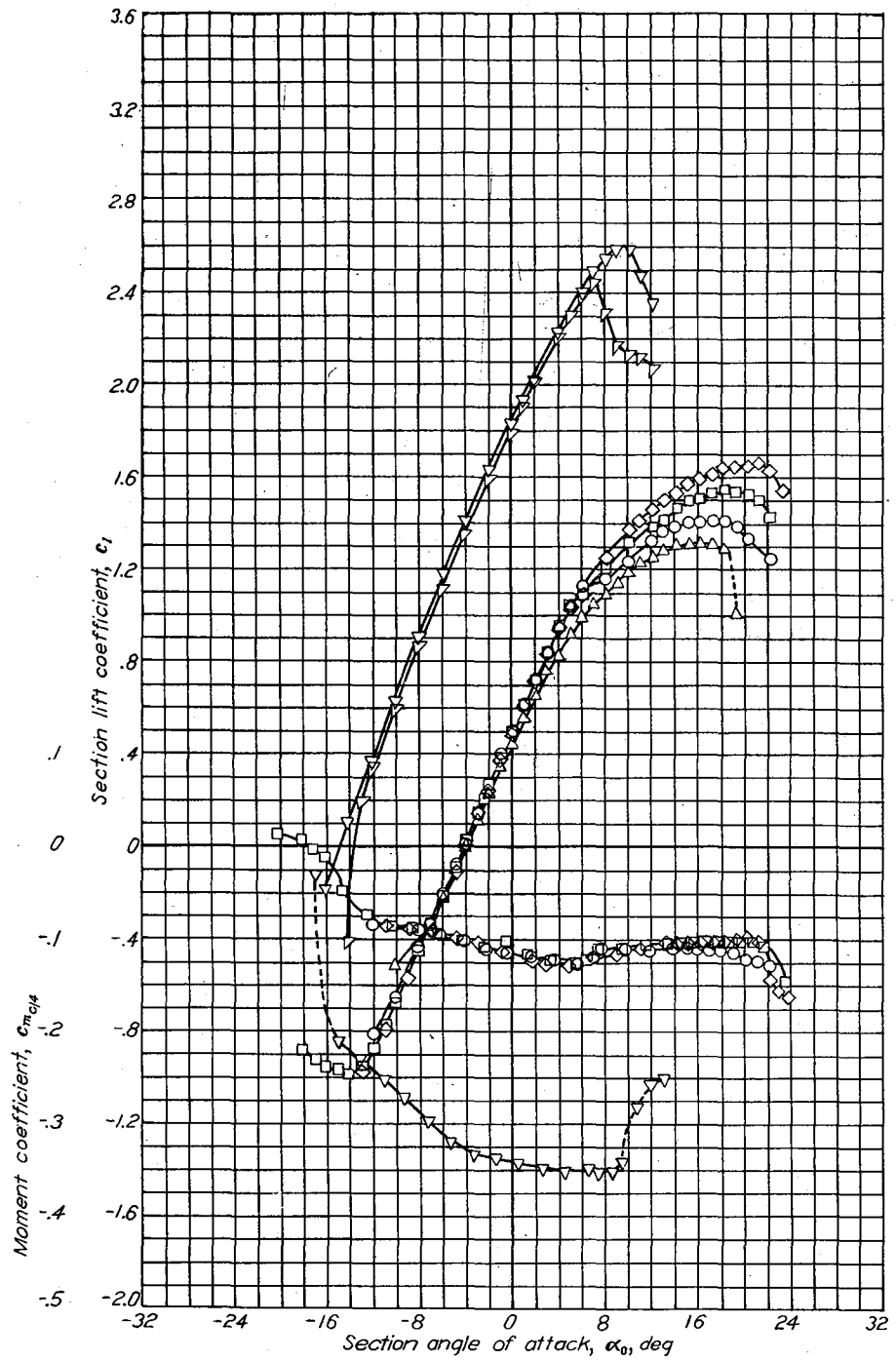




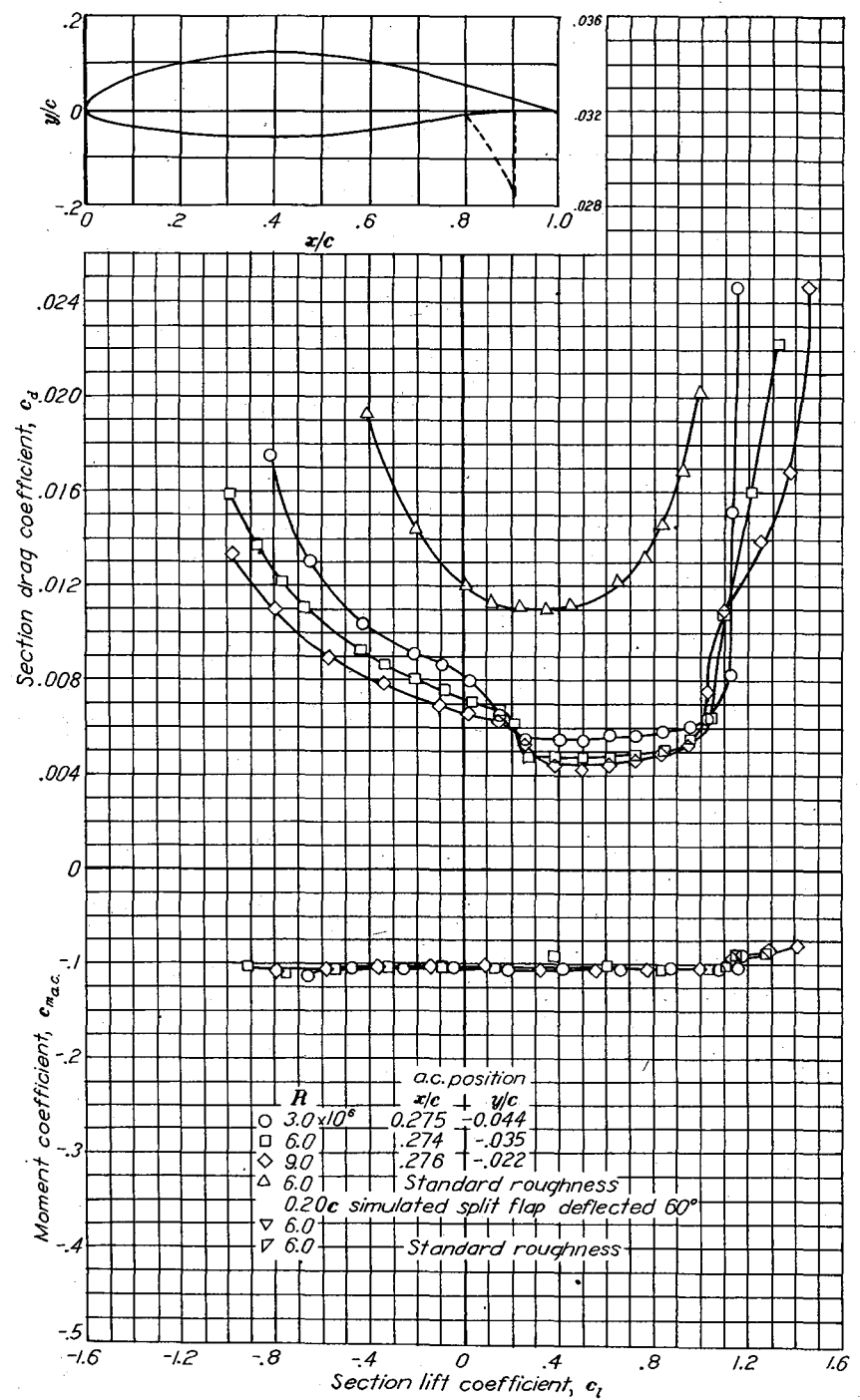
Aerodynamic characteristics of the NACA 65-418 airfoil section, 24-inch chord.



Aerodynamic characteristics of the NACA 653-418,  $\alpha = 0.5$  airfoil section, 24-inch chord.



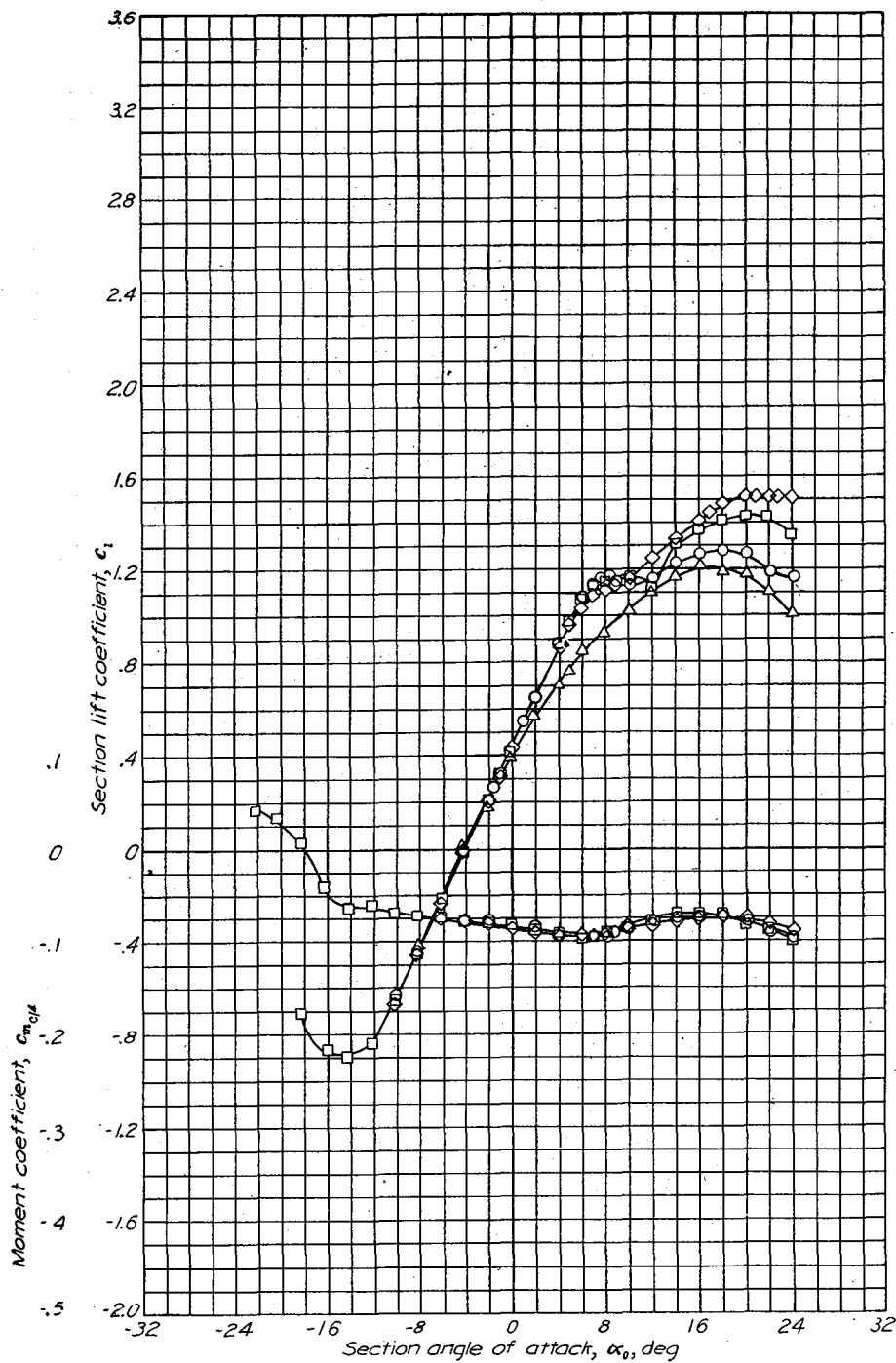
Aerodynamic characteristics of the NACA 65-618 airfoil section, 24-inch chord.



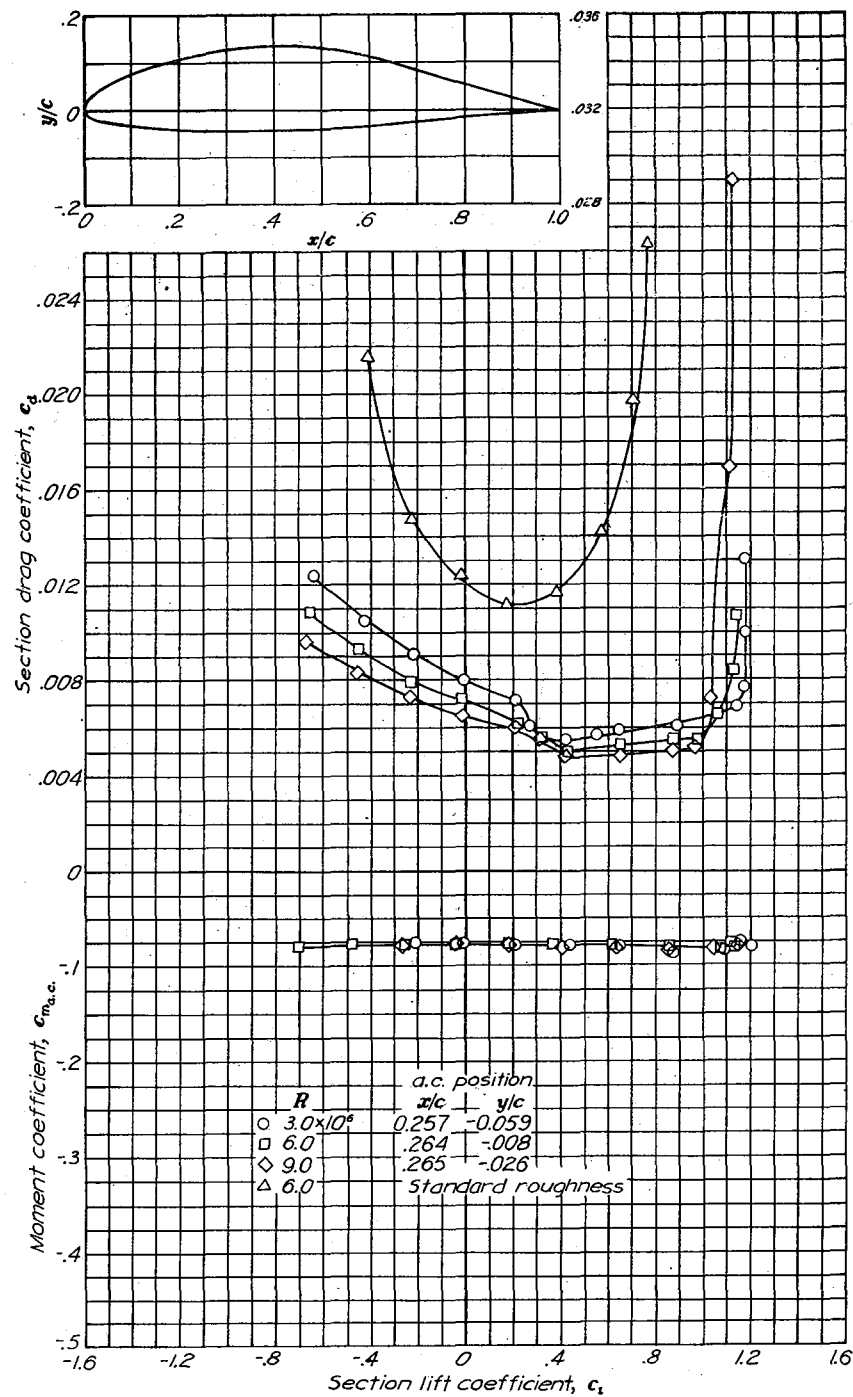
NACA 65-618

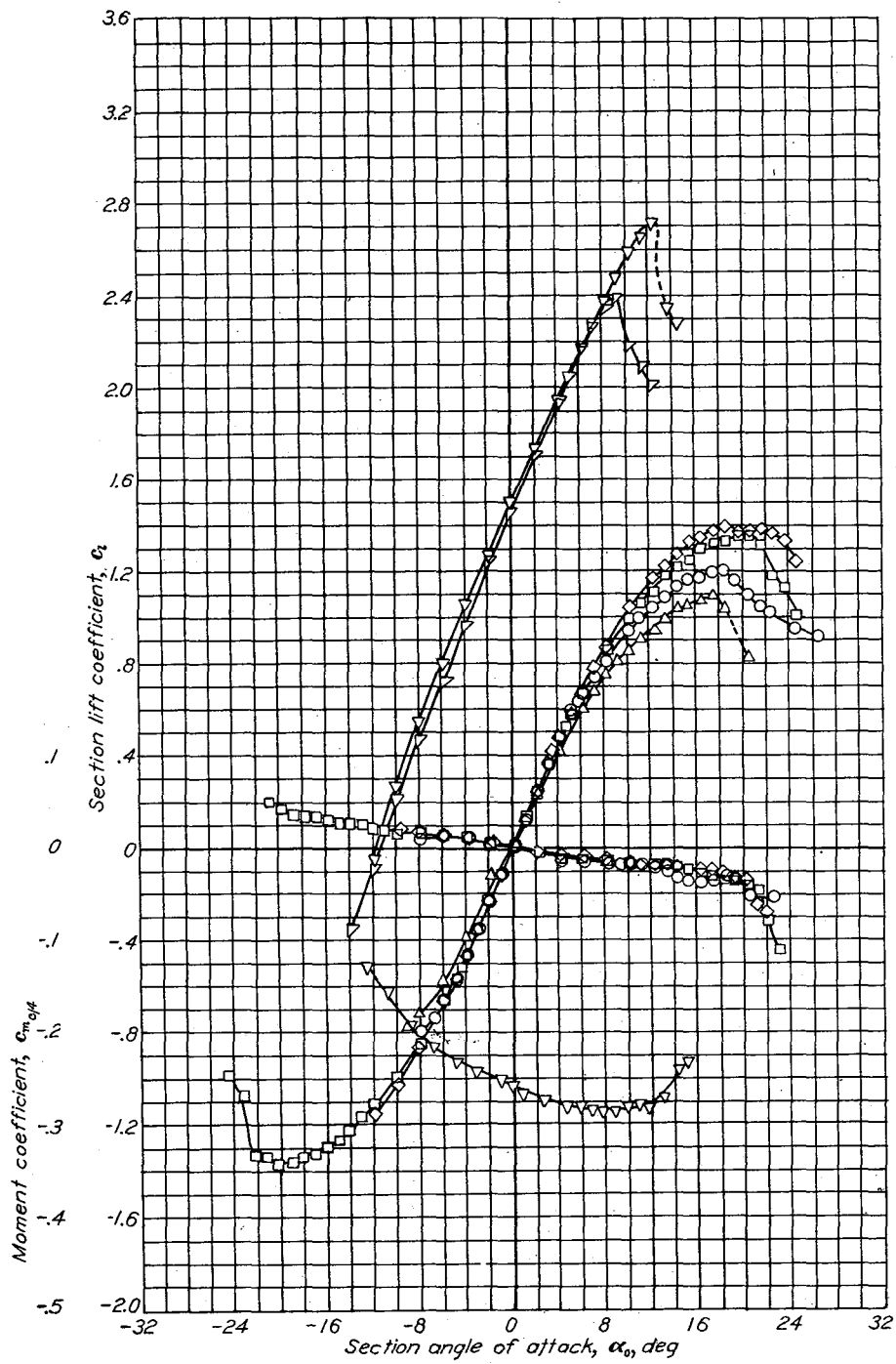
SUMMARY OF AIRFOIL DATA

NACA 65-3-618,  $\alpha = 0.5$

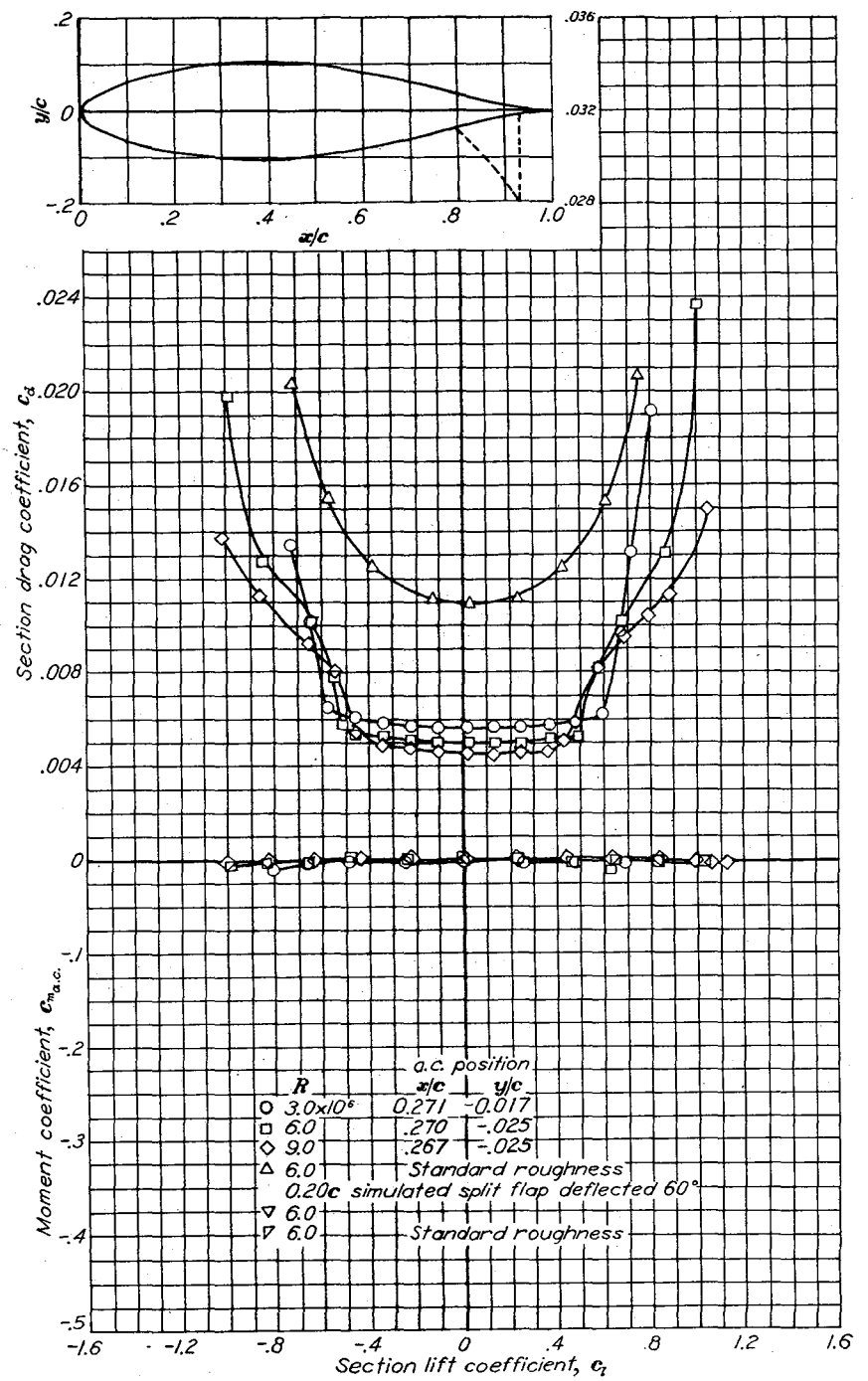


Aerodynamic characteristics of the NACA 65-618,  $\alpha=0.5$  airfoil section, 24-inch chord.

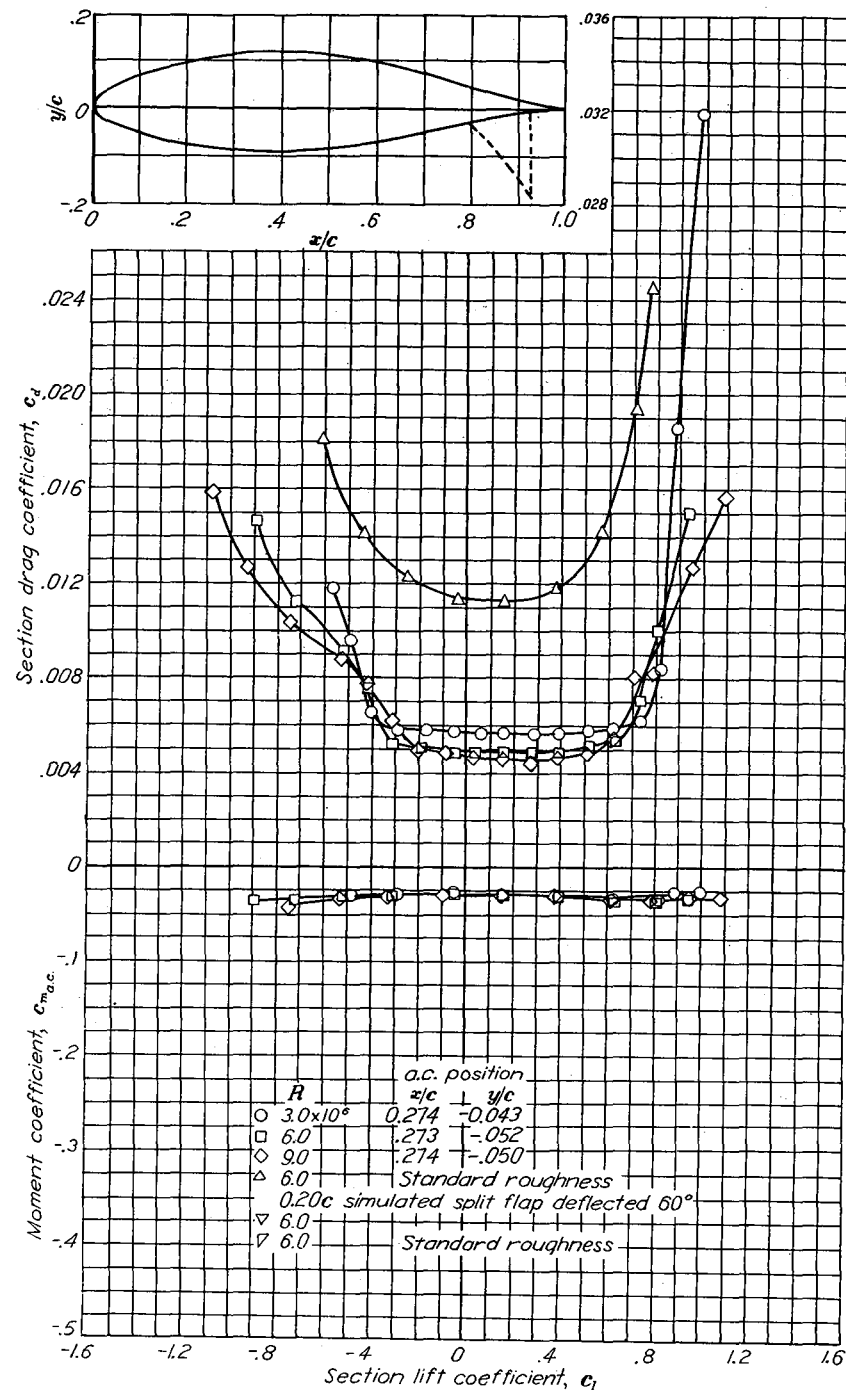
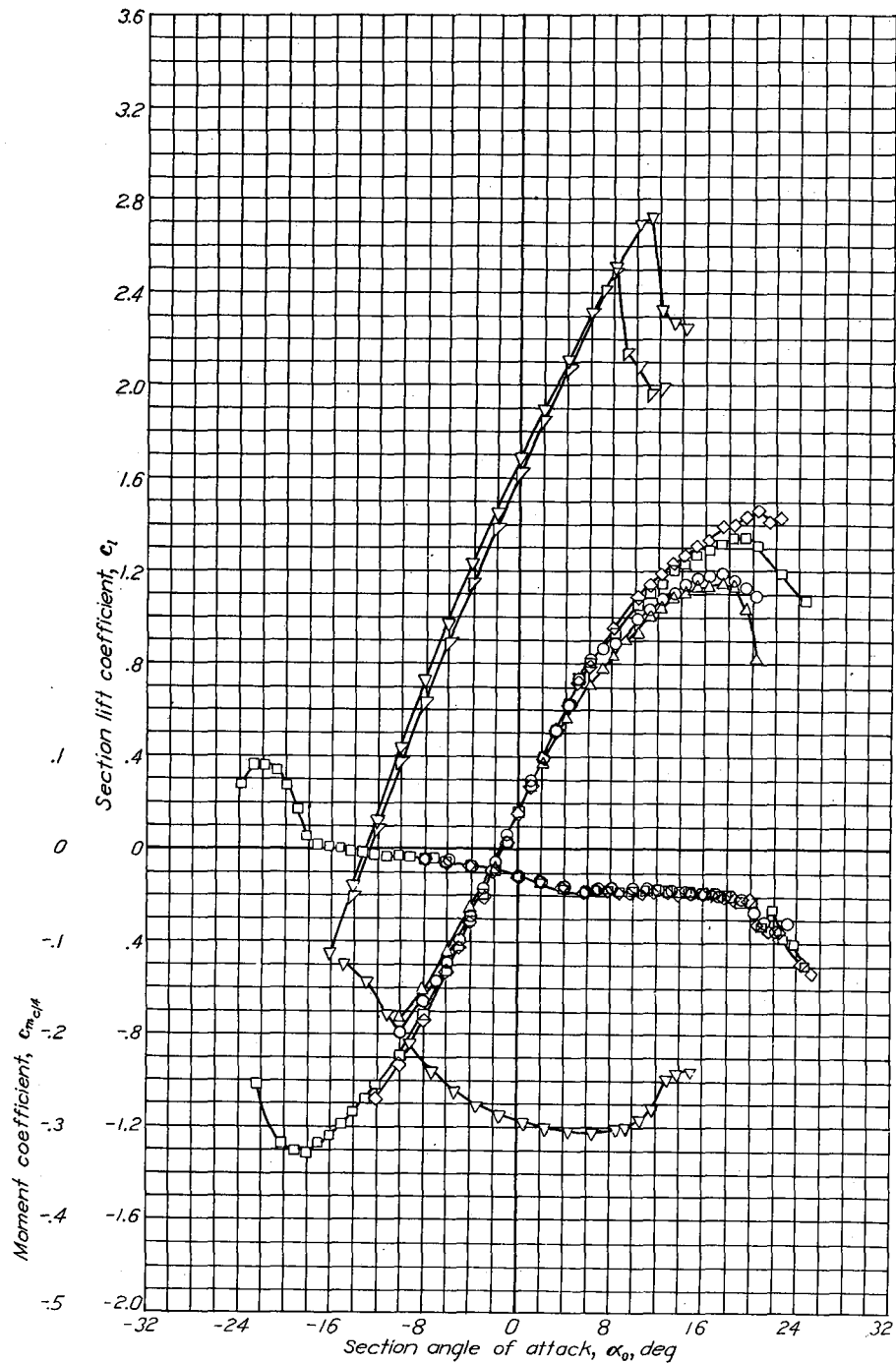




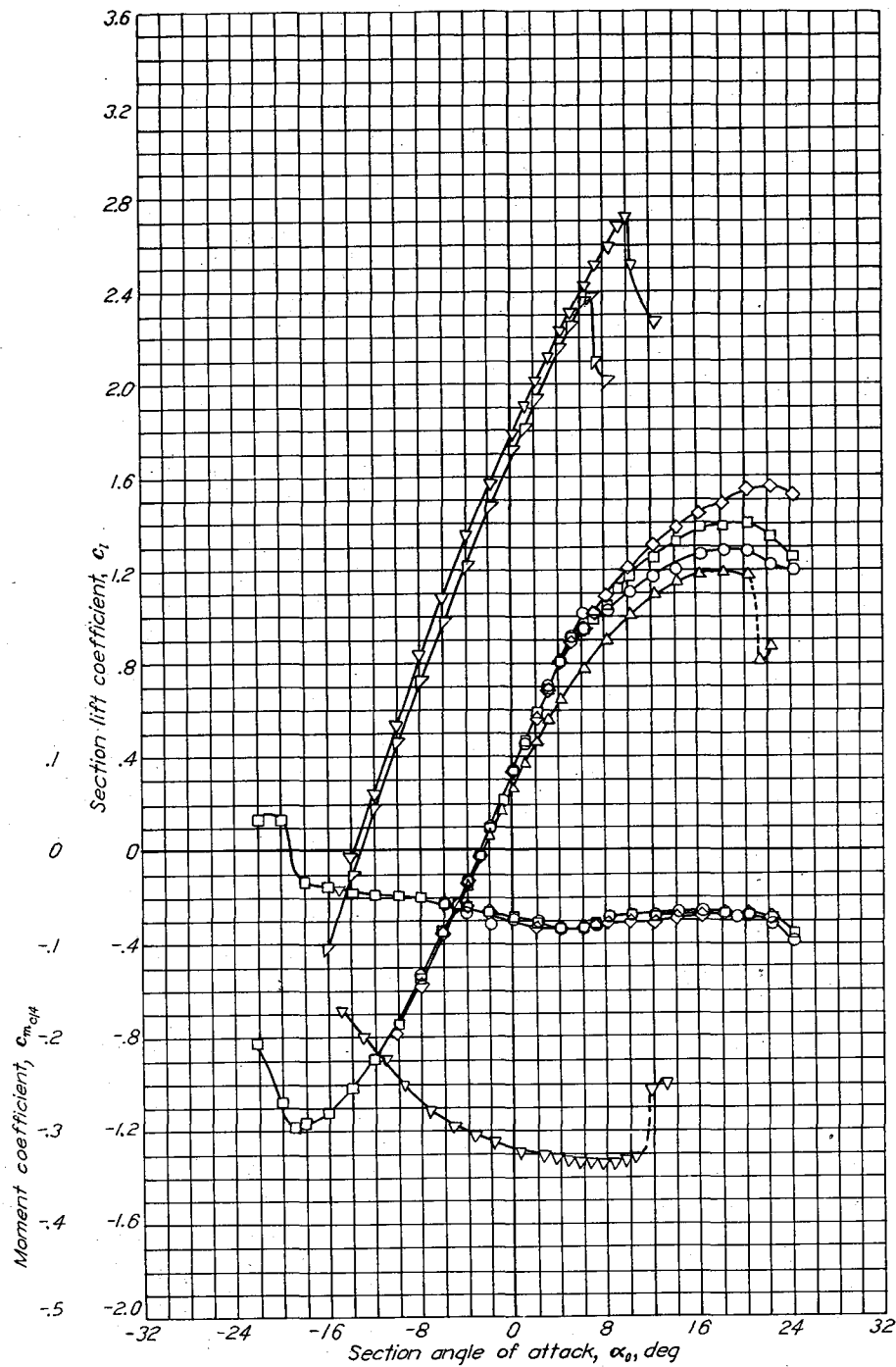
Aerodynamic characteristics of the NACA 65-021 airfoil section, 24-inch chord.



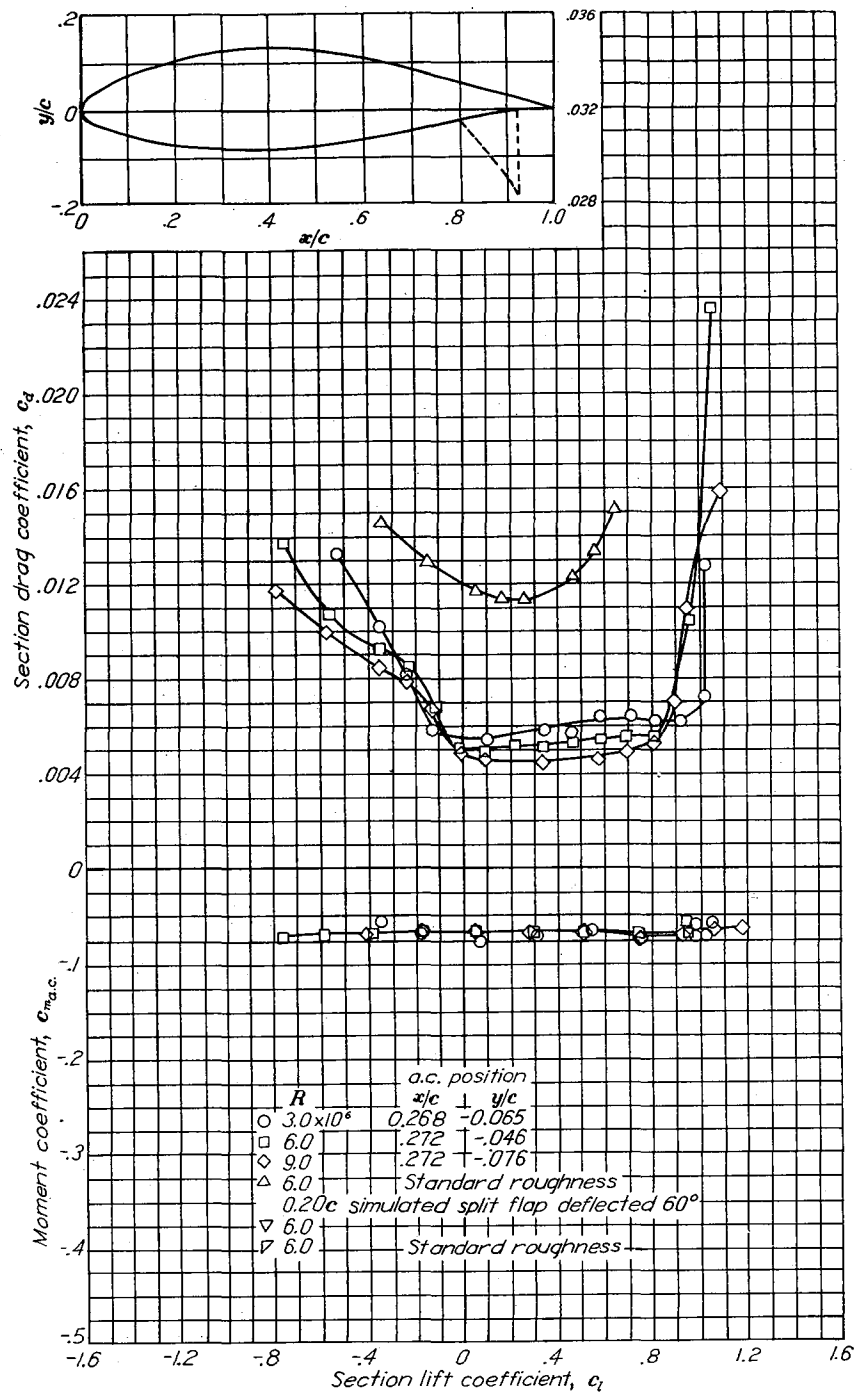
NACA 65-4-021

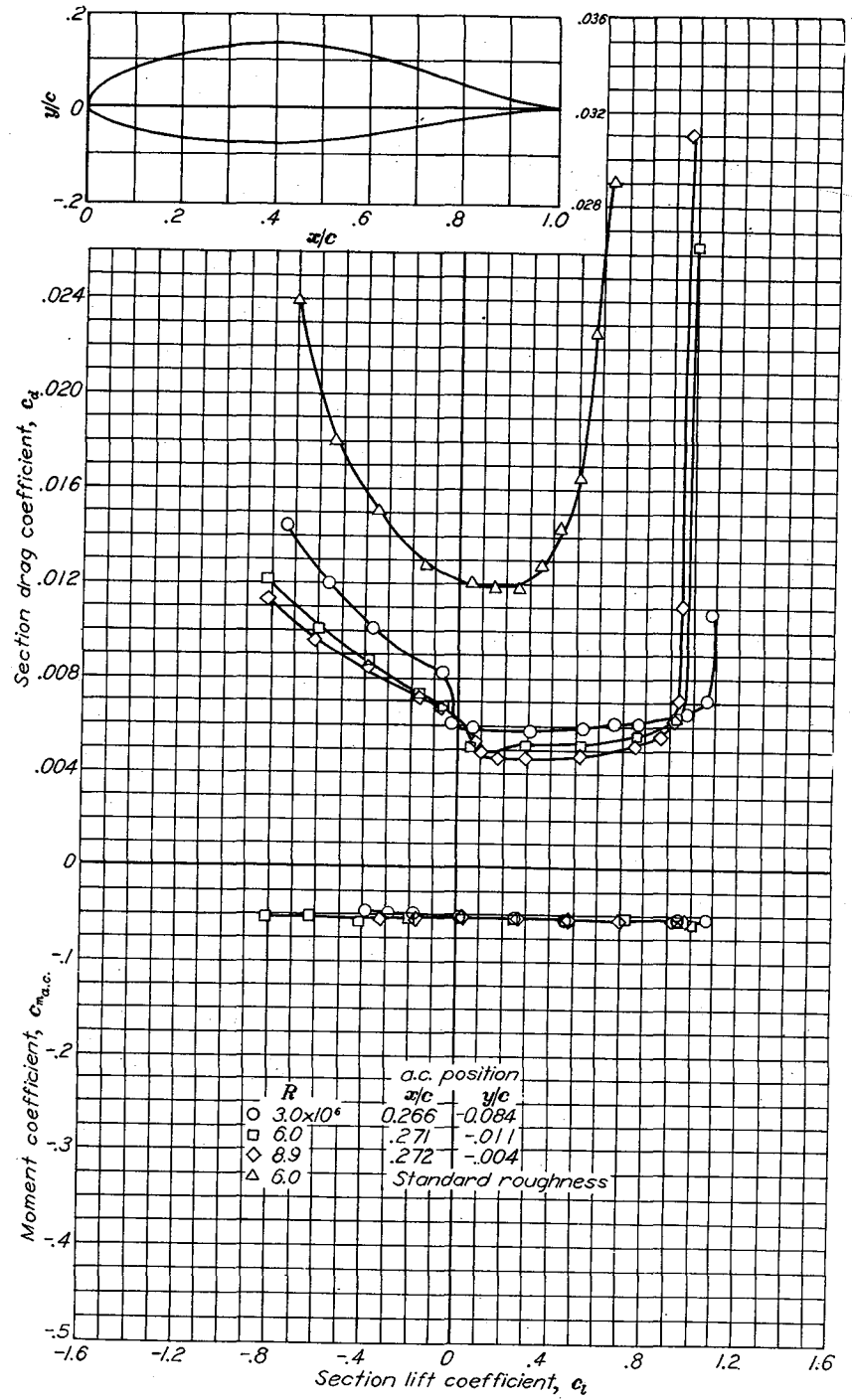
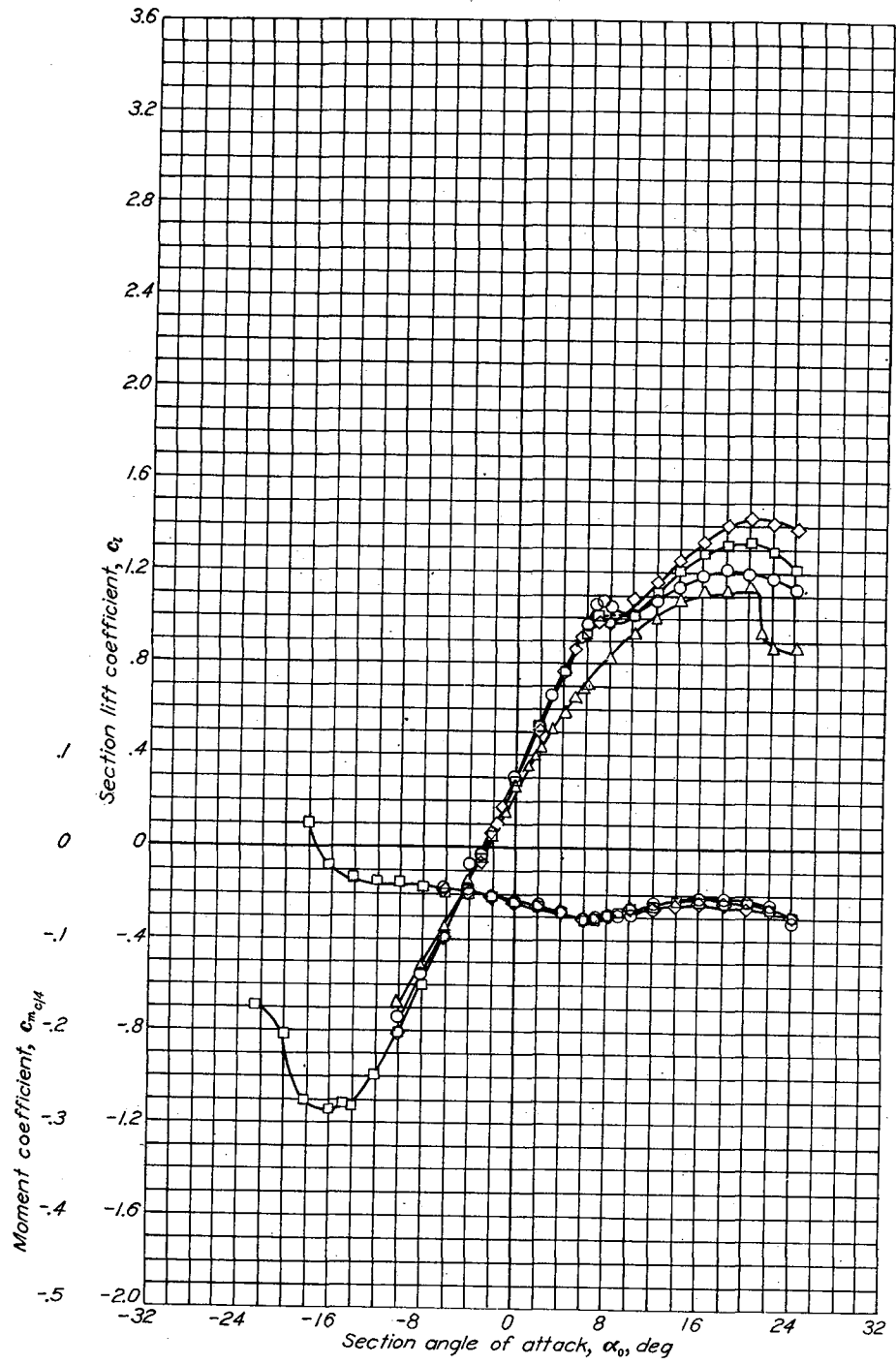


Aerodynamic characteristics of the NACA 654-221 airfoil section. 24-inch chord.



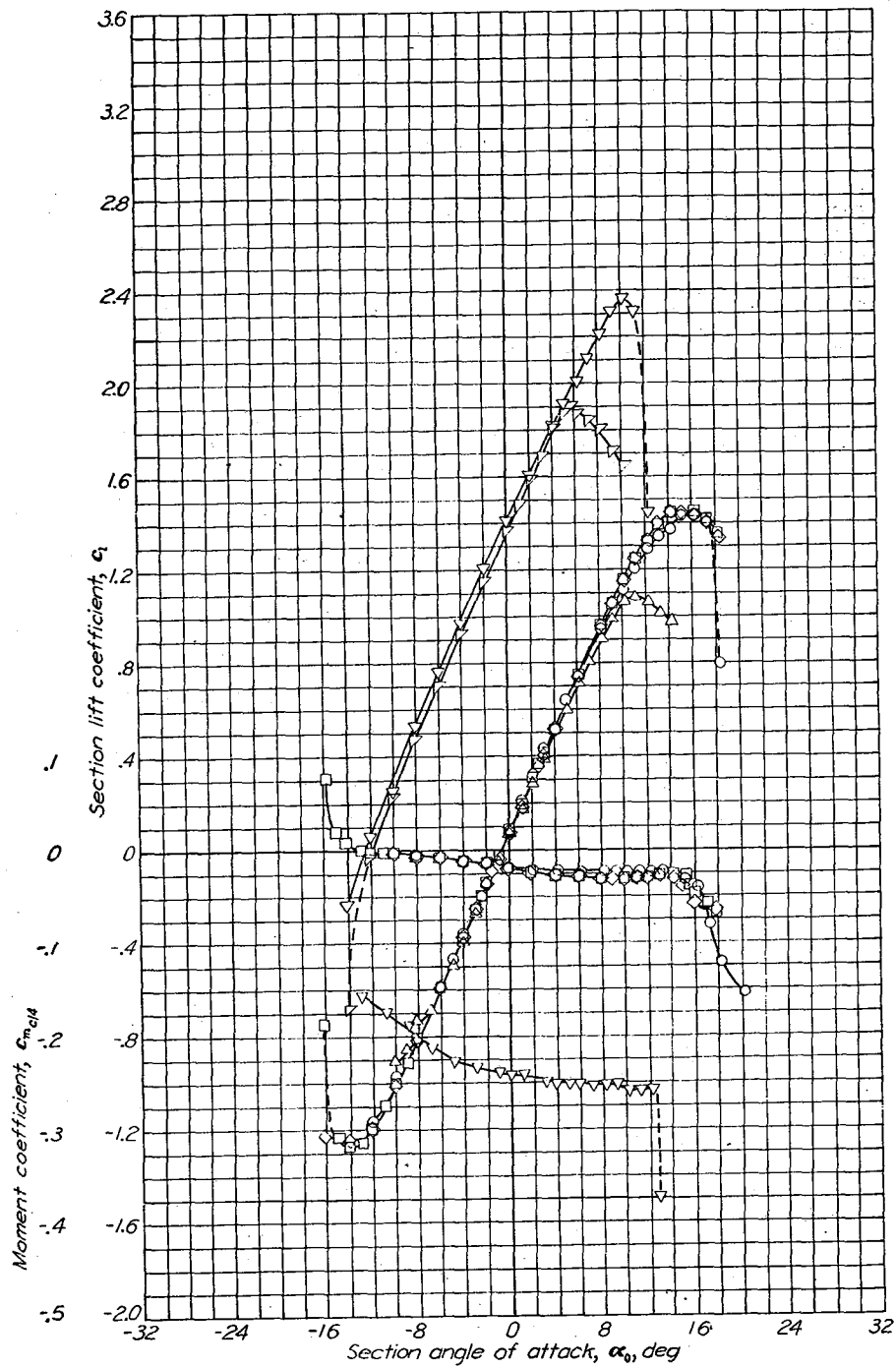
Aerodynamic characteristics of the NACA 65-421 airfoil section, 24-inch chord.



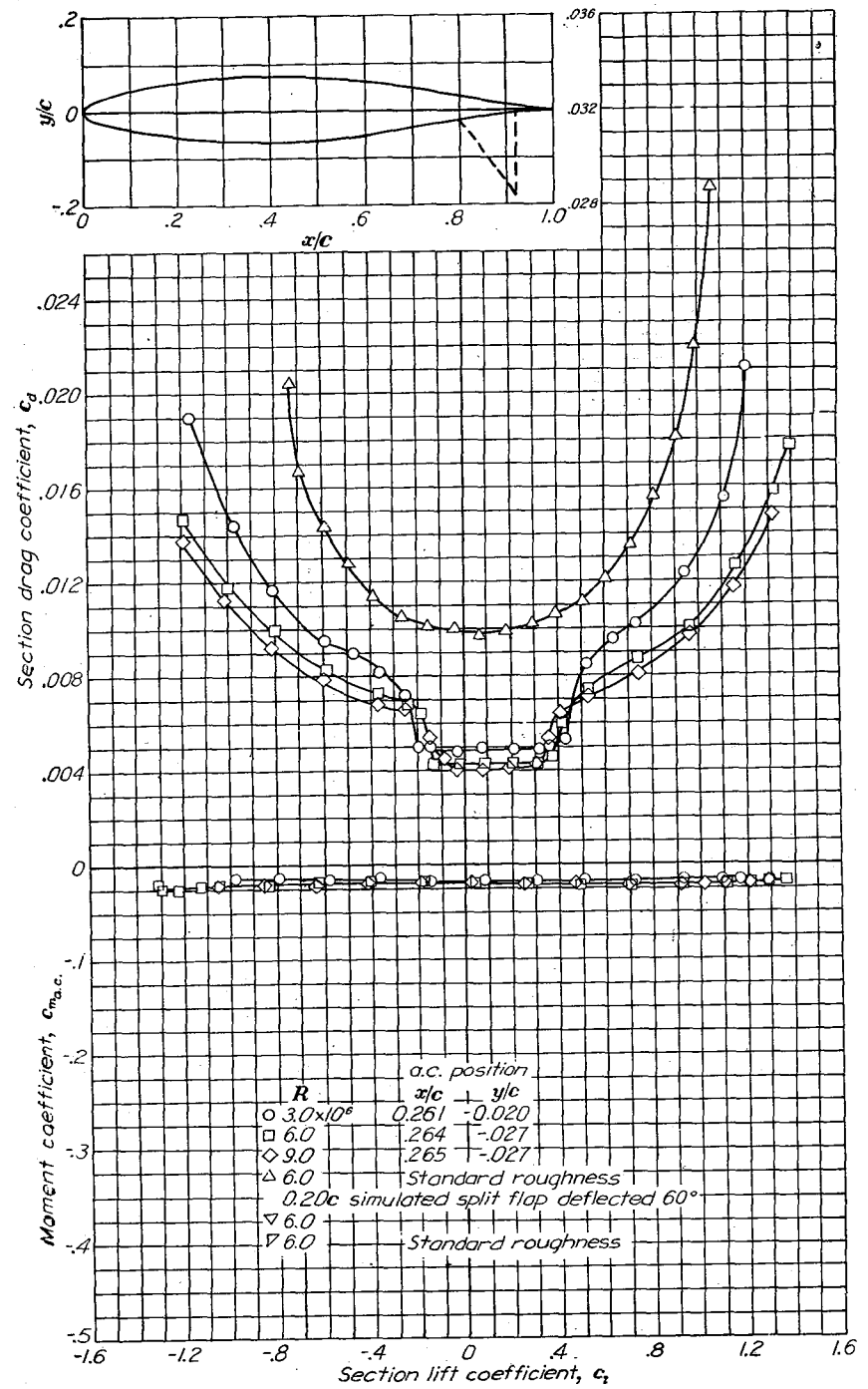


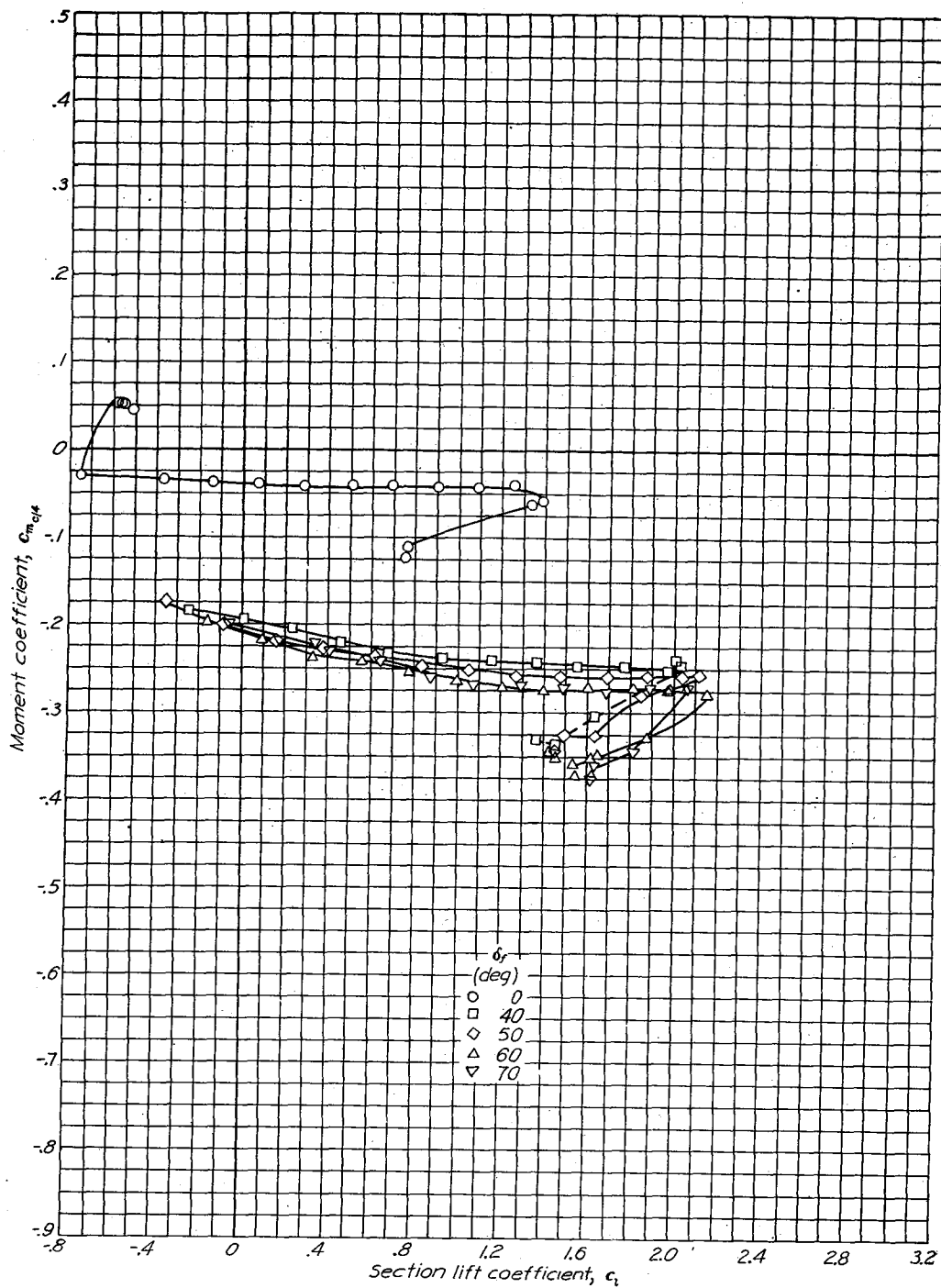
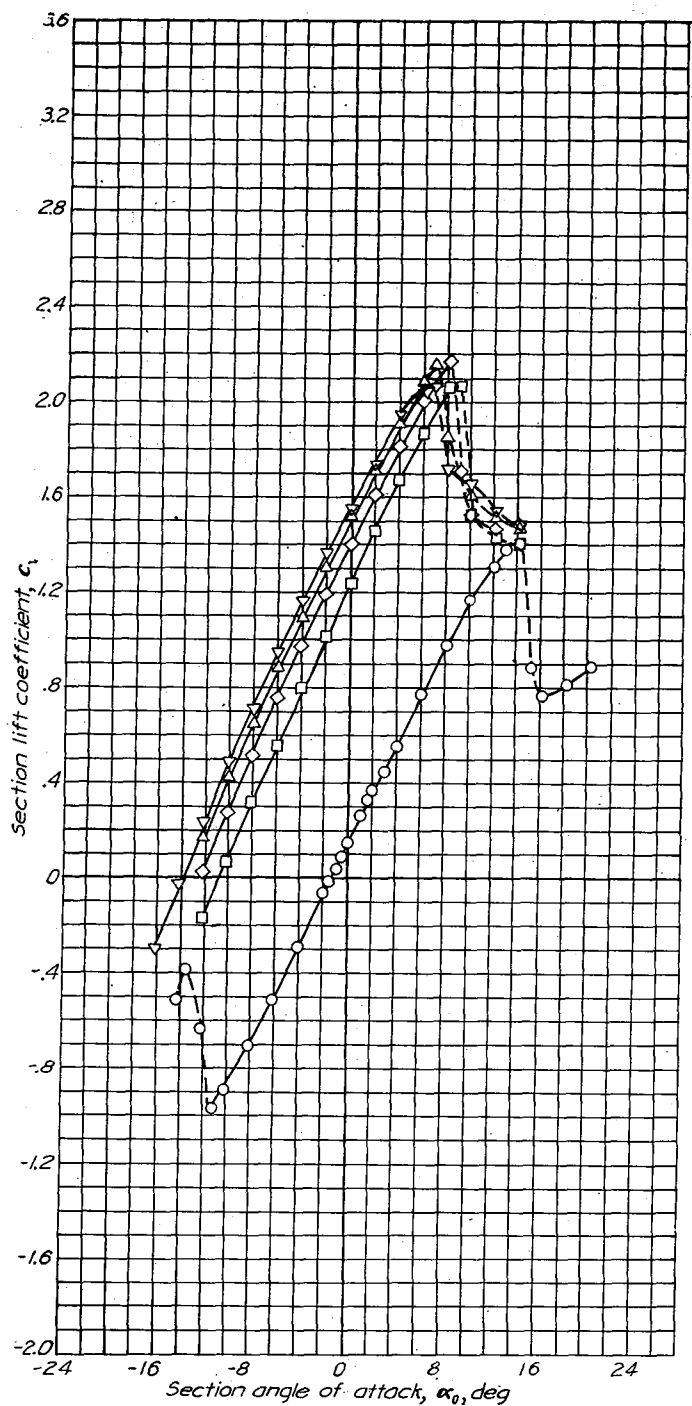
Aerodynamic characteristics of the NACA 654-421,  $\alpha = 0.5^\circ$  airfoil section, 24-inch chord.

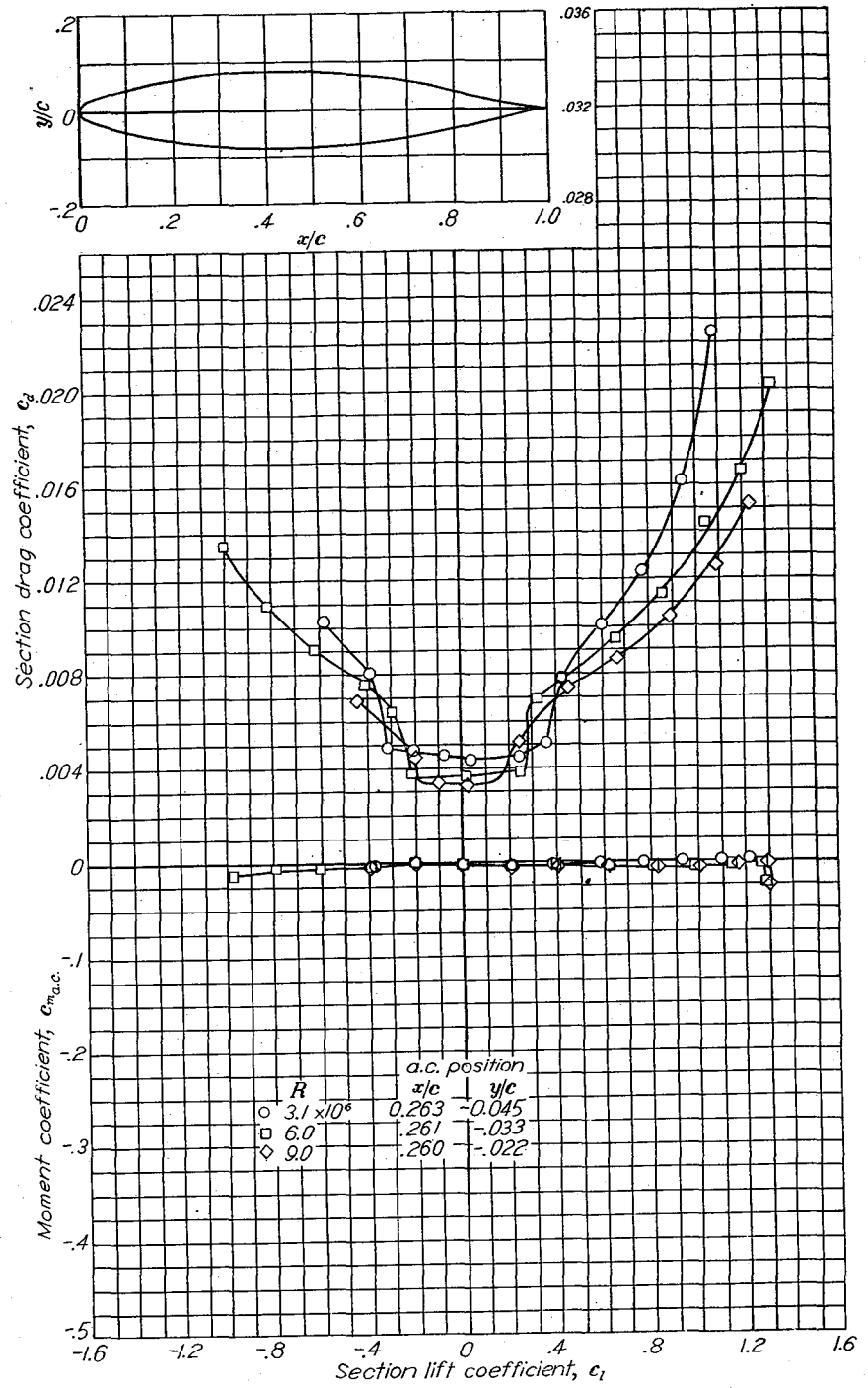
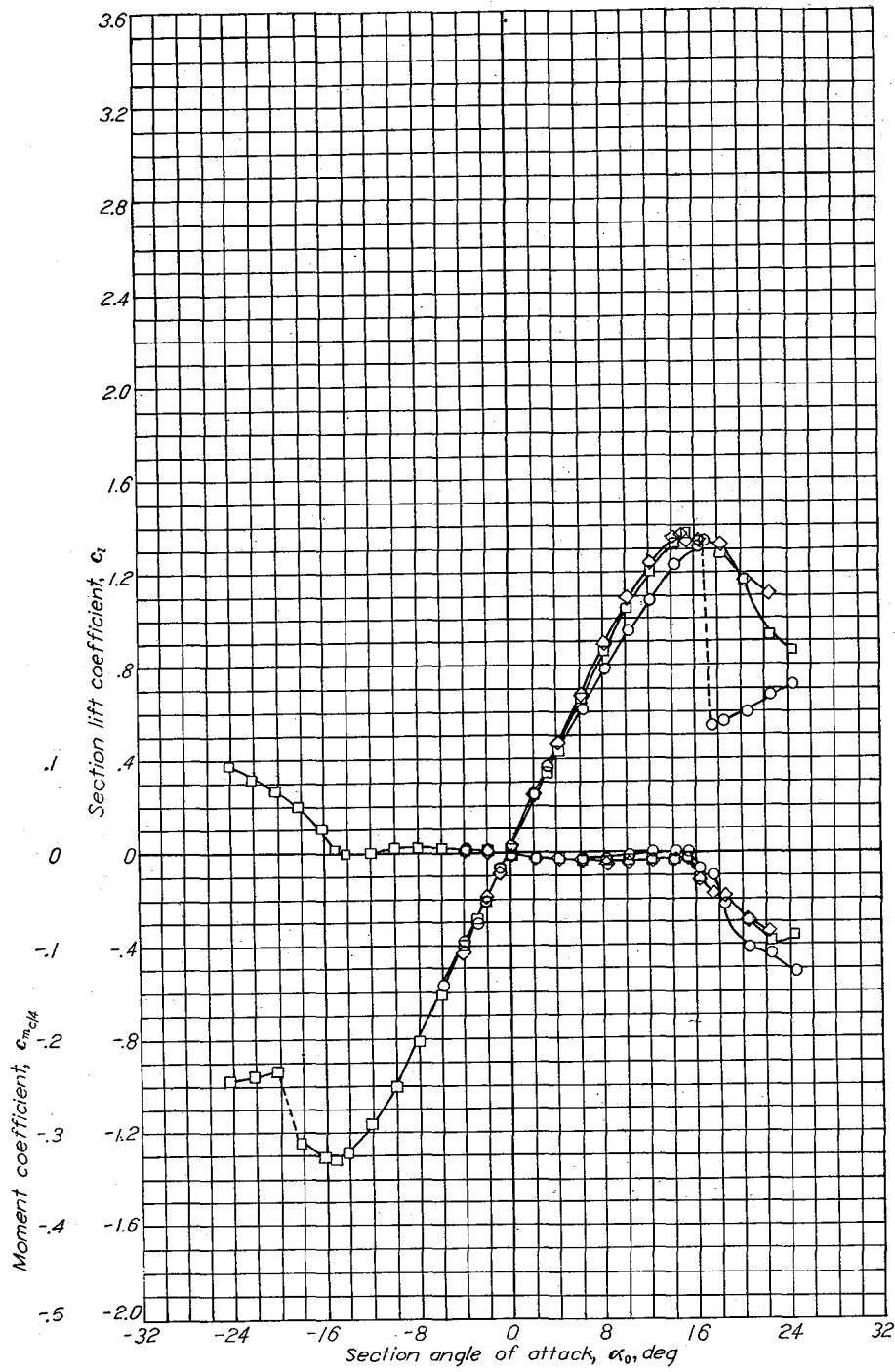




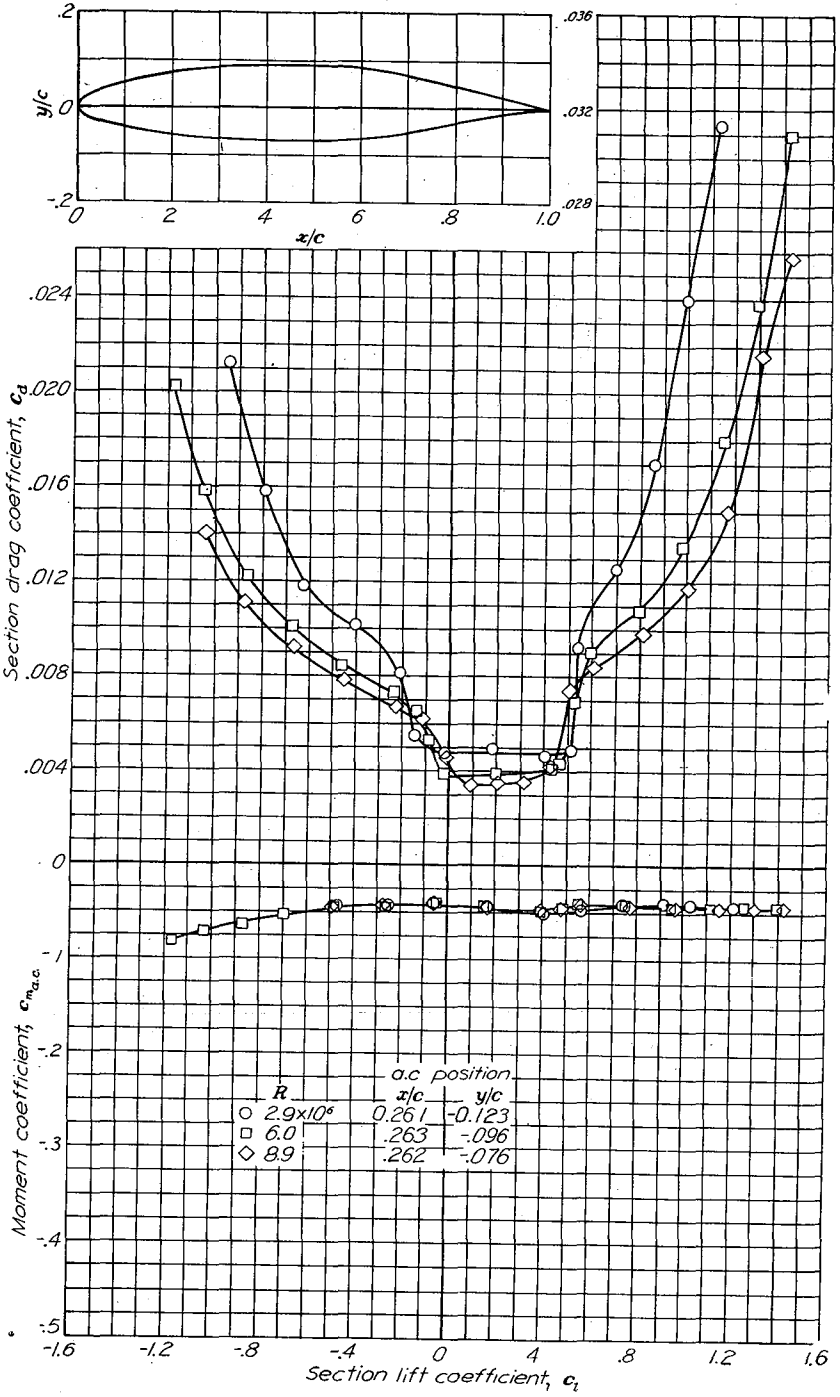
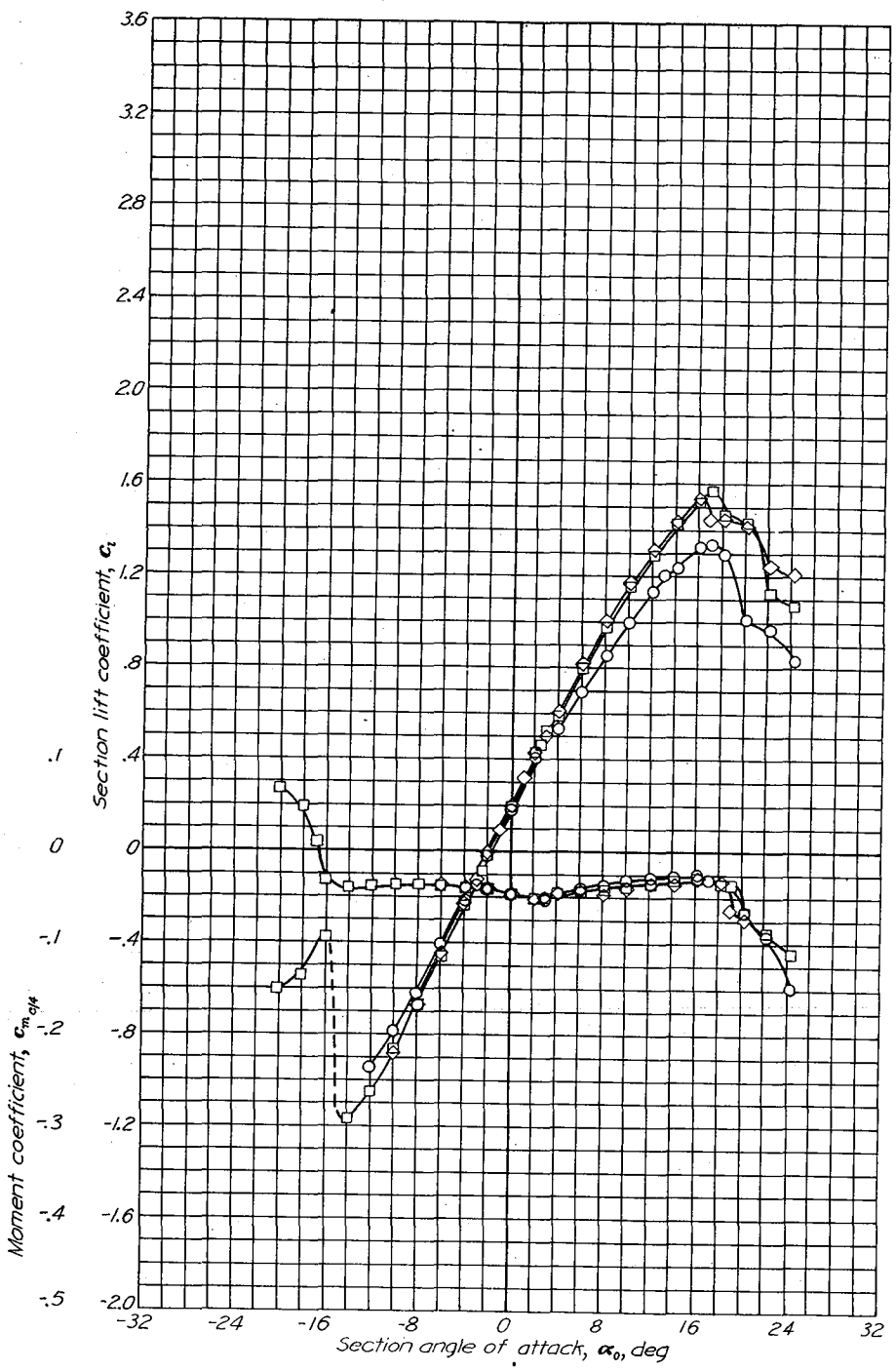
Aerodynamic characteristics of the NACA 65(215)-114 airfoil section, 24-inch chord.



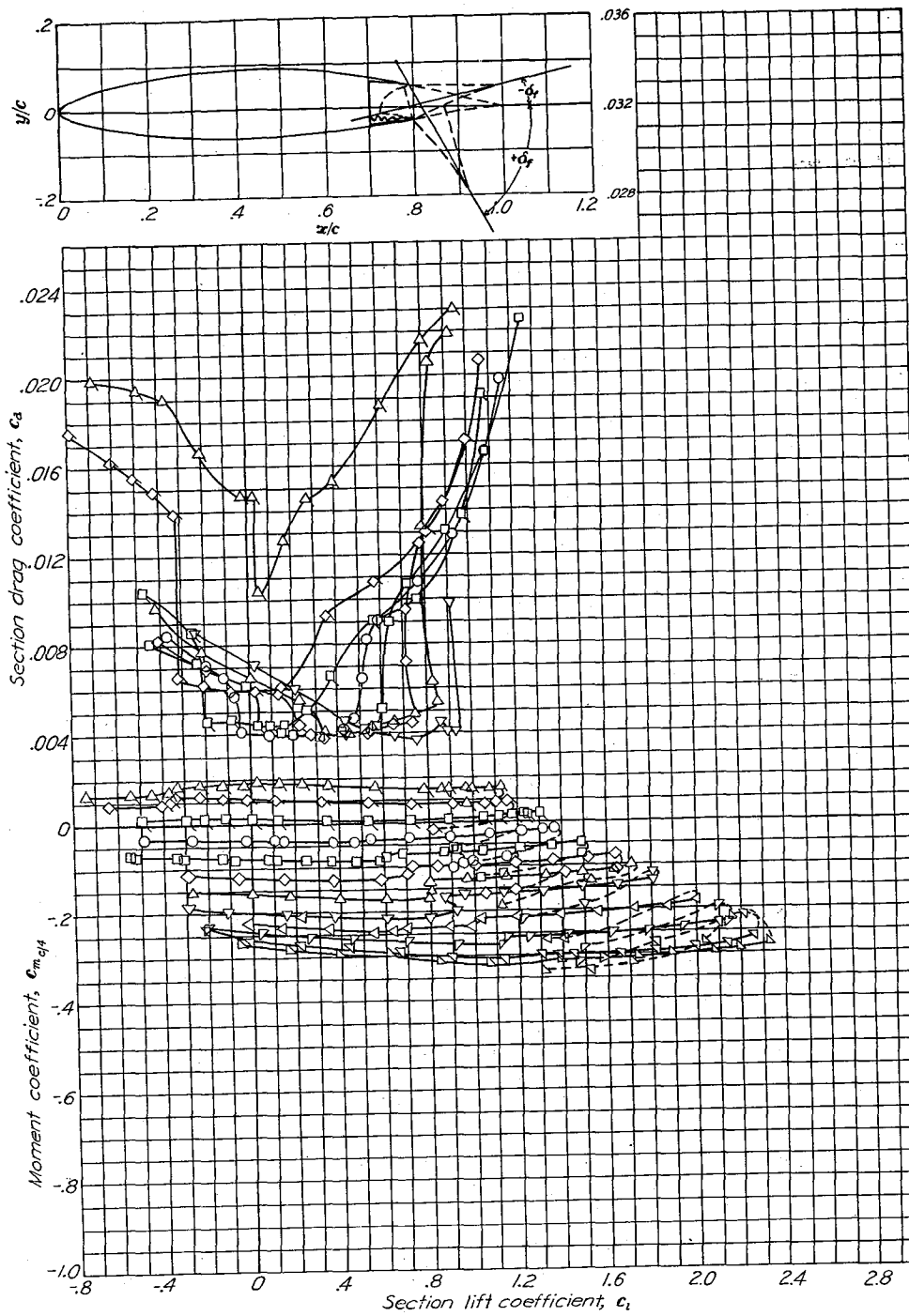
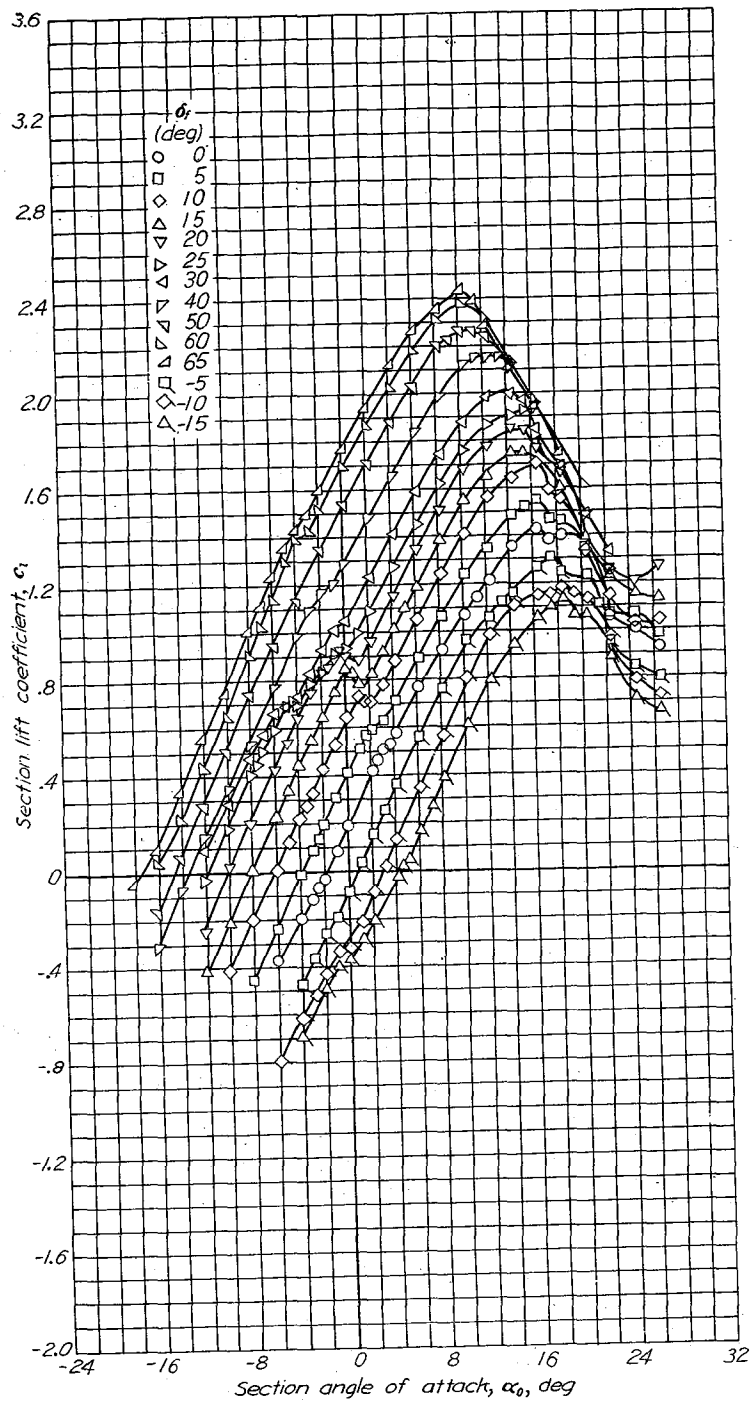
Lift and moment characteristics of the NACA 66,1-212 airfoil section with 0.20c split flap.  $R=6 \times 10^6$ .



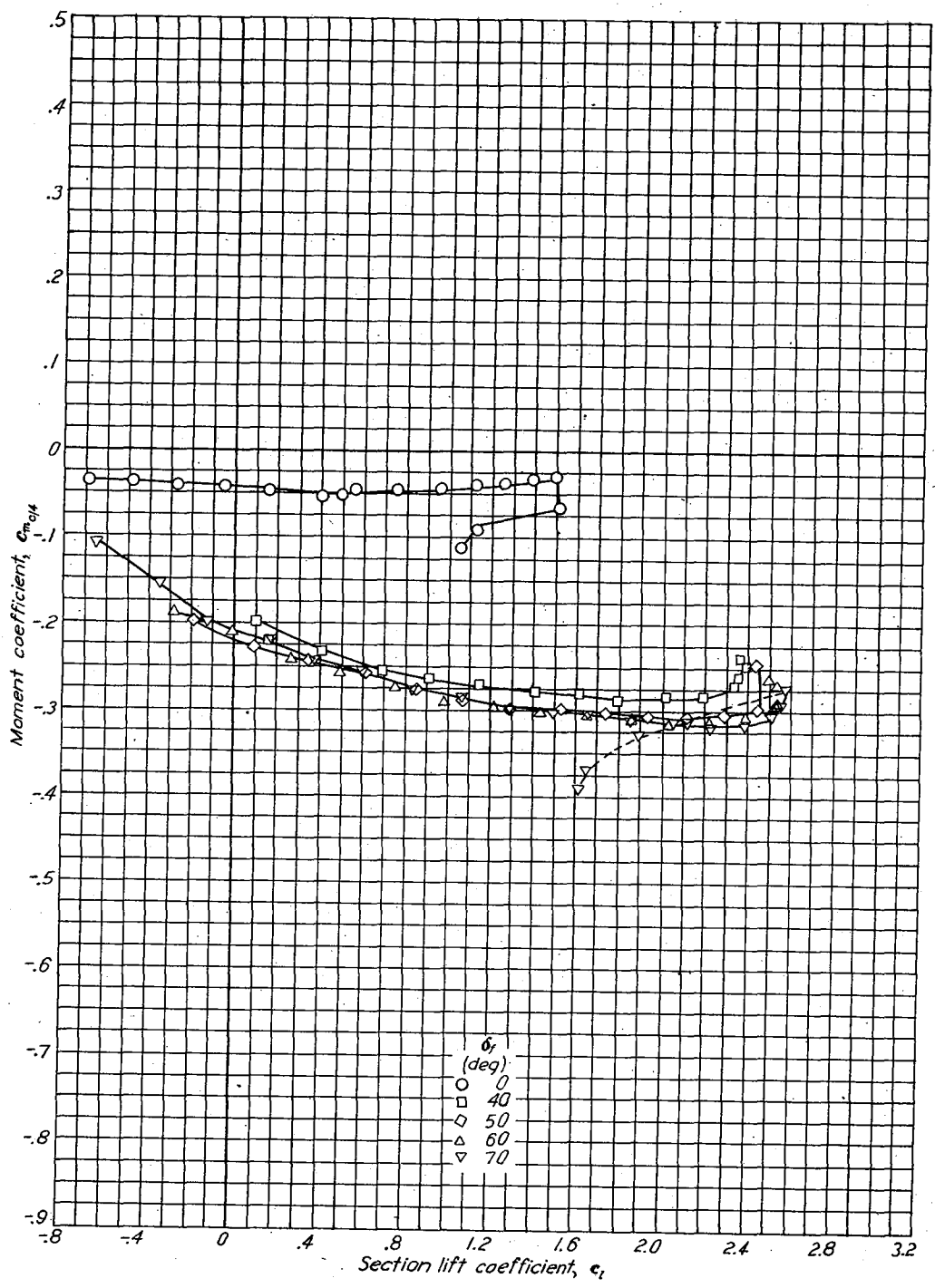
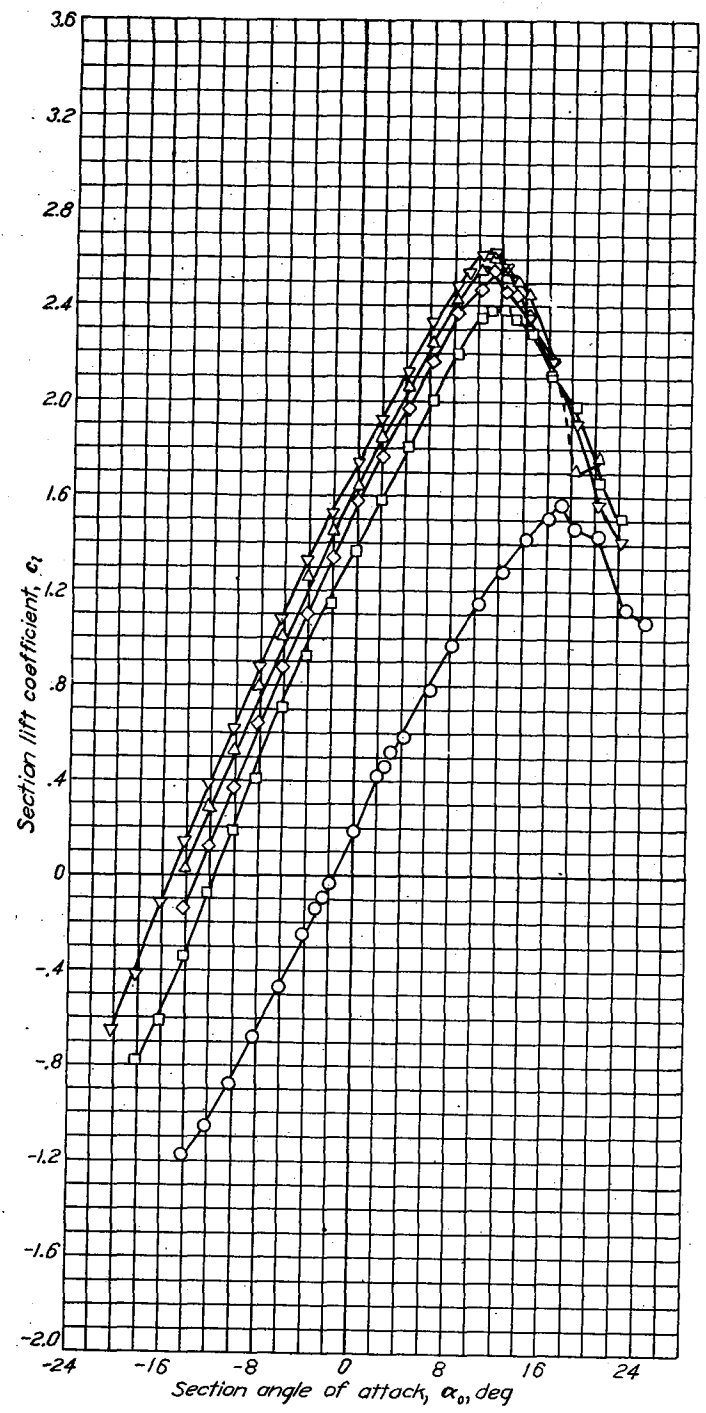
Aerodynamic characteristics of the NACA 66(215)-016 airfoil section, 24-inch chord.



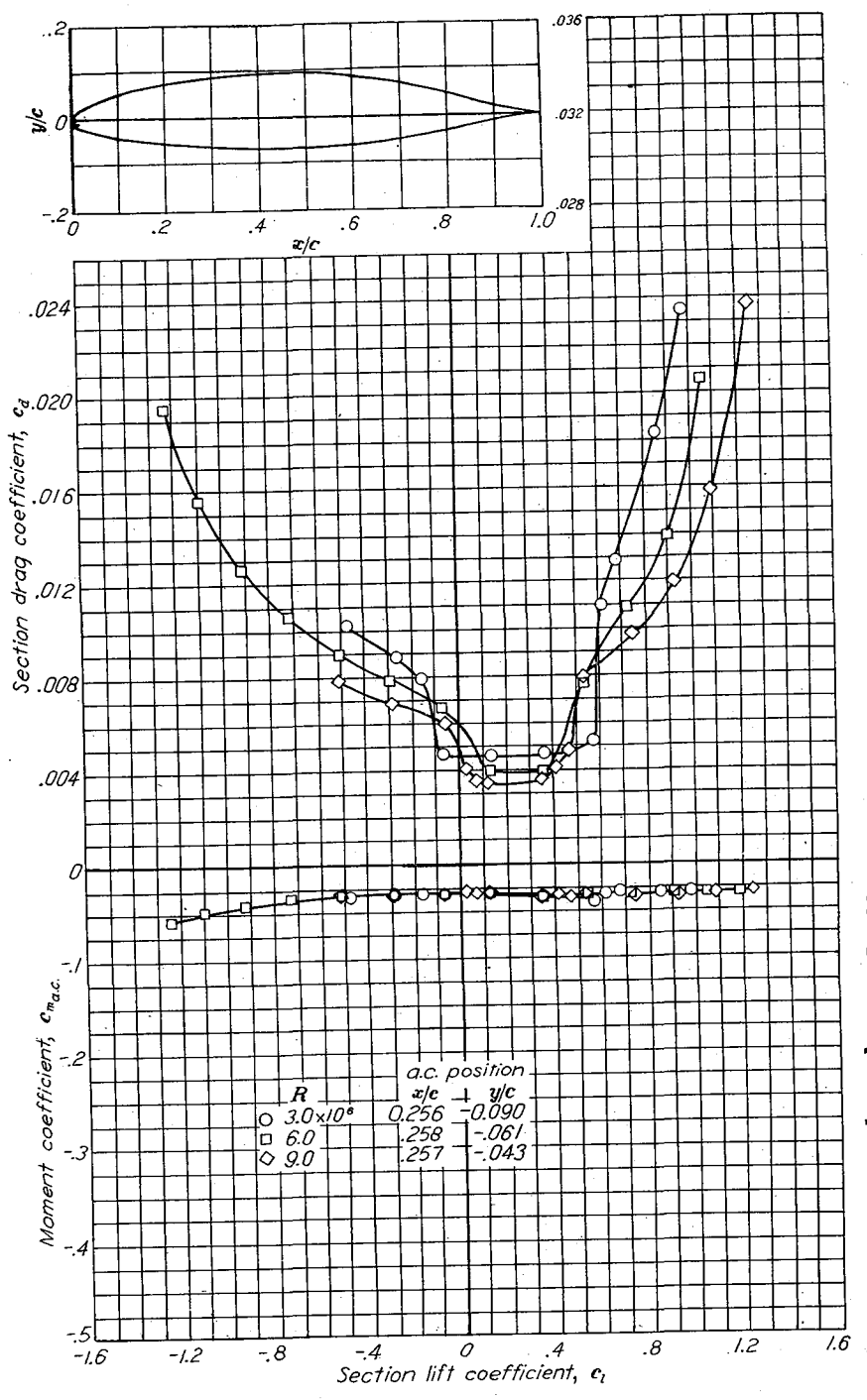
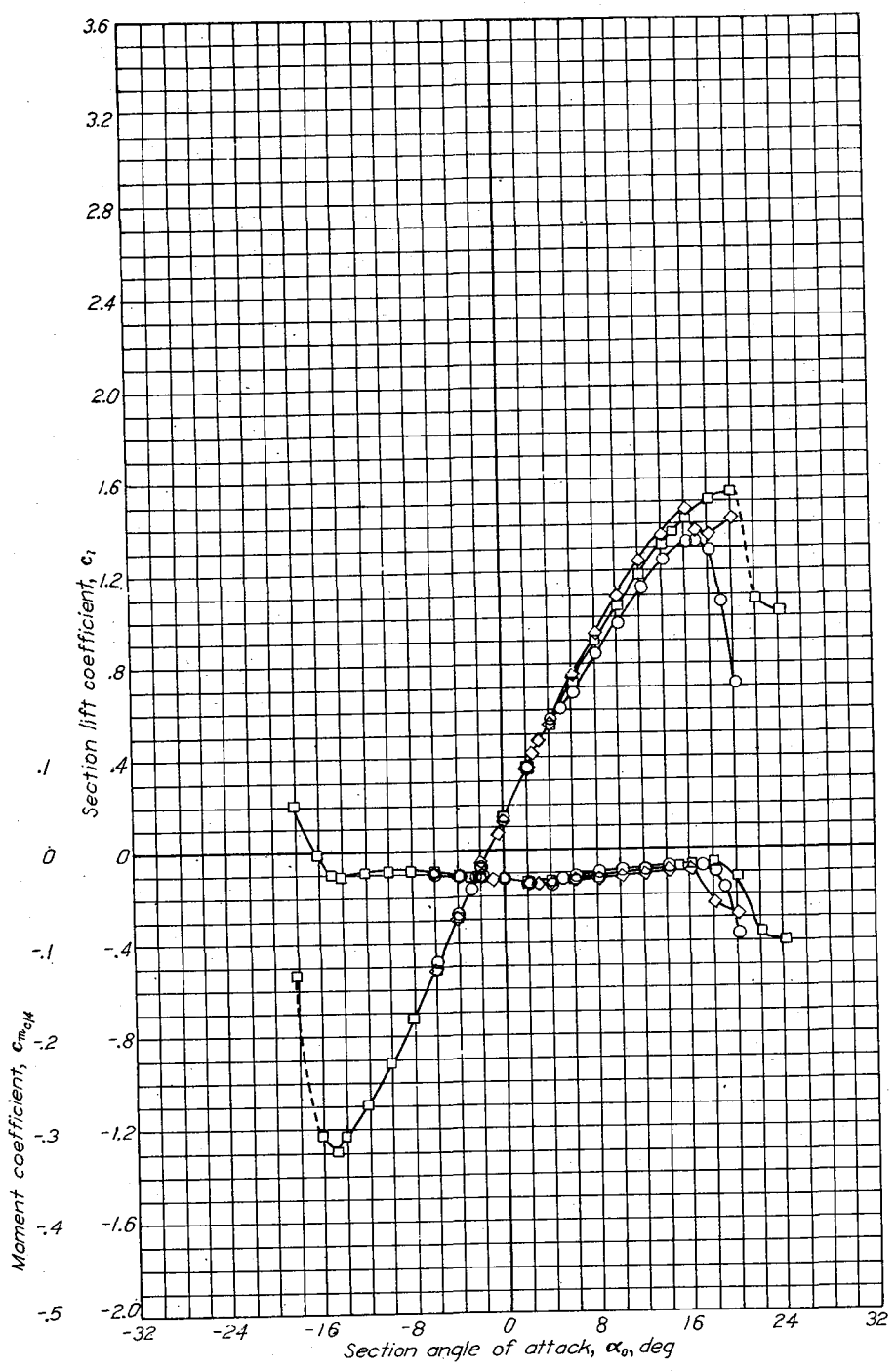
Aerodynamic characteristics of the NACA 66(215)-216 airfoil section, 24-inch chord.



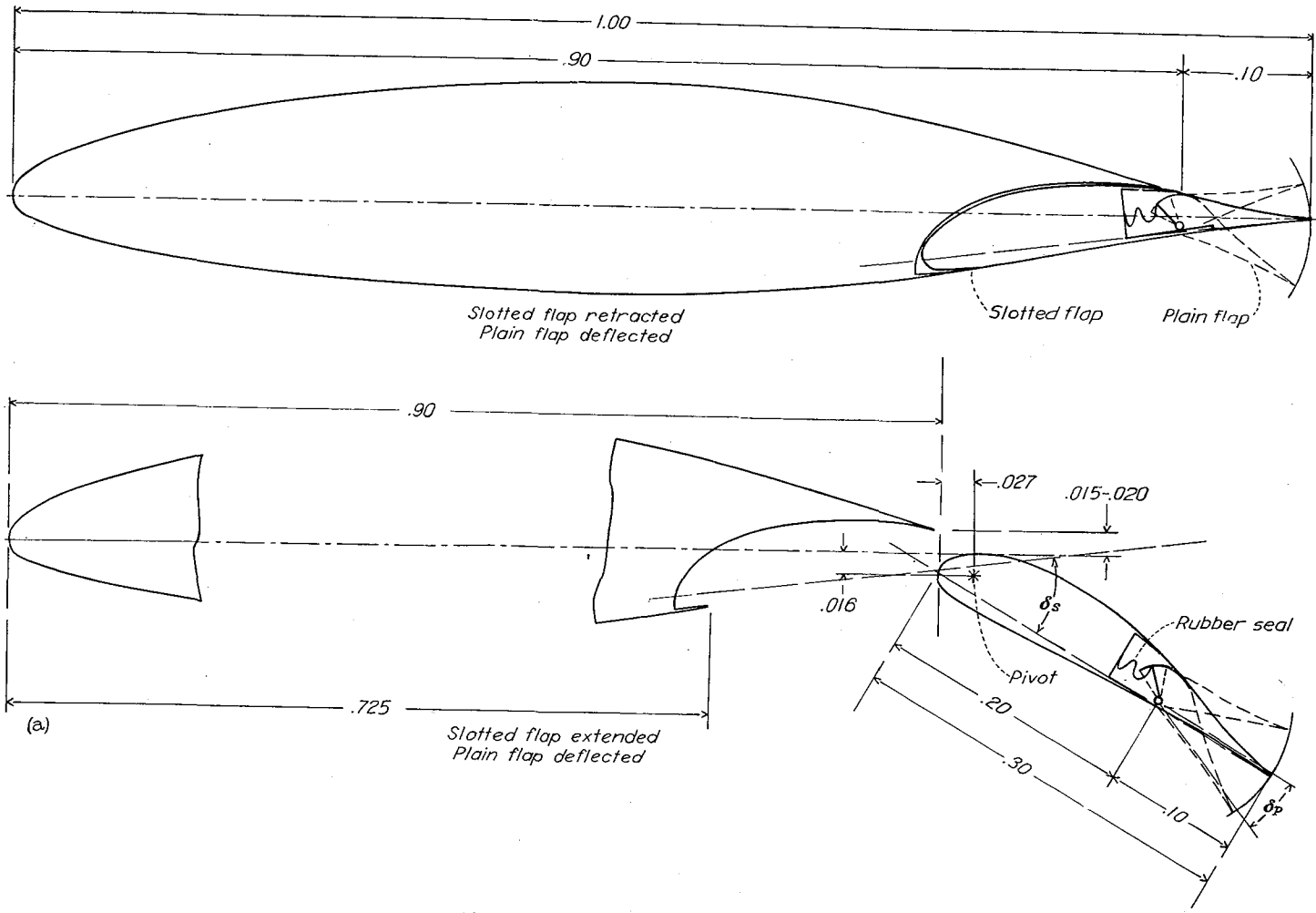
Aerodynamic characteristics of the NACA 66(215)-216 airfoil section with 0.20c sealed plain flap.  $R=6 \times 10^6$ .



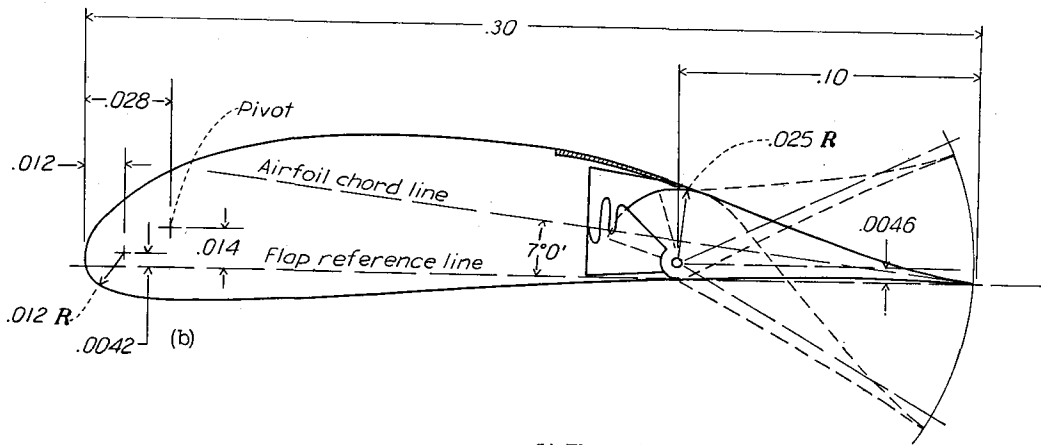
Lift and moment characteristics of the NACA 66(215)-216 airfoil section with 0.20c split flap.  $R=6 \times 10^6$ .



Aerodynamic characteristics of the NACA 66(215)-216,  $\alpha=0.6$  airfoil section, 24-inch chord.



(a) Airfoil-flap configuration.

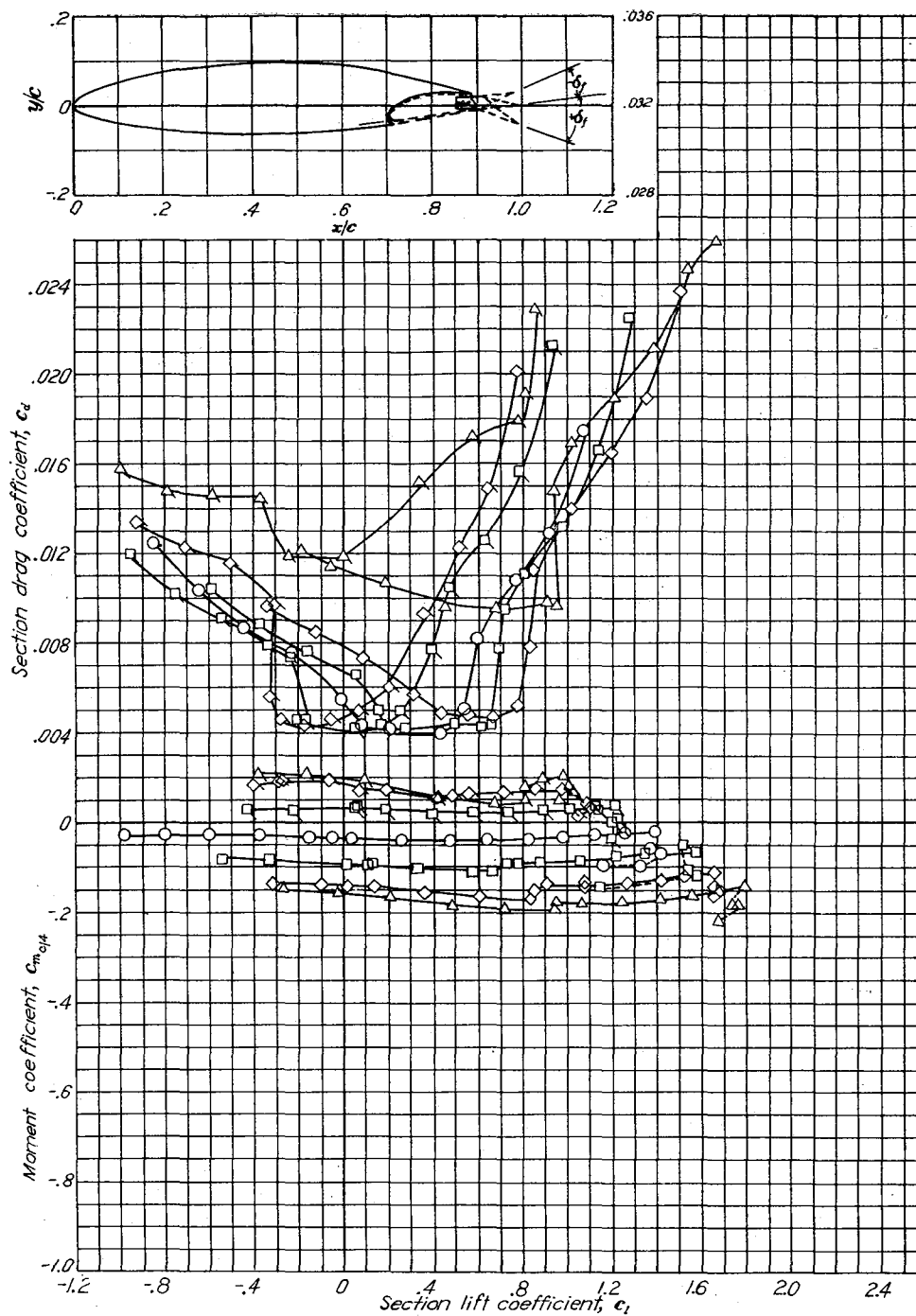
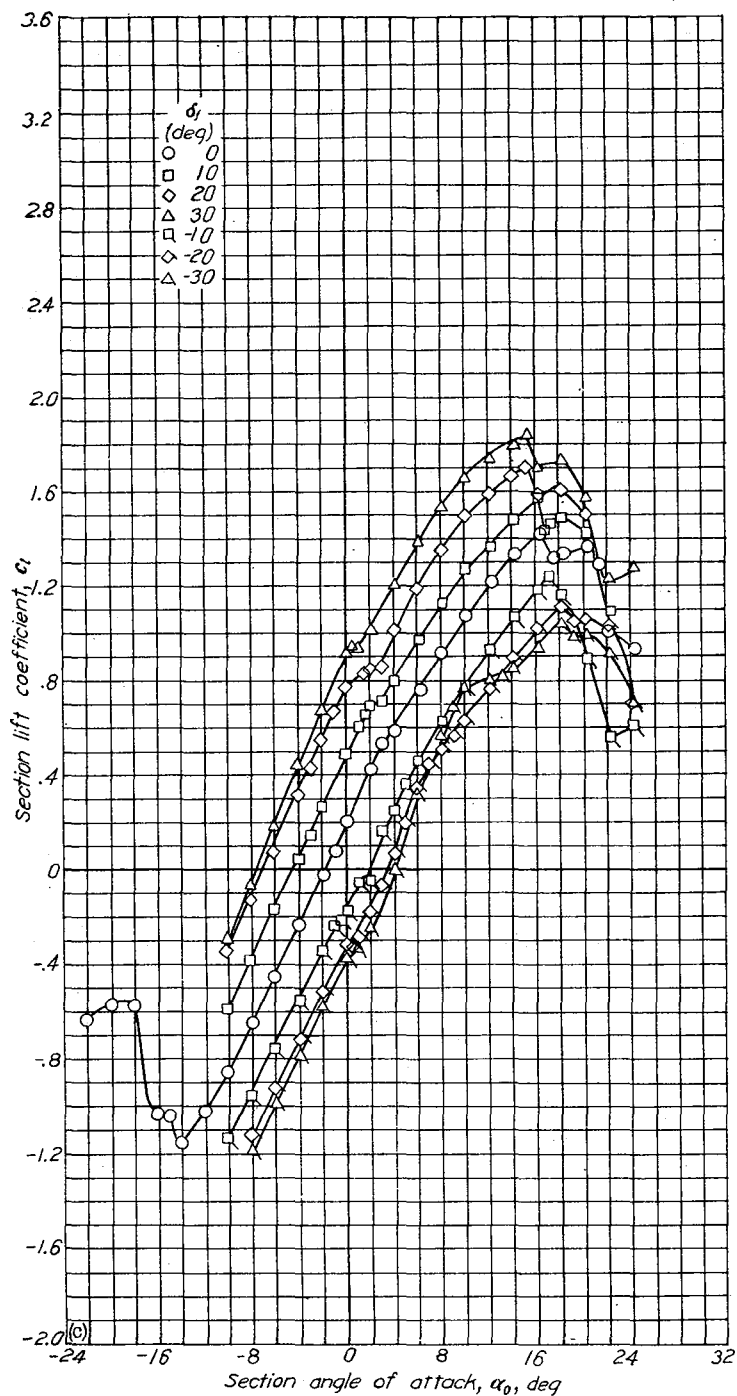


(b) Flap configuration.

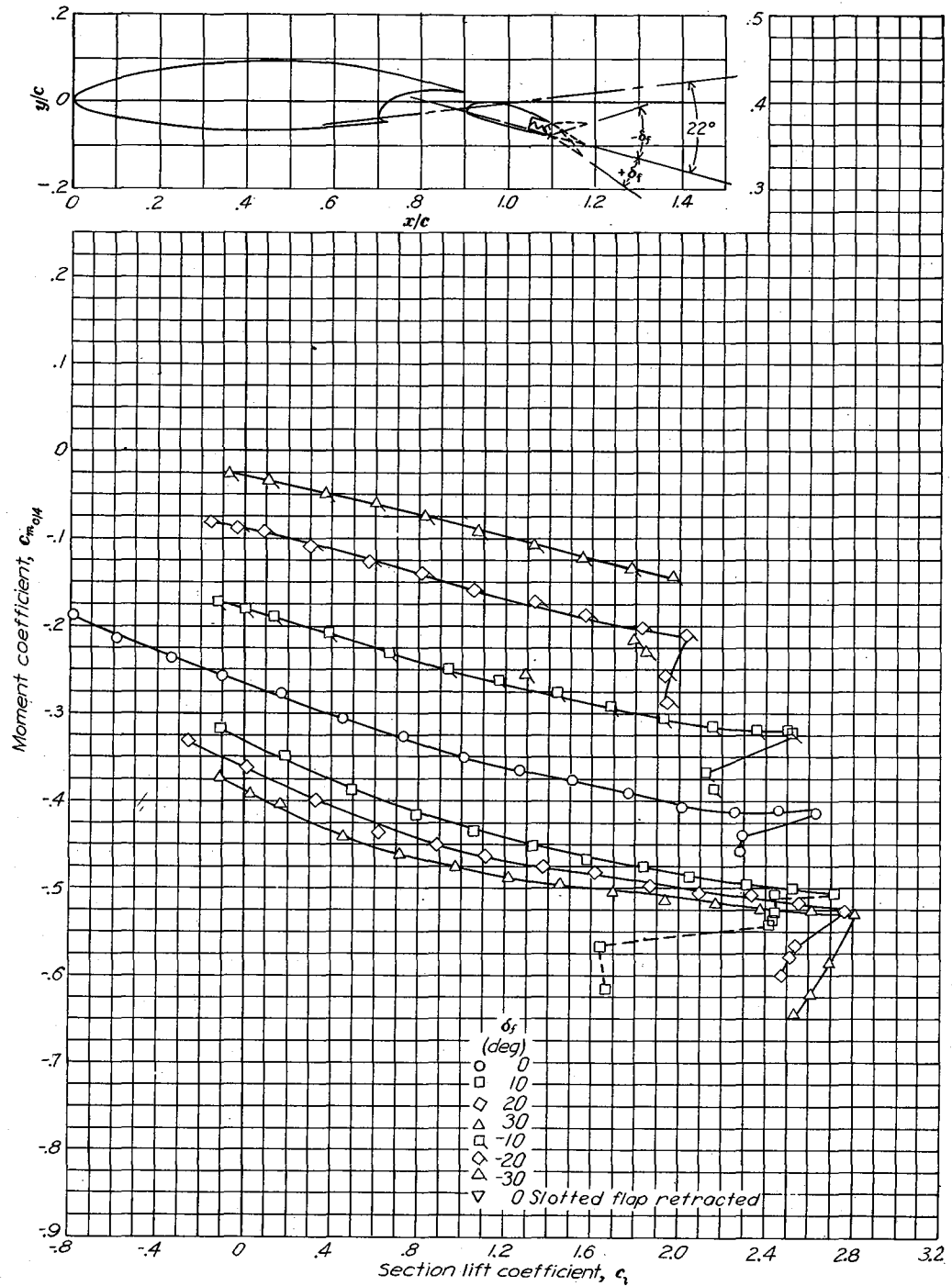
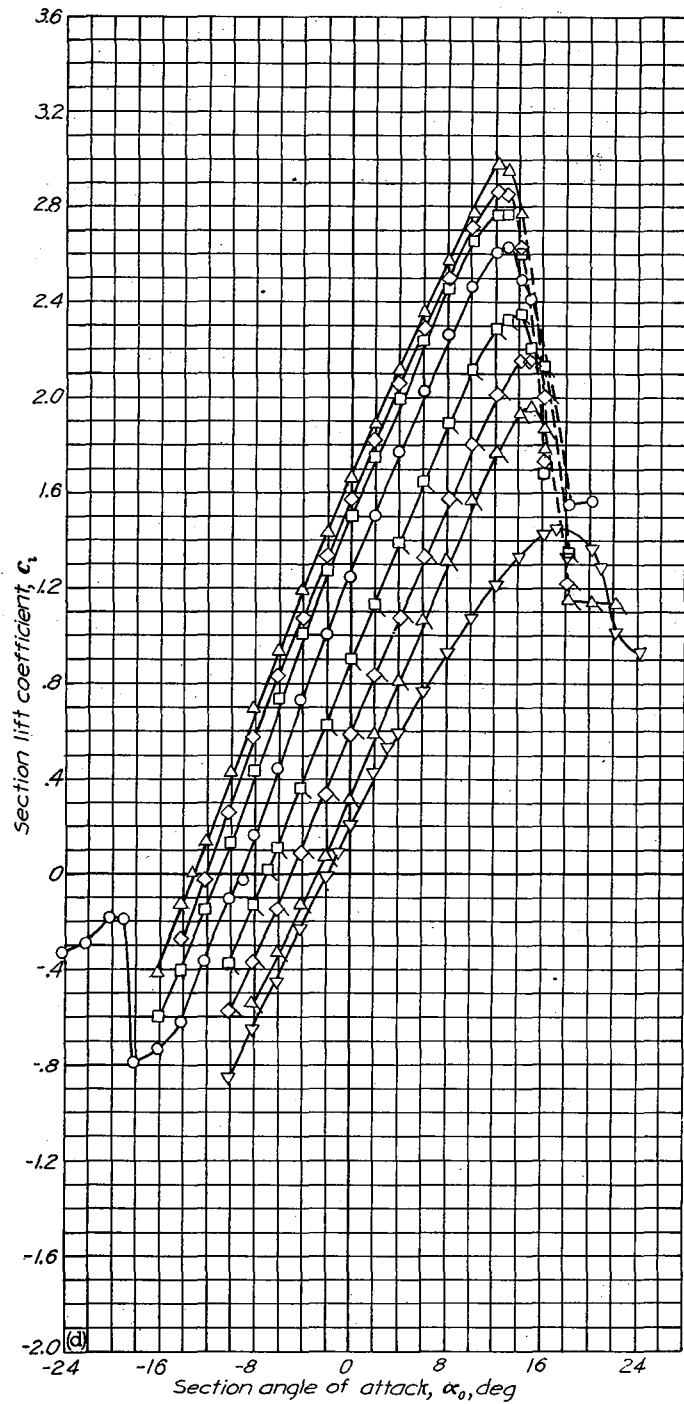
NACA 66(215)-216,  $\alpha = 0.6$  airfoil section with 0.30c slotted and 0.10c plain flap.

Flap coordinates			
Upper surface		Lower surface	
Abscissa	Ordinate	Abscissa	Ordinate
0.5	1.54	0.5	-0.58
1.04	2.04	1.04	-.83
2.08	2.75	2.08	-1.00
4.16	3.75	4.16	-.92
6.25	4.28	6.25	-.79
8.33	4.53	8.33	-.62
10.41	4.58	10.41	-.46
12.50	4.50	12.50	-.33
14.58	4.33	14.58	-.21
16.66	4.06	16.66	-.08
18.75	3.54	18.75	0
20.29	3.04	20.29	.10
22.91	2.06	22.91	.17
25.00	1.27	25.00	.14
27.08	.62	27.08	.004
29.16	.15	29.16	0
30.00	0	30.00	0

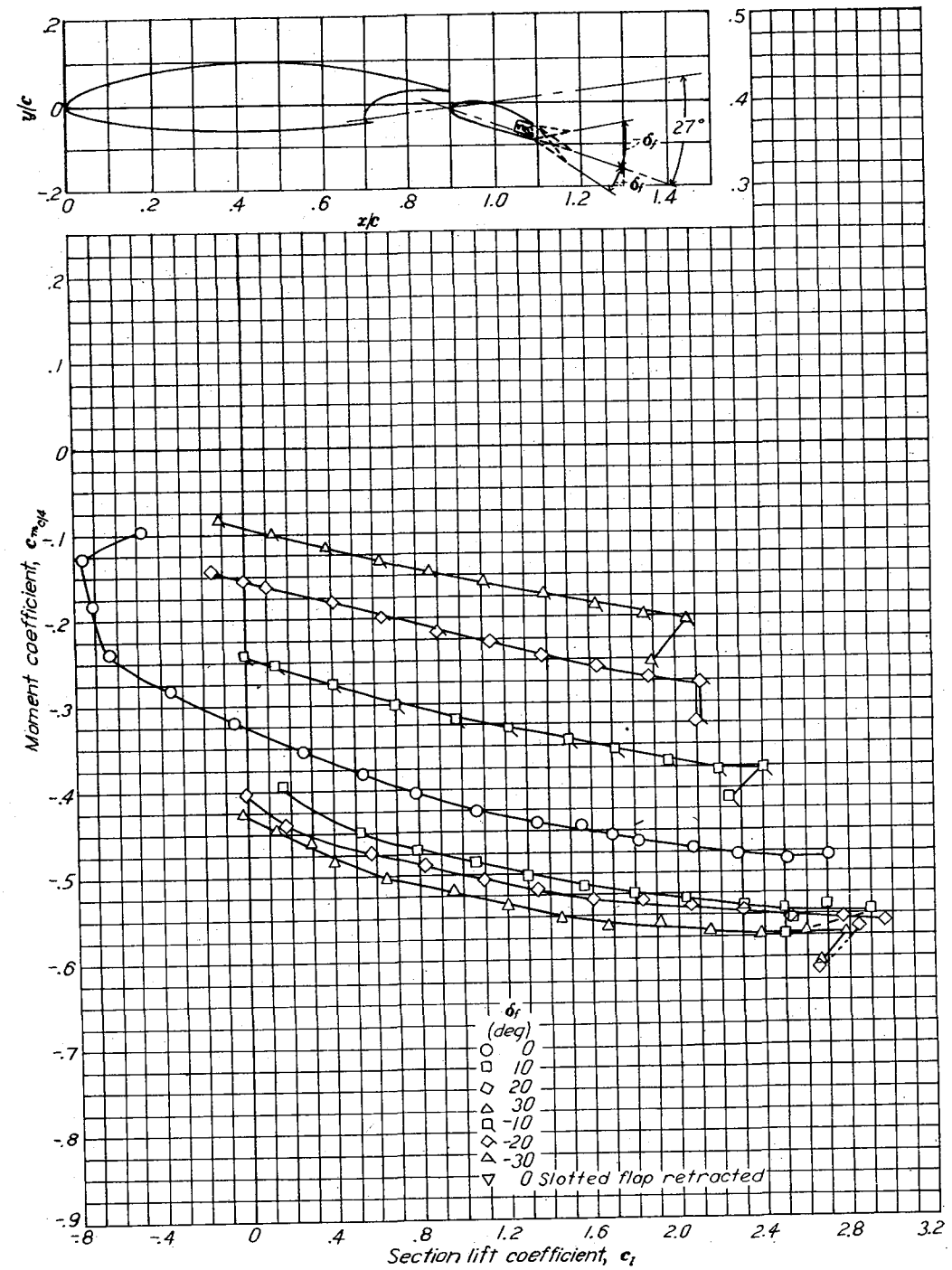
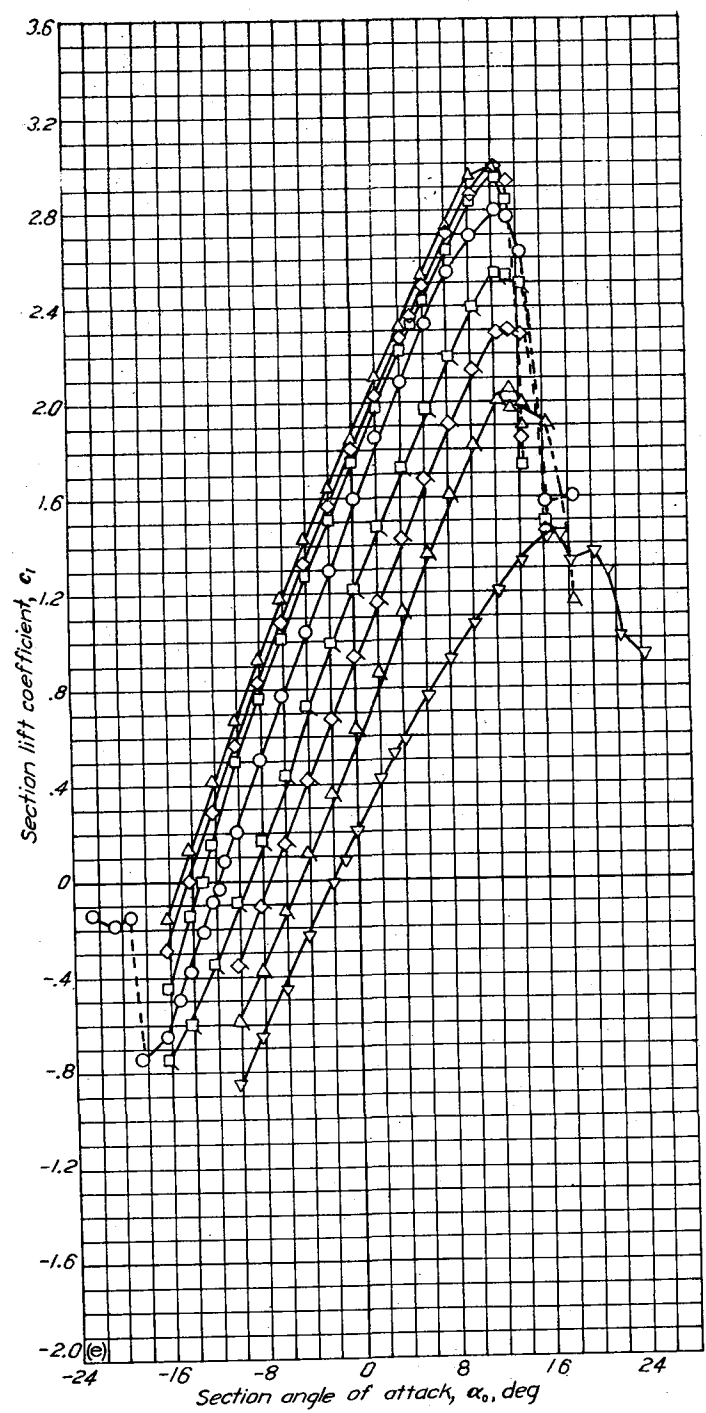




(c) Aerodynamic characteristics. Slotted flap retracted;  $R=6 \times 10^6$ .  
 NACA 66(215)-216,  $\alpha=0.6$  airfoil section with 0.30c slotted and 0.10c plain flap.

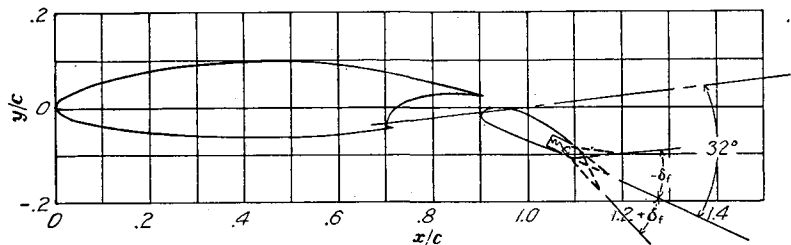
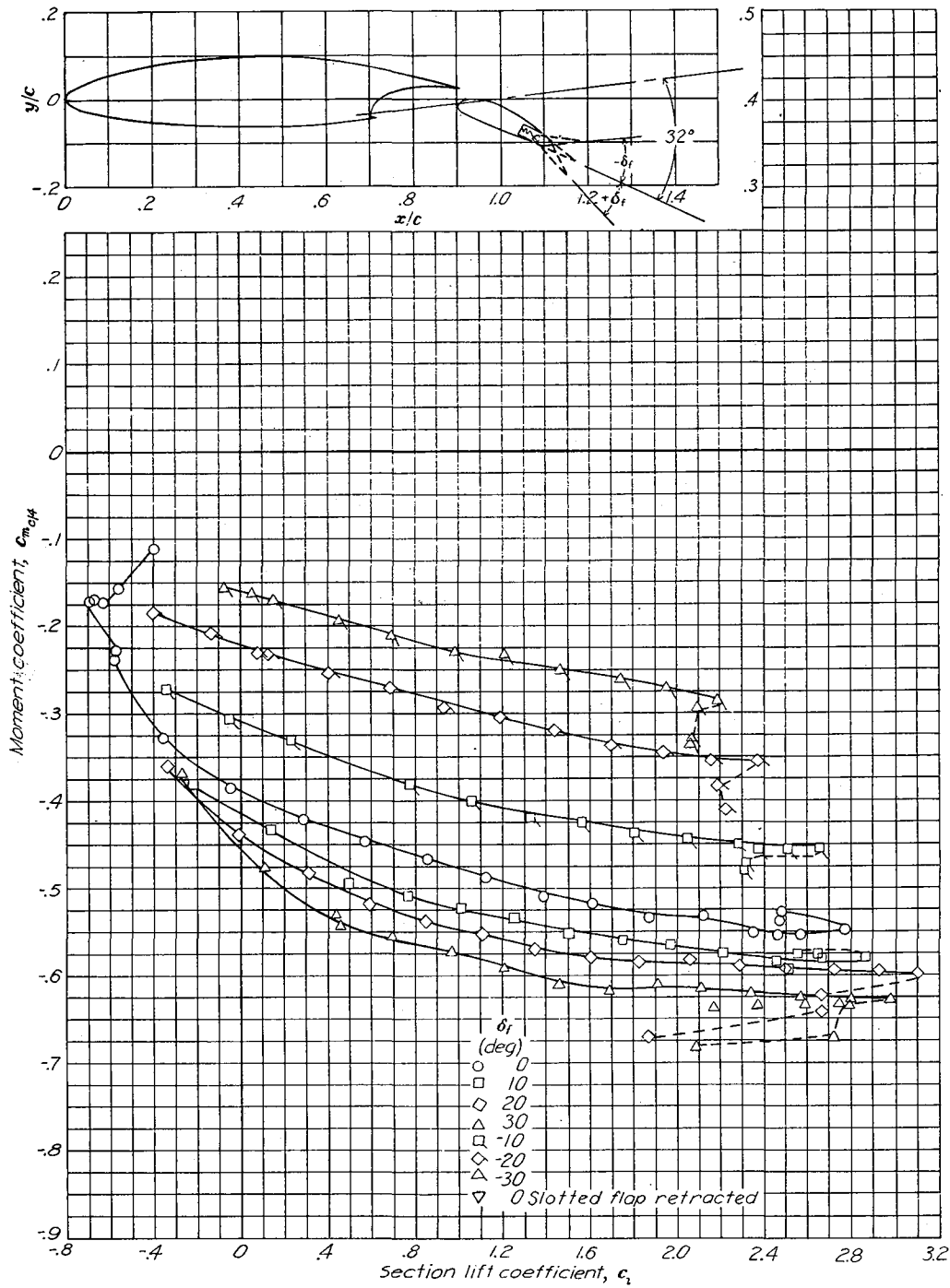
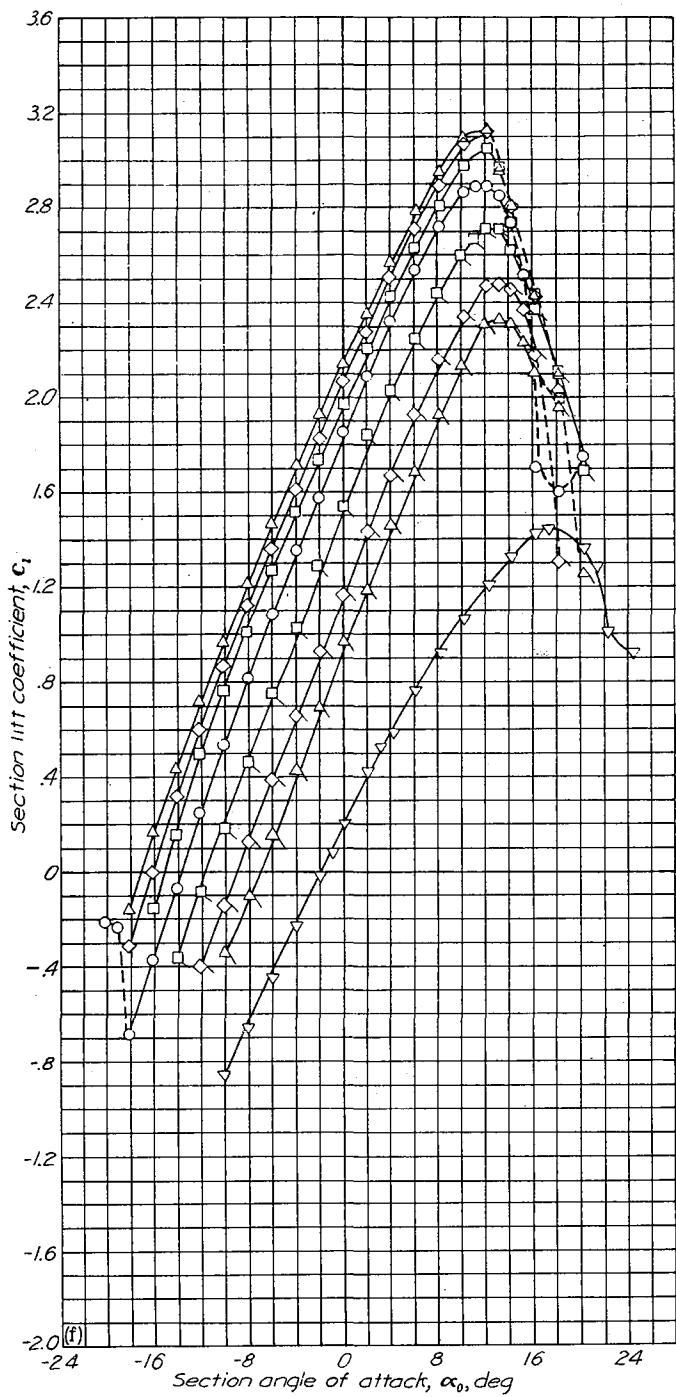
NACA 66(215)-216,  $\alpha = 0.6$  with flap

(d) Lift and moment characteristics. Slotted flap deflected  $22^\circ$ ;  $R=6 \times 10^6$ .  
 NACA 66(215)-216,  $\alpha=0.6$  airfoil section with 0.30c slotted and 0.10c plain flap

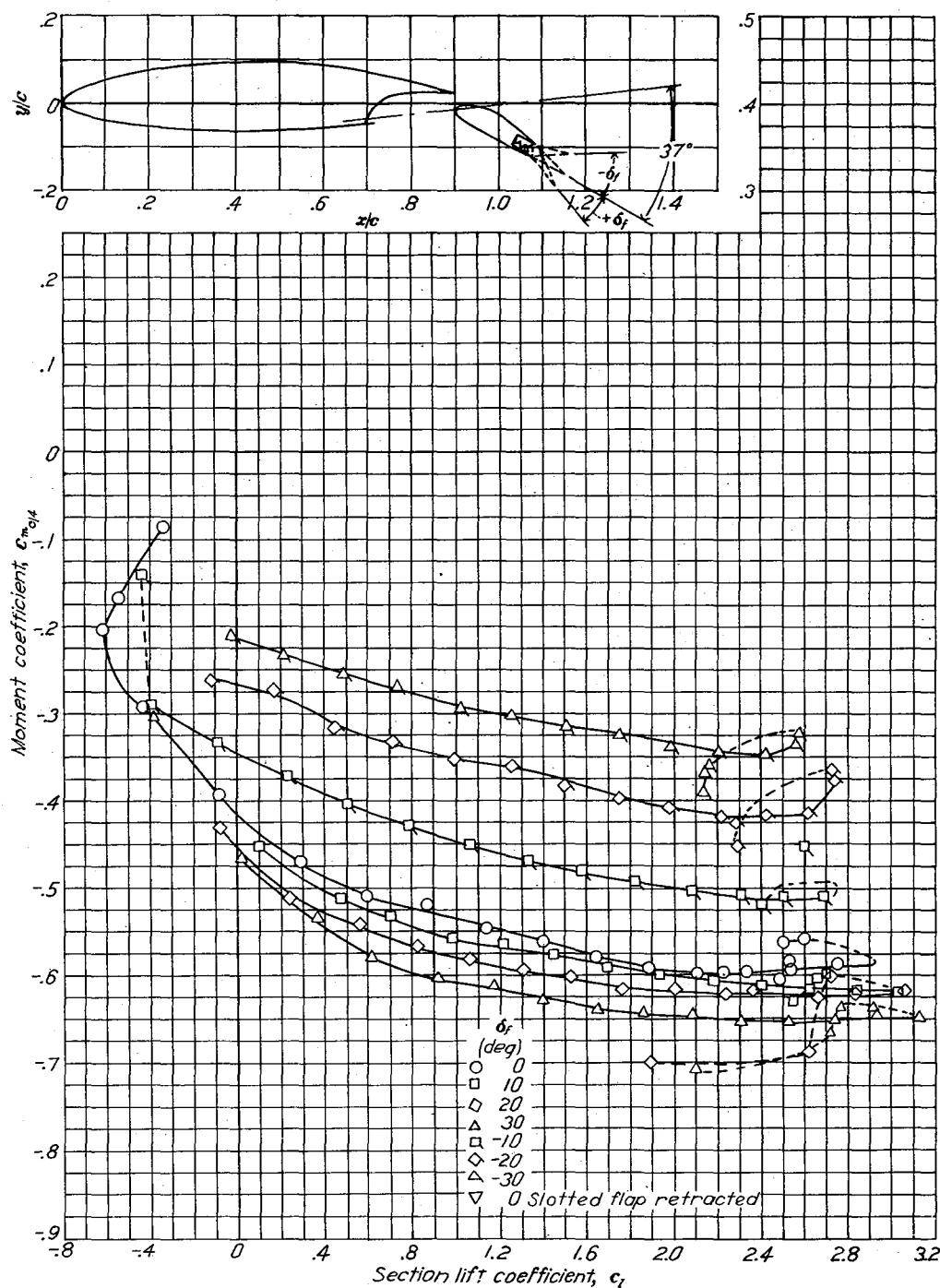
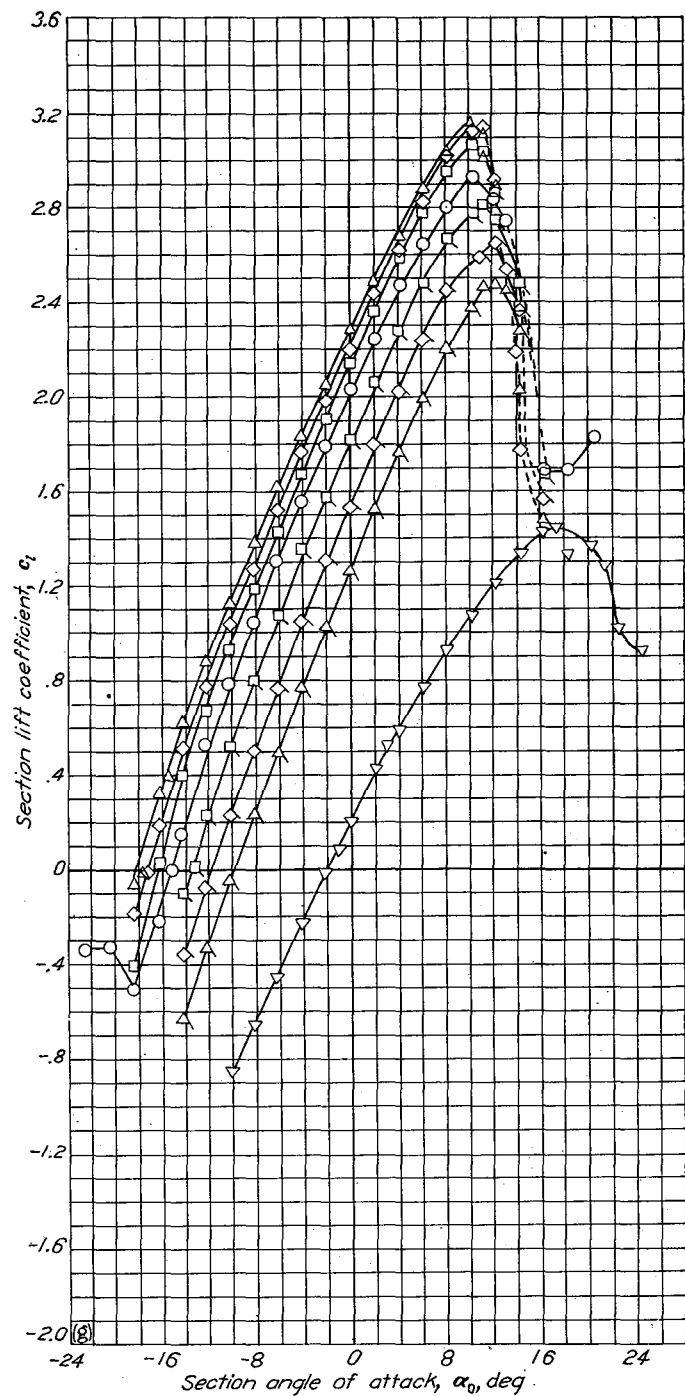


(e) Lift and moment characteristics. Slotted flap deflected 27°;  $R=6 \times 10^6$ .  
 NACA 66(215)-216,  $\alpha=0.6$  airfoil section with 0.30c slotted and 0.10c plain flap.

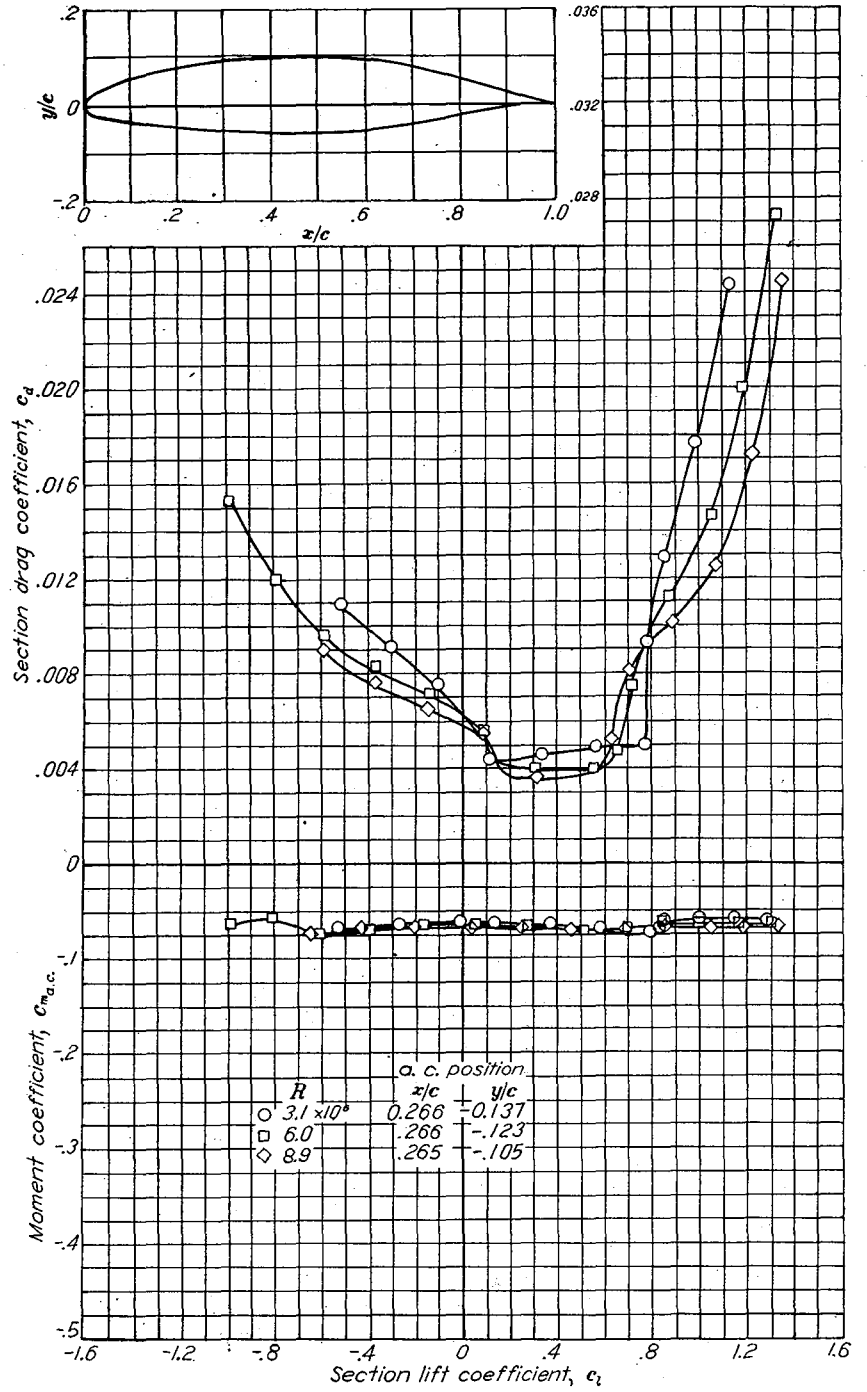
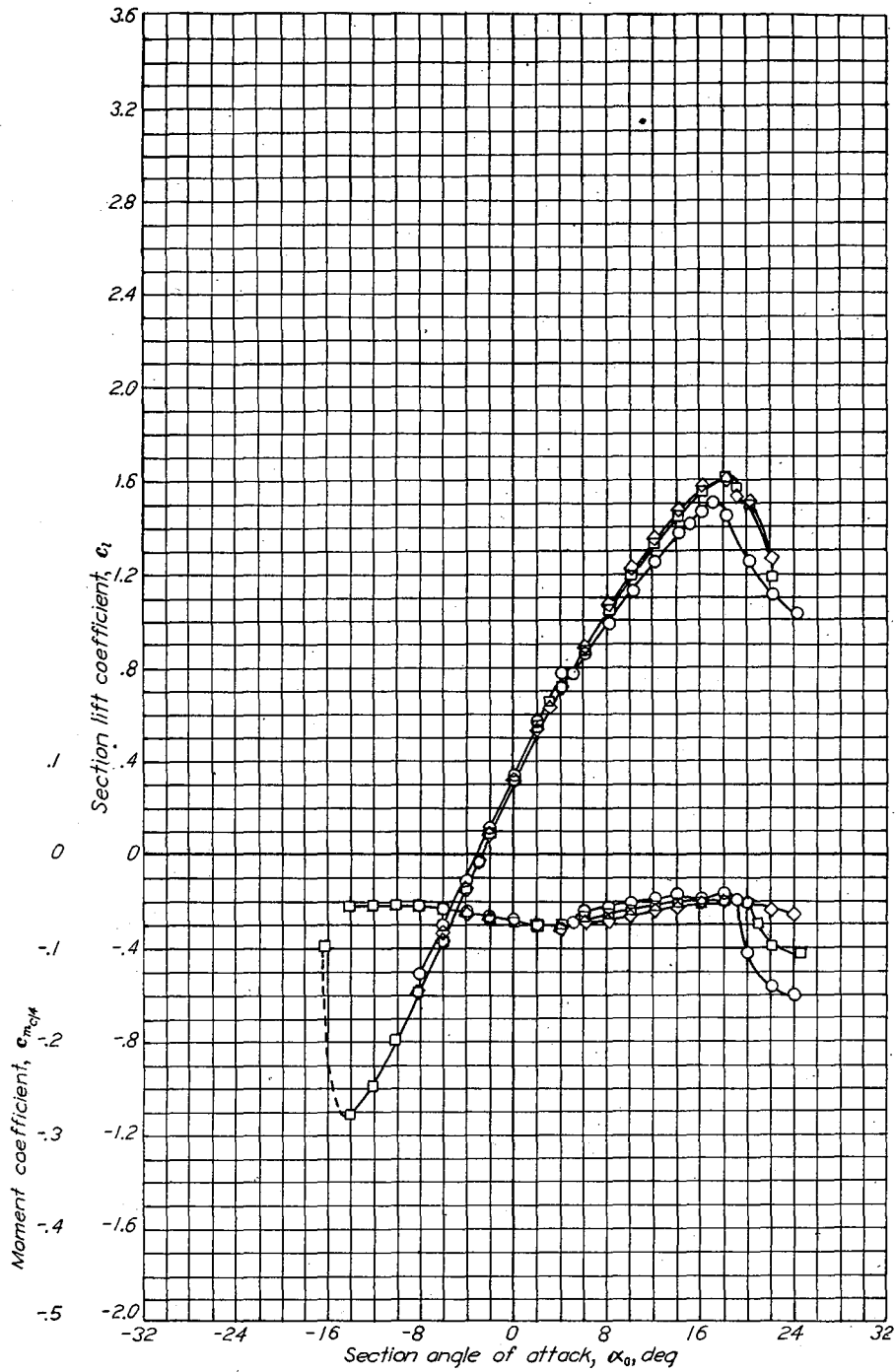
NACA 66(215)-216,  $\alpha = 0.6$  with flap



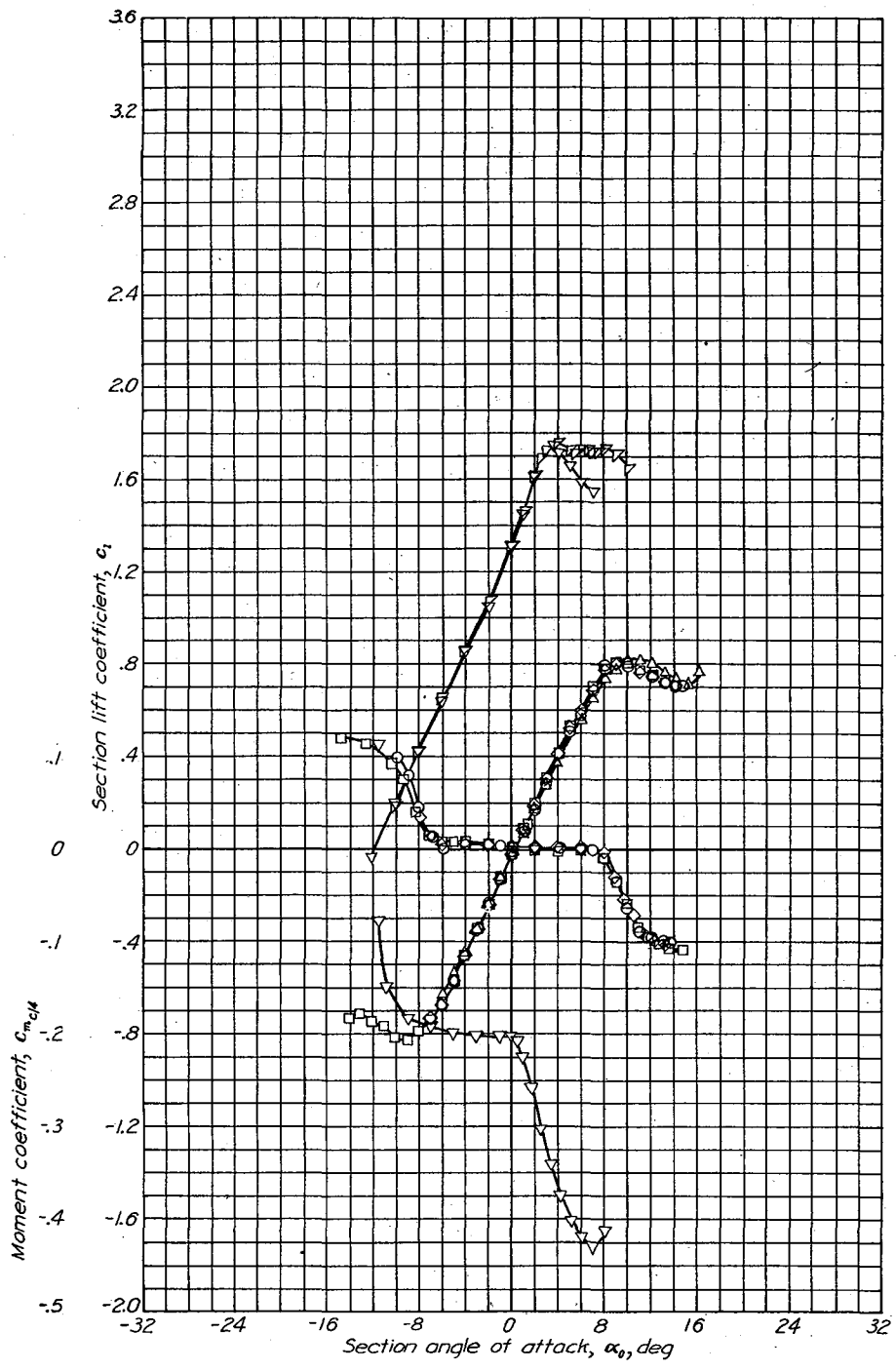
(f) Lift and moment characteristics. Slotted flap deflected  $32^\circ$ ;  $R=6 \times 10^4$ .  
 NACA 66(215)-216,  $\alpha=0.6$  airfoil section with 0.30c slotted and 0.10c plain flap.



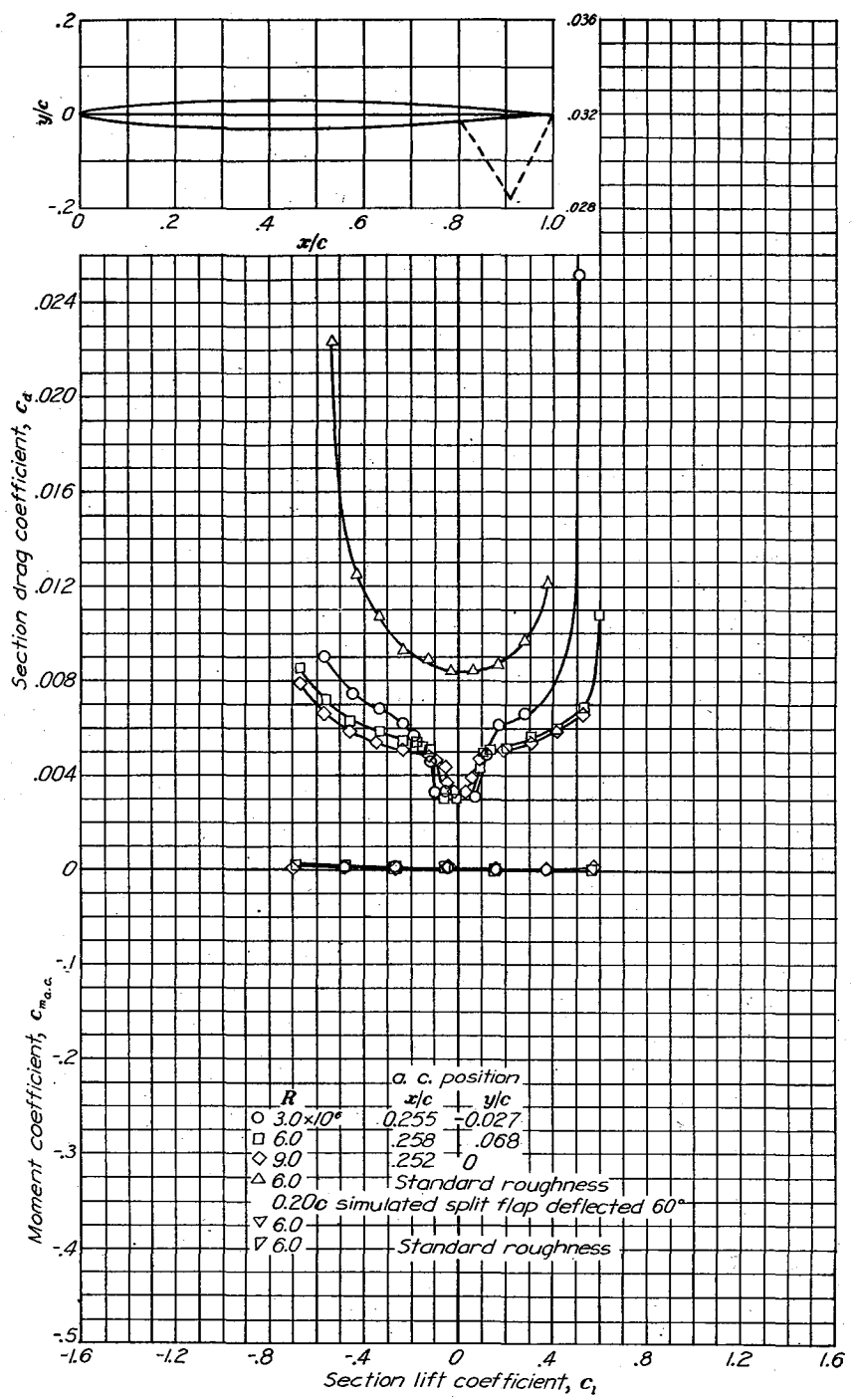
(g) Lift and moment characteristics. Slotted flap deflected  $37^\circ$ ;  $R=6 \times 10^6$ .  
 NACA 66(215)-216,  $\alpha=0.6$  airfoil section with 0.30c slotted and 0.10c plain flap.



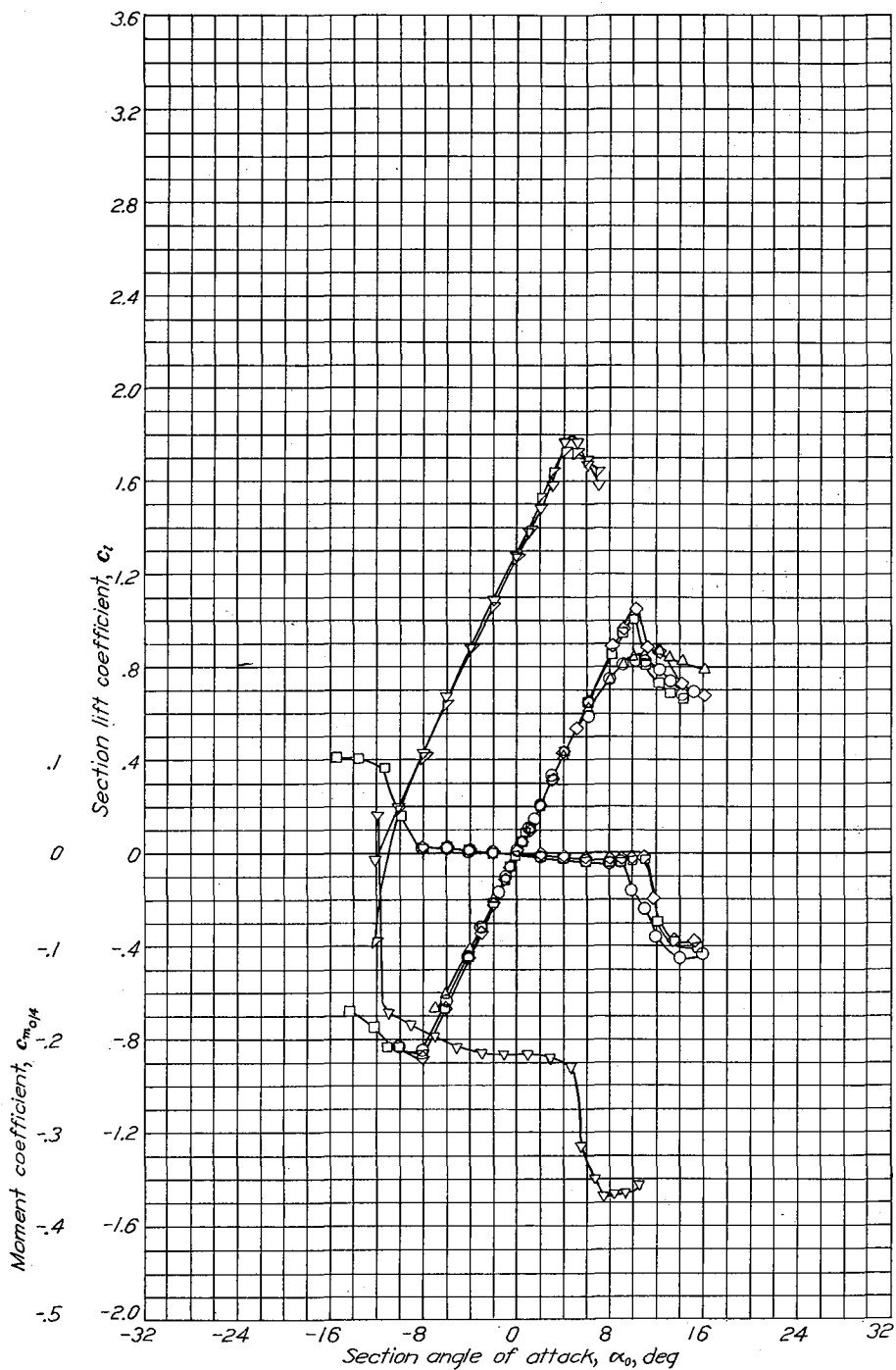
Aerodynamic characteristics of the NACA 66(215)-416 airfoil section, 24-inch chord.



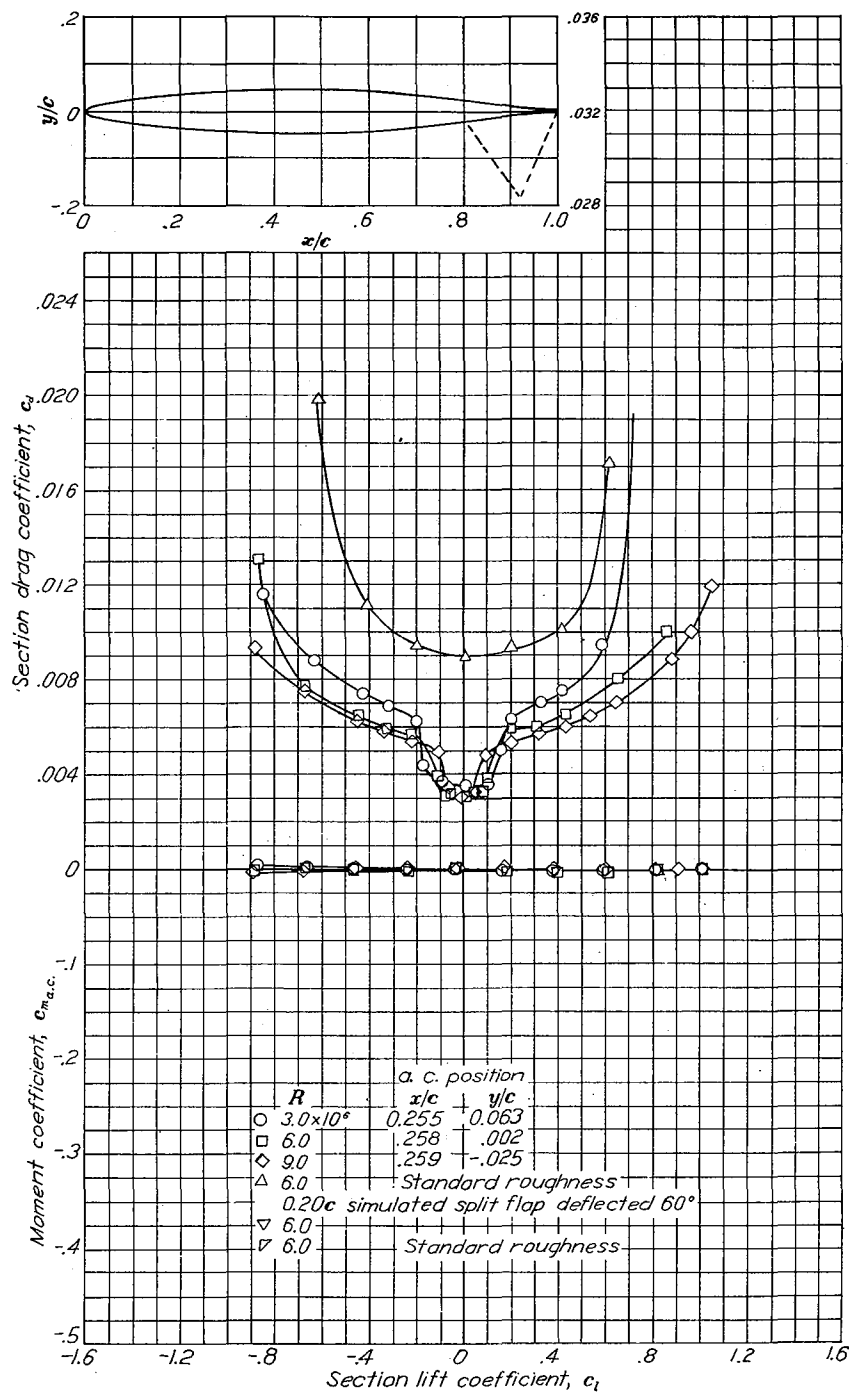
Aerodynamic characteristics of the NACA 66-006 airfoil section, 24-inch chord.



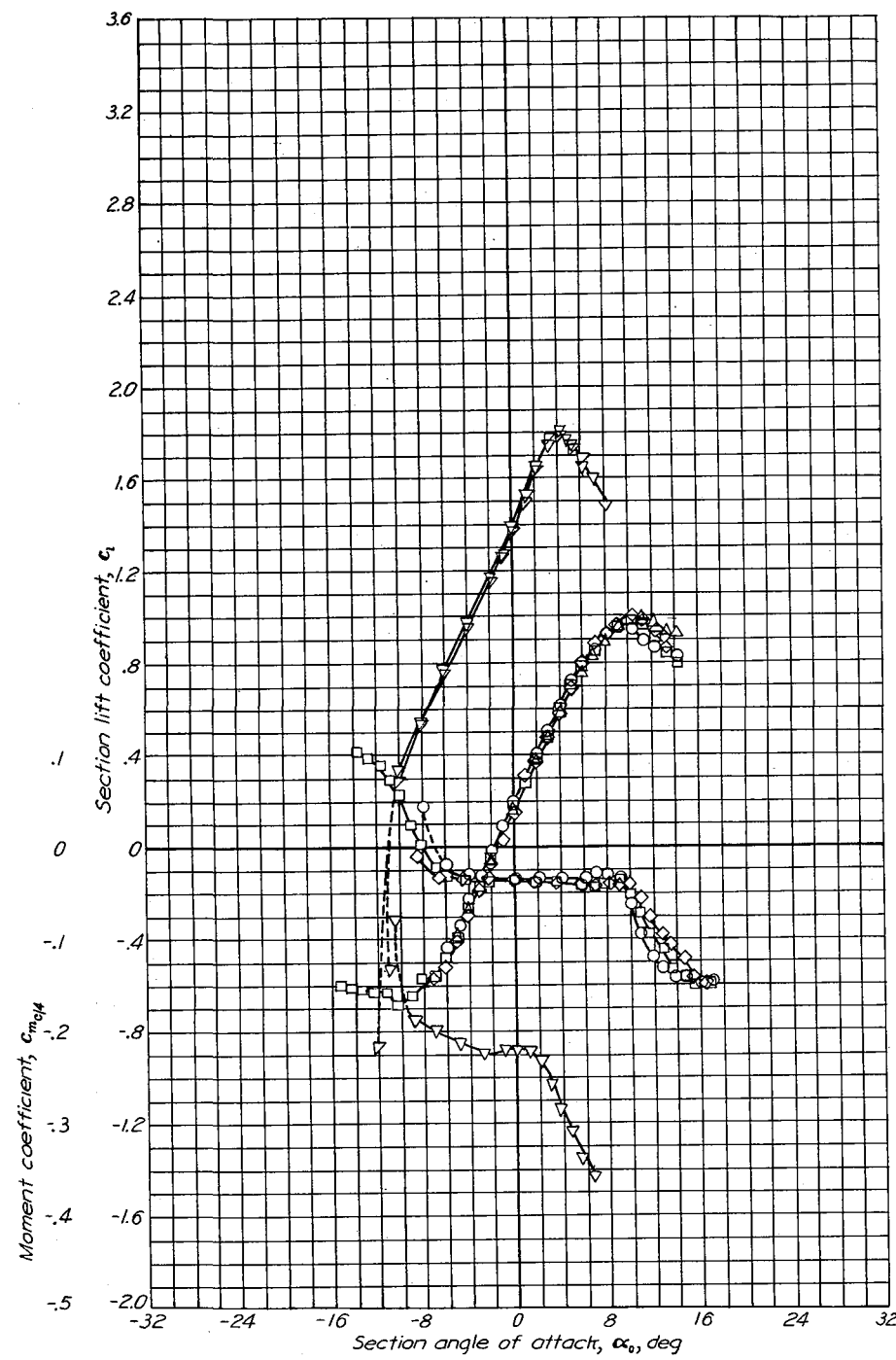
NACA 66-006



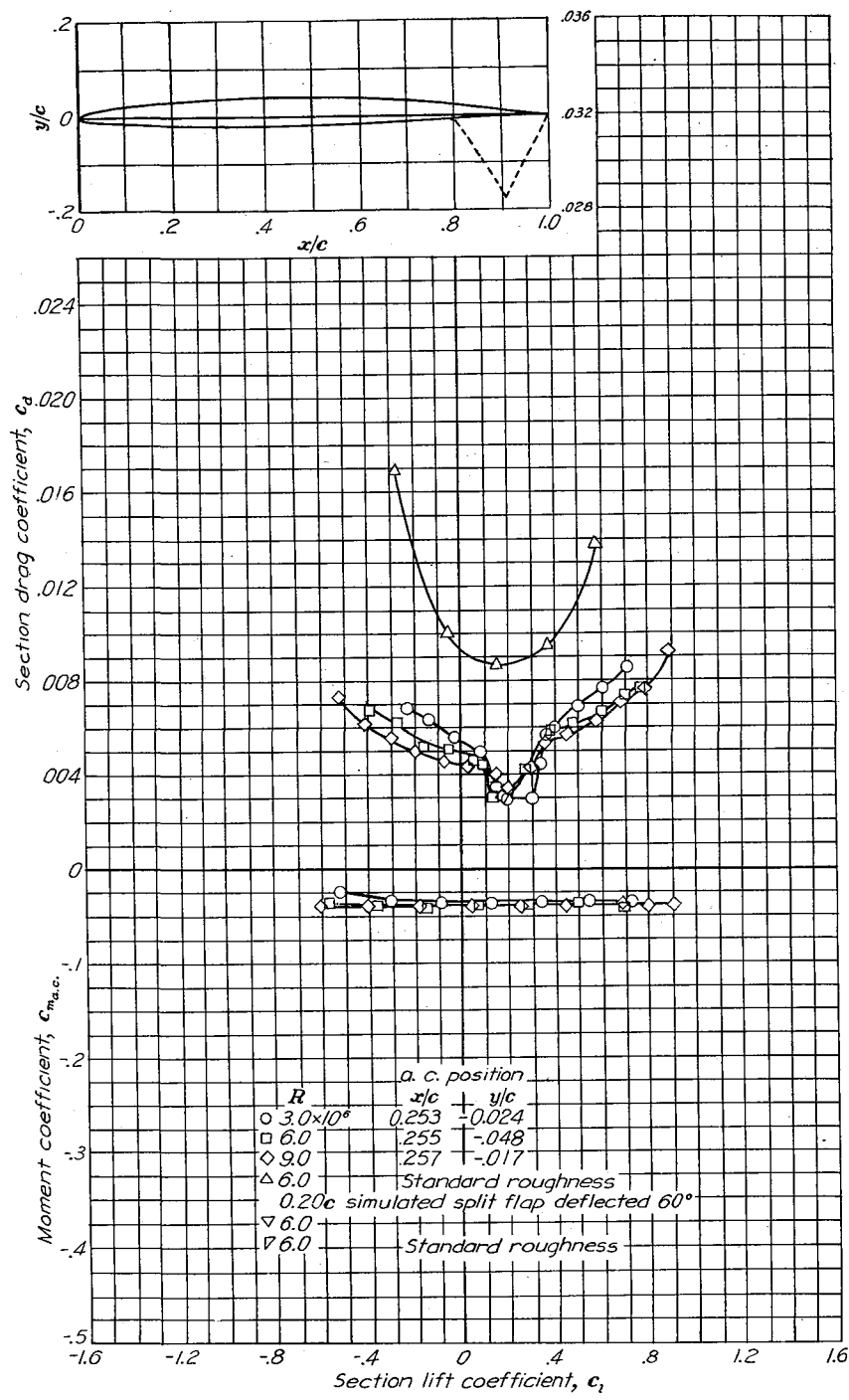
Aerodynamic characteristics of the NACA 66-009 airfoil section, 24-inch chord.

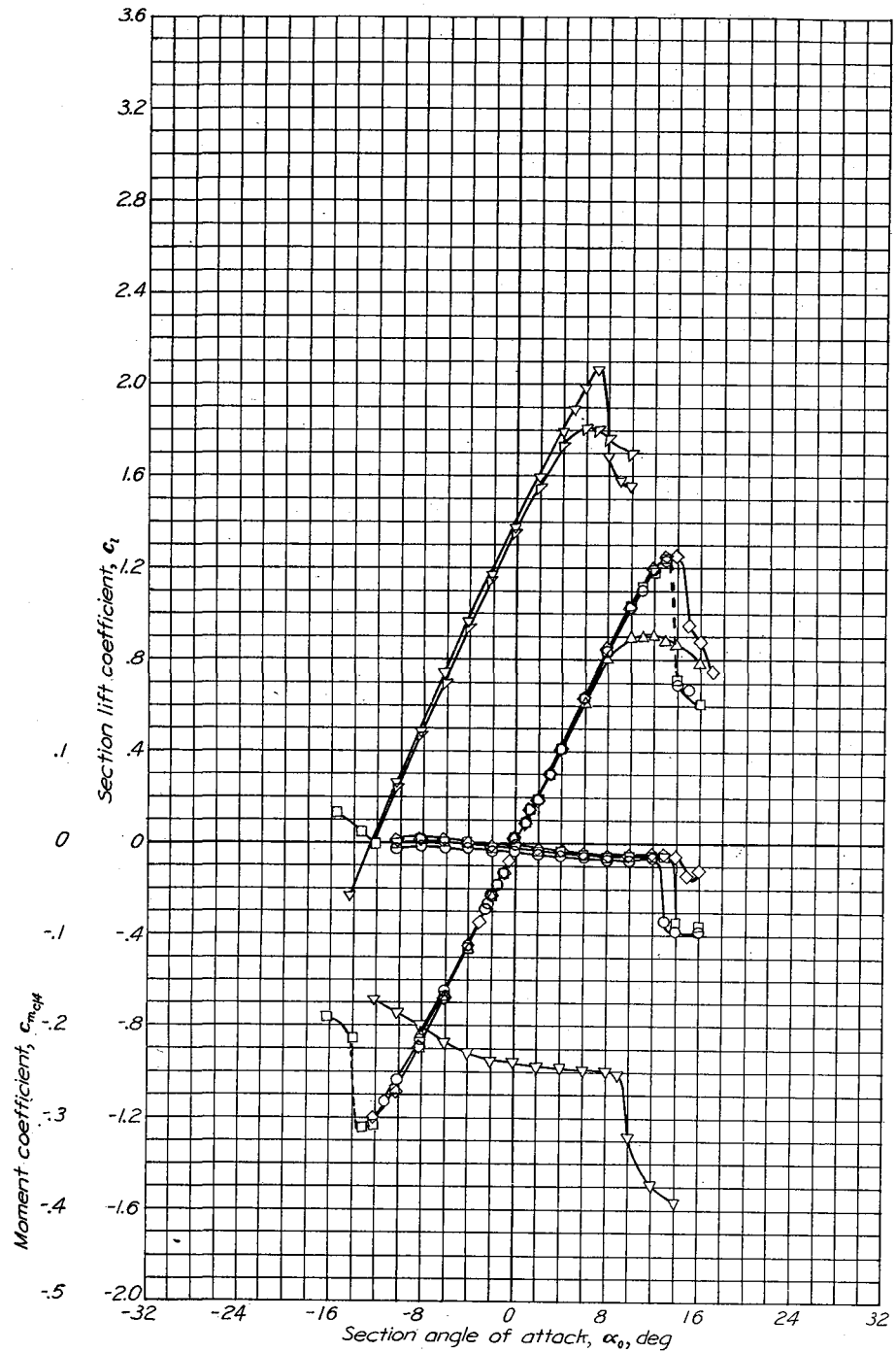




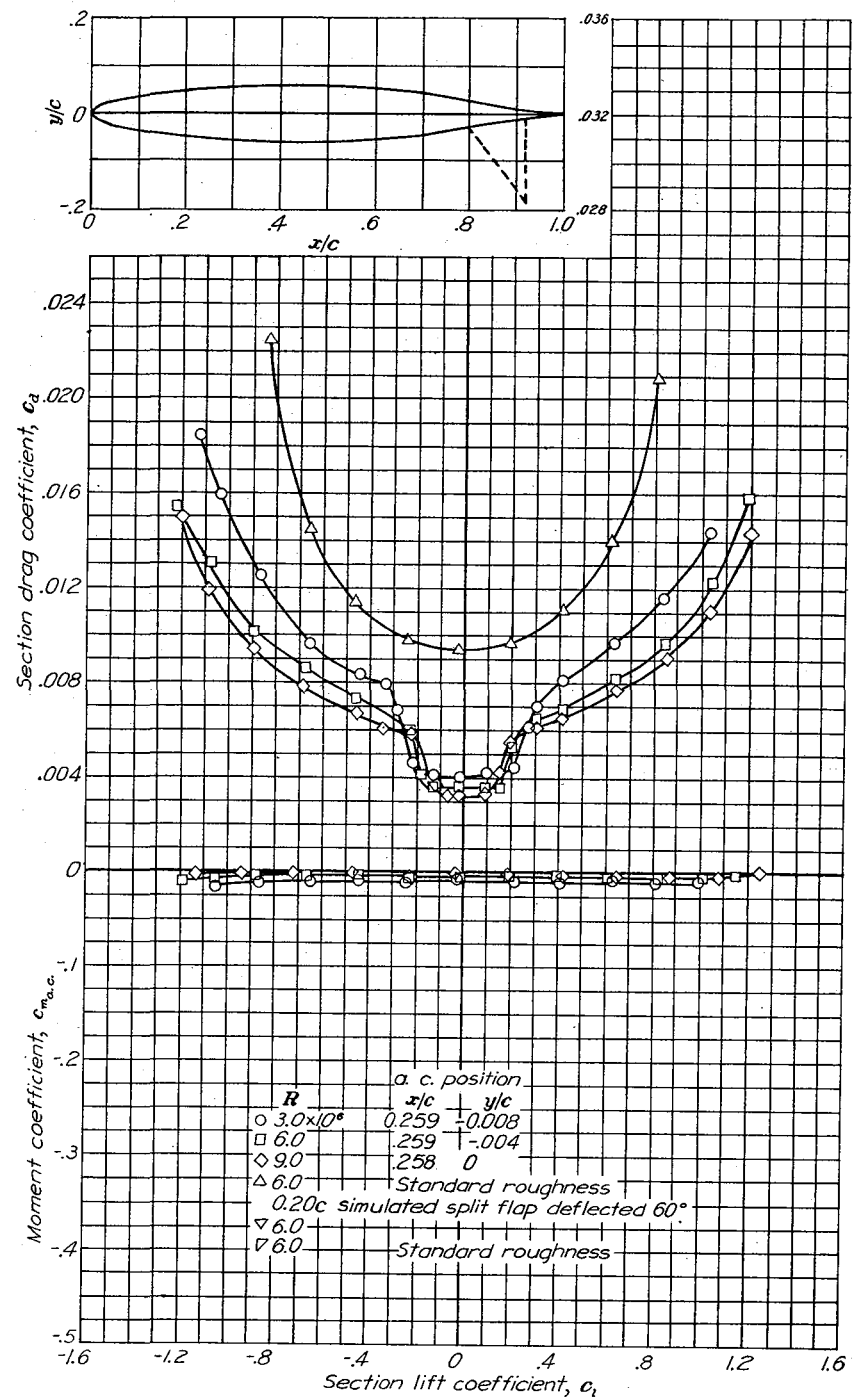


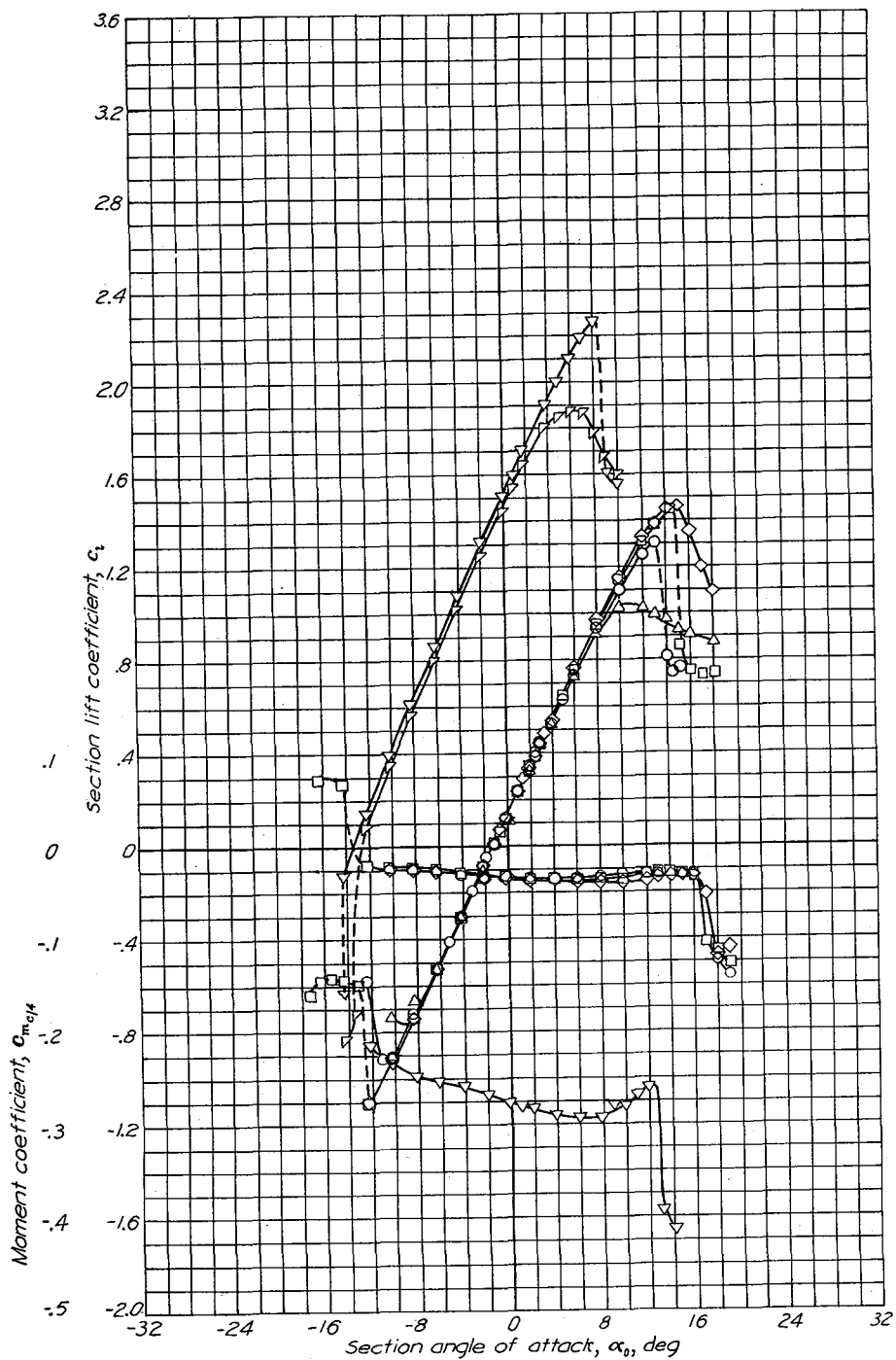
Aerodynamic characteristics of the NACA 66-206 airfoil section, 24-inch chord.



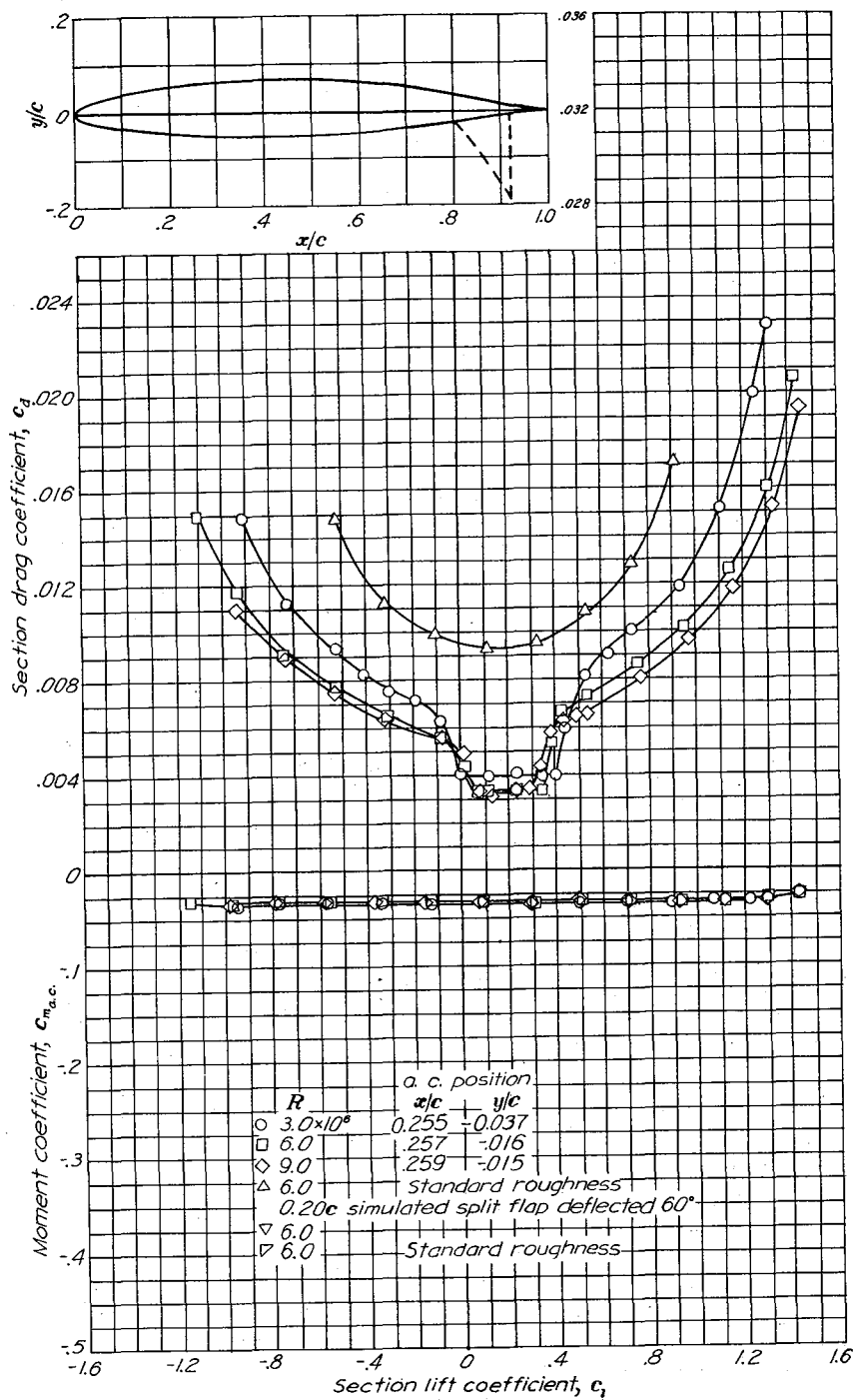


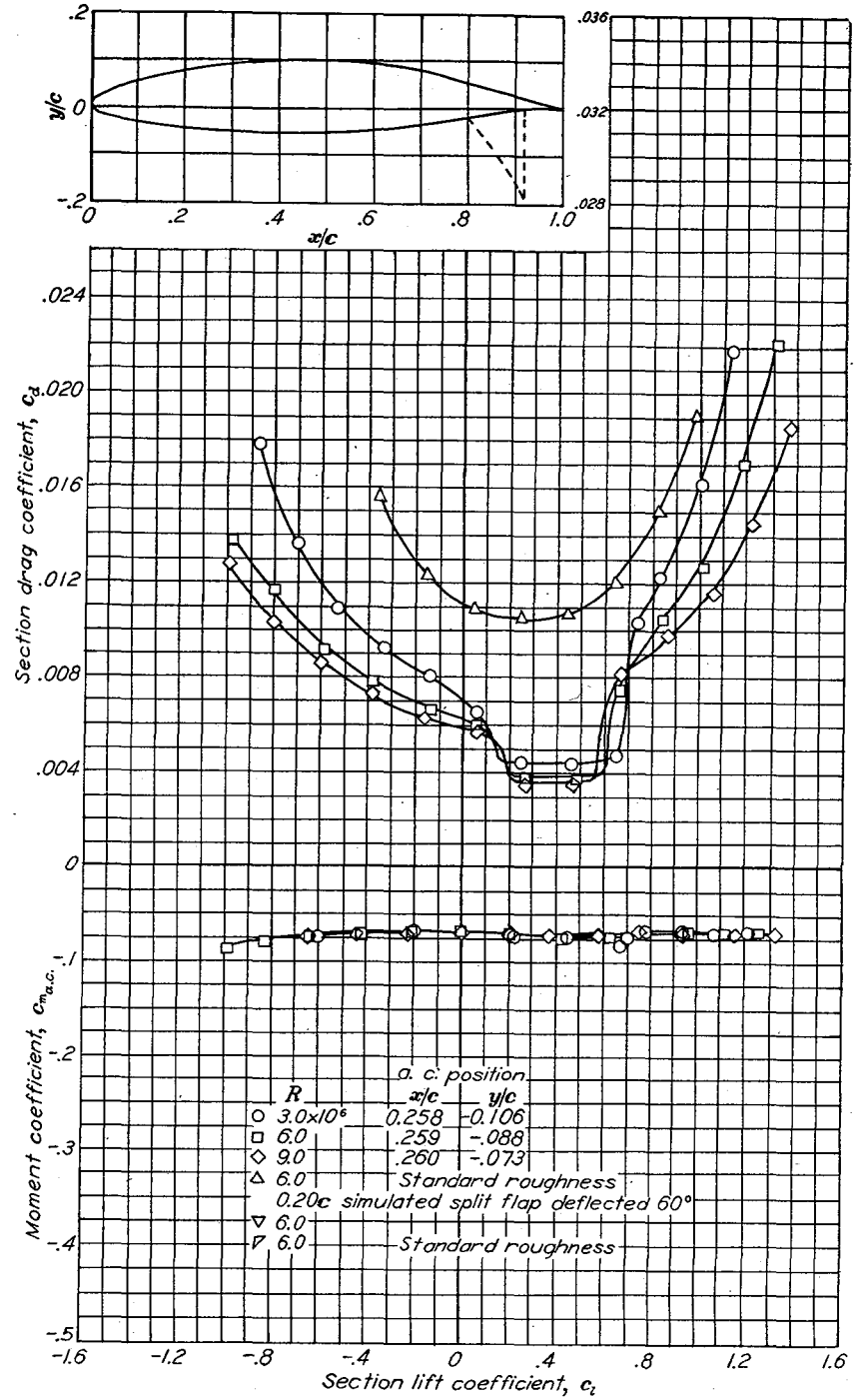
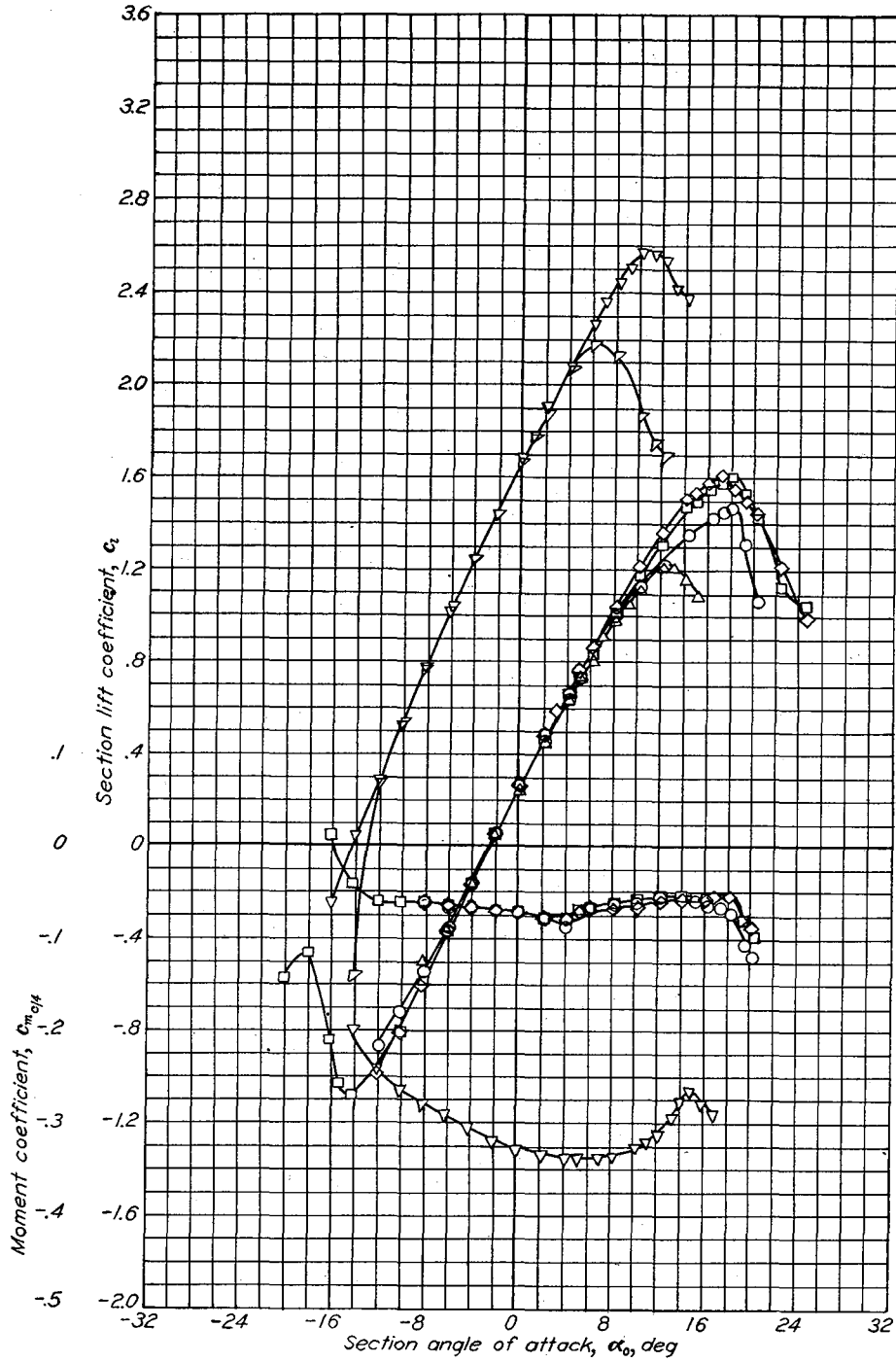
Aerodynamic characteristics of the NACA 661-012 airfoil section, 24-inch chord.



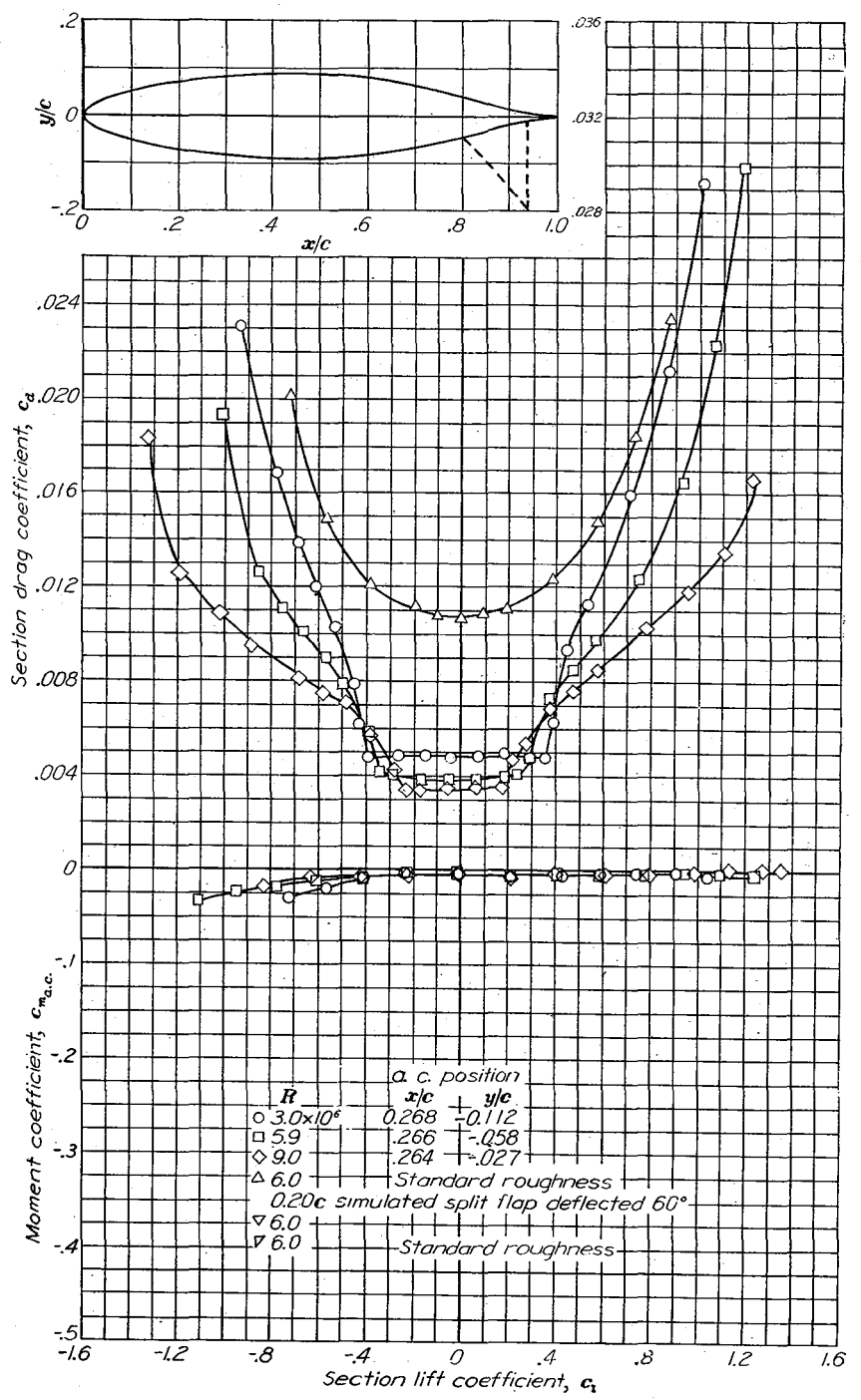
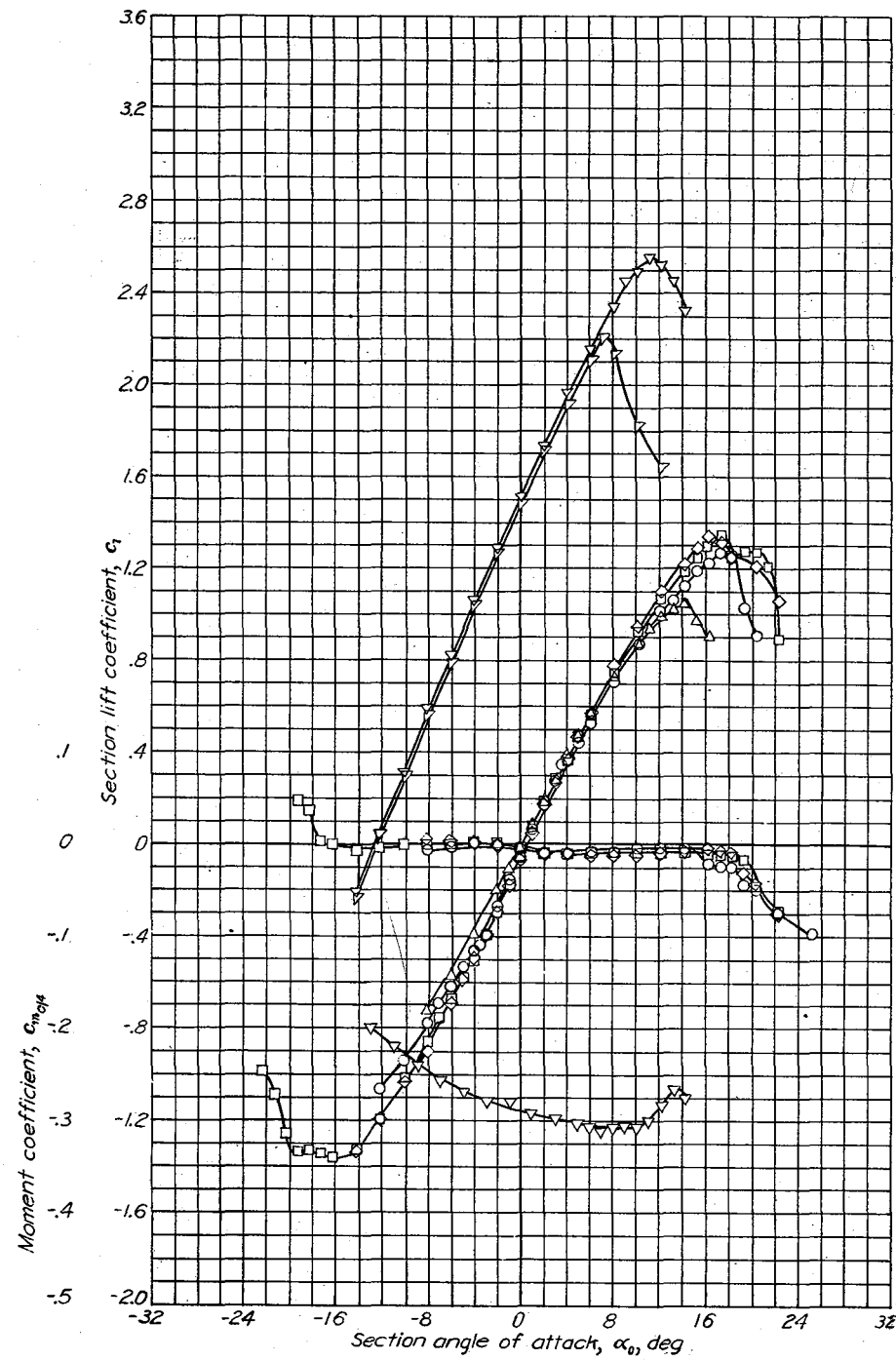


Aerodynamic characteristics of the NACA 661-212 airfoil section, 24-inch chord.

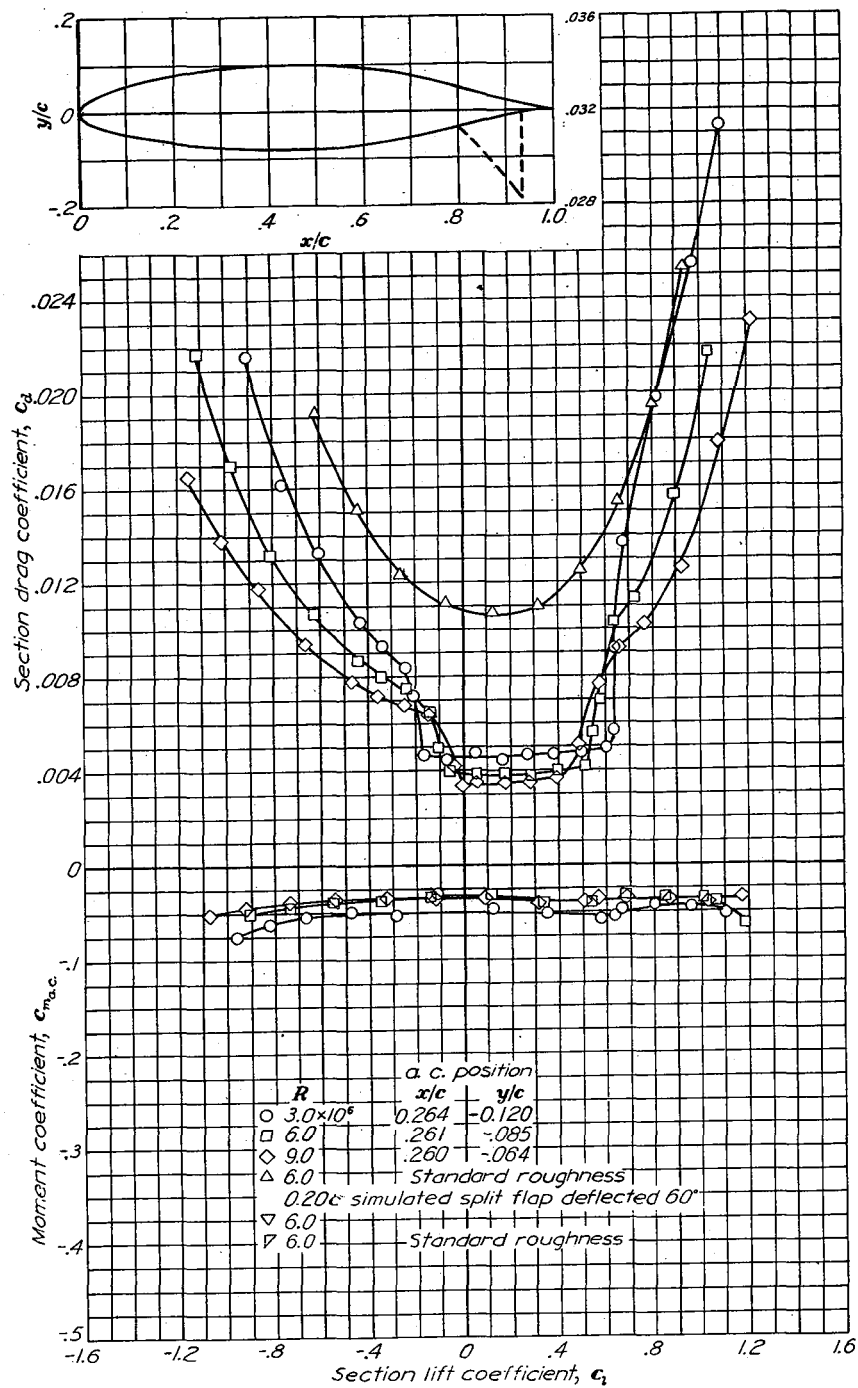
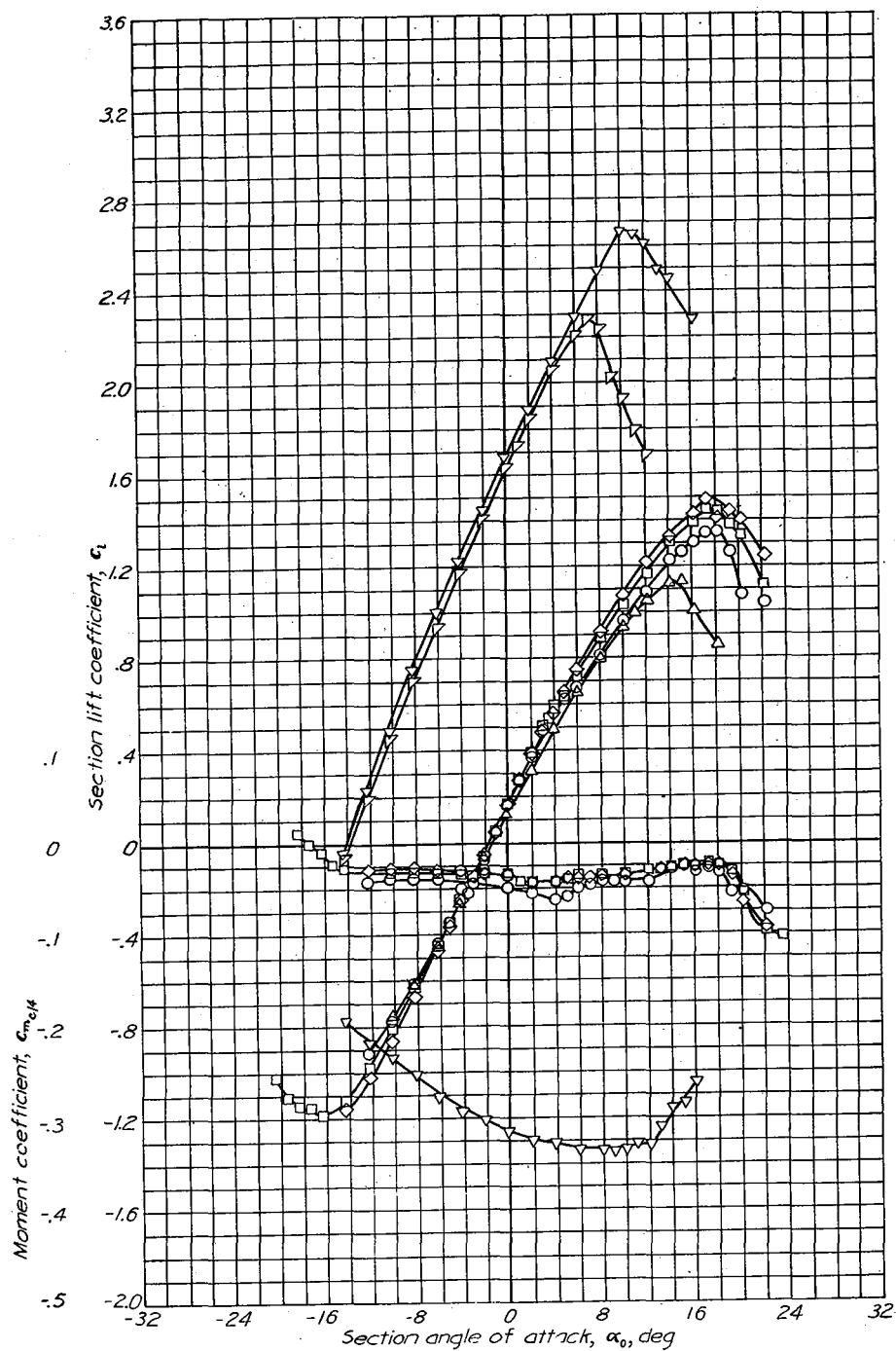




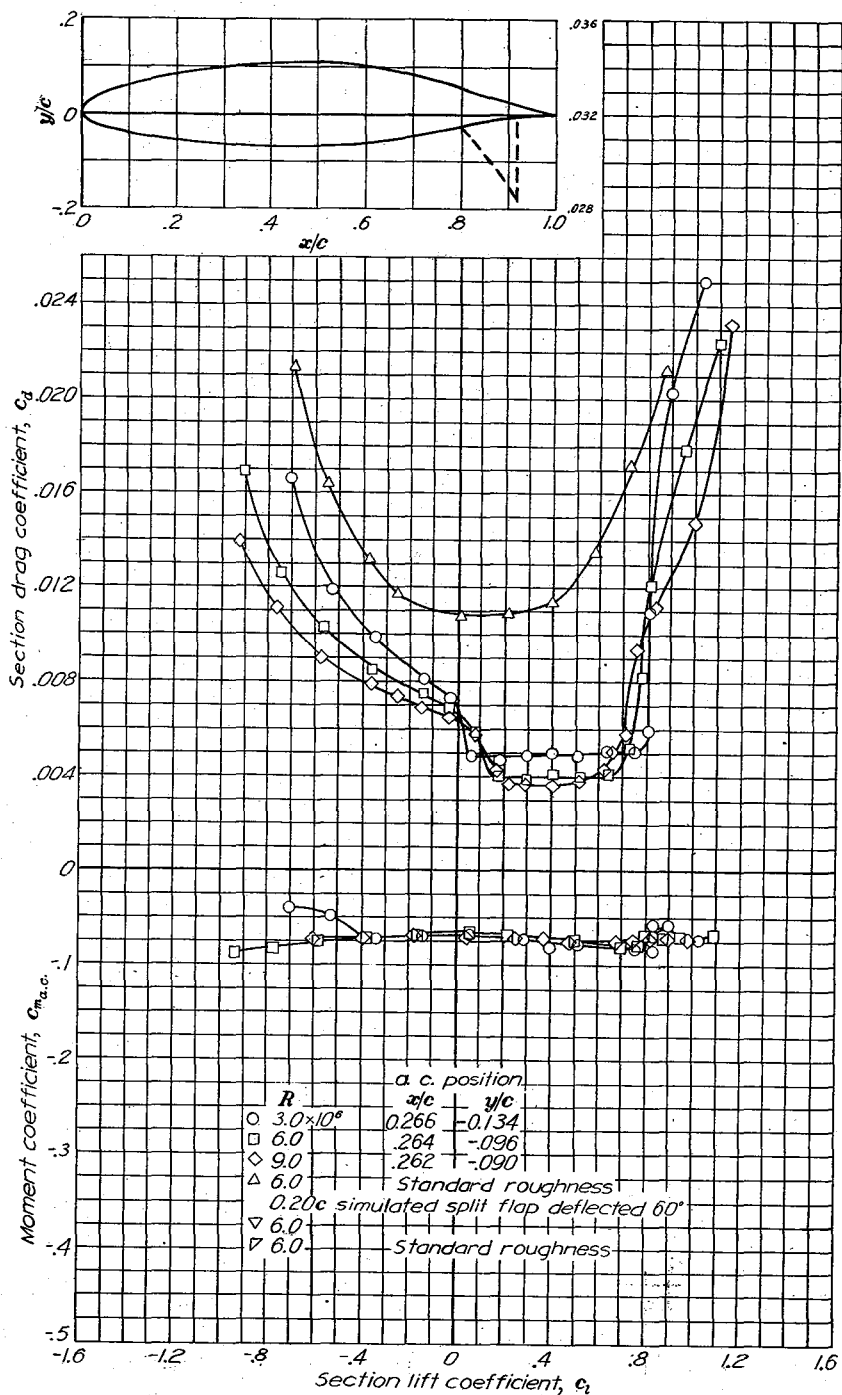
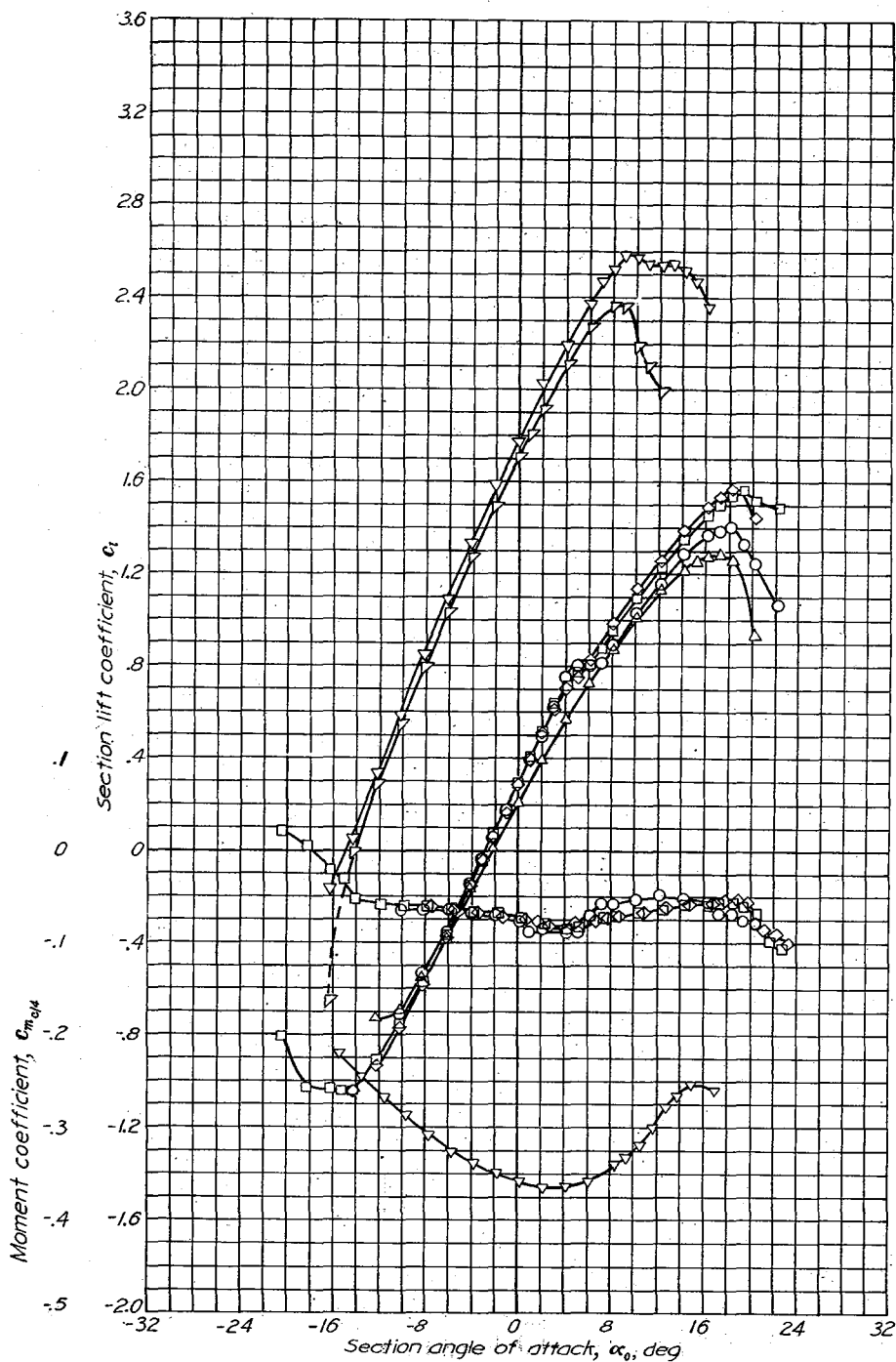
Aerodynamic characteristics of the NACA 662-415 airfoil section. 24-inch chord.



Aerodynamic characteristics of the NACA 663-018 airfoil section, 24-inch chord.

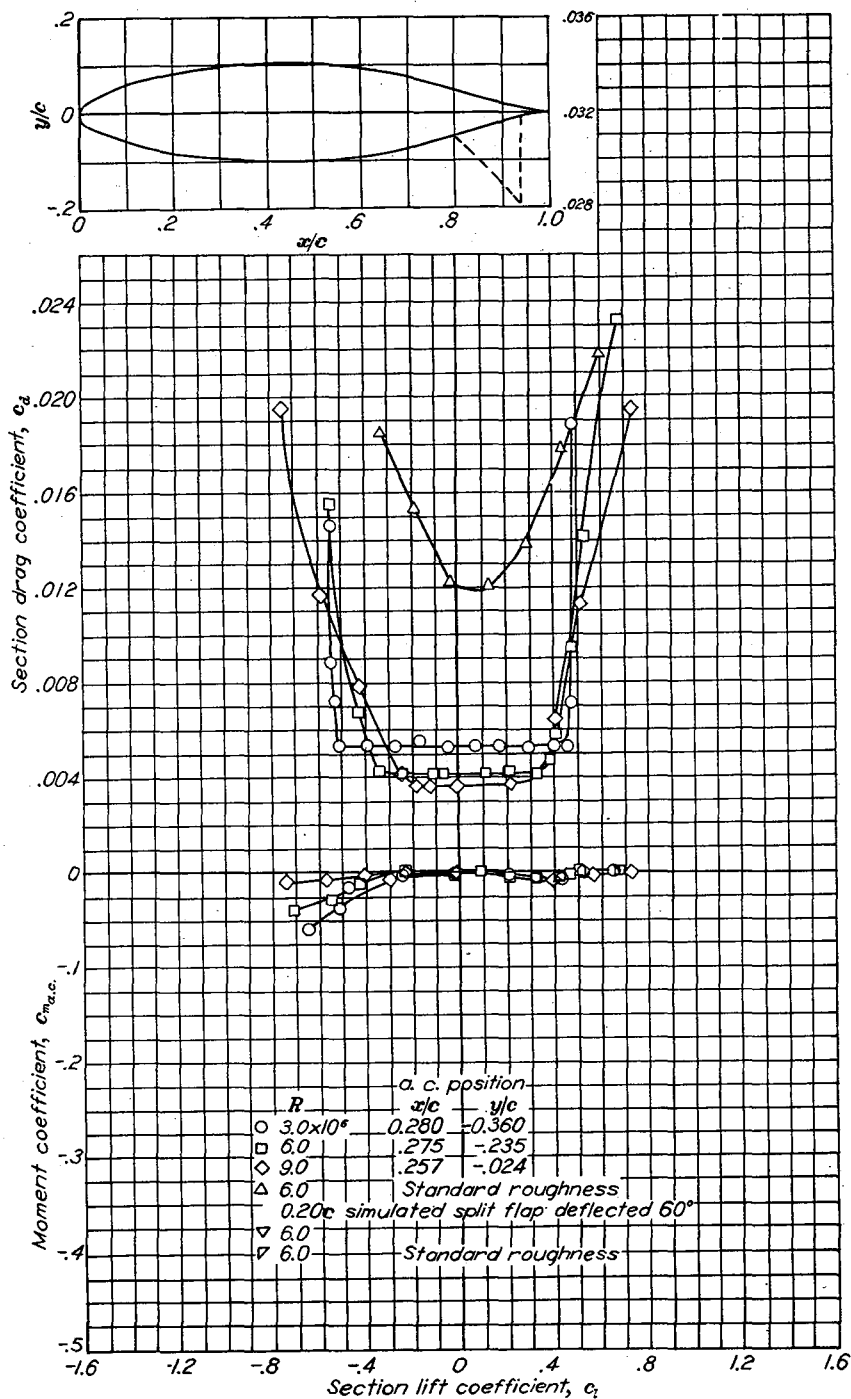
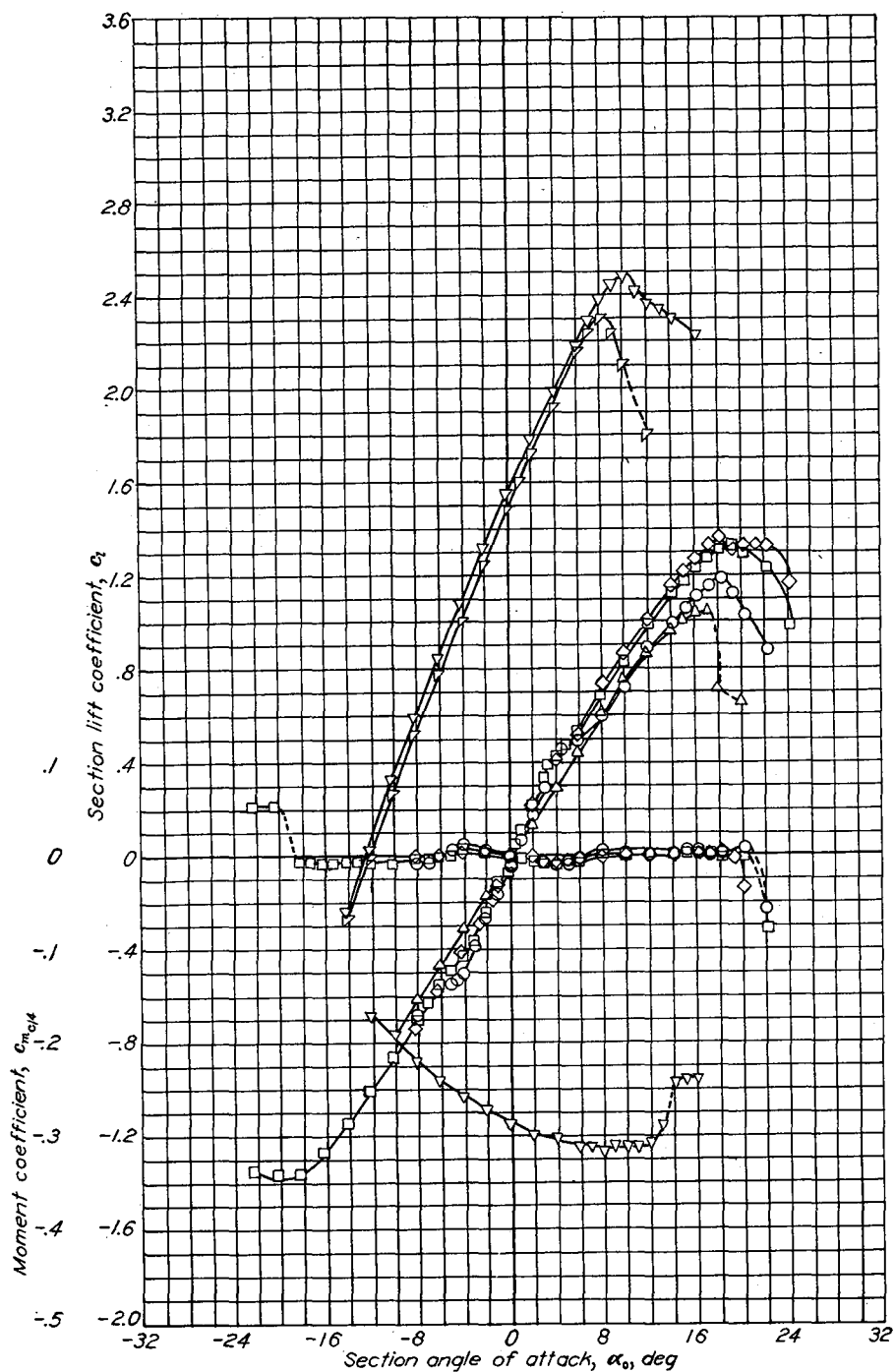


Aerodynamic characteristics of the NACA 663-218 airfoil section, 24-inch chord.



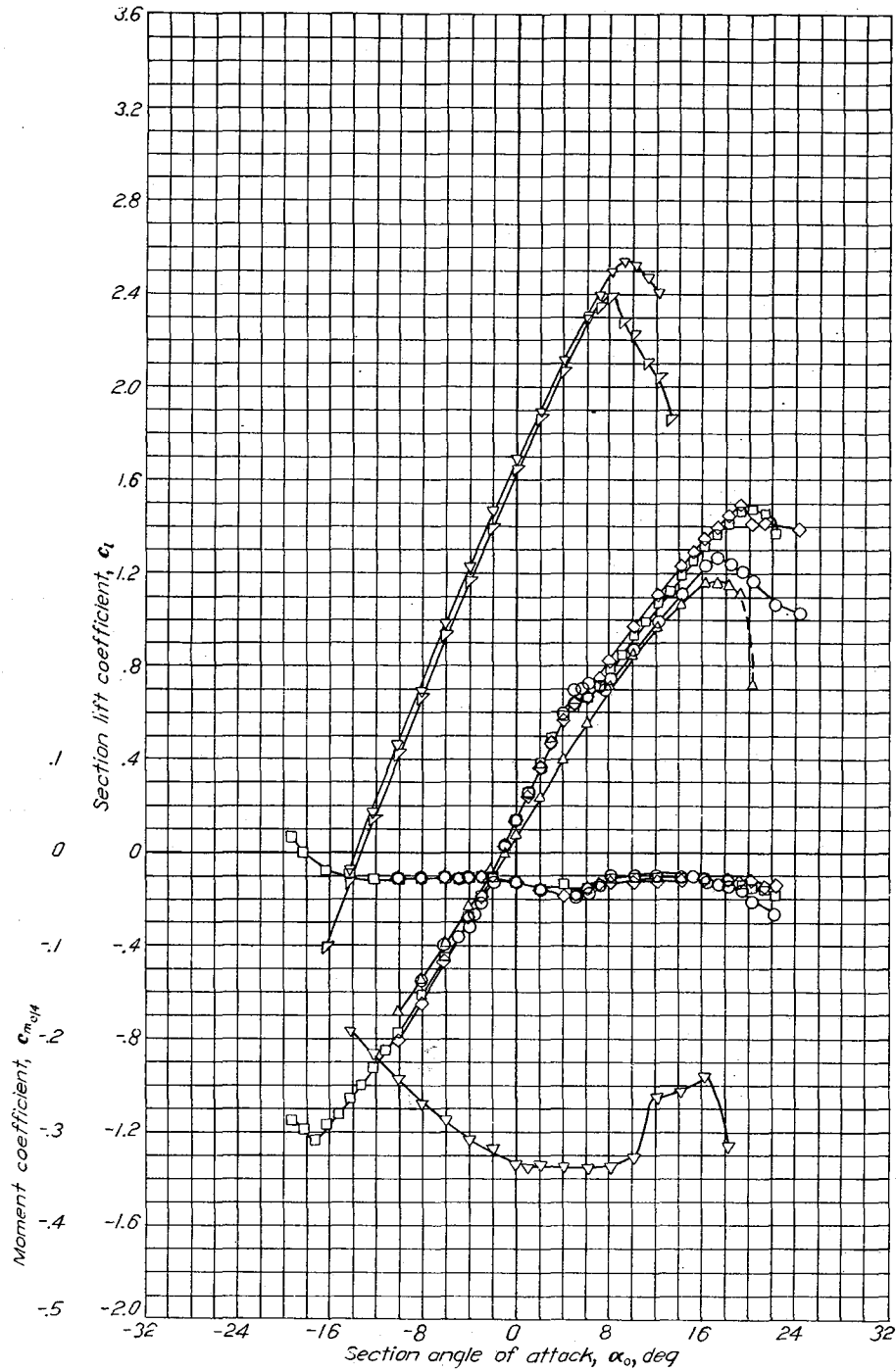
Aerodynamic characteristics of the NACA 663-418 airfoil section, 24-inch chord.

NACA 664-021

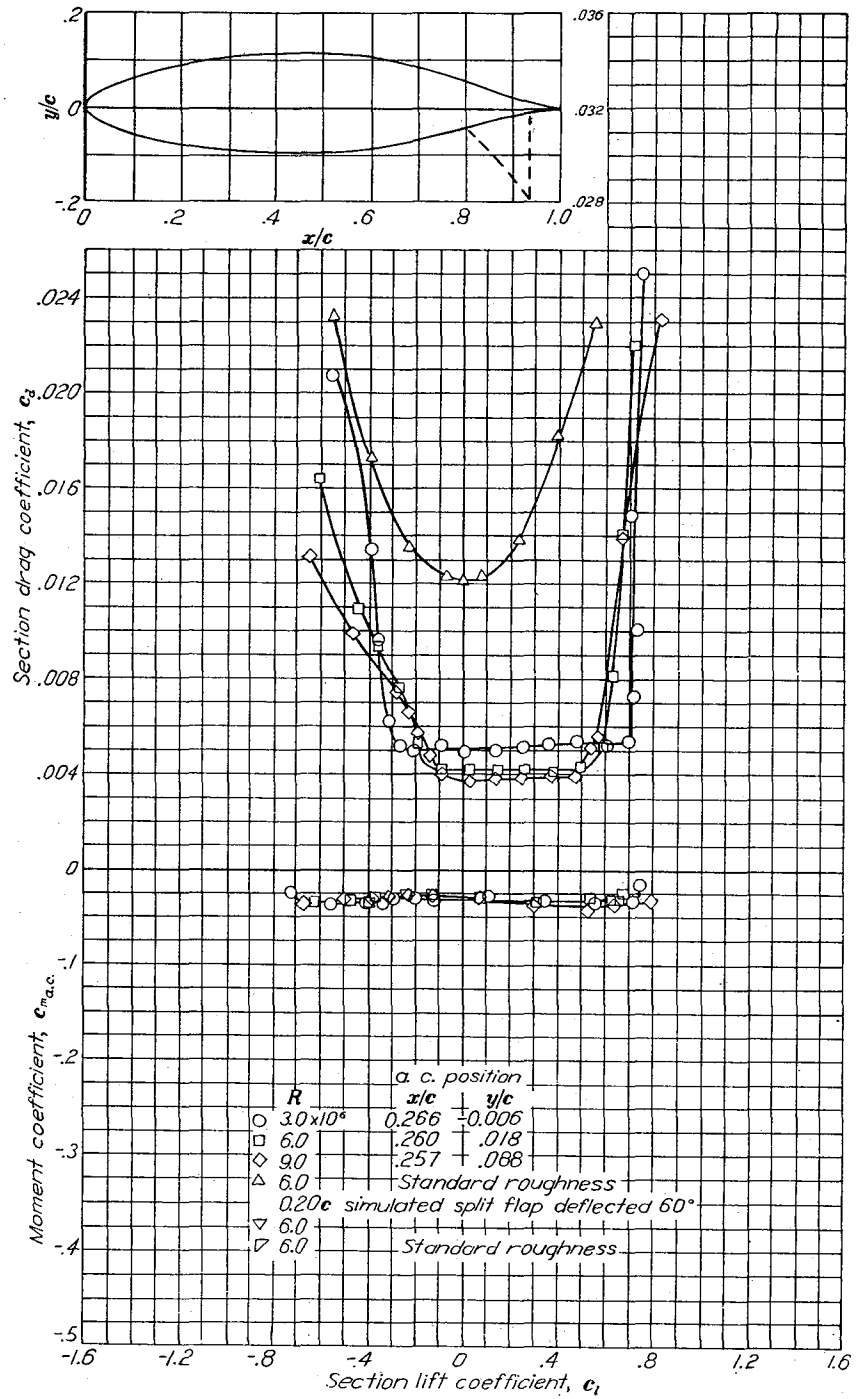


Aerodynamic characteristics of the NACA 664-021 airfoil section, 24-inch chord.

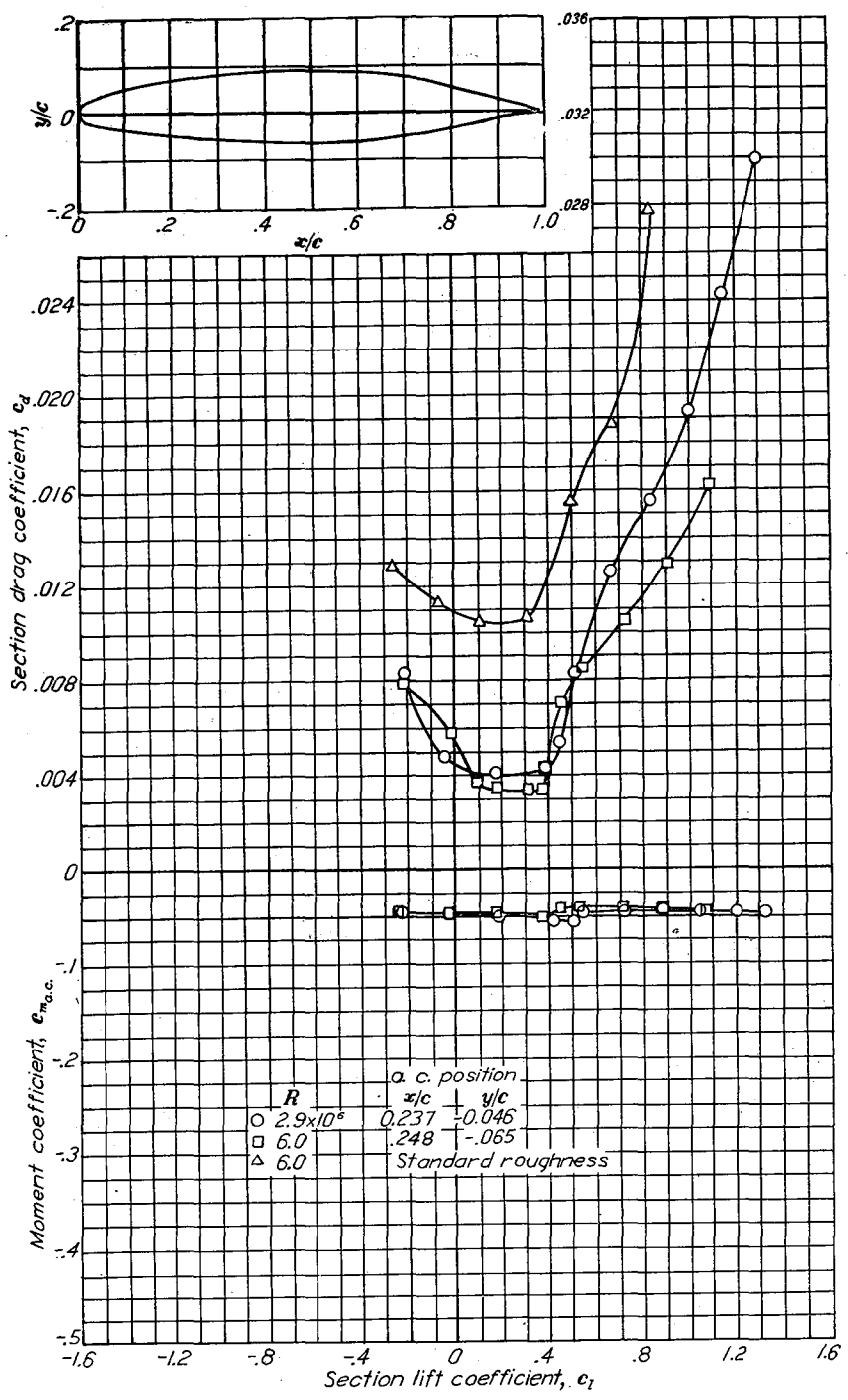
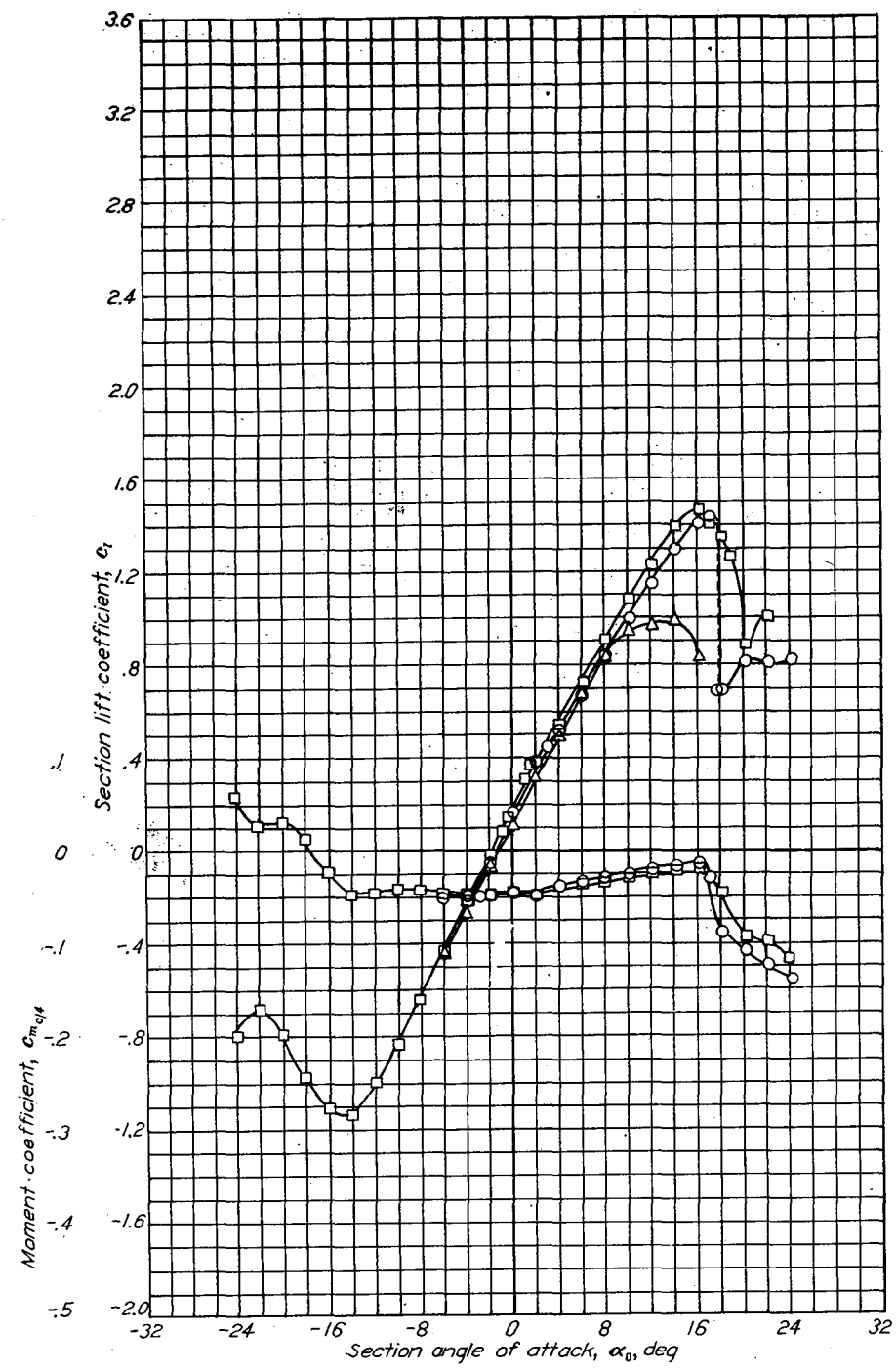




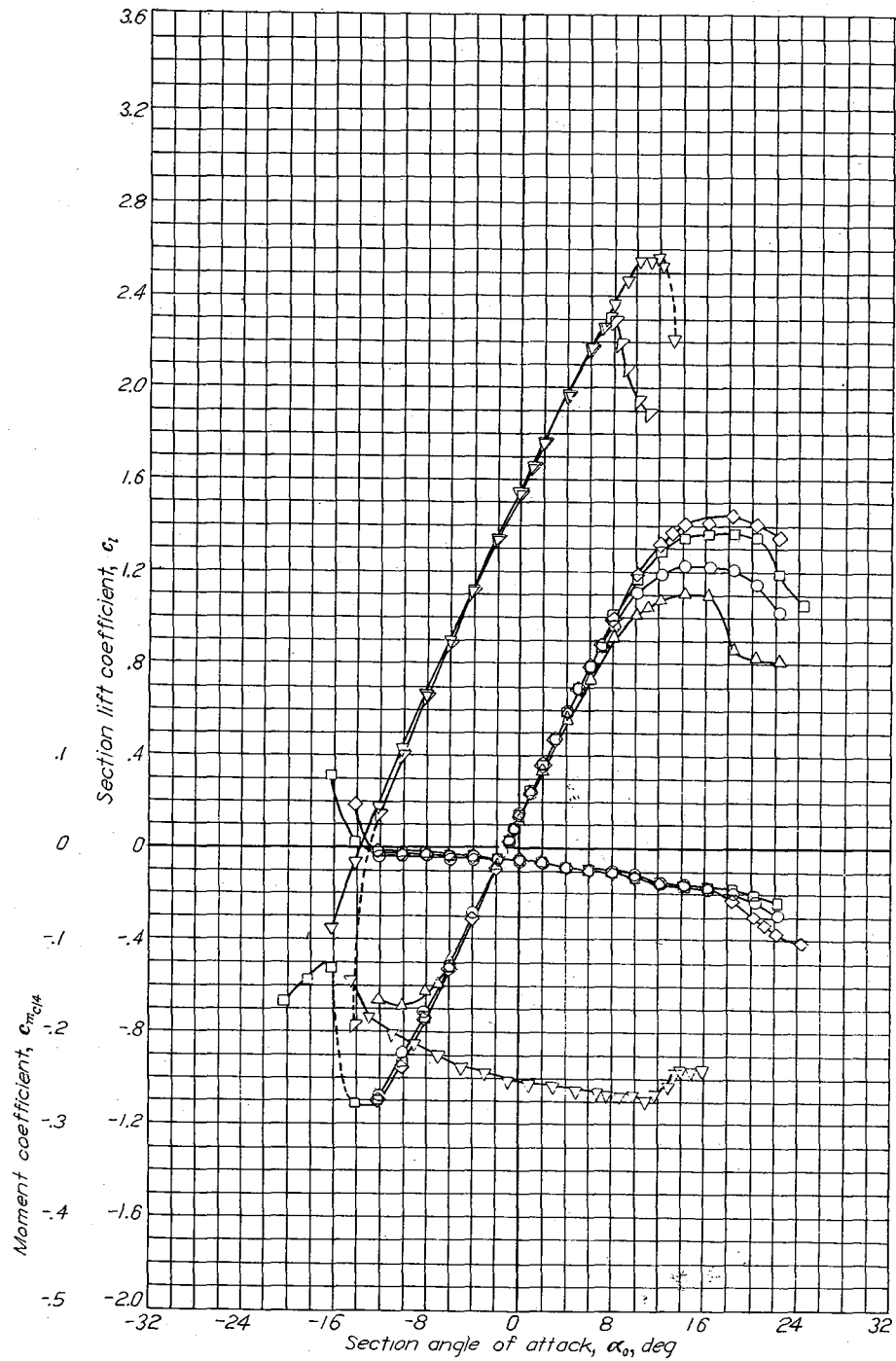
Aerodynamic characteristics of the NACA 66-221 airfoil section, 24-inch chord.



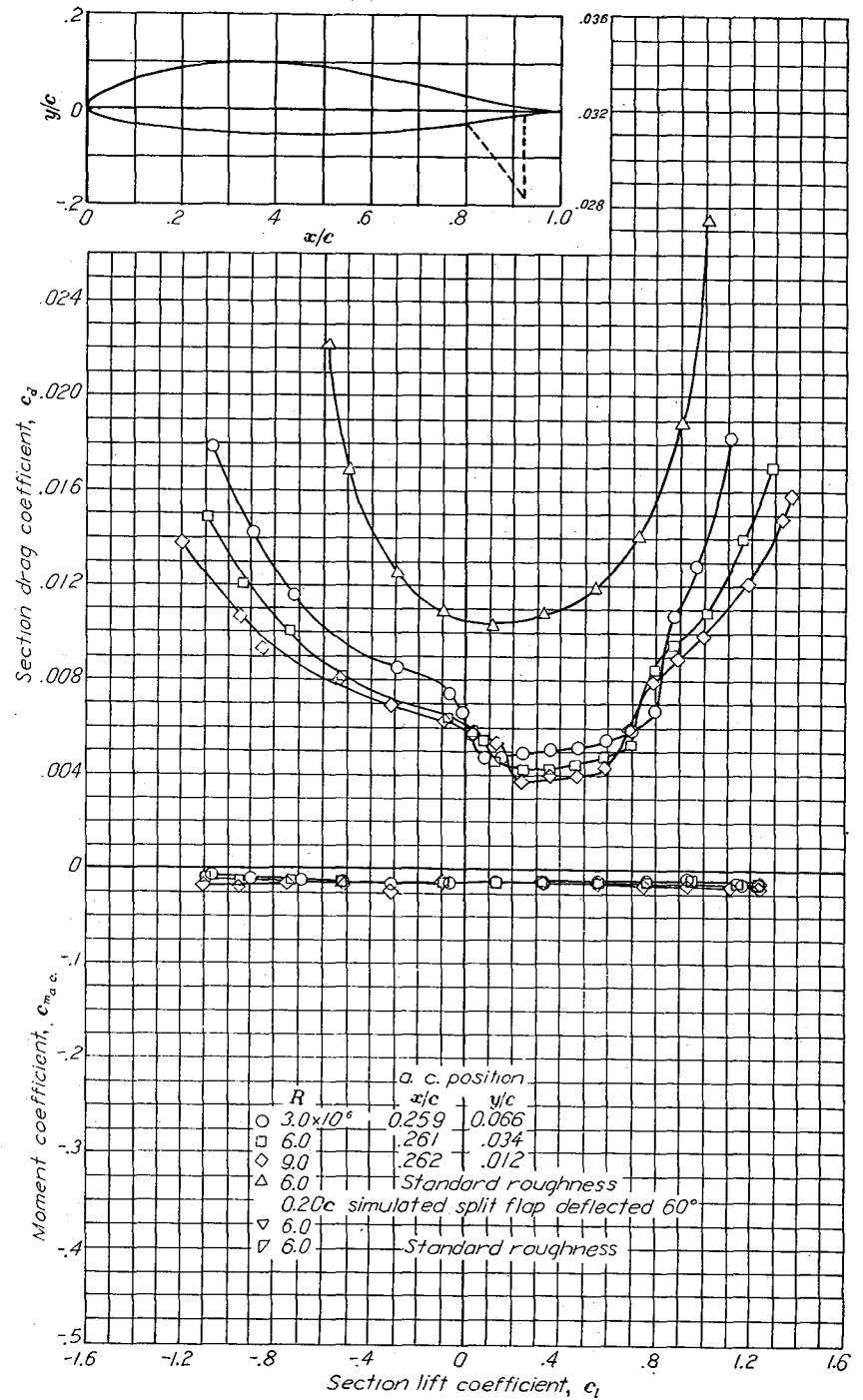
NACA 66-221

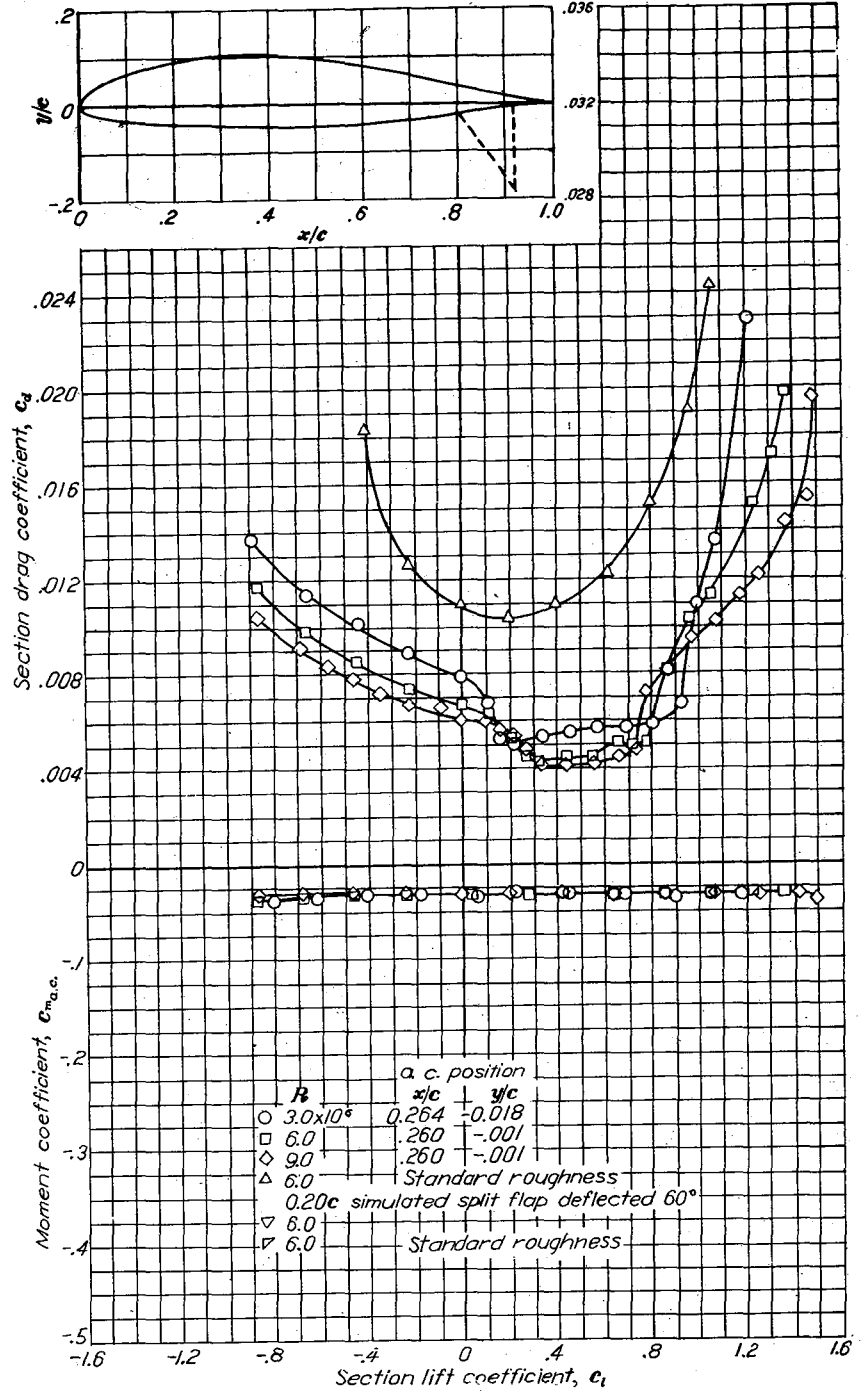
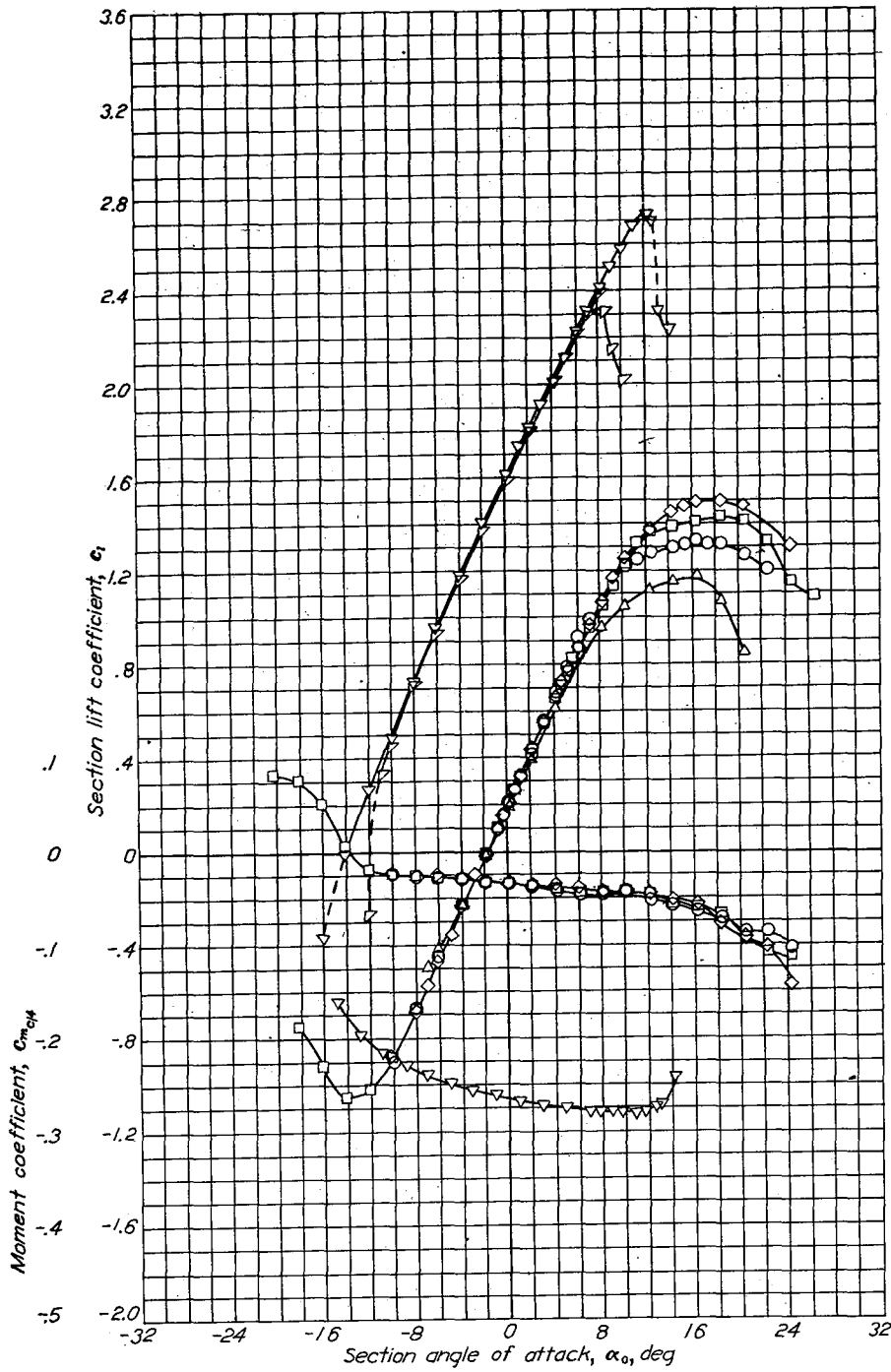


Aerodynamic characteristics of the NACA 67,1-215 airfoil section, 24-inch chord.

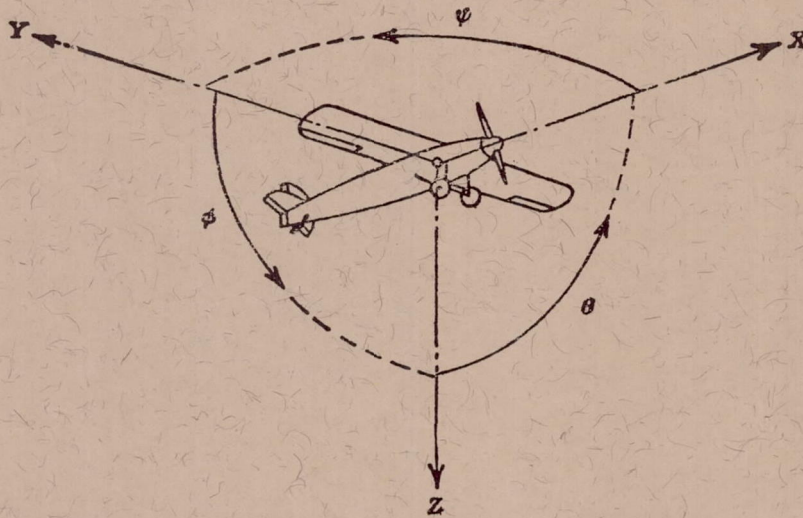


Aerodynamic characteristics of the NACA 747A315 airfoil section, 24-inch chord.





Aerodynamic characteristics of the NACA 747A415 airfoil section, 24-inch chord.



Positive directions of axes and angles (forces and moments) are shown by arrows

Axis		Force (parallel to axis) symbol	Moment about axis			Angle		Velocities	
Designation	Sym- bol		Designation	Sym- bol	Positive direction	Designa- tion	Sym- bol	Linear (compo- nent along axis)	Angular
Longitudinal.....	X	X	Rolling.....	L	Y → Z	Roll.....	φ	u	p
Lateral.....	Y	Y	Pitching.....	M	Z → X	Pitch.....	θ	v	q
Normal.....	Z	Z	Yawing.....	N	X → Y	Yaw.....	ψ	w	r

Absolute coefficients of moment

$$C_l = \frac{L}{qbS} \quad C_m = \frac{M}{qcS} \quad C_n = \frac{N}{qbS}$$

(rolling)      (pitching)      (yawing)

Angle of set of control surface (relative to neutral position),  $\delta$ . (Indicate surface by proper subscript.)

#### 4. PROPELLER SYMBOLS

$D$  Diameter  
 $p$  Geometric pitch  
 $p/D$  Pitch ratio  
 $V'$  Inflow velocity  
 $V_s$  Slipstream velocity  
 $T$  Thrust, absolute coefficient  $C_T = \frac{T}{\rho n^2 D^4}$   
 $Q$  Torque, absolute coefficient  $C_Q = \frac{Q}{\rho n^2 D^5}$

$P$  Power, absolute coefficient  $C_P = \frac{P}{\rho n^3 D^5}$   
 $C_s$  Speed-power coefficient  $= \sqrt[5]{\frac{\rho V^5}{P n^2}}$   
 $\eta$  Efficiency  
 $n$  Revolutions per second, rps  
 $\Phi$  Effective helix angle  $= \tan^{-1}\left(\frac{V}{2\pi r n}\right)$

#### 5. NUMERICAL RELATIONS

1 hp = 76.04 kg-m/s = 550 ft-lb/sec  
 1 metric horsepower = 0.9863 hp  
 1 mph = 0.4470 mps  
 1 mps = 2.2369 mph

1 lb = 0.4536 kg  
 1 kg = 2.2046 lb  
 1 mi = 1,609.35 m = 5,280 ft  
 1 m = 3.2808 ft